METABOLIC ALTERATIONS IN NEURODEGENERATIVE DISORDERS

EDITED BY: David Baglietto-Vargas, Kristine Freude, Ines Moreno-Gonzalez and Carlos J. Rodriguez-Ortiz

PUBLISHED IN: Frontiers in Aging Neuroscience

frontiers Research Topics

ISSN 1664-8714
ISBN 978-2-88974-672-9
DOI 10.3389/978-2-88974-672-9

About Frontiers

Frontiers is more than just an open-access publisher of scholarly articles: it is a pioneering approach to the world of academia, radically improving the way scholarly research is managed. The grand vision of Frontiers is a world where all people have an equal opportunity to seek, share and generate knowledge. Frontiers provides immediate and permanent online open access to all its publications, but this alone is not enough to realize our grand goals.

Frontiers Journal Series

The Frontiers Journal Series is a multi-tier and interdisciplinary set of open-access, online journals, promising a paradigm shift from the current review, selection and dissemination processes in academic publishing. All Frontiers journals are driven by researchers for researchers; therefore, they constitute a service to the scholarly community. At the same time, the Frontiers Journal Series operates on a revolutionary invention, the tiered publishing system, initially addressing specific communities of scholars, and gradually climbing up to broader public understanding, thus serving the interests of the lay society, too.

Dedication to Quality

Each Frontiers article is a landmark of the highest quality, thanks to genuinely collaborative interactions between authors and review editors, who include some of the world's best academicians. Research must be certified by peers before entering a stream of knowledge that may eventually reach the public - and shape society; therefore, Frontiers only applies the most rigorous and unbiased reviews.
Frontiers revolutionizes research publishing by freely delivering the most outstanding research, evaluated with no bias from both the academic and social point of view. By applying the most advanced information technologies, Frontiers is catapulting scholarly publishing into a new generation.

What are Frontiers Research Topics?

Frontiers Research Topics are very popular trademarks of the Frontiers Journals Series: they are collections of at least ten articles, all centered on a particular subject. With their unique mix of varied contributions from Original Research to Review Articles, Frontiers Research Topics unify the most influential researchers, the latest key findings and historical advances in a hot research area! Find out more on how to host your own Frontiers Research Topic or contribute to one as an author by contacting the Frontiers Editorial Office: frontiersin.org/about/contact

METABOLIC ALTERATIONS IN NEURODEGENERATIVE DISORDERS

Topic Editors:
David Baglietto-Vargas, University of Malaga, Spain
Kristine Freude, University of Copenhagen, Denmark
Ines Moreno-Gonzalez, University of Malaga, Spain
Carlos J. Rodriguez-Ortiz, University of California, Irvine, United States

Citation: Baglietto-Vargas, D., Freude, K., Moreno-Gonzalez, I., Rodriguez-Ortiz, C. J., eds. (2022). Metabolic Alterations in Neurodegenerative Disorders. Lausanne: Frontiers Media SA. doi: 10.3389/978-2-88974-672-9

Table of Contents

frontiers in Aging Neuroscience

EDITORIAL
published: 18 February 2022
doi: 10.3389/fnagi.2022.833109

Editorial: Metabolic Alterations in Neurodegenerative Disorders

Kristine K. Freude[1], *Ines Moreno-Gonzalez*[2,3], *Carlos J. Rodriguez-Ortiz*[4] *and David Baglietto-Vargas*[2,3]*

[1] Department of Veterinary and Animal Sciences, Faculty of Health and Medical Sciences, University of Copenhagen, Frederiksberg, Denmark, [2] Departamento Biologia Celular, Genetica y Fisiologia, Instituto de Investigacion Biomedica de Malaga, Facultad de Ciencias, Universidad de Malaga, Malaga, Spain, [3] Centro de Investigacion Biomedica en Red Sobre Enfermedades Neurodegenerativas, Madrid, Spain, [4] Institute for Memory Impairments and Neurological Disorders, University of California, Irvine, Irvine, CA, United States

Keywords: neurodegenerative disorders, hyperlipidemia, metabolism, blood-brain barrier, astrocytes, ceramides, probiotics, anesthesia

Editorial on the Research Topic

Metabolic Alterations in Neurodegenerative Disorders

The world's population is growing larger and older due to extended life span, resulting from improved medical intervention possibilities, assistance, and overall quality of life. However, associated with this increased life expectancy, the number of neurodegenerative disorders (NDDs) such as Alzheimer's disease (AD), Parkinson's disease (PD), Huntington's disease (HD), and many other diseases has increased exponentially in the past few decades, causing a progressive and irreversible deterioration of the brain and disturbing the daily activity of affected individuals and their families (Dugger and Dickson, 2017). Novel evidence has indicated that these NDDs are intimately connected to metabolic alterations, which facilitate or trigger the progression of these disorders (Muddapu et al., 2020). Therefore, this special issue focuses on investigating the factors and mechanisms by which metabolic alterations trigger the onset and enhance the progression of NDDs. As such, Hefner et al., highlighted the impact of metabolic alterations such as type 2 diabetes mellitus (T2DM), obesity and non-alcoholic fatty liver disease (NAFLD) into the development of different proteinopathies such as AD. Specifically, this review argues that cardiometabolic disorders are able to rise amyloid beta (Aβ) peptide levels in the periphery and subsequently cross the blood brain barrier and increase the Aβ levels in the brain. Furthermore, Li et al., demonstrate that T2DM increases iron concentration in several brain areas, causing neurotoxicity, which can lead to multiple neuronal diseases such as PD, AD, and HD. Overall, these studies highlight the importance of specific cardiometabolic diseases affecting both peripheral and central nervous system (CNS) through diverse mechanisms, triggering the onset, and progression of multiple NDDs.

One of the earliest pathological changes in many NDDs, including AD, affects cell metabolism and, more specifically, glucose metabolism in neurons (Gordon et al., 2018). In addition, emerging evidence supports the notion that glia cells play a profound role in stable brain metabolism and functionality of neurons. Consequently, studies investigating the glial contribution besides glucose metabolism could reveal functional insights into altered metabolic features in AD brains. In this special issue, Salcedo et al. investigate the role of branched-chain amino acids (BCAAs) in both primary astrocytes derived from familial AD (fAD) mouse models and from astrocytes derived from human induced pluripotent stem cells (hiPSCs). BCAA's are central to neurotransmitter cycling (Yudkoff et al., 1996) and the authors elegantly show that BCAA's are highly metabolized in astrocytes in order to synthesize glutamine. Moreover, they show that hiPSC-derived astrocytes carrying fAD mutations display a reduction in synthesis of neuroactive amino acids. These

OPEN ACCESS

Edited by:
Kyoungho Suk, Kyungpook National University, South Korea

Reviewed by:
Ruqayya Afridi, Kyungpook National University, South Korea
Md Habibur Rahman, The State University of New Jersey, United States

***Correspondence:**
David Baglietto-Vargas
d.baglietto@uma.es

Specialty section:
This article was submitted to Alzheimer's Disease and Related Dementias, a section of the journal Frontiers in Aging Neuroscience

Received: *10 December 2021*
Accepted: *25 January 2022*
Published: *18 February 2022*

Citation:
Freude KK, Moreno-Gonzalez I, Rodriguez-Ortiz CJ and Baglietto-Vargas D (2022) Editorial: Metabolic Alterations in Neurodegenerative Disorders. Front. Aging Neurosci. 14:833109. doi: 10.3389/fnagi.2022.833109

findings underline the importance of decreased alternative substrate usage in AD within the glia compartments of the brain and thereby, contribution to the overall hypometabolism present early on in AD pathology. Another interesting aspect presented in this special issue is the link between APOE status, abundance of ceramides and gender. Ceramides are central to sphingolipid metabolism and whilst reduced ceramide levels promote neuronal survival and fitness; an increase in ceramides, as observed in AD postmortem brains, leads to the opposite and damages neurons (Czubowicz and Strosznajder, 2014). Even though den Hoedt et al. showed limited associations between the APOE4 status and presences of long-chain ceramides [Cer(d18:1/24:0)], they were able to pinpoint another interesting correlation, which includes the observation that the female gender of the mice was affecting ceramide levels in a much stronger way than the APOE4 genotype. This study opens up a future venue of research, which could link specific metabolic alterations to the gender bias observed in AD, with females being twice as likely affected than males.

Another highly relevant study with focus on metabolic substrate and cognitive decline is the clinical study by Kreuzer et al., which identified brain metabolic asymmetric alterations as a common factor coupling neuronal degeneration and cognitive function. In addition, Tang et al. demonstrated that Gamma-Glutamyl transferase, a key enzyme used as indicator of potential hepatic or biliary illness, is commonly upregulated in obese women with mild cognitive decline. In general, these studies highlight the importance of metabolic alterations as a major causative factor leading to cognitive impairments in NDDs.

This collection also includes a review report by Fang et al., summarizing the critical role of Silent information regulator-1 (SIRT1) in the regulation of important biological processes in cellular homeostasis, such as cell growth, apoptosis, inflammation, differentiation, metabolism, and senescence. In regards to energy stress, the study highlights the relevant role of SIRT1 maintaining mitochondrial proper function and biogenesis. Similarly, Tyagi et al., demonstrate that hyperlipidemia, a hallmark characteristic of metabolic syndrome (MetS), may contribute to further alterations in metabolism, inflammation and damage of the blood-brain barrier (BBB) by lowering the level of SIRT3. Thus, these findings support the idea that the SIRT family of signaling proteins are important effectors of metabolic alterations driving several downstream pathological mechanisms resulting in major risks to develop NNDs.

Mitochondrial dysfunction and the formation of reactive oxygen species (ROS) are both common pathological mechanisms that trigger neurodegeneration in several dementia-associated diseases, including AD and PD (Buccellato et al., 2021). Therefore, interventions that mitigate these pathologies are often the focus of studies evaluating potential therapies for NDDs. In this regard, Nurrahma et al. performed a preclinical assay where rat models of PD were supplemented with probiotics in an effort to ameliorate energy metabolism impairments. They reported that rats treated with probiotic supplementation showed amelioration of motor deficits along with restored muscle mass. Additionally, treated animals displayed lower dopaminergic degeneration, elevated mitochondrial function and energy metabolism, and reduced PD pathology. Although ROS species formation is a major pathological event triggering AD and PD, little is known about this in HD. A novel study led by Villegas et al. discusses the importance of NADPH oxidases (NOXs) in neuronal cells and how NOX contributes to redox levels and affects important biological processes, such as neurogenesis, neurite outgrowth, and synaptic plasticity. These studies highlight ROS as a major harmful factor in NDDs, and how modulating NOX levels, as well as probiotic supplementation, could represent a novel therapeutic intervention to mitigate ROS.

General anesthetics is a common medical approach in many surgical procedure, however, recent clinical evidences have shown that patients under anesthesia can develop profound cognitive alterations, including post-operative delirium (POD) (Cottrell and Hartung, 2020). In regard with this, Lin et al. has showed that hip replacement, one of the most common medical procedure, is associated with clinical cognitive disorders. In addition, new scientific evidences showed that metabolic alterations and T2DM aggravate the risk to suffer POD (Hudetz et al., 2011). In this sense, Peng et al., have demonstrated that mice on a high fat diet (HFD) and under long-term exposure to the anesthetic isoflurane, developed significant insulin resistance (IR), and cognitive impairments. Metformin, an antidiabetic compound, could reverse the observed phenotypes of IR, tau hyperphosphorylation and cognitive deficits in mice. These studies demonstrate that general anesthetic procedure is a risk factor for development or progression of cognitive decline, which is aggravated when metabolic alterations are present in the patients.

Overall, this special issue contains a series of compelling studies that provide critical view into the mechanisms and pathological processes by which metabolic alterations drive the development of several NDDs.

AUTHOR CONTRIBUTIONS

KF, IM-G, CR-O, and DB-V have contributed to the manuscript writing and editing. DB-V has coordinated, reviewed, and submitted the editorial manuscript. All authors contributed to the article and approved the submitted version.

FUNDING

This study was supported by awards from the Innovation Fund Denmark (BrainStem, 4108-00008B) (KF), Novo Nordisk Foundation (GliAD—NNF18OC0052369 and NNF19OC0058399) (KF), Spanish Ministry of Science and Innovation PID2019-108911RA-100 (DB-V) and PID2019-107090RA-100 (IM-G), Beatriz Galindo program BAGAL18/00052 (DB-V), RYC-2017-21879 (IM-G), UMA20-FEDERJA-104 (IM-G), and B1-2019_06 (IM-G).

REFERENCES

Buccellato, F. R., D'Anca, M., Fenoglio, C., Scarpini, E., and Galimberti, D. (2021). Role of oxidative damage in Alzheimer's disease and neurodegeneration: from pathogenic mechanisms to biomarker discovery. *Antioxidants (Basel)* 10:1353. doi: 10.3390/antiox10091353

Cottrell, J. E., and Hartung, J. (2020). Anesthesia and cognitive outcome in elderly patients: a narrative viewpoint. *J. Neurosurg. Anesthesiol.* 32, 9–17. doi: 10.1097/ANA.0000000000000640

Czubowicz, K., and Strosznajder, R. (2014). Ceramide in the molecular mechanisms of neuronal cell death. The role of sphingosine-1-phosphate. *Mol. Neurobiol.* 50, 26–37. doi: 10.1007/s12035-013-8606-4

Dugger, B. N., and Dickson, D. W. (2017). Pathology of neurodegenerative diseases. *Cold Spring Harb. Perspect. Biol.* 9:a028035. doi: 10.1101/cshperspect.a028035

Gordon, B. A., Blazey, T. M., Su, Y., Hari-Raj, A., Dincer, A., Flores, S., et al. (2018). Spatial patterns of neuroimaging biomarker change in individuals from families with autosomal dominant Alzheimer's disease: a longitudinal study. *Lancet Neurol.* 17, 241–250. doi: 10.1016/S1474-4422(18)30028-0

Hudetz, J. A., Patterson, K. M., Amole, O., Riley, A. V., and Pagel, P. S. (2011). Postoperative cognitive dysfunction after noncardiac surgery: effects of metabolic syndrome. *J. Anesth.* 25, 337–344. doi: 10.1007/s00540-011-1137-0

Muddapu, V. R., Dharshini, S. A. P., Chakravarthy, V. S., and Gromiha, M. M. (2020). Neurodegenerative diseases - is metabolic deficiency the root cause? *Front. Neurosci.* 14:213. doi: 10.3389/fnins.2020.00213

Yudkoff, M., Daikhin, Y., Grunstein, L., Nissim, I., Stern, J., Pleasure, D., et al. (1996). Astrocyte leucine metabolism: significance of branched-chain amino acid transamination. *J. Neurochem.* 66, 378–385. doi: 10.1046/j.1471-4159.1996.66010378.x

Conflict of Interest: The authors declare that the research was conducted in the absence of any commercial or financial relationships that could be construed as a potential conflict of interest.

Publisher's Note: All claims expressed in this article are solely those of the authors and do not necessarily represent those of their affiliated organizations, or those of the publisher, the editors and the reviewers. Any product that may be evaluated in this article, or claim that may be made by its manufacturer, is not guaranteed or endorsed by the publisher.

frontiers in Aging Neuroscience

ORIGINAL RESEARCH
published: 02 February 2021
doi: 10.3389/fnagi.2021.611595

Detection Gap of Right-Asymmetric Neuronal Degeneration by CERAD Test Battery in Alzheimer's Disease

*Annika Kreuzer[1], Julia Sauerbeck[1], Maximilian Scheifele[1], Anna Stockbauer[1], Sonja Schönecker[2], Catharina Prix[2], Elisabeth Wlasich[2], Sandra V. Loosli[2], Philipp M. Kazmierczak[3], Marcus Unterrainer[1,3], Cihan Catak[4], Daniel Janowitz[4], Oliver Pogarell[5], Carla Palleis[2,6], Robert Perneczky[5,6,7,8], Nathalie L. Albert[1], Peter Bartenstein[1,7], Adrian Danek[2], Katharina Buerger[4,6], Johannes Levin[2,6], Andreas Zwergal[2], Axel Rominger[1,7,9], Matthias Brendel[1,7] and Leonie Beyer[1]**

[1]Department of Nuclear Medicine, University Hospital, Ludwig-Maximilians-University Munich, Munich, Germany, [2]Department of Neurology, University Hospital, Ludwig-Maximilians-University, Munich, Germany, [3]Department of Radiology, University Hospital, Ludwig-Maximilians-University, Munich, Germany, [4]Institute for Stroke and Dementia Research, University Hospital, Ludwig-Maximilians-University, Munich, Germany, [5]Department of Psychiatry, University Hospital, Ludwig-Maximilians-University, Munich, Germany, [6]DZNE—German Center for Neurodegenerative Diseases, Munich, Germany, [7]Munich Cluster for Systems Neurology (SyNergy), Munich, Germany, [8]Ageing Epidemiology (AGE) Research Unit, School of Public Health, Imperial College, London, United Kingdom, [9]Department of Nuclear Medicine Inselspital, University of Bern, Bern, Switzerland*

OPEN ACCESS

Edited by:
Carlos J. Rodriguez-Ortiz, University of California, Irvine, United States

Reviewed by:
Takahito Yoshizaki, Keio University, Japan
Claudia Jacova, Pacific University, United States

***Correspondence:**
Leonie Beyer
leonie.beyer@med.uni-muenchen.de

Received: *29 September 2020*
Accepted: *04 January 2021*
Published: *02 February 2021*

Citation:
Kreuzer A, Sauerbeck J, Scheifele M, Stockbauer A, Schönecker S, Prix C, Wlasich E, Loosli SV, Kazmierczak PM, Unterrainer M, Catak C, Janowitz D, Pogarell O, Palleis C, Perneczky R, Albert NL, Bartenstein P, Danek A, Buerger K, Levin J, Zwergal A, Rominger A, Brendel M and Beyer L (2021) Detection Gap of Right-Asymmetric Neuronal Degeneration by CERAD Test Battery in Alzheimer's Disease. Front. Aging Neurosci. 13:611595. doi: 10.3389/fnagi.2021.611595

Objectives: Asymmetric disease characteristics on neuroimaging are common in structural and functional imaging of neurodegenerative diseases, particularly in Alzheimer's disease (AD). However, a standardized clinical evaluation of asymmetric neuronal degeneration and its impact on clinical findings has only sporadically been investigated for F-18-fluorodeoxyglucose positron emission tomography (F-18-FDG-PET). This study aimed to evaluate the impact of lateralized neuronal degeneration on the detection of AD by detailed clinical testing. Furthermore, we compared associations between clinical evaluation and lateralized neuronal degeneration between FDG-PET hypometabolism and hippocampal atrophy. Finally, we investigated if specific subtests show associations with lateralized neuronal degeneration.

Methods: One-hundred and forty-six patients with a clinical diagnosis of AD (age 71 ± 8) were investigated by FDG-PET and the "Consortium to Establish a Registry for Alzheimer's disease" (CERAD) test battery. For assessment of neuronal degeneration, FDG-PET hypometabolism in brain regions typically affected in AD were graded by visual (3D-surface projections) and semiquantitative analysis. Asymmetry of the hippocampus (left-right) in magnetic resonance tomography (MRI) was rated visually by the Scheltens scale. Measures of asymmetry were calculated to quantify lateralized neuronal degeneration and asymmetry scores were subsequently correlated with CERAD.

Results: Asymmetry with left-dominant neuronal degeneration to FDG-PET was an independent predictor of cognitive impairment (visual: $\beta = -0.288$, $p < 0.001$; semiquantitative: $\beta = -0.451$, $p < 0.001$) when controlled for age, gender, years of education and total burden of neuronal degeneration, whereas hippocampal asymmetry

to MRI was not ($\beta = -0.034$; $p = 0.731$). Direct comparison of CERAD-PET associations in cases with right- and left-lateralized neuronal degeneration estimated a detection gap of 2.7 years for right-lateralized cases. Left-hemispheric neuronal degeneration was significantly associated with the total CERAD score and multiple subscores, whereas only MMSE (semiquantitative: $\beta = 0.429$, $p < 0.001$) and constructional praxis (semiquantitative: $\beta = 0.292$, $p = 0.008$) showed significant associations with right-hemispheric neuronal degeneration.

Conclusions: Asymmetry of deteriorated cerebral glucose metabolism has a significant impact on the coupling between neuronal degeneration and cognitive function. Right dominant neuronal degeneration shows a delayed detection by global CERAD testing and requires evaluation of specific subdomains of cognitive testing.

Keywords: cognitive performance, Alzheimer's disease, FDG-PET, hippocampal atrophy, asymmetry

INTRODUCTION

Alzheimer's disease (AD) is the most common neurodegenerative disease, causing an enormous burden on patients, relatives, and caregivers, and the whole health care system (De Deyn et al., 2011; Colucci et al., 2014; Peña-Longobardo and Oliva-Moreno, 2015; Mareˇcová and Zahálková, 2016). Accurate early diagnosis and prediction of further cognitive deterioration is essential. F-18-fluorodeoxyglucose positron emission tomography (F-18-FDG-PET) of the brain has been a decisive diagnostic tool for several years (Sperling et al., 2011; Perani et al., 2014; Salmon et al., 2015; Brugnolo et al., 2019) and has been recommended for differential diagnosis of AD especially in clinically ambiguous or early cases by the Delphi consensus of the European Association of Nuclear Medicine (EANM) and the European Academy of Neurology (EAN; Nobili et al., 2018).

To support the clinical diagnosis, a biomarker-based diagnostic scheme has been proposed for AD including categorization for amyloid, tau, and existing neuronal degeneration (ATN scheme; Jack and Holtzman, 2013; Jack et al., 2016, 2018). Neuronal degeneration in AD can be assessed by cranial magnetic resonance imaging (MRI) or FDG-PET (Jack et al., 2016), often presenting with asymmetric patterns. Hippocampal atrophy has been predominantly found in the left hemisphere in subjects with mild cognitive impairment (MCI) and AD (Shi et al., 2009) and asymmetry of the hippocampus, amygdala, caudate and cortex was predictive of disease progression from MCI to AD (Wachinger et al., 2016) and associated with AD-related single nucleotide polymorphisms (Wachinger et al., 2018). Asymmetric neuronal degeneration is correlated with asymmetries of amyloid burden, both concordant with lateralized cognitive symptoms (Frings et al., 2015). However, only a few studies are dealing with the clinical impact of asymmetric neuronal degeneration patterns.

The "Consortium to Establish a Registry for Alzheimer's disease" (CERAD) test battery is a widespread and well recognized clinical neuropsychological testing method for determining AD (Welsh et al., 1994). Total CERAD scores, published by Chandler et al. (2005) also allow judging the severity of AD, which is an advantage over screening methods like Mini-Mental-State-Examination (MMSE; Chandler et al., 2005; Ehrensperger et al., 2010; Wolfsgruber et al., 2014). We previously found that FDG-PET abnormalities in AD-typical brain regions and CERAD total scores are well associated with clinical AD (Beyer et al., 2019). Earlier results indicated that individual scores of the CERAD battery provide a good representation of the left-hemispheric dysfunction in AD patients but impairment of the right hemisphere appears to be only poorly represented (Teipel et al., 2006).

This study aimed to evaluate the impact of lateralized neuronal degeneration on the detection of AD by detailed clinical testing with the integration of the timeline of clinical progression. Furthermore, we compared associations between clinical evaluation and lateralized neuronal degeneration between FDG-PET and hippocampal atrophy to structural MRI. Finally, we investigated if specific subtests of the CERAD battery show associations with lateralized neuronal degeneration.

MATERIALS AND METHODS

Study Design Patient Enrolment

The study included 146 patients with a clinical diagnosis of AD. All suspected AD cases were confirmed in clinical follow-up (23.7 ± 13.8 months) and a subset of $n = 49$ received repeated neuropsychological testing including the CERAD test battery. The subjects were recruited and scanned in a clinical setting at the University of Munich (Department of Nuclear Medicine) between 2010 and 2016. Patients had been referred by the Departments of Neurology, Psychiatry, and Institute for Stroke and Dementia Research. The majority of patients were recruited *via* specialized outpatient clinics. Data analysis was approved by the local ethics committee (19-004). All subjects underwent clinical dementia workup, including detailed cognitive testing and FDG-PET. Data on handedness was available in 104/146 patients.

Clinical Assessment and Cognitive Testing

Neurological examination and neuropsychological testing were performed including the CERAD battery plus Trail-Making Test

A and B and verbal fluency tests (CERAD+; Morris et al., 1989), resulting in raw values and *Z*-scores for all subtests. We created a total CERAD score by summing up the raw values from the individual CERAD subtests by inclusion of subtests as described earlier (Chandler et al., 2005; Beyer et al., 2019): verbal fluency (maximum score = 24), modified BNT (maximum score = 15), word list learning (maximum score = 30), constructional praxis (maximum score = 11), word list recall (maximum score = 10), word list recognition discriminability (maximum score = 10). Thus, the maximum achievable score was 100 (Chandler et al., 2005). For patients with clinical follow-up examination, the annual change of total CERAD was calculated. Age, gender, and years of education (YoE) were obtained as covariates.

MRI

MRI (1.5/3.0 Tesla magnets) using a T1w sequence for hippocampal atrophy evaluation was available from 96/146 included patients. The Scheltens scale, a score for medial temporal lobe atrophy which ranges from 0 to 4, was rated visually by an expert in Radiology (Minoshima et al., 1995). A summed score was built for both hippocampi and asymmetry was quantified as the difference between left and right scoring.

FDG-PET

FDG-PET Acquisition

FDG was purchased commercially. All FDG-PET images were created using either a 3-dimensional GE Discovery 690 PET/CT scanner or a Siemens ECAT EXACT HR+ PET scanner. Each subject fasted for at least 6 h, resulting in a plasma glucose level less than 120 mg/dl (6.7 mM) at the time of the tracer administration. All patients were injected i.v. with a dose of 142 ± 8 MBq FDG as a slow bolus while sitting quietly in a room with a low noise level and dimmed light. A static emission frame was acquired from 30 to 60 min p.i. for the Siemens ECAT EXACT HR+ PET scanner, respectively from 30 to 45 min p.i. for the Discovery 690 PET/DT. For attenuation correction, a transmission scan with external 68Ge-sources (Siemens) or a low-dose CT was performed before the static acquisition. PET data were reconstructed iteratively (GE) or with filtered back-projection (Siemens).

Visual Analysis of FDG-PET

Three-dimensional stereotactic surface projections (3D-SSP; Minoshima et al., 1995) were created using the software Neurostat (Department of Radiology, University of Washington, Seattle, WA, USA) for visual image interpretation. Visual assessment of the 3D-SSP images was carried out by an expert in Nuclear Medicine using tracer uptake and *Z*-score maps (global mean scaling). Voxel-wise *Z*-scores were calculated in Neurostat by comparing the individual tracer uptake to historical FDG-PET images from a healthy age-matched cohort (n = 18). The reader had access to clinical information and structural imaging. A simplified approach of the *t*-sum method published by Herholz et al. (2002) was performed for visual quantification as previously published (Beyer et al., 2019). In brief, the rating was grouped into four grades of neuronal degeneration ranging from 0 to 3, where 0 is no neuronal degeneration, 1 is mild neuronal degeneration, 2 is moderate neuronal degeneration, and 3 is severe neuronal degeneration. Preselected AD-typical regions in FDG-PET were graded: the bilateral parietal lobe, bilateral temporal lobe, and bilateral posterior cingulate cortex. Summed scores were calculated for the whole brain and each hemisphere (scores 0 to 9). Asymmetry was calculated as the difference between the left and right hemisphere or subregion (left-right). A subset of half of the patients (n = 73) was rated twice by the first reader and by one additional expert in Nuclear Medicine to test for intra-/inter-rater reliability.

Semiquantitative Analysis of FDG-PET

Also, semiquantitative analysis of FDG-PET was conducted. The images have been anonymized before analysis. PMOD software (version 3.5, PMOD Technologies Limited, Zürich, Switzerland) was used for coregistration of all individual FDG-PET image volumes to an in-house FDG-PET template within the MNI space (Daerr et al., 2017). In analogy to the visual analysis, we measured the mean activity within bilateral parietal, bilateral temporal, and bilateral posterior cingulate cortex volumes of interest (VOIs) of the Hammers atlas (Hammers et al., 2003) and scaled the measured regional activities by a cerebellum reference region to generate standardized uptake value ratios (SUVr). Asymmetry was calculated by the Asymmetry-Index [AI = (left − right)/(left + right)∗100] for hemispheres and subregions.

Calculations and Statistical Analysis

Mean visual ratings, semiquantitative results, and mean asymmetries were calculated for each hemisphere and subregions (parietal, temporal, and posterior cingulate cortex). Intra-/inter-rater agreement were assessed by intra-/inter-class correlation coefficients. Visual ratings and semiquantitative results of both hemispheres and separately for the left/right hemisphere were correlated using Pearson's correlation coefficient. FDG-PET results were compared between sides using a Wilcoxon test for visual and two-sided *t*-test for semiquantitative analysis. Mean asymmetry was compared between the whole hemisphere and subregions by a one-way ANOVA. Asymmetry indices of all cortical regions were correlated with each other and the total asymmetry index using a Pearson's correlation coefficient.

Cognitive performance was correlated with the visual rating using Spearman–Rho and with the semiquantitative analysis using Pearson's correlation coefficient. Multiple regression analyses were conducted with the cognition (expressed with CERAD) as the dependent and (i) asymmetry as the independent variable or (ii) Scheltens-Scale as the independent variable, both with age, gender, years of education, and the total hypometabolism in FDG-PET (sum score of both hemispheres) as covariates for both visual and semiquantitative analyses.

For separate analysis of both right- and left-asymmetric hypometabolism, patients with (nearly) unilateral neuronal degeneration by FDG-PET ($\geq$2.0 vs. <2.0 for the contralateral side in the visual rating) were selected, and both groups were separately correlated with the CERAD total score using Spearman–Rho (visual) or Pearson's correlation coefficient (semiquantitative).

Based on the change of the total CERAD score per year and patient and the CERAD difference between correlation lines of right- and left-lateralized cases for the full range of observed neuronal degeneration, we calculated an average detection gap between the left and right hemisphere for both visual and semiquantitative FDG-PET results as following: the mean CERAD was calculated for visual/semiquantitative FDG-PET results separately for left- und right-asymmetric cases using the mean visual/semiquantitative FDG-PET results with the formula of all four correlations, respectively. The mean CERAD difference between left- and right-asymmetric cases was then divided by the mean annual decrease in CERAD of all available follow-up cases and compared against each other.

Additional regression analyses were performed using the left-/right-hemispheric hypometabolism as the dependent and all CERAD subscores separately as the independent variables with age, gender, and education as covariates controlled for multiple testing with Bonferroni correction.

All statistical analyses were performed using SPSS (version 25.0, IBM, Armonk, New York, NY, USA) and a significance level of $p < 0.05$ was applied in all analyses.

RESULTS

Demographics and Asymmetry in FDG Uptake

The study population consisted of 146 subjects (57.5% female) with a clinical diagnosis of AD (follow-up 23.7 ± 13.8 months) and available FDG-PET data. Of all patients, six patients were diagnosed with atypical AD, 133 patients with typical AD (n = 41 early-onset AD, n = 92 late-onset AD), and seven patients were not further specified. 90/104 patients (86.5%) were right-handed, 6/104 (5.8%) were left-handed and 8/104 (7.7%) claimed to be ambidextrous. For details of the study population, see **Table 1**.

TABLE 1 | Demographic and clinical data of the study population (n = 146).

Gender (♂male/♀female)	♂62/♀84
Age (y ±SD)	70.5 ± 8.0
Education (y ±SD)	12.4 ± 3.2
Handedness (n = 104)	90 right, 16 left, 8 ambidextrous
Total CERAD score (±SD)	54.3 ± 13.3
CERAD subscores (±SD)	
Verbal fluency (animals)	12.8 ± 5.4
Modified BNT	12.3 ± 2.6
MMSE (±SD)	22.7 ± 4.1
Word list learning total	11.3 ± 4.6
Word list learning 1	2.5 ± 1.5
Word list learning 2	3.8 ± 1.7
Word list learning 3	4.8 ± 1.7
Word list recall	2.1 ± 1.9
Word list intrusion	1.7 ± 2.3
Word list savings	42.1 ± 33.1
Word list recognition-discriminability (%)	82.5 ± 13.5
Constructional praxis	9.1 ± 2.3
Constructional recall	3.3 ± 3.0
Savings figures	30.0 ± 28.0
CERAD+ scores (±SD)	
Verbal fluency (S-words)	9.2 ± 5.0
TMT-A (s)	85.9 ± 40.6
TMT-B (s)	185.6 ± 85.3
TMT A/B (s)	2.9 ± 1.1
Clinical follow-up (±SD)	23.7 ± 13.8
Total CERAD score follow up (±SD, n = 49)	51.5 ± 13.7

SD, standard deviation; MMSE, mini-mental-state-examination; CERAD, Consortium to Establish a Registry for Alzheimer's disease; BNT, Boston Naming Test; TMT, Trail Making Test; y, years; m, months; s, seconds.

Asymmetries in FDG uptake were assessed by visual and semiquantitative measures (see **Table 2**). Intra- and inter-rater agreement was excellent (intra-rater: $\kappa = 0.92$ $p < 0.001$, inter-rater: $\kappa = 0.96$ $p < 0.001$). Visual ratings and semiquantitative results significantly correlated for both hemispheres ($R = 0.583$, $p < 0.001$) and separately for the left ($R = 0.700$, $p < 0.001$) and right hemisphere ($R = 0.707$, $p < 0.001$). Visual analysis showed a more pronounced hypometabolism pattern of neuronal degeneration in the left hemisphere ($p < 0.001$). Asymmetry was pronounced in the posterior cingulate cortex ($p < 0.001$), followed by the parietal lobe ($p = 0.033$) and less prominent in the temporal lobe ($p = 0.059$). The semiquantitative analysis also indicated significant differences between left and right for the posterior cingulate cortex ($p < 0.001$) and the parietal cortex ($p < 0.001$) but not for the full hemisphere ($p = 0.122$) or the temporal cortex ($p = 0.907$). ANOVA confirmed these results, revealing a significant difference between asymmetry magnitude in subregions and full hemispheres for semiquantitative assessment ($F_{(146,3)} = 6.964$; $p < 0.001$). *Post hoc* testing indicated stronger asymmetry in the posterior cingulate cortex when compared to the lateral parietal lobe ($p = 0.040$), the temporal lobe ($p < 0.001$) and entire hemispheres ($p = 0.003$). Asymmetry indices of all cortical subregions significantly correlated with each other and the total asymmetry index (visual: all $R > 0.584$, all $p < 0.01$; semiquantitative: all $R > 0.573$, all $p < 0.01$).

Asymmetry in FDG-PET as an Independent Predictor of Cognitive Impairment

Our recent findings of a significant correlation between neuronal degeneration and cognitive impairment (Beyer et al., 2019) were confirmed in the current subset and showed significant associations between deteriorated FDG-PET in bihemispheric AD target regions and the CERAD total score (visual: $\rho = 0.435$; $p < 0.001$; semiquantitative: $R = 0.442$, $p < 0.001$). Using a multiple regression analysis, asymmetry in FDG-PET was a significant predictor of current cognitive impairment (visual: $\beta = -0.288$, $p < 0.001$; semiquantitative: $\beta = -0.451$, $p < 0.001$) and explained 35.4% (visual)/32.0% (semiquantitative) of the variance in CERAD, independent from age, gender, education and total burden of neuronal degeneration to FDG-PET (see **Table 3**). Left-lateralized neuronal degeneration was associated with stronger presence of cognitive impairment. Exemplary patients with left- and right-asymmetric neuronal degeneration in FDG-PET 3D-SSP are visualized in **Figure 1**.

In contrast to FDG-PET, asymmetry of neuronal degeneration in the hippocampus to MRI as rated by Scheltens Scale (asymmetry: left-right) did not indicate an independent prediction of the current cognition

TABLE 2 | Visual and semiquantitative FDG-PET results and asymmetries.

Region		Visual FDG-PET (3DSSP-rating)	Visual asymmetries (left-right)	Semiquantitative FDG-PET (SUVr)	Semiquantitative asymmetries (AI)
Hemispheres (±SD)	Right	−3.1 ± 2.3	−0.7 ± 2.5	0.85 ± 0.07	−1.04 ± 3.63
	Left	−3.8 ± 2.2		0.83 ± 0.07	
Parietal cortex (±SD)	Right	−1.2 ± 1.0	−0.2 ± 1.0	0.87 ± 0.08	−1.33 ± 3.52
	Left	−1.4 ± 1.0		0.85 ± 0.08	
Temporal cortex (±SD)	Right	−0.7 ± 0.9	−0.2 ± 1.1	0.81 ± 0.07	−0.69 ± 4.14
	Left	−1.0 ± 0.9		0.82 ± 0.07	
Posterior cingulate cortex (±SD)	Right	−1.2 ± 0.9	−0.4 ± 0.7	0.89 ± 0.09	−2.44 ± 2.29
	Left	−1.6 ± 0.8		0.85 ± 0.08	

SD, standard deviation; FDG, F-18-fluorodesoxyglucose; PET, positron-emission-tomography; 3DSSP, three-dimensional stereotactic surface projections; SUVr, standardized uptake value ratios; AI, asymmetry index.

TABLE 3 | Multiple regression analysis for asymmetry in the visual and semiquantitative analysis based on total CERAD score.

Region	Independent variable Asymmetry β (*p*)	Covariates Age β (*p*)	Gender β (*p*)	YoE β (*p*)	Total burden FDG-PET β (*p*)
Visual					
Hemispheres	−0.288 (<0.001)	−0.168 (0.020)	0.177 (0.017)	0.220 (0.002)	0.435 (<0.001)
Parietal lobe	−0.276 (<0.001)	−0.163 (0.024)	0.168 (0.023)	0.211 (0.004)	0.440 (<0.001)
Temporal lobe	−0.262 (<0.001)	−0.181 (0.013)	0.161 (0.029)	0.231 (0.002)	0.429 (<0.001)
Posterior cingulate cortex	−0.219 (0.003)	−0.149 (0.045)	0.158 (0.037)	0.238 (0.001)	0.414 (<0.001)
Semiquantitative					
Hemispheres	−0.451 (<0.001)	−0.140 (0.049)	0.131 (0.071)	0.185 (0.012)	0.442 (<0.001)
Parietal lobe	−0.419 (<0.001)	−0.125 (0.081)	0.110 (0.129)	0.191 (0.010)	0.414 (<0.001)
Temporal lobe	−0.445 (<0.001)	−0.143 (0.046)	0.139 (0.057)	0.191 (0.010)	0.444 (<0.001)
Posterior cingulate cortex	−0.168 (0.035)	−0.089 (0.251)	0.069 (0.376)	0.269 (0.001)	0.303 (<0.001)

CERAD, Consortium to Establish a Registry for Alzheimer's disease. FDG-PET, F-18-fluorodeoxyglucose positron emission tomography.

when controlled for age, gender, education, and total semiquantitative burden of neuronal degeneration to FDG-PET ($\beta = -0.034$; $p = 0.731$).

Delayed CERAD Detection of Right-Hemispheric Neuronal Degeneration

Next, we aimed to investigate associations of neuronal degeneration and cognitive decline independently for FDG-PET results of each hemisphere. Considering all 146 cases, we observed a stronger correlation for neuronal degeneration in the left hemisphere with the total CERAD score (visual: $\rho = -0.479$, $p < 0.001$, semiquantitative: $R = 0.497$, $p < 0.001$) when compared to neuronal degeneration in the right hemisphere (visual: $\rho = -0.205$, $p = 0.013$; semiquantitative: $R = 0.282$, $p = 0.001$).

To increase specificity for the side of affection, we defined asymmetric cases with (nearly) unilateral neuronal degeneration by FDG-PET (≥2.0 vs. <2.0 for the contralateral side in the visual rating) and were able to compare 35 cases predominantly affected on the left hemisphere and 16 cases predominantly affected on the right hemisphere. Both left-hemispheric (visual: $\rho = 0.571$, $p < 0.001$; semiquantitative: $R = 0.575$, $p < 0.001$) and right-hemispheric (visual: $\rho = 0.463$, $p = 0.071$; semiquantitative: $R = 0.740$, $p = 0.001$) neuronal degeneration was associated significantly with the total CERAD score. However, the function of total CERAD score and right-lateralized neuronal degeneration ranged at a higher level when compared to the function of CERAD and left-lateralized neuronal degeneration (see **Figure 2**).

The averaged CERAD score as a function of FDG-PET of left dominant cases ranged 9.9 CERAD score units below the average of right dominant cases. Considering longitudinal CERAD data of 49 subjects of this cohort, the total CERAD score deteriorated by -3.6 ± 7.4 points per year. This hypothetical model results in an average detection gap of 2.7 years for CERAD assessment in right-lateralized cases when compared to left-lateralized cases at an equal neuronal degeneration level.

Associations of Right-Hemispheric Neuronal Degeneration With CERAD Subscores

Finally, we tested if CERAD and CERAD+ subscores may detect right-lateralized neuronal degeneration better when compared to the total CERAD score. Right-hemispheric neuronal degeneration in visual and semiquantitative analysis was significantly associated only with MMSE (semiquantitative: $\beta = 0.429$, $p < 0.001$) and constructional praxis (semiquantitative: $\beta = 0.292$, $p = 0.008$), whereas left-hemispheric hypometabolism significantly correlated with 8/18 subscores. For details of all correlations with the visual rating and semiquantitative results see **Table 4**.

DISCUSSION

In the present study, we investigated the relationship between asymmetric neuronal degeneration patterns measured by FDG-PET and cognition expressed by the CERAD test battery in clinical AD patients. We demonstrate that asymmetries

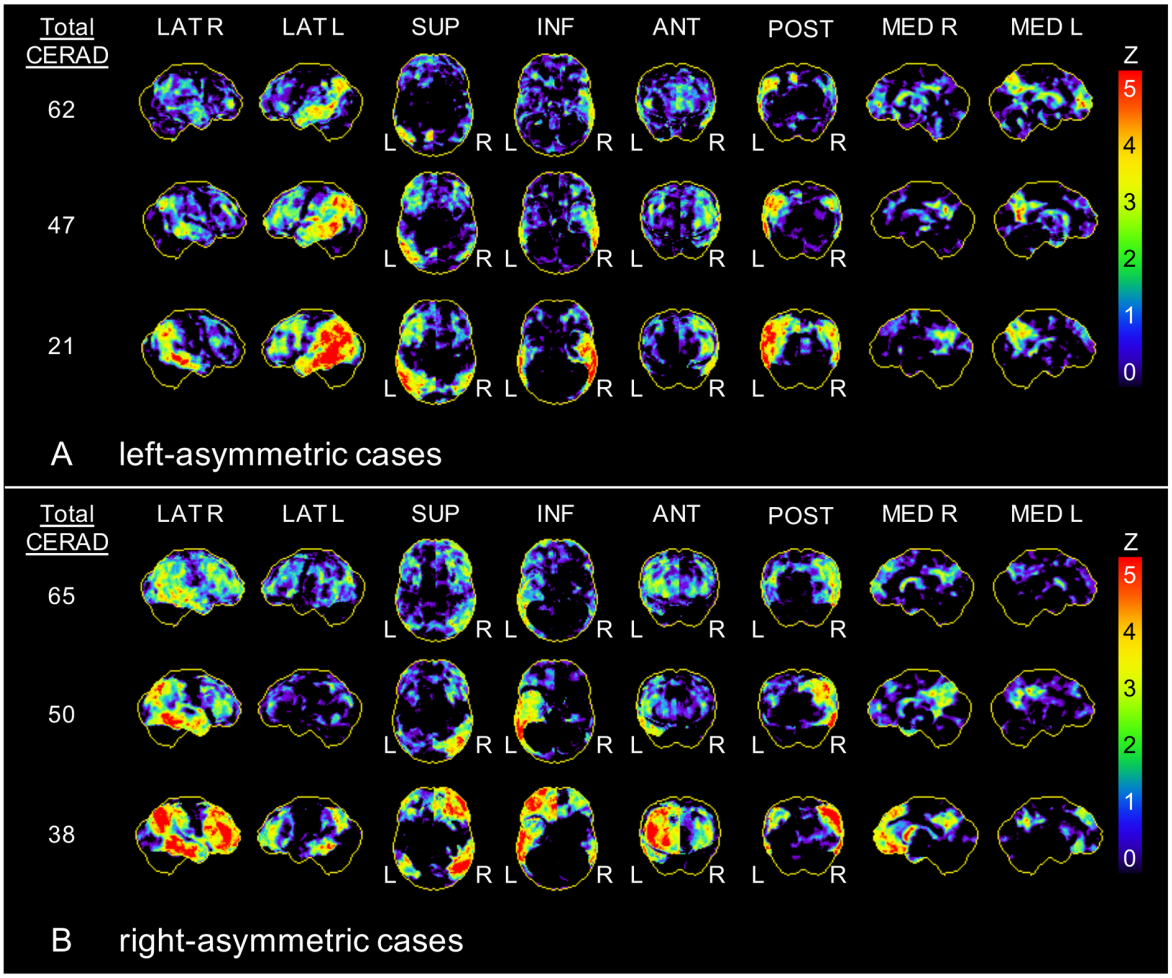

FIGURE 1 | Exemplary asymmetric hypometabolism patterns. Three-dimensional stereotactic surface projections (*Z*-score maps) of patients with **(A)** left-asymmetric and **(B)** right-asymmetric hypometabolism in F-18-fluorodeoxyglucose positron emission tomography (FDG-PET). CERAD, Consortium to establish a registry for Alzheimer's disease; R, right; L, left; LAT, lateral; SUP, superior; INF, inferior; ANT, anterior; POST, posterior; MED, medial.

in FDG-PET constitute an independent predictor of current cognitive impairment. Predominant left-hemispheric neuronal degeneration led to more severe cognitive impairment as assessed by the CERAD battery when compared to right-hemispheric neuronal degeneration. In contrast to the left hemisphere, right-hemispheric cognitive abilities are poorly represented in CERAD subscores, with only two subscores showing a significant association with right-hemispheric neuronal degeneration.

Associations of Asymmetric Neuronal Degeneration and Cognitive Function

Asymmetries of brain function are well known and the reasons for asymmetric neuronal degeneration expressed by gray matter asymmetries in aging and neurodegenerative diseases are being discussed extensively (Minkova et al., 2017). Previous smaller scaled studies showed a predominance of left hemisphere metabolic dysfunction in MCI and AD (Loewenstein et al., 1989; Murayama et al., 2016). In line with this, we found a left dominant neuronal degeneration pattern in our AD cohort when compared to the right hemisphere and also separately in distinct brain regions known to be affected in AD (parietal, temporal, and posterior cingulate cortex). Asymmetry indices of all regions significantly correlated with each other, indicating that left-/right-asymmetric asymmetry is concordant between regions on a single-patient level.

Asymmetry in FDG-PET proved to be an independent predictor of cognitive function, indicating that left-hemispheric hypometabolism is associated with a stronger presence of cognitive impairment in clinical testing. It has already been shown in patients with MCI and AD that the left-dominant group in FDG-PET had lower scores in verbal memory and a greater tendency to be diagnosed with AD rather than MCI (Murayama et al., 2016). Thus, the consistent findings in the current cohort established the basis to study the impact of asymmetry on FDG-PET evaluation in a clinical setting.

Asymmetric hippocampal atrophy in MRI rated by the Scheltens Scale did not indicate an independent prediction

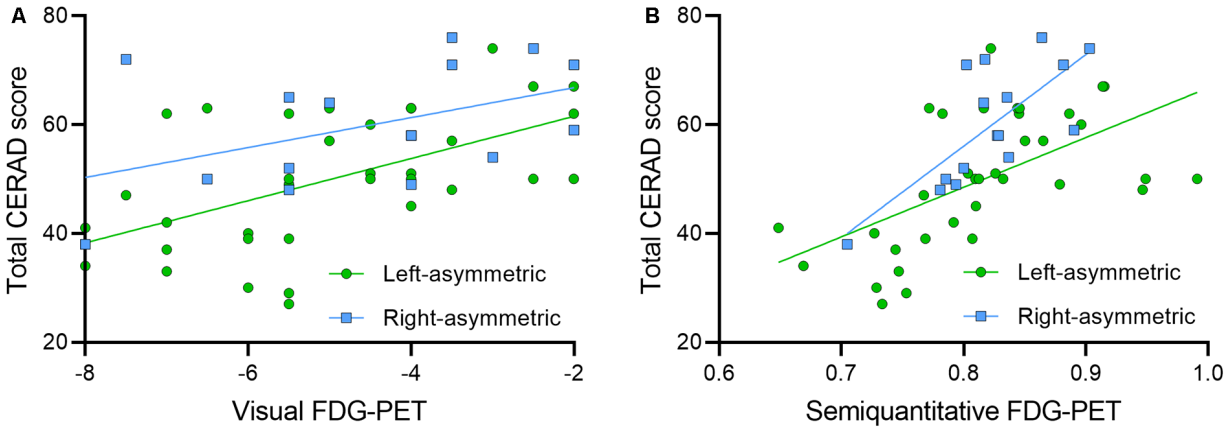

FIGURE 2 | Comparison of cases with dominant right- and left-lateralization. Correlation plots show the functions of **(A)** visual FDG-PET and **(B)** semiquantitative FDG-PET with total CERAD score for left- (n = 35, green dots) and right- (n = 16, blue squares) asymmetric cases.

TABLE 4 | Correlation of CERAD subscores with hypometabolism in FDG-PET.

Subscore	Visual		Semiquantitative	
	Left β (p)	Right β (p)	Left β (p)	Right β (p)
Verbal fluency (animals)	0.466 (<0.001)	0.142 (n.s.)	0.389 (<0.001)	0.177 (n.s.)
Modified BNT	0.262 (0.018)	0.037 (n.s.)	0.349 (<0.001)	0.194 (n.s.)
MMSE	0.520 (<0.001)	0.297 (0.018)	0.542 (<0.001)	0.429 (<0.001)
Word list learning total	0.460 (<0.001)	0.159 (n.s.)	0.446 (<0.001)	0.240 (n.s.)
Word list learning 1	0.393 (<0.001)	0.121 (n.s.)	0.437 (<0.001)	0.273 (n.s.)
Word list learning 2	0.398 (<0.001)	0.204 (n.s.)	0.339 (0.004)	0.219 (n.s.)
Word list learning 3	0.307 (0.018)	0.274 (n.s.)	0.257 (n.s.)	0.247 (n.s.)
Word list recall	0.248 (n.s.)	0.208 (n.s.)	0.130 (n.s.)	0.093 (n.s.)
Word list intrusion	0.012 (n.s.)	0.098 (n.s.)	0.031 (n.s.)	0.053 (n.s.)
Word list savings	−0.010 (n.s.)	0.185 (n.s.)	−0.103 (n.s.)	0.043 (n.s.)
Word list recognition—discriminability	0.094 (n.s.)	0.125 (n.s.)	0.088 (n.s.)	0.115 (n.s.)
Constructional praxis	0.202 (n.s.)	0.180 (n.s.)	0.259 (0.018)	0.292 (0.008)
Constructional recall	0.209 (n.s.)	0.183 (n.s.)	0.229 (n.s.)	0.217 (n.s.)
Savings figures	0.163 (n.s.)	0.165 (n.s.)	0.158 (n.s.)	0.167 (n.s.)
Verbal fluency (S-words)	0.287 (0.008)	0.004 (n.s.)	0.310 (0.003)	0.089 (n.s.)
TMT A	0.232 (n.s.)	0.162 (n.s.)	0.252 (n.s.)	0.232 (n.s.)
TMT B	0.331 (n.s.)	0.210 (n.s.)	0.152 (n.s.)	0.100 (n.s.)
TMT A/B	0.185 (n.s.)	−0.046 (n.s.)	0.011 (n.s.)	−0.088 (n.s.)

CERAD, Consortium to Establish a Registry for Alzheimer's disease; FDG, F-18-fluorodeoxyglucose; PET, positron-emission-tomography; BNT, Boston Naming Test; MMSE, mini-mental state examination; TMT, Trail Making Test; n.s., non-significant.

of cognition. We focused on a visual approach for a rating of hippocampal atrophy to generate results that can be transferred into a clinical routine setting. However, quantitative approaches with segmentation and measurement methods analyzing hippocampal subfields (Giuliano et al., 2017) and/or cortical regions could probably improve the informative value of asymmetry in MRI.

Detection Gap Between Left- and Right-Asymmetric Cases

In further disease progression, cognitive deterioration correlates with neurodegeneration biomarkers (Beyer et al., 2019) with greater cognitive impairment along the continuum from normal cognitive status to MCI and AD dementia. Asymmetries of neuronal degeneration patterns and their influence on cognition have not been considered in the diagnostic workup so far (Jack et al., 2010, 2013). It has been hypothesized that early stages of AD may be characterized by a lateralized pattern with left-hemispheric hypometabolism and decreasing differences with further disease progression (Weise et al., 2018). Also, patients with left-hemispheric dominance of neuronal degeneration are more likely to be diagnosed with MCI (Cherbuin et al., 2010), which might lead to an assignment bias in our cohort.

The reason for different neuronal degeneration patterns has not been clarified yet, but we demonstrate that left-asymmetric cases might be clinically detectable earlier than right-asymmetric cases. We found a detection gap of >2.5 years of a potential later-diagnosis of right-asymmetric patients compared to left-asymmetric patients when using the CERAD test battery. Clinical symptoms deriving from left-hemispheric neuronal degeneration seem to be stronger represented by

the CERAD battery. Consequently, left- vs. right-asymmetric neuronal degeneration patterns in FDG-PET need to be weighted differently because right-asymmetric neuronal degeneration might be insufficiently represented in clinical testing.

Representation of Asymmetric Neuronal Degeneration by CERAD Subscores

Several studies have shown that different deteriorated brain subdomains are linked to either left- or right-hemispheric neuronal degeneration. Verbal and nonverbal impairments (Zahn et al., 2004), severe dysfunction in verbal memory, general memory, and delay recall (Murayama et al., 2016), language and visuospatial deficits (Haxby et al., 1985) were associated with left-hemispheric neuronal degeneration. Right-hemispheric neuronal degeneration was associated with constructional praxis recall (Han et al., 2015) and drawing test performance (Förster et al., 2010) and, together with left-hemispheric alterations, with constructional praxis (Han et al., 2015).

For the clinical representation of the existing neuronal degeneration, the CERAD battery has been proven to adequately represent left-hemispheric dysfunction in AD, but with difficulties displaying right-hemispheric dysfunction (Welsh et al., 1994; Teipel et al., 2006). This matches our finding that despite the higher correlation of the CERAD total score with left-hemispheric hypometabolism compared to right-hemispheric hypometabolism, more CERAD subscores significantly correlated with left-, and only two correlated with right-hemispheric hypometabolism. Only the MMSE and constructional praxis subtests were found to be significantly associated with right-hemispheric neuronal degeneration. Therefore, subjects with clinical apraxia and even mild to moderate cognitive impairment (as assessed by MMSE) should be considered for FDG-PET to search for right-hemispheric neuronal degeneration.

Some studies found symmetric associations with CERAD scores (Schönknecht et al., 2011) and clusters with the involvement of both hemispheres (Staffaroni et al., 2017). Many cognitive abilities are known to derive from both left- and right-hemispheric brain areas and disruptions in brain activities in some regions of the brain consequently lead to worsening of other connected functions as well. In line with this, the constructional praxis subtest was significantly associated with the right-, but also with left-hemispheric neuronal degeneration. Also, the MMSE as a global measurement of cognitive function is significantly associated with both hemispheres. Whereas more specific subtests are available for left-hemispheric abilities, the clinical representation of the right-hemispheric neuronal degeneration is limited to these two subtests.

Additional tests included in the CERAD+ test battery (e.g., TMT, verbal fluency with S-words) as well do not sufficiently represent right-hemispheric brain functions as the represented abilities also involve both hemispheres. Furthermore, it has been pointed out that some subscores like BNT, word list recognition, or constructional praxis and recall tests should be considered less strongly for early detection of dementia because of strong ceiling effects (Luck et al., 2018).

Therefore, the early and accurate clinical assessment of right-asymmetric cases remains challenging, and additional neuropsychological testing (especially with behavioral measures) should be considered especially in cases with cognitive impairments of right-hemispheric brain functions as they might be poorly represented by CERAD. Furthermore, imaging with FDG-PET can also be considered to support clinical diagnosis.

Limitations

Among the limitations of our study, we note that correlations with neuropsychological testing are limited to CERAD test battery results. Other neuropsychological tests and behavioral measures are not included in this study and analysis of additional parameters would be of interest. While *p*-tau in the cerebrospinal fluid was available and pathologic in all of our cases, we did not have a comprehensive evaluation of Aβ in all cases. Therefore, the ATN scheme (Jack et al., 2016) could not be fulfilled with the proposed biomarkers. However, the diagnoses of AD were confirmed by long-term clinical follow-up, and only subjects with a confident clinical diagnosis of AD were included in the analysis. We focused on covariates recommended to support the diagnosis of AD, but we could not cover the full range of environmental factors, comorbidities, and apolipoprotein E status which otherwise could have influenced our results. A major strength of the study lies in the clinical setting to guarantee transferability into routine clinical scenarios.

A small subset of patients in this sample was classified as atypical AD. Asymmetry analysis in this subsample would be of great interest but was not possible due to the limited amount of cases. Data on handedness was only available in a subset of patients (n = 104) and the sample size of left-handed subjects was too small for separate analysis. Therefore, the potential effect of the difference between the dominant and minor hemisphere cannot be further investigated and might have influenced the results.

CONCLUSION

Asymmetry in FDG-PET predicts cognitive performance, but only left-hemispheric neuronal degeneration is well represented by the clinical used CERAD battery. Therefore, clinical diagnosis in patients with right-hemispheric neuronal degeneration might be delayed, calling for extended neuropsychological testing and additional diagnostic procedures in clinically unclear cases to capture cognitive impairments related to right-hemispheric neuronal degeneration.

DATA AVAILABILITY STATEMENT

The raw data supporting the conclusions of this article will be made available by the authors, upon reasonable request.

ETHICS STATEMENT

The studies involving human participants were reviewed and approved by LMU Munich ethics commitee (19-004). Written informed consent for this retrospective analysis was not

required in accordance with the national legislation and the institutional requirements.

AUTHOR CONTRIBUTIONS

AK: acquisition of data, analysis, interpretation of data, document writing, and editing. JS, MS, AS, NA, PB, and AR: acquisition of data, interpretation of molecular imaging data, and revising of the manuscript. SS, CPr, EW, SL, CC, DJ, OP, CPa, RP, AD, KB, JL, and AZ: acquisition of clinical patient data, drafting and revising of the manuscript. PK and MU: acquisition of radiological data, drafting and revising of the manuscript. MB: interpretation of molecular imaging data, conception, intellectual input, drafting and revising of the manuscript. LB: conception and design, acquisition of data, document editing, final manuscript approval for submission and publication. All authors contributed to the article and approved the submitted version.

FUNDING

LB was funded by the Munich-Clinician-Scientist-Program (LMU Munich).

ACKNOWLEDGMENTS

Parts of this article originated from the doctoral thesis of AK.

REFERENCES

Beyer, L., Schnabel, J., Kazmierczak, P., Ewers, M., Schönecker, S., Prix, C., et al. (2019). Neuronal injury biomarkers for assessment of the individual cognitive reserve in clinically suspected Alzheimer's disease. *Neuroimage Clin.* 24:101949. doi: 10.1016/j.nicl.2019.101949

Brugnolo, A., De Carli, F., Pagani, M., Morbelli, S., Jonsson, C., Chincarini, A., et al. (2019). Head-to-head comparison among semi-quantification tools of brain FDG-PET to aid the diagnosis of prodromal Alzheimer's disease. *J. Alzheimers Dis.* 68, 383–394. doi: 10.3233/JAD-181022

Chandler, M. J., Lacritz, L. H., Hynan, L. S., Barnard, H. D., Allen, G., Deschner, M., et al. (2005). A total score for the CERAD neuropsychological battery. *Neurology* 65, 102–106. doi: 10.1212/01.wnl.0000167607.63000.38

Cherbuin, N., Réglade-Meslin, C., Kumar, R., Sachdev, P., and Anstey, K. J. (2010). Mild cognitive disorders are associated with different patterns of brain asymmetry than normal aging: the PATH through life study. *Front. Psychiatry* 1:11. doi: 10.3389/fpsyt.2010.00011

Colucci, L., Bosco, M., Fasanaro, A. M., Gaeta, G. L., Ricci, G., and Amenta, F. (2014). Alzheimer's disease costs: what we know and what we should take into account. *J. Alzheimers Dis.* 42, 1311–1324. doi: 10.3233/JAD-131556

Daerr, S., Brendel, M., Zach, C., Mille, E., Schilling, D., Zacherl, M. J., et al. (2017). Evaluation of early-phase [^{18}F]-florbetaben PET acquisition in clinical routine cases. *Neuroimage Clin.* 14, 77–86. doi: 10.1016/j.nicl.2016.10.005

De Deyn, P. P., Goeman, J., Vervaet, A., Dourcy-Belle-Rose, B., Van Dam, D., and Geerts, E. (2011). Prevalence and incidence of dementia among 75-80-year-old community-dwelling elderly in different districts of Antwerp, Belgium: The Antwerp Cognition (ANCOG) Study. *Clin. Neurol. Neurosurg.* 113, 736–745. doi: 10.1016/j.clineuro.2011.07.030

Ehrensperger, M. M., Berres, M., Taylor, K. I., and Monsch, A. U. (2010). Early detection of Alzheimer's disease with a total score of the German CERAD. *J. Int. Neuropsychol. Soc.* 16, 910–920. doi: 10.1017/S1355617710000822

Förster, S., Teipel, S., Zach, C., Rominger, A., Cumming, P., Fougere, C. L., et al. (2010). FDG-PET mapping the brain substrates of visuo-constructive processing in Alzheimer's disease. *J. Psychiatr. Res.* 44, 462–469. doi: 10.1016/j.jpsychires.2009.09.012

Frings, L., Hellwig, S., Spehl, T. S., Bormann, T., Buchert, R., Vach, W., et al. (2015). Asymmetries of amyloid-β burden and neuronal dysfunction are positively correlated in Alzheimer's disease. *Brain* 138, 3089–3099. doi: 10.1093/brain/awv229

Giuliano, A., Donatelli, G., Cosottini, M., Tosetti, M., Retico, A., and Fantacci, M. E. (2017). Hippocampal subfields at ultra high field MRI: an overview of segmentation and measurement methods. *Hippocampus* 27, 481–494. doi: 10.1002/hipo.22717

Hammers, A., Allom, R., Koepp, M. J., Free, S. L., Myers, R., Lemieux, L., et al. (2003). Three-dimensional maximum probability atlas of the human brain, with particular reference to the temporal lobe. *Hum. Brain Mapp.* 19, 224–247. doi: 10.1002/hbm.10123

Han, J. Y., Byun, M. S., Seo, E. H., Yi, D., Choe, Y. M., Sohn, B. K., et al. (2015). Functional neural correlates of figure copy and recall task performances in cognitively impaired individuals: an ^{18}F-FDG-PET study. *NeuroReport* 26, 1077–1082. doi: 10.1097/WNR.0000000000000476

Haxby, J. V., Duara, R., Grady, C. L., Cutler, N. R., and Rapoport, S. I. (1985). Relations between neuropsychological and cerebral metabolic asymmetries in early Alzheimer's disease. *J. Cereb. Blood Flow Metab.* 5, 193–200. doi: 10.1038/jcbfm.1985.25

Herholz, K., Salmon, E., Perani, D., Baron, J. C., Holthoff, V., Frölich, L., et al. (2002). Discrimination between Alzheimer dementia and controls by automated analysis of multicenter FDG-PET. *NeuroImage* 17, 302–316. doi: 10.1006/nimg.2002.1208

Jack, C. R. Jr., Bennett, D. A., Blennow, K., Carrillo, M. C., Dunn, B., Haeberlein, S. B., et al. (2018). NIA-AA research framework: toward a biological definition of Alzheimer's disease. *Alzheimers Dement.* 14, 535–562. doi: 10.1016/j.jalz.2018.02.018

Jack, C. R. Jr., Bennett, D. A., Blennow, K., Carrillo, M. C., Feldman, H. H., Frisoni, G. B., et al. (2016). A/T/N: an unbiased descriptive classification scheme for Alzheimer disease biomarkers. *Neurology* 87, 539–547. doi: 10.1212/WNL.0000000000002923

Jack, C. R. Jr., and Holtzman, D. M. (2013). Biomarker modeling of Alzheimer's disease. *Neuron* 80, 1347–1358. doi: 10.1016/j.neuron.2013.12.003

Jack, C. R. Jr., Knopman, D. S., Jagust, W. J., Petersen, R. C., Weiner, M. W., Aisen, P. S., et al. (2013). Tracking pathophysiological processes in Alzheimer's disease: an updated hypothetical model of dynamic biomarkers. *Lancet Neurol.* 12, 207–216. doi: 10.1016/S1474-4422(12)70291-0

Jack, C. R. Jr., Knopman, D. S., Jagust, W. J., Shaw, L. M., Aisen, P. S., Weiner, M. W., et al. (2010). Hypothetical model of dynamic biomarkers of the Alzheimer's pathological cascade. *Lancet Neurol.* 9, 119–128. doi: 10.1016/S1474-4422(09)70299-6

Loewenstein, D. A., Barker, W. W., Chang, J. Y., Apicella, A., Yoshii, F., Kothari, P., et al. (1989). Predominant left hemisphere metabolic dysfunction in dementia. *Arch. Neurol.* 46, 146–152. doi: 10.1001/archneur.1989.00520380046012

Luck, T., Pabst, A., Rodriguez, F. S., Schroeter, M. L., Witte, V., Hinz, A., et al. (2018). Age-, sex- and education-specific norms for an extended CERAD neuropsychological assessment battery-results from the population-based LIFE-adult-study. *Neuropsychology* 32, 461–475. doi: 10.1037/neu0000440

Marešová, P., and Zahálková, V. (2016). The economic burden of the care and treatment for people with Alzheimer's disease: the outlook for the Czech Republic. *Neurol. Sci.* 37, 1917–1922. doi: 10.1007/s10072-016-2679-6

Minkova, L., Habich, A., Peter, J., Kaller, C. P., Eickhoff, S. B., and Klöppel, S. (2017). Gray matter asymmetries in aging and neurodegeneration: a review and meta-analysis. *Hum. Brain Mapp.* 38, 5890–5904. doi: 10.1002/hbm.23772

Minoshima, S., Frey, K. A., Koeppe, R. A., Foster, N. L., and Kuhl, D. E. (1995). A diagnostic approach in Alzheimer's disease using three-dimensional stereotactic surface projections of fluorine-18-FDG PET. *J. Nucl. Med.* 36, 1238–1248.

Morris, J. C., Heyman, A., Mohs, R. C., Hughes, J. P., van Belle, G., Fillenbaum, G., et al. (1989). The consortium to establish a registry for Alzheimer's disease

(CERAD). Part I. Clinical and neuropsychological assessment of Alzheimer's disease. *Neurology* 39, 1159–1165. doi: 10.1212/wnl.39.9.1159

Murayama, N., Ota, K., Kasanuki, K., Kondo, D., Fujishiro, H., Fukase, Y., et al. (2016). Cognitive dysfunction in patients with very mild Alzheimer's disease and amnestic mild cognitive impairment showing hemispheric asymmetries of hypometabolism on ^{18}F-FDG PET. *Int. J. Geriatr. Psychiatry* 31, 41–48. doi: 10.1002/gps.4287

Nobili, F., Arbizu, J., Bouwman, F., Drzezga, A., Agosta, F., Nestor, P., et al. (2018). European association of nuclear medicine and european academy of neurology recommendations for the use of brain ^{18}F-fluorodeoxyglucose positron emission tomography in neurodegenerative cognitive impairment and dementia: Delphi consensus. *Eur. J. Neurol.* 25, 1201–1217. doi: 10.1111/ene.13728

Peña-Longobardo, L. M., and Oliva-Moreno, J. (2015). Caregiver burden in Alzheimer's disease patients in spain. *J. Alzheimers Dis.* 43, 1293–1302. doi: 10.3233/JAD-141374

Perani, D., Schillaci, O., Padovani, A., Nobili, F. M., Iaccarino, L., Della Rosa, P. A., et al. (2014). A survey of FDG- and amyloid-PET imaging in dementia and GRADE analysis. *Biomed. Res. Int.* 2014:785039. doi: 10.1155/2014/785039

Salmon, E., Bernard Ir, C., and Hustinx, R. (2015). Pitfalls and limitations of PET/CT in brain imaging. *Semin. Nucl. Med.* 45, 541–551. doi: 10.1053/j.semnuclmed.2015.03.008

Schönknecht, O. D. P., Hunt, A., Toro, P., Guenther, T., Henze, M., Haberkorn, U., et al. (2011). Bihemispheric cerebral FDG PET correlates of cognitive dysfunction as assessed by the CERAD in Alzheimer's disease. *Clin. EEG Neurosci.* 42, 71–76. doi: 10.1177/155005941104200207

Shi, F., Liu, B., Zhou, Y., Yu, C., and Jiang, T. (2009). Hippocampal volume and asymmetry in mild cognitive impairment and Alzheimer's disease: meta-analyses of MRI studies. *Hippocampus* 19, 1055–1064. doi: 10.1002/hipo.20573

Sperling, R. A., Aisen, P. S., Beckett, L. A., Bennett, D. A., Craft, S., Fagan, A. M., et al. (2011). Toward defining the preclinical stages of Alzheimer's disease: recommendations from the National institute on aging-Alzheimer's association workgroups on diagnostic guidelines for Alzheimer's disease. *Alzheimers Dement.* 7, 280–292. doi: 10.1016/j.jalz.2011.03.003

Staffaroni, A. M., Melrose, R. J., Leskin, L. P., Riskin-Jones, H., Harwood, D., Mandelkern, M., et al. (2017). The functional neuroanatomy of verbal memory in Alzheimer's disease: [^{18}F]-fluoro-2-deoxy-D-glucose positron emission tomography (FDG-PET) correlates of recency and recognition memory. *J. Clin. Exp. Neuropsychol.* 39, 682–693. doi: 10.1080/13803395.2016.1255312

Teipel, S. J., Willoch, F., Ishii, K., Bürger, K., Drzezga, A., Engel, R., et al. (2006). Resting state glucose utilization and the CERAD cognitive battery in patients with Alzheimer's disease. *Neurobiol. Aging* 27, 681–690. doi: 10.1016/j.neurobiolaging.2005.03.015

Wachinger, C., Nho, K., Saykin, A. J., Reuter, M., Rieckmann, A., and Alzheimer's Disease Neuroimaging Initiative. (2018). A longitudinal imaging genetics study of neuroanatomical asymmetry in Alzheimer's disease. *Biol. Psychiatry* 84, 522–530. doi: 10.1016/j.biopsych.2018.04.017

Wachinger, C., Salat, D. H., Weiner, M., Reuter, M., and Alzheimer's Disease Neuroimaging Initiative. (2016). Whole-brain analysis reveals increased neuroanatomical asymmetries in dementia for hippocampus and amygdala. *Brain* 139, 3253–3266. doi: 10.1093/brain/aww243

Weise, C. M., Chen, K., Chen, Y., Kuang, X., Savage, C. R., Reiman, E. M., et al. (2018). Left lateralized cerebral glucose metabolism declines in amyloid-β positive persons with mild cognitive impairment. *Neuroimage Clin.* 20, 286–296. doi: 10.1016/j.nicl.2018.07.016

Welsh, K. A., Hoffman, J. M., Earl, N. L., and Hanson, M. W. (1994). Neural correlates of dementia: regional brain metabolism (FDG-PET) and the CERAD neuropsychological battery. *Arch. Clin. Neuropsychol.* 9, 395–409.

Wolfsgruber, S., Jessen, F., Wiese, B., Stein, J., Bickel, H., Mösch, E., et al. (2014). The CERAD neuropsychological assessment battery total score detects and predicts Alzheimer disease dementia with high diagnostic accuracy. *Am. J. Geriatr. Psychiatry* 22, 1017–1028. doi: 10.1016/j.jagp.2012.08.021

Zahn, R., Juengling, F., Bubrowski, P., Jost, E., Dykierek, P., Talazko, J., et al. (2004). Hemispheric asymmetries of hypometabolism associated with semantic memory impairment in Alzheimer's disease: a study using positron emission tomography with fluorodeoxyglucose-F^{18}. *Psychiatry Res.* 132, 159–172. doi: 10.1016/j.pscychresns.2004.07.006

Conflict of Interest: RP is on the advisory board for Biogen, has consulted for Eli Lilly, is a grant recipient from Janssen Pharmaceutica and Boehringer Ingelheim, and has received speaker honoraria from Janssen-Cilag, Pfizer, and Biogen. PB declares a research collaboration with GE. AR received speaker honoraria from Piramal Imaging and GE Healthcare. MB received speaker honoraria from GE healthcare and LMI and is an advisor of LMI.

The remaining authors declare that the research was conducted in the absence of any commercial or financial relationships that could be construed as a potential conflict of interest.

frontiers in Aging Neuroscience

ORIGINAL RESEARCH
published: 10 February 2021
doi: 10.3389/fnagi.2021.630409

Association Between Gamma-Glutamyl Transferase and Mild Cognitive Impairment in Chinese Women

Zhaoyang Tang[1†], Xueyu Chen[1†], Wenran Zhang[1†], Xiangfu Sun[2], Qingzhi Hou[1], Yuejin Li[1], Xia Feng[1], Yanru Chen[1], Jian Lv[1], Long Ji[1], Guoyong Ding[1*] and Dong Li[1,3*]*

[1] Department of Epidemiology, School of Public Health, Shandong First Medical University & Shandong Academy of Medical Sciences, Taian, China, [2] Taian Traffic Hospital, Taian, China, [3] The Second Affiliated Hospital of Shandong First Medical University, Taian, China

Background: Dementia, as a global public health problem, is becoming increasingly serious. As a precursor of dementia, mild cognitive impairment (MCI) plays an important role in the diagnosis and prevention of dementia. Recent studies have found a correlation between gamma-glutamyl transferase (GGT) levels and cognitive function in men. The relationship between GGT levels and cognitive function in women remains unclear because GGT activity and expression differ between the sexes.

Method: We recruited a total of 2,943 Chinese women from Jidong and Taian in 2019. We grouped the participants according to GGT levels, diagnosed MCI using the Montreal Cognitive Assessment (MOCA) scale, and modeled the study outcomes using logistic regression to explore the relationship between GGT level and MCI. We also analyzed the interaction of obesity, sleep duration, and hyperuricemia with GGT in the development of MCI.

Results: The prevalence of MCI increased with increasing GGT level, from the lowest quartile to the highest quartile of GGT: 8.4% (66/786), 14.2% (119/840), 17.6% (108/613), and 21.4% (151/704), respectively. At the same time, as GGT levels increased, so did the risk of MCI. In the fully adjusted model, compared with those for participants in the lowest GGT quartiles, the odds ratios (ORs), and 95% confidence intervals (CIs) for MCI for participants in the second, third, and fourth GGT quartiles were 1.49 (1.04–2.12), 1.53(1.06–2.21), and 1.88 (1.33–2.65), respectively. The risk of developing MCI was further increased in people with high GGT levels who were obese (OR = 1.96, 95% CI: 1.39–2.76, $P < 0.001$), slept less (OR = 1.91, 95% CI: 1.35–2.71, $P < 0.001$), had high levels of uric acid (OR = 1.55, 95% CI: 1.03–2.32, $P < 0.001$), or after menopause (OR = 2.92, 95% CI: 2.07–4.12, $P < 0.001$).

Conclusion: We found that MCI is more common in women with elevated GGT levels, so GGT could be a potential diagnostic marker for MCI. Meanwhile, our findings indicated that women with high GGT levels had an increased risk of MCI when they were obese, sleep deprived, had high serum uric acid (SUA) levels or underwent menopause.

Keywords: mild cognitive impairment, female population, diagnostic marker, cross-sectional study, gamma-glutamyl transferase

OPEN ACCESS

Edited by:
Carlos J. Rodriguez-Ortiz, University of California, Irvine, United States

Reviewed by:
Venkata Saroja Voruganti, University of North Carolina at Chapel Hill, United States
Weiping Jia, Shanghai Sixth People's Hospital, China

***Correspondence:**
Long Ji
lji@sdfmu.edu.cn
Guoyong Ding
dgy153@126.com
Dong Li
tsmcdongli@163.com

[†] These authors have contributed equally to this work

Received: *17 November 2020*
Accepted: *08 January 2021*
Published: *10 February 2021*

Citation:
Tang Z, Chen X, Zhang W, Sun X, Hou Q, Li Y, Feng X, Chen Y, Lv J, Ji L, Ding G and Li D (2021) Association Between Gamma-Glutamyl Transferase and Mild Cognitive Impairment in Chinese Women. Front. Aging Neurosci. 13:630409. doi: 10.3389/fnagi.2021.630409

INTRODUCTION

With the aging of the population, dementia has become a major global public health problem and caused a huge disease burden (WHO, 2017). The global prevalence of dementia is expected to rise from 30 million in 2010 to 106 million in 2050 (Brookmeyer et al., 2007). Mild cognitive impairment (MCI) refers to the clinical condition between normal aging and dementia in which persons experience memory loss to a greater extent than one would expect for their age, yet they do not meet currently accepted criteria for clinically probable dementia (Petersen, 2001). Therefore, MCI is regarded as the prodromal stage of dementia; when people have MCI, their rate of conversion to dementia will be considerably accelerated compared with that of healthy age-matched individuals (Petersen, 2000; Thompson and Hodges, 2002; Ding et al., 2015).

Gamma-glutamyl transferase (GGT) is routinely used in clinical practice as an indicator of potential hepatic or biliary diseases, as it is mainly found in the liver and plays an important role in maintaining the intracellular concentration of glutathione (Kristenson et al., 1985; Forman et al., 2009; Kunutsor, 2016). Recently, the serum level of GGT has been reported to be associated with vascular diseases, which are considered to have pro-oxidant and proinflammatory properties (Emdin et al., 2005; Kunutsor et al., 2014, 2015; Jeon et al., 2020). However, inflammation and oxidative stress are the most likely pathways leading to cognitive impairment (Zafrilla et al., 2006; Gackowski et al., 2008). Therefore, GGT levels might be associated with an increased risk of dementia. A previous cohort study showed that serum GGT was log-linearly associated with the risk of dementia, and the risk of dementia increases with increasing GGT level in the male population (Kunutsor and Laukkanen, 2016). Another longitudinal study of older adults also showed that increased GGT levels are associated with cognitive decline at the end of life (Praetorius Bjork and Johansson, 2018). However, the result of a population-wide genetic study could not confirm a causal effect of GGT on the risk of dementia (Kunutsor et al., 2018). Therefore, the relationship between GGT and cognitive impairment is far from clear, especially among female individuals, among whom there is a lack of related research.

A systematic review of 75 studies in 2013 showed that the prevalence of dementia was significantly higher in women, with a prevalence rate that was 1.65 times higher among women than men (Chan et al., 2013); as a result, women are more likely to suffer from cognitive impairment. At the same time, an ovariectomized mouse model found that GGT activity might be related to estrogen (Zarida et al., 1994), which suggests that women not only face a higher risk of dementia but also are more sensitive to GGT activity.

In summary, owing to the sex-specific expression of GGT and the unknown relationship between GGT and MCI (Schiele et al., 1977), we collected data on GGT levels, cognitive function and general condition information from 2,943 women from two different Chinese cities to explore the association between GGT and MCI in the female population.

METHODS

Study Participants

In 2019, a total of 8,166 participants from Jidong ($n = 6,154$) and Taian ($n = 2,012$), including 4,655 male participants and 3,511 female participants, underwent health checks. Among the 3,511 female participants, individuals with missing data on GGT, body mass index (BMI), sleep duration, serum uric acid (SUA), Montreal Cognitive Assessment (MOCA) score, or important confounders ($n = 355$, 10.1%); heavy alcoholism (defined as 30 g/day, $n = 25$, 0.7%); hepatobiliary and pancreatic diseases including cancer and viral hepatitis ($n = 119$, 3.3%); and a history of dementia ($n = 6$, 0.2%) were excluded from this study. In our study, participants with severe cognitive impairment (defined as a chief complaint of memory impairment and a MOCA score <18, $n = 66$, 1.9%) were excluded, even if they were not diagnosed with dementia. Eventually, a total of 2,943 female participants were included in our study (**Figure 1**).

The study was conducted in accordance with the guiding principles of the Helsinki Declaration and approved by the Ethics Committee of Jidong Oilfield Inc. Medical Centers and Taian Traffic Hospital. Written informed consent was obtained from all participants.

Assessment of Mild Cognitive Impairment

Previous studies have found that the MOCA scale is more sensitive in MCI screening than other scales, and the specificity is not significantly different from that of other scales (Dong et al., 2010, 2012; Kasten et al., 2010). Therefore, we decided to use the MOCA scale to evaluate MCI. In this study, using the Chinese version of the MOCA scale and cutoffs for the Chinese population. The MOCA scale is a rapid tool for detecting MCI, which is assessed from different cognitive domains, they include attention, memory, executive function, language, visuospatial ability, abstract thinking, numeracy, and orientation. Each MOCA is limited to 10 min, with a maximum score of 30. We defined no subjective cognitive decline and a MOCA score ≥26 as normal (Dong et al., 2010, 2012; Kasten et al., 2010), and complaints of memory loss and a MOCA score of more than 18 and <26 points as MCI (Nasreddine et al., 2005). Considering the effect of education on cognitive function, those with 12 years or less of education had 1 point added to their scores. The MOCA scale was administered by specially trained investigators.

Assessment of Gamma-Glutamyl Transferase (GGT) and Serum Uric Acid (SUA)

Blood samples were collected by venipuncture from the large antecubital veins in the morning after overnight fasting. All blood samples were stored in vacuum tubes containing ethylenediaminetetraacetic acid (EDTA). GGT and SUA levels were determined using an autoanalyzer (Hitachi 747; Hitachi, Tokyo, Japan) with the kinetic and uricase-peroxidase methods, respectively, in the laboratories of Jidong Oilfield Hospital and Taian Traffic Hospital.

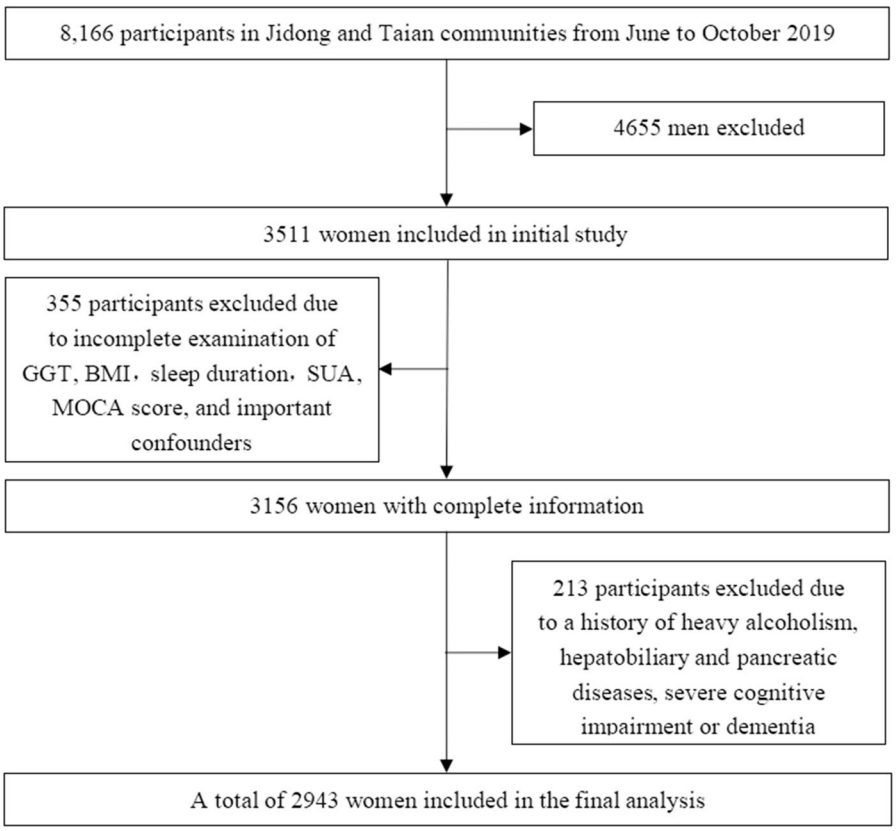

FIGURE 1 | Flow chart of the study.

Assessment of Covariates

A series of standardized questionnaires, clinical examinations, and laboratory tests were used to collect basic information (Zhang et al., 2013). A standardized questionnaire was administered by well-trained interviewers to collect subjects' information. Demographic variables, including age, sex, education level and histories of hypertension, diabetes mellitus, dyslipidemia and hepatobiliary, and pancreatic diseases, were collected through the questionnaire. We also asked them about their menstrual history to see if they had gone through menopause and their age at menopause. According to self-reported information, alcohol consumption was classified as heavy drinker (alcohol consumption $\geq$30 g/day), mild-moderate drinker (alcohol consumption $<$30 g/day) or abstainer (alcohol consumption $=$ 0 g/day) (Yoo et al., 2020), and smoking status was classified as non-smoker or having quit more than 1 year ago or current smoker or having quit $<$1 year ago. BMI was defined based on the measured height and weight and calculated as weight (kg)/height (m^2). Education was categorized into illiterate or primary school, middle school, or university or above. The Pittsburgh Sleep Quality Index Questionnaire was used to measure sleep quality and duration (Mollayeva et al., 2016). Sleep duration was classified as $<$6, 6–7, 7–8, and $>$8 h, and adequate sleep or insufficient sleep were defined based on whether the sleep duration was greater than the median of 7 h (Papandreou et al., 2019). Hypertension was defined as the use of antihypertensive drugs, a self-reported history, diastolic blood pressure $\geq$90 mmHg, or systolic blood pressure $\geq$140 mmHg. Diabetes mellitus was defined as current treatment with insulin or an oral hypoglycemic agent, presence of a history of diabetes, or fasting blood glucose level $\geq$7.0 mmol/L (126 mg/dL). Dyslipidemia was defined as current use of lipid-lowering therapy, a self-reported history, or serum levels of triglyceride (TG) $\geq$1.7 mmol/L, total cholesterol (TC) $\geq$5.18 mmol/L, high-density lipoprotein (HDL) $<$1.04 mmol/L, or low-density lipoprotein (LDL) $\geq$3.37 mmol/L (Lv et al., 2016).

Statistical Analysis

The Kolmogorov-Smirnov test was used to measure the normality of the distribution of the test variables. Continuous variables with normal distributions were expressed as the mean $\pm$ standard deviation (SD). Continuous variables that did not have a normal distribution were represented by the mean and interquartile range. Categorical variables were presented as frequencies and percentages. We compared the baseline

characteristics of different serum GGT quartile groups using one-way ANOVA or the Kruskal-Wallis rank-sum test for normally or non-normally distributed continuous variables, respectively, and the chi-square test or Fisher's exact test for categorical variables. We also compared the baseline characteristics of groups with and without MCI using Student's *t*-test or the Mann-Whitney *U*-test for normally or non-normally distributed continuous variables, respectively, and the chi-square test or Fisher's exact test for categorical variables. Logistic regression model was used to evaluate the association between risk factors (GGT, BMI, sleep duration, SUA, and estrogen level) and MCI by calculating odds ratios (ORs) with 95% confidence intervals (CIs). The 25th, 50th, and 75th percentiles of GGT nodes were selected by using the restricted cubic spline method, and the confounding factors were adjusted by using the 25th percentile (12 U/L) as the reference. A dose-response diagram was also drawn by the GGT levels as horizontal coordinates, and the corresponding OR values as vertical coordinates. Nomogram was based on the results of logistic regression analysis. We used the postestimation Wald test in the multivariable-adjusted logistic model to obtain an omnibus *P*-value for interaction, the models were adjusted for age, education, smoking status, alcohol consumption, hypertension, hyperlipidemia, and diabetes mellitus.

The statistical analyses were performed using SAS software, version 9.4 (SAS Institute Inc., Cary, NC, USA), and the significance level was set as $P < 0.05$.

RESULTS

Baseline Characteristics of the Study Participants

A total of 2,943 participants from Jidong (2,821) and Taian (122) eventually enrolled in our study (**Figure 1**). We found no statistically significant differences between the populations from the two centers in terms of GGT, sleep duration, BMI, smoking status, education level, hypertension, diabetes mellitus, dyslipidemia, SUA, total cholesterol, triglycerides, HDL-C, LDL-C, and estrogen level ($P > 0.05$). Although there was a significant difference in the age of potential subjects from the two centers, there was no significant difference in the ages of the MCI patients from the two centers (**Supplementary Table 1**). Therefore, we combined the patients from the two centers for the analysis.

We compared baseline characteristics by different quartiles of serum GGT activity (**Table 1**). There were 14 factors that were significantly associated with serum GGT levels, including age, sleep duration, BMI, smoking status, education level, hypertension, diabetes mellitus, dyslipidemia, SUA, total cholesterol, triglycerides, HDL-C, LDL-C, and estrogen level ($P < 0.05$). We considered all of these possible confounding variables when evaluating the independent relationship between GGT and MCI.

At the same time, baseline characteristics were compared in women participants with and without MCI. Significant differences were found in age, sleep duration, BMI, smoking status, education level, hypertension, diabetes mellitus, dyslipidemia, triglycerides, SUA, LDL-C, GGT, and estrogen level ($P < 0.05$). **Supplementary Table 2** clearly shows the association between baseline characteristics and MCI.

Association Between GGT and MCI in Women

The prevalence of MCI in the participants increased with increasing GGT level, being 8.4, 14.2, 17.6, and 21.4% in the lowest to highest quartiles of GGT, respectively (**Table 1**).

For the participants in the present study, compared to the lowest quartile, the highest quartile of GGT exhibited a positive association with MCI risk (OR = 1.88, 95% CI: 1.33–2.65, $P < 0.001$) in the fully adjusted model. At the same time, we found that as GGT levels increased, the ORs and 95% CIs for MCI of the participants in the second, third, and fourth GGT quartiles increased, respectively, compared with those of the participants in the lowest GGT quartile. Moreover, in all three models of the participants, the *P* for trend across quartiles was <0.001 (**Figure 2**). The dose-response relationship between GGT level and risk of MCI was analyzed by using the restricted cubic spline regression model. And the risk of MCI increased with increasing GGT level when the GGT level was below 35 μ/l, and when the GGT level was higher than 35 U/l, the risk of MCI remained high but decreased slightly with increasing GGT level (**Figure 3**).

Effect of BMI, Sleep Duration, Serum Uric Acid, and Estrogen Level on the Relationship Between GGT and the Risk of MCI

In our study, obesity, insufficient sleep, hyperuricemia, and menopause all increased the risk of MCI of the participants. The OR and 95% CI for MCI due to obesity was 1.32 (1.04–1.69) in the fully adjusted model. Likewise, insufficient sleep also increased the risk of MCI, and the OR and 95% CI for MCI due to insufficient sleep was 1.33 (1.05–1.69) in the fully adjusted model. For hyperuricemia, the OR and 95% CI for MCI was 1.34 (1.01–1.77) in the fully adjusted model. Reduced estrogen levels also affect the development of MCI in postmenopausal women, the OR and 95% CI for MCI due to menopause was 2.28 (1.78–2.91) in the fully adjusted model (**Supplementary Table 3**). We also found that obesity, insufficient sleep, hyperuricemia, and menopause were significant risk factors for MCI according to the nomogram based on the logistic regression results for all factors (**Supplementary Figure 1**).

We summarized the results of the analysis on the effects of the interactions between serum GGT and the presence of obesity, insufficient sleep, and hyperuricemia on the risk of MCI in **Figure 4**. Through interaction analysis, we found that women with high GGT levels had an increased risk of MCI when they were obese (OR = 1.96 for obese women with Q4 GGT compared to nonobese women in Q1-Q3 GGT, *P* for interaction = 0.032), lacked sleep (OR = 1.91 for women who slept less and had Q4 GGT compared to women who slept more and had Q1-Q3 GGT, *P* for interaction = 0.001), had a high level of SUA (OR = 1.55

TABLE 1 | Comparison of baseline characteristics according to quartiles of serum GGT.

Characteristic	GGT level					
	Q1 (n = 786)	Q2 (n = 840)	Q3 (n = 613)	Q4 (n = 704)	*P*	*P* for trend
GGT(U/L)	10.6 ± 1.3	14.4 ± 1.1	19.1 ± 1.7	42.6 ± 3.3	<0.001	<0.001
Age (years)	42.1 ± 12.2	45.5 ± 13.1	48.5 ± 13.5	50.1 ± 12.8	<0.001	<0.001
Education level (n, %)					<0.001	<0.001
<6 years	33 (4.2)	47 (5.6)	49 (8.0)	49 (7.0)		
6–12 years	196 (24.9)	273 (32.5)	238 (38.8)	339 (48.2)		
>12 years	557 (70.9)	520 (61.9)	326 (53.2)	316 (44.9)		
Sleep duration (n, %)					<0.001	<0.001
<7 h	281 (35.8)	356 (42.4)	296 (48.3)	329 (46.7)		
≥7 h	505 (64.2)	484 (57.6)	317 (51.7)	375 (53.3)		
BMI (n, %)					<0.001	<0.001
<25 kg/m^2	111 (14.1)	205 (24.4)	221 (36.1)	308 (43.8)		
≥25 kg/m^2	675 (85.9)	635 (75.6)	392 (63.9)	396 (56.3)		
Current smoker (n, %)	14 (1.8)	44 (5.2)	32 (5.2)	54 (7.7)	<0.001	<0.001
Mild-moderate drinking (n, %)	5 (0.6)	8 (1.0)	5 (0.8)	10 (1.4)	0.459	0.162
Hypertension (n, %)	32 (4.1)	58 (6.9)	93 (15.2)	126 (17.9)	<0.001	<0.001
Dyslipidemia (n, %)	13 (1.7)	31 (3.7)	50 (8.2)	78 (11.1)	<0.001	<0.001
Diabetes (n, %)	13 (1.7)	21 (2.5)	32 (5.2)	56 (8.0)	<0.001	<0.001
UA(umol/L)	271.4 ± 55.6	291.9± 65.2	305.1 ± 66.9	328.0 ± 76.6	<0.001	<0.001
TC (mmol/L)	4.7 ± 1.6	5.7 ± 6.8	5.6 ± 5.9	6.7± 10.7	<0.001	<0.001
Triglycerides (mmol/L)	1.1 ± 0.5	1.3 ± 0.7	1.6 ± 1.0	2.1 ± 1.7	<0.001	<0.001
HDL-C (mmol/L)	1.3 ± 0.2	1.3 ± 0.3	1.2 ± 0.3	1.2 ± 0.2	<0.001	<0.001
LDL-C (mmol/L)	1.8 ± 0.7	1.9 ± 0.7	2.1 ± 0.8	2.3 ± 0.8	<0.001	<0.001
Menopause (n, %)	168 (21.4)	268 (31.9)	254 (41.4)	302 (42.9)	<0.001	<0.001
MCI (n, %)	66 (8.4)	119 (14.2)	108 (17.6)	151 (21.4)	<0.001	<0.001

Q1, quartile 1 (n = 786): ≤12 U/L; Q2, quartile 2 (n = 840): 13-16 U/L; Q3, quartile 3 (n = 613): 17-22 U/L; Q4, quartile 4 (n = 704): >22 U/L.

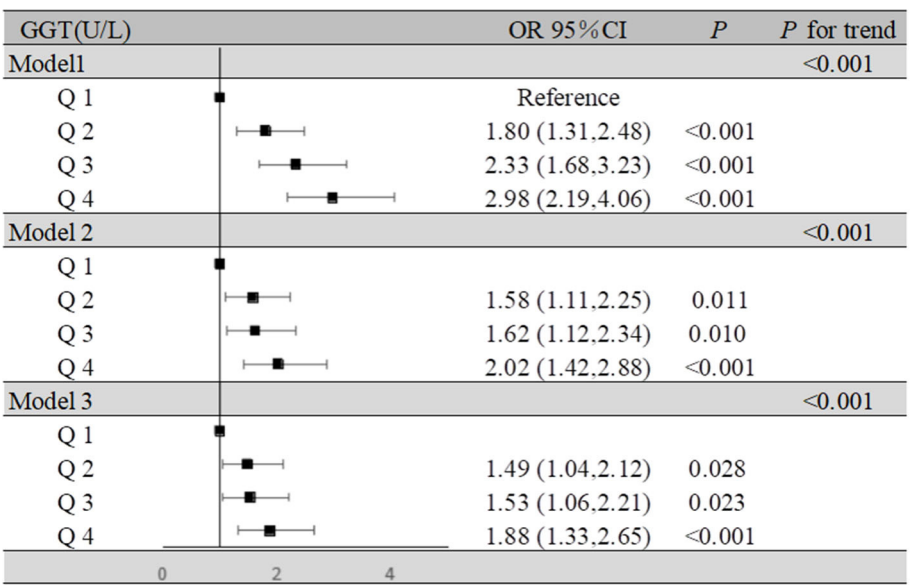

FIGURE 2 | Association of GGT levels and MCI in the participants. Model 1: unadjusted. Model 2: adjusted for age, BMI, education, sleep duration, smoking status, and alcohol consumption. Model 3: adjusted for age, BMI, education, sleep duration, smoking status, alcohol consumption, hypertension, hyperlipidemia, diabetes mellitus, serum uric acid, and estrogen level.

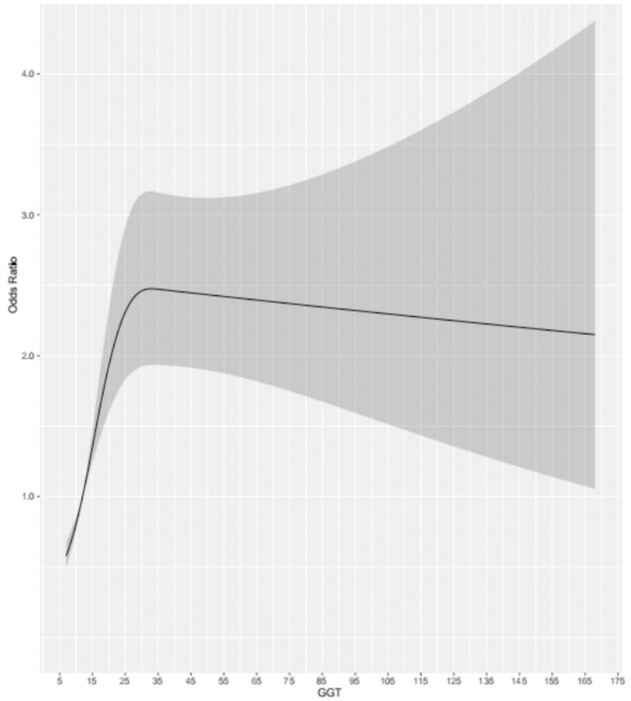

FIGURE 3 | Dose-response relationship between the risk of MCI and changes in GGT level.

for women with high UA levels and Q4 GGT compared to women with low UA levels and Q1-Q3 GGT, *P* for interaction = 0.037) or after menopause (OR = 2.92 for postmenopausal women and Q4 GGT compared to premenopausal women and Q1-Q3 GGT, *P* for interaction <0.001). Considering women with high GGT levels, when they were obese, lack of sleep, had high levels of uric acid or after menopause, we obtained higher OR values than that we did for women with high GGT levels alone (OR = 1.19, 95% CI: 1.07–1.33). So obesity, lack of sleep, hyperuricemia, and menopause all had subadditive effects on the increased risk of MCI associated with GGT (**Supplementary Table 3**, **Figure 4**).

DISCUSSION

In our study, we found that GGT might be an independent risk factor for MCI in the female population, and as GGT levels increased, so did the risk of MCI. At the same time, we also found that women with high GGT levels were at increased risk of developing MCI when they were obese, lacked sleep, had high levels of uric acid or after menopause. BMI, sleep duration and uric acid may interact with GGT in the development of MCI.

Our study found an association between higher GGT and higher risk of cognitive impairment in the female population, which is consistent with previous studies in the male population (Kunutsor and Laukkanen, 2016). A study of GGT and Parkinson's disease is also consistent with our finding, that GGT may contribute to neurodegenerative disease in the female population (Yoo et al., 2020). However, contrary to our findings, a genetic study found no clear link between GGT and cognitive function (Kunutsor et al., 2018), possibly because that study did not include a subgroup analysis based on sex, which is essential because of the finding from previous study that estrogen may affect GGT activity in the body (Zarida et al., 1994).

The potential proinflammatory and pro-oxidative effects of GGT might be an important cause of the increased risk of MCI related to GGT (Kunutsor et al., 2014, 2015). Additionally, GGT levels were directly involved in atheromatous plaque formation, which has also been implicated as an underlying link in the pathogenesis of cognitive impairment (Breteler, 2000; Paolicchi et al., 2004; Franzini et al., 2009).

Through the analysis of the baseline data, we found that the differences in age, education, sleep duration, BMI, hypertension, dyslipidemia, diabetes, SUA, triglycerides. LDL-C, and estrogen decline were statistically significant not only in the MCI and non-MCI groups (**Supplementary Table 2**), but also in the different GGT level groups (**Table 1**). However, previous studies found that only BMI (Carter et al., 2019; Cho et al., 2019), sleep (D'Rozario et al., 2020; Zhang et al., 2020), uric acid (Zhang et al., 2015; Ya et al., 2017; Tana et al., 2018) and estrogen level (D'Rozario et al., 2020; Zhang et al., 2020) affected both GGT and MCI. Moreover, after we used logistic regression to establish the nomogram, we found that obesity, lack of sleep, high uric acid levels, and menopause were risk factors for MCI. Therefore, the effects of the interaction of obesity, lack of sleep, high uric acid levels, and menopause with GGT on MCI was analyzed by demographic, lifestyle, and biochemical parameters. Interestingly, when we constructed nomograms, we found that mild-moderate alcohol consumption may have a weak protective effect on MCI, consistent with previous research on the relationship between alcohol consumption and Alzheimer's disease (AD) (Venkataraman et al., 2016).

Direct release in the context of hepatocyte injury is not the sole cause of serum GGT elevation. GGT elevation may also be due to factors such as obesity related to serum GGT activities that occur and lead to increased expression or decreased breakdown. A previous study showed that the level of GGT expression in obese people may be different from that in normal people (Carter et al., 2019). Moreover, obesity also plays an important role in neurodegenerative diseases by inducing insulin resistance (Pugazhenthi et al., 2017). These findings make it possible for BMI and GGT to play a synergistic role in the development of MCI.

Sleep may cause changes in GGT levels because of its interaction with obesity, and a recent nematode model study demonstrated a synergistic effect between insomnia and obesity (Grubbs et al., 2020; Zhang et al., 2020). Therefore, lack of sleep may also lead to GGT elevation. In the same way, lack of sleep is a major cause of cognitive impairment. In summary, the mechanism of sleep deprivation affecting MCI may be partially enhanced by GGT.

The levels of serum UA, an important natural antioxidant, may parallel the levels of serum GGT due to their relationship with oxidative stress, as reported in the Chinese population,

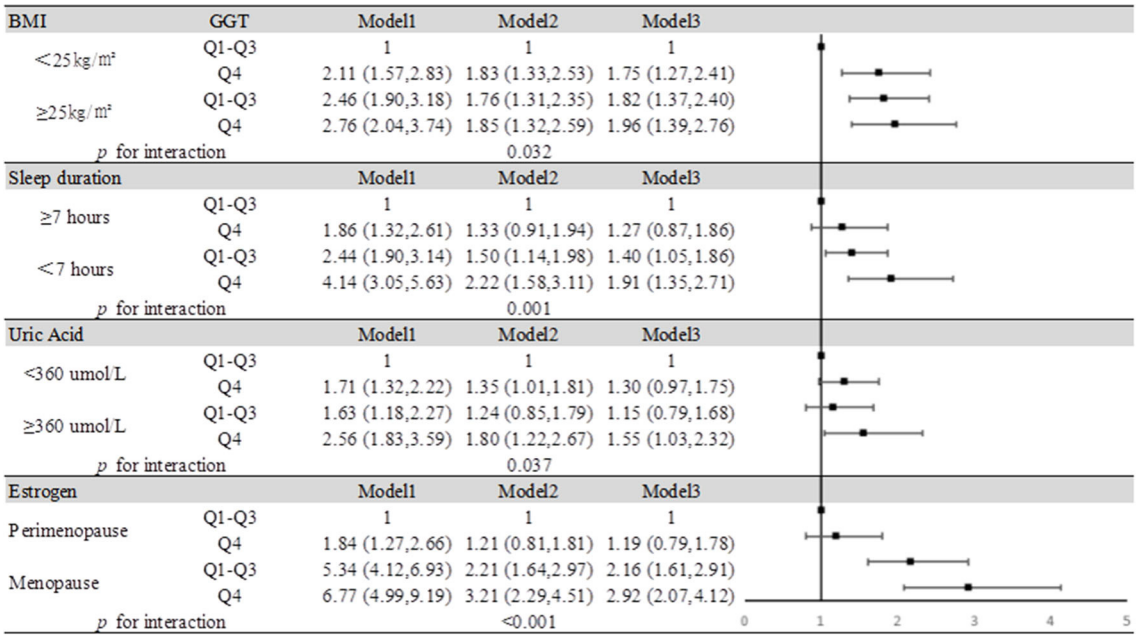

FIGURE 4 | Impact of serum GGT level on MCI according to BMI, sleep duration, uric acid, and estrogen. Model 1: unadjusted. Model 2: adjusted for age, education, smoking status, and alcohol consumption. Model 3: adjusted for age, education, smoking status, alcohol consumption, hypertension, hyperlipidemia, and diabetes mellitus.

especially in Chinese females (Zhang et al., 2015; Ya et al., 2017). Large cohort studies completed in recent years have found that high uric acid levels may increase the risk of cognitive impairment, possibly because uric acid is more damaging to vascular tissue than it is productive of antioxidant effects (Latourte et al., 2018; Singh and Cleveland, 2018). Therefore, the synergistic effect of GGT and SUA in MCI may be due to their effect on the risk of cardiovascular disease. In addition, a previous study found that increased SUA in women increases the risk of non-alcoholic fatty liver disease and that fatty liver disease development leads to increased GGT secretion, which might be an important reason for the parallel relationship between GGT and SUA levels (Chen et al., 2019).

In animal study, GGT levels have been found to increase significantly after ovariectomy, suggesting that estrogen levels have a significant effect on GGT expression (Zarida et al., 1994). At the same time, studies have shown that endogenous estrogens are associated with better cognitive performance, and our study found that a decrease in estrogens and an increase in GGT both affect MCI, this is of positive significance for the study of cognitive impairment in postmenopausal women (Fink et al., 2018; Shimizu et al., 2019).

In our study, we found that MCI is more common in women with elevated GGT levels, so GGT could be a potential diagnostic marker for MCI. Meanwhile, our findings indicated that women with high GGT levels had an increased risk of MCI when they were overweight, sleep deprived, or had high uric acid levels.

LIMITATIONS

Since we performed a cross-sectional study, we could not refute the conclusion reached in previous studies that there is no causal link between GGT and MCI (Kunutsor et al., 2018). However, there has been no previous research into the relationship between GGT and cognitive function in the female population, so our results are significant in terms of the diagnosis and early indication of MCI in the female population. In addition, because our study only included Chinese women, the results may not be generalizable to the entire population. However, at the same time, our study was a two-center study that integrated analysis of different populations, and the conclusions are more representative and extrapolatable in Chinese female population.

DATA AVAILABILITY STATEMENT

The raw data supporting the conclusions of this article will be made available by the authors, without undue reservation.

ETHICS STATEMENT

The study was conducted in accordance with the guiding principles of the Helsinki Declaration and approved by the Ethics Committee of Oilfield Inc. Medical Centers and Taian Traffic Hospital. Written informed consent was obtained from all participants.

AUTHOR CONTRIBUTIONS

All authors listed have made a substantial, direct and intellectual contribution to the work, and approved it for publication.

FUNDING

The author(s) disclosed receipt of the following financial support for the research, authorship, and/or publication of this article: This work was supported by the National Natural Science Foundation of China (81973138) and National Key Research and Development Project of China (2017YFE0118800).

SUPPLEMENTARY MATERIAL

The Supplementary Material for this article can be found online at: https://www.frontiersin.org/articles/10.3389/fnagi.2021.630409/full#supplementary-material

REFERENCES

Breteler, M. (2000). Vascular risk factors for Alzheimer's disease: an epidemiologic perspective. *Neurobiol. Aging* 21, 153–160. doi: 10.1016/S0197-4580(99)00110-4

Brookmeyer, R., Johnson, E., Ziegler-Graham, K., and Arrighi, H. (2007). Forecasting the global burden of Alzheimer's disease. *Alzheimer's Dementia* 3, 186–191. doi: 10.1016/j.jalz.2007.04.381

Carter, A., Borges, M., Benn, M., Tybjaerg-Hansen, A., Davey Smith, G., Nordestgaard, B., et al. (2019). Combined association of body mass index and alcohol consumption with biomarkers for liver injury and incidence of liver disease: a mendelian randomization study. *JAMA Network Open* 2:e190305. doi: 10.1001/jamanetworkopen.2019.0305

Chan, K., Wang, W., Wu, J., Liu, L., Theodoratou, E., Car, J., et al. (2013). Epidemiology of Alzheimer's disease and other forms of dementia in China, 1990-2010: a systematic review and analysis. *Lancet* 381, 2016–2023. doi: 10.1016/S0140-6736(13)60221-4

Chen, Y., Huang, Q., Ai, P., Liu, H., Chen, X., Xu, X., et al. (2019*).* Association between serum uric acid and non-alcoholic fatty liver disease according to different menstrual status groups. *Canad. J. Gastroenterol. Hepatol.* 2019:2763093. doi: 10.1155/2019/2763093

Cho, G., Hwang, S., Lee, K., Choi, K., Hyun Baik, S., Kim, T., et al. (2019). Association between waist circumference and dementia in older persons: a nationwide population-based study. *Obesity* 27, 1883–1891. doi: 10.1002/oby.22609

Ding, D., Zhao, Q., Guo, Q., Meng, H., Wang, B., Luo, J., et al. (2015). Prevalence of mild cognitive impairment in an urban community in China: a cross-sectional analysis of the Shanghai Aging Study. *Alzheimer's Dementia* 11, 300–309 e302. doi: 10.1016/j.jalz.2013.11.002

Dong, Y., Lee, W., Basri, N., Collinson, S., Merchant, R., Venketasubramanian, N., et al. (2012). The montreal cognitive assessment is superior to the Mini-Mental State Examination in detecting patients at higher risk of dementia. *Int. Psychogeriat.* 24, 1749–1755. doi: 10.1017/S1041610212001068

Dong, Y., Sharma, V., Chan, B., Venketasubramanian, N., Teoh, H., Seet, R., et al. (2010). The Montreal Cognitive Assessment (MoCA). is superior to the Mini-Mental State Examination (MMSE). for the detection of vascular cognitive impairment after acute stroke. *J. Neurol. Sci.* 299, 15–18. doi: 10.1016/j.jns.2010.08.051

D'Rozario, A., Chapman, J., Phillips, C., Palmer, J., Hoyos, C., Mowszowski, L., et al. (2020). Objective measurement of sleep in mild cognitive impairment: a systematic review and meta-analysis. *Sleep Med. Rev.* 52:101308. doi: 10.1016/j.smrv.2020.101308

Emdin, M., Pompella, A., and Paolicchi, A. (2005). Gamma-glutamyltransferase, atherosclerosis, and cardiovascular disease: triggering oxidative stress within the plaque. *Circulation* 112, 2078–2080. doi: 10.1161/CIRCULATIONAHA.105.571919

Fink, H., Jutkowitz, E., McCarten, J., Hemmy, L., Butler, M., Davila, H., et al. (2018). Pharmacologic interventions to prevent cognitive decline, mild cognitive impairment, and clinical Alzheimer-Type dementia: a systematic review. *Ann. Internal Med.* 168, 39–51. doi: 10.7326/M17-1529

Forman, H., Zhang, H., and Rinna, A. (2009). Glutathione: overview of its protective roles, measurement, and biosynthesis. *Mol. Aspects Med.* 30, 1–12. doi: 10.1016/j.mam.2008.08.006

Franzini, M., Corti, A., Martinelli, B., Del Corso, A., Emdin, M., Parenti, G., et al. (2009). Gamma-glutamyltransferase activity in human atherosclerotic plaques–biochemical similarities with the circulating enzyme. *Atherosclerosis* 202, 119–127. doi: 10.1016/j.atherosclerosis.2008.03.023

Gackowski, D., Rozalski, R., Siomek, A., Dziaman, T., Nicpon, K., Klimarczyk, M., et al. (2008). Oxidative stress and oxidative DNA damage is characteristic for mixed Alzheimer disease/vascular dementia. *J. Neurol. Sci.* 266, 57–62. doi: 10.1016/j.jns.2007.08.041

Grubbs, J., Lopes, L., van der Linden, A., and Raizen, D. (2020). A salt-induced kinase is required for the metabolic regulation of sleep. *PLoS Biol.* 18:e3000220. doi: 10.1371/journal.pbio.3000220

Jeon, J., Kim, D., Kim, W., Choi, D., Jung, K., and Jang, S. (2020). Dose-response relationship between gamma-glutamyltransferase and the risk of atherosclerotic cardiovascular diseases in Korean adults. *Atherosclerosis* 292, 152–159. doi: 10.1016/j.atherosclerosis.2019.11.004

Kasten, M., Bruggemann, N., Schmidt, A., and Klein, C. (2010). Validity of the MoCA and MMSE in the detection of MCI and dementia in Parkinson disease. *Neurology* 75:478. doi: 10.1212/WNL.0b013e3181e7948a

Kristenson, H., Hood, B., Peterson, B., and Trell, E. (1985). Prevention of alcohol-related problems in urban middle-aged males. *Alcohol* 2, 545–549. doi: 10.1016/0741-8329(85)90132-6

Kunutsor, S. (2016). Gamma-glutamyltransferase-friend or foe within? *Liver Int.* 36, 1723–1734. doi: 10.1111/liv.13221

Kunutsor, S., Apekey, T., and Khan, H. (2014). Liver enzymes and risk of cardiovascular disease in the general population: a meta-analysis of prospective cohort studies. *Atherosclerosis* 236, 7–17. doi: 10.1016/j.atherosclerosis.2014.06.006

Kunutsor, S., Bakker, S., Kootstra-Ros, J., Gansevoort, R., and Dullaart, R. (2015). Circulating gamma glutamyltransferase and prediction of cardiovascular disease. *Atherosclerosis* 238, 356–364. doi: 10.1016/j.atherosclerosis.2014.12.045

Kunutsor, S., and Laukkanen, J. (2016). Gamma glutamyltransferase and risk of future dementia in middle-aged to older Finnish men: a new prospective cohort study. *Alzheimer's Dementia* 12, 931–941. doi: 10.1016/j.jalz.2016.03.003

Kunutsor, S., Laukkanen, J., and Burgess, S. (2018). Genetically elevated gamma-glutamyltransferase and Alzheimer's disease. *Exp. Gerontol.* 106, 61–66. doi: 10.1016/j.exger.2018.03.001

Latourte, A., Soumare, A., Bardin, T., Perez-Ruiz, F., Debette, S., and Richette, P. (2018). Uric acid and incident dementia over 12 years of follow-up: a population-based cohort study. *Ann. Rheumatic Dis.* 77, 328–335. doi: 10.1136/annrheumdis-2016-210767

Lv, H., Yang, X., Zhou, Y., Wu, J., Liu, H., Wang, Y., et al. (2016). Parity and serum lipid levels: a cross-sectional study in chinese female adults. *Sci. Rep.* 6:33831. doi: 10.1038/srep33831

Mollayeva, T., Thurairajah, P., Burton, K., Mollayeva, S., Shapiro, C., and Colantonio, A. (2016). The Pittsburgh sleep quality index as a screening tool for sleep dysfunction in clinical and non-clinical samples: a systematic review and meta-analysis. *Sleep Med. Rev.* 25, 52–73. doi: 10.1016/j.smrv.2015.01.009

Nasreddine, Z., Phillips, N., Bédirian, V., Charbonneau, S., Whitehead, V., Collin, I., et al. (2005). The Montreal Cognitive Assessment, MoCA: a brief screening tool for mild cognitive impairment. *J. Am. Geriatr. Soc.* 53, 695–699. doi: 10.1111/j.1532-5415.2005.53221.x

Paolicchi, A., Emdin, M., Ghliozeni, E., Ciancia, E., Passino, C., Popoff, G., et al. (2004). Images in cardiovascular medicine. human atherosclerotic plaques

contain gamma-glutamyl transpeptidase enzyme activity. *Circulation* 109:1440. doi: 10.1161/01.CIR.0000120558.41356.E6

Papandreou, C., Babio, N., Diaz-Lopez, A., Martinez-Gonzalez, M., Becerra-Tomas, N., Corella, D., et al. (2019). Sleep duration is inversely associated with serum uric acid concentrations and uric acid to creatinine ratio in an elderly mediterranean population at high cardiovascular risk. *Nutrients* 11:761. doi: 10.3390/nu11040761

Petersen, R., (2000). Aging, mild cognitive impairment, and Alzheimer's disease. *Neurol. Clin*. 18, 789–806. doi: 10.1016/S0733-8619(05)70226-7

Petersen, R., Doody, R., Kurz, A., Mohs, R., Morris, J., Rabins, P., et al., (2001). Current concepts in mild cognitive impairment. *Arch. Neurol.* 58, 1985–1992. doi: 10.1001/archneur.58.12.1985

Praetorius Bjork, M., and Johansson, B. (2018). Gamma-Glutamyltransferase (GGT). as a biomarker of cognitive decline at the end of life: contrasting age and time to death trajectories. *Int. Psychogeriat.* 30, 981–990. doi: 10.1017/S1041610217002393

Pugazhenthi, S., Qin, L., and Reddy, P. (2017). Common neurodegenerative pathways in obesity, diabetes, and Alzheimer's disease. *Biochim. Biophys. Acta Mol. Basis Dis.* 1863, 1037–1045. doi: 10.1016/j.bbadis.2016.04.017

Schiele, F., Guilmin, A., Detienne, H., and Siest, G. (1977). Gamma-glutamyltransferase activity in plasma: statistical distributions, individual variations, and reference intervals. *Clin. Chem.* 23, 1023–1028. doi: 10.1093/clinchem/23.6.1023

Shimizu, Y., Sawada, N., Iwasaki, M., Shikimoto, R., Nozaki, S., Mimura, M., et al. (2019). Reproductive history and risk of cognitive impairment in Japanese women. *Maturitas* 128, 22–28. doi: 10.1016/j.maturitas.2019.06.012

Singh, J., and Cleveland, J. (2018). Gout and dementia in the elderly: a cohort study of Medicare claims. *BMC Geriat.* 18:281. doi: 10.1186/s12877-018-0975-0

Tana, C., Ticinesi, A., Prati, B., Nouvenne, A., and Meschi, T. (2018). Uric acid and cognitive function in older individuals. *Nutrients* 10:975. doi: 10.3390/nu10080975

Thompson, S., and Hodges, J. (2002). Mild cognitive impairment: a clinically useful but currently ill-defined concept? *Neurocase* 8, 405–410. doi: 10.1076/neur.8.5.405.16182

Venkataraman, A., Kalk, N., Sewell, G., Ritchie, C W., and Lingford-Hughes A. (2016). Alcohol and Alzheimer's disease does alcohol dependence contribute to beta-amyloid deposition,neuroinflammation and neurodegeneration in Alzheimer's disease. *Alcohol Alcohol.* 52:158. doi: 10.1093/alcalc/agw101

WHO (2017). *Dementia a Public Health Priority*. Geneva: WHO.

Ya, Z., Fei, L., Yue, Z., Dan, L., Neng-Bo, L., Yi, L., et al. (2017). Association between serum gamma-glutamyl transferase and serum uric acid levels in Chinese females: a cross-sectional study. *Endocrine Res.* 42, 296–301. doi: 10.1080/07435800.2017.1300809

Yoo, D., Kim, R., Jung, Y., Han, K., Shin, C., and Lee, J. (2020). Serum gamma-glutamyltransferase activity and Parkinson's disease risk in men and women. *Sci. Rep*. 10:1258. doi: 10.1038/s41598-020-58306-x

Zafrilla, P., Mulero, J., Xandri, J., Santo, E., Caravaca, G., and Morillas, J. (2006). Oxidative stress in Alzheimer patients in different stages of the disease. *Curr. Med. Chem*. 13, 1075–1083. doi: 10.2174/092986706776360978

Zarida, H., Wan Zurinah, W., Zanariah, J., Michael, L., and Khalid, B. (1994). Effect of ovariectomy and sex hormones replacement on tumour marker enzymes under administration of chemical carcinogens in the rat. *Exp. Toxicol. Pathol.* 46, 31–36. doi: 10.1016/S0940-2993(11)80010-2

Zhang, J., Xiang, G., Xiang, L., and Dong, J. (2015). Serum gamma-glutamyl transferase is associated with the elevated uric acid levels in normotensive Chinese adults. *Clin. Chim. Acta* 441, 122–126. doi: 10.1016/j.cca.2014.12.031

Zhang, L., Zhang, X., Meng, H., Li, Y., Han, T., and Wang, C. (2020). Obstructive sleep apnea and liver injury in severely obese patients with nonalcoholic fatty liver disease. *Sleep Breath*. 24, 1515–1521. doi: 10.1007/s11325-020-02018-z

Zhang, Q., Zhou, Y., Gao, X., Wang, C., Zhang, S., Wang, A., et al. (2013). Ideal cardiovascular health metrics and the risks of ischemic and intracerebral hemorrhagic stroke. *Stroke* 44, 2451–2456. doi: 10.1161/STROKEAHA.113.678839

Conflict of Interest: The authors declare that the research was conducted in the absence of any commercial or financial relationships that could be construed as a potential conflict of interest.

frontiers in Aging Neuroscience

ORIGINAL RESEARCH
published: 14 April 2021
doi: 10.3389/fnagi.2021.611891

Iron Deposition Characteristics of Deep Gray Matter in Elderly Individuals in the Community Revealed by Quantitative Susceptibility Mapping and Multiple Factor Analysis

*Jing Li[1], Qihao Zhang[2], Yena Che[3], Nan Zhang[4] and Lingfei Guo[4]**

[1] Department of Radiology, Beijing Friendship Hospital, Capital Medical University, Beijing, China, [2] Department of Radiology, Weill Cornell Medical College, Cornell University, New York City, NY, United States, [3] Department of Clinical Laboratory, Shandong Provincial Hospital Affiliated to Shandong First Medical University, Jinan, Shandong, China, [4] Department of Radiology, Shandong Provincial Hospital Affiliated to Shandong First Medical University, Jinan, Shandong, China

Purpose: The objective of this study was to determine which factors influence brain iron concentrations in deep gray matter in elderly individuals and how these factors influence regional brain iron concentrations.

Methods: A total of 105 elderly individuals were enrolled in this study. All participants underwent detailed magnetic resonance imaging (MRI) examinations from October 2018 to August 2019. Among them, 44 individuals had undergone a previous MRI examination from July 2010 to August 2011. Quantitative susceptibility mapping (QSM) was utilized as an indirect quantitative marker of brain iron, and the susceptibility values of deep gray matter structures were obtained. Univariate analysis and multiple linear regression analysis were used to investigate 11 possible determinants for cerebral iron deposition.

Results: Our results showed no sex- or hemisphere-related differences in susceptibility values in any of the regions studied. Aging was significantly correlated with increased insusceptibility values in almost all analyzed brain regions (except for the thalamus) when we compared the susceptibility values at the two time points. In a cross-sectional analysis, the relationship between gray matter nucleus susceptibility values and age was conducted using Pearson's linear regression. Aging was significantly correlated with the susceptibility values of the globus pallidus (GP), putamen (Put), and caudate nucleus (CN), with the Put having the strongest correlations. In multiple linear regression models, associations with increased susceptibility values were found in the CN, Put, red nucleus, and dentate nucleus for individuals with a history of type 2 diabetes mellitus (T2DM). However, the patients with hypertension showed significantly reduced susceptibility values in the red nucleus and dentate nucleus. Our data suggested that smokers had increased susceptibility values in the thalamus. No significant associations were found for individuals with a history of hypercholesterolemia and Apolipoprotein E4 carrier status.

OPEN ACCESS

Edited by:
David Baglietto-Vargas, University of Malaga, Spain

Reviewed by:
Mikko T. Huuskonen, University of Southern California, United States
Kristine Freude, University of Copenhagen, Denmark

***Correspondence:**
Lingfei Guo
glfsci@163.com

Received: *29 September 2020*
Accepted: *15 March 2021*
Published: *14 April 2021*

Citation:
Li J, Zhang Q, Che Y, Zhang N and Guo L (2021) Iron Deposition Characteristics of Deep Gray Matter in Elderly Individuals in the Community Revealed by Quantitative Susceptibility Mapping and Multiple Factor Analysis. Front. Aging Neurosci. 13:611891. doi: 10.3389/fnagi.2021.611891

Conclusion: Our data revealed that aging, T2DM, and smoking could increase iron deposition in some deep gray matter structures. However, hypertension had the opposite effects in the red nuclei and dentate nuclei. Brain iron metabolism could be influenced by many factors in different modes. In future studies, we should strictly control for confounding factors.

Keywords: quantitative susceptibility mapping, multiple factor analysis, magnetic resonance imaging, iron deposition, deep gray matter

INTRODUCTION

Iron is the most abundant trace element in the human body. Iron in the nervous system is also involved in many fundamental biological processes, including oxygen transportation, DNA synthesis, catecholamine neurotransmitters, and myelin formation. Iron homeostasis is needed to maintain normal physiological brain function, whereas dysregulation of iron homeostasis can cause neurotoxicity through different mechanisms (Ward et al., 2014). Abnormal increases in iron content have been reported to be associated with many neural diseases, such as Parkinson's disease, Alzheimer's disease (AD), and Huntington's disease (Wu et al., 2012), but restless leg syndrome is characterized by reduced iron concentrations in the substantia nigra (SN) (Rizzo and Plazzi, 2018). In Parkinson's disease, an increase in iron concentration is noted in the SN (Faucheux et al., 2003); however, pantothenate kinase-associated neurodegeneration is characterized by an excess of iron mainly in the globus pallidus (GP), leading to a typical MRI pattern called the eye of the tiger (Kruer et al., 2011). These facts illustrate that brain iron patterns are characteristic of disease or disease stages; therefore, investigating the physiological distribution of iron in the normal brain is very important to better understand the disease-related changes that involve iron deposition.

In addition to aging, many studies have revealed that total iron concentrations increase with age in the SN, putamen (Put), GP, caudate nucleus (CN), and cortex (Xu et al., 2008; Ramos et al., 2014), but few studies have focused specifically on elderly individuals. Age-related accumulation of iron might be an important factor that contributes to neurodegenerative processes. Because many neurodegenerative disorders involve elderly people, we selected elderly individuals in the community as our target population in this study. We expect our results to present some constructive suggestions for future studies to better investigate the complex pathophysiological processes underlying neurological disorders. Previous MRI studies that focused on differences in brain iron levels between sexes reported inconsistent findings. Whereas one study reported lower iron levels in the thalamus (Thal) and red nucleus (RN) in females than in males (Gong et al., 2015), another study did not observe any difference (Xu et al., 2008). The other objective of the present study was to detect the effects of sex on regional brain iron concentrations. Many elderly people have histories of hypertension, diabetes mellitus (DM), or hypercholesterolemia. Cerebral microbleeds (CMBs), white matter hyperintensities (WMHs), and cerebral microinfarcts are also common brain MRI findings of elderly people (Valdés Hernández et al., 2016; van Veluw et al., 2017; Haller et al., 2018). Furthermore, we estimated the influence of these factors on brain iron levels in this study.

The emergence of the quantitative susceptibility mapping (QSM) technique over the past decade (Wang and Liu, 2015) has enabled accurate and reproducible *in vivo* measurements of local brain iron levels under both normal and pathological conditions (Acosta-Cabronero et al., 2016; Wang et al., 2017). Many neurodegenerative disorders with brain iron accumulation are usually associated with excess iron accumulation in deep gray matter (DGM) (Schipper, 2012), and DGM plays a crucial role in regulating movements and in various types of learning (Seger, 2008). In addition, DGM has the highest iron content (Peterson et al., 2019), and susceptibility values calculated from QSM have been reported to have a strong correlation with iron concentration in the human brain, especially in DGM (Hinoda et al., 2015). Accordingly, the objective of this study was to utilize QSM as a quantitative marker of brain iron to detect possible factors influencing the iron levels of the DGM [Thal, CN, Put, GP, SN, RN, and dentate nucleus (DN)] to accurately map iron in elderly individuals in the community, which might help us to better control confounding factors in future research.

MATERIALS AND METHODS

Participants

The volunteers of this study were recruited from the community. The participants signed an informed consent form approved by the Institutional Review Board of Shandong Medical Imaging Research Institute Affiliated to Shandong University (ID: 2018-002). Subjects were excluded if they had a history of neurological disease or neurological ailment, including immune, metabolic, toxic, and infectious diseases or head trauma. If the subjects had other diseases, such as malignant tumors, renal insufficiency, alcoholism, or autoimmune disease, they were excluded. All MR images were evaluated by an experienced neuroradiologist for signs of space-occupying lesions and cerebrovascular diseases. Subjects with evidence of infarct (except for lacunar infarcts) or cerebral hemorrhages (except for CMBs) were excluded from further analysis.

The final sample consisted of 105 participants (57 females and 48 males) with a mean age of 65.26 $\pm$ 6.33 years (range 50–80) and a mean education level of 11.39 $\pm$ 2.57 years (range 6–16).

The history of diabetes, hypertension, hypercholesterolemia, and smoking status was taken from the participants' self-reported medical history. Individuals with a history of type 2 DM (T2DM) or hypertension were referred to as diagnosed with T2DM or hypertensive individuals who were taking hypoglycemic drugs or antihypertensive drugs when an MRI scan was conducted. In our study, 59 (56.19%) participants had hypertension, 23 (21.90%) participants had T2DM, 32 (30.48%) participants had hyperlipidemia, and 26 (24.76%) participants smoked (details are shown in **Table 1**).

Among these 105 participants, 44 individuals had undergone another MRI scan in our hospital between July 2010 and December 2011, thereby providing us with an opportunity to study the age-related accumulation of brain iron using a longitudinal approach (details in **Table 1**). During the research, we fully considered the influence of gadolinium intake on the susceptibility values in the brain. We carefully reviewed the clinical and imaging data of 44 participants, and we followed up by telephone patients who underwent two MRI examinations. None of these patients had an enhanced MRI scan with gadolinium contrast agent.

TABLE 1 | Description of demographic characteristics and risk factors [mean ± SD or n (%)].

Variable		Participants (had one MR scan)	Participants (had two MR scans)
No. of participants		105	44
Age (years)		65.25 ± 6.33	59.19 ± 5.31
Education (years)		11.38 ± 2.57	11.91 ± 2.64
Gender	M	48 (45.71)	22 (50.00)
	F	57 (54.29)	22 (50.00)
Hypertension	No	46 (43.81)	12 (27.27)
	Yes	59 (56.19)	32 (72.73)
Diabetes	No	82 (78.10)	31 (70.45)
	Yes	23 (21.90)	13 (29.55)
Hyperlipidemia	No	73 (69.52)	27 (61.36)
	Yes	32 (30.48)	17 (38.64)
Smoking	No	79 (75.24)	34 (77.27)
	Yes	26 (24.76)	10 (22.73)
WMHs	No	31 (29.52)	28 (63.64)
	Yes	74 (70.48)	16 (36.36)
Lacunes	No	89 (84.76)	43 (97.73)
	Yes	16 (15.24)	1 (2.27)
CMBs	No	83 (79.05)	30 (68.18)
	Yes	22 (20.95)	14 (31.82)
E4 gene	No	88 (86.27)	38 (86.36)
	Yes	14 (13.73)	6 (13.64)

Participants who had one MR examination were referred to as individuals who had an MRI brain scan from October 2018 to August 2019. Participants who had two MR examinations were referred to as individuals who had MRI scans at two time points: the first was from July 2010 to December 2011, the second was from October 2018 to August 2019, and the time interval was approximately 8 years. The Apolipoprotein E4 (APOE4) gene carrier status of 102 patients was determined by using blood samples obtained from October 2018 to August 2019. Individuals with E4 alleles were coded as Yes, and individuals without E4 alleles were coded as No. CMBs, cerebral microbleeds; WMHs, white matter hyperintensities.

MRI Acquisition

From October 2018 to August 2019, all subjects were imaged on a MAGNETOM Skyra 3.0 T MR scanner (Siemens Healthcare, Erlangen, Germany) using a product 32-channel head coil for signal reception. The brain scanning protocol consisted of a 3D T1-weighted (T1W) magnetization-prepared rapid gradient-echo (MPRAGE) sequence for anatomic structures [repetition time (TR) = 2,300 ms, echo time (TE) = 2.3 ms, inversion time (TI) = 900 ms, flip angle = 9°, and isotropic voxel size = 1 mm^3] and a 3D multiecho gradient-echo (ME-GRE) sequence for QSM (TR = 50 ms, first TE = 6.8 ms, TE interval = 4.1 ms, number of echoes = 10, flip angle = 15°, and voxel size = 1 mm × 1 mm × 2 mm). In addition, T2-weighted (T2W) turbo spin-echo images (TR = 3,700 ms, TE = 109 ms, TI = 900 ms, flip angle = 15°, and slice thickness = 5 mm), T2W fluid-attenuated inversion recovery (FLAIR) images (TR = 8,000 ms, TE = 81 ms, TI = 2,370 ms, flip angle = 15°, and slice thickness = 5 mm), diffusion-weighted images (DWIs) (TR = 3,700 ms, TE = 65 ms, flip angle = 18°, and slice thickness = 5 mm), and susceptibility-weighted images (SWIs) (TR = 27 ms, TE = 20 ms, flip angle = 15°, and slice thickness = 5 mm) were acquired to detect brain abnormalities.

From July 2010 to December 2011, 44 participants were evaluated on a Signa 3.0T MRI scanner (Signa, HDx, General Electric Healthcare, Milwaukee, WI, United States) with an eight-channel array coil. The scanning sequences included conventional MRI sequences (T2W imaging, T2-FLAIR, and DWI), 3D T1W imaging for anatomic structure, and enhanced 3D multiecho GE T2*-weighted angiography (ESWAN) sequences for QSM. 3D T1W images were acquired using a T1W volumetric fast spoiled gradient recalled-echo (FSPGR) sequence with the following parameters: TR = 7.3 ms, TE = 2.7 ms, TI = 850 ms, flip angle = 13°, and isotropic voxel size = 1 mm^3; ESWAN sequences were acquired using a 3D-enhanced T2*-weighted contrast flow-compensated (i.e., the gradient moment was null in all three orthogonal directions) ME-GRE (12 different TEs) sequence with the following parameters: TR = 51.6 ms, first TE = 4.4 ms, TE = 4.4–38.2 ms, TE interval = 4.8 ms, number of echoes = 8, flip angle = 20°, and voxel size = 1 mm × 1 mm × 2 mm.

Quantitative Susceptibility Mapping Preprocessing and Quantitative Analysis

Brain QSM maps were computed from ME-GRE complex image data using morphology-enabled dipole inversion with an automatic uniform cerebrospinal fluid (CSF) zero reference algorithm (MEDI + 0) (Liu et al., 2018). Briefly, a non-linear fitting of the multiecho data was performed to estimate the total field, followed by spatial field unwrapping and background field removal using the projection onto dipole fields (PDF) algorithm to compute the local field (Liu et al., 2011), which was then inverted to obtain the final susceptibility map. Structural priors (edges) within the lateral ventricles derived from the magnitude image and with a regularization term enforcing a uniform susceptibility distribution of the CSF were used in the numerical inversion to improve QSM quality and to provide

CSF as an automatic susceptibility reference. The CSF mask was determined by thresholding the R2* map computed from the ME-GRE magnitude data and imposing voxel connectivity (Liu et al., 2018). The conventional images (T1W, T2W, and FLAIR) were processed with an automated FMRIB Software Library (FSL) pipeline, which consisted of brain data extraction using the Brain Extraction Tool (BET) algorithm (Smith, 2002), bias field correction using FMRIB's Automated Segmentation Tool (FAST) (Zhang et al., 2001), and linear coregistration to the ME-GRE magnitude image (which is in the same space as QSM) using FMRIB's Linear Registration Tool (FLIRT) with six degrees of freedom (Jenkinson et al., 2002). For the region of interest (ROI) analysis, FMRIB's Integrated Registration Segmentation Tool (FIRST) (Patenaude et al., 2011) was used to segment selected subcortical GM structures (Thal, CN, Put, GP, RN, SN, and DN) on T1W images, and the resulting segmentation masks were linearly coregistered to QSM. These masks were then visually inspected and manually edited by an experienced neuroradiologist if necessary (e.g., to remove veins or CMBs with high positive susceptibility values) on QSM images using ITK-SNAP v3.8 software[1]. The mean susceptibility value within each ROI was recorded (**Figure 1**).

Conventional MRI Assessment

According to the Standards for Reporting Vascular Changes on Neuroimaging (STRIVE) criteria (Wardlaw et al., 2013a), WMHs were signal abnormalities of variable size, defined as white matter hyperintense lesions on FLAIR images. Lacunes were round or ovoid, subcortical small lesions (3–15 mm in diameter) that were hypointense on T1W images and hyperintense on T2W images and had a perilesional halo on FLAIR images. CMBs were defined as small signal voids (≤10 mm in diameter) with associated blooming on T2*-weighted images. The severity of CMBs, lacunes, and WMHs was assessed using a simple scoring method (Amin Al Olama et al., 2020). In a binary fashion (i.e., presence or absence), individuals with lacunar infarcts, WMHs, or CMBs were coded as 1; and individuals without these MRI findings were coded as 0.

APOE Genotyping

Apolipoprotein E (APOE) genotyping was conducted using standard real-time fluorescence polymerase chain reaction (PCR) methods (Calero et al., 2009). APOE4 carrier status was determined: individuals with E4 alleles were coded as 1, and individuals without E4 alleles were coded as 0.

Statistical Analysis

Statistical analysis was performed using Statistical Package for the Social Sciences software (Version 21.0 for Windows; SPSS, Chicago, IL, United States). The measurement data are presented as the mean ± standard deviation. The count data were represented in the form of n (%). The effect of different hemispheric locations was compared using a paired

[1]www.itksnap.org

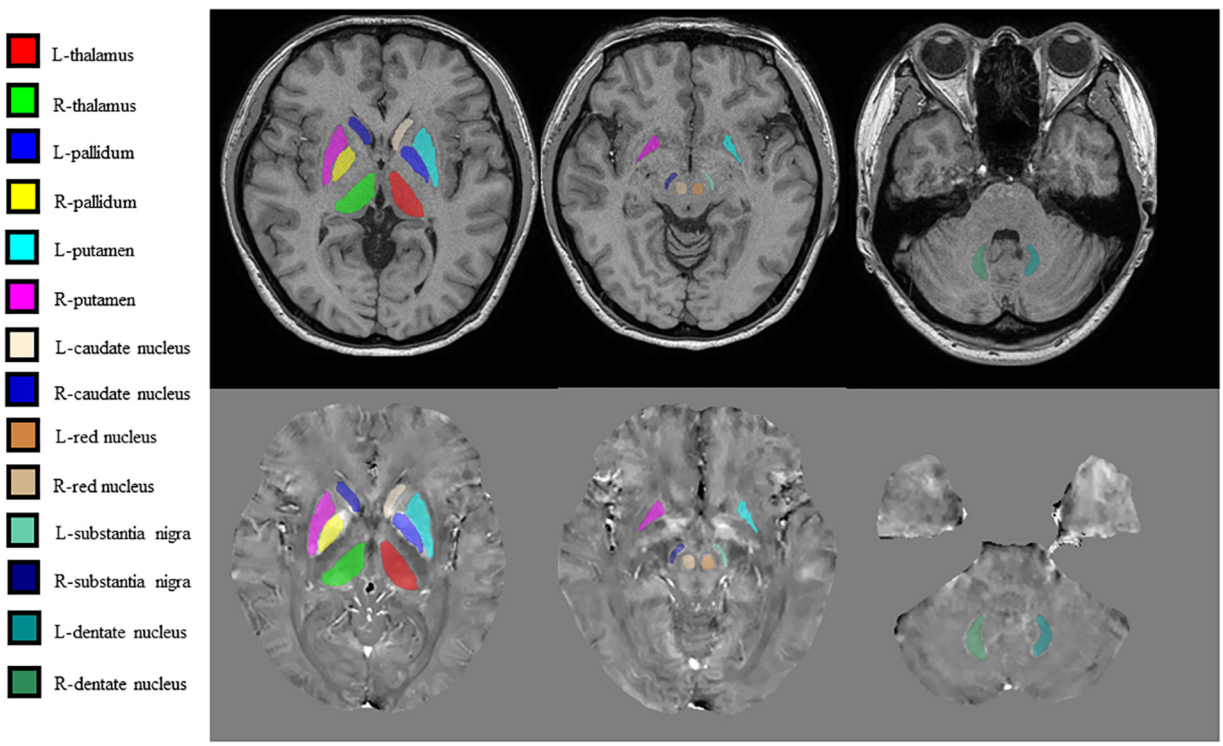

FIGURE 1 | Regions of interest (ROIs) were traced directly on the quantitative susceptibility mapping (QSM) image and T1-weighted (T1W) images to remove veins with high positive susceptibility values on QSM.

TABLE 2 | Comparison of the susceptibility values of the gray matter nuclei between the left and right hemispheres (mean ± SD).

	Mean value	Left	Right	*t*	*p*
Thalamus	0.04 ± 14.37	0.40 ± 14.53	0.33 ± 15.96	0.724	0.470
Globus pallidus	185.82 ± 47.47	184.08 ± 48.25	187.57 ± 49.78	−1.461	0.147
Putamen	98.79 ± 31.49	97.45 ± 33.09	100.12 ± 33.05	−1.358	0.178
Caudate nucleus	83.24 ± 22.94	83.89 ± 23.78	82.59 ± 24.13	0.967	0.336
Red nucleus	149.58 ± 42.62	148.19 ± 44.53	150.98 ± 44.36	−1.13	0.261
Substantia nigra	158.96 ± 39.90	159.13 ± 43.10	158.78 ± 40.06	0.152	0.879
Dentate nucleus	111.16 ± 40.86	111.88 ± 42.38	110.42 ± 41.12	0.871	0.386

t-test. To test the independent association between variables and susceptibility values in DGM, we performed multiple regression analyses. Considering that our sample size is not large enough, we made variable selection before doing the multiple linear regression analysis. First, we performed a univariate analysis using an independent sample *t*-test and Pearson correlation analysis. Only variables for which a univariate association with susceptibility values at a p-value < 0.1 was seen were entered into the multiple regression models as independent variables (Pirpamer et al., 2016). Second, for every ROI, the multiple linear relationships between the independent parameters and the susceptibility values were estimated with a stepwise regression method, and the best multiple linear regression models were selected.

After univariate analysis, for the Thal, variables of smoking status, history of T2DM and hypertension, APOE carrier status, and whether having CMBs in the brain were introduced to the following multiple linear regression analysis. For the Put, variables of aging, history of T2DM, and whether having CMBs in the brain were introduced to the following multivariate analysis. For the CN, the variables are aging and history of T2DM; for the RN, the variables are aging, history of T2DM and hypertension, whether having lacunes in the brain; for the SN, the variables are aging and history of hypertension; for the DN, the variables are aging, gender, history of T2DM, and hypertension.

Among these 105 participants, 44 patients received two MRI examinations at two different time points. Hence, the age-related accumulation of brain iron could be analyzed longitudinally with paired *t*-tests. Because multiple hypotheses were tested, we used the Bonferroni method for correction to avoid type I errors.

RESULTS

For susceptibility values, no significant effect of hemispheric location in the seven ROIs was found. Therefore, in the

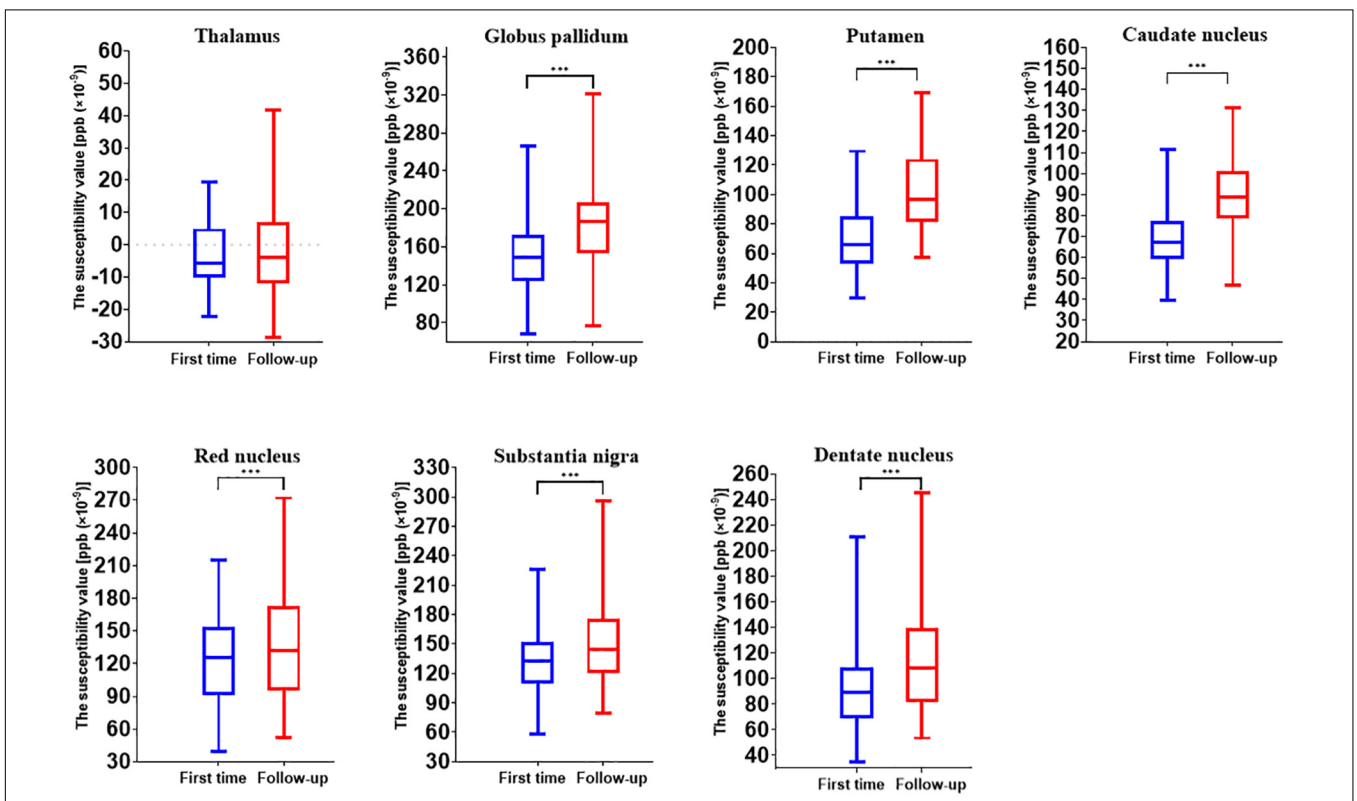

FIGURE 2 | Comparison results of susceptibility values of gray matter nuclei between two time points (first time, July 2010 to December 2011; follow-up, October 2018 to August 2019). ***$p < 0.001$.

following analysis, we used the mean values of the left and right hemispheres (**Table 2**).

The longitudinal analysis of 44 individuals who had two MRI scans showed the age-related accumulation of brain iron in the GP (t = 10.763, $p < 0.001$), Put (t = 20.657, $p < 0.001$), CN (t = 10.308, $p < 0.001$), RN (t = 3.497, p = 0.001), SN (t = 4.976, $p < 0.001$), and DN (t = 8.576, $p < 0.001$) but not in the Thal (t = 0.659, p = 0.513) (**Figure 2**).

In the univariate analysis for each region, the factors with p values less than 0.1 are highlighted in italics (**Table 3**). Pearson's correlation analysis showed increased rates of susceptibility values with aging varying among these regions. Put exhibited the highest rate of increase in susceptibility with aging (**Table 4**). Scatter plots illustrated a linear age dependency of iron concentration as measured by mean QSM susceptibility values (**Figure 3**).

Because the longitudinal analysis showed that age played a key role in susceptibility values in the DGM (except for the Thal), age was introduced into the subsequent multiple linear regression analysis. After the multiple linear regression analysis, we found that the influencing factor for Thal was smoking status (t = 2.166, p = 0.033). Regarding Put, CN, RN, and DN, the influencing factors included a history of T2DM (t = -3.094, p = 0.003; t = 2.682, p = 0.009; t = 2.069, p = 0.041; and t = 2.682, p = 0.009, respectively) and age (t = 4.257, p = 0.000; t = 2.897, p = 0.005; t = 3.164, p = 0.001; and t = 3.126, p = 0.002, respectively). In these regions, the results showed that T2DM patients had increased iron deposition. Age-related increases in susceptibility values could also be detected, and the rates of increase with aging varied among these regions. For RN and DN, a history of hypertension also influenced the susceptibility values (t = −3.236, p = 0.002; t = −2.818, p = 0.006, respectively), and patients with hypertension showed significantly lower iron content in these regions. Details of the multiple linear regression models are listed in **Table 5**.

We analyzed interaction effects by introducing three new factors: age × history of hypertension, age × history of DM, and history of hypertension × history of DM. In the Put, CN, and RN, no interaction effects were found. However, an interaction effect was found in the DN. Aging was associated with susceptibility values only in the participants who had no hypertension or DM (data not shown).

DISCUSSION

In this study, using the QSM method, we investigated some factors and their effects on brain iron content. These factors included hemispheric location, sex, aging, smoking status, APOE carrier status, history of T2DM, hypertension, hyperlipidemia, and some important MRI features (CMBs, WMHs, and cerebral microinfarcts) in elderly people in the community. We expect that this knowledge will help us to gain more insight into the potential abnormalities of magnetic susceptibility that arise from various neurological diseases and neural degeneration. Similar to many other studies, our data indicated significant effects of age on susceptibility values in the DGM. In the cross-sectional analysis,

TABLE 3 | Determinants of susceptibility values in gray matter structures: results of univariate analysis.

		Thalamus			Globus pallidus			Putamen			Caudate nucleus			Red nucleus			Substantia nigra			Dentate nucleus		
		Susceptibility value	Statistical value		Susceptibility value	Statistical value		Susceptibility value	Statistical value		Susceptibility value	Statistical value		Susceptibility value	Statistical value		Susceptibility value	Statistical value		Susceptibility value	Statistical value	
			t	p		t	p		t	p		t	p		t	p		t	p		t	p
CMBs	No (83)	-1.52 ± 13.60	-2.190	*0.031*	186.96 ± 48.35	0.476	0.635	95.53 ± 29.41	-2.094	*0.039*	82.33 ± 22.03	-0.786	0.434	148.94 ± 40.14	-0.301	0.794	159.58 ± 37.54	0.309	0.758	111.47 ± 42.60	0.154	0.878
	Yes (22)	5.89 ± 15.97			181.52 ± 44.77			111.09 ± 36.54			86.67 ± 26.37			152.03 ± 51.92			156.61 ± 48.73			109.95 ± 34.34		
WMH	0 (31)	0.20 ± 15.27	0.076	0.940	181.69 ± 43.50	-0.575	0.566	93.74 ± 30.00	-1.064	0.290	83.47 ± 25.15	0.068	0.946	152.68 ± 40.24	0.480	0.632	162.26 ± 38.45	0.548	0.585	109.13 ± 44.13	-0.327	0.744
	1 (74)	-0.03 ± 14.08			187.55 ± 49.21			100.90 ± 32.06			83.14 ± 22.12			148.29 ± 43.78			157.57 ± 40.66			112.00 ± 39.70		
Lacunes	0 (89)	-0.49 ± 14.84	-0.893	0.374	187.52 ± 48.55	0.865	0.389	97.49 ± 31.83	-1.000	0.320	83.25 ± 23.08	0.010	0.992	153.17 ± 41.23	2.065	*0.041*	160.87 ± 38.29	1.163	0.248	112.91 ± 42.36	1.042	0.300
	1 (16)	2.99 ± 11.36			176.36 ± 41.02			106.04 ± 29.43			83.18 ± 22.88			129.64 ± 46.03			148.29 ± 47.88			101.36 ± 30.44		
Hypertension	No (46)	2.13 ± 15.85	1.325	0.188	190.74 ± 46.77	0.936	0.351	97.61 ± 30.60	-0.338	0.736	83.78 ± 24.38	0.213	0.831	161.25 ± 36.39	2.541	*0.013*	165.95 ± 38.43	1.599	0.113	118.90 ± 44.04	1.732	*0.086*
	Yes (59)	-1.60 ± 13.00			182.00 ± 48.05			99.71 ± 32.41			82.81 ± 21.95			140.49 ± 45.14			153.50 ± 40.49			105.11 ± 37.47		
Diabetes	No (82)	-1.33 ± 14.26	-1.858	*0.066*	186.54 ± 48.46	0.292	0.711	95.54 ± 33.36	-2.024	*0.046*	80.21 ± 23.18	-2.623	*0.010*	145.53 ± 43.31	-1.860	*0.066*	156.87 ± 38.16	-1.014	0.313	106.12 ± 41.18	-2.440	*0.016*
	Yes (23)	4.90 ± 14.00			183.20 ± 44.64			110.36 ± 23.92			94.02 ± 18.77			164.02 ± 37.45			166.41 ± 45.93			129.10 ± 34.91		
Hyperlipidemia	No (73)	-0.15 ± 15.29	-0.199	0.842	190.50 ± 51.98	1.534	0.128	97.64 ± 33.19	-0.565	0.574	82.44 ± 23.92	-0.533	0.595	152.52 ± 42.57	1.029	0.306	161.42 ± 37.99	0.956	0.341	112.35 ± 44.07	0.451	0.653
	Yes (32)	0.46 ± 12.23			175.16 ± 33.38			101.42 ± 27.55			85.04 ± 20.77			143.12 ± 42.69			153.33 ± 44.07			108.42 ± 32.85		
E4 gene	No (88)	-0.94 ± 14.05	-1.792	*0.076*	185.64 ± 48.92	-0.229	0.819	99.30 ± 29.95	-0.274	0.785	83.53 ± 21.37	-0.859	0.392	150.21 ± 41.33	0.208	0.835	159.67 ± 40.66	0.466	0.642	115.12 ± 41.81	1.619	0.109
	Yes (14)	6.48 ± 16.46			188.82 ± 35.75			101.75 ± 37.98			89.00 ± 26.77			147.62 ± 53.22			154.23 ± 40.31			96.36 ± 27.89		
Smoke	No (79)	-1.55 ± 12.81	-2.004	*0.048*	184.30 ± 43.97	-0.572	0.568	95.98 ± 28.33	-1.606	0.111	82.50 ± 20.95	-0.571	0.569	148.68 ± 41.95	-0.379	0.706	157.27 ± 36.68	-0.753	0.453	112.81 ± 43.35	0.725	0.470
	Yes (26)	4.86 ± 17.75			190.46 ± 57.54			107.33 ± 39.00			85.47 ± 28.50			152.34 ± 45.34			164.08 ± 48.88			106.10 ± 32.35		
Gender	M (48)	1.49 ± 16.18	0.949	0.345	192.50 ± 52.27	-0.657	0.513	97.19 ± 35.03	-0.476	0.635	81.67 ± 24.39	-0.641	0.523	146.74 ± 40.93	-0.626	0.533	161.60 ± 44.49	0.622	0.533	103.47 ± 41.56	-1.786	*0.077*
	F (57)	-1.19 ± 12.66			188.62 ± 43.29			100.14 ± 28.43			84.56 ± 21.77			151.98 ± 44.21			156.73 ± 35.84			117.62 ± 39.47		

Significant p-values < 0.10 are highlighted in italics.
CMBs, cerebral microbleeds; WMH, white matter hyperintensity.

TABLE 4 | The Pearson linear relationship between susceptibility values of DGM and age.

	Thalamus	Globus pallidus	Putamen	Caudate nucleus	Red nucleus	Substantia nigra	Dentate nucleus
r	−0.060	0.306	0.383	0.270	0.112	0.113	0.221
p	0.570	0.002	0.000	0.005	0.257	0.252	0.024

The Bonferroni method was used for multiple hypothesis correction to avoid type I error, and the new p-value level was adjusted to 0.007.
DGM, deep gray matter.

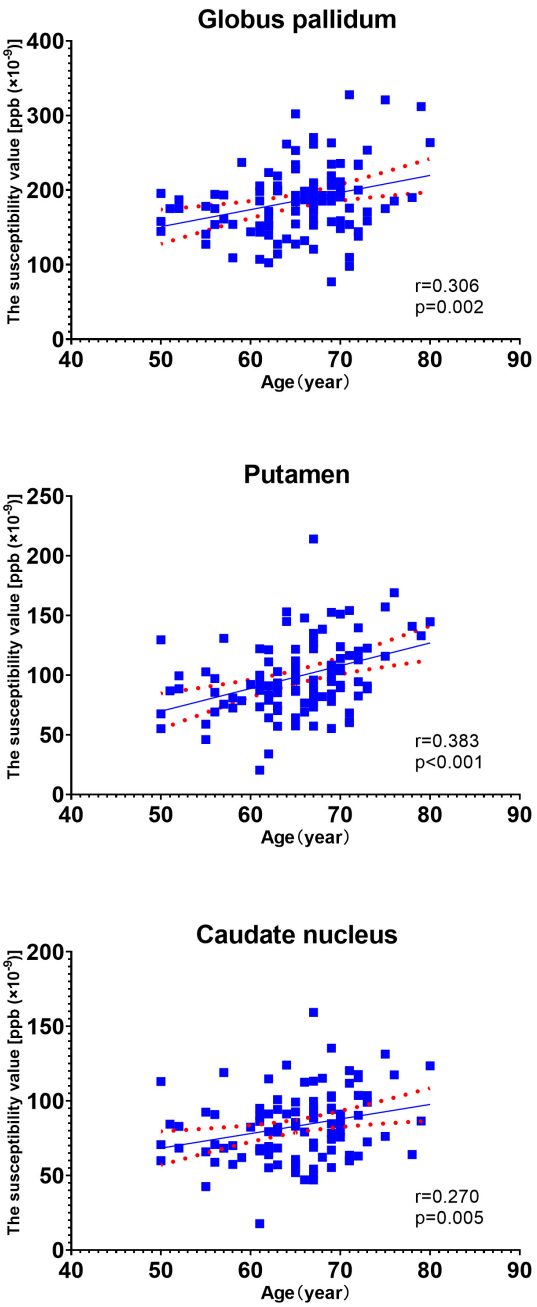

FIGURE 3 | Scatter plots illustrating a linear age dependency of iron concentration as measured by mean quantitative susceptibility mapping (QSM) susceptibility values. The putamen exhibited the highest rate of increase in susceptibility values with aging.

age-related iron deposition was found in the GN, Put, CN, and DN (Xu et al., 2008; Li et al., 2014; Gong et al., 2015). Based on the knowledge that QSM is reproducible across scanner makers, models, field strengths, and sites and could be used in clinical investigations both longitudinally and across centers (Hinoda et al., 2015; Wang et al., 2017; Wicaksono et al., 2020), the MR measures of QSM were accurate and consistent across repeated measurements and between platforms (Hobson et al., 2020). We performed a longitudinal analysis of age-related iron deposition despite different scanners in the two examinations. The results showed significant age-related increases in GN, Put, CN, RN, SN, and DN but not in Thal (**Figures 4**, **5**). Notably, the rate of increase varies among these regions, reflecting a heterogeneous accumulation of iron in different brain tissues. The highest rate of increase was found in the Put. Our results showed no support for a linear age-related change in iron content in the Thal, consistent with some previous studies (Bilgic et al., 2012; Gong et al., 2015; Persson et al., 2015). These findings illustrated that when we intend to study the iron deposition of neurological diseases involving the DGM, especially the Put; age, as a confounding factor, should be controlled more strictly.

In this study, we found that brain iron was abnormally deposited in patients with T2DM in several DGM, including the Put, CN, RN, and DN (**Figure 6**). A previous study investigated the deposition of iron in the brain in T2DM patients with mild cognitive impairment using QSM and showed similar results. They found that susceptibility values in the right CN and SN and the left Put increased and that the susceptibility of these regions was closely correlated with cognitive impairment, suggesting that iron deposition may play an important role in the process of T2DM cognitive impairment (Yang et al., 2018). The precise mechanisms underlying the higher iron concentration in T2DM are not understood, but hyperglycemia could lead to neuronal damage. Neurons have a continuous high glucose demand, and unlike muscle cells, they cannot accommodate episodic glucose uptake under the influence of insulin. Neuronal glucose uptake depends on the extracellular concentration of glucose, and cellular damage can ensue after persistent episodes of hyperglycemia (Tomlinson and Gardiner, 2008). Iron accumulation could occur as an epiphenomenon of demyelination, axonal damage, and/or neurodegeneration (Raz et al., 2015). Insulin resistance leads to high permeability of the blood–brain barrier (BBB) and triggers cognitive decline in a diabetic insulin resistance mouse model and in an AD model (Takechi et al., 2017). Increased permeability with leakage of material into the vessel wall and perivascular tissue could cause inflammation (Wardlaw et al., 2013b), and the inflammatory status of the brain could influence brain iron metabolism and

TABLE 5 | Determinants of susceptibility values in gray matter structures: results of multiple linear stepwise regression analysis.

	Factors	*r*	Adjusted *r*	*T*	*p*	*R* of model	*F* of model	*P* of model
Thalamus	Smoking	7.120	0.212	2.166	0.033	0.212	4.692	0.033
Putamen	Age	1.895	0.381	4.257	0.000	0.428	11.447	0.000
	Diabetes	14.494	0.191	2.137	0.035			
Caudate nucleus	Age	0.967	0.267	2.897	0.005	0.366	7.882	0.001
	Diabetes	13.643	0.247	2.682	0.009			
Red nucleus	Age	1.533	0.310	3.164	0.001	0.392	5.170	0.000
	Diabetes	19.459	0.185	2.069	0.041			
	Hypertension	−27.122	−0.317	−3.236	0.002			
Dentate nucleus	Age	1.917	0.297	3.126	0.002	0.409	6.657	0.000
	Diabetes	23.972	0.244	2.682	0.009			
	Hypertension	−21.968	−0.268	−2.818	0.006			

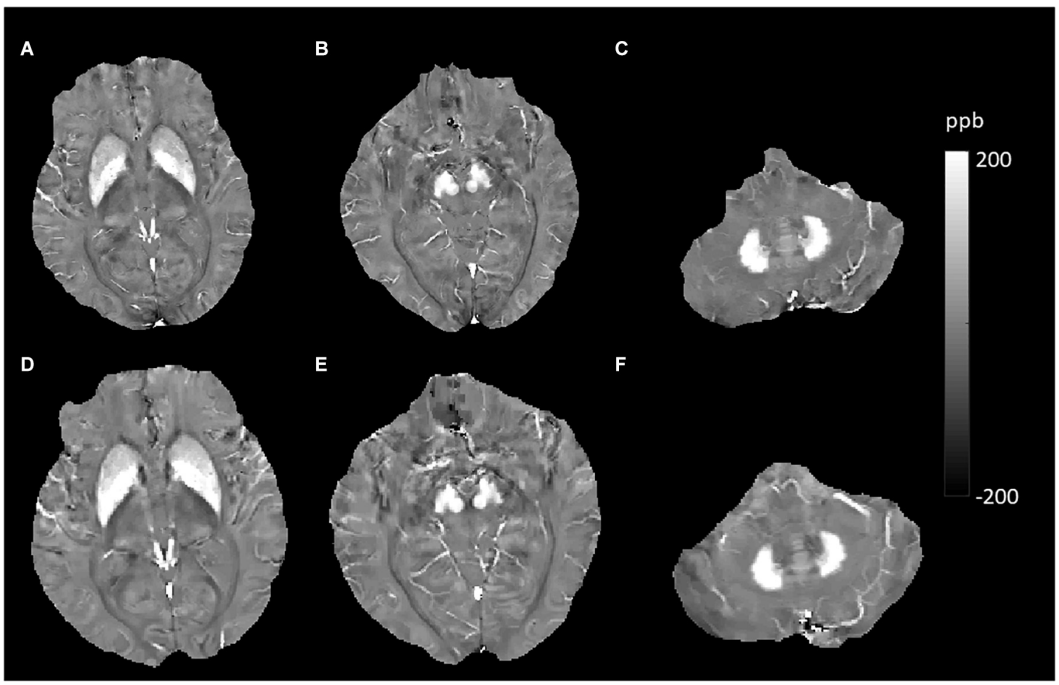

FIGURE 4 | Evolution of susceptibility values with age in the caudate nucleus, putamen, globus pallidus, red nucleus, substantia nigra, and dentate nucleus. These images were from an 80-year-old male non-smoker without hypertension and type 2 diabetes mellitus (T2DM). The upper row **(A–C)** shows quantitative susceptibility mapping (QSM) images acquired in 2010, and the bottom row **(D–F)** shows QSM images acquired in 2019. Susceptibility values of the gray matter nuclei increased significantly over time.

lead to iron deposition (McCarthy et al., 2018). Therefore, we speculate that neuronal damage caused by hyperglycemia and permeability of the BBB caused by insulin resistance may be the reasons for iron accumulation in T2DM, but this inference needs to be substantiated by more studies.

In addition to brain iron dysmetabolism in patients with hypertension, we initially speculated that the brain iron content would be increased in hypertensive patients. Conversely, we observed decreased susceptibility in the RN and DN. Many studies have suggested that increased systolic blood pressure (SBP) is associated with injury to the white matter microstructure and gray matter atrophy (Maillard et al., 2012; Fennema-Notestine et al., 2016; Carnevale et al., 2018). Few studies have examined the effect of hypertension on regional brain iron deposition. A study reported that hypertensive participants had significantly greater iron content in the hippocampus, CN, Put, entorhinal cortex, superior frontal gyrus, and primary visual cortex (Rodrigue et al., 2011). One study of cognitively

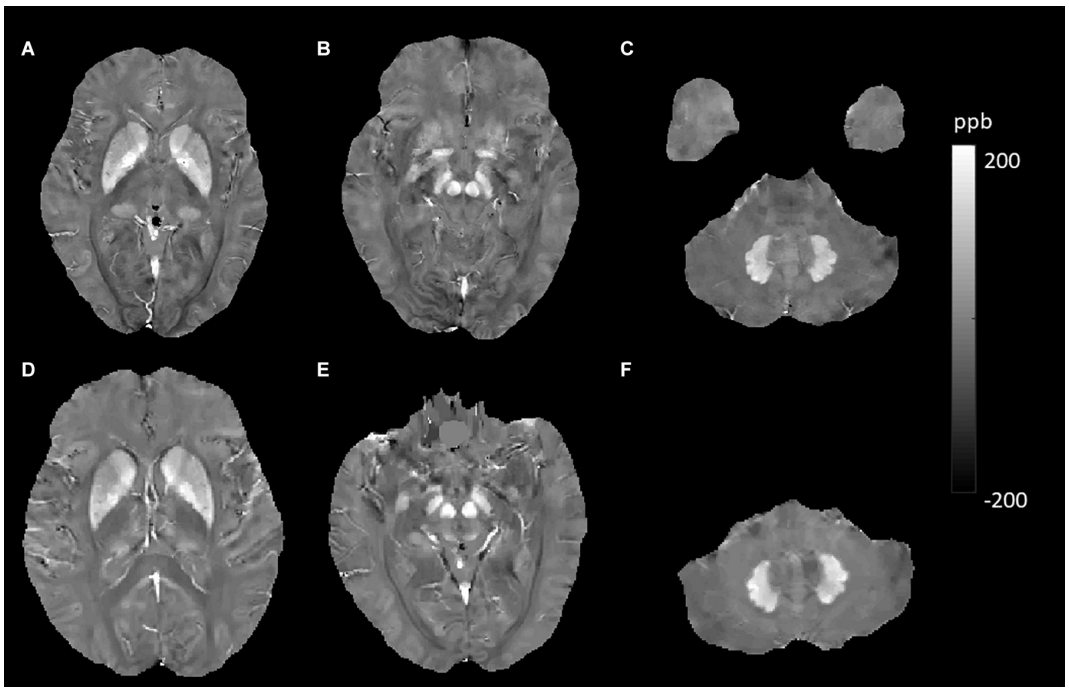

FIGURE 5 | Evolution of susceptibility values with age in the caudate nucleus, putamen, globus pallidus, red nucleus, substantia nigra, and dentate nucleus. These images were from a 64-year-old female non-smoker without hypertension and type 2 diabetes mellitus (T2DM). The upper row **(A–C)** shows quantitative susceptibility mapping (QSM) images acquired in 2011, and the bottom row **(D–F)** shows QSM images acquired in 2019. Susceptibility values of the gray matter nuclei increased significantly over time.

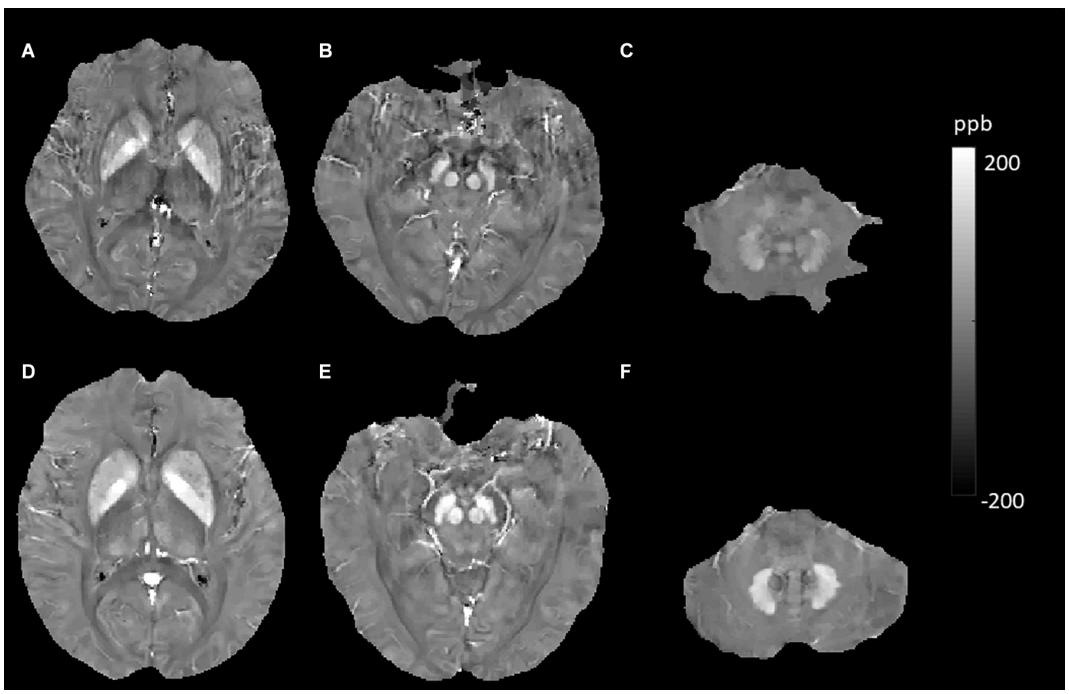

FIGURE 6 | Evolution of susceptibility values with type 2 diabetes mellitus (T2DM) effect in the putamen, caudate nucleus, red nucleus, and dentate nucleus. The upper row **(A–C)** shows susceptibility images of a 55-year-old male non-smoker without hypertension and T2DM (first). The bottom row **(D–F)** shows quantitative susceptibility mapping (QSM) images of a 52-year-old male non-smoker with T2DM but without hypertension (second). Susceptibility values of the putamen, caudate nucleus, red nucleus, and dentate nucleus were higher in the second participant than in the first participant.

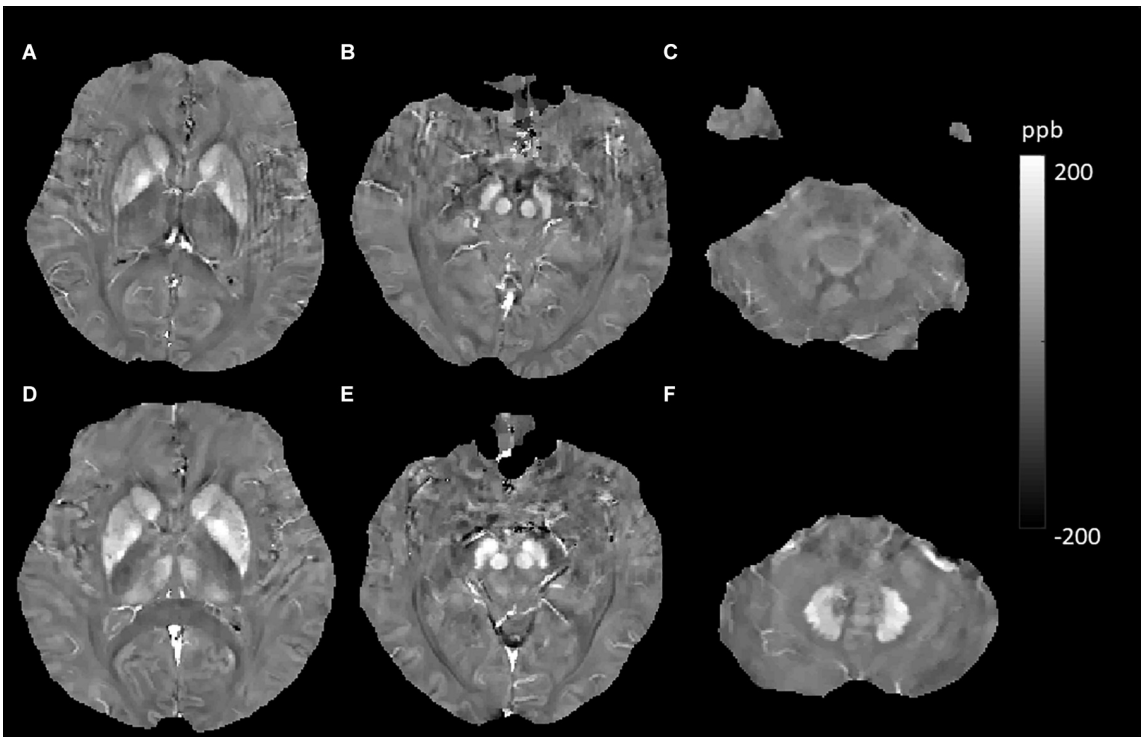

FIGURE 7 | Evolution of susceptibility values with smoking effects in the thalamus. The upper row **(A–C)** shows susceptibility images of a 56-year-old male non-smoker without hypertension and type 2 diabetes mellitus (T2DM) (first). The bottom row **(D–F)** shows quantitative susceptibility mapping (QSM) images of a 55-year-old male smoker without hypertension and T2DM (second). The susceptibility value of the thalamus was higher in the second participant than in the first participant.

impaired patients showed that DM-positive patients had lower susceptibility values, indicative of lower brain iron content, than DM-negative patients in the hippocampus and pulvinar of the Thal (Park et al., 2018); however, in that study, hypertension was more frequently found in DM-positive patients (69.6% vs. 39.1%). It was unclear whether hypertension might be the cause of the lower brain iron content that caused the mixed effects of hypertension and DM to lead to the different results. These heterogeneous results suggested that hypertension or other neurological diseases may cause complicated iron redistribution, and the white matter, cortex, and DGM may show different or completely opposite changes. This hypothesis has been verified by a study that found decreased iron levels in the temporal cortex in postmortem human brains with Parkinson's disease (Yu et al., 2013).

Our data represented that smokers had increased brain iron levels in the Thal (**Figure 7**). Active and passive tobacco smoking (TS) has been associated with vascular endothelial dysfunction in a causative and dose-dependent manner primarily related to the release of reactive oxygen species (ROS), and ROS can also induce cerebral inflammation (Kaisar et al., 2018). Brain inflammation and BBB impairment could cause iron accumulation, which might lead to extraordinarily increased susceptibility values in Thal smokers. A study reporting brain iron accumulation in unexplained fetal and infant death victims with mothers who were smokers also supported our results (Lavezzi et al., 2011). In the Thal, we found that individuals who carried APOE4 had higher susceptibility values (6.48 vs. -0.94). This suggested that the APOE4 gene might aggravate brain iron deposits. Previous studies suggest that APOE4 is a major genetic risk factor for AD and poor neurological outcomes after traumatic brain injury and hemorrhage (Bell et al., 2012). APOE4 could lead to accelerated BBB breakdown and thereby cause neuronal and synaptic dysfunction (Montagne et al., 2020). These findings indicate that brain iron overload in APOE4 carriers comes from destroyed cerebrovascular integrity. However, the p-value was 0.076 (close to 0.05) in our study. This might be because the sample of APOE4 carriers was not large enough, as only 14 subjects carried the APOE4 gene in our participants. This inference requires a larger sample size to be confirmed.

We found a slightly lower susceptibility value of the Thal than other studies, and some individuals even had negative values. We think that it may be different from the research population and related to the different ROI tracking methods. Low susceptibility in DGM was also reported in two previous QSM analyses (Kim et al., 2017; Uchida et al., 2019). These results may suffer from systematic errors in QSM reconstruction or white noise. Furthermore, all QSM images were generated using the MEDI + 0 method, which uses the value in CSF as a zero reference; this could partly eliminate the effect of systematic error and background white noise.

Previous MRI studies that focused on differences in brain iron levels between sexes and hemispheric locations reported different results (Xu et al., 2008; Gong et al., 2015; Persson et al., 2015; Chai et al., 2019; Peterson et al., 2019). However, our data showed no sex- or hemisphere-related differences in iron levels in any of the regions studied. These heterogeneous results might be caused by the differences in the characteristics of the populations studied. With more data or by using a meta-analysis (reasonably merging data from different studies), we might elucidate the sex- and hemisphere-related effects more powerful and effectively. We did not find that CMBs, WMHs, or cerebral microinfarcts influenced the brain iron levels in the studied regions; we speculated that these common brain MR findings in elderly people were caused by hypertension, T2DM, aging, or other factors related to common vascular risk factors; thus, they did not directly influence brain iron levels.

Our present study has several limitations. First, this is mainly cross-sectional research, and the sample size of the longitudinal study was relatively small. In the future, we will follow up with more individuals and provide more powerful evidence demonstrating which factors influence iron accumulation. Second, we measured iron content in brain regions that have both calcification and iron accumulation (such as the GP), which may have affected the accuracy of the iron content measurement. Third, we did not investigate white matter. Because the brain injury caused by hypertension was closely related to the white matter microstructure, iron metabolism of white matter should be evaluated in more detail in the future. Fourth, other influencing factors, such as body mass index (BMI), serum iron concentrations, and the usage of hypoglycemic drugs and antihypertensive drugs, may also induce changes in regional susceptibility values and should be investigated in the future.

CONCLUSION

Our data confirmed the significant effects of age on susceptibility values in DGM. The highest rate of iron deposition with aging was observed in the Put. T2DM and hypertension had the opposite effects on iron metabolism in the DGM. Our data confirmed that smokers had increased brain iron levels in the Thal. These results showed that iron metabolism is complicated and that different diseases have different patterns. These results also indicate that in future studies, we should not only pay attention to conventional factors, such as age and sex, but also consider other confounding factors, including disease history and smoking status, to better elucidate the underlying mechanisms of iron-related neurodegenerative diseases.

DATA AVAILABILITY STATEMENT

The raw data supporting the conclusions of this article will be made available by the authors, without undue reservation.

ETHICS STATEMENT

The studies involving human participants were reviewed and approved by the Institutional Review Board of Shandong Medical Imaging Research Institute Affiliated to Shandong University. The patients/participants provided their written informed consent to participate in this study.

AUTHOR CONTRIBUTIONS

JL and LG wrote the main manuscript text. QZ and YC prepared the imaging data, **Figures 1**–**7**, and the tables. NZ prepared the clinical data. LG revised the main manuscript text. All the authors reviewed the manuscript.

FUNDING

This work was supported by grants from the National Natural Science Foundation of China (81800840), the Natural Science Foundation of Shandong Province (ZR2020MH288), Technology Development Plan of Jinan (201302049, 201602206, and 201907052), Medical and Health Science and Technology Development Project of Shandong Province (2016WS0529 and 2019WS544), and Funding for Study Abroad Program by Shandong Province (201803059).

REFERENCES

Acosta-Cabronero, J., Betts, M. J., Cardenas-Blanco, A., Yang, S., and Nestor, P. J. (2016). In vivo MRI mapping of brain iron deposition across the adult lifespan. *J. Neurosci.* 36, 364–374. doi: 10.1523/jneurosci.1907-15.2016

Amin Al Olama, A., Wason, J. M. S., Tuladhar, A. M., van Leijsen, E. M. C., Koini, M., Hofer, E., et al. (2020). Simple MRI score aids prediction of dementia in cerebral small vessel disease. *Neurology* 94, e1294–e1302.

Bell, R. D., Winkler, E. A., Singh, I., Sagare, A. P., Deane, R., Wu, Z., et al. (2012). Apolipoprotein E controls cerebrovascular integrity via cyclophilin A. *Nature* 485, 512–516. doi: 10.1038/nature11087

Bilgic, B., Pfefferbaum, A., Rohlfing, T., Sullivan, E. V., and Adalsteinsson, E. (2012). MRI estimates of brain iron concentration in normal aging using quantitative susceptibility mapping. *NeuroImage* 59, 2625–2635. doi: 10.1016/j.neuroimage.2011.08.077

Calero, O., Hortigüela, R., Bullido, M. J., and Calero, M. (2009). Apolipoprotein E genotyping method by real time PCR, a fast and cost-effective alternative to the TaqMan and FRET assays. *J. Neurosci. Methods* 183, 238–240. doi: 10.1016/j.jneumeth.2009.06.033

Carnevale, L., D'Angelosante, V., Landolfi, A., Grillea, G., Selvetella, G., Storto, M., et al. (2018). Brain MRI fiber-tracking reveals white matter alterations in hypertensive patients without damage at conventional neuroimaging. *Cardiovasc. Res.* 114, 1536–1546. doi: 10.1093/cvr/cvy104

Chai, C., Wang, H., Liu, S., Chu, Z. Q., Li, J., Qian, T., et al. (2019). Increased iron deposition of deep cerebral gray matter structures in hemodialysis patients: a longitudinal study using quantitative susceptibility mapping. *J. Magn. Reson. Imaging.* 49, 786–799. doi: 10.1002/jmri.26226

Faucheux, B. A., Martin, M. E., Beaumont, C., Hauw, J. J., Agid, Y., and Hirsch, E. C. (2003). Neuromelanin associated redox-active iron is increased in the substantia nigra of patients with Parkinson's disease. *J. Neurochem.* 86, 1142–1148. doi: 10.1046/j.1471-4159.2003.01923.x

Fennema-Notestine, C., McEvoy, L. K., Notestine, R., Panizzon, M. S., Yau, W. W., Franz, C. E., et al. (2016). White matter disease in midlife is heritable, related to hypertension, and shares some genetic influence with systolic blood pressure. *NeuroImage Clin*. 12, 737–745. doi: 10.1016/j.nicl.2016.10.001

Gong, N. J., Wong, C. S., Hui, E. S., Chan, C. C., and Leung, L. M. (2015). Hemisphere, gender and age-related effects on iron deposition in deep gray matter revealed by quantitative susceptibility mapping. *NMR Biomed*. 28, 1267–1274. doi: 10.1002/nbm.3366

Haller, S., Vernooij, M. W., Kuijer, J. P. A., Larsson, E. M., Jäger, H. R., and Barkhof, F. (2018). Cerebral microbleeds: imaging and clinical significance. *Radiology* 287, 11–28. doi: 10.1148/radiol.2018170803

Hinoda, T., Fushimi, Y., Okada, T., Fujimoto, K., Liu, C., Yamamoto, A., et al. (2015). Quantitative susceptibility mapping at 3 T and 1.5 T: evaluation of consistency and reproducibility. *Invest. Radiol*. 50, 522–530. doi: 10.1097/rli.0000000000000159

Hobson, N., Polster, S. P., Cao, Y., Flemming, K., Shu, Y., Huston, J., et al. (2020). Phantom validation of quantitative susceptibility and dynamic contrast-enhanced permeability MR sequences across instruments and sites. *J. Magn. Reson. Imaging*. 51, 1192–1199. doi: 10.1002/jmri.26927

Jenkinson, M., Bannister, P., Brady, M., and Smith, S. (2002). Improved optimization for the robust and accurate linear registration and motion correction of brain images. *Neuroimage* 17, 825–841. doi: 10.1006/nimg.2002.1132

Kaisar, M. A., Sivandzade, F., Bhalerao, A., and Cucullo, L. (2018). Conventional and electronic cigarettes dysregulate the expression of iron transporters and detoxifying enzymes at the brain vascular endothelium: in vivo evidence of a gender-specific cellular response to chronic cigarette smoke exposure. *Neurosci. Lett*. 682, 1–9. doi: 10.1016/j.neulet.2018.05.045

Kim, H. G., Park, S., Rhee, H. Y., Lee, K. M., Ryu, C. W., Rhee, S. J., et al. (2017). Quantitative susceptibility mapping to evaluate the early stage of Alzheimer's disease. *NeuroImage Clin*. 16, 429–438. doi: 10.1016/j.nicl.2017.08.019

Kruer, M. C., Hiken, M., Gregory, A., Malandrini, A., Clark, D., Hogarth, P., et al. (2011). Novel histopathologic findings in molecularly-confirmed pantothenate kinase-associated neurodegeneration. *Brain* 134(Pt 4), 947–958. doi: 10.1093/brain/awr042

Lavezzi, A. M., Mohorovic, L., Alfonsi, G., Corna, M. F., and Matturri, L. (2011). Brain iron accumulation in unexplained fetal and infant death victims with smoker mothers–the possible involvement of maternal methemoglobinemia. *BMC Pediatr*. 11:62. doi: 10.1186/1471-2431-11-62

Li, W., Wu, B., Batrachenko, A., Bancroft-Wu, V., Morey, R. A., Shashi, V., et al. (2014). Differential developmental trajectories of magnetic susceptibility in human brain gray and white matter over the lifespan. *Hum. Brain Mapp*. 35, 2698–2713. doi: 10.1002/hbm.22360

Liu, T., Khalidov, I., de Rochefort, L., Spincemaille, P., Liu, J., Tsiouris, A. J., et al. (2011). A novel background field removal method for MRI using projection onto dipole fields (PDF). *NMR Biomed*. 24, 1129–1136. doi: 10.1002/nbm.1670

Liu, Z., Spincemaille, P., Yao, Y., Zhang, Y., and Wang, Y. (2018). MEDI+0: morphology enabled dipole inversion with automatic uniform cerebrospinal fluid zero reference for quantitative susceptibility mapping. *Magn. Reson. Med*. 79, 2795–2803. doi: 10.1002/mrm.26946

Maillard, P., Seshadri, S., Beiser, A., Himali, J. J., Au, R., Fletcher, E., et al. (2012). Effects of systolic blood pressure on white-matter integrity in young adults in the Framingham heart study: a cross-sectional study. *Lancet Neurol*. 11, 1039–1047. doi: 10.1016/s1474-4422(12)70241-7

McCarthy, R. C., Sosa, J. C., Gardeck, A. M., Baez, A. S., Lee, C. H., and Wessling-Resnick, M. (2018). Inflammation-induced iron transport and metabolism by brain microglia. *J. Biol. Chem*. 293, 7853–7863. doi: 10.1074/jbc.ra118.001949

Montagne, A., Nation, D. A., Sagare, A. P., Barisano, G., Sweeney, M. D., Chakhoyan, A., et al. (2020). APOE4 leads to blood-brain barrier dysfunction predicting cognitive decline. *Nature* 581, 71–76. doi: 10.1038/s41586-020-2247-3

Park, M., Moon, W. J., Moon, Y., Choi, J. W., Han, S. H., and Wang, Y. (2018). Region-specific susceptibility change in cognitively impaired patients with diabetes mellitus. *PLoS One* 13:e0205797. doi: 10.1371/journal.pone.0205797

Patenaude, B., Smith, S. M., Kennedy, D. N., and Jenkinson, M. (2011). A Bayesian model of shape and appearance for subcortical brain segmentation. *Neuroimage* 56, 907–922. doi: 10.1016/j.neuroimage.2011.02.046

Persson, N., Wu, J., Zhang, Q., Liu, T., Shen, J., Bao, R., et al. (2015). Age and sex related differences in subcortical brain iron concentrations among healthy adults. *NeuroImage* 122, 385–398. doi: 10.1016/j.neuroimage.2015.07.050

Peterson, E. T., Kwon, D., Luna, B., Larsen, B., Prouty, D., De Bellis, M. D., et al. (2019). Distribution of brain iron accrual in adolescence: evidence from cross-sectional and longitudinal analysis. *Hum. Brain Mapp*. 40, 1480–1495. doi: 10.1002/hbm.24461

Pirpamer, L., Hofer, E., Gesierich, B., De Guio, F., Freudenberger, P., Seiler, S., et al. (2016). Determinants of iron accumulation in the normal aging brain. *Neurobiol. Aging* 43, 149–155. doi: 10.1016/j.neurobiolaging.2016.04.002

Ramos, P., Santos, A., Pinto, N. R., Mendes, R., Magalhães, T., and Almeida, A. (2014). Iron levels in the human brain: a post-mortem study of anatomical region differences and age-related changes. *J. Trace Elem. Med. Biol*. 28, 13–17. doi: 10.1016/j.jtemb.2013.08.001

Raz, E., Branson, B., Jensen, J. H., Bester, M., Babb, J. S., Herbert, J., et al. (2015). Relationship between iron accumulation and white matter injury in multiple sclerosis: a case-control study. *J. Neurol*. 262, 402–409. doi: 10.1007/s00415-014-7569-3

Rizzo, G., and Plazzi, G. (2018). Neuroimaging applications in restless legs syndrome. *Int. Rev. Neurobiol*. 143, 31–64.

Rodrigue, K. M., Haacke, E. M., and Raz, N. (2011). Differential effects of age and history of hypertension on regional brain volumes and iron. *NeuroImage* 54, 750–759. doi: 10.1016/j.neuroimage.2010.09.068

Schipper, H. M. (2012). Neurodegeneration with brain iron accumulation – clinical syndromes and neuroimaging. *Biochim. Biophys. Acta* 1822, 350–360. doi: 10.1016/j.bbadis.2011.06.016

Seger, C. A. (2008). How do the basal ganglia contribute to categorization? their roles in generalization, response selection, and learning via feedback. *Neurosci. Biobehav. Rev*. 32, 265–278. doi: 10.1016/j.neubiorev.2007.07.010

Smith, S. M. (2002). Fast robust automated brain extraction. *Hum. Brain Mapp*. 17, 143–155. doi: 10.1002/hbm.10062

Takechi, R., Lam, V., Brook, E., Giles, C., Fimognari, N., Mooranian, A., et al. (2017). Blood-Brain barrier dysfunction precedes cognitive decline and neurodegeneration in diabetic insulin resistant mouse model: an implication for causal link. *Front. Aging Neurosci*. 9:399. doi: 10.3389/fnagi.2017.00399

Tomlinson, D. R., and Gardiner, N. J. (2008). Glucose neurotoxicity. *Nat. Rev. Neurosci*. 9, 36–45. doi: 10.1038/nrn2294

Uchida, Y., Kan, H., Sakurai, K., Arai, N., Kato, D., Kawashima, S., et al. (2019). Voxel-based quantitative susceptibility mapping in Parkinson's disease with mild cognitive impairment. *Mov. Disord*. 34, 1164–1173. doi: 10.1002/mds.27717

Valdés Hernández, M., Allerhand, M., Glatz, A., Clayson, L., Muñoz Maniega, S., Gow, A., et al. (2016). Do white matter hyperintensities mediate the association between brain iron deposition and cognitive abilities in older people? *Eur. J. Neurol*. 23, 1202–1209. doi: 10.1111/ene.13006

van Veluw, S. J., Shih, A. Y., Smith, E. E., Chen, C., Schneider, J. A., Wardlaw, J. M., et al. (2017). Detection, risk factors, and functional consequences of cerebral microinfarcts. *Lancet Neurol*. 16, 730–740. doi: 10.1016/s1474-4422(17)30196-5

Wang, Y., and Liu, T. (2015). Quantitative susceptibility mapping (QSM): decoding MRI data for a tissue magnetic biomarker. *Magn. Reson. Med*. 73, 82–101. doi: 10.1002/mrm.25358

Wang, Y., Spincemaille, P., Liu, Z., Dimov, A., Deh, K., Li, J., et al. (2017). Clinical quantitative susceptibility mapping (QSM): biometal imaging and its emerging roles in patient care. *J. Magn. Reson. Med*. 46, 951–971. doi: 10.1002/jmri.25693

Ward, R. J., Zucca, F. A., Duyn, J. H., Crichton, R. R., and Zecca, L. (2014). The role of iron in brain ageing and neurodegenerative disorders. *Lancet Neurol*. 13, 1045–1060. doi: 10.1016/s1474-4422(14)70117-6

Wardlaw, J. M., Smith, C., and Dichgans, M. (2013b). Mechanisms of sporadic cerebral small vessel disease: insights from neuroimaging. *Lancet* 12, 483–497. doi: 10.1016/s1474-4422(13)70060-7

Wardlaw, J. M., Smith, E. E., Biessels, G. J., Cordonnier, C., Fazekas, F., Frayne, R., et al. (2013a). Neuroimaging standards for research into small vessel disease and its contribution to ageing and neurodegeneration. *Lancet Neurol*. 12, 822–838.

Wicaksono, K. P., Fushimi, Y., Nakajima, S., Yokota, Y., Oshima, S., Otani, S., et al. (2020). Two-minute quantitative susceptibility mapping from three-dimensional echo-planar imaging: accuracy, reliability, and detection

performance in patients with cerebral microbleeds. *Invest. Radiol.* 56, 69–77. doi: 10.1097/rli.0000000000000708

Wu, B., Li, W., Guidon, A., and Liu, C. (2012). Whole brain susceptibility mapping using compressed sensing. *Magn. Reson. Med.* 67, 137–147. doi: 10.1002/mrm.23000

Xu, X., Wang, Q., and Zhang, M. (2008). Age, gender, and hemispheric differences in iron deposition in the human brain: an in vivo MRI study. *NeuroImage* 40, 35–42. doi: 10.1016/j.neuroimage.2007.11.017

Yang, Q. F., Zhou, L. N., Liu, C., Liu, D. H., Zhang, Y., Li, C., et al. (2018). Brain iron deposition in type 2 diabetes mellitus with and without mild cognitive impairmentan in vivo susceptibility mapping study. *Brain Imaging Behav.* 12, 1479–1487. doi: 10.1007/s11682-017-9815-7

Yu, X., Du, T., Song, N., He, Q., Shen, Y., Jiang, H., et al. (2013). Decreased iron levels in the temporal cortex in postmortem human brains with Parkinson disease. *Neurology* 80, 492–495. doi: 10.1212/wnl.0b013e31827f0ebb

Zhang, Y., Brady, M., and Smith, S. (2001). Segmentation of brain MR images through a hidden Markov random field model and the expectation-maximization algorithm. *IEEE Trans. Med. Imaging* 20, 45–57. doi: 10.1109/42.906424

Conflict of Interest: The authors declare that the research was conducted in the absence of any commercial or financial relationships that could be construed as a potential conflict of interest.

frontiers in Aging Neuroscience

ORIGINAL RESEARCH
published: 07 May 2021
doi: 10.3389/fnagi.2021.668775

Probiotic Supplementation Facilitates Recovery of 6-OHDA-Induced Motor Deficit via Improving Mitochondrial Function and Energy Metabolism

Bira Arumndari Nurrahma[1†], Shu-Ping Tsao[2†], Chieh-Hsi Wu[2,3], Tu-Hsueh Yeh[4,5], Pei-Shan Hsieh[6], Binar Panunggal[7,8] and Hui-Yu Huang[1]*

[1] Graduate Institute of Metabolism and Obesity Sciences, College of Nutrition, Taipei Medical University, Taipei City, Taiwan, [2] Ph.D. Program in Drug Discovery and Development Industry, College of Pharmacy, Taipei Medical University, Taipei City, Taiwan, [3] School of Pharmacy, College of Pharmacy, Taipei Medical University, Taipei City, Taiwan, [4] Department of Neurology, Taipei Medical University Hospital, Taipei City, Taiwan, [5] Department of Neurology, College of Medicine and Taipei Neuroscience Institute, Taipei Medical University, Taipei City, Taiwan, [6] Bioflag Biotech Co., Ltd., Tainan City, Taiwan, [7] School of Nutrition and Health Sciences, College of Nutrition, Taipei Medical University, Taipei City, Taiwan, [8] Department of Nutrition Science, Faculty of Medicine, Diponegoro University, Central Java, Indonesia

OPEN ACCESS

Edited by:
Ines Moreno-Gonzalez, University of Malaga, Spain

Reviewed by:
Andrii Domanskyi, Orion Corporation (Finland), Finland
Vanessa Castelli, University of L'Aquila, Italy

***Correspondence:**
Hui-Yu Huang
maggieh323@tmu.edu.tw

[†] These authors have contributed equally to this work and share first authorship

Received: *17 February 2021*
Accepted: *12 April 2021*
Published: *07 May 2021*

Citation:
Nurrahma BA, Tsao S-P, Wu C-H, Yeh T-H, Hsieh P-S, Panunggal B and Huang H-Y (2021) Probiotic Supplementation Facilitates Recovery of 6-OHDA-Induced Motor Deficit via Improving Mitochondrial Function and Energy Metabolism. Front. Aging Neurosci. 13:668775. doi: 10.3389/fnagi.2021.668775

Parkinson's disease (PD) is a neurodegenerative disease associated with progressive impairment of motor and non-motor functions in aging people. Overwhelming evidence indicate that mitochondrial dysfunction is a central factor in PD pathophysiology, which impairs energy metabolism. While, several other studies have shown probiotic supplementations to improve host energy metabolism, alleviate the disease progression, prevent gut microbiota dysbiosis and alter commensal bacterial metabolites. But, whether probiotic and/or prebiotic supplementation can affect energy metabolism and cause the impediment of PD progression remains poorly characterized. Therefore, we investigated 8-weeks supplementation effects of probiotic [*Lactobacillus salivarius* subsp. *salicinius* AP-32 (AP-32)], residual medium (RM) obtained from the AP-32 culture medium, and combination of AP-32 and RM (A-RM) on unilateral 6-hydroxydopamine (6-OHDA)-induced PD rats. We found that AP-32, RM and A-RM supplementation induced neuroprotective effects on dopaminergic neurons along with improved motor functions in PD rats. These effects were accompanied by significant increases in mitochondrial activities in the brain and muscle, antioxidative enzymes level in serum, and altered SCFAs profile in fecal samples. Importantly, the AP-32 supplement restored muscle mass along with improved motor function in PD rats, and produced the best results among the supplements. Our results demonstrate that probiotic AP-32 and A-RM supplementations can recover energy metabolism via increasing SCFAs producing and mitochondria function. This restoring of mitochondrial function in the

brain and muscles with improved energy metabolism might additionally be potentiated by ROS suppression by the elevated generation of antioxidants, and which finally leads to facilitated recovery of 6-OHDA-induced motor deficit. Taken together, this work demonstrates that probiotic AP-32 supplementation could be a potential candidate for alternate treatment strategy to avert PD progression.

Keywords: Parkinson's disease, 6-hydroxydopamine, probiotic, prebiotic, *Lactobacillus salivarius* AP-32, mitochondrial function, energy metabolism

INTRODUCTION

The Parkinson's disease (PD) is a widespread neurodegenerative disease in aging individuals, marked by a gradual loss of dopaminergic neurons in the SNc pars compacta (SNc) region of the midbrain. The gradual loss of dopaminergic neurons reduces dopamine turnover in the motor circuit of the brain leading to motor dysfunctions, such as bradykinesia, rigidity, tremor, and postural. Simultaneously, non-motor impairments, such as gut dysfunction, sleep disorder, depression, and dysphagia, are also associated with PD instability (Kalia and Lang, 2015; Maiti et al., 2017). PD patients also suffer from loss of body weight and skeletal muscles (Garber and Friedman, 2003; Falvo et al., 2008; Stevens-Lapsley et al., 2012), which all together worsen the life quality of PD individuals over time.

Although PD pathogenesis remains unclear, several risk factors are known to be associated with PD such as aging, environmental factors, and genetic mutations (Kalia and Lang, 2015; Maiti et al., 2017). Importantly, mitochondrial function is known to be disrupted in PD patients (Schapira et al., 1990). This disruption leads to decreased respiratory enzyme activity, decreased ATP production and energy failure (Verstreken et al., 2005). In a functional mitochondrion, a large antioxidant defense capacity balances the generation of reactive oxygen species (ROS). Mitochondrial damage with decrease of antioxidant defense capacity is imperative of net ROS production. Functionally compromised mitochondria, as in the state of PD, creates an imbalance between ROS production and removal, resulting in net ROS production along with detrimental effects on the anti-oxidative defense system. In effect, there is an increase in oxidative stress resulting from the increased ROS production, and accumulation with simultaneous decrease in oxidative stress-related antioxidant enzymes. Prolonged oxidative stress can further exacerbate mitochondria damage and eventually lead to dopaminergic neurons degeneration (Federico et al., 2012; Subramaniam and Chesselet, 2013; Tait and Green, 2013). An increase in glycolysis can counteract energy failure and dopaminergic cell death induced by malfunctioning mitochondria (Smith et al., 2018). However, neurons have limited capability to up regulate glycolysis. Augmenting the ATP deficit by stimulating glycolysis with pharmacological interventions has shown to attenuate PD progression (Cai et al., 2019).

Several recent studies show a link between PD pathogenesis and gut microbiota dysbiosis (Sun and Shen, 2018). Compared to healthy people, the gut microbiota of individuals with PD have been consistently reported to be abundant with more pro-inflammatory bacteria and less abundant with anti-inflammatory bacteria (Unger et al., 2016). Such changes in the abundance and diversity of microbial flora result in altered production of microbe-derived metabolites in the GI tract. Microbial metabolites beneficial to host immune system and energy metabolism, particularly the short-chain fatty acids (SCFAs), are found to be reduced in PD patients (Unger et al., 2016). The SCFAs (acetate, propionate, and butyrate) are used by host as substrates for lipid, cholesterol, and glucose metabolism which are eventually utilized for the production of energy via Krebs cycle in mitochondria (LeBlanc et al., 2017). Therefore, SCFAs play an important role as precursors for energy metabolism in host. This understanding has led to an ongoing hypothesis that gut microbiota could play an important role in PD pathogenesis, where SCFAs could be the key mediator between gut microbiota and brain bidirectional axis (Ferrante et al., 2003; Monti et al., 2010; Koh et al., 2016; Lei et al., 2016; Schonfeld and Wojtczak, 2016).

Probiotics are live microorganisms that, when administered in appropriate amounts, confer a beneficial effect on the host (Gazerani, 2019). Whereas, prebiotics are non-digestible nutrients that can influence gut microbiota growth and activity, including the production of SCFAs (Franco-Robles and López, 2015). *Lactobacillus,* is a popular probiotic known to exhibit neuroprotective effects (Castelli et al., 2020; Hsieh et al., 2020), decrease neuroinflammation, increase synaptic plasticity, alter gut microbiota (Bonfili et al., 2017), immunomodulatory effects, barrier function promoter and pathogen inhibitor functions (Hsieh et al., 2013). Besides probiotics, studies have also shown that the metabolites produced by the bacteria fermentation process could generate similar therapeutic effects (Koh et al., 2016). The residues obtained from probiotics culture medium are an alternate source of microbe-derived metabolites, which may contain beneficial nutrients, such as SCFAs. Therefore, the residual medium from probiotic culture can alternatively be utilized as prebiotic supplements.

In this study, we tested the hypothesis that probiotic and potential prebiotic from probiotic residual medium might perform a beneficial role in preventing neurodegeneration in PD condition, we also try to investigate and explore the possible mechanism underlying beneficial effects of a probiotic [*Lactobacillus salivarius* subsp. *salicinius* AP-32 (AP-32)], a potential prebiotic [AP-32 residual medium (RM)], and a symbiotic [the combination between AP-32 and its residual medium (A-RM)] supplementation in 6-OHDA PD rat model.

MATERIALS AND METHODS

Probiotic and Prebiotic

Probiotic *Lactobacillus salivarius* subsp. *salicinius* AP-32 (AP-32) and the prebiotic residues of microbial culture medium (RM) were provided by Bioflag Biotech Co., Ltd., Tainan, Taiwan. *L. salivarius* subsp. *salicinius* AP-32 was isolated from healthy human gut and deposited in Food Industry Research and Development Institute, Taiwan (ID: BCRC 910437) and in Wuhan University, China (ID: CCTCC-M2011127). Probiotic AP-32 consists of 10^{11} colony-forming unit (CFU)/g. Probiotic AP-32 was selected due to its capacity to regulate inflammatory function and genus *Lactobacillus* function to promote neuroprotective effects (Bonfili et al., 2017; Castelli et al., 2020; Hsieh et al., 2020). RM powder was derived from the supernatant obtained from probiotic AP-32 fermented medium. Briefly, after the probiotic AP-32 were grown in the medium, the fermented medium was centrifuged to remove the bacteria. The supernatant was spray dried. 4 L of supernatant liquid RM upon spray-drying yielded 60 g of RM powders. The RM consists of carbohydrates, proteins, fats, amino acids, and SCFAs (**Supplementary Table 1**). A-RM was a mixture of probiotic AP-32 (1.03×10^9 CFU/kgBW of AP-32) and RM (62 mg/kgBW of RM). Fresh stock solution of AP-32, RM, and A-RM were prepared before oral gavage everyday by dissolving each powder in distilled water to final concentration of 1 mg/ml. The final gavage volume was calculated as per the body weight of rats.

Animal Grouping

Male Sprague-Dawley (SD) rats (8 weeks old, 280-300 g) were purchased from BioLASCO Taiwan Co., Ltd. (Taiwan) and were housed two rats per cage at Laboratory Animal Center (LAC) Taipei Medical University under a controlled environment (12/12-h light/dark cycle, 22°C–24°C, 40%–60% humidity) with free access to food and water. Rats were randomly assigned to normal control (NC, $n = 5$) and PD groups ($n = 30$). PD rats were obtained by unilateral 6-OHDA injection into the right medial forebrain bundle (MFB). To reduce variability among groups, we performed apomorphine-induced rotation test at 6 weeks after unilateral 6-OHDA lesions and confirmed 25 PD rats (contralateral rotation more than 100 rotations/hour (Kaminska et al., 2017)). The confirmed PD rats were equally assigned into the following 5 groups: untreated PD (PD, $n = 5$), L-DOPA-treated PD (L, $n = 5$), AP-32-treated PD (AP-32, $n = 5$), RM-treated PD (RM, $n = 5$), and A-RM-treated PD (A-RM, $n = 5$). One-way ANOVA was performed after grouping to ensure the equal animal grouping. After the animal grouping, rats were given either AP-32 (1.03×10^9 CFU/kgBW), RM (62 mg/kgBW), or A-RM (1.03×10^9 CFU/kgBW of AP-32 mixed with 62 mg/kgBW of RM) once a day for 8 weeks by oral gavage administration. L-DOPA treatment (8 mg/kgBW of L-DOPA + 15 mg/kgBW benserazide dissolved in 0.9% NaCl) was performed by intraperitoneal (i.p.) injection 3 times/week (Sgroi et al., 2014)started from animal grouping until 8 consecutive weeks. Every day, the food and water intakes by rats were recorded, and their bodyweights (BW) were measured weekly. Apomorphine-induced rotation test was repeated at 4 and 8 weeks after supplementations. Catwalk-gait analysis and body composition were evaluated after 8 weeks of supplementations. Rats were sacrificed afterward. The timeline of the study is shown in **Figure 1**. All animal procedures were approved by the Taipei Medical University Animal Care and Use Committee of Panel (IACUC/IACUP) (approval no. LAC-2020-0183) and were conducted in accordance with the Taiwan code of practice for the care and use of animals for scientific purposes.

Unilateral 6-OHDA Injection Into the Right MFB

Induction of PD using unilateral 6-OHDA injection into the right MFB was modified from Hoffer et al. (1994). Rats were anesthetized through i.p. injection of tiletamine with zolazepam (20–40 mg/kgBW) (Zoletil®, Virbac, New Zealand) and xylazine (5–10 mg/kgBW) (Rompun®, Bayer HealthCare, Germany). Then, rats were fixed in a stereotaxic apparatus (David Kopf Instruments, Tujunga, CA, United States) by positioning their forehead flat. After exposing the skull by surgical incision, 1-mm burr hole was drilled into the right medial forebrain bundle (MFB) with the coordinates: anteroposterior (AP) −4.4 mm from the bregma; mediolateral (ML) 1.2 mm from the midline; and dorsoventral (DV) −7.8 mm. Subsequently, 6−OHDA (9 μg per rat in 3 μl of 0.9% NaCl + 0.02% (w/v) ascorbic acid) (Sigma-Aldrich, Darmstadt, Germany) was infused by an infusion pump through a 10 μl Hamilton syringe at 0.2 μl/min, constant flow rate. The implanted syringe was left still for an additional 5 min after infusion and then retracted slowly. Sham−operated rats underwent the same procedure with 3 μl of the vehicle (0.9% NaCl + 0.02% (w/v) ascorbic acid). To reduce variability caused by 6-OHDA degradation, the 6-OHDA solution was freshly prepared in ascorbic acid solution, kept at 4°C, and protected from light (Sanchez et al., 2009). The fresh solution was used within 1 h. During the surgery and recovery procedures, animals were maintained warm using a heating pad.

Serum Biochemical Analysis

Blood was immediately collected by cardiac puncture, and the rats were immediately sacrificed after 8-weeks of supplementation. Blood was centrifuged at 3,500 x *g* for 10 min at 4°C to obtain the serum. Serum total cholesterol (TCHO), triglycerides (TG), high-density lipoprotein cholesterol (HDL), aspartate aminotransferase (AST), alanine aminotransferase (ALT), albumin (ALB), and total protein (TP) were measured using an autoanalyzer (Fujifilm NX500i, Tokyo, Japan).

Evaluation of Neurodegeneration Process and Motor Function

Apomorphine-Induced Rotation Test

Apomorphine-induced rotation test was performed at 6 weeks after unilateral 6-OHDA lesions to assess the variability of the unilateral 6-OHDA-induced PD rats. Rats were assigned separately into a square cage. A dopamine receptor agonist,

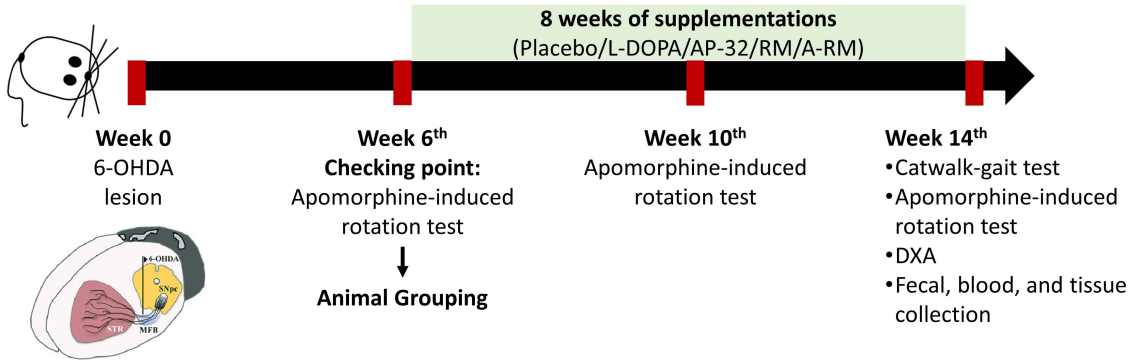

FIGURE 1 | Timeline of the study.

apomorphine (0.5 mg/kgBW in 0.9% NaCl and 1% ascorbic acid) (Sigma-Aldrich, Darmstadt, Germany), was injected subcutaneously to trigger contralateral rotation. Contralateral rotations were recorded for 1 hour. Contralateral rotations induced by apomorphine reflect the dopaminergic neuron loss. The test was repeated at 4 and 8 weeks after supplementations to assess the supplementations effects.

Immunohistochemistry Staining and Image Analysis

Immunohistochemistry staining was used to evaluate tyrosine hydroxylase (TH) presence in the striatum and SNc. TH is the specific marker to determine dopaminergic neuron number. Briefly, each brain was cut into coronal slices containing striatum (interaural 9.20 mm and bregma 0.20 mm) and SNc (interaural 3.40 mm and bregma −5.60 mm), then incubated in 4% formaldehyde. The free-floating sections were incubated in a 0.3% hydrogen peroxide solution for 10 min under light-protected condition light, to block internal peroxidases. After that, sections were incubated in PBS containing 0.5% Triton X-100, 4% BSA at room temperature for one hour. Sections were then left to incubate with rabbit polyclonal anti-TH (1:300) (Elabscience, US, Cat. No. E-AB-70077) in PBS containing 0.4% Triton X-100 at 4°C overnight. The primary antibody was omitted in control sections. After incubation for two hours at room temperature with goat anti-rabbit IgGHRP (Sigma, B7401), 1:100 in PBS containing 0.4% Triton X100, immunocomplexes were revealed using 3,3′-diamino-benzidine (DAB Substrate Kit for Peroxidase, Vector) as the chromogen. After washing extensively, the sections were dehydrated and mounted on slides using Permount (Fisher Scientific, United States) mounting media. Slides imaging was performed using pathology slide scanner Motic EasyScan hardware and software (Motic, Hong Kong). The intensity of TH + level was then quantified using ImageJ. The intensity of TH + level of lesioned side was standardized with the respected non-lesioned side (contralateral side).

Catwalk Quantitative Gait Analysis Test

A Catwalk-gait test was performed to evaluate the gait performance after 8 weeks of supplementations. The Catwalk-gait test was done on a quantitative gait analysis system, GaitLab ViewPoint (ViewPoint, China) hardware and software. The apparatus consisted of a raised glass floor with a green light. On the bottom floor of the walkway, a high-speed video camera is placed to record the green light reflected from each point of contact with the animal at 100 frames per second. The pattern of green light was interpreted by custom software and translated into a quantitative assessment of the rat's paw print. The following variables were obtained from Catwalk-gait analysis: speed (speed started from entering until leaving the walkway, cm/s), stride length (distance between the same paw, cm), stride frequency (number of strides per second, strides/sec), stance time (the time the animal lays a paw on floor, secs), duty factor (ratio of a paw frequency and total time), asymmetry gait analysis (left pair lag, secs; right pair lag, secs; left pair gap, cm; right pair gap, cm), and intensity sum.

Evaluation of Mitochondrial Function and Energy Metabolism

Mitochondrial Function by Seahorse Bioscience XFe24 Extracellular Flux Analysis

Mitochondrial function was evaluated by measuring real time basal oxygen consumption rates (OCR) and extracellular acidification rate (ECAR) with Seahorse Bioscience XFe24 extracellular flux analyzer. OCR measures mitochondrial respiration efficacy and ECAR measures glycolysis efficacy. After sacrifice, fresh brains and left soleus muscles were transferred into an XFe24 islet capture microplate (Seahorse Bioscience, United States, Cat. No. 101122-100). The Seahorse XFe24 performs repeated measurement of oxygen and proton concentrations surrounding tissues in the assay medium using oxygen and hydrogen ion-sensitive fluorophores. Briefly, inside a non-carbon dioxide incubator the assay cartridge plate (Seahorse Bioscience, United States, Cat. No. 100867-100) was hydrated using an XF calibration solution (Seahorse Bioscience, United States, Cat. No. 100867-000) for overnight at 37°C. For the experiments, Seahorse XF Assay medium (Seahorse Bioscience, United States, Cat. No. 102365-100), containing 5.0 mmol/l glucose and 2.0 mmol/l pyruvate at pH 7.4 and 37°C, was used to minimize any movement

during the assay, isolated tissues were placed at the bottom of the islet plates and covered with a screen. 525 μl of XF assay medium was then added into the wells and maintained at 37°C in a non-carbon dioxide incubator for 20 min. After the incubation, the islet plate was placed inside the analyzer instrument. Three cycles were performed to obtain basal mitochondria respiration and glycolysis rate. After the Seahorse experiment, protein concentration in each well was then determined. The tissues from all islet plate wells were transferred into individual 1.5 ml microtubes containing 5 μl/ml (each) of NP40 lysis buffer (Invitrogen, Frederick, MD), proteinase, and phosphatase inhibitor at 4°C (Sigma Aldrich, St. Louis, MO). Tissues were homogenized and then centrifuged for 10 min at 1,000 x *g*. The supernatant was separated and then used for the Bradford protein quantification assay (Thermo Scientific, Rockford, IL). Sample duplicates and bovine serum albumin (BSA) standards (Sigma-Aldrich, Darmstadt, Germany) were load into a 96-well plate with the following concentrations (mg/ml): 0, 25, 125, 250, 500, 750, 1,000, 1,500, and 2,000. The Bradford reagents (Sigma-Aldrich, Darmstadt, Germany) were added to the wells containing either samples or standards. Afterward, the plate was incubated for 5 min at room temperature, and 595 nm was used to read the absorbance of the samples and standards. Concentration of samples was finally calculated by using standard curve and interpolation technique.

Dual-Energy X-Ray Absorptiometry (DXA)

After 8 weeks of supplementation, the body composition of each rat was assessed to determine total body fat, muscle mass, and bone mineral density by using DXA (Lunar Hologic, GE Healthcare, Wisconsin, United States) hardware and software. To ensure rats were motionless during scanning, rats were anesthetized using zoletil (20-40 mg/kgBW) and xylazine (5–10 mg/kgBW) by i.p. injection. With their face facing downwards, the rats were placed on the scanning bed. Nose to tail scanning was conducted to obtain complete body composition measurement.

Antioxidant Activity

Glutathione peroxidase (GPx) and superoxide dismutase (SOD) activities were measured in serum using colorimetric assay using GPx and SOD assay kits (BioVision, California, United States) according to the manufacturer's instructions. The GPx and SOD activities were calculated using an equation obtained from linear regression of the standard curve.

Fecal Microbial Metabolites Analysis by High-Performance Liquid Chromatography (HPLC)

Fresh fecal samples were collected during the eighth week. Determination of microbial metabolites consisted of six SCFAs (acetic, propionic, isobutyric, butyric, isovaleric, and valeric acids). SCFAs were determined by HPLC, following a previous study (Granado-Serrano et al., 2019). Briefly, SCFAs were extracted using 70% ethanol (5 mL of ethanol for 200 mg of the sample), then mixed and centrifuged at 20°C, 2500 rpm, 10 min. The supernatant was mixed with 2-ethylbutyric acid, pyridine, 1-EDC-HCl, and 2-NPH-HCl, then re-acted to 60°C for 20 min. The mixture was then mixed with potassium hydroxide, reacted at 60°C for 20 min, and cooled down. Next, the mixture was shaken with a phosphoric acid aqueous solution and ether for 3 min, then centrifuged to collect the ether layer. The ether layer was shaken with water for 3 min then centrifuged. Nitrogen gas was used to eliminate ether. Lastly, HPLC (column temperature 50°C, a flow rate of 1.1 mL/min, measurement wavelength 400 nm) was used after dissolving the obtained fatty acid hydrazide with methanol.

Statistical Analyses

Statistical analyses were performed using SPSS Statistics 19 software. Differences were evaluated using one-way ANOVA followed by Tukey HSD *post hoc* test. Results are expressed as mean ± standard error of the mean (SEM). Significance was determined as $p < 0.05$.

RESULTS

Serum Biochemical Profiles After 8 Weeks of AP-32, RM, and A-RM Supplementation

Levels of TCHO, TG, HDL, AST, ALT, ALB, and TP were measured in serum after 8-weeks of treatment. There was no significant difference among groups in serum bio-chemical profiles (**Table 1**), suggesting that AP-32, RM, and A-RM will not affect the serum biochemical value.

Supplementation of Probiotic *L. salivarius* AP-32, Prebiotic RM, and Combination A-RM Attenuated Neurodegenerative Process Apomorphine-Induced Rotation

Contralateral rotation induced by apomorphine could reflect the dopaminergic neuron loss after unilateral 6-OHDA injection into MFB. Six weeks after the injection, rats were exhibited more than 200 contralateral rotations/hour (**Table 2**). After 4 weeks of supplementations, contralateral rotations were decreased by 31.6 ± 7.3% in AP-32, 29.1 ± 12% in RM, and 27.9 ± 6.3% in A-RM-treated group. The contralateral rotations continuously decreased after 8 weeks of supplementations, with reduction of 66.7 ± 10.7%, 51.3 ± 8.8%, and 60.1 ± 8.3% in AP-32, RM, and A-RM, respectively. Compared to untreated PD group, supplementation of AP-32, RM, and A-RM significantly decreased contralateral rotations after 4- and 8-weeks supplementation. There is no significant difference between untreated PD and L-DOPA-treated group.

Neuroprotective Effect

Dopaminergic neurons were evaluated using a specific marker, TH. TH + level of the untreated PD group showed dramatic

TABLE 1 | The effects of AP-32, RM, and A-RM on serum biochemical profiles after 8 weeks of treatment in 6-OHDA-induced PD rats.

Biochemistry levels	NC	PD	L	AP-32	RM	A-RM
TCHO (mg/dL)	81.8 ± 21.2	84.4 ± 14.7	75.8 ± 13.6	85 ± 17.5	71.7 ± 11.1	77.3 ± 11.1
TG (mg/dL)	108.8 ± 46.7	94 ± 44.7	96.8 ± 46.2	104.7 ± 25.6	107.7 ± 14.9	95.0 ± 56.4
HDL (mg/dL)	44.8 ± 9.6	46.7 ± 15.0	46.8 ± 6.3	39.2 ± 6.0	39.7 ± 11.1	33.3 ± 3.8
AST (u/L)	183.3 ± 54.5	247 ± 55.3	185 ± 52.0	141.3.8 ± 31.1	274.3 ± 50.5	318.0 ± 50.8
ALT (u/L)	47.8 ± 4.1	54.3 ± 8.0	43.5 ± 5.2	43 ± 3.7	46.7 ± 5.3	59.3 ± 9.9
ALB (g/dL)	4.6 ± 0.9	3.7 ± 0.2	4.3 ± 0.7	3.9 ± 0.4	3.5 ± 0.1	3.8 ± 0.2
TP (g/dL)	7.2 ± 0.8	6.4 ± 0.3	6.8 ± 0.6	6.4 ± 0.3	6.1 ± 0.2	6.4 ± 0.2

All data are expressed mean ± SEM (n = 5 rats/group). There is no significant difference between groups. NC, normal control; PD, untreated PD as negative control; L, PD treated with 8 mg of L-DOPA as a positive control; AP-32, PD treated with 1.03 × 109 CFU/kg BW of AP-32; RM, PD treated with 62 mg/kgBW of residues of microbial culture medium RM; A-RM, PD treated with AP-32 and 62 mg/kgBW of residues of microbial culture medium RM. TCHO, Total Cholesterol; TG, Triglycerides; HDL, High Density Lipoprotein-Cholesterol; AST, Aspartate Aminotransferase; ALT, Alanine Aminotransferase; ALB, Albumin; TP, Total Protein.

TABLE 2 | AP-32, RM, and A-RM decreased contralateral rotation in apomorphine-induced rotation test after 4 and 8 weeks.

Week	NC	PD	L	AP-32	RM	A-RM
6th	0.0 ± 0.0	221.0 ± 13.9#	220.4 ± 9.3	223.8 ± 16.1	221.0 ± 12.1	214.8 ± 12.4
10th	0.0 ± 0.0	258.2 ± 31.3#	233.6 ± 20.6	187.6 ± 24.8*	191.4 ± 27.6*	194.0 ± 20.8*
14th	0.0 ± 0.0	269.6 ± 29.5#	258.4 ± 23.3	90.2 ± 24.6*	131.4 ± 20.8*	107.0 ± 21.2*

*Apomorphine-induced rotation test was conducted at 6, 10, and 14 weeks after 6-OHDA lesion. Data are expressed mean ± SEM (n = 5 rats/group). #p < 0.05 PD group compared to NC group. *p < 0.05 L, AP-32, RM, and A-RM groups compared to PD group. There is no significant difference between AP-32, RM, and A-RM. One-way ANOVA with Tukey's post hoc test. BW, Bodyweight; FCE, Food Consumption Efficiency (an increase of BW/total calorie intake).*

reductions in striatum (**Figures 2A,B**) and SNc (**Figures 2C,D**) of the 6-OHDA-lesioned side. Supplementation of AP-32 and its combination with residual medium (A-RM) prevented the loss of TH + intensity level in the striatum and SNc induced by unilateral 6-OHDA injection, indicating neuroprotective effects performed by these supplementations. A significant increase in the TH + level of the RM group was only observed in the SNc but not in the striatum. Supplementation of AP-32 for 8 weeks showed slightly higher TH + level in the striatum and SNc than RM. Here we also noted that RM seemed to have a suppression effect on AP-32, as seen in a slight decrease of TH + level in a group supplemented with A-RM.

Evaluation of Gait Function

Unilateral 6-OHDA MFB injection induced gait dysfunction as seen in dynamic parameters in Catwalk-gait analysis (**Figure 3**). Significant decreases of speed (**Figure 3A**) and stride length (**Figure 3B**) were found in untreated PD group. However, supplementation of probiotic AP-32, RM, and A-RM for 8 weeks could significantly increase the locomotor speed and stride length of PD rats. AP-32 supplementation shows better speed performance than RM and A-RM. Stride frequency (**Figure 3C**) was high in untreated PD group and decreased in AP-32, RM, A-RM, and L-DOPA-treated group. Stance time (**Figure 3D**) was increased by unilateral 6-OHDA injection but significantly reduced by AP-32 and A-RM supplementation. Altogether, the gait analysis results suggest that unilateral 6-OHDA injection into MFB impaired the gait function by decreasing the ability to move faster and further. But supplementation of AP-32, RM, and A-RM showed improvement of the gait function. Furthermore, supplementation of AP-32 and A-RM showed reduced left pair lag compared to the untreated PD group (**Figure 3G**). This result is corresponded with the preserved TH + level in AP-32 and A-RM-treated group, suggesting that unilateral 6-OHDA injection induced asymmetry gait dysfunction and both supplementations could alter the dysfunction.

Supplementation of Probiotic *L. salivarius* AP-32, Prebiotic RM, and Combination A-RM Restored Mitochondrial Function and Energy Metabolism

Mitochondrial Function Analysis

Mitochondrial function was evaluated in the brain and soleus muscle through measuring OCR and ECAR. In the brain, including striatum and SNc, mitochondrial function was decreased in the untreated PD group, marked by decreases in OCR and ECAR (**Figures 4A,B**). However, supplementation of AP-32 and A-RM in-creased OCR and ECAR. Group treated with L-DOPA and RM only showed an in-crease in ECAR and not in OCR. Supplementation of AP-32 significantly showed the highest OCR and ECAR in the brain compared to RM and A-RM, indicating that AP-32 could improve mitochondrial function in the brain better than RM and A-RM. This is consistent with TH immunohistochemistry results that show AP-32 exerted the best neuroprotective effect among all supplementation groups. Subsequently, the untreated PD group shows a decrease in mitochondrial function in the soleus muscles as evaluated by OCR and ECAR values (**Figures 4C,D**). Supplementation of AP-32, RM, and A-RM could reverse the decreases induced by 6-OHDA, with AP-32 showed the best results. The OCR and ECAR results in the brain and soleus muscle further supported an evidence that AP-32 exerted better effects than RM and A-RM.

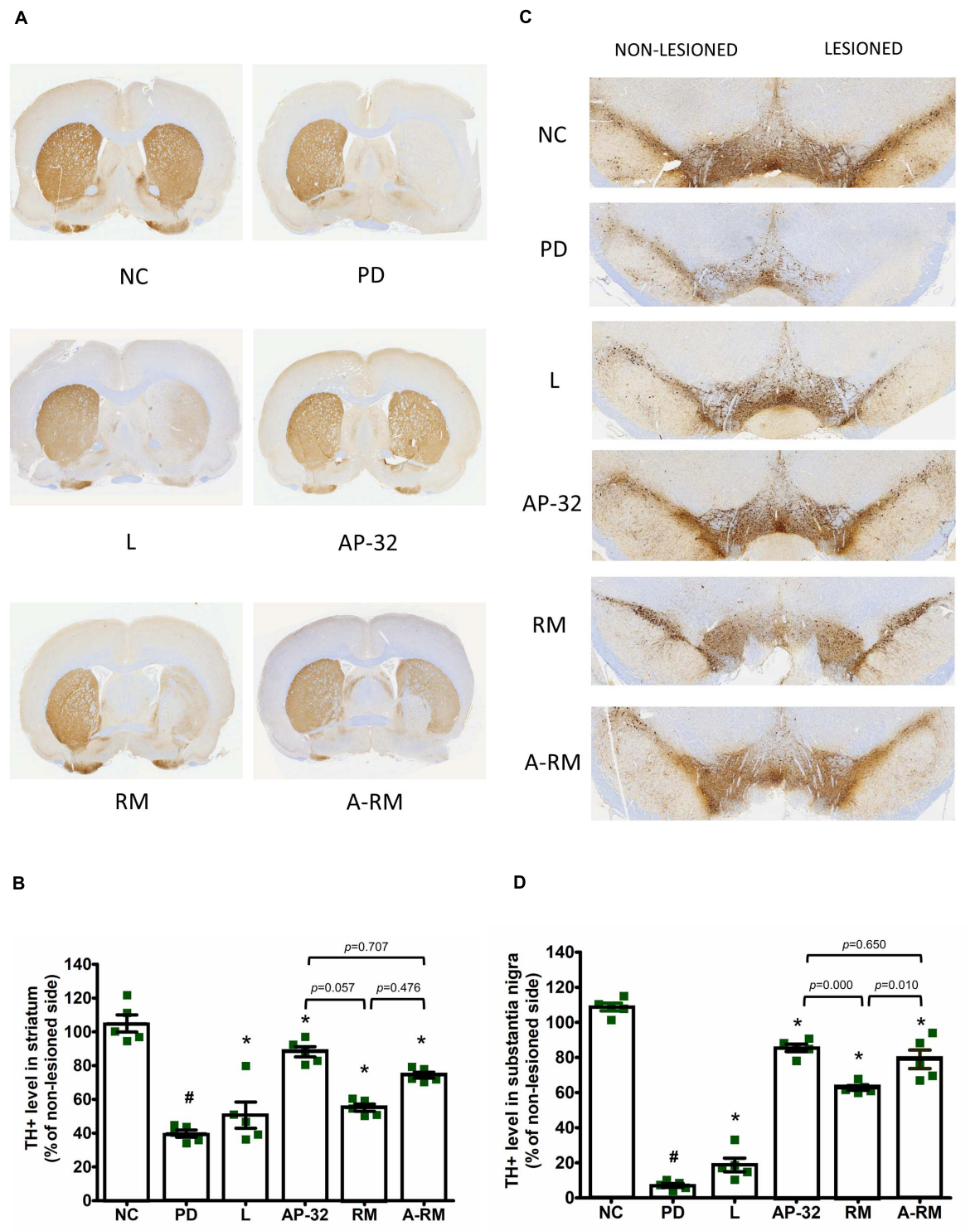

FIGURE 2 | Supplementation of AP-32, RM, and A-RM rescued the 6-OHDA-mediated reduction of dopaminergic neurons in the striatum and substantia nigra pars compacta (SNc) after 8-weeks of supplementations. **(A)** A representative of the immunohistochemical staining for TH (dopaminergic neuron marker) in the striatum. **(B)** Quantitative analysis of the number of TH-positive cells in the striatum. **(C)** A representative of the immunohistochemical staining for TH in SNc. **(D)** Quantitative analysis of the number of TH-positive cells in the SNc. The intensity of the lesioned side was standardized with the non-lesioned side and reported as mean ± SEM (n = 5 rats/group). #$p < 0.05$ PD group compared to NC group. *$p < 0.05$ L, AP-32, RM, and A-RM groups compared to PD group. Data were evaluated by one-way ANOVA with Tukey's *post hoc* test.

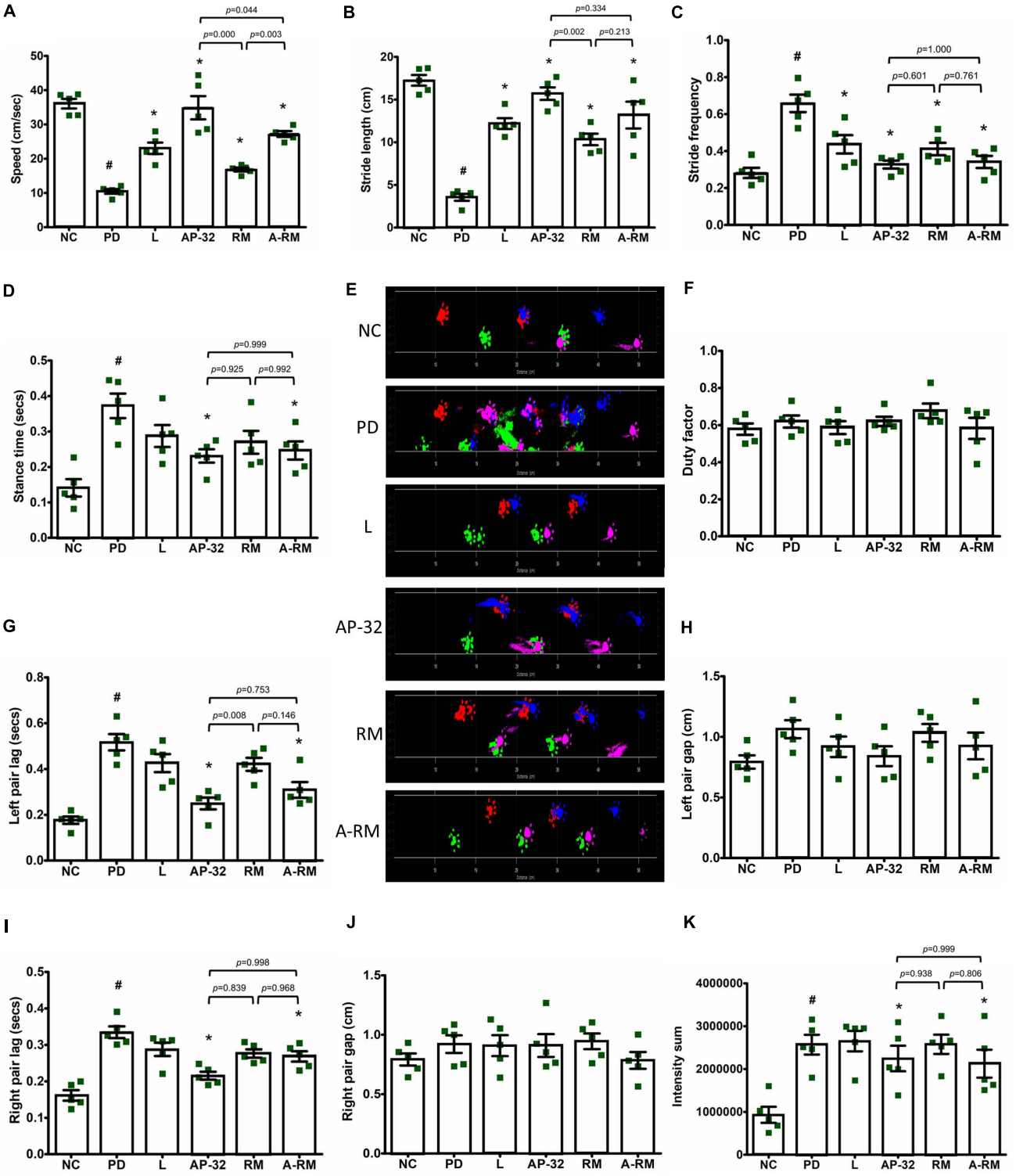

FIGURE 3 | Dynamic parameters for gait analysis in 6-OHDA-induced PD rats. **(A)** Speed started from entering until leaving the walkway. **(B)** Stride length. **(C)** Stride frequency. **(D)** Stance time. **(E)** Section from original footprints recorded after 8-weeks supplementations; pink, front left; blue, front right; green, hind left; red, hind right. **(F)** Duty factor. **(G)** Left pair lag. **(H)** Left pair gap. **(I)** Right pair lag. **(J)** Right pair gap. **(K)** Intensity sum. All data are expressed as mean ± SEM (n = 5 rats/group). $^{\#}p < 0.05$ PD group compared to NC group. $^{*}p < 0.05$ L, AP-32, RM, and A-RM groups compared to PD group. Data were evaluated by one-way ANOVA with Tukey's *post hoc* test.

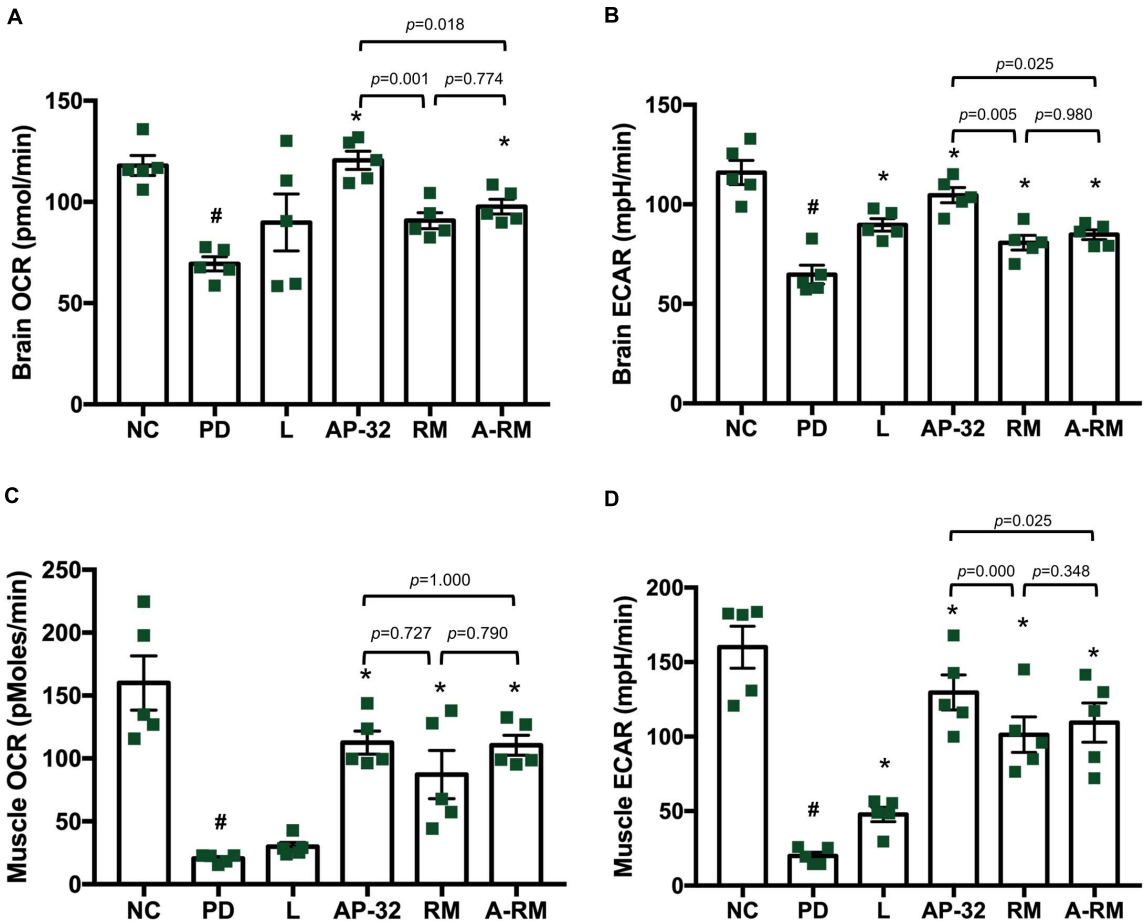

FIGURE 4 | The effect of AP-32, RM, and A-RM on mitochondrial function in the brain and soleus muscle after 8-weeks of supplementation. Mitochondrial function was evaluated by basal mitochondria respiration, oxygen consumption rate (OCR), and basal glycolysis rate, and basal extracellular acidification flux (ECAR). **(A,B)** The mitochondrial activates in the brain, including striatum and SNc. **(C,D)** The mitochondrial actives in the soleus muscle. All data are expressed as mean ± SEM (n = 5 rats/group). #$p < 0.05$ PD group compared to NC group. *$p < 0.05$ L, AP-32, RM, and A-RM groups compared to PD group. Data were evaluated by one-way ANOVA with Tukey's *post hoc* test.

BW Gain, Food Consumption Efficiency (FCE), Water Intake, and Body Composition

The BW of the rats was observed after 6-OHDA injection. Each group gained BW during the experiment period. However, the untreated PD group showed less BW gain than other groups (**Table 3**). Probiotic *L. salivarius* AP-32 and combination A-RM treatment group showed significantly higher BW gain than the untreated PD group. The supplementation of AP-32 for 8 weeks also resulted in greater BW gain than RM and A-RM. It indicated that AP-32 could prevent BW loss better than RM and A-RM.

There is no significant difference in water and food intake between groups (**Table 3**). The untreated PD group shows the lowest FCE compared to other groups. These results indicated

TABLE 3 | The effect of AP-32, RM, and A-RM on BW gain, food intake, food conversion efficiency, and water intake in 6-OHDA-induced PD rats.

Parameter	NC	PD	L	AP-32	RM	A-RM
BW gain (g)/rat	320.2 ± 9.5	127.6 ± 14.2$^{\#}$	200.8 ± 14.7*	295.0 ± 25.4*	227.6 ± 8.5*$^{\$}$	250.4 ± 14.7*$^{\$}$
Food intake (Kcal)/day/rat	112.8 ± 14.4	101.4 ± 9.2	107.1 ± 9.3	105.0 ± 7.7	103.5 ± 8.4	102.8 ± 6.9
FCE (%)	2.9 ± 0.3	1.3 ± 0.2$^{\#}$	1.9 ± 0.2*	2.8 ± 0.3*	2.2 ± 0.2*$^{\$}$	2.4 ± 0.1*
Water intake (ml)/day/rat	34.2 ± 2.7	33.9 ± 1.4	34.2 ± 1.7	34.9 ± 2.1	32.3 ± 3.2	34.3 ± 2.6

Data are expressed mean ± SEM (n = 5 rats/group). #*p < 0.05 PD group compared to NC group.* **p < 0.05 L, AP-32, RM, and A-RM groups compared to PD group.* $^{\$}$*p < 0.05 RM and A-RM groups compared to AP-32 group. One-way ANOVA with Tukey's post hoc test. BW, Bodyweight; FCE, Food Consumption Efficiency (an increase of BW/total calorie intake).*

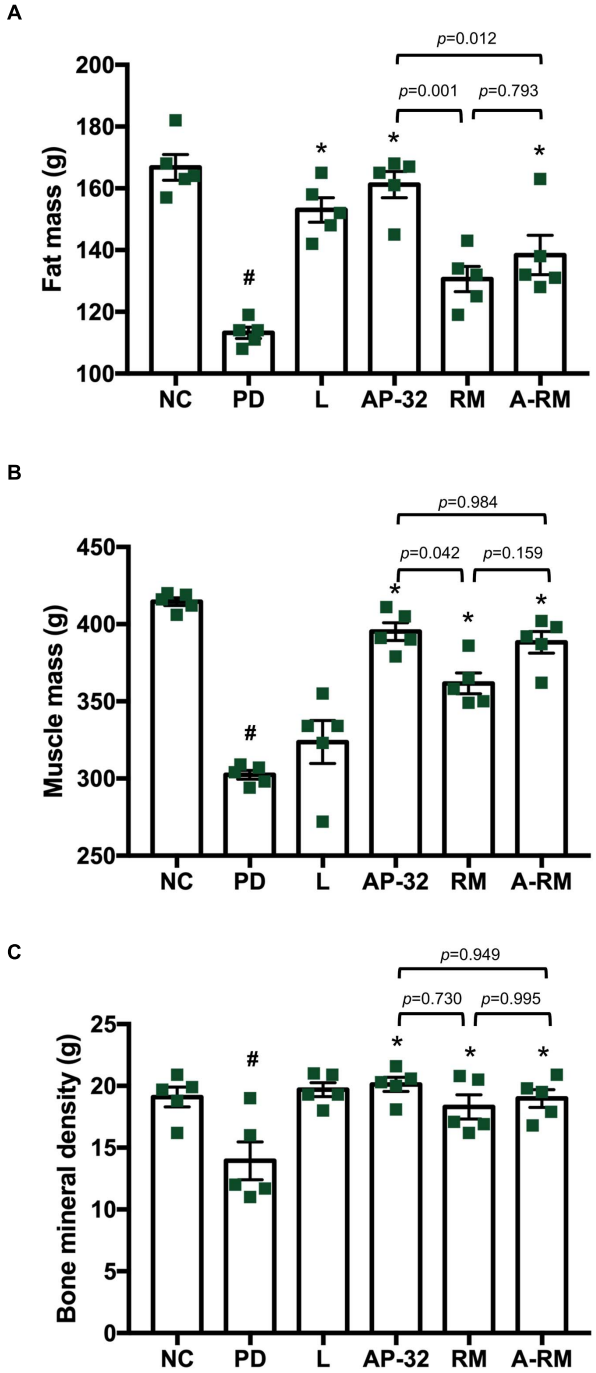

FIGURE 5 | Body composition of rats after 8 weeks of treatments. Body composition was evaluated by Dual-Energy X-Ray Absorptiometry (DXA), which includes **(A)** fat mass, **(B)** muscle mass, and **(C)** bone mineral density. All data are expressed as mean ± SEM (n = 5 rats/group). $^{*}p < 0.05$ compared to PD group. Data were evaluated by one-way ANOVA with Tukey's *post hoc* test. $^{\#}p < 0.05$ PD group compared to NC group.

that probiotic AP-32, prebiotic RM, and combination A-RM could increase the efficiency of food consumption and attenuate BW loss induced by 6-OHDA.

Consistent with BW declines, body composition measured through DXA (**Figure 5**) showed that the untreated PD group had lower total fat mass, muscle mass, and bone mineral density than the healthy group. Supplementation of probiotic AP-32 and RM prevented the decreases, with AP-32 performed the best among all treatments, followed by A-RM and RM. Muscle mass was preserved in groups treated with AP-32, RM, and RM, indicating their ability to prevent muscle atrophy in 6-OHDA-induced PD rats. Together, these results suggest that AP-32, RM, and A-RM could prevent BW loss, increase FCE, and maintain body composition, with AP-32 showed the best result among supplementation groups. Here we also observed significant increases of fat mass and bone mineral density mass, but not muscle mass in L-DOPA-treated group.

Supplementation of Probiotic *L. salivarius* AP-32 Enhanced Antioxidative Enzyme Activities

Serum antioxidative enzyme activities of GPx and SOD were decreased in 6-OHDA-induced PD groups (**Figure 6**). Treatment of AP-32, RM, A-RM, and L-DOPA significantly increased GPx activity in serum. However, only the PD group treated with AP-32 showed significant improvement in SOD activity. The combination of AP-32 and RM could not exert the similar effects exerted by supplementation of AP-32 alone. It suggests that AP-32 was the better supplement in increasing antioxidative enzyme activities compared to RM and A-RM. The results are also consistent with results of TH immunohistochemistry and gait function evaluation which indicate that AP-32 performed the best among all treatments.

The Fecal SCFAs Were Increased by Supplementation of Probiotic *L. salivarius* AP-32, Prebiotic RM, and Combination A-RM

Induction of PD with 6-OHDA neurotoxin reduced microbial metabolites, SCFAs, in fecal samples (**Table 4**). Supplementation of AP-32, RM, and their combination (A-RM) elevated SCFAs. AP-32, RM, and A-RM supplementations showed significantly higher total acid, propionic acid, and butyric acid than the untreated PD group. Isovaleric acid only increased by supplementation of AP-32 and RM. Meanwhile, isobutyric acid only elevated in the group supplemented with AP-32. Among all supplementation group, AP-32 showed slightly higher isobutyric acid, butyric acid, and valeric acid.

DISCUSSION

In this study, we found that the 8-week supplementation of probiotic [*Lactobacillus salivarius* subsp. *salicinius* AP-32 (AP-32)], prebiotic [residual medium (RM)], and the symbiotic [combination of AP-32 and RM (A-RM)] significantly prevented dopaminergic neuron loss along with improved motor function in PD rats. Along with their neuroprotective effects, the supplementations induced marked increase in the following:

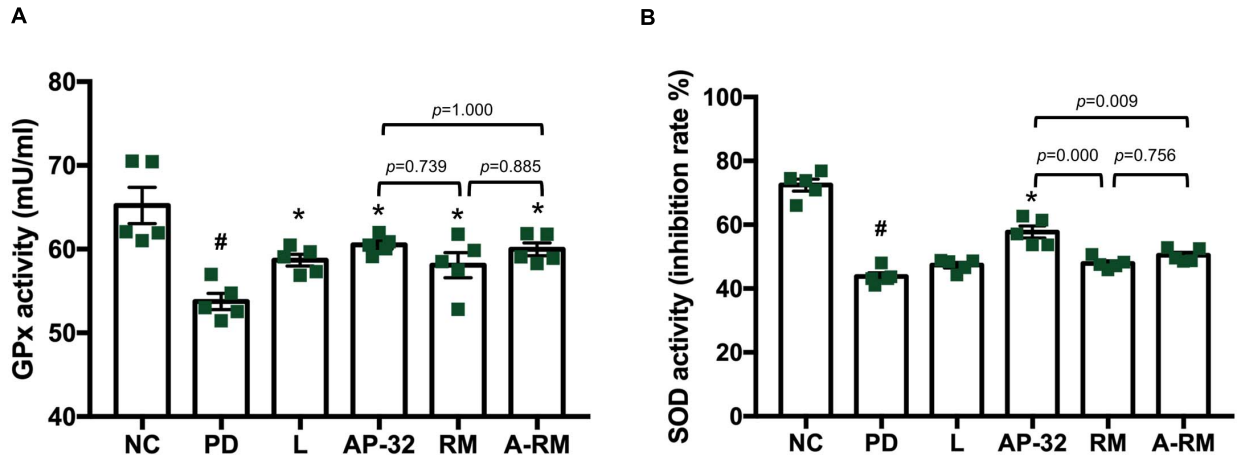

FIGURE 6 | The effect of AP-32, RM, and ARM on antioxidative enzyme activities in serum. **(A)** Glutathione peroxidase (GPx) activity, **(B)** superoxide dismutase (SOD) activity. Data are expressed as mean ± SEM (n = 5 rats/group). #$p < 0.05$ PD group compared to NC group. *$p < 0.05$ L, AP-32, RM, and A-RM groups compared to PD group. All data were evaluated by one-way ANOVA with Tukey's *post hoc* test.

TABLE 4 | The effect of AP-32, RM, and A-RM on fecal SCFAs profiles after 8 weeks of treatments.

SCFAs (mM)	NC	PD	L	AP-32	RM	A-RM
Total acid	6.43 ± 0.64	4.48 ± 1.37#	5.38 ± 1.28	6.39 ± 0.42*	6.42 ± 0.87*	6.50 ± 1.73*
Acetic acid	4.33 ± 0.61	3.63 ± 1.36	3.99 ± 0.92	4.49 ± 0.53	4.96 ± 0.79	4.92 ± 0.90
Propionic acid	1.06 ± 0.06	0.58 ± 0.16#	0.95 ± 0.12*	0.93 ± 0.10*	1.00 ± 0.07*	1.16 ± 0.37*
Isobutyric acid	0.03 ± 0.01	0.03 ± 0.00	0.03 ± 0.01	0.05 ± 0.01*	0.04 ± 0.02	0.04 ± 0.01
Butyric acid	1.80 ± 0.13	0.54 ± 0.11#	0.90 ± 0.38	1.57 ± 0.38*	1.23 ± 0.21*	1.21 ± 0.61*
Isovaleric acid	0.02 ± 0.00	0.01 ± 0.00	0.01 ± 0.01	0.03 ± 0.01*	0.03 ± 0.01*	0.02 ± 0.00
Valeric acid	0.08 ± 0.01	0.06 ± 0.01	0.05 ± 0.01	0.07 ± 0.02	0.05 ± 0.03	0.05 ± 0.02

*Data are expressed as mean ± SEM (n = 5 rats/group). #p < 0.05 PD group compared to NC group. *p < 0.05 L, AP-32, RM, and A-RM groups compared to PD group. There is no significant difference between AP-32, RM, and A-RM. One-way ANOVA with Tukey's post hoc test. SCFAs, short-chain fatty acids.*

mitochondrial activities and glycolysis in the brain and muscle, antioxidative enzymes activities in the serum, and altered SCFAs profile in fecal samples. We noted that the supplementations also resulted in restoration of muscle mass and accompanied improvement of motor function. Overall, the supplementations were found to prevent the 6-OHDA-induced progression of PD and its associated symptoms, where AP-32 supplementation was found to yield the best results. The probiotic supplementation could play as an active modulator in regulating the onset of motor deficit progression in unilateral 6-OHDA-induced PD rats. The possible neurorestoration molecular pathway of probiotic is shown in **Figure 7**.

From our understanding, there could be two possible pathways underlying the neuroprotective effects of probiotic AP-32, prebiotic RM, and symbiotic A-RM. First, the increases of mitochondrial activities and glycolysis (**Figure 4**) by supplementation of probiotic AP-32, prebiotic RM, and symbiotic A-RM might increase energy metabolism in the brain and muscle, thus prevented the loss of dopaminergic neurons (**Figure 2**) and muscle atrophy (**Figure 5**). Second, the modulation of the SCFAs production (**Table 4**) and increase in antioxidative enzyme activities (**Figure 6**) induced by these supplementations might have played a vital role in protecting the mitochondria against reactive oxygen species (ROS).

Neurodegenerative diseases, like PD, have been associated with impaired energy metabolism in the brain, which results in excessive neuronal deaths. Mitochondrial respiration and glycolysis are the two important metabolic pathways during energy metabolism in neurons. In a PD brain, mitochondrial electron transport chain reaction in tricarboxylic acid (TCA) cycle is known to malfunction, which results in decreased mitochondrial respiration (Schapira et al., 1990). Also, the reduction in glycolysis process is associated with many of neurodegenerative diseases. Dysfunctions in mitochondrial respiration and glycolysis reduction lead to declined ATP production (Tait and Green, 2013). As neurons are high energy demanding cells (Verstreken et al., 2005), the deficit in energy production and high energy demand can lead to energy starvation in the neurons, impairing their function and eventual death via apoptotic pathway (Tait and Green, 2013). In this study, we found that there were increases in mitochondrial respiration activities and glycolysis in the brain and muscle of rats supplemented with probiotic AP-32, prebiotic RM, and symbiotic A-RM (**Figure 4**). Thus, our findings indicate that these supplements might facilitate the modulation of energy metabolism for meeting the energy demand in the brain and muscles, which might have prevented the dopaminergic neuron loss and muscle atrophy.

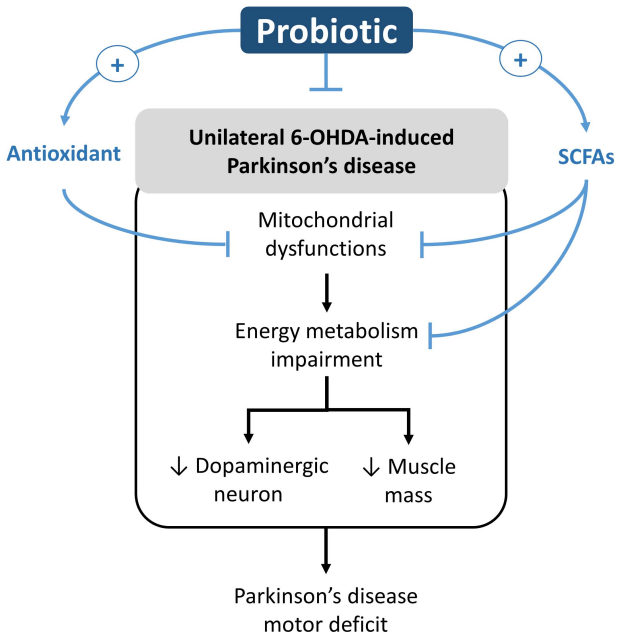

FIGURE 7 | Potential neurorestoration molecular pathway of probiotic in facilitating recovery of motor deficit in unilateral 6-OHDA-induced Parkinson's disease.

Mitochondrial dysfunctions can lead to increased oxidative stress from the generation of ROS, such as superoxide anion and hydrogen peroxide. This can further increase neuronal deaths, a characteristic typically found in neurodegenerative diseases (Shukla et al., 2011; Federico et al., 2012; Subramaniam and Chesselet, 2013). In normal conditions, antioxidants such as SOD and GPx are innately produced to neutralize the oxidative stress. However, in the pathological state of PD, neurons fail to produce sufficient levels of antioxidants to counterbalance the ROS (Di Pietro et al., 2014; Cho et al., 2016; Feuerstein et al., 2016). The cumulative increase of oxidative stress damages the mitochondria and interferes with the energy production process (Shukla et al., 2011). Therefore, restoring the balance between ROS and antioxidants can be crucial for preventing the damage in dopaminergic neurons of PD (Shukla et al., 2011; Poewe et al., 2017). In our study, we observed that 6-OHDA decreased oxidative stress-related antioxidant enzymes, SOD and GPx, in the serum (**Figure 6**). However, long-term supplementation of probiotic AP-32 resulted in increase of SOD and GPx activity levels in the serum of 6-OHDA treated rats. The increase of serum antioxidant enzymes indicates that these supplementations could indirectly have a protective effect against ROS to decrease oxidative stress in the brain (Cho et al., 2016). It was observed that prebiotic RM and symbiotic A-RM could only significantly elevate GPx level. The results thus indicate that supplementing pure AP-32 can generate a better antioxidant production capacity *in vivo* than only supplementing the prebiotic metabolites (RM) extracted from its culture.

Upon analyzing the fecal samples obtained from the rats, it was determined that the probiotic AP-32, prebiotic RM, and symbiotic A-RM supplementation altered the SCFAs levels in the rodent's gut (**Table 4**). SCFAs (e.g., acetate, propionate, and butyrate) generated from fermentation by gut microbiota in the large intestine are known to exert antioxidant properties, immunomodulatory function, and regulate energy metabolism (Koh et al., 2016; Schonfeld and Wojtczak, 2016; LeBlanc et al., 2017). The observed increases of butyric acid and propionic acid are likely to be involved in the elevation of antioxidative enzymes (SOD and GPx) in the group treated with AP-32 (and increase of GPx in RM and A-RM group). This suggests that AP-32 might reduce oxidative stress by increasing host antioxidant enzyme activities. Probiotics can decrease oxidative stress by producing anti-oxidative enzymes, stimulating antioxidant metabolites (e.g., folate, glutathione), up-regulate host anti-oxidative enzymes activities, trigger other signaling pathways (e.g., NFkB, PKC, MAPK, Nrf2), and down-regulate ROS-producing enzymes activities (Wang et al., 2017). Also, the antioxidant capacity induced by SCFAs might be involved in counteracting the mitochondria-destroying oxidative stress prevailing in a PD brain. With reduced oxidative stress, mitochondria could function properly to supply energy in the brain and muscles, supported by the finding of increased OCR and ECAR in the PD group treated with AP-32, RM, and A-RM (**Figures 4A,B**). In addition, SCFAs could up-regulate energy metabolism in the brain and muscle by serving as energy substrates (Lei et al., 2016; Schonfeld and Wojtczak, 2016; LeBlanc et al., 2017). Specifically, butyric acid is known to enhance mitochondrial activity by increasing oxygen consumption and glucose uptake (Clark and Mach, 2017), which could facilitate enhanced energy utilization in the brain. Thus, the prevention of dopaminergic neurons loss in striatum and SNc along with reduced of motor dysfunction could be a synergistic effect originating from the enhanced anti-oxidative enzymes, improved mitochondria activities, and up-regulated energy utilization in the brain and muscles.

We also noted that AP-32, RM, and A-RM supplementation prevented the 6-OHDA induced loss of bodyweight (**Table 3**), muscle atrophy, and bone density deprivation (**Figure 5**) in rats. The reduced muscle atrophy in the soleus muscle was also accompanied with improved gait function evaluated by the Catwalk-gait test (**Figure 3**). Supplementation of AP-32, RM, and A-RM increased mitochondrial function in soleus muscle (**Figures 4C,D**). Several studies have described that PD patients also suffer from loss of bodyweight, muscle atrophy and concomitant impairments in motor functions (Garber and Friedman, 2003; Falvo et al., 2008; Stevens-Lapsley et al., 2012). There is also a known association between PD progression and decreased bone density (Handa et al., 2019). Consistent with these findings, our 6-OHDA treated rats reproduced the marked decreases in muscle mass and bodyweight (Kim and Choe, 2010; Choe et al., 2011, 2012; Minalyan et al., 2019) as well as bone density (Ali et al., 2019; Handa et al., 2019) in neurotoxin-induced PD animal model. Supplementation of the probiotic AP-32 prevented muscle atrophy, weight loss, and bone density deprivation, without affecting the food and water consumption behavior in the rats (**Table 3**). These effects by AP-32 and RM might rely on their capacity to modulate gut microbiota composition and microbiota metabolites. Supplementation of

AP-32 might favor the commensal bacteria inside the intestine and their metabolites, which influence energy production, redox balance, immune response, and mitochondrial biogenesis (Clark and Mach, 2017). Increases in SCFAs production could up-regulate energy metabolism in the muscle by serving as energy substrates (Newman and Verdin, 2014; Kesl et al., 2016; Lei et al., 2016). Butyric acid enhances mitochondrial activity by increasing oxygen consumption and glucose uptake (Gao et al., 2009), which could increase energy supply in the muscle. The up-regulation of mitochondria and energy utilization indicates the ability of probiotic AP-32 and its RM in preventing body weight loss and muscle atrophy (Gao et al., 2009; Hock and Kralli, 2009). This restored muscle mass might also contribute to the improvement of motor function (Visser et al., 2005; Curcio et al., 2016). Regarding restored bone density in groups supplemented with AP-32, RM, and A-RM, it might also be another benefit of an increase in SCFAs production upon AP-32 and RM supplementation. SCFAs are known to protect bone density mass through downregulation osteoclastogenesis and bone resorption (Lucas et al., 2018). Additionally, SCFAs can increase the absorption of calcium, which is important in bone formation, through calcium and hydrogen exchange in the gut (Trinidad et al., 1996).

In this study, we found that supplementation of bacterial RM and A-RM could also reduce dopaminergic neuron loss, motor dysfunctions, and muscle atrophy, along with increased GPx and fecal SCFAs. The observed increases of propionic acid and butyric acid in PD groups supplemented with RM and A-RM could enhance antioxidant capacity (Koh et al., 2016; Schonfeld and Wojtczak, 2016), as seen in elevated serum GPx activity. As the RM contained SCFAs and various amino acids, including branched-chain amino acids (BCAAs) (**Supplementary Table 1**), the BCAAs can increase mitochondrial energy production rate and mitochondrial DNA abundance (Tatpati et al., 2010), which might explain the increase in mitochondrial activity. Thus, supplementation of RM and A-RM could also preserve dopaminergic neuron and muscle mass, possibly through enhancing GPx, SCFAs, and energy metabolism.

Although all supplementation groups showed significant neuroprotective effects, but from the Catwalk results, SOD activity, bodyweight and mitochondrial activities, AP-32 showed the best results compared to RM and A-RM groups. After comparing the protective effects of AP-32 and A-RM, we concluded that AP-32 has a better performance on Catwalk results (**Figure 3**), SOD activity (**Figure 6**), bodyweight (**Table 3**) and mitochondrial activities (**Figure 4**). Only the speed parameter was found to significantly decrease in RM and A-RM while the other parameters also followed the same trend but no significant difference. From those observations, it appears that RM may affect the function of AP-32. It needs more experiment to gain more deep understanding the interaction between AP-32 and RM.

Here we also observed effects of L-DOPA treatment on serum GPx activity ECAR in the brain and soleus muscle, fat mass, and bone mineral density. L-DOPA has been described to exert antioxidative effects (Han et al., 1996; Exner et al., 2003; Jodko-Piórecka and Litwinienko, 2015; Recky et al., 2021), including glutathione (Zhu et al., 2020). The upregulated GPx might affect the energy metabolism and bone mineral density. Further, previous study reported that L-DOPA administration could increase relative 2-deoxyglucose uptake in unilateral 6-OHDA injected substantia nigra pars reticulata rats (Trugman and Wooten, 1986). This result might explain our observation shown in **Figures 4B,D** because L-DOPA could increase relative 2-deoxyglucose uptake which might increase the glucose utilization in SNc. The result presented in this study is also supported by Adams et al. (2008) in which they reported levodopa/benserazide treatment increased lactate and pyruvate accumulation in human skeletal muscle, along with reduced lactate-to-pyruvate ratio, indicating increased aerobic glycolysis. Since L-DOPA can inhibit glycogen synthesis, then the decreased glycogen synthase could result in intracellular accumulation of glucose-6-phosphate (G6P) (Smith et al., 2004). As the cell could not store it as glycogen, it might lead to glucose utilization pathway, glycolysis (increased ECAR). In adipose tissue, L-DOPA is known to decrease dialysate glycerol, which suggest lipolysis inhibition (Adams et al., 2008). It might explain the preserved fat mass in PD group treated with L-DOPA.

We observed significantly higher bone mineral density in L-DOPA-treated group than the PD group. This result is contradictive with previous studies which suggest L-DOPA treatment induces bone loss by increasing homocysteine (Hcy), catechol O-methyltransferase (COMT)-stimulated L-DOPA metabolite (Yasui et al., 2003; Gjesdal et al., 2006). However, Hcy-induced bone loss can be caused by oxidative stress that triggers osteoclastic bone resorption (Koh et al., 2006). In our data, L-group also show higher GPX activity than the PD group. The increase of GPX activity might reduce the oxidative stress and promote the osteoclastic bone resorption. Additionally, study by Wang et al. demonstrate that the protective effect of glutathione against 6-OHDA-induced bone marrow stromal cell death (Wang et al., 2011). Furthermore, dopamine deprivation can lead to bone loss in PD as the system failed to prevent hyperprolactinemia (Ali et al., 2019; Handa et al., 2019). In *in vivo* study by Handa et al. (2019), higher dose of L-DOPA indeed increased Hcy, suggesting that L-DOPA might affect bone density in dose-dependent manner.

Further experiments are required to establish a more direct mechanism in the brain with respect to the AP-32, RM, and A-RM effects, including gut microbiota composition. Our ongoing study is now focused on the effects of probiotics on gut function and gut microbiota composition alterations. In summary, long-term supplementation of AP-32 was found to be the best treatment for protecting dopaminergic neurons and improve motor functions in 6-OHDA-induced PD rats. This supplementation enhanced SCFAs in the gut along with increased anti-oxidative enzymes in the systemic system, which probably was responsible for the reduction of oxidative stress in the brain. The elevated production of these fatty acids in the gut could be responsible for the increased mitochondrial activities in the brain and muscles, and directly involved in increased energy utilization. Recovery of these functions possibly underlie the decreased dopaminergic neuron loss and muscle loss prevention leading to improved motor functions in 6-OHDA-induced PD rats.

CONCLUSION

The results obtained from our study reveal that long-term supplementation of probiotic *Lactobacillus salivarius* subsp. *salicinius* AP-32 (AP-32), prebiotic residual medium (RM) from AP-32 cultured medium, and their combination (A-RM) performed neuroprotective effects against dopaminergic neuron loss and motor dysfunction in a unilateral 6-OHDA-induced PD rat model. These supplementations increased mitochondrial activities and glycolysis which might increase energy metabolism in the brain and muscle, thus prevented dopaminergic neuron loss and muscle atrophy. Additionally, these supplementations modulated SCFAs production and increased antioxidative enzyme activities which might play important role in protecting mitochondria against reactive oxygen species (ROS). Supplementation of AP-32 showed the best performances among all supplementation groups. Therefore, AP-32 is the potential alternative as nutritional supplements in the treatment of PD. However, more detailed studies are required to investigate the mechanistic role of *Lactobacillus salivarius* subsp. *salicinius* AP-32 and prebiotic RM in attenuating PD progression.

DATA AVAILABILITY STATEMENT

The original contributions presented in the study are included in the article/**Supplementary Material**, further inquiries can be directed to the corresponding author/s.

ETHICS STATEMENT

The animal study was reviewed and approved by Taipei Medical University Animal Care and Use Committee of Panel (IACUC/IACUP) (approval no. LAC-2020-0183).

AUTHOR CONTRIBUTIONS

H-YH designed and supervised the experiments. BAN, S-PT, and BP performed the experiments. C-HW and P-SH contributed reagents, materials, and analysis platforms. BAN and S-PT analyzed the data. BAN, S-PT, H-YH, and T-HY interpreted the results. S-PT prepared the figures. BAN and H-YH drafted the manuscript. All authors have read and agreed to the published version of the manuscript.

FUNDING

This study was supported by the Taipei Medical University - New Professor Research grant (grant no. TMU108-AE1- B27), Taipei Medical University - University and Industry Collaboration Project (grant no. A-109-065). The authors also declare that this study received funding from Bioflag Biotech Co., Ltd., Tainan, Taiwan. The funder was not involved in the study design, collection, analysis, interpretation of data, the writing of this article or the decision to submit it for publication.

ACKNOWLEDGMENTS

The authors are grateful for the assistance of graduate students at the College of Kinesiology, the University of Taipei, for their technical assistance in conducting animal experiments.

SUPPLEMENTARY MATERIAL

The Supplementary Material for this article can be found online at: https://www.frontiersin.org/articles/10.3389/fnagi.2021.668775/full#supplementary-material

REFERENCES

Adams, F., Boschmann, M., Lobsien, E., Kupsch, A., Lipp, A., Franke, G., et al. (2008). Influences of levodopa on adipose tissue and skeletal muscle metabolism in patients with idiopathic parkinson's disease. *Eur. J. Clin. Pharmacol.* 64, 863–870. doi: 10.1007/s00228-008-0532-4

Ali, S. J., Ellur, G., Khan, M. T., and Sharan, K. (2019). Bone loss in MPTP mouse model of Parkinson's disease is triggered by decreased osteoblastogenesis and increased osteoclastogenesis. *Toxicol. Appl. Pharmacol.* 363, 154–163. doi: 10.1016/j.taap.2018.12.003

Bonfili, L., Cecarini, V., Berardi, S., Scarpona, S., Suchodolski, J. S., Nasuti, C., et al. (2017). Microbiota modulation counteracts Alzheimer's disease progression influencing neuronal proteolysis and gut hormones plasma levels. *Sci. Rep.* 7:2426. doi: 10.1038/s41598-017-02587-2

Cai, R., Zhang, Y., Simmering, J. E., Schultz, J. L., Li, Y. H., Fernandez-Carasa, I., et al. (2019). Enhancing glycolysis attenuates Parkinson's disease progression in models and clinical databases. *J. Clin. Invest.* 129, 4539–4549. doi: 10.1172/Jci129987

Castelli, V., D'Angelo, M., Lombardi, F., Alfonsetti, M., Antonosante, A., Catanesi, M., et al. (2020). Effects of the probiotic formulation SLAB51 in in vitro and in vivo parkinson's disease models. *Aging U.S.* 12, 4641–4659. doi: 10.18632/aging.102927

Cho, C. H., Kim, E. A., Kim, J., Choi, S. Y., Yang, S. J., and Cho, S. W. (2016). N-Adamantyl-4-methylthiazol-2-amine suppresses amyloid β-induced neuronal oxidative damage in cortical neurons. *Free Radic. Res.* 50, 678–690. doi: 10.3109/10715762.2016.1167277

Choe, M. A., An, G. J., Koo, B. S., and Jeon, S. (2011). Effect of DHEA on recovery of muscle atrophy induced by parkinson's disease. *J. Korean Acad. Nurs.* 41, 834–842. doi: 10.4040/jkan.2011.41.6.834

Choe, M. A., Koo, B. S., An, G. J., and Jeon, S. (2012). Effects of treadmill exercise on the recovery of dopaminergic neuron loss and muscle Atrophy in the 6-OHDA lesioned parkinson's disease rat model. *Korean J. Physiol. Pharmacol.* 16, 305–312. doi: 10.4196/kjpp.2012.16.5.305

Clark, A., and Mach, N. (2017). The crosstalk between the gut microbiota and mitochondria during exercise. *Front. Physiol.* 8:319. doi: 10.3389/fphys.2017.00319

Curcio, F., Basile, C., Liguori, I., Della-Morte, D., Gargiulo, G., Galizia, G., et al. (2016). Tinetti mobility test is related to muscle mass and strength in non-institutionalized elderly people. *Age* 38, 525–533. doi: 10.1007/s11357-016-9935-9

Di Pietro, V., Lazzarino, G., Amorini, A. M., Tavazzi, B., D'Urso, S., Longo, S., et al. (2014). Neuroglobin expression and oxidant/antioxidant balance after graded traumatic brain injury in the rat. *Free Radic. Biol. Med.* 69, 258–264. doi: 10.1016/j.freeradbiomed.2014.01.032

Exner, M., Hermann, M., Hofbauer, R., Kapiotis, S., and Gmeiner, B. M. (2003). Free and peptide-bound DOPA can inhibit initiation of low density lipoprotein oxidation. *Free Radic. Res.* 37, 1147–1156. doi: 10.1080/10715760310001595766

Falvo, M. J., Schilling, B. K., and Earhart, G. M. (2008). Parkinson's disease and resistive exercise: rationale, review, and recommendations. *Mov. Disord.* 23, 1–11. doi: 10.1002/mds.21690

Federico, A., Cardaioli, E., Da Pozzo, P., Formichi, P., Gallus, G. N., and Radi, E. (2012). Mitochondria, oxidative stress and neurodegeneration. *J. Neurol. Sci.* 322, 254–262. doi: 10.1016/j.jns.2012.05.030

Ferrante, R. J., Kubilus, J. K., Lee, J., Ryu, H., Beesen, A., Zucker, B., et al. (2003). Histone deacetylase inhibition by sodium butyrate chemotherapy ameliorates the neurodegenerative phenotype in Huntington's disease mice. *J. Neurosci.* 23, 9418–9427. doi: 10.1523/JNEUROSCI.23-28-09418.2003

Feuerstein, D., Backes, H., Gramer, M., Takagaki, M., Gabel, P., Kumagai, T., et al. (2016). Regulation of cerebral metabolism during cortical spreading depression. *J. Cereb. Blood Flow Metab.* 36, 1965–1977. doi: 10.1177/0271678x15612779

Franco-Robles, E., and López, M. G. (2015). Implication of fructans in health: immunomodulatory and antioxidant mechanisms. *Sci. World J.* 2015:289267. doi: 10.1155/2015/289267

Gao, Z. G., Yin, J., Zhang, J., Ward, R. E., Martin, R. J., Lefevre, M., et al. (2009). Butyrate improves insulin sensitivity and increases energy expenditure in mice. *Diabetes* 58, 1509–1517. doi: 10.2337/db08-1637

Garber, C. E., and Friedman, J. H. (2003). Effects of fatigue on physical activity and function in patients with Parkinson's disease. *Neurology* 60, 1119–1124. doi: 10.1212/01.wnl.0000055868.06222.ab

Gazerani, P. (2019). Probiotics for Parkinson's disease. *Int. J. Mol. Sci.* 20, 4121. doi: 10.3390/ijms20174121

Gjesdal, C. G., Vollset, S. E., Ueland, P. M., Refsum, H., Drevon, C. A., Gjessing, H. K., et al. (2006). Plasma total homocysteine level and bone mineral density – The Hordaland homocysteine study. *Arch. Int. Med.* 166, 88–94. doi: 10.1001/archinte.166.1.88

Granado-Serrano, A. B., Martín-Garí, M., Sánchez, V., Riart Solans, M., Berdún, R., Ludwig, I. A., et al. (2019). Faecal bacterial and short-chain fatty acids signature in hypercholesterolemia. *Sci. Rep.* 9:1772. doi: 10.1038/s41598-019-38874-3

Han, S.-K., Mytilineou, C., and Cohen, G. (1996). l-DOPA up-regulates glutathione and protects mesencephalic cultures against oxidative stress. *J. Neurochem.* 66, 501–510. doi: 10.1046/j.1471-4159.1996.66020501.x

Handa, K., Kiyohara, S., Yamakawa, T., Ishikawa, K., Hosonuma, M., Sakai, N., et al. (2019). Bone loss caused by dopaminergic degeneration and levodopa treatment in parkinson's disease model mice. *Sci. Rep.* 9:13768. doi: 10.1038/s41598-019-50336-4

Hock, M. B., and Kralli, A. (2009). Transcriptional control of mitochondrial biogenesis and function. *Annu. Rev. Physiol.* 71, 177–203. doi: 10.1146/annurev.physiol.010908.163119

Hoffer, B. J., Hoffman, A., Bowenkamp, K., Huettl, P., Hudson, J., Martin, D., et al. (1994). Glial-cell line-derived neurotrophic factor reverses toxin-induced injury to midbrain dopaminergic-neurons in-vivo. *Neurosci. Lett.* 182, 107–111. doi: 10.1016/0304-3940(94)90218-6

Hsieh, P. S., An, Y., Tsai, Y. C., Chen, Y. C., Chuang, C. J., Zeng, C. T., et al. (2013). Potential of probiotic strains to modulate the inflammatory responses of epithelial and immune cells in vitro. *N. Microbiol.* 36, 167–179.

Hsieh, T. H., Kuo, C. W., Hsieh, K. H., Shieh, M. J., Peng, C. W., Chen, Y. C., et al. (2020). Probiotics alleviate the progressive deterioration of motor functions in a mouse model of Parkinson's disease. *Brain Sci.* 10:206. doi: 10.3390/brainsci10040206

Jodko-Piórecka, K., and Litwinienko, G. (2015). Antioxidant activity of dopamine and L-DOPA in lipid micelles and their cooperation with an analogue of α-tocopherol. *Free Radic. Biol. Med.* 83, 1–11. doi: 10.1016/j.freeradbiomed.2015.02.006

Kalia, L. V., and Lang, A. E. (2015). Parkinson's disease. *Lancet* 386, 896–912. doi: 10.1016/s0140-6736(14)61393-3

Kaminska, K., Lenda, T., Konieczny, J., Czarnecka, A., and Lorenc-Koci, E. (2017). Depressive-like neurochemical and behavioral markers of parkinson's disease after 6-OHDA administered unilaterally to the rat medial forebrain bundle. *Pharmacol. Rep.* 69, 985–994. doi: 10.1016/j.pharep.2017.05.016

Kesl, S. L., Poff, A. M., Ward, N. P., Fiorelli, T. N., Ari, C., Van Putten, A. J., et al. (2016). Effects of exogenous ketone supplementation on blood ketone, glucose, triglyceride, and lipoprotein levels in Sprague-Dawley rats. *Nutr. Metab.* 13:9. doi: 10.1186/s12986-016-0069-y

Kim, Y., and Choe, M. A. (2010). Effect of decreased locomotor activity on hindlimb muscles in a rat model of parkinson's disease. *J. Korean Acad. Nurs.* 40, 580–588. doi: 10.4040/jkan.2010.40.4.580

Koh, A., De Vadder, F., Kovatcheva-Datchary, P., and Backhed, F. (2016). From dietary fiber to host physiology: Short-chain fatty acids as key bacterial metabolites. *Cell* 165, 1332–1345. doi: 10.1016/j.cell.2016.05.041

Koh, J. M., Lee, Y. S., Kim, Y. S., Kim, D. J., Kim, H. H., Park, J. Y., et al. (2006). Homocysteine enhances bone resorption by stimulation of osteoclast formation and activity through increased intracellular ROS generation. *J. Bone Miner. Res.* 21, 1003–1011. doi: 10.1359/jbmr.060406

LeBlanc, J. G., Chain, F., Martin, R., Bermudez-Humaran, L. G., Courau, S., and Langella, P. (2017). Beneficial effects on host energy metabolism of short-chain fatty acids and vitamins produced by commensal and probiotic bacteria. *Microb. Cell Fact.* 16:79. doi: 10.1186/s12934-017-0691-z

Lei, E., Vacy, K., and Boon, W. C. (2016). Fatty acids and their therapeutic potential in neurological disorders. *Neurochem. Int.* 95, 75–84. doi: 10.1016/j.neuint.2016.02.014

Lucas, S., Omata, Y., Hofmann, J., Böttcher, M., Iljazovic, A., Sarter, K., et al. (2018). Short-chain fatty acids regulate systemic bone mass and protect from pathological bone loss. *Nat. Commun.* 9:55. doi: 10.1038/s41467-017-02490-4

Maiti, P., Manna, J., and Dunbar, G. L. (2017). Current understanding of the molecular mechanisms in parkinson's disease: targets for potential treatments. *Transl. Neurodegener.* 6:28. doi: 10.1186/s40035-017-0099-z

Minalyan, A., Gabrielyan, L., Pietra, C., Taché, Y., and Wang, L. (2019). Multiple beneficial effects of ghrelin agonist, HM01 on homeostasis alterations in 6-hydroxydopamine model of parkinson's disease in male rats. *Front. Integr. Neurosci.* 13:13. doi: 10.3389/fnint.2019.00013

Monti, B., Gatta, V., Piretti, F., Raffaelli, S. S., Virgili, M., and Contestabile, A. (2010). Valproic acid is neuroprotective in the rotenone rat model of parkinson's disease: involvement of alpha-synuclein. *Neurotox. Res.* 17, 130–141. doi: 10.1007/s12640-009-9090-5

Newman, J. C., and Verdin, E. (2014). Ketone bodies as signaling metabolites. *Trends Endocrinol. Metab.* 25, 42–52. doi: 10.1016/j.tem.2013.09.002

Poewe, W., Seppi, K., Tanner, C. M., Halliday, G. M., Brundin, P., Volkmann, J., et al. (2017). Parkinson disease. *Nat. Rev. Dis. Primers* 3:17013. doi: 10.1038/nrdp.2017.13

Recky, J. R. N., Serrano, M. P., Dantola, M. L., and Lorente, C. (2021). Oxidation of tyrosine: antioxidant mechanism of L-DOPA disclosed. *Free Radic. Biol. Med.* 165, 360–367. doi: 10.1016/j.freeradbiomed.2021.01.037

Sanchez, B., Relova, J. L., Gallego, R., Ben-Batalla, I., and Perez-Fernandez, R. (2009). 1,25-Dihydroxyvitamin D3 administration to 6-hydroxydopamine-lesioned rats increases glial cell line-derived neurotrophic factor and partially restores tyrosine hydroxylase expression in substantia nigra and striatum. *J. Neurosci. Res.* 87, 723–732. doi: 10.1002/jnr.21878

Schapira, A. H., Cooper, J. M., Dexter, D., Clark, J. B., Jenner, P., and Marsden, C. D. (1990). Mitochondrial complex I deficiency in parkinson's disease. *J. Neurochem.* 54, 823–827. doi: 10.1111/j.1471-4159.1990.tb02325.x

Schonfeld, P., and Wojtczak, L. (2016). Short- and medium-chain fatty acids in energy metabolism: the cellular perspective. *J. Lipid Res.* 57, 943–954. doi: 10.1194/jlr.R067629

Sgroi, S., Kaelin-Lang, A., and Capper-Loup, C. (2014). Spontaneous locomotor activity and L-DOPA-induced dyskinesia are not linked in 6-OHDA parkinsonian rats. *Front. Behav. Neurosci.* 8:331. doi: 10.3389/fnbeh.2014.00331

Shukla, V., Mishra, S. K., and Pant, H. C. (2011). Oxidative stress in neurodegeneration. *Adv. Pharmacol. Sci.* 2011:572634. doi: 10.1155/2011/572634

Smith, A. M., Depp, C., Ryan, B. J., Johnston, G. I., Alegre-Abarrategui, J., Evetts, S., et al. (2018). Mitochondrial dysfunction and increased glycolysis in prodromal and early parkinson's blood cells. *Mov. Disord.* 33, 1580–1590. doi: 10.1002/mds.104

Smith, J. L., Ju, J. S., Saha, B. M., Racette, B. A., and Fisher, J. S. (2004). Levodopa with carbidopa diminishes glycogen concentration, glycogen synthase activity, and insulin-stimulated glucose transport in rat skeletal muscle. *J. Appl. Physiol.* 97, 2339–2346. doi: 10.1152/japplphysiol.01219.2003

Stevens-Lapsley, J., Kluger, B. M., and Schenkman, M. (2012). Quadriceps muscle weakness, activation deficits, and fatigue with parkinson disease.

Neurorehabil. Neural Repair 26, 533–541. doi: 10.1177/1545968311425925

Subramaniam, S. R., and Chesselet, M. F. (2013). Mitochondrial dysfunction and oxidative stress in parkinson's disease. *Prog. Neurobiol.* 106–107, 17–32. doi: 10.1016/j.pneurobio.2013.04.004

Sun, M. F., and Shen, Y. Q. (2018). Dysbiosis of gut microbiota and microbial metabolites in parkinson's disease. *Aging Res. Rev.* 45, 53–61. doi: 10.1016/j.arr.2018.04.004

Tait, S. W., and Green, D. R. (2013). Mitochondrial regulation of cell death. *Cold Spring Harb. Perspect. Biol.* 5:a008706. doi: 10.1101/cshperspect.a008706

Tatpati, L. L., Irving, B. A., Tom, A., Bigelow, M. L., Klaus, K., Short, K. R., et al. (2010). The effect of branched chain amino acids on skeletal muscle mitochondrial function in young and elderly adults. *J. Clin. Endocrinol. Metab.* 95, 894–902. doi: 10.1210/jc.2009-1822

Trinidad, T., Wolever, T., and Thompson, L. (1996). Effect of acetate and propionate on Ca absorption from the rectum and distal colon of humans. *Am. J. Clin. Nutr.* 63, 574–578. doi: 10.1093/ajcn/63.4.574

Trugman, J. M., and Wooten, G. F. (1986). The effects of L-DOPA on regional cerebral glucose utilization in rats with unilateral lesions of the substantia nigra. *Brain Res.* 379, 264–274. doi: 10.1016/0006-8993(86)90780-8

Unger, M. M., Spiegel, J., Dillmann, K. U., Grundmann, D., Philippeit, H., Burmann, J., et al. (2016). Short chain fatty acids and gut microbiota differ between patients with parkinson's disease and age-matched controls. *Parkinson. Relat. Disord.* 32, 66–72. doi: 10.1016/j.parkreldis.2016.08.019

Verstreken, P., Ly, C. V., Venken, K. J., Koh, T. W., Zhou, Y., and Bellen, H. J. (2005). Synaptic mitochondria are critical for mobilization of reserve pool vesicles at *Drosophila* neuromuscular junctions. *Neuron* 47, 365–378. doi: 10.1016/j.neuron.2005.06.018

Visser, M., Goodpaster, B. H., Kritchevsky, S. B., Newman, A. B., Nevitt, M., Rubin, S. M., et al. (2005). Muscle mass, muscle strength, and muscle fat infiltration as predictors of incident mobility limitations in well-functioning older persons. *J. Gerontol. Series A Biol. Sci. Med. Sci.* 60, 324–333. doi: 10.1093/gerona/60.3.324

Wang, H. H., Luo, W. F., Wang, X. X., Qin, X. L., and Bao, S. Y. (2011). Reduced glutathione alleviates the toxic effect of 6-hydroxydopamine on bone marrow stromal cells. *Neural Regen. Res.* 6, 1691–1695. doi: 10.3969/j.issn.1673-5374.2011.22.002

Wang, Y., Wu, Y., Wang, Y., Xu, H., Mei, X., Yu, D., et al. (2017). Antioxidant properties of probiotic bacteria. *Nutrients* 9:521. doi: 10.3390/nu9050521

Yasui, K., Nakaso, K., Kowa, H., Takeshima, T., and Nakashima, K. (2003). Levodopa-induced hyperhomocysteinaemia in parkinson's disease. *Acta Neurol. Scandinav.* 108, 66–67. doi: 10.1034/j.1600-0404.2003.00135.x

Zhu, J., Sun, L., Zhang, L., Wang, H., Fan, A., Yang, B., et al. (2020). Prevalence and influencing factors of anxiety and depression symptoms in the first-line medical staff fighting against COVID-19 in gansu. *Front. Psychiatry* 11:386. doi: 10.3389/fpsyt.2020.00386

Conflict of Interest: P-SH was employed by the company Bioflag Biotech Co., Ltd., Tainan City, Taiwan.

The remaining authors declare that the research was conducted in the absence of any commercial or financial relationships that could be construed as a potential conflict of interest.

frontiers in Aging Neuroscience

ORIGINAL RESEARCH
published: 11 June 2021
doi: 10.3389/fnagi.2021.680672

Subjective Cognitive Decline May Be Associated With Post-operative Delirium in Patients Undergoing Total Hip Replacement: The PNDABLE Study

Xu Lin[1†], *Fanghao Liu*[1†], *Bin Wang*[1†], *Rui Dong*[2], *Lixin Sun*[1], *Mingshan Wang*[1] and *Yanlin Bi*[1*]

[1] Department of Anesthesiology, Qingdao Municipal Hospital Affiliated to Qingdao University, Qingdao, China, [2] Department of Anesthesiology, Nanjing Drum Tower Hospital, Nanjing, China

Objective: Subjective cognitive decline (SCD) is associated with an increased risk of clinical cognitive disorders. Post-operative delirium (POD) is a common complication after total hip replacement. We aimed to investigate the relationship between SCD and POD in patients undergoing total hip replacement.

Methods: Our study recruited 214 cognitively intact individuals from the Perioperative Neurocognitive Disorder And Biomarker Lifestyle (PNDABLE) study in the final analysis. SCD was diagnosed with Subjective Cognitive Decline Scale (SCDS), Mini-Mental State Examination (MMSE), and Montreal Cognitive Assessment (MoCA). The incidence of POD was evaluated by using Confusion Assessment Method (CAM), and POD severity was measured by using the Memorial Delirium Assessment Scale (MDAS). Preoperative cerebrospinal fluid (CSF) Aβ40, Aβ42, T-tau, and P-tau levels were measured by enzyme-linked immune-sorbent assay (ELISA).

Results: Overall, the incidence of POD was 26.64% (57/214), including 32.43% (36/111) in the SCD group and 20.39% (21/103) in the NC group. With the increase of age, the incidence of POD in all age groups increased ($P < 0.05$). Logistic regression analysis showed that after adjusting for SCD, Aβ42, Aβ40, P-tau, and T-tau, SCD (OR 2.32, CI 1.18–4.55, $P = 0.01$) and the increased CSF level of P-tau (OR 1.04, CI 1.01–1.06, $P < 0.001$) were risk factors for POD, while the level of aβ42 (OR 0.99, CI 0.99–1.00, $P < 0.001$) was a protective factor for POD.

Conclusion: SCD is one of the preoperative risk factors for POD.

Clinical Trial Registration: This study was registered at China Clinical Trial Registry (Chictr200033439).

Keywords: subjective cognitive decline, post-operative delirium, total hip replacement, cerebrospinal fluid, biomarker

OPEN ACCESS

Edited by:
Kristine Freude,
University of Copenhagen, Denmark

Reviewed by:
Heidi Lindroth,
Mayo Clinic, United States
Lingling Sun,
Shenzhen Sixth People's Hospital, China

***Correspondence:**
Yanlin Bi
pndable2021@sina.com

[†] These authors have contributed equally to this work

Received: *15 March 2021*
Accepted: *07 May 2021*
Published: *11 June 2021*

Citation:
Lin X, Liu F, Wang B, Dong R, Sun L, Wang M and Bi Y (2021) Subjective Cognitive Decline May Be Associated With Post-operative Delirium in Patients Undergoing Total Hip Replacement: The PNDABLE Study. Front. Aging Neurosci. 13:680672. doi: 10.3389/fnagi.2021.680672

INTRODUCTION

Post-operative delirium (POD) is a common complication in the surgical patients. It is characterized by acute changes in the patients' mental state, involving impairment of cognition, attention, and consciousness levels, and tends to occur within 1 week after surgery (or before discharge) (Evered et al., 2018). POD is affected by a variety of factors, with the incidence ranging from 4 to 65% (Rudolph and Marcantonio, 2011), and 17% after total hip replacement (Oh et al., 2021). Previous studies have confirmed that POD has a high morbidity and mortality and at the same time reduces the quality of patients' life, prolongs the length of hospital stay, and increases the burden on families and society (Eckenhoff et al., 2020). So far, the pathogenesis of POD is still unclear. It was found that biomarkers such as amyloid (Aβ) and Tau protein in cerebrospinal fluid (CSF) have become strong predictors of POD (Jia et al., 2019; Bassil et al., 2020). However, there was no independent preoperative subjective cognitive status to predict POD. Therefore, it is crucial to identify an independent preoperative subjective cognitive status associated with POD that may be predicted in the preoperative settings.

Subjective cognitive decline (SCD) refers to a condition in which an individual's memory and/or other cognitive abilities are significantly reduced relative to one's previous performance level in the absence of an objective neuropsychological deficit (Jessen et al., 2014). The evidence shows that SCD increases the risk of future pathological cognitive declining (Cheng et al., 2017). However, to date, preoperative SCD has not been assessed as a risk factor of POD. Moreover, there is hardly any research on the relationship between SCD and POD and their related mechanisms.

Therefore, we planned to conduct a prospective, observational cohort study to investigate the relationship between SCD and POD and their related mechanisms, as well as whether there was a difference in the incidence of POD in SCD patients aged from 40 to 90 years old, so as to find a new way for the early prevention of POD. For these purposes, we make the hypothesis that preoperative SCD is a risk factor of POD in patients and that the significance of SCD may vary in different age groups. Three analyses were then performed. Firstly, the relationship between SCD and POD was assessed. Secondly, the relationship between Aβ40, Aβ42, T-tau, P-tau, and POD or SCD was analyzed. Thirdly, the incidence of SCD and POD in patients of different age groups was observed and analyzed.

MATERIALS AND METHODS

The PNDABLE Study

Participants were recruited from the Perioperative Neurocognitive Disorder And Biomarker Lifestyle (PNDABLE) study, which is a large cohort study conducted in 2018 to analyze the risk factors and biomarkers of perioperative neurocognitive impairment in the Han population in northern China for the early diagnosis and prevention of the disease. The study has been registered with the China Clinical Trial Registry (clinical registration number: Chictr200033439), and ethical approval for this study (Ethical Committee N°2020 PRO FORMA Y number 005) was provided by the Ethical Committee Qingdao Municipal Hospital affiliated to Qingdao University, Qingdao, China (Chairman Prof Yang), on May 21, 2020. All patients were informed of the purpose of participation in the study and of the procedure (blood and CSF collection) and had signed an informed consent form prior to inclusion. Cognitive function was evaluated by subjective cognitive decline scale (SCDS), Mini-Mental State Examination (MMSE), and Montreal Cognitive Assessment (MOCA); the patients were diagnosed as normal cognitive (NC), SCD, mild cognitive impairment (MCI) and Alzheimer's disease (AD) according to the different scores. The patients of the NC group and SCD group were selected as the main study objects.

Study Participants

This is a prospective, observational, cohort study of patients undergoing total hip replacement. Three hundred eligible patients who were between 40 and 90 years of age and scheduled to have total hip replacement under combined spinal and epidural anesthesia, between June 2020 and December 2020 in Qingdao Municipal Hospital affiliated to Qingdao University, were included in this study. The inclusion criteria of this study include (1) age 40–90 years; (2) Han Nationality Patients in north China; (3) American Society of Anesthesiologists (ASA) score 1 or 2; (4) preoperative cognitive status was good with no language communication disorder; and (5) educational level was enough to complete preoperative cognitive function test. The exclusion criteria include (1) central nervous system infection, head trauma, epilepsy, multiple sclerosis, and other major neurological diseases; (2) major psychological dysfunction; (3) severe systemic diseases (such as malignant tumors) that may affect the levels of POD biomarkers (Aβ and Tau) in CSF; (4) genetic family history; (5) preoperative MMSE scores of 23 or less or MOCA scores of 26 or less; (6) ASA score [a global score that assesses the physical status of patients before surgery, ranging from 1 (normal health) to 5 (moribund)] (Davenport et al., 2006) >2; (7) severe visual and hearing disorders; and (8) unwillingness to comply with the protocol or procedures.

Data of 214 patients were analyzed in this study (see **Figure 1**, flow diagram).

Neuropsychological Testing

SCDS, MMSE, and MOCA scores were used to evaluate the cognitive function of the patients the day before the operation by a neurologist. Patients were asked whether their memory and/or other cognitive abilities were significantly reduced relative to their previous performance level in the absence of an objective neuropsychological deficit (Jessen et al., 2014), which was for diagnosing SCD, meanwhile, by the SCDS: (1) Compared with the past, the ability of conscious memory decreased which worried patients, which was the basic condition for diagnosis of SCD; (2) other conditions that ultimately determine SCD include normal MMSE scores of 24 or more, MoCA scores of 27 or more, and exclusion from other neuropsychiatric disorders, medical disorders, and drug or other substance abuse (Jorm et al., 1997; Jessen et al., 2014; Molinuevo et al., 2017). POD was defined by the Confusion Assessment Method (CAM), and POD

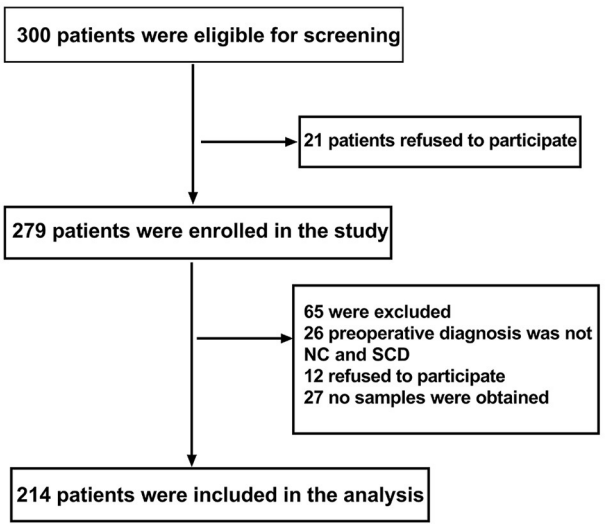

FIGURE 1 | Flow diagram. The flow diagram shows that 300 patients were initially screened for the studies, and 214 patients were finally included in the data analysis.

severity was measured using the Memorial Delirium Assessment Scale (MDAS) (Inouye et al., 1990; Schuurmans et al., 2003) at 10 a.m. and 2 p.m. twice a day on 1–7 days (or before discharge) by an anesthesiologist post-operatively. The above assessments performed by a neurologist and an anesthesiologist were not involved in intraoperative management of the patients. The diagnosis of POD included the following four clinical criteria: (1) acute onset and fluctuation process; (2) inattention; (3) disorganized thinking; and (4) change of consciousness level. POD can be diagnosed if it meets the standards 1, 2, and 3 or 4 at the same time. The CAM and MDAS in Chinese research have been proven to have good reliability and validity (Leung et al., 2008; Shi et al., 2014). Therefore, CAM and MDAS positive scores on patients post-operatively on 1–7 days (or before discharge) were recorded.

Anesthesia and Surgery

All patients who underwent total hip replacement under combined spinal and epidural anesthesia used the same surgical team to avoid the impact of different surgical techniques. During anesthesia, oxygen saturation, electrocardiography, non-invasive blood pressure, and pulse oximetry were continuously monitored, which were recorded at fixed intervals of 3 min. However, glucocorticoid drugs, dexmedetomidine non-steroidal analgesics, and midazolam were avoided during surgeries.

Post-operatively, the visual analog scale (VAS) score of 0–10 (lower score indicating lower level of pain) (Chung et al., 2016) was used to assess the pain at the same time. Patient-controlled intravenous analgesia (PCIA) was used post-operatively for 48 h by all patients. The PCIA opioid consisted of 2.5 $\mu g \cdot kg^{-1}$ sufentanil and 5 mg tropisetron (total volume of 100 ml, including 0.9% normal saline, bolus 2 ml, basal rate 2 ml/h, and lockout time 15 min). If patients need it, they were given non-opioid drugs for analgesia, which was recorded.

Sample Collection

The CSF (2 ml) was collected in a polypropylene centrifugal tube during spinal-epidural joint block prior to administration of the local anesthetic, which were centrifuged immediately at 2000 g for 10 min at room temperature (Bakr et al., 2017; Pérez-Ruiz et al., 2018) and then stored at −80°C for further analysis.

Elisa

The concentrations of Aβ40, Aβ42, T-tau, and P-tau were detected from 1.5 ml CSF using Aβ40 (BioVendor, Ghent, Belgium Lot: No. 292-6230), Aβ42 (BioVendor, Ghent, Belgium Lot: No. 296-64401), P-tau (BioVendor, Ghent, Belgium Lot: QY-PF9092), and T-tau (BioVendor, Ghent, Belgium Lot: No. EK-H12242) assay kit in accordance with the manufacturer's protocol. Finally, the optical density value (OD value) of each hole was measured at the wavelength of 450 m with an enzyme marker (EnSpire, PerkinElmer, Waltham, MA, USA) (Bakr et al., 2017; Pérez-Ruiz et al., 2018). All samples were assayed by the same laboratory assistant who was blinded to the group assignment.

Study Size

No formal power analysis was performed, but we have a large cohort size which has included 1,905 patients in the PNDABLE study to decrease the risk of underpowered analyses.

Data Analysis

SPSS statistical software, version 21.0 (SPSS, Inc., Chicago, IL, USA), and GraphPad Prism software, version 6.01 (GraphPad Software, Inc., La Jolla, CA, USA), were used for data analysis. The K–S test was used to determine whether the measurement data conformed to the normal distribution. The measurement data that conformed to the normal distribution was expressed by mean ± standard deviation (SD); the median and interquartile range (IQR, 25–75 percentile) or a number (%) to express the data. Independent sample *t*-test was used for comparison among groups, and χ^2 test was used for counting data. Binary logistic regression analysis of SCD and POD, Aβ40, Aβ42, T-tau, and P-tau was performed. SCD, Aβ40, Aβ42, T-tau, and P-tau based on the univariate analysis were chosen as covariates in multivariate logistic regression analysis. $P < 0.05$ was statistically significant.

RESULTS

Characteristics of Included Participants in PNDABLE

This study enrolled 300 participants. Two hundred fourteen ($n = 214$) were eligible for analysis, and 86 participants were excluded. The criteria for exclusion are shown in **Figure 1**. The demographic and clinical data are summarized in **Table 1**.

The incidence of POD was observed in 26.64% ($n = 57/214$), with 32.43% ($n = 36/111$) in the SCD group and 20.39% ($n = 21/103$) in the NC group. Among the patients diagnosed with SCD, there was no significant difference in preoperative MMSE

TABLE 1 | Characteristics of participants.

	SCD group (*N* = 111)	NC group (*N* = 103)	*P*-value
Age (year), mean ± SD	60.52 ± 10.63	63.06 ± 10.50	0.08
Male, n (%)	57 (51.35)	62 (60.19)	0.19
Years of education, n (%)			
0	8 (7.21)	7 (6.80)	0.10
1–9	49 (44.14)	45 (43.69)	0.57
10–13	26 (23.42)	25 (24.27)	0.35
14–17	18 (16.22)	17 (16.50)	0.21
>17	10 (9.01)	9 (8.74)	0.17
Height (cm), mean ± SD	169.61 ± 7.23	168.41 ± 5.43	0.86
Body weight (kg), mean ± SD	68.23 ± 8.63	65.17 ± 10.72	0.72
BMI (kg/m^2), mean ± SD	26.23 ± 3.61	24.62 ± 2.53	0.08
ASA class, n (%)			
I	48 (43.24)	45 (43.69)	0.77
II	63 (56.76)	58 (56.31)	0.55
Dependence on smoking (n), n (%)	31 (27.93)	35 (33.98)	0.34
Alcohol abuse, n (%)	31 (27.93)	33 (32.04)	0.51
Coronary heart disease, n (%)	33 (29.73)	35 (33.98)	0.51
Hypertension, n (%)	38 (34.23)	40 (38.83)	0.49
Diabetes, n (%)	15 (13.51)	18 (17.48)	0.42
Family history of dementia, n (%)	5 (4.50)	4 (3.88)	1.00
Time of anesthesia (min), mean ± SD	141.38 ± 25.41	147.82 ± 23.41	0.76
Time of surgery (min), mean ± SD	133.14 ± 25.35	136.76 ± 31.73	0.88
Estimated volume of infusion (ml), mean ± SD	911.27 ± 33.86	922.45 ± 36.89	0.74
Estimated blood loss (ml), mean ± SD	111.97 ± 5.45	120.28 ± 7.79	0.59
Preoperative the highest MMSE score, median, and 25–75 percentile	24 (22–27)	25 (23–28)	0.31
Preoperative the highest MoCA score, median, and 25–75 percentile	27 (25–29)	28 (26–30)	0.18
Post-operative the highest MDAS score, median, and 25–75 percentile	13 (10–15)	12 (9–15)	0.79
Post-operative the highest VAS score, median, and 25–75 percentile	2 (1–3)	3 (2–5)	0.61

The length of anesthesia was defined from the time that the anesthesiologists started the spinal anesthesia in the patients to the time when the patients were sent to the post-anesthesia care unit. The length of surgery was defined from the time of initial incision to the time of the closure of the skin. BMI, Body Mass Index; ASA, American Society of Anesthesiologists; cm, centimeter; min, minute; kg, kilogram; ml, milliliter; SD, standard deviation; MMSE, Mini-Mental State Examination; MOCA, Montreal cognitive assessment; MDAS, Memorial Delirium Assessment Scale; VAS, visual analog scale.

score [24 (22–27)] compared with patients diagnosed with NC [25 (23–28), $P = 0.31$]. Similarly, the preoperative MoCA score [27 (25–29)] in the SCD group was not significantly different from the score [28 (26–30), $P = 0.18$] in the NC group. In this study, it has been found that the POD and its severity were primarily diagnosed by CAM and MDAS scores on post-operative day 1 and day 2, which is consistent with previous studies (Lin et al., 2020). Moreover, MDAS scores [13 (10–15)] were not significantly different from the patients who were diagnosed as NC [12 (9–15), $P = 0.79$]. Additionally, the post-operative highest VAS scores are the same in the SCD group 2 (1–3) and NC group [3 (2–5), $P = 0.61$].

Comparison of CSF Biomarker Levels Between Two Groups

Compared with the NC group, the differences in CSF levels of Aβ40, Aβ42, T-tau, and P-tau of the SCD group were statistically significant ($P < 0.05$), as shown in **Table 2**.

TABLE 2 | Comparison of CSF biomarker levels between the two groups.

Biomarkers	SCD group (*N* = 111)	NC group (*N* = 103)	*P*-value
Aβ40 (pg/ml, ± s)	4751.09 ± 2425.44	6233.88 ± 3450.97	< 0.001
Aβ42 (pg/ml, ± s)	186.81 ± 136.24	233.33 ± 123.59	0.009
P-tau (pg/ml, ± s)	41.42 ± 16.99	35.43 ± 12.23	0.003
T-tau (pg/ml, ± s)	224.55 ± 146.39	167.56 ± 71.13	< 0.001

SCD, subjective cognitive decline; NC, normal cognitive; CSF, cerebrospinal fluid.

Logistic Regression Analysis of the Influencing Factors of POD and SCD

In this study, logistic regression analysis showed that patients with SCD were more prone to POD. SCD and the increased CSF level of P-tau were risk factors for POD; however, the increased CSF level of Aβ42 was a protective factor for POD by univariate analysis. After adjustment for SCD, Aβ42, Aβ40, P-tau, and T-tau,

multivariate logistic regression analysis showed that SCD and the increased CSF level of P-tau were still risk factors for POD; the increased CSF level of Aβ42 was still a protective factor for POD, as shown in **Table 3**.

TABLE 3 | Analyze the influencing factors of POD and SCD by logistic regression.

Factors of interest	Unadjusted		Adjusted	
	OR (95%CI)	*P*-value	OR (95%CI)	*P*-value
SCD	1.87 (1.01–3.49)	0.04	2.32 (1.18–4.55)	0.01
Aβ42	0.10 (0.99–1.00)	0.00	0.99 (0.99–1.00)	0.00
Aβ40	1.00 (0.99–1.00)	0.07	1.00 (0.99–1.00)	0.04
P-tau	1.04 (1.02–1.06)	<0.001	1.04 (1.01–1.06)	0.00
T-tau	1.00 (1.00–1.01)	0.00	1.00 (1.00–1.01)	0.01

OR, relative risk; CI, confidence interval. After adding SCD, Aβ42, Aβ40, P-tau, T-tau, multivariate regression analysis was performed.

TABLE 4 | Relationship between SCD and biomarkers in CSF by logistic regression.

Biomarkers	Unadjusted		Adjusted	
	OR (95%CI)	*P*-value	OR (95%CI)	*P*-value
Aβ42	1.00 (0.99–1.00)	0.01	1.00 (0.99–1.00)	0.02
Aβ40	1.00 (0.99–1.00)	0.00	1.00 (0.99–1.00)	0.00
P-tau	1.03 (1.01–1.05)	0.01	1.04 (1.01–1.06)	0.00
T-tau	1.01 (1.00–1.01)	0.00	1.01 (1.00–1.01)	<0.001

OR, relative risk; CI, confidence interval; CSF, cerebrospinal fluid. After adding Aβ42, Aβ40, P-tau, T-tau, multivariate regression analysis was performed.

Relationship Between SCD and Biomarkers in CSF by Logistic Regression

The SCD was taken as the dependent variable; logistic regression analysis was carried out to explore the influencing factors. The results showed that the CSF levels of P-tau and T-tau were risk factors for SCD by univariate analysis. After adjustment for Aβ42, Aβ40, P-tau, and T-tau, the CSF levels of P-tau and T-tau were still risk factors for SCD by multivariate logistic regression analysis, as shown in **Table 4**.

Comparison of POD Incidence in Different Age Groups With SCD

There were no statistical significance differences in the mean age between the SCD and NC group in **Table 1**. Further, the patients with SCD were divided into five different age groups: 40–49 years old (Group A), 50–59 years old (Group B), 60–69 years old (Group C), 70–79 years old (Group D), and 80–90 years old (Group E). The results showed that the incidence of POD increased with age in SCD patients, as shown in **Figure 2**.

DISCUSSION

In this study, we found that SCD is one of the preoperative risk factors for POD.

POD is a syndrome with subjective variability and numerous influencing factors, and it is a product of the interaction of patients' demographic factors, basic disease factors, and anesthesia and surgery factors (Aldecoa et al., 2017). Its pathogenesis is complex, including the cholinergic theory of the cholinergic nerve, the theory of inflammatory response, the theory of exogenous toxin and free radical damage, the theory of Tau protein hyperphosphorylation, and the theory of Aβ protein abnormal deposition.

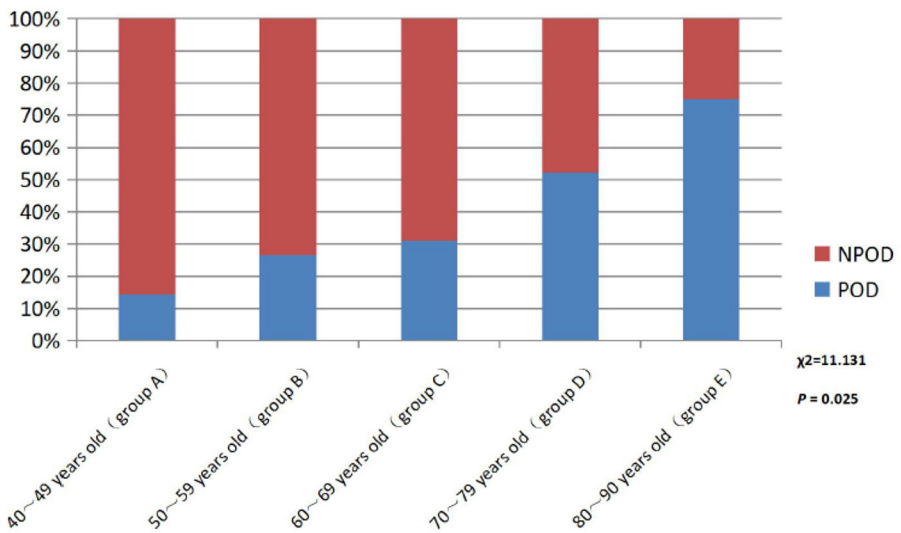

FIGURE 2 | Comparison of POD incidence in different age groups patients with SCD. POD, post-operative delirium; NPOD, non-post-operative delirium.

Previous studies have confirmed that the concentration of biomarkers such as Aβ42, Aβ40, T-tau, and P-tau in patients can be used as an important basis for clinical research and diagnosis of POD (McKhann et al., 2011). However, CSF is considered to be the best source of these biomarkers, because it is in direct contact with the brain and can better reflect the pathophysiological changes occurring in the central nervous system (CNS) (Olsson et al., 2016). Therefore, after controlling for age, gender, height, weight, BMI, years of education, history of smoking, history of drinking, hypertension, diabetes, coronary heart disease, ASA class, and other confounding factors, this study included patients undergoing total hip replacement under elective combined spinal and epidural anesthesia; preoperative CSF was measured by biochemical index assessment, and the concentration of related biomarkers was detected to further verify their important diagnostic value for POD.

SCD, also known as subjective memory impairment (SMI) and subjective cognitive impairment (SCI), was first established on the basis of AD research and was considered as the preclinical stage of AD (Jessen et al., 2014). Epidemiological studies have shown that the prevalence of SCD ranges from 10 to 88% and increases with age: 20% in people 65 years and younger, 25–50% in people 65 years and older, and 88% in people over 85 years of age (Gifford et al., 2015). For SCD, memory decline is the most common symptom, and at the same time it can be accompanied by visual–spatial impairment, language impairment, attention deficit, and other symptoms (Si et al., 2020). According to statistics, an estimated 27% of SCD patients will develop MCI in the future, and another 14% will eventually be diagnosed with cognitive impairment (Mitchell et al., 2014). At present, with the deepening of people's understanding of neuropathology, neuropsychology, neuroimaging, and pathophysiology, the study of SCD is no longer limited to AD but extends to the field of perioperative neurocognitive disorder (PND).

The results of this study showed that there were significant differences in the expression of Aβ40, Aβ42, P-tau, and T-tau in CSF between SCD Group and NC Group ($P < 0.05$), indicating an increased risk of POD in patients with SCD. Further logistic regression analysis of biomarkers in CSF showed that the increased concentrations of P-tau were a risk factor for POD, consistent with previous findings (Jia et al., 2019). At the same time, the concentrations of P-tau decreased, which indicated that the changes of biomarkers such as P-tau in CSF were also risk factors for SCD. There was an evidence that an increased tau protein in CSF deposition in SCD patients results in a decrease in glucose metabolism in the brain (Perrotin et al., 2012; Snitz et al., 2015; Buckley et al., 2017), a decrease in medial temporal lobe volume (Scheef et al., 2012), and a thinner cortex (Jessen et al., 2006; Saykin et al., 2006). In addition, the deposition of Tau proteins may be associated with the neurodegeneration that SCD patients are experiencing, and they interact to reduce CNS tolerance and ultimately accelerate the destruction of cognitive function (Hu et al., 2019). Combined with the results of this study, we hypothesized that the changes in the level of related biomarkers in patients with CSF might be one of the mechanisms of POD in patients with SCD.

A large number of studies have confirmed that advanced age is the main risk factor for SCD and POD. The reasons may be as follows: (1) in the elderly, brain atrophy, decreased number of neurons, degeneration of the central cholinergic system, and relative reduction of specific receptors and neurotransmitters lead to decreased learning, memory, and cognitive reserve. (2) The function of abnormal microglia or being in a "pre-excitation" state is more likely to be stimulated by surgery, anesthesia, and inflammation of peripheral tissues, leading to central inflammatory response. (3) Low organ function reserve, decreased vitality and increased vulnerability, and poor tolerance to anesthesia and surgery are prone to adverse drug reactions. (4) The permeability of the endothelium and blood–brain ridge fluid barrier is increased, and peripheral inflammatory factors enter the CNS to activate the central inflammatory response (Lucin et al., 2013; Rundshagen, 2014). In this study, patients will be included for stratified analysis according to their age. The study found that the incidence rate of POD in the SCD group increased with age, which was also confirmed to be an independent risk factor for POD in patients with SCD.

The limitations of this study are as follows: First, the number of patients was limited and more eligible patients would be included in future studies. Second, this study was a single-center study, which could be further validated by multicenter studies in the future. Third, this study only focused on the relationship between SCD and the biomarkers in patients' CSF and did not involve other related pathogenesis of POD, which depended on further research.

In conclusion, SCD is one of the preoperative risk factors for POD, which provides new insight into the prevention of POD. The early prevention of POD could improve the quality of patients' life and reduce the length of hospital stay and the burden on families and society.

DATA AVAILABILITY STATEMENT

The raw data supporting the conclusions of this article will be made available by the authors, without undue reservation.

ETHICS STATEMENT

Ethical approval for this study (Ethical Committee N°2020 PRO FORMA Y number 005) was provided by the Ethical Committee Qingdao Municipal Hospital affiliated to Qingdao University, Qingdao, China (Chairman Prof Yang) on 21 May 2020. The patients/participants provided their written informed consent to participate in this study. Written informed consent was obtained from the individual(s) for the publication of any potentially identifiable images or data included in this article.

AUTHOR CONTRIBUTIONS

XL contributed to the study design, data collection, statistical analysis, and manuscript preparation. FL performed ELISA. BW was involved in the data collection. RD performed the

neuropsychological testing. YB and MW contributed to the study concept and design, as well as manuscript preparation and review. XL and LS performed the statistical analysis. All authors contributed to the article and approved the submitted version.

FUNDING

This study was supported by grants from the National Natural Science Foundation of China (No. 91849126).

REFERENCES

Aldecoa, C., Bettelli, G., Bilotta, F., Sanders, R. D., Audisio, R., Borozdina, A., et al. (2017). European society of anaesthesiology evidence-based and consensus-based guideline on postoperative delirium. *Eur. J. Anesthesiol.* 34, 192–214. doi: 10.1097/EJA.0000000000000594

Bakr, A., Silva, D., Cramb, R., Flint, G., and Foroughi, M. (2017). Outcomes of CSF spectrophotometry in cases of suspected subarachnoid haemorrhage with negative CT: two years retrospective review in a Birmingham hospital. *Br. J. Neurosurg.* 31, 223–226. doi: 10.1080/02688697.2016.1265089

Bassil, F., Brown, H. J., Pattabhiraman, S., Iwasyk, J. E., Maghames, C. M., Meymand, E. S., et al. (2020). Amyloid-Beta (Aβ) plaques promote seeding and spreading of alpha-synuclein and tau in a mouse model of lewy body disorders with Aβ pathology. *Neuron* 105, 260–275. doi: 10.1016/j.neuron.2019.10.010

Buckley, R. F., Hanseeuw, B., Schultz, A. P., Vannini, P., Aghjayan, S. L., Properzi, M. J., et al. (2017). Region-Specific association of subjective cognitive decline with tauopathy independent of global beta-Amyloid burden. *JAMA Neurol.* 74, 1455–1463. doi: 10.1001/jamaneurol.2017.2216

Cheng, Y. W., Chen, T. F., and Chiu, M. J. (2017). From mild cognitive impairment to subjective cognitive decline: conceptual and methodological evolution. *Neuropsychiat. Dis. Treat.* 13, 491–498. doi: 10.2147/NDT.S123428

Chung, D., Sue, A., Hughes, S., Simmons, J., Hailu, T., Swift, C., et al. (2016). Impact of race/ethnicity on pain management outcomes in a community-based teaching hospital following inpatient palliative care consultation. *Cureus* 8:e823. doi: 10.7759/cureus.823

Davenport, D. L., Bowe, E. A., Henderson, W. G., Khuri, S. F., and Mentzer, R. M. Jr. (2006). National Surgical Quality Improvement Program (NSQIP) risk factors can be used to validate American Society of Anesthesiologists Physical Status Classification (ASA PS) levels. *Ann. Surg.* 243, 636–641. discussion: 641–634. doi: 10.1097/01.sla.0000216508.95556.cc

Eckenhoff, R. G., Maze, M., Xie, Z., Culley, D. J., Goodlin, S. J., Zuo, Z., et al. (2020). Perioperative neurocognitive disorder: state of the preclinical science. *Anesthesiology* 132, 55–68. doi: 10.1097/ALN.0000000000002956

Evered, L., Silbert, B., Knopman, D. S., Scott, D. A., DeKosky, S. T., Rasmussen, L. S., et al. (2018). Recommendations for the nomenclature of cognitive change associated with anaesthesia and surgery-2018. *Br. J. Anesthesia* 121, 1005–1012. doi: 10.1097/ALN.0000000000002334

Gifford, K. A., Liu, D., Romano, R. III, Jones, R. N., and Jefferson, A. L. (2015). Development of a subjective cognitive decline questionnaire using item response theory: a pilot study. *Alzheimers Dement.* 1, 429–439. doi: 10.1016/j.dadm.2015.09.004

Hu, X., Teunissen, C. E., Spottke, A., Heneka, M. T., Düzel, E., Peters, O., et al. (2019). Smaller medial temporal lobe volumes in individuals with subjective cognitive decline and biomarker evidence of Alzheimer's disease-Data from three memory clinic studies. *Alzheimers Dement.* 15, 185–193. doi: 10.1016/j.jalz.2018.09.002

Inouye, S. K., van Dyck, C. H., Alessi, C. A., Balkin, S., Siegal, A. P., and Horwitz, R. I. (1990). Clarifying confusion: the confusion assessment method. A new method for detection of delirium. *Ann. Intern. Med.* 113, 941–948. doi: 10.7326/0003-4819-113-12-941

Jessen, F., Amariglio, R. E., van Boxtel, M., Breteler, M., Ceccaldi, M., Chételat, G., et al. (2014). A conceptual framework for research on subjective cognitive decline in preclinical Alzheimer's disease. *Alzheimers Dement.* 10, 844–852. doi: 10.1016/j.jalz.2014.01.001

Jessen, F., Feyen, L., Freymann, K., Tepest, R., Maier, W., Heun, R., et al. (2006). Volume reduction of the entorhinal cortex in subjective memory impairment. *Neurobiol. Aging* 27, 1751–1756. doi: 10.1016/j.neurobiolaging.2005.10.010

Jia, L., Qiu, Q., Zhang, H., Chu, L., Du, Y., Zhang, J., et al. (2019). Concordance between the assessment of Abeta42, T-tau, and P-T181-tau in peripheral blood neuronal-derived exosomes and cerebrospinal fluid. *Alzheimer's Dement.* 15, 1071–1080. doi: 10.1016/j.jalz.2019.05.002

Jorm, A. F., Christensen, H., Korten, A. E., Henderson, A. S., Jacomb, P. A., and Mackinnon, A. (1997). Do cognitive complaints either predict future cognitive decline or reflect past cognitive decline? a longitudinal study of an elderly community sample. *Psychol. Med.* 27, 91–98. doi: 10.1017/S0033291796003923

Leung, J., Leung, V., Leung, C. M., and Pan, P. C. (2008). Clinical utility and validation of two instruments (the confusion assessment method algorithm and the Chinese version of nursing delirium screening scale) to detect delirium in geriatric inpatients. *Gen. Hosp. Psychiatry* 30, 171–176. doi: 10.1016/j.genhosppsych.2007.12.007

Lin, X., Tang, J., Liu, C., Li, X., Cao, X., Wang, B., et al. (2020). Cerebrospinal fluid cholinergic biomarkers are associated with postoperative delirium in elderly patients undergoing Total hip/knee replacement: a prospective cohort Study. *BMC Anesthesiol.* 20:246. doi: 10.1186/s12871-020-01166-9

Lucin, K. M., O'Brien, C. E., Bieri, G., Czirr, E., Mosher, K. I., Abbey, R. J., et al. (2013). Microglial beclin 1 regulates retromer trafficking and phagocytosis and is impaired in Alzheimer's disease. *Neuron* 79, 873–886. doi: 10.1016/j.neuron.2013.06.046

McKhann, G. M., Knopman, D. S., Chertkow, H., Hyman, B. T., Jack, C. R. Jr, Kawas, C. H., Klunk, W. E., et al. (2011). The diagnosis of dementia due to Alzheimer's disease: Recommendations from the National Institute on Aging-Alzheimer's Association workgroups on diagnostic guidelines for Alzheimer's disease. *Alzheimers Dement.* 7, 263–269. doi: 10.1016/j.jalz.2011.03.005

Mitchell, A. J., Beaumont, H., Ferguson, D., Yadegarfar, M., and Stubbs, B. (2014). Risk of dementia and mild cognitive impairment in older people with subjective memory complaints: meta-analysis. *Acta Psychiatr. Scand.* 130, 439–451. doi: 10.1111/acps.12336

Molinuevo, J. L., Rabin, L. A., Amariglio, R., Buckley, R., Dubois, B., Ellis, K. A., et al. (2017). Implementation of subjective cognitive decline criteria in research studies. *Alzheimers Dement.* 13, 296–311. doi: 10.1016/j.jalz.2016.09.012

Oh, C. S., Lim, H. Y., Jeon, H. J., Kim, T. H., Park, H. J., Piao, L., et al. (2021). Postoperative delirium in elderly patients undergoing total hip replacement: a prospective single-blind randomised controlled trial. *Eur. J. Anesthesiol.* 38(Suppl. 1), S58–S66. doi: 10.1097/EJA.0000000000001414

Olsson, B., Lautner, R., Andreasson, U., Öhrfelt, A., Portelius, E, Bjerke, M., Hölttä, M., et al. (2016). CSF and blood biomarkers for the diagnosis of Alzheimer's disease: a systematic review and meta-analysis. *Lancet Neurol.* 15, 673–684. doi: 10.1016/S1474-4422(16)00070-3

Pérez-Ruiz, E., Decrop, D., Ven, K., Tripodi, L., Leirs, K., Rosseels, J., et al. (2018). Digital ELISA for the quantification of attomolar concentrations of Alzheimer's disease biomarker protein tau in biological samples. *Anal. Chim. Acta* 1015, 74–81. doi: 10.1016/j.aca.2018.02.011

Perrotin, A., Mormino, E. C., Madison, C. M., Hayenga, A. O., and Jagust, W. J. (2012). Subjective cognition and amyloid deposition imaging: a Pittsburgh Compound B positron emission tomography study in normal elderly individuals. *Arch. Neurol.* 69, 223–229. doi: 10.1001/archneurol.2011.666

Rudolph, J. L., and Marcantonio, E. R. (2011). Review articles: postoperative delirium: acute change with long-term implications. *Anesthesia Analg.* 112, 1202–1211. doi: 10.1213/ANE.0b013e3182147f6d

Rundshagen, I. (2014). Postoperative cognitive dysfunction. *Dtsch. Arztebl. Int.* 111, 119–125. doi: 10.3238/arztebl.2014.0119

Saykin, A. J., Wishart, H. A., Rabin, L. A., Santulli, R. B., Flashman, L. A., West, J. D., et al. (2006). Older adults with cognitive complaints show brain atrophy similar to that of amnestic MCI. *Neurology* 67, 834–842. doi: 10.1212/01.wnl.0000234032.77541.a2

Scheef, L., Spottke, A., Daerr, M., Joe, A., Striepens, N., Kölsch, H., et al. (2012). Glucose metabolism, gray matter structure, and memory

decline in subjective memory impairment. *Neurology* 79, 1332–1339. doi: 10.1212/WNL.0b013e31826c1a8d

Schuurmans, M. J., Deschamps, P. I., Markham, S. W., Shortridge-Baggett, L. M., and Duursma, S. A. (2003). The measurement of delirium: review of scales. *Res. Theory Nurs. Pract.* 17, 207–224. doi: 10.1891/rtnp.17.3.207.53186

Shi, Z., Wu, Y., Li, C., Fu, S., Li, G., Zhu, Y., et al. (2014). Using the Chinese version of memorial delirium assessment scale to describe postoperative delirium after hip surgery. *Front. Aging Neurosci.* 6:297. doi: 10.3389/fnagi.2014.00297

Si, T., Xing, G., and Han, Y. (2020). Subjective cognitive decline and related cognitive deficits. *Front. Neurol.* 11:247. doi: 10.3389/fneur.2020.00247

Snitz, B. E., Lopez, O. L., McDade, E., Becker, J. T., Cohen, A. D., Price, J. C., et al. (2015). Amyloid-beta imaging in older adults presenting to a memory clinic with subjective cognitive decline: a pilot study. *J. Alzheimers Dis.* 48(Suppl. 1), S151–S159. doi: 10.3233/JAD-150113

Conflict of Interest: The authors declare that the research was conducted in the absence of any commercial or financial relationships that could be construed as a potential conflict of interest.

frontiers in Aging Neuroscience

ORIGINAL RESEARCH
published: 28 July 2021
doi: 10.3389/fnagi.2021.716616

Effects of Lipotoxicity in Brain Microvascular Endothelial Cells During Sirt3 Deficiency-Potential Role in Comorbid Alzheimer's Disease

*Alpna Tyagi[1,2], Carol Mirita[1], Iman Shah[1], P. Hemachandra Reddy[3] and Subbiah Pugazhenthi[1,2]**

[1] Rocky Mountain Regional VA Medical Center, Aurora, CO, United States, [2] Department of Medicine, University of Colorado Anschutz Medical Campus, Aurora, CO, United States, [3] Internal Medicine Department and Garrison Institute on Aging, Texas Tech University Health Sciences Center, Lubbock, TX, United States

Silence information regulator 3 (SIRT3) is an NAD^+ dependent deacetylase enzyme that enhances the function of key mitochondrial proteins. We have earlier demonstrated that deletion of Sirt3 gene leads to downregulation of metabolic enzymes, mitochondrial dysfunction and neuroinflammation in the brain, the major causes of Alzheimer's disease (AD). We also reported recently that Sirt3 gene deletion in Alzheimer's transgenic mice leads to exacerbation of neuroinflammation, amyloid plaque deposition and microglial activation. AD often coexists with other brain lesions caused by comorbidities which can exert their deleterious effects through the neurovascular unit. This unit consists of brain microvascular endothelial cells (BMECs), end feet of astrocytes, and pericytes. BMECs are uniquely different from other vascular endothelial cells because they are glued together by tight-junction proteins. BMECs are in constant contact with circulating factors as they line the luminal side. Therefore, we hypothesized that vascular endothelial injury caused by comorbidities plays a significant role in neuroinflammation. Herein, we investigated the effects of lipotoxicity in BMECs and how Sirt3 deficiency facilitate the deleterious effects of lipotoxicity on them using *in vivo* and *in vitro* models. We observed decreases in the levels of SIRT3 and tight junction proteins in the brain samples of western diet-fed APP/PS1 mice. Similar observations were obtained with Alzheimer's post-mortem samples. Exposure of BEND3 cells, mouse brain-derived Endothelial cells3, to a combination of high glucose and palmitic acid resulted in significant ($P < 0.01$-$P < 0.001$) decreases in the levels of SIRT3, claudin-5 and ZO-1. Induction of inflammatory mediators, including Cox-2, CXCL1, RANTES, and GADD45β was also observed in these treated cells. Interestingly, the induction was more with Sirt3-silenced BEND3 cells, suggesting that Sirt3 deficiency exacerbates inflammatory response. Palmitic acid was more potent in inducing the inflammatory mediators. Significant cytotoxicity and changes in microglial morphology were observed when cocultures of Sirt3-silenced BEND3 and Sirt3-silenced BV2 cells were exposed to palmitic acid.

OPEN ACCESS

Edited by:
David Baglietto-Vargas, University of Malaga, Spain

Reviewed by:
Malgorzata Burek, Julius Maximilian University of Würzburg, Germany
Ramasamy Thangavel, University of Missouri, United States

***Correspondence:**
Subbiah Pugazhenthi
subbiah.pugazhenthi@cuanschutz.edu

Received: *28 May 2021*
Accepted: *08 July 2021*
Published: *28 July 2021*

Citation:
Tyagi A, Mirita C, Shah I, Reddy PH and Pugazhenthi S (2021) Effects of Lipotoxicity in Brain Microvascular Endothelial Cells During Sirt3 Deficiency-Potential Role in Comorbid Alzheimer's Disease. Front. Aging Neurosci. 13:716616. doi: 10.3389/fnagi.2021.716616

Transendothelial electrical resistance measurement with these cocultures suggested decreased barrier integrity. The findings of this study suggest that hyperlipidemia in comorbidities can compromise blood brain barrier integrity by inducing inflammatory mediators and decreasing tight junction proteins in the vascular endothelial cells of the AD brain, leading to activation of microglia.

Keywords: blood brain barrier, brain micro endothelial cells, lipotoxicity, inflammation, sirt3, microglia

INTRODUCTION

Blood brain barrier (BBB) protects the brain parenchyma from circulating toxins, immune cells, and pathogens while regulating the transport of essential nutrients. BBB is vital to homeostasis of the brain, and with aging its integrity begins to decrease. An MRI study has provided direct evidence to show BBB breakdown in the aging human brain (Montagne et al., 2015). Therefore, BBB breakdown is also associated with aging-associated neurodegenerative diseases (Sweeney et al., 2019). BBB dysfunction is reported to be both cause and consequences of Alzheimer's disease (AD) (Erickson and Banks, 2013). Two-hit vascular hypothesis suggests that a primary cerebrovascular dysfunction (first hit) can cause BBB damage-induced defective Aβ clearance (second hit), leading to the neurodegenerative cascade (Zlokovic, 2005). The breakdown of BBB has been observed in 5XFAD mice, a transgenic Alzheimer's mouse model with amyloid pathology, at 4 months of age and it was shown to be mimicked in a cell culture model with cerebral endothelial cells (Liu et al., 2020). Previous studies have reported that consumption of calorie-rich western diet leads to compromise BBB integrity (Kanoski et al., 2010; Hsu and Kanoski, 2014; Hargrave et al., 2016). Western diet consists of saturated fat and simple sugars. The effect of these components on BBB disruption and associated biological effects in brain microvascular endothelial cells (BMECs) remained mostly unidentified.

Blood brain barrier consists of BMECs, end feet of astrocytes, and pericytes, collectively known as neurovascular unit (NVU) (Iadecola, 2017). Unlike other vascular endothelial cells, BMECs are glued together by tight-junction (TJ) proteins (e.g., occludins and claudins) and scaffolding proteins- zona occludens (e.g., ZO-1 and ZO-2) (Haseloff et al., 2015). Particularly, claudins are essential to guard the barrier functions, as loss of them increases barrier permeability. While, scaffolding proteins (ZO-1 and ZO-2) are important for binding claudins to the TJs (Hartsock and Nelson, 2008; Daneman and Prat, 2015). BMECs are uniquely positioned at the interface between peripheral blood circulation and the central nervous system (CNS). Circulating factors in aged mice have been shown to induce inflammatory mediators through upregulation of vascular cell adhesion molecule 1 (VCAM1) and intercellular adhesion molecule-1 (ICAM1) (Su et al., 2012; Yousef et al., 2019). Increased inflammation reduced TJ proteins namely claudin-5, ZO1 and occludins. Further, BBB breakdown caused microglial reactivity, neuroinflammation, and cognitive deficits in aged mice, which were counteracted by systemic administration of anti-VCAM-1 antibody or by genetic silencing of VCAM1.

Alzheimer's disease often coexists with other brain lesions caused by comorbidities which can exert their deleterious CNS effects through NVU. The precondition for the comorbidities is called metabolic syndrome (MetS), a highly prevalent condition among adult population (Aguilar et al., 2015). MetS can be caused by the downregulation of silence information regulator 3 (SIRT3), a deacetylase enzyme that enhances the function of key mitochondrial proteins (Hirschey et al., 2011). We have reported that deletion of Sirt3 gene leads to downregulation of metabolic enzymes, mitochondrial dysfunction and neuroinflammation in the brain, the main causes of Alzheimer's disease (Tyagi et al., 2018). In a subsequent recent publication, we reported that SIRT3 deficiency in AD mice exacerbates brain insulin resistance, neuroinflammation, amyloid plaque deposition and proliferation of glial cells (Tyagi et al., 2020). Because 20% of total energy consumption is in the brain, it is highly vascularized to facilitate the uptake of oxygen and nutrients. Studies have revealed that to meet the high energy requirement for active transport across BBB, endothelial cells contain a large number of mitochondria, and they are susceptible to oxidative stress (Navaratna et al., 2013). BMECs also have high metabolic activity because of their active transport function. Therefore, under conditions of metabolic dysregulation as observed during diet-induced obesity, BMECs can be susceptible to injury. A study, by Hargrave et al. (2016) showed that diet-induced obesity in rats leads to BBB leakage in multiple regions of hippocampus along with cognitive dysfunction.

Loss of BBB integrity can lead to dysregulation of microglia, the immune cells of the brain. Microglia in their entire life span, do not directly encounter the systemic circulation because of the BBB (Crotti and Ransohoff, 2016). Although microglial regulation is primarily by brain intrinsic events, changes in the periphery are known to modulate microglial behavior (Dilger and Johnson, 2008). Increased BBB permeability can lead to fibrinogen infiltration and microglial activation (Ryu and McLarnon, 2009). Dual opposing effects of microglia have been demonstrated during systemic inflammation by *in vivo* imaging (Haruwaka et al., 2019). In this study, microglia were shown to migrate to the cerebral vasculature and enhance

Abbreviations: AD, Alzheimer's disease; BBB, blood brain barrier; BMECs, brain microvascular endothelial cells; BEND3, mouse brain-derived Endothelial cells3; Cox, cyclooxygenase; CNS, central nervous system; CRP, C-reactive protein; HG, high glucose; HBMECs, human brain microvascular endothelial cells; ICAM1, intercellular adhesion molecule-1; IL-1β, interleukin-1beta; MetS, metabolic syndrome; MMP-9, matrix metallopeptidase 9; NF-kB, nuclear factor kappa-light-chain-enhancer of activated B; NVU, neurovascular unit; PA, palmitic acid; PGs, prostaglandins; shSirt3, Sirt3-silenced; SIRT, silence information regulator; TJ, tight junction; TEER, transendothelial electrical resistance; VaD, Vascular dementia; VCAM, vascular cell adhesion molecule; ZO, zona occludens.

BBB integrity by increasing the expression of claudin-5 in response to systemic inflammation. However, during sustained inflammation, microglia phagocytosed astrocytic end-feet and cause BBB injury.

Thus, findings from previous studies suggest that changes at the systemic level can affect the internal milieu of the brain when BBB permeability is increased. We hypothesized that comorbidities may exacerbate Alzheimer's pathogenesis by a mechanism involving BBB, specifically BMECs. Therefore, the objective of this study was to determine how the circulating factors in comorbidities act at the level of BBB and regulate microglia.

MATERIALS AND METHODS

AD Post-mortem Samples

Post-mortem brain samples of 70–90-year-old AD cases and controls were obtained from Garrison Institute of Aging, Lubbock, TX, United States. Both groups were age and sex matched. The Alzheimer's cases were at the Braak stage of 5 or 6 and these brain samples were positive for amyloid plaques and neurofibrillary tangles while they were absent in control group. The post-mortem intervals were between 2 and 5 h for all brain samples used for the study.

Western Diet Feeding of APP/PS1 Mice

Animal care and the experimental procedures were approved by IACUC at Rocky Mountain Regional Veteran Affairs Medical Center, Aurora CO, United States. C57BL/6 (wild type; WT) and APP/PS1 (AD mice, stock # 5864) mice in C57BL/6 genetic background were obtained from Jackson Laboratory (Bar Harbor, ME, United States). To generate the WT and AD mice for experimentation, female C57BL/6 mice were crossed with male APP/PS1 mice. Tail snips from each offspring were subjected to genotyping for PSEN1. Six-weeks old male mice (WT and AD, 6/group) were fed *ad libitum*, a standard diet (TD.2018 Envigo, Indianapolis, IN, United States) or a calorie rich western diet (TD.08811, Envigo, Indianapolis, IN, United States) for 7 months. Western diet contained 17.3% protein, 47.6% carbohydrate and 23.2% fat by weight which generate 14.7% kcal, 40.7% kcal, and 44.6% kcal, respectively. While composition of standard diet was 18.6% protein (24% kcal), 44.2% carbohydrate (58% kcal) and 6.2% fat (18% kcal). At the end of the study, mice were subjected to CO2 asphyxiation followed by euthanasia. Blood was collected by cardiac puncture in BD Microtainer tubes coated with K2 EDTA followed by centrifugation at 4°C for 15 min at 2000 rpm, and separated plasma was stored at – 80°C for analysis. The brain was snap frozen in liquid nitrogen and stored at – 80°C for RNA and protein analyses.

Cell Cultures

Mouse Brain Endothelial Cells (BEND3) and Human Brain Microvascular Endothelial Cells (HBMECs) were obtained from American Type Culture Collection (Cat # CRL-2299, Manassas, VA, United States) and NEUROMICS (Cat # HEC02, Edina, MN, United States), respectively. BV2 cells, mouse microglial cell line, cells were a kind gift from Dr. Dennis Selkoe (Harvard Medical School, Boston, MA, United States). BEND3 and BV2 cells were cultured in advanced DMEM/F12 medium (Cat # 12634-010, Gibco, Gaithersburg, MD, United States) containing 10% fetal bovine serum and 1% penicillin-streptomycin under standard culture conditions, and Endo-Growth Media (Cat # MED001, NEUROMICS, Edina, MN, United States) was used to grow HBMECs. **Generation of Sirt3-silenced cell lines:** BEND3 and BV2 cells were infected with Sirt3 shRNA Lentiviral particles (Cat # sc 61556) or control shRNA Lentiviral particles (Cat # sc 108080) using polybrene (0.5 μg/ml; Cat # sc 134220). Stable infected cells were selected using puromycin dihydrochloride (8 μg/ml, Cat # sc 10807) in DMEM media supplemented with 10% FBS for 4 weeks, and cells were pooled and maintained in the same medium. All the reagents, used for transfection, were from Santa Cruz Biotechnology (Dallas, TX, United States). Silencing of Sirt3 gene was confirmed by western blot analysis in stable infected cells.

RNA Isolation, PCR Array and RT-PCR Analysis

Total RNA was isolated from BEND3 and Sirt3-silenced (shSirt3) BEND3 cells exposed to high glucose and palmitic acid, using Versagene RNA isolation kit (Thermo Fisher Scientific, Hampton, NH, United States). RNA samples were treated with DNase and then converted to cDNA as described earlier (Velmurugan et al., 2012). The cocktail for PCR array was prepared by adding 1278 μl of the RT^2 qPCR SYBR Green master mix and 1173 μl H_20 to 102 μl of the diluted cDNA and 25 μl of this cocktail was added to each well of the 96-well PCR array plate (SABiosciences, Frederick, MD, United States) containing primers for the 84 genes in mouse inflammatory pathway, 5 housekeeping control genes and 3 RNA and PCR quality controls as in our previous study (Qin et al., 2016). The mRNA levels of Cox-2, CXCL1 RANTES, and GADD45β were measured by real-time quantitative RT-PCR using Taqman probes. Amplicons corresponding the amplification sequence was synthesized and used as standards in the RT-PCR analysis and the mRNA levels of chemokines were expressed in attograms (ag) per pg of GAPDH.

Western Blot Analysis

Cell/tissue lysates, from cultured cells, frontal cortical tissue of mice, and post-mortem human brain of AD patients and age-matched controls, were prepared with mammalian protein extraction buffer (Pierce, Rockford, IL, United States), supplemented with phosphatase and protease inhibitors as described previously (Pugazhenthi et al., 2013; Tyagi et al., 2018). The total protein concentration was determined by using Bradford assay Kit (Cat # 5000001, Bio-Rad, Hercules, CA, United States) in the supernatant of cell/tissue lysates. Briefly, equal amount of protein (∼30–50 μg/well) was resolved on a gradient 4–20% SDS-PAGE and separated proteins were then transferred to PVDF membrane. The membranes were blocked in blocking buffer (5% non-fat milk in TBST) for 1 h at room temperature. Subsequently, membranes were incubated with primary antibodies (1:1000) overnight on shaker

at 4°C, followed by alkaline phosphatase conjugated appropriate secondary antibody for 1 h. Signals were visualized by CDP-star reagent (Sigma Aldrich-St Louis, MO, United States) using ChemiDoc Imaging System (Bio-Rad, Hercules, CA, United States). The band intensities were quantified with reference to β-actin control bands, using Image Lab software from Bio-Rad. Primary antibodies, SIRT1 (Cat # 9475), SIRT3 (Cat # 5490), SIRT5 (Cat # 8782), SIRT6 (Cat # 12486), SIRT7 (Cat # 5360), Cox-2 (Cat # 12282), IKB-α (Cat # 4814), NF-κB p65 (Cat # 8242), Matrix metallopeptidase 9 (MMP-9; Cat # 13667) and β-actin (Cat # 4967) from Cell Signaling Technology (Danvers, MA, United States); claudin-5 (Cat # ab15106), Occludin (Cat # ab167161), ZO-1 (Cat # ab59720), CXCL1 (Cat # ab86436) and RANTES (Cat # ab189841) from AbCam (Cambridge, MA, United States); GADD45β (Cat # MBS821452) from MyBioSource (San Diego, CA, United States), were used for immunoblotting.

Immunofluorescent Staining

Cells were fixed in 4% paraformaldehyde for 20 min followed by gentle rinsing three times for 5 min each with PBS. The cells were permeabilized with 5% BSA and 0.2% Triton X-100 in PBS for 60 min and then incubated with primary antibodies, rabbit anti-claudin-5 (Cat # ab15106; 1:1000 dilution), rabbit anti-ZO-1 (Cat # ab59720; 1:1000 dilution) or rabbit anti-Iba1 (Cat # 019-19741, Wako, Richmond, VA, United States;1:2000 dilution), overnight at 4°C in a humidified chamber. Next day, following three washes with PBS, cells were incubated with appropriate secondary antibodies conjugated to Alexa Fluor (Alexa Flour 488 or Alexa flour 594) and DAPI (2 μg/ml; nuclear stain) in dark for 1 h followed by three washes with PBS. The immuno-stained cells were mounted with Prolong Gold Antifade reagent, and images of stained cells were captured with the Leica SP8 confocal microscope with white laser, using a Leica HC PL APO 40 × 1.30 NA oil objective.

Microglial - Endothelial Cocultures and TEER Measurement

Transendothelial electrical resistance (TEER) is an important measure of BBB integrity, using a cell culture model. To determine how the interactions between microglia and BMEC lead to compromised BBB integrity, and further to identify how silencing Sirt3 gene in these cells affects BBB, thus these cells were cocultured as shown in **Figure 6A**. BV2 or shSirt3-BV2 cells were cultured on the bottom well of a 6-well dish. In parallel, BEND3 or shSirt3-BEND3 cells were cultured on coated transwell inserts, placed in another 6-well dish. When the cell culture reached ∼70% confluence, the inserts were placed in over cultured microglia. First, the inserts were placed in the dish without microglia to measure background resistance at 37°C with heating plate using EVOM resistance meter (World Precision Instrument, Sarasota, FL, United States). Then the inserts with endothelial cells were placed in dishes with microglia and treated with high glucose (30 mM), palmitic acid (300 μM) or the combination of both for 48 h. In another set of similar experiment, we exposed BV2 cells to a combination of cytokines (20 ng/ml TNF-α, 20 ng/ml IL-1β, and 20 ng/ml IFNγ) and the coculture was continued for 6 days. Resistance was measured at 24 h time intervals. Altered endothelial cell permeability was determined from the TEER values.

Plasma Assays

Insulin levels were determined using mouse Insulin ELISA kit (Cat # 80-INSMS-EO1, ALPCO, Salem, NH, United States). C-reactive protein (CRP) and interleukin-1beta (IL-1β) were measured using CRP (Cat # MCRP00) and IL-1β (Cat # MLB00C) mouse ELISA kit, respectively, from R &D systems (Minneapolis, MN, United States). Plasma triglycerides were assayed using a colorimetric kit (Cat # ab65336) from Abcam, Cambridge, MA, United States. Assays were performed following the manufacture's protocol.

Statistical Analysis

All statistical analyses were carried out using GraphPad software. Significant differences between groups were determined by one-way ANOVA followed by Dunnett's test, and two-sided P values of < 0.05 were considered significant.

RESULTS

Western Diet Induces Insulin Resistance and Neuroinflammation and Reduces the BBB Integrity in APP/PS1 Mice

Having characterized a genetic model for comorbid AD previously (Tyagi et al., 2020), herein we examined a lifestyle-based AD model with metabolic syndrome (MetS). As expected, western diet feeding in wild type mice resulted in 2–2.7-fold increase ($P < 0.01$) in plasma levels of insulin, triglycerides, CRP and IL-1β (**Figure 1A**). APP/PS1 mice were also characterized by significant hyperinsulinemia ($P < 0.01$) and modest increases in the levels of IL-1β ($P < 0.05$). The combination of western diet and amyloid pathology resulted in significant increases in the circulating levels of insulin (3.8-fold, $P < 0.001$), triglycerides (2.8-fold, $P < 0.001$), CRP (2.0-fold, $P < 0.01$), and IL-1β (3.0-fold, $P < 0.01$) as compared to wild type mice fed standard diet (**Figure 1A**), suggesting diet-induced exacerbation of insulin resistance and inflammation. Further examination of the brain frontal cortical samples by Western blot analysis (**Figure 1B**), followed by quantitation (**Figure 1C**) revealed 52% ($P < 0.01$) decrease SIRT3 levels in the western diet-fed wild type mice. IkBα levels decreased by 58%, ($P < 0.01$) suggesting NF-kB activation. BMECs are an important component of BBB. The uniqueness of BMECs is due to TJs proteins, including claudin-5. There was a 38% decrease ($P < 0.01$) in claudin-5 levels in western diet-fed mice. SIRT3 and claudin-5 did not change significantly in APP/PS1 mouse brain whereas they were significantly reduced in western-diet-fed APP/PS1 mouse brain, compared to wild type mouse brain. However, IkBα expression was significantly less (42%, $P < 0.01$) in APP/PS1 mice, and further its levels decreased by 77% ($P < 0.001$) in western diet-fed APP/PS1 mice, as compared to wild type control mice.

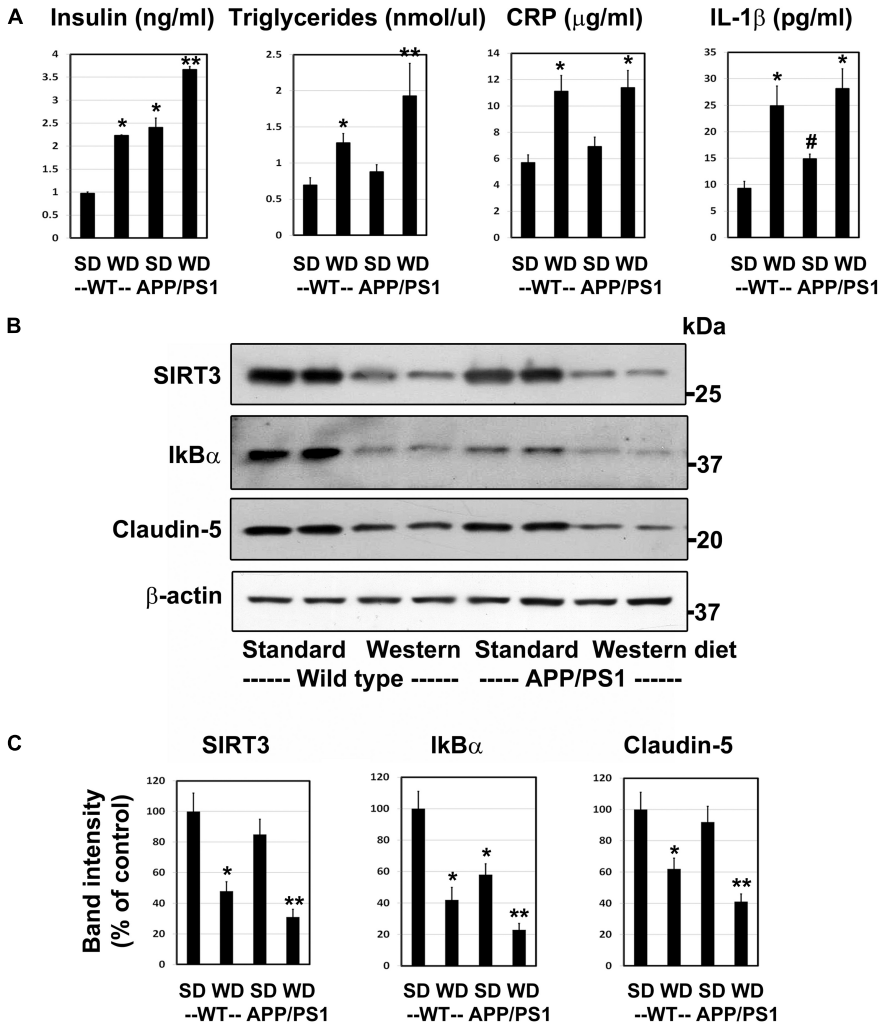

FIGURE 1 | Western diet induces insulin resistance and neuroinflammation and reduces the BBB integrity in APP/PS1 mice. **(A)** 6 weeks-old Wild type (WT) and APP/PS1 male mice were fed on standard diet (SD) or energy-rich western diet (WD) for 7 months. Plasma levels of insulin, CRP and IL-1β were assayed by ELISA. Plasma triglycerides levels were determined calorimetrically using assay kit. All assays were performed following the manufactures' protocol. **(B)** Mouse cortical samples from the four groups of mice were collected for the Western blot analysis of SIRT3, IkBα and claudin-5. The blots were re-probed for β-actin. **(C)** The band intensities were determined by scanning, corrected for β-actin levels, and expressed as percent of control. Data are expressed as mean of ± SE (n = 6) for each group. $^{\#}$, $P < 0.05$; *, $P < 0.01$; **, $P < 0.001$ vs WT mice on standard diet.

Overall, western diet-fed APP/PS1 mice were characterized by hyperinsulinemia, and neuroinflammation like our previously reported genetic model of comorbid AD (Tyagi et al., 2020). In addition, western diet reduced the levels of claudin-5, suggesting compromised BBB integrity.

Downregulation of Sirtuin Pathway and Compromised BBB Integrity in the Human Alzheimer Post-mortem Brain

To determine if the findings in mouse models of comorbid AD are observed in human AD, we examined post-mortem human brain samples of AD cases and age-matched controls by Western blot analysis (**Figure 2A**). The sirtuin family of proteins were significantly reduced in Alzheimer's patients compared to age-matched controls (**Figure 2B**). The levels of SIRT1, 3, 6, and 7 decreased by 33–53% ($P < 0.01$). SIRT5 was nearly absent (88%, $P < 0.001$) in AD brain samples. These findings are like our observations in APP/PS1/Sirt3$^{-/-}$ mouse brain (Tyagi et al., 2020). Damage to BBB is another well-known feature of AD brain (Erickson and Banks, 2013; Sweeney et al., 2019). As expected, the levels of TJ proteins claudin-5, occludin and ZO-1 decreased by 36–66% ($P < 0.01$-$P < 0.001$), suggesting compromised BBB integrity in the AD brain. MMP-9 is an enzyme that belongs to zinc metalloproteinases family which plays a key role in the degradation of the extracellular matrix of BBB (Van Dyken and Lacoste, 2018). The levels of the active cleaved MMP-9 (lower band) increased by 66% ($P < 0.01$) in the Alzheimer's brain. This enzyme may play an additional role in increasing BBB permeability in this neurodegenerative disease. These two sets

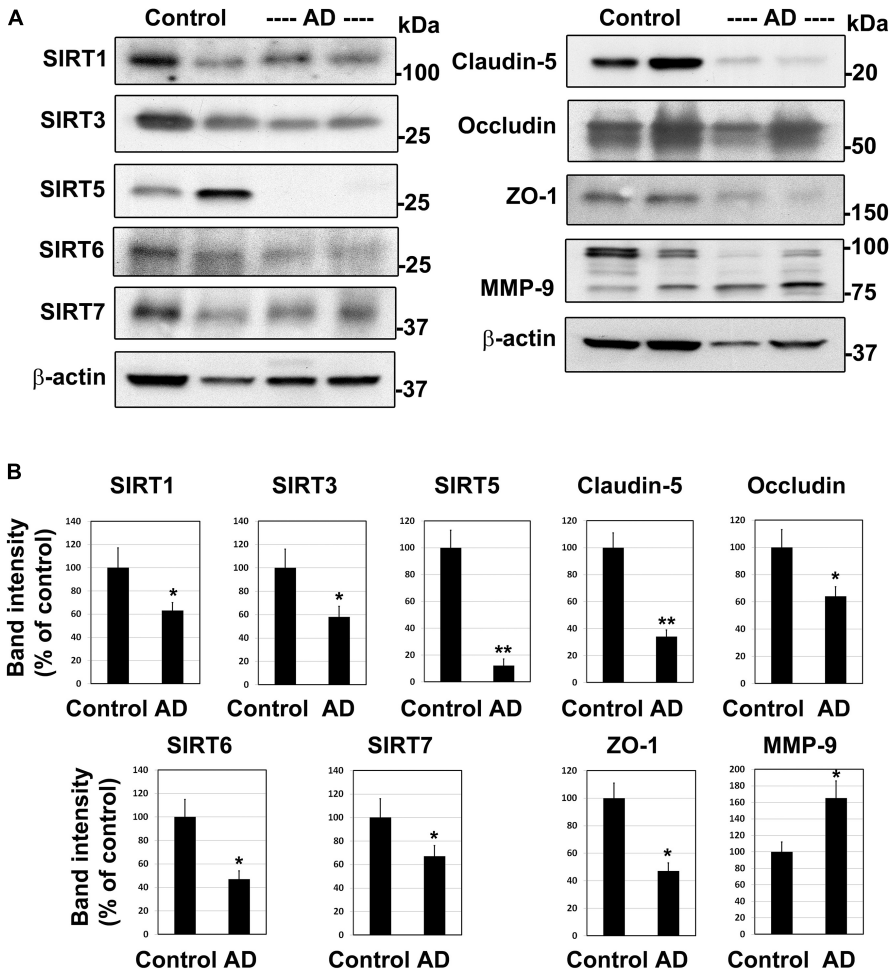

FIGURE 2 | Downregulation of sirtuin pathway and compromised BBB integrity in the human Alzheimer post-mortem brain. **(A)** Post-mortem brain samples of AD cases and age-matched controls were obtained from Garrison Institute of Aging, Lubbock, TX. Western blot analysis was performed for SIRT1, SIRT3, SIRT5, SIRT6, SIRT7, MMP-9 and tight junction proteins, claudin-5, occludin and ZO-1. The blots were re-probed for β-actin. Representative images of 20 samples are presented. **(B)** The band intensities were determined by scanning, corrected for the levels of β-actin and expressed as percent of control. *, $P < 0.01$; **, $P < 0.001$ vs control. AD, Alzheimer's disease.

of findings on sirtuins, involved in metabolic regulation and TJ proteins, markers of BBB integrity raise a key question of whether they are causally linked. Therefore, we used cell culture studies to address the link between these two pathways.

Glucolipotoxicity-Mediated BMEC Injury

Under conditions of MetS, endothelial cells are constantly exposed to high glucose and dyslipidemia, resulting in vascular injury. To determine the effects of glucolipotoxicity on BMECs, we performed cell culture studies with BEND3 cells, a mouse brain microvascular endothelial cell line. Following exposure of these cells to high glucose (30 mM) and palmitic acid (300 μM), we examined the levels of SIRT3 and TJ proteins by Western blot analysis. Palmitic acid decreased the levels of SIRT3 (35%; $P < 0.05$), claudin-5 (47%; $P < 0.01$) and ZO-1 (62%; $P < 0.001$) (**Figure 3A**). Surprisingly, high glucose did not change their levels. With the combination of high glucose and palmitic acid, the decreases in SIRT3 and TJ proteins were by 50–68% ($P < 0.01$-$P < 0.001$). Overall, palmitic acid was found to be more toxic to BEND3 cells compared to high glucose. In addition, we exposed primary human BMECs to high glucose and palmitic acid and examined the TJ proteins by immunofluorescent staining. We observed significant loss of claudin-5 (upper panel) and ZO-1 (lower panel) when the endothelial cells were exposed to palmitic acid (**Figure 3B**). High glucose did not have any effect on TJ proteins.

Induction of Inflammatory Genes in Endothelial Cells Exposed to Glucolipotoxicity

To determine if BMECs stressed in MetS release inflammatory mediators in the brain, we exposed BEND3 and shSirt3-BEND3 cells to a combination of high glucose and palmitic acid. Subsequently performed pathway-specific array for NF-kB target

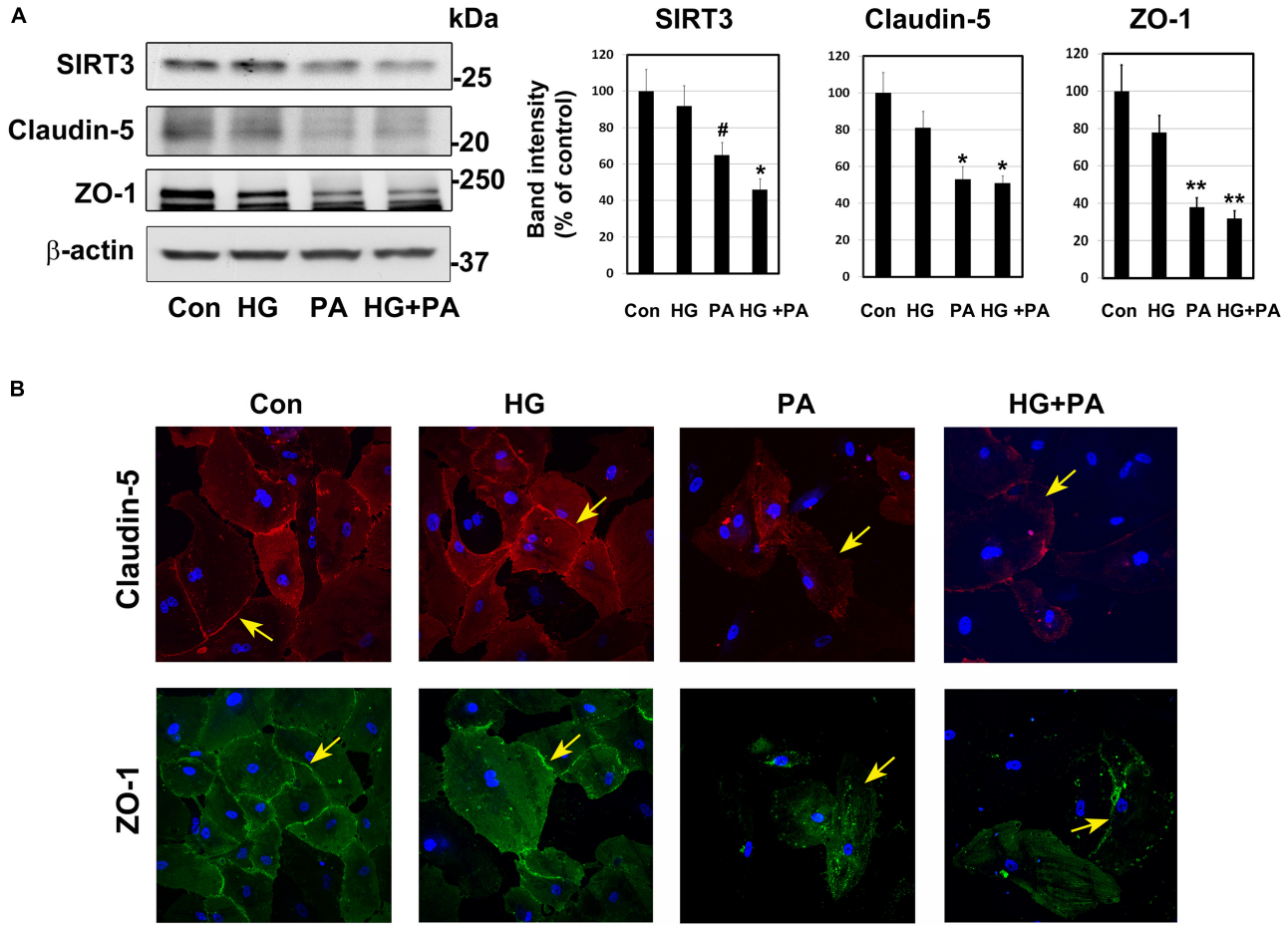

FIGURE 3 | Glucolipotoxicity-mediated BMEC injury. **(A)** BEND3 cells, a mouse brain endothelial cell line, were exposed to HG, PA or the combination of both for 48 h and processed for the immunoblotting of SIRT3, claudin-5 and ZO-1. The blots were re-probed for β-actin. The bands were scanned and corrected for the levels of β-actin. $^{\#}$, $P < 0.05$; *, $P < 0.01$; **, $P < 0.001$ compared to untreated controls. **(B)** BMECs isolated from human fetal brain (Neuromics) were cultured in the presence of HG, PA or combination of both for 24 h. The cells were fixed and immunostained for claudin-5 with Alexa flour 594 (red; upper panel) or for ZO-1 with Alexa flour 488 (green; lower panel). The nuclei were stained blue with DAPI. Images of stained cells were captured with the Leica SP8 confocal microscope with white laser, using a Leica HC PL APO 40 × 1.30 NA oil objective. HG, high glucose (30 mM); PA, palmitic acid (300 μm).

genes with these treated cells. We observed strong induction of several genes in the inflammatory pathway following exposure to high glucose and palmitic acid (**Table 1**). There was a 124-fold induction of Cox-2 gene and 28-fold induction of CXCL1 in BMECs exposed to a combination of high glucose and palmitic acid. Other chemokines including RANTES (CCL5), GADD455β and CXCL10 were also induced significantly. In general, the induction was significantly more with Sirt3-silenced endothelial cells, suggesting that MetS exacerbates the inflammatory response. To further confirm the induction of selected inflammatory genes, we performed quantitative RT-PCR analysis, using Taqman probes. For this experiment, the cells were treated with high glucose, palmitic acid or the combination of them. Interestingly, the induction was observed only with palmitic acid and not with glucose (**Figure 4A**). Cox-2 was induced by 96 and 204 folds ($P < 0.001$) in BEND3 and shSirt3-BEND3 cells, respectively. Similar induction of CXCL1 by the fatty acid was observed in these cells. Exacerbated induction in Sirt3-silenced BEND3 cells suggest that these cells are more prone for inflammatory response under conditions of SIRT3 deficiency which will be seen in MetS. The mRNA levels of RANTES and GADD45β were also elevated significantly ($P < 0.01$-$P < 0.001$), following exposure to palmitic acid although to a smaller extent. Next, we examine the levels of induced inflammatory mediators at the protein levels, we performed Western blot analysis with BEND3/shSirt3-BEND3 cells incubated in the presence of high glucose, palmitic acid or in combination of both (**Figure 4B**). Fivefold increase in the levels of Cox-2 protein was observed following exposure to palmitic acid to BEND3 cells ($P < 0.001$). In the case of shSirt3-BEND3 cells, palmitic acid increased Cox-2 levels by eightfolds ($P < 0.001$, **Figure 4C**). Surprisingly, in the case of other inflammatory mediators, CXCL1, RANTES, and GADD45β, we did not observe any significant change at the protein level, suggesting impairment of translation or stability of their mRNA.

TABLE 1 | BEND3 and shSirt3-BEND3 cells were incubated in the absence (control) and presence of a combination of high glucose (30 mM) and palmitic acid (300 μM) for 48 h.

	PCR array of NF-κB target genes			
	————BEND3————		————shSirt3-BEND3————	
	Control	HG + PA	Control	HG + PA
Cox-2	1	124	2.4	256
CXCL1	1	27.9	1.01	39.9
RANTES	1	6.1	1.8	15
GADD45β	1	6.8	−1.14	10.9
Adrenomedullin	1	7.4	−1.04	10.9
CXCL10	1	2.2	1.2	5.5
NQO1	1	3.0	1.6	3.1
Myc	1	2.6	−1.05	2.4
NF-κBIA	1	2.3	1.2	2.3

The cells were processed for RNA isolation and pathway-specific gene expression array was performed. Fold inductions over BEND3-control are presented. shSirt3, Sirt3-silenced.

Effects of SIRT3 Deficiency on Microglial and Endothelial Cell Interactions

To determine if SIRT3 deficiency dysregulates interactions between microglia and endothelial cells in the presence of high glucose and palmitic acid, we performed mixed cultures of BV2/BEND3 and shSirt3-BV2/shSirt3-BEND3 cell lines. Western blot analysis showed significant reduction (∼ 75%) in SIRT3 protein levels in the shSirt3-BEND3 and shSirt3-BV2 stable cell lines (**Figure 5A**). Immunofluorescent staining for microglial cells in the mixed culture showed changes in microglial morphology, suggesting activation, following exposure to a combination of high glucose and palmitic acid (**Figure 5B**). In the case of mixed cultures with Sirt3-silenced cell lines, glucolipotoxicity was more along with enhanced microglial activation, suggesting that microglial and endothelial interactions may be dysregulated during MetS.

Measurement of Barrier Function in Endothelial Cells (TEER)

Brain microvascular endothelial cells are unique compared to other endothelial cells because they are joined together by TJ proteins which play a key role in BBB integrity. TEER measurement is a standard method to determine electrical resistance across BMECs.To determine if interactions between BMECs and microglia affects BBB permeability and if SIRT3 plays a role in this interaction, we performed coculture of BEND3 and BV2 cells as shown in **Figure 6A**. Similar coculture was also performed with shSirt3-BEND3 and shSirt3-BV2 cells. When these cocultures were exposed to palmitic acid, there was a modest decreases ($P < 0.05$) in TEER values (**Figure 6B**). Interestingly, TEER values were slightly higher (not significant) when cells were exposed to high glucose + palmitic acid, suggesting high glucose might be protecting the cells from lipotoxicity effect of palmitic acid (**Figure 6B**). Similar results were observed with coculture of shSirt3-BEND3 and shSirt3-BV2 cells. Because there was toxicity to the cells with palmitic acid after 48 h, we designed another long-term exposure with a combination of cytokines, as a model for chronic inflammation. We observed that permeability across BMECs increased (decreased TEER) in a time-dependent manner when cocultured with microglial cells, exposed to a mixture of cytokines (**Figure 6C**). The decrease was more when Sirt3-silenced cells (BV2 and BMECs) were used for coculture.

DISCUSSION

Several prior studies have suggested that the pure form of AD is rare, and it coexists with the brain lesions caused by comorbidities namely obesity, diabetes, hypertension, and cardiovascular disease (Montine et al., 2012; Kawas et al., 2015; Baglietto-Vargas et al., 2016; White et al., 2016). In a recent study, we reported the generation of a genetically induced comorbid AD mouse model with amyloid pathology and MetS (Tyagi et al., 2020). In this comorbid mouse model, exacerbation of MetS, neuroinflammation, and Alzheimer's pathology were observed. MetS, a cluster of risk factors, is the early phase of comorbidities. There are multiple pathways through which MetS can interact with CNS and dysregulate homeostasis of the brain. MetS can cause vascular injury in the brain, leading to BBB breakdown, neuroinflammation and microglial activation (Newcombe et al., 2018; Zlokovic et al., 2020). In the current study, we examined the effects of MetS on BMECs by *in vivo* and *in vitro* studies. Our main findings suggest the involvement of BMECs and microglia (**Figure 7A**). Particularly, we demonstrate that hyperlipidemia, observed in MetS and obesity modulate BMECs tight junction and induces inflammatory mediators which activate microglia, resident immune cells of the brain (**Figure 7B**).

Having characterized a genetic model of comorbid AD (Tyagi et al., 2020), herein we examined a life-style-based model. Following the feeding of APP/PS1 mice with western diet, enriched with saturated fat and simple sugars, we observed markers of MetS in this comorbid AD mice. These mice were characterized by hyperinsulinemia, hypertriglyceridemia and elevated levels of CRP. These findings are like our observations in APP/PS1/Sirt3$^{-/-}$ mouse brain (Tyagi et al., 2020). Damage to BBB is another well-known feature of AD brain (Erickson and Banks, 2013; Sweeney et al., 2019). Previous studies have examined the role of BBB permeability in AD (Yamazaki et al., 2019; Huang et al., 2020) as well as during diet-induced obesity (Ouyang et al., 2014). Therefore, we examined the levels of claudin-5 (TJ protein) with brain samples and observed additive effects of AD and diet-induced obesity (**Figure 1B**). Similar additive effects were seen with SIRT3 levels. Examination of AD post-mortem samples revealed downregulation of sirtuin pathway and decreases in the levels of TJ proteins (**Figure 2**). MMP-9 is an enzyme that belongs to zinc metalloproteinases family which plays a key role in the degradation of the extracellular matrix of BBB (Van Dyken and Lacoste, 2018). We also observed elevation of the active cleaved fragment of MMP-9 which degrades TJs proteins. SIRT3 deficiency is

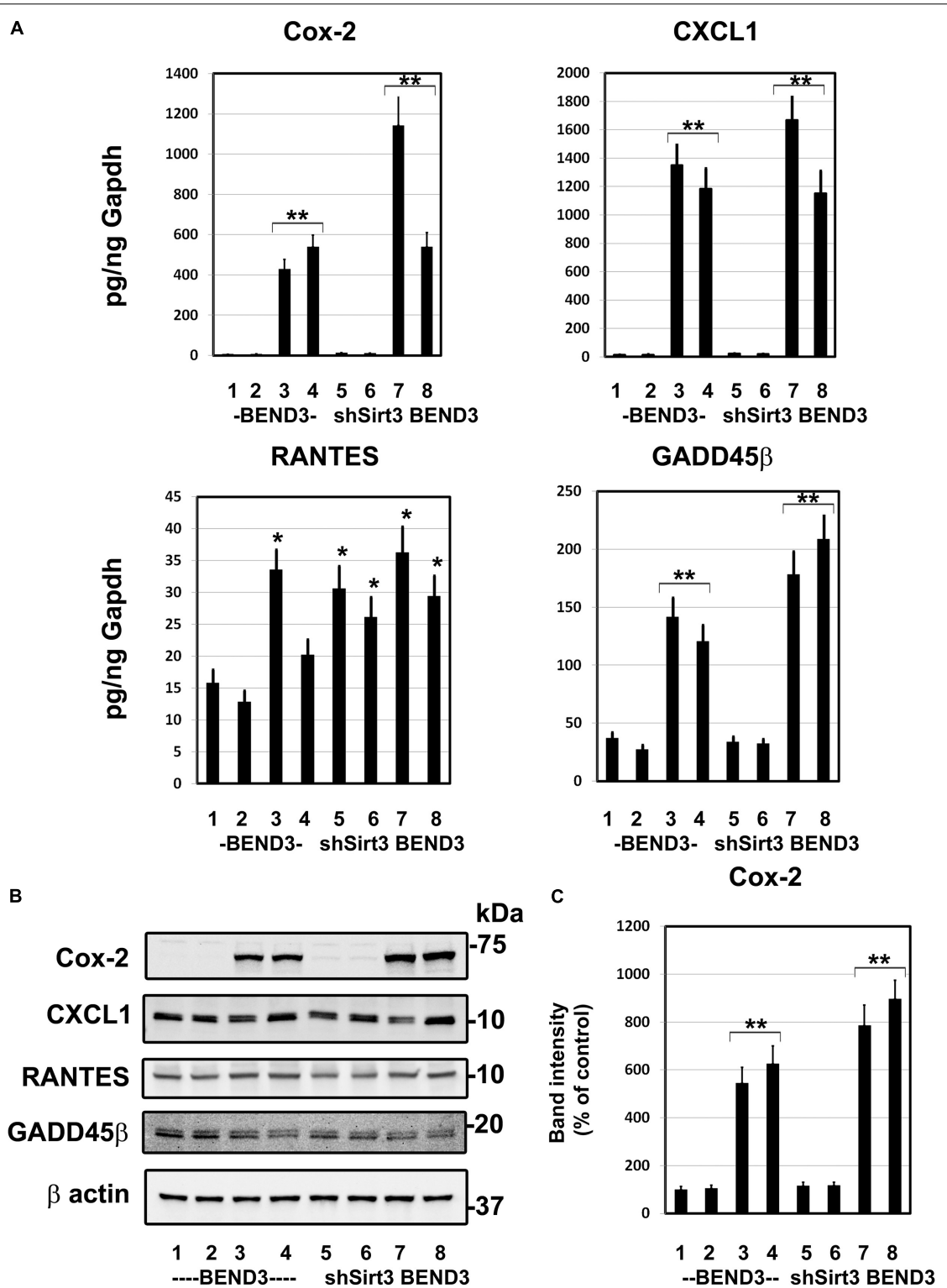

FIGURE 4 | Induction of inflammatory genes in endothelial cells exposed to glucolipotoxicity. **(A)** BEND3 and shSirt3- BEND3 cells were cultured in the absence (1) or presence of 30 mM glucose (2), 300 μM palmitic acid (3) or combination of both (4) for 48 h. The cells were processed for RNA isolation and RT-PCR analysis of Cox-2, CXCL1, RANTES, and GADD45β. mRNA levels of chemokines were expressed in attograms (ag) per pg of GAPDH. **(B)** BEND3 and shSirt3-BEND3 cells were cultured in the absence (1) or presence of 30 mM glucose (2), 300 μM palmitic acid (3) or combination of both (4) for 48 h. The cell lysates were prepared and immunoblotted for Cox-2, CXCL1, RANTES and GADD45β. The blots were re-probed for β-actin. **(C)** The bands for Cox-2 were scanned and corrected for the levels of β-actin. *, $P < 0.01$; **, $P < 0.001$ vs untreated controls. shSirt3, Sirt3-silenced.

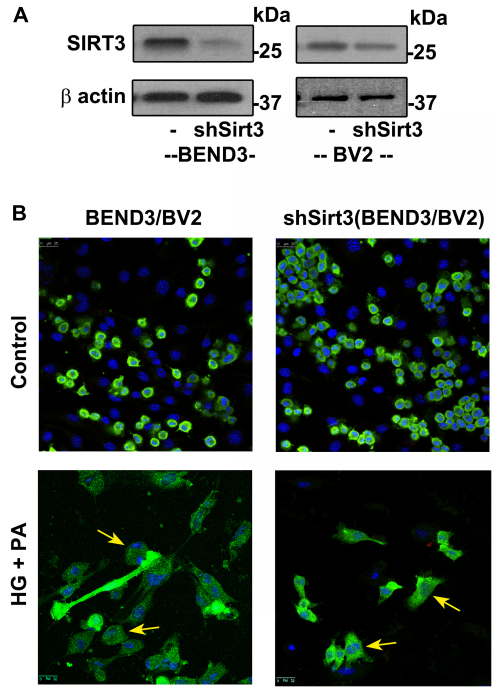

FIGURE 5 | Effects of SIRT3 deficiency on microglial and endothelial cell interactions. **(A)** Lysates, from BEND3, shSirt3-BEND3, BV2, and shSirt3-BV2 cells, were immunoblotted for SIRT3 and β-actin. **(B)** Mixed cultures of BEND3/BV2 and shSirt3-BEND3/shSirt3-BV2 were incubated in the absence and presence of high glucose (HG 30 mM) and palmitic acid (PA 300 μm) for 48 h. The treated cells were fixed and immunostained for Iba1 with Alexa Flour 488 (green). Nuclei were stained blue with DAPI. Images of stained cells were captured with the Leica SP8 confocal microscope with white laser, using a Leica HC PL APO 40 × 1.30 NA oil objective. shSirt3, Sirt3-silenced.

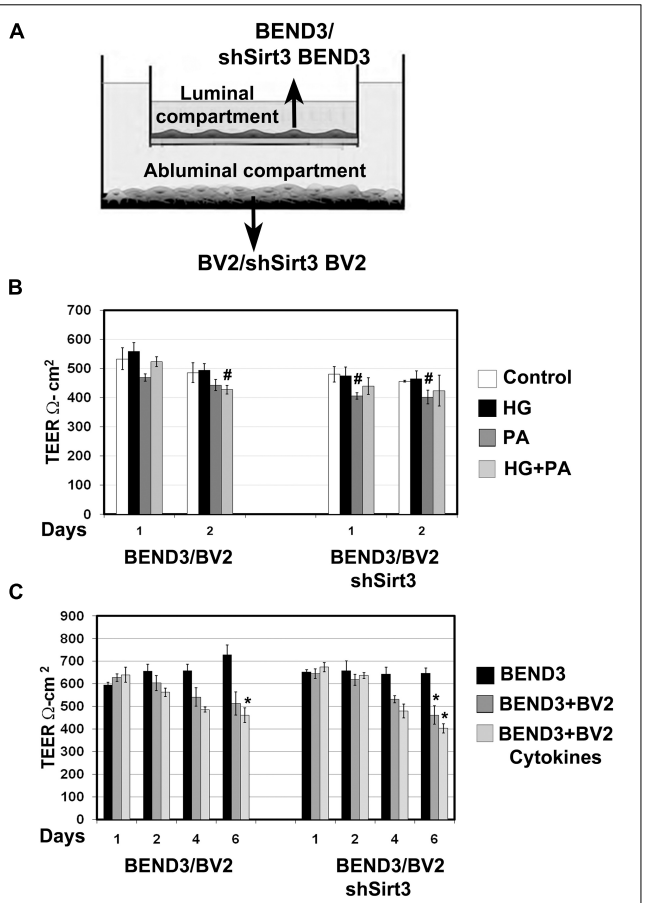

FIGURE 6 | Measurement of barrier function in endothelial cells (TEER). **(A)** An *In vitro* co-culture model of microglial and endothelial cells: Culture of BEND3 or shSirt3-BEND3 cells in the Boyden chamber inserts, while BV2 or shSirt3-BV2 cells in the bottom wells were performed. **(B)** The cocultures were incubated in the absence and presence of high glucose (HG 30 mM), palmitic acid (PA 300 μm), or combination of both for 24 h and 48 h. TEER was measured, using EVOM resistance meter after 24 h and 48 h. **(C)** The cocultures were exposed to a combination of cytokines (20 ng/ml each of TNF-α, IL-1β, and IFN-γ) for 6 days, followed by TEER measurement. #, $P < 0.05$; *, $P < 0.01$ vs untreated controls. shSirt3, Sirt3-silenced.

known to accelerate the progression of MetS (Hirschey et al., 2011). Calorie restriction by fasting upregulates SIRT3 expression (Nogueiras et al., 2012). Brain vasculature is critical for cognition. Vascular dementia (VaD) is the second most common form of dementia after AD. However, significant overlap between these two forms is being recognized. The overlap ranges from AD with vascular dysfunction to mixed type of dementia (Iadecola, 2013). When cerebrovascular lesions are often observed in aged brains, it is difficult to consider VaD as a distinct type (Gorelick et al., 2011). Deteriorating vascular function and the progressive neurodegenerative process need to be viewed as converging pathogenic mechanisms.

There were elevated plasma levels of IL-1β and triglycerides in western diet-fed mice (**Figure 1A**). Cytokines are known to pass through BBB and induce the secondary inflammatory pathway in the brain (Banks, 2005; Yarlagadda et al., 2009). Induction of cytokines and chemokines in hippocampus is observed following systemic challenge with IL-1β and TNFα in mice (Skelly et al., 2013). Microglia are known to be primed in the aging brain and they respond to peripheral inflammation with greater severity and duration (Dilger and Johnson, 2008). Although dyslipidemia has been shown to correlate with BBB impairment in Alzheimer's patients (Bowman et al., 2012), its effects on the CNS, especially as a potential cause of neuroinflammation has not been investigated. Our current study focused on the role of lipotoxicity observed during diet-induced obesity. In this study, we demonstrate that palmitic acid induces an array of inflammatory mediators in cultured BEND3 cells. Induction of gene expression of inflammatory mediators, including Cox-2, CXCL1, RANTES, and GADD45β were observed in these treated cells. Cox, a rate limiting enzyme in the synthesis of prostaglandins (PGs), catalyzes the conversation of arachidonic acid to PGs. While Cox-1 is constitutively expressed, Cox-2 is the inducible form. This enzyme is known to play a key role in the development of vascular inflammation (Grace et al., 2014; Voyvodic et al., 2014). Induction of Cox-2 is known to further induce inflammatory mediators in neurodegenerative diseases (Minghetti, 2004). We observed strong induction of Cox-2 at the mRNA and protein levels in BEND3 cells exposed

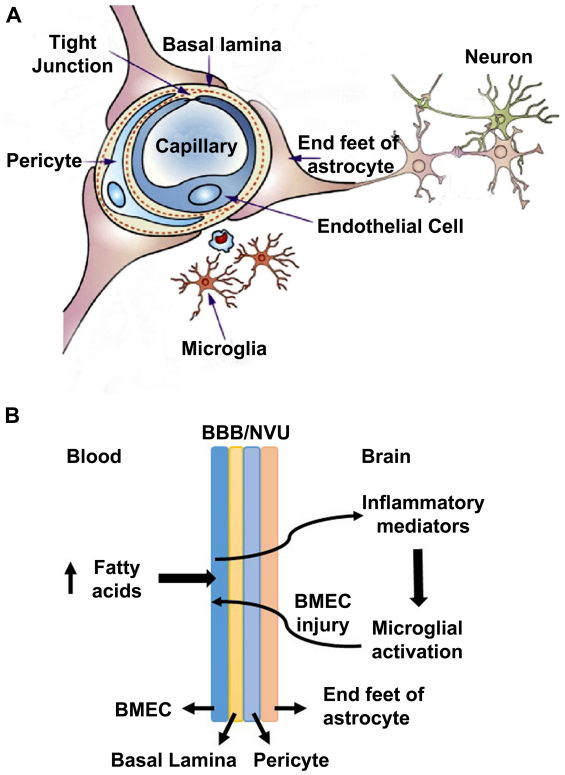

FIGURE 7 | A model for the interactions of obesity with BBB **(A)** A schematic diagram for the neurovascular unit (NVU) is presented here. NVU comprises of brain microvascular endothelial cells (BMECs), end feet of astrocytes and pericytes. BMECs are glued together by tight-junction (TJ) proteins, which form the blood brain barrier to maintain the homeostasis of the brain. **(B)** A potential mechanism is presented here, based on the findings of this study. High concentration of saturated fatty acids in blood, as observed in obesity, acts on BMECs and induces the expression of inflammatory mediators, which activate microglia. Activated microglia, in turn acts on BMECs, leading to a vicious cycle.

to palmitic acid (**Figure 4**). Interestingly, the induction was more with Sirt3-silenced BEND3 cells, suggesting that Sirt3 deficiency exacerbates inflammatory response. Although Cox-2 mRNA levels closely mirror protein levels, surprisingly, the robust induction of other inflammatory mediators by palmitic acid was not reflected at their corresponding protein level. This discrepancy can be explained by posttranscriptional regulation of mRNA, as it is reported to vary among different cytokines/chemokines. Previous studies have suggested that the mRNA stability of cytokines and chemokines are highly regulated, and posttranscriptional regulation of their mRNA has a role in governing the inflammation (Herman and Autieri, 2017).

Previous studies have suggested that sirtuins play a role in BBB integrity. Increased BBB permeability, decreased expression of TJs protein (claudin-5) along with decreases in mRNA levels of Sirt1 in the brain microvessels have been reported in aged mice (Stamatovic et al., 2019). This study also demonstrated the loss of BBB integrity in Sirt1-silenced mice. Another study reported minocycline-mediated improvement in BBB integrity by a mechanism involving SIRT3 by *in vivo* and *in vitro* studies under hypoxic conditions (Yang et al., 2015). Minocycline decreased BBB permeability to Evans Blue in rats and increased TEER in cultured HBMECs after hypoxia. These effects were lost following the silencing of Sirt3. AMPAR antagonist perampanel has been shown to protect NVU by a mechanism involving Sirt3 (Chen et al., 2021). However, the role of sirtuins have not been examined under conditions of comorbid AD. Our findings on the dysregulation of microglial and BMEC interactions are significant in the context of SIRT3 deficiency in comorbidities which further induces an inflammatory response. We have previously reported the formation of inflammasomes in the brain samples of Sirt3$^{-/-}$ mice (Tyagi et al., 2018).

Significant cytotoxicity and changes in microglial morphology were observed when cocultures of shSirt3-BEND3 and shSirt3-BV2 cells were exposed to HG and PA. TEER measurement with these cocultures suggested decreased barrier integrity. Previous studies have reported that microglia through their distinct phenotypes regulate BBB integrity (Ronaldson and Davis, 2020). Microglia play biphasic roles in terms of BBB integrity in a context dependent manner (Ronaldson and Davis, 2020). Following BBB injury juxtavascular microglia migrated to the site and close the leak through their processes with P2RY12 receptor (Lou et al., 2016). However, proinflammatory cytokines released from activated microglia are also known to decrease the expression of TJs and increase the expression of MMP-9 which degrades TJ proteins (Wiggins-Dohlvik et al., 2014). Perivascular microglia cause necroptosis of endothelial cells, following ischemic/reperfusion injury by a mechanism involving TNF-α (Chen et al., 2019). Aβ-stimulated microglia decrease the levels of TJ proteins in cocultured BEND3 cells whereas unstimulated microglia increased their content (Mehrabadi et al., 2017). Inflammatory signals have been shown to be amplified by communications between BMECs and glial cells (Krasnow et al., 2017). LPS-activated microglia increase the permeability of BMECs by a mechanism involving NADPH oxidase (Matsumoto et al., 2012). IL-1β induced induction of proinflammatory cytokines in microglia was significantly more when cocultured with BMECs (Zhu et al., 2019). During BBB damage, fibrinogen leakage can induce clustering of microglia near the perivascular region, leading to neuronal injury (Davalos et al., 2012).

CONCLUSION

The findings of this study suggest that hyperlipidemia in comorbidities of AD can compromise BBB integrity by inducing inflammatory mediators and decreasing TJ proteins in the vascular endothelial cells of the AD brain, leading to activation of microglia. We propose a model (**Figure 7**) in which BMECs serve as a gateway in the crosstalk between peripheral and central inflammation. As BMECs line the luminal side, they are in constant contact with circulating factors and in communication with circulating immune cells. These cerebrovascular endothelial cells are critical sensors of peripheral inflammation and mediators of microglial activation. In this model, elevated circulating fatty acids during diet-induced obesity act on

BMECs and induce inflammatory mediators which activate microglia. Under conditions of Sirt3 deficiency this microglial and endothelial interactions are further exacerbated.

DATA AVAILABILITY STATEMENT

The original contributions presented in the study are included in the article/**Supplementary Material**, further inquiries can be directed to the corresponding author/s.

ETHICS STATEMENT

The animal study and the experimental procedures were approved by IACUC at Rocky Mountain Regional Veteran Affairs Medical Center, Aurora, CO.

AUTHOR CONTRIBUTIONS

AT and SP designed the experiments and wrote the manuscript. AT supervised the mouse experiments, sacrificed the animals, collected the tissues, and performed the immunofluorescent staining. IS did the Immunoblotting. CM contributed to the microscopic image capture and analysis. PHR provided the human post-mortem brain samples of AD cases and age-matched controls. All authors reviewed and approved the manuscript.

FUNDING

This study was supported by a Merit Review grant NEUD-004-07F from the Veterans Administration (to SP).

ACKNOWLEDGMENTS

This work was carried out with the use of resources and facilities at the Rocky Mountain Regional Veterans Administration Medical Center. Confocal microscopy was carried out at the VA Microscopy Core Facility.

SUPPLEMENTARY MATERIAL

The Supplementary Material for this article can be found online at: https://www.frontiersin.org/articles/10.3389/fnagi.2021.716616/full#supplementary-material

REFERENCES

Aguilar, M., Bhuket, T., Torres, S., Liu, B., and Wong, R. J. (2015). Prevalence of the metabolic syndrome in the United States, 2003-2012. *JAMA* 313, 1973–1974. doi: 10.1001/jama.2015.4260

Baglietto-Vargas, D., Shi, J., Yaeger, D. M., Ager, R., and LaFerla, F. M. (2016). Diabetes and Alzheimer's disease crosstalk. *Neurosci. Biobehav. Rev.* 64, 272–287. doi: 10.1016/j.neubiorev.2016.03.005

Banks, W. A. (2005). Blood-brain barrier transport of cytokines: a mechanism for neuropathology. *Curr. Pharm. Des.* 11, 973–984. doi: 10.2174/1381612053381684

Bowman, G. L., Kaye, J. A., and Quinn, J. F. (2012). Dyslipidemia and blood-brain barrier integrity in Alzheimer's disease. *Curr. Gerontol. Geriatr. Res.* 2012:184042. doi: 10.1155/2012/184042

Chen, A. Q., Fang, Z., Chen, X. L., Yang, S., Zhou, Y. F., Mao, L., et al. (2019). Microglia-derived TNF-alpha mediates endothelial necroptosis aggravating blood brain-barrier disruption after ischemic stroke. *Cell Death Dis.* 10:487. doi: 10.1038/s41419-019-1716-9

Chen, T., Liu, W. B., Qian, X., Xie, K. L., and Wang, Y. H. (2021). The AMPAR antagonist perampanel protects the neurovascular unit against traumatic injury via regulating Sirt3. *CNS Neurosci. Ther.* 27, 134–144. doi: 10.1111/cns.13580

Crotti, A., and Ransohoff, R. M. (2016). Microglial physiology and pathophysiology: insights from genome-wide transcriptional profiling. *Immunity* 44, 505–515. doi: 10.1016/j.immuni.2016.02.013

Daneman, R., and Prat, A. (2015). The blood-brain barrier. *Cold Spring Harb. Perspect. Biol.* 7:a020412. doi: 10.1101/cshperspect.a020412

Davalos, D., Ryu, J. K., Merlini, M., Baeten, K. M., Le Moan, N., Petersen, M. A., et al. (2012). Fibrinogen-induced perivascular microglial clustering is required for the development of axonal damage in neuroinflammation. *Nat. Commun.* 3:1227. doi: 10.1038/ncomms2230

Dilger, R. N., and Johnson, R. W. (2008). Aging, microglial cell priming, and the discordant central inflammatory response to signals from the peripheral immune system. *J. Leukoc Biol.* 84, 932–939. doi: 10.1189/jlb.0208108

Erickson, M. A., and Banks, W. A. (2013). Blood-brain barrier dysfunction as a cause and consequence of Alzheimer's disease. *J. Cereb. Blood Flow Metab.* 33, 1500–1513. doi: 10.1038/jcbfm.2013.135

Gorelick, P. B., Scuteri, A., Black, S. E., Decarli, C., Greenberg, S. M., Iadecola, C., et al. (2011). Vascular contributions to cognitive impairment and dementia: a statement for healthcare professionals from the american heart association/american stroke association. *Stroke* 42, 2672–2713. doi: 10.1161/STR.0b013e3182299496

Grace, P. M., Ramos, K. M., Rodgers, K. M., Wang, X., Hutchinson, M. R., Lewis, M. T., et al. (2014). Activation of adult rat CNS endothelial cells by opioid-induced toll-like receptor 4 (TLR4) signaling induces proinflammatory, biochemical, morphological, and behavioral sequelae. *Neuroscience* 280, 299–317. doi: 10.1016/j.neuroscience.2014.09.020

Hargrave, S. L., Davidson, T. L., Zheng, W., and Kinzig, K. P. (2016). Western diets induce blood-brain barrier leakage and alter spatial strategies in rats. *Behav. Neurosci.* 130, 123–135. doi: 10.1037/bne0000110

Hartsock, A., and Nelson, W. J. (2008). Adherens and tight junctions: structure, function and connections to the actin cytoskeleton. *Biochim. Biophys. Acta* 1778, 660–669. doi: 10.1016/j.bbamem.2007.07.012

Haruwaka, K., Ikegami, A., Tachibana, Y., Ohno, N., Konishi, H., Hashimoto, A., et al. (2019). Dual microglia effects on blood brain barrier permeability induced by systemic inflammation. *Nat. Commun.* 10:5816. doi: 10.1038/s41467-019-13812-z

Haseloff, R. F., Dithmer, S., Winkler, L., Wolburg, H., and Blasig, I. E. (2015). Transmembrane proteins of the tight junctions at the blood-brain barrier: structural and functional aspects. *Semin. Cell Dev. Biol.* 38, 16–25. doi: 10.1016/j.semcdb.2014.11.004

Herman, A. B., and Autieri, M. V. (2017). Inflammation-regulated mRNA stability and the progression of vascular inflammatory diseases. *Clin. Sci.* 131, 2687–2699. doi: 10.1042/CS20171373

Hirschey, M. D., Shimazu, T., Jing, E., Grueter, C. A., Collins, A. M., Aouizerat, B., et al. (2011). SIRT3 deficiency and mitochondrial protein hyperacetylation accelerate the development of the metabolic syndrome. *Mol. Cell* 44, 177–190. doi: 10.1016/j.molcel.2011.07.019

Hsu, T. M., and Kanoski, S. E. (2014). Blood-brain barrier disruption: mechanistic links between Western diet consumption and dementia. *Front. Aging Neurosci.* 6:88. doi: 10.3389/fnagi.2014.00088

Huang, Z., Wong, L. W., Su, Y., Huang, X., Wang, N., Chen, H., et al. (2020). Blood-brain barrier integrity in the pathogenesis of Alzheimer's disease. *Front. Neuroendocrinol.* 59:100857. doi: 10.1016/j.yfrne.2020.100857

Iadecola, C. (2013). The pathobiology of vascular dementia. *Neuron* 80, 844–866. doi: 10.1016/j.neuron.2013.10.008

Iadecola, C. (2017). The neurovascular unit coming of age: a journey through neurovascular coupling in health and disease. *Neuron* 96, 17–42. doi: 10.1016/j.neuron.2017.07.030

Kanoski, S. E., Zhang, Y., Zheng, W., and Davidson, T. L. (2010). The effects of a high-energy diet on hippocampal function and blood-brain barrier integrity in the rat. *J. Alzheimers Dis.* 21, 207–219. doi: 10.3233/JAD-2010-091414

Kawas, C. H., Kim, R. C., Sonnen, J. A., Bullain, S. S., Trieu, T., and Corrada, M. M. (2015). Multiple pathologies are common and related to dementia in the oldest-old: the 90+ Study. *Neurology* 85, 535–542. doi: 10.1212/WNL.0000000000001831

Krasnow, S. M., Knoll, J. G., Verghese, S. C., Levasseur, P. R., and Marks, D. L. (2017). Amplification and propagation of interleukin-1beta signaling by murine brain endothelial and glial cells. *J. Neuroinflammation* 14, 133. doi: 10.1186/s12974-017-0908-4

Liu, Y., Huber, C. C., and Wang, H. (2020). Disrupted blood-brain barrier in 5xFAD mouse model of Alzheimer's disease can be mimicked and repaired *in vitro* with neural stem cell-derived exosomes. *Biochem. Biophys. Res. Commun.* S0006-291X, 30342–30349. doi: 10.1016/j.bbrc.2020.02.074

Lou, N., Takano, T., Pei, Y., Xavier, A. L., Goldman, S. A., and Nedergaard, M. (2016). Purinergic receptor P2RY12-dependent microglial closure of the injured blood-brain barrier. *Proc. Natl. Acad. Sci. U.S.A.* 113, 1074–1079. doi: 10.1073/pnas.1520398113

Matsumoto, J., Dohgu, S., Takata, F., Nishioku, T., Sumi, N., Machida, T., et al. (2012). Lipopolysaccharide-activated microglia lower P-glycoprotein function in brain microvascular endothelial cells. *Neurosci. Lett.* 524, 45–48. doi: 10.1016/j.neulet.2012.07.004

Mehrabadi, A. R., Korolainen, M. A., Odero, G., Miller, D. W., and Kauppinen, T. M. (2017). Poly(ADP-ribose) polymerase-1 regulates microglia mediated decrease of endothelial tight junction integrity. *Neurochem. Int.* 108, 266–271. doi: 10.1016/j.neuint.2017.04.014

Minghetti, L. (2004). Cyclooxygenase-2 (COX-2) in inflammatory and degenerative brain diseases. *J. Neuropathol. Exp. Neurol.* 63, 901–910. doi: 10.1093/jnen/63.9.901

Montagne, A., Barnes, S. R., Sweeney, M. D., Halliday, M. R., Sagare, A. P., Zhao, Z., et al. (2015). Blood-brain barrier breakdown in the aging human hippocampus. *Neuron* 85, 296–302. doi: 10.1016/j.neuron.2014.12.032

Montine, T. J., Sonnen, J. A., Montine, K. S., Crane, P. K., and Larson, E. B. (2012). Adult Changes in Thought study: dementia is an individually varying convergent syndrome with prevalent clinically silent diseases that may be modified by some commonly used therapeutics. *Curr. Alzheimer Res.* 9, 718–723. doi: 10.2174/156720512801322555

Navaratna, D., Fan, X., Leung, W., Lok, J., Guo, S., Xing, C., et al. (2013). Cerebrovascular degradation of TRKB by MMP9 in the diabetic brain. *J. Clin. Invest.* 123, 3373–3377. doi: 10.1172/JCI65767

Newcombe, E. A., Camats-Perna, J., Silva, M. L., Valmas, N., Huat, T. J., and Medeiros, R. (2018). Inflammation: the link between comorbidities, genetics, and Alzheimer's disease. *J. Neuroinflammation* 15, 276. doi: 10.1186/s12974-018-1313-3

Nogueiras, R., Habegger, K. M., Chaudhary, N., Finan, B., Banks, A. S., Dietrich, M. O., et al. (2012). Sirtuin 1 and sirtuin 3: physiological modulators of metabolism. *Physiol. Rev.* 92, 1479–1514. doi: 10.1152/physrev.00022.2011

Ouyang, S., Hsuchou, H., Kastin, A. J., Wang, Y., Yu, C., and Pan, W. (2014). Diet-induced obesity suppresses expression of many proteins at the blood-brain barrier. *J. Cereb. Blood Flow Metab.* 34, 43–51. doi: 10.1038/jcbfm.2013.166

Pugazhenthi, S., Zhang, Y., Bouchard, R., and Mahaffey, G. (2013). Induction of an inflammatory loop by interleukin-1beta and tumor necrosis factor-alpha involves NF-kB and STAT-1 in differentiated human neuroprogenitor cells. *PLoS One* 8:e69585. doi: 10.1371/journal.pone.0069585

Qin, L., Chong, T., Rodriguez, R., and Pugazhenthi, S. (2016). Glucagon-like peptide-1-mediated modulation of inflammatory pathways in the diabetic brain: relevance to Alzheimer's disease. *Curr. Alzheimer Res.* 13, 1346–1355.

Ronaldson, P. T., and Davis, T. P. (2020). Regulation of blood-brain barrier integrity by microglia in health and disease: a therapeutic opportunity. *J. Cereb. Blood Flow Metab.* 40, S6–S24. doi: 10.1177/0271678X20951995

Ryu, J. K., and McLarnon, J. G. (2009). A leaky blood-brain barrier, fibrinogen infiltration and microglial reactivity in inflamed Alzheimer's disease brain. *J. Cell Mol. Med.* 13, 2911–2925. doi: 10.1111/j.1582-4934.2008.00434.x

Skelly, D. T., Hennessy, E., Dansereau, M. A., and Cunningham, C. (2013). A systematic analysis of the peripheral and CNS effects of systemic LPS, IL-1beta, [corrected] TNF-alpha and IL-6 challenges in C57BL/6 mice. *PLoS One* 8:e69123. doi: 10.1371/journal.pone.0069123

Stamatovic, S. M., Martinez-Revollar, G., Hu, A., Choi, J., Keep, R. F., and Andjelkovic, A. V. (2019). Decline in Sirtuin-1 expression and activity plays a critical role in blood-brain barrier permeability in aging. *Neurobiol Dis* 126, 105–116. doi: 10.1016/j.nbd.2018.09.006

Su, Y., Lei, X., Wu, L., and Liu, L. (2012). The role of endothelial cell adhesion molecules P-selectin, E-selectin and intercellular adhesion molecule-1 in leucocyte recruitment induced by exogenous methylglyoxal. *Immunology* 137, 65–79. doi: 10.1111/j.1365-2567.2012.03608.x

Sweeney, M. D., Zhao, Z., Montagne, A., Nelson, A. R., and Zlokovic, B. V. (2019). Blood-brain barrier: from physiology to disease and back. *Physiol. Rev.* 99, 21–78. doi: 10.1152/physrev.00050.2017

Tyagi, A., Mirita, C., Taher, N., Shah, I., Moeller, E., Tyagi, A., et al. (2020). Metabolic syndrome exacerbates amyloid pathology in a comorbid Alzheimer's mouse model. *Biochim. Biophys. Acta Mol. Basis Dis.* 1866:165849. doi: 10.1016/j.bbadis.2020.165849

Tyagi, A., Nguyen, C. U., Chong, T., Michel, C. R., Fritz, K. S., Reisdorph, N., et al. (2018). SIRT3 deficiency-induced mitochondrial dysfunction and inflammasome formation in the brain. *Sci. Rep.* 8, 17547. doi: 10.1038/s41598-018-35890-7

Van Dyken, P., and Lacoste, B. (2018). Impact of metabolic syndrome on neuroinflammation and the blood-brain barrier. *Front. Neurosci.* 12:930. doi: 10.3389/fnins.2018.00930

Velmurugan, K., Bouchard, R., Mahaffey, G., and Pugazhenthi, S. (2012). Neuroprotective actions of glucagon-like peptide-1 in differentiated human neuroprogenitor cells. *J. Neurochem.* 123, 919–931. doi: 10.1111/jnc.12036

Voyvodic, P. L., Min, D., Liu, R., Williams, E., Chitalia, V., Dunn, A. K., et al. (2014). Loss of syndecan-1 induces a pro-inflammatory phenotype in endothelial cells with a dysregulated response to atheroprotective flow. *J. Biol. Chem.* 289, 9547–9559. doi: 10.1074/jbc.M113.541573

White, L. R., Edland, S. D., Hemmy, L. S., Montine, K. S., Zarow, C., Sonnen, J. A., et al. (2016). Neuropathologic comorbidity and cognitive impairment in the Nun and Honolulu-Asia Aging Studies. *Neurology* 86, 1000–1008. doi: 10.1212/WNL.0000000000002480

Wiggins-Dohlvik, K., Merriman, M., Shaji, C. A., Alluri, H., Grimsley, M., Davis, M. L., et al. (2014). Tumor necrosis factor-alpha disruption of brain endothelial cell barrier is mediated through matrix metalloproteinase-9. *Am. J. Surg.* 208, 954–960. discussion 960. doi: 10.1016/j.amjsurg.2014.08.014

Yamazaki, Y., Shinohara, M., Shinohara, M., Yamazaki, A., Murray, M. E., Liesinger, A. M., et al. (2019). Selective loss of cortical endothelial tight junction proteins during Alzheimer's disease progression. *Brain* 142, 1077–1092. doi: 10.1093/brain/awz011

Yang, F., Zhou, L., Wang, D., Wang, Z., and Huang, Q. Y. (2015). Minocycline ameliorates hypoxia-induced blood-brain barrier damage by inhibition of HIF-1alpha through SIRT-3/PHD-2 degradation pathway. *Neuroscience* 304, 250–259. doi: 10.1016/j.neuroscience.2015.07.051

Yarlagadda, A., Alfson, E., and Clayton, A. H. (2009). The blood brain barrier and the role of cytokines in neuropsychiatry. *Psychiatry* 6, 18–22.

Yousef, H., Czupalla, C. J., Lee, D., Chen, M. B., Burke, A. N., Zera, K. A., et al. (2019). Aged blood impairs hippocampal neural precursor activity and activates microglia via brain endothelial cell VCAM1. *Nat. Med.* 25, 988–1000. doi: 10.1038/s41591-019-0440-4

Zhu, L., Liu, X., Nemeth, D. P., DiSabato, D. J., Witcher, K. G., McKim, D. B., et al. (2019). Interleukin-1 causes CNS inflammatory cytokine expression via endothelia-microglia bi-cellular signaling. *Brain Behav. Immun.* 81, 292–304. doi: 10.1016/j.bbi.2019.06.026

Zlokovic, B. V. (2005). Neurovascular mechanisms of Alzheimer's neurodegeneration. *Trends Neurosci.* 28, 202–208. doi: 10.1016/j.tins.2005.02.001

Zlokovic, B. V., Gottesman, R. F., Bernstein, K. E., Seshadri, S., McKee, A., Snyder, H., et al. (2020). Vascular contributions to cognitive impairment and dementia (VCID): a report from the 2018 National Heart, Lung, and Blood Institute and National Institute of Neurological Disorders and Stroke Workshop. *Alzheimers Dement.* 16, 1714–1733. doi: 10.1002/alz.12157

Conflict of Interest: The authors declare that the research was conducted in the absence of any commercial or financial relationships that could be construed as a potential conflict of interest.

Publisher's Note: All claims expressed in this article are solely those of the authors and do not necessarily represent those of their affiliated organizations, or those of the publisher, the editors and the reviewers. Any product that may be evaluated in this article, or claim that may be made by its manufacturer, is not guaranteed or endorsed by the publisher.

frontiers in Aging Neuroscience

REVIEW
published: 23 August 2021
doi: 10.3389/fnagi.2021.721858

Cardiometabolic Modification of Amyloid Beta in Alzheimer's Disease Pathology

*Marleigh Hefner[1], Vineet Baliga[2], Kailinn Amphay[1], Daniela Ramos[1] and Vijay Hegde[1]**

[1]Obesity and Metabolic Health Laboratory, Department of Nutritional Sciences, Texas Tech University, Lubbock, TX, United States, [2]College of Arts and Sciences, University of North Carolina, Chapel Hill, Chapel Hill, NC, United States

In recent years, several studies have suggested that cardiometabolic disorders, such as diabetes, obesity, hypertension, and dyslipidemia, share strong connections with the onset of neurodegenerative disorders such as Parkinson's and Alzheimer's disease (AD). However, establishing a definitive link between medical disorders with coincident pathophysiologies is difficult due to etiological heterogeneity and underlying comorbidities. For this reason, amyloid β (Aβ), a physiological peptide derived from the sequential proteolysis of amyloid precursor protein (APP), serves as a crucial link that bridges the gap between cardiometabolic and neurodegenerative disorders. Aβ normally regulates neuronal synaptic function and repair; however, the intracellular accumulation of Aβ within the brain has been observed to play a critical role in AD pathology. A portion of Aβ is believed to originate from the brain itself and can readily cross the blood-brain barrier, while the rest resides in peripheral tissues that express APP required for Aβ generation such as the liver, pancreas, kidney, spleen, skin, and lungs. Consequently, numerous organs contribute to the body pool of total circulating Aβ, which can accumulate in the brain and facilitate neurodegeneration. Although the accumulation of Aβ corresponds with the onset of neurodegenerative disorders, the direct function of periphery born Aβ in AD pathophysiology is currently unknown. This review will highlight the contributions of individual cardiometabolic diseases including cardiovascular disease (CVD), type 2 diabetes (T2D), obesity, and non-alcoholic fatty liver disease (NAFLD) in elevating concentrations of circulating Aβ within the brain, as well as discuss the comorbid association of Aβ with AD pathology.

Keywords: obesity, diabetes, cardiovascular disease, NAFLD, Alzheimer's disease, amyloid precursor protein, amyloid beta

OPEN ACCESS

Edited by:
Carlos J. Rodriguez-Ortiz, University of California, Irvine, United States

Reviewed by:
Ian James Martins, University of Western Australia, Australia
Alain Buisson, Université Grenoble Alpes, France

****Correspondence:***
Vijay Hegde
vijay.hegde@ttu.edu

Received: *07 June 2021*
Accepted: *26 July 2021*
Published: *23 August 2021*

Citation:
Hefner M, Baliga V, Amphay K, Ramos D and Hegde V (2021) Cardiometabolic Modification of Amyloid Beta in Alzheimer's Disease Pathology. Front. Aging Neurosci. 13:721858. doi: 10.3389/fnagi.2021.721858

INTRODUCTION

Cardiometabolic disease (CMD) pathology is a complex subject due to the intersection of various metabolic, genetic, behavioral, and environmental factors (Stanhope et al., 2018). For these reasons, the rising prevalence of cardiometabolic diseases including cardiovascular disease (CVD), type 2 diabetes (T2D), obesity, and non-alcoholic fatty liver disease (NAFLD), has become a growing concern across the globe (**Table 1**; Bertoni et al., 2002; Thorpe and Ferraro, 2004; Perumpail et al., 2017; Taylor et al., 2017; Centers for Disease Control and Prevention, 2018; Jardim et al., 2019; Villarroel et al., 2019; Alzheimer's Association Report, 2020;

TABLE 1 | Alzheimer's and cardiometabolic disease prevalence in the US, 1998 to 2020.

Disease	Prevalence (Millions)	% Total population	% Population >65 years	Mortality rate >65 years
Obesity	139[a]	42.4	42.8	19.6[f]
Type II Diabetes	34[b]	10.5	26.8	62.3[g]
Pre-Diabetes	88[b]	26.9	71.0	—
Cardiovascular Disease	85[c]	12.1	68.5	40[h]
Non-Alcoholic Fatty Liver Disease	64[d]	19.5	27.6	68.7[i]
Alzheimer's Disease	5.8[e]	2	10	25.4[j]

[a]*Hales et al. (2020)*
[b]*Centers for Disease Control and Prevention (2020)*
[c]*Mozaffarian et al. (2016)*
[d]*Mitra et al. (2020)*
[e]*Centers for Disease Control and Prevention (2018)*
[f]*Thorpe and Ferraro (2004)*
[g]*Bertoni et al. (2002)*
[h]*North and Sinclair (2012)*
[i]*Perumpail et al. (2017) and*
[j]*Taylor et al. (2017).*

Hales et al., 2020; Mitra et al., 2020; Centers for Disease Control and Prevention, 2020). The cost of cardiometabolic diseases associated with poor diet accounts for an estimated $50.4 billion (Jardim et al., 2019) and affects 47 million (Wang et al., 2014) individuals across the United States.

These costs are expected to dramatically rise in the future as the elderly population in developed nations continues to increase. It is estimated that by 2050, the elderly population of the United States (individuals aged >65 years) will be double that of the population of youth aged <14 years (Lau et al., 2007). The visibility of age-related neurodegenerative diseases becomes more prevalent as domestic birth rates decline in tandem with a growing elderly population, as seen by an estimated 50 million Americans displaying such symptoms each year (Brown et al., 2005). However, there is evidence to suggest the existence of an underlying relationship between deteriorating metabolic health and age-related neurodegenerative disease risk. In elderly populations, mid-life obesity, T2D, and various CVD are associated with an increased risk of dementia development (de Bruijn and Ikram, 2014), supporting the trend that the onset of age intensifies the complications and progression of neurodegenerative diseases over time.

Age-related neurodegenerative diseases, particularly dementia, progress incrementally over time. An example of this trend between age and dementia progression is observed through mild cognitive impairments, which serve as clinical precursors that characterize the stages of advanced dementias (Roberts and Knopman, 2013). Individuals diagnosed with these impairments are at an increased risk for developing dementias compared to cognitively healthy subjects, with a conversion rate ranging between 10–15% in specialty clinics (Michaud et al., 2017). It is possible for individuals with mild cognitive impairment to improve or maintain their cognitive health: however, permanent and accelerated cognitive decline is considered inevitable once an impairment proceeds toward advanced stages of dementia such as those typical to AD (Michaud et al., 2017).

Alzheimer's disease (AD) is the most common age-related neurodegenerative disease and is the 4th leading cause of death (Estrada et al., 2019) in the developed world, accounting for 60–80% of all dementia-related cases (Alzheimer's Association, 2008). The direct medical cost of AD-related dementias across the developed world is projected to increase from $109 billion in 2010 to $259 billion in 2040 even if the prevalence of AD were to remain constant (Deb et al., 2017). However, the sum of the economic, social, and emotional burden of AD cannot be truly quantified.

The objective of this review is to explore how major cardiometabolic diseases (T2D, obesity, and NAFLD) contribute to AD pathology. Due to its growing importance to medical systems, public policy, and health economics, AD will be the primary lens through which the relationship between age, metabolism, and neurodegenerative disease progression will be discussed.

ASSOCIATION OF THE MAJOR CARDIOMETABOLIC DISEASES AND ALZHEIMER'S DISEASE

Type 2 Diabetes and Obesity

T2D is a metabolic disease of abnormal insulin function that leads to chronic hyperglycemia and impacts roughly 26 million individuals in the United States, with an estimated additional 79 million facing pre-diabetes conditions (Blair, 2016). T2D incidence is projected to increase 50% by 2040, representing a total of 640 million new cases (Zheng et al., 2018). The exponential rise in T2D cases poses significant economic and social burdens for global health systems and individuals. A crucial relationship between T2D and AD is observed in the context of chronic peripheral hyperinsulinemia and impaired insulin sensitivity being identified in patients with AD, though research on their translation to brain hyperinsulinemia and brain insulin resistance is in its infancy (Verdile et al., 2015). Promising data from fluorodeoxyglucose-positron emission tomography (also known as FDG-PET) imaging studies have observed reductions in brain glucose metabolism under conditions of hyperinsulinemia within brains afflicted with AD (Verdile et al., 2015).

Insulin signaling regulates major metabolic processes within the liver, adipose tissue, and skeletal muscle. This relationship

between insulin signaling and other CMD is supported by an estimated 61% of T2D cases simultaneously correlate with obesity, therefore making obesity a strong risk factor for the development of T2D (Zheng et al., 2018). Over the last 25 years, obesity rates have risen exponentially to the extent that obesity is now classified as an epidemic affecting 1 in 3 adults in the United States (Lee, 2011). Obesity is formally defined as a metabolic disorder in which body mass index >30 kg/m^2 (Walker and Harrison, 2015; Pugazhenthi et al., 2017) and is characterized by chronic hyperglycemia, elevated concentrations of free fatty acids in the blood *via* overnutrition, and physical inactivity (Guzman et al., 2016; Pugazhenthi et al., 2017). As lipids accumulate in adipose tissue, numerous adverse complications arise such as increases in peripheral inflammation, insulin resistance, dyslipidemia, and higher concentrations of inflammatory cytokines that play key roles in overactivation of immune response mechanisms (Lee, 2011; Verdile et al., 2015; Walker and Harrison, 2015; Pugazhenthi et al., 2017).

Obesity is also considered a catalyst for dementia, but there is an ongoing debate regarding the extent of the relationship between the two disorders. Midlife (40–59 years) has been identified as the time period with the highest risk of developing dementia for obese individuals compared to any other point in life (Walker and Harrison, 2015). The location of adipose tissue accumulation is equally as critical since abdominal adiposity is known to contribute substantially to the risk of developing insulin resistance, T2D, heart attack, heart failure, high blood pressure, and neurodegenerative diseases when compared to overall BMI (Yusuf et al., 2005; Meisinger et al., 2006; Nicklas et al., 2006; Racette et al., 2006; Yoon et al., 2012; Nurdiantami et al., 2018). Obesity is also associated with decreased hippocampal volume and a reduction of brain gray matter (Arvanitakis et al., 2004). A systematic review conducted by Albanese et al. reinforces this point by identifying that the probability of developing dementia dramatically increases as BMI increases, particularly in midlife (Albanese et al., 2017).

Cardiovascular Disease

CVD is a large category of diseases that centers around impairment of the cardiovascular system through complications arising within heart and blood vessels that reduces functional capacity (Francula-Zaninovic and Nola, 2018). This impairment manifests in many forms ranging from heart-centric disorders such as arrythmia, valve malfunctions, heart attacks, and stroke to circulatory diseases such as coronary artery disease, deep vein thrombosis, hypertension, and atherosclerosis (Matheny et al., 2011; de Bruijn and Ikram, 2014).

CVD comprises the leading cause of death in the United States and Europe with a mortality rate of 35.2% and 48%, respectively, and is on a trajectory to average 23.6 million deaths per year globally by 2030 (Willis et al., 2012; Francula-Zaninovic and Nola, 2018). Disorders related to CVD can develop within individuals of any age; however, the risk of developing CVD rises abruptly with ages after 45 and disproportionately impacts a far greater number of individuals 65 years or older (40% mortality; **Table 1**, North and Sinclair, 2012). Common conditions associated with increased risks of CVD include obesity, increased blood pressure, dyslipidemia, adverse behaviors (lack of exercise, tobacco, and alcohol usage), and T2D (Willis et al., 2012). CVD does not exist in a vacuum, and individuals experiencing it are likely to develop, or be at risk of developing hypercholesterolemia, dyslipidemia, hypertension, and T2D, which increase the severity of unfavorable health outcomes (Fillit et al., 2008). With the pattern of CVD incidence strongly correlating with age, it is common to see individuals with CVD also exhibit symptoms of other age-related or neurodegenerative disorders. This is primarily due to CVD disruptions in blood circulation. These disruptions reduce oxygen and nutrient delivery to the brain as well as removal of toxic byproducts, exacerbating progressive cognitive decline associated with common neurodegenerative diseases, such as AD (Matheny et al., 2011; de Bruijn and Ikram, 2014). The risk of AD is reported to double every 5 years after age 60, and more than 30% of people over the age of 80 are likely to suffer from both AD and CVD (Tini et al., 2020).

Non-alcoholic Fatty Liver Disease

The liver is responsible for a variety of complex metabolic processes, including macronutrient metabolism, regulation of blood volume, detoxification, immune system function, lipid and cholesterol homeostasis, and the metabolism of many drugs (Trefts et al., 2017; Estrada et al., 2019). Macronutrient metabolism is among the most critical liver functions. Additionally, the liver is involved in lipid oxidation, packaging of excess lipids for storage in adipose tissue, and ketogenesis (Trefts et al., 2017). The health of the liver is critical to wellbeing. Therefore, disruptions in the functionality of the liver through exogenous or endogenous conditions can have life-threatening consequences. One such adverse consequence is manifested in NAFLD, a disorder that results in the excessive accumulation of fat within the liver of individuals who consume little to no alcohol, the most common type of liver disease (Sheka et al., 2020). Patients experiencing NAFLD display the presence of hepatic steatosis—at least 5–10% of the liver's weight being fat—without competing liver disease etiologies such as excess alcohol consumption or viral hepatitis (Younossi et al., 2016). Approximately 20% of individuals diagnosed with NAFLD also experience inflammation originating from increased accumulation of fat within the liver or nonalcoholic steatohepatitis (NASH; Sheka et al., 2020). Consequences of NAFLD/NASH include reduced whole-body hepatic and adipose tissue insulin sensitivity (Bugianesi et al., 2010) as well as an increased risk of cardiovascular events (Targher et al., 2020), T2D, and all-cause mortality (Targher et al., 2020). Thus, such a cascade strengthens the hypothesis that NAFLD/NASH carries a degree of influence on the incidence of other metabolic disorders such as obesity, T2D, and CVD. According to Hurjui et al., NAFLD should be considered a piece of a multi-organ system disturbance of insulin sensitivity, which explains why NAFLD episodes are closely linked with the onset of diabetes, metabolic syndrome, and CVD (Hurjui et al., 2012). Although the precise mechanism for the association between NAFLD and insulin resistance is not fully understood, current evidence indicates NAFLD alters the secretion of hepatokines, lipids, and

non-coding RNA, of which the latter play a critical role in regulating gene expression (Sulaiman et al., 2019; Yoshino and Dwivedi, 2020).

As mentioned, alterations in lipid metabolism has been linked to AD risk, and due in part to the role of the liver in maintaining lipid homeostasis, the liver has been identified as a novel target for AD treatment (Stampfer, 2006; Estrada et al., 2019). In addition, researchers have identified 189 genes mutually expressed in conditions of both AD and NAFLD, and have recently linked the liver to the brain *via* the blood-brain barrier (Estrada et al., 2019). Specifically, the low-density lipoprotein receptor-related protein 1 (LRP1) is a transport protein expressed in both the blood-brain barrier and the liver, functioning to clear brain and periphery-derived amyloid β (Aβ), which is a key protein involved in AD pathogenesis. Aβ, its contribution to AD, and its relationship with metabolic health, will be discussed at length in the remainder of this review. In this review, findings from the relationship between liver dysfunction and AD will serve as the first indication that metabolic disorders, such as NAFLD, T2D, obesity, and CVD, may be a common link to AD pathology *via* Aβ modification.

SIMILARITIES IN CARDIOMETABOLIC DISEASE ETIOLOGY WITH ALZHEIMER'S DISEASE PATHOLOGY

It is important to note that the major CMD have similar risk factors, which illustrates the challenges in definitively attributing observational epidemiological studies to a single disorder. Recently, numerous studies have linked insulin resistance, a key pathophysiological feature of NAFLD, T2D, and obesity, to several neurodegenerative mechanisms of AD. These mechanisms include oxidative stress, mitochondrial dysfunction, and inflammation by dysregulated insulin signaling, along with impairments to signal transduction and gene expression (Estrada et al., 2019). Hepatic fibrosis has also been shown to lead to reduced insulin clearance, insulin resistance, and T2D (Utzschneider and Kahn, 2006). It is well established that hepatic, adipose, and muscle tissue insulin resistance and decreased pancreatic insulin production result from hyperglycemia brought about by excessive liver gluconeogenesis (Bazotte et al., 2014), which are all predictors of both T2D and NAFLD. In conditions of obesity, liver lipid accumulation has been associated with NAFLD pathophysiology (Utzschneider and Kahn, 2006); it is estimated that up to 80% of NAFLD patients are clinically obese and up to 70% of liver disease patients are overweight (Milic et al., 2014; Meex and Watt, 2017). Chronic low-grade peripheral inflammation from excess visceral adipose tissue and a surplus of circulating free fatty acids are not only two key contributors to liver damage and progression of NAFLD, but also exemplify the conditions of obesity (Milic et al., 2014). Similarly, abnormal lipid metabolism commonly found in obesogenic conditions parallels an increased risk for AD development and reinforces how dyslipidemia typical to T2D and obesity possesses significant overlap with AD. Therefore, dyslipidemia can serve as a credible risk factor that measures the metabolic irregularities that facilitate the onset of neurodegenerative disorders. This overlap of dyslipidemia between CMD and AD points to the crucial role the liver serves as the main peripheral organ responsible for lipid metabolism and indirectly links the conditions of NAFLD with AD progression (Estrada et al., 2019).

An association between NAFLD and increased CVD prevalence has also been identified (Martins and Oliveira, 2018). Much of the evidence suggests that CVD is the most common cause of mortality among patients with NAFLD (Martins and Oliveira, 2018). Mildly elevated serum gamma-glutamyltransferase concentrations independently predict the occurrence of CVD-related events and NAFLD is associated with a higher incidence of high-risk coronary atherosclerotic plaques and coronary artery inflammation (Choi et al., 2018; Wojcik-Cichy et al., 2018; Rahmani et al., 2019). The definitive contribution of NASH or NAFLD to excess CVD risk remains unanswered, but a 2010 meta-analysis by Musso et al. suggests that NAFLD patients experienced roughly twice the risk of fatal and non-fatal CVD events compared to control populations (Musso et al., 2011). Additionally, anti-aging genes might be a link between CMD and AD pathology, particularly the NAD-dependent deacetylase SIRT1. SIRT1 has protective effects against CVD and regulates blood pressure, atherosclerosis, oxidative stress and cardiac cell survival through its deacetylase activity (Tanno et al., 2012). The hallmark of AD is the accumulation of amyloid beta plaques, which result from the sequential cleavage of APP by the beta and gamma-secretases (Tanzi and Bertram, 2005). However, studies show that SIRT1 expression avoids the production of amyloid beta peptides by alternate cleavage of APP by the alpha and gamma-secretases (Postina et al., 2004; Kojro and Fahrenholz, 2005), which possible reduces brain generated amyloid beta plaques. Therefore, SIRT1 could have a therapeutic role in CMD associated neurodegenerative diseases (Martins, 2018). In summary, the human body is made up of intertwined system that cause different diseased states to have significant similarities in their presentation and etiology. Furthermore, each chronic disorder covered in this review, including obesity, T2D, NAFLD, and CVD, has been linked to AD pathology in overlapping and independent ways, which we will discuss in detail moving forward.

THE ROLE OF Aβ IN ALZHEIMER'S DISEASE

AD is a disorder characterized by a progressive, irreversible, gradual decline in cognitive function. It is neuropathologically defined by progressive neuronal and synaptic loss as well as the progressive aggregation of neurofibrillary tangles and senile plaques (Schapira, 2007). The prevalence of AD is rapidly escalating worldwide, primarily among people that exceed 65 years of age. At such rates, cases of AD incidence are projected to double by 2050 from the current 55–88 million cases globally (Hebert et al., 2001). Collectively, these data warn of the morbidity associated with AD, and the significant rise in AD cases being observed has the potential to place significant economic burden on the global healthcare apparatus.

The current understanding of AD pathogenesis is multifaceted, but this review will focus on the fundamental processes most affected by CMD health, namely extracellular Aβ deposition and intracellular tau protein hyper-accumulation. The accumulation of Aβ and tau protein are not only two key markers of AD, but also have considerable involvement with neurodegenerative mechanisms. Aβ is a major component of senile plaques and the insoluble tau protein is a major component of neurofibrillary tangles (Hebert et al., 2001). Aβ consists of 36–43 peptides that are aggregated within the large transmembrane protein, amyloid precursor protein (APP). Aβ is produced by neurons, microglia, and astrocytes in the brain and outside the blood-brain barrier by platelets, fibroblasts, osteoblasts, and skeletal muscle cells (Wang et al., 2017). Hence, a portion of Aβ is believed to originate from the brain itself, while the rest resides in peripheral tissues such as the liver, pancreas, kidney, spleen, skin, and lungs; each of these tissues express APP required for Aβ generation. Under normal conditions, APP within the brain will produce nonamyloidogenic Aβ products by α-secretase. However, amyloidogenic Aβ can accumulate as a result of enzymatic β-site APP cleaving enzymes BACE-1 and multi-protein γ-secretase (**Figure 1**; Chow et al., 2010). Defective clearance of Aβ during the cleavage of APP is understood to result in the accumulation of insoluble Aβ (Chow et al., 2010). Initially, Aβ monomers polymerize into soluble oligomers and then into larger insoluble fragments like Aβ42 that can precipitate as amyloid fibrils (Younkin, 1998). The Aβ fragments have the potential to assume a variety of different lengths, though the average length is 40 residues (Aβ 1 to 40) with a small, but considerable portion possessing lengths of 42 residues (Aβ 1 to 42; Younkin, 1998).

The neurotoxicity of Aβ is understood to originate from the extra two amino acids on Aβ 1–42 which have a higher tendency to misfold and aggregate (Ahmed et al., 2010). The Aβ monomers, which ultimately polymerize into insoluble fragments, like Aβ42, that can precipitate into amyloid fibrils (Younkin, 1998) are most commonly associated with AD (Mayeux et al., 1999). However, the amount of Aβ deposited and its distribution weakly parallels with the clinical expression of the disease, and the causal role of Aβ in AD pathology remains under debate due to accumulating evidence that supports other alternative views of etiology (Pimplikar et al., 2010; Castellani and Smith, 2011; Chételat, 2013; Moreno-Treviño et al., 2015; Tse and Herrup, 2017; de la Torre, 2018). Among these possible alternative explanations, Aβ may in fact exert its effects early on, and trigger a cascade of degenerative processes, which act independently even when Aβ is therapeutically removed (Holtzman, 2008). Additionally, Aβ is considered polymorphic, producing different conformational forms or pools of Aβ, which vary in their relevance to disease pathology (Murphy and LeVine, 2010). Even though Aβ is substantially degraded in the brain, a significant amount remains undisturbed and is transported across the blood-brain barrier into the peripheral circulation. The net concentration of Aβ transported across the blood-brain barrier is thought to determine the degree of Aβ deposited in the brain, although concrete data from human subjects is lacking (DeMattos et al., 2002). The presence of this bidirectional Aβ flow suggests that disruption of Aβ degradation

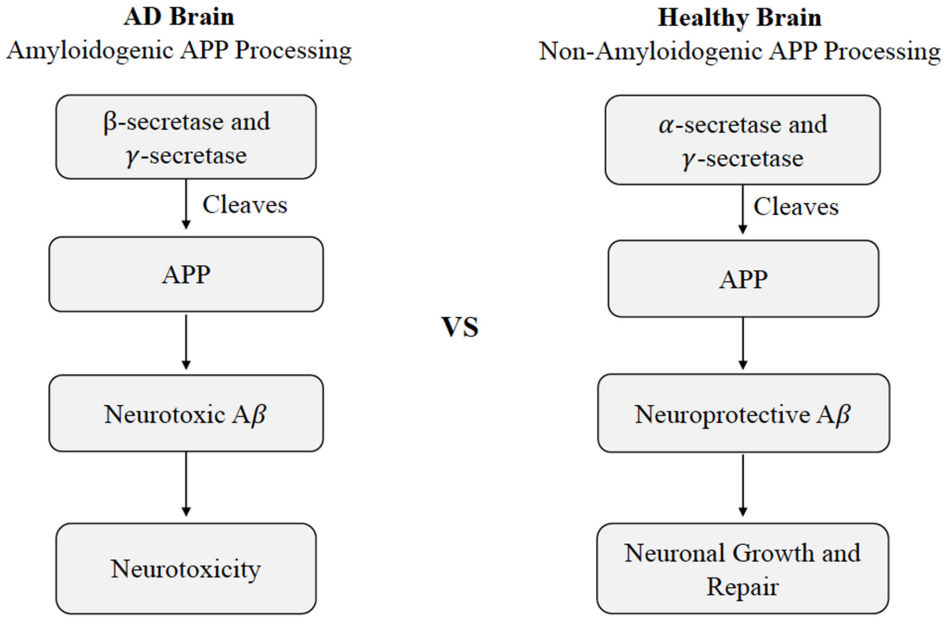

FIGURE 1 | Cleavage of APP in healthy vs. Alzheimer's disease states. Differences in non-amyloidogenic cleavage of APP in a healthy brain compared to amyloidogenic cleavage of APP AD brain. In a healthy brain, APP is cleaved by γ-secretase and γ-secretase to produce neuroprotective Aβ, leading to neuronal growth and repair. In an AD brain, APP is cleaved by Aβ β- and γ-secretase, leading to neurotoxicity. Abbreviations: APP, amyloid precursor protein; AD, Alzheimer's disease; Aβ, amyloid beta.

in peripheral tissues by cardiometabolic impairments can contribute to the comorbid brain Aβ pathology in AD. There have been numerous studies elucidating the pathogenesis, the molecular and clinical mechanisms, the association of diabetes and metabolic syndromes, and the broad range of consequences, yet no single or combined treatment has shown to have satisfactory levels of efficiency to delay or completely prevent AD pathogenesis. Overall, AD is a complex disorder with multiple pathological contributors, some of which remain to be fully understood. As a consequence of the substantial effects that cardiometabolic modifications can have on Aβ metabolism, Aβ will be the component of AD pathology central to this review.

ALTERED Aβ METABOLISM IN TYPE 2 DIABETES AND OBESITY

Due to their etiological similarities, T2D and obesity-induced conditions, including hyperinsulinemia, insulin resistance, hyperglycemia, altered insulin signaling, and inflammation, and their relationship with Aβ metabolism will be discussed concurrently. Other diseased states, such as NAFLD, will also be included in the following discussion but only as they contribute to such T2D and obesity-related conditions.

Hyperinsulinemia and Insulin Resistance

As mentioned previously in this review, dysregulation of glucose homeostasis is associated with an increased risk of neurodegenerative disease development (Blázquez et al., 2014). Interestingly, in metabolically healthy individuals, it has been established that basal insulin concentration in the brain and insulin receptor affinity are significantly reduced with age (Baranowska-Bik and Bik, 2017). Therefore, one of the chief pathological features that links AD with peripheral metabolic health appears to be altered insulin metabolism (Tumminia et al., 2018). For instance, T2D is associated with impaired insulin and insulin-like growth factor-1 signaling, which has been suggested as a risk factor for cognitive impairment and dementia (Westwood et al., 2014). Hyperinsulinemia has been linked to both CMD dysfunction and AD pathology, and it highlights the close relationship between Aβ and insulin *via* insulin degrading enzyme (IDE). During hyperinsulinemia, Aβ and insulin both compete for IDE action, resulting in Aβ accumulation and plaque formation (Kawamura et al., 2012). However, isolating the individual metabolic effects of chronic hyperinsulinemia and insulin resistance is a difficult task as these phenomena tend to occur in tandem. It has been theorized that hyperinsulinemia emerged as a consequence of the insulin resistance that typifies T2D (Shanik et al., 2008), though more recent research suggests that NAFLD can serve as a significant driver of hyperinsulinemia through the pancreas even in the absence of T2D or insulin resistance (Godoy-Matos et al., 2020). In addition, it is important to note that prolonged hyperinsulinemia can result in hypoinsulinemia secondary to pancreatic beta cell fatigue.

Hyperinsulinemic conditions can also occur as a result of liver dysfunction. The excessive accumulation of fat within and around the liver induced by NAFLD can also facilitate inflammation, leading to hepatic cirrhosis and pancreatic necrosis due to their interconnected relationship (Yoon et al., 2017). For example, Yoon et al. studied 285 hospital patients diagnosed with pancreaticobiliary disease and reported that fatty liver changes matched trends associated with the development of acute pancreatitis and hepatic cirrhosis, as well as higher rates of adverse complications like mortality and organ failure (Yoon et al., 2017). A possible explanation of such conclusions is that cirrhosis induced by NAFLD can inhibit glycogenesis, which can lead to higher circulating blood glucose, bringing rise to T2D-related complications of chronic hyperinsulinemia (Yoon et al., 2017).

Furthermore, since pancreatic islet cells produce both insulin and APP, the precursor protein to Aβ, pancreatic dysfunction characterized by changes in APP concentrations is of particular interest (Yoon et al., 2017). Pancreatic dysfunction leading to altered APP cleavage and potentially neurodegenerative Aβ production has been investigated in human and animal models of AD. These studies generally suggest that increased expression of APP in the pancreas leads to increased insulin secretion in AD mice (Kulas et al., 2017). Increased concentrations of APP are among a slew of consequences of pancreatitis. On a separate but related matter, liver fat accumulation is also understood to exacerbate inflammation, contributing to the overactivation of hormonal production sites, such as the Islets of Langerhans (Yoon et al., 2017). This hormonal overactivation can lead to abnormal metabolic activity that reduces pancreatic and digestive functionality but favors overproduction of insulin from the pancreas, exacerbating conditions of increased circulating insulin that typifies chronic hyperinsulinemia (Yoon et al., 2017).

Hyperinsulinemia and its relationship with AD will be further investigated throughout this review, but this relationship is introduced in **Figure 2** (Qiu and Folstein, 2006). As hyperinsulinemic conditions prevail, the demand placed on the body and brain to clear insulin increases. Therefore, there is increased competition for IDE in the brain and peripheral tissues. IDE is an ubiquitously expressed enzyme dually equipped to degrade not only excess insulin, but also excess Aβ (Pivovarova et al., 2016). When IDE is occupied degrading excess insulin in conditions of hyperinsulinemia, Aβ is left to steadily accumulate in both peripheral circulation and centrally, intensifying the conditions of AD induced by Aβ accumulation (**Figure 3**). It is this mechanism that highlights the interconnected relationship between T2D conditions and AD pathology. Common trends between hyperglycemia, brain insulin resistance, and improper function of the IDE have been recognized in a variety of studies tracking the pathological features of AD (Tumminia et al., 2018).

Lastly, cerebrospinal insulin concentrations are correlated with peripheral insulin concentrations, suggesting pancreatic insulin makes up the majority of brain insulin (Arnold et al., 2018) and strengthens emphasis on peripheral organ system health in AD prevention and treatment. It is important to note that the ratio of the concentration of insulin in cerebrospinal fluid compared to the periphery is lower in both aging patients with AD and those with insulin resistance compared to healthy subjects. This relationship may be related to decreased transport of insulin across the blood-brain barrier since insulin

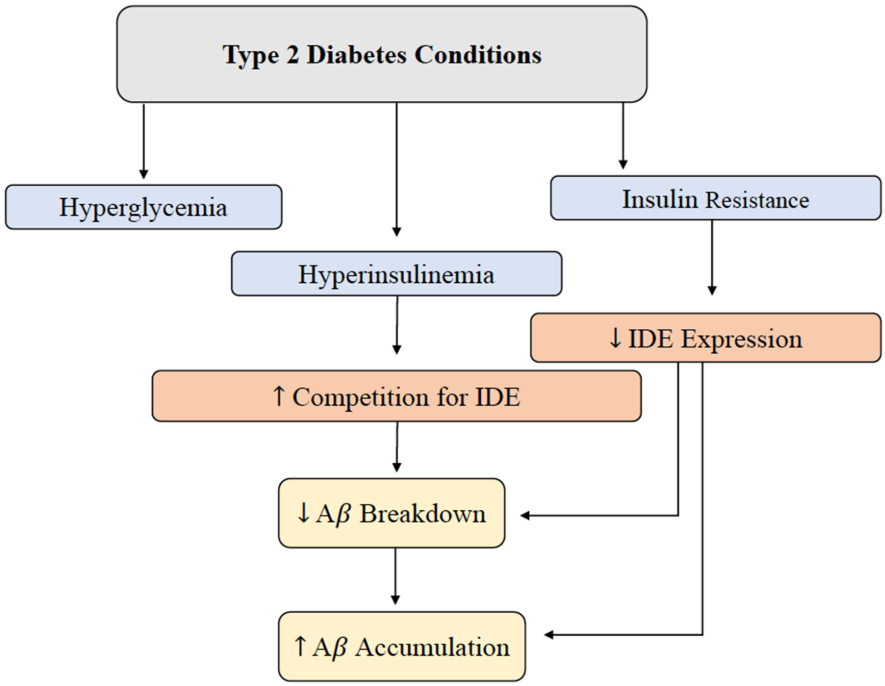

FIGURE 2 | Brain Aβ accumulation induced by T2D conditions. IDE is responsible for the degradation of excess insulin and Aβ in the brain. Hyperglycemia, hyperinsulinemia, and insulin resistance are abnormal symptoms present in T2D, and this alteration in metabolism leads to a decrease in IDE expression and increased competition for IDE. Decreased IDE activity and increased IDE competition leads to decreased Aβ and insulin breakdown. In addition, hyperinsulinemia contributes to a build-up of Aβ peptides in the brain. Abbreviations: IDE, insulin-degrading enzyme; T2D, type 2 diabetes; Aβ, amyloid beta.

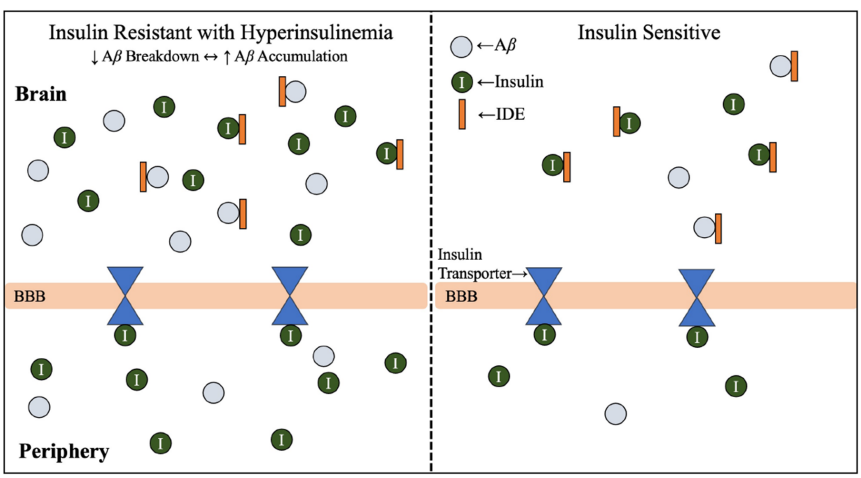

FIGURE 3 | Insulin resistance and hyperinsulinemia increases competition for IDE. Mechanism by which T2D conditions of insulin resistance and hyperinsulinemia contribute to increased competition for IDE, and therefore increased accumulation of Aβ. As introduced in **Figure 2**, IDE is responsible for the degradation of excess insulin and Aβ in the brain. Hyperglycemia, hyperinsulinemia, and insulin resistance are symptoms of T2D, and the combined effect of hyperinsulinemia and Aβ accumulation leads to increased competition for IDE, resulting in accumulation of both Aβ and insulin in the brain. Abbreviations: Aβ, amyloid beta; AD, Alzheimer's disease; IDE, insulin degrading enzyme; T2D, type 2 diabetes; BBB, blood-brain barrier.

transport is affected by inflammation, obesity, hyperglycemia, and hypertriglyceridemia (Banks et al., 2012). However, the ratio of cerebrospinal fluid to peripheral insulin may not be as crucial as the total concentration of insulin in the body.

Hyperglycemia and Altered Insulin Signaling

It has also been theorized that chronic hyperglycemia may contribute to the production of advanced glycation end products

(AGE), which interact with specialized AGE receptors on the endothelial lining of the blood-brain barrier that mediate Aβ influx to the brain (Li et al., 2019). Aβ is considered an AGE receptor ligand and therefore can effectively bind to these receptors and signal an influx across the blood-brain barrier from the circulatory pathways (**Figure 5**; Murphy and LeVine, 2010; Li et al., 2019).

Another dimension of the relationship between insulin and Aβ includes genetic and structural disruptions within the insulin signaling pathway *via* receptor-level inhibition. As concentrations of insulin increase, more insulin receptor sites are occupied; however, chronic exposure to insulin reduces the proportion of short, higher-affinity isoforms of insulin receptors relative to the long, lower-affinity isoforms (Shanik et al., 2008). In addition, serine rather than tyrosine phosphorylation of the insulin response element has been associated with insulin resistance related to decreased activation of downstream insulin-signaling proteins (**Figure 4**; Copps and White, 2012). This alteration of insulin signal pathways intricately links peripheral insulin resistance to brain insulin resistance, in addition to the discovery that insulin receptors are widely expressed in the brain (Pomytkin et al., 2018). Brain insulin and glucose metabolism play an important role in synaptic function of neurons (**Figure 4**) and Aβ degradation (**Figure 3**), in addition to their chief role of glucose uptake (Freude et al., 2005; De Felice et al., 2014; Bedse et al., 2015; Arnold et al., 2018). In summary, glucose metabolism dysfunction in the form of hyperinsulinemia, insulin resistance, hyperglycemia, and altered insulin signaling are all metabolic factors that can be individually and holistically linked to Aβ metabolism, and therefore AD risk.

Inflammation

Chronic inflammation is prevalent in multiple metabolic diseases, including T2D and obesity, and may serve as another possible risk factor in appraising AD risk (Murphy and LeVine, 2010). Increased concentrations of pro-inflammatory cytokines produced in the presence of chronic inflammation can lead to pancreatic β-cell damage and impaired insulin secretion (Murphy and LeVine, 2010). These cytokines, such as tumor necrosis factor-α (TNF-α), have the ability to cross the blood-brain barrier to contribute to the progression of AD (**Figure 4**; Wang et al., 2015). In addition, it has been established *in vivo* since the 1990's that when the interleukin-1 is elevated in the brain, less hippocampal acetylcholine is produced, and this can contribute to neurological deficits (Rada et al., 1991; **Figure 6**).

Oxidative stress is understood to begin with the production of reactive oxygen species, which are molecules that contain oxygen free radicals and are formed during normal cellular processes (de la Monte, 2012). This production of free radicals contributes to oxidative stress and cellular damage. Due to the brain's elevated lipid concentration, lack of antioxidant defense mechanisms, and high oxygen requirements make the brain especially vulnerable to oxidative stress, which is a well-established early contributor to AD-related neurodegeneration (Verdile et al., 2015). Furthermore, inflammation-induced oxidative stress in the brain can lead to altered brain glucose metabolism and reduced ATP synthesis, which promotes neural dysfunction, synapse loss, and neurodegeneration (Verdile et al., 2015). *In vitro* evidence also suggests that Aβ may increase the generation of reactive oxygen species; however, it is unclear whether Aβ are the cause or result of oxidative stress when *in vivo* evidence is presented (Yao et al., 2009). Furthermore, the primary site for reactive oxygen species generation is the mitochondria, and mitochondrial dysfunction has been suggested as an early contributor to AD, particularly in mouse models (Verdile et al., 2015). Chronic inflammation is an important component of altered Aβ metabolism through the lens of obesity as well.

In a corresponding manner, adipose tissues release adipokines, such as leptin and adiponectin that function in a similar manner to that of cytokines with regards to oxidative stress and inflammation (Verdile et al., 2015). Interestingly, leptin, the primary regulator of appetite and energy homeostasis is related to insulin resistance and the development of obesity when produced in excess (Gruzdeva et al., 2019). As tissues become less sensitive to leptin, a condition known as leptin resistance, the failure of leptin feedback mechanisms lead to continued production by adipose tissues despite the already synthesized leptin being unable to carry out its function or participate in signaling cascades. Leptin resistance and excess leptin production result in abnormal appetite, hyperinsulinemia, hypothalamic inflammation, obesity, dyslipidemia, altered blood-brain barrier transport, and the emergence of other metabolic disorders (Gruzdeva et al., 2019). Leptin can cross the blood-brain barrier to evoke the classical appetite-suppressing and thermogenesis-initiating signals to the hypothalamus (Banks, 2001). Increased concentrations of circulating leptin in obesity are known to increase neuroendocrine dysfunction exacerbated by hypothalamic leptin resistance, which leads to the down regulation of appetite-suppressing and energy-expending signals, contributing to obesogenic conditions (Waterson and Horvath, 2015).

Although leptin receptors are heavily concentrated within the hypothalamus, other regions of the brain associated with learning and memory, such as the hippocampus, express leptin receptors as well, which explains why these regions are widely focused on in AD and obesity-related research (Murphy and LeVine, 2010). In fact, direct injection of leptin within the hippocampus of mice has been shown to modulate long-term nerve impulse strength and synaptic plasticity, as well as dramatically improved memory processing in both time-dependent and dose-dependent conditions (Li et al., 2016). In human studies, decreased leptin levels is associated with increased Aβ deposition and memory impairment, reinforcing how leptin resistance within the brain may exacerbate AD-related pathologies (Li et al., 2016; Forny-Germano et al., 2018). Collectively, the evidence suggests leptin may play a role in neuroprotection and the effects of obesity on neurodegenerative disorders.

Beyond chronic inflammation induced by inflammatory adipokines and cytokines, the current understanding of altered

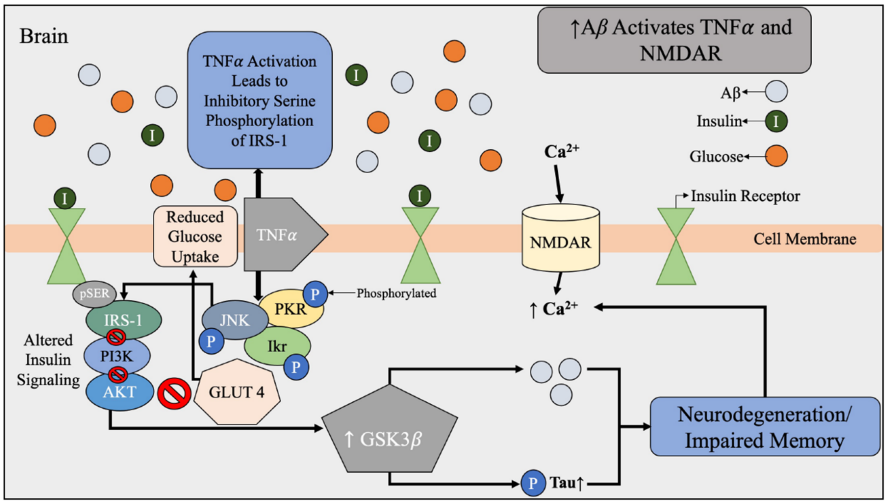

FIGURE 4 | Aβ dysfunction contributing to alterations in brain insulin signaling beginning with the activation of TNFα and NMDAR by Aβ. During Aβ accumulation found in AD brains, there is increased expression of TNFα and activation of NMDAR. NMDAR activation results in an influx of Ca^{2+} that leads to oxidative stress and synaptic dysfunction of the brain. Under normal conditions, Aβ is used to regulate the calcium flow that is required for synaptic transmission. Increased expression of TNFα and stress kinases leads to inhibitory serine phosphorylation of IRS-1 and PI3K therefore reduced glucose uptake. The effects of Aβ accumulation and toxic stress triggers a cascade of impaired insulin signaling. Abbreviations: Aβ, amyloid beta; TNFα, tumor necrosis factor α; NMDAR, N-Methyl-D aspartate receptor; IRS-1, insulin receptor substrate-1; PI3k, phosphatidylinositol-3-kinase; AKT, protein kinase B; pTau, hyperphosphorylated tau; GLUT4, glucose transporter 4; JNK, N-terminal kinases; PKR, protein kinase R; Ikr, rapid-component delayed-rectifier potassium channel.

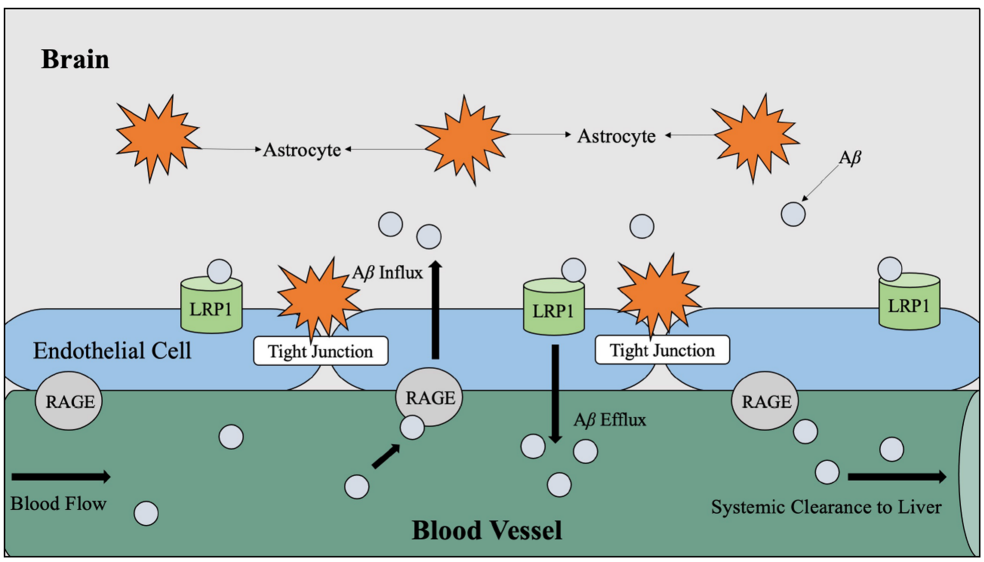

FIGURE 5 | LRP1 and RAGE-mediated Aβ transport across the BBB. Aβ travels through the blood vessels to cross the BBB for systemic clearance by the liver. In the periphery, Aβ binds to RAGE, which is the receptor for AGE believed to be produced as a result of hyperglycemia. When Aβ binds to RAGE, Aβ influxes into the brain *via* endothelial cells. Counteracting Aβ influx into the brain, Aβ efflux into the periphery is mediated by LRP1. Abbreviations: LRP1, lipoprotein receptor-related protein; RAGE, receptor for advanced glycation end products; Aβ, amyloid beta; BBB, blood-brain barrier; AGE, advanced glycation end products.

Aβ metabolism in the context of obesity is related to T2D due to the similarities in the pathophysiology of each condition. Most relevant to dysfunctional Aβ metabolism is the mutual presence of insulin resistance in conditions of obesity and T2D. Therefore, the mechanism of altered Aβ metabolism in the context of insulin resistance is identical for both T2D and obesity. Obesity is unique in its contribution to insulin resistance compared to T2D because excess adiposity is understood to result in insulin resistance, whereas T2D conditions often begin with insulin resistance. Nevertheless, there is a considerable lack of evidence that excess adiposity alone may contribute to Aβ metabolism.

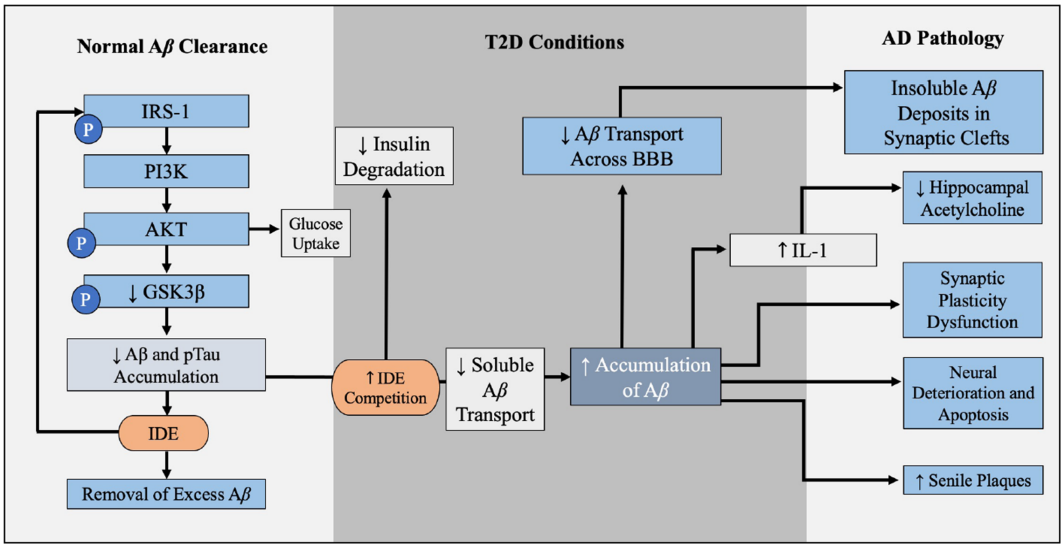

FIGURE 6 | Contribution of T2D conditions to Aβ accumulation and AD pathology. In the healthy brain insulin signaling pathway, insulin binds to PI3K which is degraded to AKT, leading to GLUT4-mediated glucose uptake and phosphorylation (inactivation) of GSK3β. GSK3β inactivation leads to decreased Aβ and pTau accumulation, and IDE degrades excess insulin and Aβ in the brain. When IR and hyperinsulinemia is developed during T2D, this increased competition for IDE, leading to Aβ and insulin accumulation, further illustrated in **Figure 4**. Increased Aβ accumulation leads to increased decreased soluble Aβ transport across BBB, leaving insoluble Aβ deposits trapped within the synaptic clefts, promoting inflammation and oxidative stress and increasing NF-kB. Increased levels of NF-kB increases IL-1 expression, which reduces hippocampal acetylcholine. Excess Aβ decreases synaptic plasticity, promotes neural deterioration and apoptosis, and promotes Aβ plaques. Aβ plaques is a well-established contributors to AD. Abbreviations: Aβ, amyloid beta; T2D, type 2 diabetes; AD, Alzheimer's disease; PI3K, phosphoinositide 3-kinase; AKT, protein kinase B; GLUT4, glucose transporter 4; GSK3β, glycogen synthase kinase 3 β; pTau, hyperphosphorylated tau; IDE, insulin degrading enzyme; IR, insulin resistance; BBB, blood-brain barrier.

ALTERED Aβ METABOLISM IN CARDIOVASCULAR DISEASE

CVD pathology can be summarized as elevated levels of blood lipids paired with atherosclerosis, the buildup of lipids, cholesterols, and plaques within arterial walls, that can lead to arterial stiffness and rigidity and obstruct blood flow and increase blood pressure (de Bruijn and Ikram, 2014). Elevated blood pressure damages arteries and other blood vessels which can lead to chronic inflammation (Fioranelli et al., 2018). In addition, chronic inflammation drastically reduces the functional surface area of blood vessels due to their inability to completely repair. Reduced functional surface area can lead to the deposition and accumulation of proteins like pTau and Aβ secondary to microglial cells lacking the adequate oxygen and glucose to perform routine excretory functions at maximum efficiency (Fioranelli et al., 2018). As cardiovascular circulatory efficiency diminishes, brain atrophy can increase, which is understood to be related to inefficient Aβ clearance and removal (Murphy and LeVine, 2010). Furthermore, brain Aβ concentrations are proportional to cholesterol concentrations, and Aβ accumulation within heart and blood vessels is understood to contribute to arterial stiffening, atherosclerosis, and cardiac dysfunction (Yeung et al., 2014; Fioranelli et al., 2018). In addition, Aβ1–40 was found to be 100 times more abundant in aortic atherosclerotic plaques than anywhere else in the body (Yeung et al., 2014). This accumulation of Aβ occurs when lymphatic capillaries fail to adequately drain due to the atherosclerosis, contributing to greater Aβ1–40 deposits within cardiovascular structures that induce cell damage and inflammation (Yeung et al., 2014).

A New York Heart Association study of 939 patients exhibiting early signs of heart failure indicated that higher concentrations of circulating Aβ1–40 resulted in higher mortality rates and greater frequency of diastolic dysfunction (Stakos et al., 2020). These adverse outcomes are likely due to elevated Aβ1–40 hindering the blood supply by disrupting normal vascular development. As the blood supply decreases, APP is upregulated, leading to increased vasoconstriction that inhibits the functionality of endothelium that is necessary in maintaining adequate blood supply to critical organs by vasodilation (Stakos et al., 2020). A similar experiment exploring the relationship between Aβ and diastolic dysfunction involving 3,266 patients discovered that lower stroke volume corresponds with higher concentrations of Aβ, reinforcing the results of the first (Stakos et al., 2020).

Furthermore, knockout mice for the APP gene (APP−/−) displayed 75–90% smaller arterial plaque thickness, significantly fewer arterial lesions, and a lower pro-inflammatory response measured by a low macrophage content than the APP+/+ mice (Karisetty et al., 2020; Tini et al., 2020). Therefore, APP, and subsequently Aβ, may play a role in the vascular inflammation that exacerbates cognitive impairment (Stakos et al., 2020). Although the aforementioned studies do shed light on the relationship between CVD conditions and Aβ metabolism independent of neurodegenerative outcomes, additional research

is required to determine a direct relationship between CVD pathology and AD risk.

ALTERED Aβ METABOLISM IN NON-ALCOHOLIC FATTY LIVER DISEASE

The liver has been identified as a key organ involved in the pathology and progression of AD due to its role in Aβ clearance (Estrada et al., 2019). It has been observed that Aβ solubility, as well as functionality of Aβ transport proteins, is of great importance with regards to transport across the blood-brain barrier when the liver enters a diseased state. In addition, evidence suggests that the solubility of Aβ is a critical aspect of clinical manifestations of AD (Murphy and LeVine, 2010).

The main enzyme responsible for Aβ production is BACE1, which is primarily expressed in the brain and can be found in peripheral organs (Murphy and LeVine, 2010). Under normal physiological conditions, Aβ is produced to support synaptic plasticity and regulate the calcium flow required for the transmission of synaptic communication(Karisetty et al., 2020). In the periphery, Aβ clearance is an essential contributor to AD progression since inadequate removal of Aβ from blood contributes to Aβ accumulation in the brain (Wang et al., 2006). Although enzymes such as IDE and neprilysin are responsible for degrading excess Aβ within the brain (**Figure 3**), much of the Aβ remains intact. Therefore, the efflux of soluble Aβ across the blood-brain barrier to the periphery exists as a mechanism for enhanced Aβ clearance (Murphy and LeVine, 2010).

As introduced in **Figure 5**, it is hypothesized that the facilitation of soluble Aβ efflux across the blood-brain barrier is controlled by the low-density lipoprotein receptor-related protein 1 (LRP1) on the "brain side" and receptors for advanced glycation end products (RAGE) on the "blood side" (Murphy and LeVine, 2010). The LRP1 is understood to be the mediator for Aβ uptake by hepatocytes (Wang et al., 2017). Theoretically, the proper flow of Aβ across the blood-brain barrier for clearance by the liver reduces Aβ burden on the brain since it is estimated that 60% (Wang et al., 2017) of brain-derived Aβ is cleared by the periphery; however, insoluble Aβ is a characteristic of AD pathology and cannot cross the blood-brain barrier (Murphy and LeVine, 2010). Therefore, soluble Aβ is considered more toxic than insoluble Aβ (Li et al., 2019).

In the periphery, soluble Aβ clearance is an essential component to AD progression since inadequate removal of Aβ from blood circulation contributes to Aβ buildup in the brain (Wang et al., 2006). Impaired removal of Aβ has been proposed as a potential link between peripheral metabolic dysfunction and AD; therefore, peripheral organs may be a vital component of excess Aβ removal. The liver, in particular, is unique in that it promotes Aβ clearance by protein degradation or bile excretion (Estrada et al., 2019). Liver disease is associated with high concentrations of circulating Aβ as a consequence of diminished detoxification ability (Wang et al., 2017). To counteract this effect, the administration of treatments that enhance LRP1-mediated Aβ clearance by the liver result in both improved cognition and mitigate the potentially damaging effects of Aβ within the brain (Tamaki et al., 2007; Sehgal et al., 2012). Hence, therapeutic intervention focused on the liver emerges as a promising target for AD intervention and therapy.

AD TREATMENTS AND FUTURE DIRECTIONS

Currently Available Alzheimer's Disease Treatments

At present, there are only two drug classifications for AD treatment that are clinically proven to improve memory and alertness, but do not increase life expectancy or slow AD progression. These drugs are cholinesterase inhibitors and memantine (**Table 2**, Weller and Budson, 2018). Cholinesterase inhibitors (donepezil, rivastigmine, and galantamine) are prescribed for the specific treatment of various stages of AD, whereas memantine is reserved for moderate or severe cases of AD (Weller and Budson, 2018). Memantine medications have been experimentally shown to over stimulate the extra synaptic N-methyl-D-aspartate receptor (NMDA), which is understood to contribute to neuronal excitotoxicity and death (Wang and Reddy, 2017), however, clinically, the effect of memantine appears to be more of an antagonistic effect on the whole population of NMDA receptors (Liu et al., 2019).

Though the purpose of the following section of this review is not to systematically synthesize all approved and pending AD treatments, it is critical to have a general understanding of the AD therapy-related research being conducted. The nature of this review focuses on the amyloid hypothesis, which hypothesizes that the accumulation of Aβ within brain parenchyma drives synaptic dysfunction and neurodegeneration leading to the manifestation of AD (van Dyck, 2018); however, both anti-amyloid and non-anti-amyloid treatments under

TABLE 2 | Approved Alzheimer's disease treatments.

Reference	Drug class	Mechanism	Key findings
Sharma (2019)	Cholinesterase inhibitors	Blocks cholinesterase, which degrades acetylcholine.	Limited efficacy, high doses associated with negative side effects, such as worsened cognition.
Matsunaga et al. (2015)	Memantine	Blocks NMDA receptors, preventing neuron loss.	More promising efficacy, some improvements in cognition, well tolerated, but small effect sizes of clinical studies limit evidence.

Abbreviation: NMDA, N-Methyl-D-aspartic acid or N-Methyl-D-aspartate.

TABLE 3 | Major anti-amyloid AD treatments under investigation.

Reference	Drug class	Mechanism	Key findings
Moussa-Pacha et al. (2020)	BACE1	BACE inhibitor, reduces Aβ production.	Insignificant physiological effects, some shown to worsen cognition. Several early phase trials ongoing.
Hung and Fu (2017)	pTau	Derivative of methyl blue shown to inhibit tau aggregation.	Phase 2 clinical trial suggests improvement in cognition at low doses. Research ongoing.
Hung and Fu (2017)	pTau	Enhancing immunotherapy pTau clearance *via* synthetic peptide of truncated and misfolded tau.	All early phase trials. No data yet but research ongoing.
Hung and Fu (2017)	pTau	Microtubule stabilizing agents.	Several failed due to toxic side effects. Additional clinical trials in early phase.
Boada et al. (2020)	Albumin 1 Immunoglobulin Plasma Exchange	Removal of Aβ bound to albumin plasma.	New therapy. Suggests greater effect on cognition in moderate stages of AD, additional research needed.
Deane (2012)	RAGE	Antagonist of RAGE receptors transporting circulating Aβ to brain.	Clinical trials not effective.
van Dyck (2018)	Aβ	Human monoclonal anti-Aβ antibodies provide passive immunity against Aβ accumulation.	Completed trials have yielded either failed or seen non-significant outcomes. Aducanumab specifically shows more promise for improving MMSE and CDR but is in early phase testing.
Hung and Fu (2017)	Aβ	Aβ clearance enhanced by active immunotherapy from Aβ peptides.	Several trials discontinued due to adverse immune responses. Additional trials ongoing in early phases.
Hung and Fu (2017)	γ-secretase	γ-secretase inhibitors shift APP cleavage toward production of shorter, less toxic Aβ peptides.	Clinical trials discontinued due to adverse side effects. One small unpublished study suggested some improvement in cognition.
Hung and Fu (2017)	Intravenous Immunoglobin	A naturally occurring antibody from the plasma of healthy donors. IVIG may direct antibodies against Aβ.	No beneficial effects observed.
Avgerinos et al. (2018)	Intranasal Insulin	Brains affected by AD show decreased concentration of insulin and increased concentration of insulin receptors, modulated Aβ in early AD.	Some positive results in function status and ADL but no other cognitive indicators. Has been suggested that different insulin types and doses may have variable effects on different APOE patients.

Abbreviations: BACE1, β-secretase 1; pTau, hyperphosphorylated tau; Aβ, amyloid beta; AD, Alzheimer's disease; RAGE, receptor for advanced glycation end products; MMSE, Mini Mental State Examination; CDR, Clinical Dementia Rating; APP, Amyloid Precursor Protein; APOE, Apolipoprotein E; APOE ε4 allele is a risk factor for AD.

investigation have been included as this review emphasizes the potential for combination therapies (**Table 3**) for effective AD treatment. Aβ is considered the initiator of the AD cascade, beginning with Aβ-induced amyloid plaques, neurofibrillary tangles from pTau, neurodegeneration, synaptic damage, neuron loss, and other pathological hallmarks of AD (Chen et al., 2017). As a result, anti-amyloid therapies have an extensive history of intervention attempts. AD patients have also displayed deficiency in the enzyme choline acetyltransferase, hence, cholinergic-based therapies were created (Sharma, 2019). Acetylcholine plays a sizable role in learning and memory, which is why it is now classified as a key biomarker in late-term AD pathology.

Alzheimer's Disease Treatments Under Investigation

Since 2019, AD drug intervention research seems to have shifted away from anti-amyloid therapies. In addition to the major non-anti-amyloid therapies (**Table 4**), new experimental treatments and therapies are focusing on inducing ketosis, partial agonists of dopamine, microglial activation inhibitors, RAGE antagonists, bacterial protease inhibitors, serotonin uptake inhibitors, γ-secretase inhibitors, antioxidant and anti-neuroinflammatory agents, anti-diabetes medications, tyrosine kinase inhibitors, and PPAR-γ agonists (Huang et al., 2020).

Additional AD hypotheses, including the cholinergic hypothesis and tau hypothesis, have been targeted for anti-AD treatments. The latter can be summarized by pTau causing an accumulation of neurofibrillary tangles within nerve cells, which interact with cellular proteins and prevent them from executing their normal function (Maccioni et al., 2010; Bakota and Brandt, 2016). The cholinergic hypothesis can be summarized as a reduction in acetylcholine synthesis, which inhibits biological activity of acetylcholinesterase (Sharma, 2019). A loss of cholinergic neurons are thought to encourage excessive influx of calcium into cells, resulting in neuronal damage (Sharma, 2019). Hence, acetylcholinesterase inhibitors are utilized for treatment to limit acetylcholine degradation, increasing the function of neural cells by increasing the concentration of acetylcholine (Sharma, 2019). Still, focusing on Aβ, pTau, or

TABLE 4 | Major non-anti-amyloid AD treatments under investigation.

Reference	Drug target	Mechanism	Brief conclusions
Fitz et al. (2019)	Retinoid X Receptors	Important for APOE expression, retinoid acid-mediated signaling, neuronal plasticity, and memory; anti-inflammatory effects of RXR/LXR.	Research is focused on activating LXR/RXR in the brain using nonsteroid synthetic ligands. Mice studies have seen variable outcomes.
Fitz et al. (2019)	Liver X Receptors	Include LRXα and LRXβ. LRXs are transcriptional regulators of lipid metabolism and inflammation. LRXβ is expressed in brain and spinal cord as the brain is the most cholesterol-rich organ and peripheral cholesterol cannot cross BBB. LRXβ K/O mice display motor neuron degeneration and impaired coordination.	Early phases of research; still needs validation in animal studies but has shown reduced levels of insoluble Aβ in mice. Research is focused on activating LXR/RXR in the brain using nonsteroid synthetic ligands.
Fitz et al. (2019)	Nuclear Receptors	Widely expressed in the brain. By directly binding to PPARs and LXRs, nuclear receptors ultimately induce stabilization of nuclear complexes that promote neuro- and peripheral inflammatory genes.	Early phases of research; still needs validation in animal studies.

Abbreviations: RXR, retinoid X receptors; APOE, apolipoprotein E; LXR, liver X receptors; BBB, blood-brain-barrier; K/O, knock-out; PPAR, peroxisome proliferator-activated receptor.

acetylcholine alone is unlikely in addressing the complete range of symptoms associated with neurological disease pathology (Fessel, 2018).

Overall, Aβ therapies have not yielded promising results in clinical trials (Panza et al., 2019a). Several anti-amyloid drug therapies since 2016 have failed due to lack of efficacy, toxicity, and worsening cognition (Huang et al., 2020). There is, however, evidence that Aβ and tau pathology, currently accepted as trademark biomarkers for AD, are only a piece of the full pathogenesis of AD (Bednar, 2019). Therefore, the greatest potential for a complete and robust AD treatment lies in combination therapies individualized to each patient care based on their specific clinical manifestations of AD and from learning more about the mechanisms of pathogenesis, which can vary greatly between patients (Bednar, 2019). Instead, the barrier that AD researchers face may not be that AD treatment candidates are entirely unsuccessful, but that they are simply only addressing one aspect of an extremely complex disorder that possesses numerous overlaps with other non-neurological disorders like NAFLD and T2D that lack thoroughly understood links to AD.

Anti-diabetes Medications for Alzheimer's Disease Treatment

Anti-diabetes drug therapies have been investigated for their efficacy as AD therapies due to the current understanding of the mechanisms that closely link glucose metabolism dysfunction with AD (Boccardi et al., 2019). It remains unclear which anti-diabetic medications holistically improves the outcome of AD patients; therefore, it is important to identify which diabetes medications lead to improvement of cognitive function and whether these benefits supersede risk factors.

According to a systematic review of randomized controlled trials by Avgerinos et al., intranasal insulin delivers insulin to the brain more rapidly than subcutaneous or intravenous insulin due to its unique ability to cross the blood-brain barrier independent of a transport process (Avgerinos et al., 2018). Intranasal insulin in patients without existing hyperinsulinemia, has been shown to alleviate the symptoms that link AD and T2D, including Aβ accumulation, synaptotoxicity, and oxidative stress (Avgerinos et al., 2018). Overall, increasing insulin in the brain of hypoinsulinemic patients translates to decreased Aβ-induced memory loss, reduces neuronal apoptosis, and increases synaptic plasticity (Boccardi et al., 2019). Data from the same systematic review also discovered that patients with the APOE4(+) gene remained stable or declined cognitively after intranasal insulin was administered, while those with the APOE4(-) gene showed more cognitive gains after administration (Avgerinos et al., 2018). However, additional research is needed to determine whether intranasal insulin alone is a sufficient treatment for AD.

Thiazolidinediones (TZDs) containing dipeptidyl peptidase-4 (DPP-4) inhibitors and glucagon-like peptide 1 (GLP-1) receptor agonists have been shown to counteract hyperglycemia, insulin resistance, and a variety of oxidative stressors, which are all precursor metabolic processes that contribute to Aβ and pTau accumulation (Boccardi et al., 2019). The peripheral effects of these antihyperglycemic medications include improving insulin signaling and reducing inflammation and oxidative stress (Boccardi et al., 2019). Centrally, these medications increase neuroprotection, neurogenesis, and synaptic plasticity and alleviate neuroinflammation (Boccardi et al., 2019). In addition, thiazolidinediones are insulin sensitizers and agonists of the peroxisome proliferator-activated receptor gamma (PPARγ; Boccardi et al., 2019). PPARγ is a possible mechanism for AD treatment due to existing evidence that PPARγ agonists decrease Aβ accumulation and inflammation (Avgerinos et al., 2018). In addition, PPARγ agonists play a key role in regulating calcium metabolism in the hippocampus, resulting in decreased oxidative stress and other stress-activated protein kinases that contribute to insulin resistance in the brain (Avgerinos et al., 2018). TZDs have also been shown to improve cerebral blood flow *via* anti-inflammatory and insulin-sensitizing effects, which

translated to increased memory in AD patients (Boccardi et al., 2019). TZDs also inactivate GSK3γ and decrease tau production (**Figure 4**). They do not prevent AD *per se*, but seem to slow AD progression (Boccardi et al., 2019). Like thiazolidinediones, GLP-1 receptor agonists are a group of anti-diabetic medications that have anti-hyperglycemic effects which may have beneficial effects on AD progression. GLP-1 is a short-acting insulinotropic peptide that enhances insulin gene expression while suppressing glucagon secretion in the pancreas (Boccardi et al., 2019). In *in vivo* models of AD, injection of GLP-1 receptor agonist was shown to decrease overburden of the hippocampus and improve spatial memory, and in a mouse model of T2D mice, GLP-1 injection decreased Aβ plaque in the cortex, restored peripheral and brain insulin sensitivity, and improved tau hyperphosphorylation, which are all significant features of AD (Boccardi et al., 2019).

It is important to note that healthy lifestyle choices can amplify the effects of anti-diabetic medication effectiveness. For patients suffering from hyperinsulinemia due to T2D and competition for IDE from Aβ, exercise can function as an alternative in regulating blood insulin and glucose levels as skeletal muscles possess a non-insulin-dependent ability to absorb glucose when their glycogen stores deplete post-exercise. This peripheral glucose uptake and insulin utilization has the potential to reduce hyperinsulinemia and decrease the competition for IDE discussed extensively in this review (**Figure 3**).

Potential Future Directions for Alzheimer's Disease Treatments

Neuroinflammation in response to glial cell accumulation has been recently considered as another key factor in AD pathology since amyloid plaques and neurofibrillary tangles are understood to be possible catalysts for the inflammatory response in the brain (Briggs et al., 2016). Meta analyses have suggested steroidal and non-steroidal anti-inflammatory drugs induce negligible effects on AD in symptomatic patients, but perhaps show potential for early-stage prevention of the disease (Briggs et al., 2016). Immune-based interventions, however, are predicted to lead to future preventive or therapeutic interventions for AD (Ozben and Ozben, 2019).

Stem cell therapies have been tested but have not yielded clinical efficacy yet, but more sophisticated studies are currently underway (Kang et al., 2016). Similarly, antibacterial therapy is considered another link to AD in which gut dysbiosis and neuroinflammation from the periphery exacerbate increased permeability of the gut and the blood-brain barrier (Panza et al., 2019b). At present, researchers have not finalized the safety of antibacterial therapy to AD as it is currently unknown which specific bacterial population in the gut of patients diagnosed with AD are overrepresented (Panza et al., 2019b).

In summary, there seems to be rationale for further research involving neuroinflammation and anti-diabetes-based interventions in the context of combination therapy, though it is impossible to rule out Aβ, pTau, and cholinergic focused interventions that have been tested only in solidarity. Until AD treatment can be identified, the importance of metabolic health, especially liver and glucose metabolism health, to prevent peripheral contribution of Aβ and pTau (Bharadwaj et al., 2017; Maarouf et al., 2018; Xin et al., 2018) should be emphasized by healthcare professionals (**Figure 6**). Research efforts for the development of AD interventions to be utilized in combination therapies may best be spent targeting Aβ clearance by decreasing LRP-1 transport of Aβ to the brain, improving Aβ clearance *via* the liver, or increasing IDE's affinity for Aβ in the brain. In addition, low-risk preventative measures, such as eating a balanced and nutrient-dense diet, engaging in regular aerobic exercise, and supplementation for nutrient deficiencies are recommended (Mendiola-Precoma et al., 2016). As nutrition scientists know, nutrition research is challenging and often puzzling as humans are subject to behavioral, environmental, and social factors, which can rarely be accurately or reliably predicted (Bednar, 2019).

CONCLUSION

The relationship between cardiometabolic health and AD pathologies are dynamic and interwoven. Aβ, one of the major pathologies of AD, served as the focus of this review. The central theme of this review was the unique relationship between Aβ and cardiometabolic health. Namely, we assessed not only how Aβ can alter cardiometabolic health, but also how cardiometabolic health can modify Aβ metabolism. Collectively, it appears insulin and inflammation are the two features common to all major CMDs and altered Aβ metabolism. This pattern reinforcing the importance of monitoring peripheral organ health in preventative neurological treatments and interventions. Based off these observations, there is reasonable evidence to suggest a collective association between AD and cardiometabolic health.

Potential novel mechanisms for AD therapies in patients with peripheral hyperinsulinemia include reducing the load of insulin on IDE in the brain, either by increasing the affinity of IDE for Aβ or by decreasing brain insulin concentrations. Furthermore, due to its central role in both Aβ clearance and hormonal regulation, the liver should be considered as a focal point of future cardiometabolic treatments targeting AD. To be effective, these therapies should improve Aβ clearance while simultaneously reducing hyperinsulinemia by drug or lifestyle interventions. Based on our findings, the pancreas may also serve as an important organ to study due to its inter-connectedness with liver function and its role in insulin synthesis as well as APP production. Lastly, future research should consider focusing on quantifying the contribution of periphery-born Aβ on AD outcomes. Overall, this review advocates for a shift towards greater emphasis on cardiometabolic health, cause-specific treatment, and combination therapies in the interest of offering the most promising interventions for AD.

AUTHOR CONTRIBUTIONS

MH and VB researched data and reviewed/edited manuscript. KA and DR researched data and reviewed manuscript.

VH conceived the idea, contributed to discussion, researched data and reviewed/edited manuscript. All authors contributed to the article and approved the submitted version.

REFERENCES

Ahmed, M., Davis, J., Aucoin, D., Sato, T., Ahuja, S., Aimoto, S., et al. (2010). Structural conversion of neurotoxic amyloid-β(1–42) oligomers to fibrils. *Nat. Struct. Mol. Biol.* 17, 561–567. doi: 10.1038/nsmb.1799

Albanese, E., Launer, L. J., Egger, M., Prince, M. J., Giannakopoulos, P., Wolters, F. J., et al. (2017). Body mass index in midlife and dementia: systematic review and meta-regression analysis of 589,649 men and women followed in longitudinal studies. *Alzheimers Dement.* 8, 165–178. doi: 10.1016/j.dadm.2017.05.007

Alzheimer's Association. (2008). 2008 Alzheimer's disease facts and figures. *Alzheimers Dement.* 4, 33–110. doi: 10.1016/j.jalz.2008.02.005

Alzheimer's Association Report (2020). 2020 Alzheimer's disease facts and figures. *Alzheimers Dement.* 16, 391–460. doi: 10.1002/alz.12068

Arnold, S. E., Arvanitakis, Z., Macauley-Rambach, S. L., Koenig, A. M., Wang, H. Y., Ahima, R. S., et al. (2018). Brain insulin resistance in type 2 diabetes and Alzheimer disease: concepts and conundrums. *Nat. Rev. Neurol.* 14, 168–181. doi: 10.1038/nrneurol.2017.185

Arvanitakis, Z., Wilson, R. S., Bienias, J. L., Evans, D. A., and Bennett, D. A. (2004). Diabetes mellitus and risk of Alzheimer disease and decline in cognitive function. *Arch. Neurol.* 61, 661–666. doi: 10.1001/archneur.61.5.661

Avgerinos, K. I., Kalaitzidis, G., Malli, A., Kalaitzoglou, D., Myserlis, P. G., and Lioutas, V. A. (2018). Intranasal insulin in Alzheimer's dementia or mild cognitive impairment: a systematic review. *J. Neurol.* 265, 1497–1510. doi: 10.1007/s00415-018-8768-0

Bakota, L., and Brandt, R. (2016). Tau biology and tau-directed therapies for Alzheimer's disease. *Drugs* 76, 301–313. doi: 10.1007/s40265-015-0529-0

Banks, W. A. (2001). Leptin transport across the blood-brain barrier: implications for the cause and treatment of obesity. *Curr. Pharm. Des.* 7, 125–133. doi: 10.2174/1381612013398310

Banks, W. A., Owen, J. B., and Erickson, M. A. (2012). Insulin in the brain: there and back again. *Pharmacol. Ther.* 136, 82–93. doi: 10.1016/j.pharmthera.2012.07.006

Baranowska-Bik, A., and Bik, W. (2017). Insulin and brain aging. *Prz. Menopauzalny* 16, 44–46. doi: 10.5114/pm.2017.68590

Bazotte, R. B., Silva, L. G., and Schiavon, F. P. (2014). Insulin resistance in the liver: deficiency or excess of insulin? *Cell Cycle* 13, 2494–2500. doi: 10.4161/15384101.2014.947750

Bednar, M. M. (2019). Combination therapy for Alzheimer's disease and related dementias. *Prog. Mol. Biol. Transl. Sci.* 168, 289–296. doi: 10.1016/bs.pmbts.2019.10.001

Bedse, G., Di Domenico, F., Serviddio, G., and Cassano, T. (2015). Aberrant insulin signaling in Alzheimer's disease: current knowledge. *Front. Neurosci.* 9:204. doi: 10.3389/fnins.2015.00204

Bertoni, A. G., Krop, J. S., Anderson, G. F., and Brancati, F. L. (2002). Diabetes-related morbidity and mortality in a national sample of U.S. elders. *Diabetes Care* 25, 471–475. doi: 10.2337/diacare.25.3.471

Bharadwaj, P., Wijesekara, N., Liyanapathirana, M., Newsholme, P., Ittner, L., Fraser, P., et al. (2017). The link between type 2 diabetes and neurodegeneration: roles for amyloid-β, amylin, and tau proteins. *J. Alzheimers Dis.* 59, 421–432. doi: 10.3233/JAD-161192

Blair, M. (2016). Diabetes mellitus review. *Urol. Nurs.* 36, 27–36. doi: 10.7257/1053-816X.2016.36.1.27

Blázquez, E., Velázquez, E., Hurtado-Carneiro, V., and Ruiz-Albusac, J. M. (2014). Insulin in the brain: its pathophysiological implications for States related with central insulin resistance, type 2 diabetes and Alzheimer's disease. *Front. Endocrinol.* 5:161. doi: 10.3389/fendo.2014.00161.

Boada, M., López, O. L. , Olazarán, J., Núñez, L., Pfeffer, M., and Paricio, M. (2020). A randomized, controlled clinical trial of plasma exchange with albumin replacement for Alzheimer's disease: Primary results of the AMBAR Study. *Alzheimer's Dement.* 16, 1412–1415. doi: 10.1002/alz.12137

Boccardi, V., Murasecco, I., and Mecocci, P. (2019). Diabetes drugs in the fight against Alzheimer's disease. *Ageing Res. Rev.* 54:100936. doi: 10.1016/j.arr.2019.100936

Briggs, R., Kennelly, S. P., and O'Neill, D. (2016). Drug treatments in Alzheimer's disease. *Clin. Med.* 16, 247–253. doi: 10.7861/clinmedicine.16-3-247

Brown, R. C., Lockwood, A. H., and Sonawane, B. R. (2005). Neurodegenerative diseases: an overview of environmental risk factors. *Environ. Health Perspect.* 113, 1250–1256. doi: 10.1289/ehp.7567

Bugianesi, E., Moscatiello, S., Ciaravella, M. F., and Marchesini, G. (2010). Insulin resistance in nonalcoholic fatty liver disease. *Curr. Pharm. Des.* 16, 1941–1951. doi: 10.2174/138161210791208875

Castellani, R. J., and Smith, M. A. (2011). Compounding artefacts with uncertainty and an amyloid cascade hypothesis that is 'too big to fail'. *J. Pathol.* 224, 147–152. doi: 10.1002/path.2885

Centers for Disease Control and Prevention. (2018). *Alzheimer's Disease: Promoting Health and Independence for an Aging Population, 2018*. Atlanta, GA: Department of Health and Human Services.

Centers for Disease Control and Prevention. (2020). *National Diabetes Statistics Report*. Atlanta, GA: U.S. Department of Health and Human Services.

Chen, G.-F., Xu, T.-H., Yan, Y., Zhou, Y.-R., Jiang, Y., Melcher, K., et al. (2017). Amyloid β: structure, biology and structure-based therapeutic development. *Acta Pharmacol. Sin.* 38, 1205–1235. doi: 10.1038/aps.2017.28

Chételat, G. (2013). Alzheimer disease: Aβ-independent processes-rethinking preclinical AD. *Nat. Rev. Neurol.* 9, 123–124. doi: 10.1038/nrneurol.2013.21

Choi, K. M., Han, K., Park, S., Chung, H. S., Kim, N. H., Yoo, H. J., et al. (2018). Implication of liver enzymes on incident cardiovascular diseases and mortality: a nationwide population-based cohort study. *Sci. Rep.* 8:3764. doi: 10.1038/s41598-018-19700-8

Chow, V. W., Mattson, M. P., Wong, P. C., and Gleichmann, M. (2010). An overview of APP processing enzymes and products. *Neuromol. Med.* 12, 1–12. doi: 10.1007/s12017-009-8104-z

Copps, K. D., and White, M. F. (2012). Regulation of insulin sensitivity by serine/threonine phosphorylation of insulin receptor substrate proteins IRS1 and IRS2. *Diabetologia* 55, 2565–2582. doi: 10.1007/s00125-012-2644-8

Deane, R. J. (2012). Is RAGE still a therapeutic target for Alzheimer's disease? *Future Med. Chem.* 4, 915–925. doi: 10.4155/fmc.12.51

de Bruijn, R. F., and Ikram, M. A. (2014). Cardiovascular risk factors and future risk of Alzheimer's disease. *BMC Med.* 12:130. doi: 10.1186/s12916-014-0130-5

De Felice, F. G., Lourenco, M. V., and Ferreira, S. T. (2014). How does brain insulin resistance develop in Alzheimer's disease? *Alzheimers Dement.* 10, S26–S32. doi: 10.1016/j.jalz.2013.12.004

de la Monte, S. M. (2012). Contributions of brain insulin resistance and deficiency in amyloid-related neurodegeneration in Alzheimer's disease. *Drugs* 72, 49–66. doi: 10.2165/11597760-000000000-00000

de la Torre, J. (2018). The vascular hypothesis of Alzheimer's disease: a key to preclinical prediction of dementia using neuroimaging. *J. Alzheimers Dis.* 63, 35–52. doi: 10.3233/JAD-180004

Deb, A., Thornton, J. D., Sambamoorthi, U., and Innes, K. (2017). Direct and indirect cost of managing alzheimer's disease and related dementias in the United States. *Expert Rev. Pharmacoecon. Outcomes Res.* 17, 189–202. doi: 10.1080/14737167.2017.1313118

DeMattos, R. B., Bales, K. R., Cummins, D. J., Paul, S. M., and Holtzman, D. M. (2002). Brain to plasma amyloid-β efflux: a measure of brain amyloid burden in a mouse model of Alzheimer's disease. *Science* 295, 2264–2267. doi: 10.1126/science.1067568

Estrada, L. D., Ahumada, P., Cabrera, D., and Arab, J. P. (2019). Liver dysfunction as a novel player in Alzheimer's progression: looking outside the brain. *Front. Aging Neurosci.* 11:174. doi: 10.3389/fnagi.2019.00174

Fessel, J. (2018). Alzheimer's disease combination treatment. *Neurobiol. Aging* 63:165. doi: 10.1016/j.neurobiolaging.2017.10.022

FUNDING

This work was supported by American Heart Association AIREA grant (20AIREA35170031) to VH.

Fillit, H., Nash, D. T., Rundek, T., and Zuckerman, A. (2008). Cardiovascular risk factors and dementia. *Am. J. Geriatr. Pharmacother.* 6, 100–118. doi: 10.1016/j.amjopharm.2008.06.004

Fioranelli, M., Bottaccioli, A. G., Bottaccioli, F., Bianchi, M., Rovesti, M., and Roccia, M. G. (2018). Stress and inflammation in coronary artery disease: a review psychoneuroendocrineimmunology-based. *Front. Immunol.* 9:2031. doi: 10.3389/fimmu.2018.02031

Fitz, N. F., Nam, K. N., Koldamova, R., and Lefterov, I. (2019). Therapeutic targeting of nuclear receptors, liver X and retinoid X receptors, for Alzheimer's disease. *Br. J. Pharmacol.* 176, 3599–3610. doi: 10.1111/bph.14668

Forny-Germano, L., De Felice, F. G., and Vieira, M. (2018). The role of leptin and adiponectin in obesity-associated cognitive decline and Alzheimer's disease. *Front. Neurosci.* 12:1027. doi: 10.3389/fnins.2018.01027

Francula-Zaninovic, S., and Nola, I. A. (2018). Management of measurable variable cardiovascular disease' risk factors. *Curr. Cardiol. Rev.* 14, 153–163. doi: 10.2174/1573403X14666180222102312

Freude, S., Plum, L., Schnitker, J., Leeser, U., Udelhoven, M., Krone, W., et al. (2005). Peripheral hyperinsulinemia promotes tau phosphorylation *in vivo*. *Diabetes* 54, 3343–3348. doi: 10.2337/diabetes.54.12.3343

Godoy-Matos, A. F., Silva Júnior, W. S., and Valerio, C. M. (2020). NAFLD as a continuum: from obesity to metabolic syndrome and diabetes. *Diabetol. Metab. Syndr.* 13:60. doi: 10.1186/s13098-020-00570-y

Gruzdeva, O., Borodkina, D., Uchasova, E., Dyleva, Y., and Barbarash, O. (2019). Leptin resistance: underlying mechanisms and diagnosis. *Diabetes Metab. Syndr. Obes.* 12, 191–198. doi: 10.2147/DMSO.S182406

Guzman, D. C., Olguin, H. J., García, E. H., Herrera, M. O., and Brizuela, N. O. (2016). Moieties in antidiabetic drugs as a target of insulin receptors in association with common neurological disorders. *Biomed. Rep.* 4, 395–399. doi: 10.3892/br.2016.616

Hales, C. M., Fryar, C. D., and Ogden, C. L. (2020). *Prevalence of Obesity and Severe Obesity Among Adults: United States, 2017–2018, NCHS Data Brief, no. 360.* Hyattsville, MD: National Center for Health Statistics.

Hebert, L. E., Beckett, L. A., Scherr, P. A., and Evans, D. A. (2001). Annual incidence of Alzheimer disease in the United States projected to the years 2000 through 2050. *Alzheimer Dis. Assoc. Disord.* 15, 169–173. doi: 10.1097/00002093-200110000-00002

Holtzman, D. M. (2008). Alzheimer's disease: moving towards a vaccine. *Nature* 454, 418–420. doi: 10.1038/454418a

Huang, L.-K., Chao, S.-P., and Hu, C.-J. (2020). Clinical trials of new drugs for Alzheimer disease. *J. Biomed. Sci.* 27:18. doi: 10.1186/s12929-019-0609-7

Hung, S.-Y., and Fu, W.-M. (2017). Drug candidates in clinical trials for Alzheimer's disease. *J. Biomed. Sci.* 24:47. doi: 10.1186/s12929-017-0355-7

Hurjui, D. M., Nita, O., Graur, L. I., Mihalache, L., Popescu, D. S., and Graur, M. (2012). The central role of the non alcoholic fatty liver disease in metabolic syndrome. *Rev. Med. Chir. Soc. Med. Nat. Iasi* 116, 425–431.

Jardim, T. V., Mozaffarian, D., Abrahams-Gessel, S., Sy, S., Lee, Y., Liu, J., et al. (2019). Cardiometabolic disease costs associated with suboptimal diet in the United States: a cost analysis based on a microsimulation model. *PLoS Med.* 16:e1002981. doi: 10.1371/journal.pmed.1002981

Kang, J. M., Yeon, B. K., Cho, S.-J., and Suh, Y.-H. (2016). Stem cell therapy for Alzheimer's disease: a review of recent clinical trials. *J. Alzheimers Dis.* 54, 879–889. doi: 10.3233/JAD-160406

Karisetty, B. C., Bhatnagar, A., Armour, E. M., Beaver, M., Zhang, H., and Elefant, F. (2020). Amyloid-β peptide impact on synaptic function and neuroepigenetic gene control reveal new therapeutic strategies for Alzheimer's disease. *Front. Mol. Neurosci.* 13:577622. doi: 10.3389/fnmol.2020.577622

Kawamura, T., Umemura, T., and Hotta, N. (2012). Cognitive impairment in diabetic patients: can diabetic control prevent cognitive decline? *J. Diabetes Investig.* 3, 413–423. doi: 10.1111/j.2040-1124.2012.00234.x

Kojro, E., and Fahrenholz, F. (2005). The non-amyloidogenic pathway: structure and function of α-secretases. *Subcell. Biochem.* 38, 105–127. doi: 10.1007/0-387-23226-5_5

Kulas, J. A., Puig, K. L., and Combs, C. K. (2017). Amyloid precursor protein in pancreatic islets. *J. Endocrinol.* 235, 49–67. doi: 10.1530/JOE-17-0122

Lau, F. C., Shukitt-Hale, B., and Joseph, J. A. (2007). Nutritional intervention in brain aging: reducing the effects of inflammation and oxidative stress. *Subcell. Biochem.* 42, 299–318. doi: 10.1007/1-4020-5688-5_14

Lee, E. B. (2011). Obesity, leptin, and Alzheimer's disease. *Ann. N Y Acad. Sci.* 1243, 15–29. doi: 10.1111/j.1749-6632.2011.06274.x

Li, X.-M., Yan, H.-J., Guo, Y.-S., and Wang, D. (2016). The role of leptin in central nervous system diseases. *Neuroreport* 27, 350–355. doi: 10.1097/WNR.0000000000000546

Li, R., Zhang, Y., Rasool, S., Geetha, T., and Babu, J. R. (2019). Effects and underlying mechanisms of bioactive compounds on type 2 diabetes mellitus and Alzheimer's disease. *Oxid. Med. Cell. Longev.* 2019:8165707. doi: 10.1155/2019/8165707

Liu, J., Chang, L., Song, Y., Li, H., and Wu, Y. (2019). The role of NMDA receptors in Alzheimer's disease. *Front. Neurosci.* 13:43. doi: 10.3389/fnins.2019.00043

Maarouf, C. L., Walker, J. E., Sue, L. I., Dugger, B. N., Beach, T. G., and Serrano, G. E. (2018). Impaired hepatic amyloid-β degradation in Alzheimer's disease. *PLoS One* 13:e0203659. doi: 10.1371/journal.pone.0203659

Maccioni, R. B., Farías, G., Morales, I., and Navarrete, L. (2010). The revitalized tau hypothesis on Alzheimer's disease. *Arch. Med. Res.* 41, 226–231. doi: 10.1016/j.arcmed.2010.03.007

Martins, I. J. (2018). Sirtuin 1, a diagnostic protein marker and its relevance to chronic disease and therapeutic drug interventions. *EC Pharmacol. Toxicol.* 6.4, 209–215.

Martins, E., and Oliveira, A. (2018). NAFLD and cardiovascular disease. *Porto Biomed. J.* 3:e2. doi: 10.1016/j.pbj.0000000000000002

Matheny, M., McPheeters, M. L., Glasser, A., Mercaldo, N., Weaver, R. B., Jerome, R. N., et al. (2011). *Systematic Review of Cardiovascular Disease Risk Assessment Tools.* Rockville, MD: Agency for Healthcare Research and Quality.

Matsunaga, S., Kishi, T., and Iwata, N. (2015). Memantine monotherapy for Alzheimer's disease: a systematic review and meta-analysis. *PLoS One* 10:e0123289. doi: 10.1371/journal.pone.0123289

Mayeux, R., Tang, M. X., Jacobs, D. M., Manly, J., Bell, K., Merchant, C., et al. (1999). Plasma amyloid β-peptide 1–42 and incipient Alzheimer's disease. *Ann. Neurol.* 46, 412–416. doi: 10.1002/1531-8249(199909)46:3<412::aid-ana19>3.0.co;2-a

Meex, R. C. R., and Watt, M. J. (2017). Hepatokines: linking nonalcoholic fatty liver disease and insulin resistance. *Nat. Rev. Endocrinol.* 13, 509–520. doi: 10.1038/nrendo.2017.56

Meisinger, C., Doring, A., Thorand, B., Heier, M., and Lowel, H. (2006). Body fat distribution and risk of type 2 diabetes in the general population: are there differences between men and women? The MONICA/KORA Augsburg cohort study. *Am. J. Clin. Nutr.* 84, 483–489. doi: 10.1093/ajcn/84.3.483

Mendiola-Precoma, J., Berumen, L. C., Padilla, K., and Garcia-Alcocer, G. (2016). Therapies for prevention and treatment of Alzheimer's disease. *Biomed. Res. Int.* 2016:2589276. doi: 10.1155/2016/2589276

Michaud, T. L., Su, D., Siahpush, M., and Murman, D. L. (2017). The risk of incident mild cognitive impairment and progression to dementia considering mild cognitive impairment subtypes. *Dement. Geriatr. Cogn. Dis. Extra* 7, 15–29. doi: 10.1159/000452486

Milić, S., Lulić, D., and Štimac, D. (2014). Non-alcoholic fatty liver disease and obesity: biochemical, metabolic and clinical presentations. *World J. Gastroenterol.* 20, 9330–9337. doi: 10.3748/wjg.v20.i28.9330

Mitra, S., De, A., and Chowdhury, A. (2020). Epidemiology of non-alcoholic and alcoholic fatty liver diseases. *Transl. Gastroenterol. Hepatol.* 5:16. doi: 10.21037/tgh.2019.09.08

Moreno-Treviño, M. G., Castillo-López, J., and Meester, I. (2015). Moving away from amyloid β to move on in Alzheimer research. *Front. Aging Neurosci.* 7:2. doi: 10.3389/fnagi.2015.00002

Moussa-Pacha, N. M., Abdin, S. M., Omar, H. A., Alniss, H., and Al-Tel, T. H. (2020). BACE1 inhibitors: current status and future directions in treating Alzheimer's disease. *Med. Res. Rev.* 40, 339–384. doi: 10.1002/med.21622

Mozaffarian, D., Benjamin, E. J., Go, A. S., Arnett, D. K., Blaha, M. J., Cushman, M., et al. (2016). Heart disease and stroke statistics—2016 update. A report from the American Heart Association. *Circulation* 133, e38–e360. doi: 10.1161/CIR.0000000000000350

Murphy, M. P., and LeVine, H. III. (2010). Alzheimer's disease and the amyloid-β peptide. *J. Alzheimers Dis.* 19, 311–323. doi: 10.3233/JAD-2010-1221

Musso, G., Gambino, R., Cassader, M., and Pagano, G. (2011). Meta-analysis: natural history of non-alcoholic fatty liver disease (NAFLD) and diagnostic accuracy of non-invasive tests for liver disease severity. *Ann. Med.* 43, 617–649. doi: 10.3109/07853890.2010.518623

Nicklas, B. J., Cesari, M., Penninx, B. W., Kritchevsky, S. B., Ding, J., Newman, A., et al. (2006). Abdominal obesity is an independent risk factor for chronic heart failure in older people. *J. Am. Geriatr. Soc.* 54, 413–420. doi: 10.1111/j.1532-5415.2005.00624.x

North, B. J., and Sinclair, D. A. (2012). The intersection between aging and cardiovascular disease. *Circ. Res.* 110, 1097–1108. doi: 10.1161/CIRCRESAHA.111.246876

Nurdiantami, Y., Watanabe, K., Tanaka, E., Pradono, J., and Anme, T. (2018). Association of general and central obesity with hypertension. *Clin. Nutr.* 37, 1259–1263. doi: 10.1016/j.clnu.2017.05.012

Ozben, T., and Ozben, S. (2019). Neuro-inflammation and anti-inflammatory treatment options for Alzheimer's disease. *Clin. Biochem.* 72, 87–89. doi: 10.1016/j.clinbiochem.2019.04.001

Panza, F., Lozupone, M., Logroscino, G., and Imbimbo, B. P. (2019a). A critical appraisal of amyloid-β-targeting therapies for Alzheimer disease. *Nat. Rev. Neurol.* 15, 73–88. doi: 10.1038/s41582-018-0116-6

Panza, F., Lozupone, M., Solfrizzi, V., Watling, M., and Imbimbo, B. P. (2019b). Time to test antibacterial therapy in Alzheimer's disease. *Brain* 142, 2905–2929. doi: 10.1093/brain/awz244

Perumpail, B. J., Khan, M. A., Yoo, E. R., Cholankeril, G., Kim, D., and Ahmed, A. (2017). Clinical epidemiology and disease burden of nonalcoholic fatty liver disease. *World J. Gastroenterol.* 23, 8263–8276. doi: 10.3748/wjg.v23.i47.8263

Pimplikar, S. W., Nixon, R. A., Robakis, N. K., Shen, J., and Tsai, L.-H. (2010). Amyloid-independent mechanisms in Alzheimer's disease pathogenesis. *J. Neurosci.* 30, 14946–14954. doi: 10.1523/JNEUROSCI.4305-10.2010

Pivovarova, O., Höhn, A., Grune, T., Pfeiffer, A. F., and Rudovich, N. (2016). Insulin-degrading enzyme: new therapeutic target for diabetes and Alzheimer's disease? *Ann. Med.* 48, 614–624. doi: 10.1080/07853890.2016.1197416

Pomytkin, I., Costa-Nunes, J. P., Kasatkin, V., Veniaminova, E., Demchenko, A., Lyundup, A., et al. (2018). Insulin receptor in the brain: mechanisms of activation and the role in the CNS pathology and treatment. *CNS Neurosci. Ther.* 24, 763–774. doi: 10.1111/cns.12866

Postina, R., Schroeder, A., Dewachter, I., Bohl, J., Schmitt, U., Kojro, E., et al. (2004). A disintegrin-metalloproteinase prevents amyloid plaque formation and hippocampal defects in an Alzheimer disease mouse model. *J. Clin. Invest.* 113, 1456–1464. doi: 10.1172/JCI20864

Pugazhenthi, S., Qin, L., and Reddy, P. H. (2017). Common neurodegenerative pathways in obesity, diabetes, and Alzheimer's disease. *Biochim. Biophys. Acta Mol. Basis Dis.* 1863, 1037–1045. doi: 10.1016/j.bbadis.2016.04.017

Qiu, W. Q., and Folstein, M. F. (2006). Insulin, insulin-degrading enzyme and amyloid-β peptide in Alzheimer's disease: review and hypothesis. *Neurobiol. Aging* 27, 190–198. doi: 10.1016/j.neurobiolaging.2005.01.004

Racette, S. B., Evans, E. M., Weiss, E. P., Hagberg, J. M., and Holloszy, J. O. (2006). Abdominal adiposity is a stronger predictor of insulin resistance than fitness among 50–95 year olds. *Diabetes Care* 29, 673–678. doi: 10.2337/diacare.29.03.06.dc05-1605

Rada, P., Mark, G. P., Vitek, M. P., Mangano, R. M., Blume, A. J., Beer, B., et al. (1991). Interleukin-1 β decreases acetylcholine measured by microdialysis in the hippocampus of freely moving rats. *Brain Res.* 550, 287–290. doi: 10.1016/0006-8993(91)91330-4

Rahmani, J., Miri, A., Namjoo, I., Zamaninour, N., Maljaei, M. B., Zhou, K., et al. (2019). Elevated liver enzymes and cardiovascular mortality: a systematic review and dose-response meta-analysis of more than one million participants. *Eur. J. Gastroenterol. Hepatol.* 31, 555–562. doi: 10.1097/MEG.0000000000001353

Roberts, R., and Knopman, D. S. (2013). Classification and epidemiology of MCI. *Clin. Geriatr. Med.* 29, 753–772. doi: 10.1016/j.cger.2013.07.003

Schapira, A. H. (2007). Mitochondria in the etiology of Parkinson's disease. *Handb. Clin. Neurol.* 83, 479–491. doi: 10.1016/S0072-9752(07)83022-3

Sehgal, N., Gupta, A., Valli, R. K., Joshi, S. D., Mills, J. T., Hamel, E., et al. (2012). Withania somnifera reverses Alzheimer's disease pathology by enhancing low-density lipoprotein receptor-related protein in liver. *Proc. Natl. Acad. Sci. U S A* 109, 3510–3515. doi: 10.1073/pnas.1112209109

Shanik, M. H., Xu, Y., Skrha, J., Dankner, R., Zick, Y., and Roth, J. (2008). Insulin resistance and hyperinsulinemia: is hyperinsulinemia the cart or the horse? *Diabetes Care* 31, S262–S268. doi: 10.2337/dc08-s264

Sharma, K. (2019). Cholinesterase inhibitors as Alzheimer's therapeutics (Review). *Mol. Med. Rep.* 20, 1479–1487. doi: 10.3892/mmr.2019.10374

Sheka, A. C., Adeyi, O., Thompson, J., Hameed, B., Crawford, P. A., and Ikramuddin, S. (2020). Nonalcoholic steatohepatitis: a review. *JAMA* 323, 1175–1183. doi: 10.1001/jama.2020.2298

Stakos, D. A., Stamatelopoulos, K., Bampatsias, D., Sachse, M., Zormpas, E., Vlachogiannis, N. I., et al. (2020). The Alzheimer's disease amyloid-β hypothesis in cardiovascular aging and disease: JACC focus seminar. *J. Am. Coll. Cardiol.* 75, 952–967. doi: 10.1016/j.jacc.2019.12.033

Stampfer, M. J. (2006). Cardiovascular disease and Alzheimer's disease: common links. *J. Intern. Med.* 260, 211–123. doi: 10.1111/j.1365-2796.2006.01687.x

Stanhope, K. L., Goran, M. I., Bosy-Westphal, A., King, J. C., Schmidt, L. A., Schwarz, J. M., et al. (2018). Pathways and mechanisms linking dietary components to cardiometabolic disease: thinking beyond calories. *Obes. Rev.* 19, 1205–1235. doi: 10.1111/obr.12699

Sulaiman, S. A., N.Muhsin, I. A., and Jamal, R. (2019). Regulatory non-coding RNAs network in non-alcoholic fatty liver disease. *Front. Physiol.* 10:279. doi: 10.3389/fphys.2019.00279

Tamaki, C., Ohtsuki, S., and Terasaki, T. (2007). Insulin facilitates the hepatic clearance of plasma amyloid β-peptide (1 40) by intracellular translocation of low-density lipoprotein receptor-related protein 1 (LRP-1) to the plasma membrane in hepatocytes. *Mol. Pharmacol.* 72, 850–855. doi: 10.1124/mol.107.036913

Tanno, M., Kuno, A., Horio, Y., and Miura, T. (2012). Emerging beneficial roles of sirtuins in heart failure. *Basic Res. Cardiol.* 107:273. doi: 10.1007/s00395-012-0273-5

Tanzi, R. E., and Bertram, L. (2005). Twenty years of the Alzheimer's disease amyloid hypothesis: a genetic perspective. *Cell* 120, 545–555. doi: 10.1016/j.cell.2005.02.008

Targher, G., Byrne, C. D., and Tilg, H. (2020). NAFLD and increased risk of cardiovascular disease: clinical associations, pathophysiological mechanisms and pharmacological implications. *Gut* 69, 1691–1705. doi: 10.1136/gutjnl-2020-320622

Taylor, C. A., Greenlund, S. F., McGuire, L. C., Lu, H., and Croft, J. B. (2017). Deaths from Alzheimer's disease—United States, 1999–2014. *MMWR Morb. Mortal. Wkly. Rep.* 66, 521–526. doi: 10.15585/mmwr.mm6620a1

Thorpe, R. J. Jr., and Ferraro, K. F. (2004). Aging, obesity, and mortality: misplaced concern about obese older people? *Res. Aging* 26, 108–129. doi: 10.1177/0164027503258738

Tini, G., Scagliola, R., Monacelli, F., La Malfa, G., Porto, I., Brunelli, C., et al. (2020). Alzheimer's disease and cardiovascular disease: a particular association. *Cardiol. Res. Pract.* 2020:2617970. doi: 10.1155/2020/2617970

Trefts, E., Gannon, M., and Wasserman, D. H. (2017). The liver. *Curr. Biol.* 27, R1147–R1151. doi: 10.1016/j.cub.2017.09.019

Tse, K.-H., and Herrup, K. (2017). Re-imagining Alzheimer's disease—the diminishing importance of amyloid and a glimpse of what lies ahead. *J. Neurochem.* 143, 432–444. doi: 10.1111/jnc.14079

Tumminia, A., Vinciguerra, F., Parisi, M., and Frittitta, L. (2018). Type 2 diabetes mellitus and Alzheimer's disease: role of insulin signalling and therapeutic implications. *Int. J. Mol. Sci.* 19:3306. doi: 10.3390/ijms19113306

Utzschneider, K. M., and Kahn, S. E. (2006). Review: the role of insulin resistance in nonalcoholic fatty liver disease. *J. Clin. Endocrinol. Metab.* 91, 4753–4761. doi: 10.1210/jc.2006-0587

van Dyck, C. H. (2018). Anti-amyloid-β monoclonal antibodies for Alzheimer's disease: pitfalls and promise. *Biol. Psychiatry* 83, 311–319. doi: 10.1016/j.biopsych.2017.08.010

Verdile, G., Keane, K. N., Cruzat, V. F., Medic, S., Sabale, M., Rowles, J., et al. (2015). Inflammation and oxidative stress: the molecular connectivity between insulin resistance, obesity and Alzheimer's disease. *Mediators Inflamm.* 2015:105828. doi: 10.1155/2015/105828

Villarroel, M., Blackwell, D., and Jen, A. (2019). *Tables of Summary Health Statistics for U.S. Adults: 2018 National Health Interview Survey*. Hyattsville, MD: National Center for Health Statistics.

Walker, J. M., and Harrison, F. E. (2015). Shared neuropathological characteristics of obesity, type 2 diabetes and Alzheimer's disease: impacts on cognitive decline. *Nutrients* 7, 7332–7357. doi: 10.3390/nu7095341

Wang, G., Chen, Z., Bartell, T., and Wang, X. (2014). Early life origins of metabolic syndrome: the role of environmental toxicants. *Curr. Environ. Health Rep.* 1, 78–89. doi: 10.1007/s40572-013-0004-6

Wang, J., Gu, B. J., Masters, C. L., and Wang, Y. J. (2017). A systemic view of Alzheimer disease—insights from amyloid-β metabolism beyond the brain. *Nat. Rev. Neurol.* 13:703. doi: 10.1038/nrneurol.2017.147

Wang, R., and Reddy, P. H. (2017). Role of glutamate and NMDA receptors in Alzheimer's disease. *J. Alzheimers Dis.* 57, 1041–1048. doi: 10.3233/JAD-160763

Wang, W.-Y., Tan, M.-S., Yu, J.-T., and Tan, L. (2015). Role of pro-inflammatory cytokines released from microglia in Alzheimer's disease. *Ann. Transl. Med.* 3:136. doi: 10.3978/j.issn.2305-5839.2015.03.49

Wang, Y.-J., Zhou, H.-D., and Zhou, X.-F. (2006). Clearance of amyloid-β in Alzheimer's disease: progress, problems and perspectives. *Drug Discov. Today* 11, 931–938. doi: 10.1016/j.drudis.2006.08.004

Waterson, M. J., and Horvath, T. L. (2015). Neuronal regulation of energy homeostasis: beyond the hypothalamus and feeding. *Cell Metab.* 22, 962–970. doi: 10.1016/j.cmet.2015.09.026

Weller, J., and Budson, A. (2018). Current understanding of Alzheimer's disease diagnosis and treatment. *F1000Res.* 7:F1000 Faculty Rev-1161. doi: 10.12688/f1000research.14506.1

Westwood, A. J., Beiser, A., Decarli, C., Harris, T. B., Chen, T. C., He, X. M., et al. (2014). Insulin-like growth factor-1 and risk of Alzheimer dementia and brain atrophy. *Neurology* 82, 1613–1619. doi: 10.1212/WNL.0000000000000382

Willis, A., Davies, M., Yates, T., and Khunti, K. (2012). Primary prevention of cardiovascular disease using validated risk scores: a systematic review. *J. R. Soc. Med.* 105, 348–356. doi: 10.1258/jrsm.2012.110193

Wojcik-Cichy, K., Koslinska-Berkan, E., and Piekarska, A. (2018). The influence of NAFLD on the risk of atherosclerosis and cardiovascular diseases. *Clin. Exp. Hepatol.* 4, 1–6. doi: 10.5114/ceh.2018.73155

Xin, S. H., Tan, L., Cao, X., Yu, J. T., and Tan, L. (2018). Clearance of amyloid β and tau in Alzheimer's disease: from mechanisms to therapy. *Neurotox. Res.* 34, 733–748. doi: 10.1007/s12640-018-9895-1

Yao, J., Irwin, R. W., Zhao, L., Nilsen, J., Hamilton, R. T., and Brinton, R. D. (2009). Mitochondrial bioenergetic deficit precedes Alzheimer's pathology in female mouse model of Alzheimer's disease. *Proc. Natl. Acad. Sci. U S A* 106, 14670–14675. doi: 10.1073/pnas.0903563106

Yeung, E. H., Robledo, C., Boghossian, N., Zhang, C., and Mendola, P. (2014). Developmental origins of cardiovascular disease. *Curr. Epidemiol. Rep.* 1, 9–16. doi: 10.1007/s40471-014-0006-4

Yoon, D. H., Choi, S. H., Yu, J. H., Ha, J. H., Ryu, S. H., and Park, D. H. (2012). The relationship between visceral adiposity and cognitive performance in older adults. *Age Ageing* 41, 456–461. doi: 10.1093/ageing/afs018

Yoon, S. B., Lee, I. S., Choi, M. H., Lee, K., Ham, H., Oh, H. J., et al. (2017). Impact of fatty liver on acute pancreatitis severity. *Gastroenterol. Res. Pract.* 2017:4532320. doi: 10.1155/2017/4532320

Yoshino, Y., and Dwivedi, Y. (2020). Non-coding RNAs in psychiatric disorders and suicidal behavior. *Front. Psychiatry* 11:543893. doi: 10.3389/fpsyt.2020.543893

Younkin, S. G. (1998). The role of A β 42 in Alzheimer's disease. *J. Physiol. Paris* 92, 289–292. doi: 10.1016/s0928-4257(98)80035-1

Younossi, Z. M., Koenig, A. B., Abdelatif, D., Fazel, Y., Henry, L., and Wymer, M. (2016). Global epidemiology of nonalcoholic fatty liver disease-Meta-analytic assessment of prevalence, incidence and outcomes. *Hepatology* 64, 73–84. doi: 10.1002/hep.28431

Yusuf, S., Hawken, S., Ounpuu, S., Bautista, L., Franzosi, M. G., Commerford, P., et al. (2005). Obesity and the risk of myocardial infarction in 27,000 participants from 52 countries: a case-control study. *Lancet* 366, 1640–1649. doi: 10.1016/S0140-6736(05)67663-5

Zheng, Y., Ley, S. H., and Hu, F. B. (2018). Global aetiology and epidemiology of type 2 diabetes mellitus and its complications. *Nat. Rev. Endocrinol.* 14, 88–98. doi: 10.1038/nrendo.2017.151

Conflict of Interest: The authors declare that the research was conducted in the absence of any commercial or financial relationships that could be construed as a potential conflict of interest.

Publisher's Note: All claims expressed in this article are solely those of the authors and do not necessarily represent those of their affiliated organizations, or those of the publisher, the editors and the reviewers. Any product that may be evaluated in this article, or claim that may be made by its manufacturer, is not guaranteed or endorsed by the publisher.

frontiers in Aging Neuroscience

ORIGINAL RESEARCH
published: 25 August 2021
doi: 10.3389/fnagi.2021.686506

Amelioration of Hippocampal Insulin Resistance Reduces Tau Hyperphosphorylation and Cognitive Decline Induced by Isoflurane in Mice

Liangyu Peng[1†], Xin Fang[1†], Fangxia Xu[1], Shuai Liu[1], Yue Qian[1], Xiangdan Gong[1], Xin Zhao[2,3], Zhengliang Ma[1], Tianjiao Xia[2,4*] and Xiaoping Gu[1*]*

[1] Department of Anesthesiology, Affiliated Drum Tower Hospital of Medical Department of Nanjing University, Nanjing, China, [2] Medical School of Nanjing University, Nanjing, China, [3] Department of Anesthesiology, Nanjing Stomatological Hospital, Medical School of Nanjing University, Nanjing, China, [4] Jiangsu Key Laboratory of Molecular Medicine, Nanjing University, Nanjing, China

OPEN ACCESS

Edited by:
Ines Moreno-Gonzalez, University of Malaga, Spain

Reviewed by:
Chun-Ling Dai, New York State Institute for Basic Research in Developmental Disabilities, United States
Bin Xu, North Carolina Central University, United States

***Correspondence:**
Zhengliang Ma
mazhengliang1964@nju.edu.cn
Tianjiao Xia
tjxia@nju.edu.cn
Xiaoping Gu
xiaopinggu@nju.edu.cn

[†] *These authors have contributed equally to this work*

Received: 27 March 2021
Accepted: 12 May 2021
Published: 25 August 2021

Citation:
Peng L, Fang X, Xu F, Liu S, Qian Y, Gong X, Zhao X, Ma Z, Xia T and Gu X (2021) Amelioration of Hippocampal Insulin Resistance Reduces Tau Hyperphosphorylation and Cognitive Decline Induced by Isoflurane in Mice. Front. Aging Neurosci. 13:686506. doi: 10.3389/fnagi.2021.686506

General anesthetics can induce cognitive impairments and increase the risk of Alzheimer's disease (AD). However, the underlying mechanisms are still unknown. Our previous studies shown that long-term isoflurane exposure induced peripheral and central insulin resistance (IR) in adult mice and aggravated IR in type 2 diabetes mellitus (T2DM) mice. Clinical and preclinical studies revealed an association between impaired insulin signaling and tau pathology in AD and other tauopathies. We investigated if alleviation of hippocampal IR by the antidiabetic agent metformin could reduce tau hyperphosphorylation and cognitive decline induced by isoflurane in mice. The effects of prolonged (6 h) isoflurane anesthesia on hippocampal IR, hippocampal tau hyperphosphorylation, and hippocampus-dependent cognitive function were evaluated in wild type (WT) adult mice and the high-fat diet plus streptozotocin (HFD/STZ) mouse model of T2DM. Here we shown that isoflurane and HFD/STZ dramatically and synergistically induced hippocampal IR and fear memory impairment. Metformin pretreatment strongly ameliorated hippocampal IR and cognitive dysfunction caused by isoflurane in WT mice, but was less effective in T2DM mice. Isoflurane also induced hippocampal tau hyperphosphorylation and metformin reversed this effect. In addition, isoflurane significantly increased blood glucose levels in both adult and T2DM mice, and metformin reversed this effect as well. Administration of 25% glucose to metformin-pretreated mice induced hyperglycemia, but surprisingly did not reverse the benefits of metformin on hippocampal insulin signaling and fear memory following isoflurane anesthesia. Our findings show hippocampal IR and tau hyperphosphorylation contribute to acute isoflurane-induced cognitive dysfunction. Brief metformin treatment can mitigate these effects through a mechanism independent of glycemic control. Future studies are needed to investigate whether long-term metformin treatment can also prevent T2DM-induced hippocampal IR and cognitive decline.

Keywords: cognitive impairment, isoflurane, insulin resistance, metformin, hippocampus, blood glucose

INTRODUCTION

About 10–50% of patients receiving surgery under anesthesia demonstrate cognitive impairments occurring between 1 month and 1 year after surgery following treatment, termed postoperative cognitive dysfunction (POCD) (James, 2020). POCD is not a transient phenomenon but associated with prolonged hospitalization, functional decline, less likely to live independently, and increased mortality (Moller et al., 1998; Steinmetz et al., 2009). Intraoperative hypoxia, inflammation, and the pharmacological effects of anesthetics are implicated in POCD pathogenesis, and older age is the strongest risk factor (Moller et al., 1998). Further, accumulating clinical and experimental evidence suggest that surgery under general anesthesia increases the risk of developing Alzheimer's disease (AD) and other forms of dementia (James, 2020). Our previous studies confirmed that long-term isoflurane exposure can induce cognitive impairment in adult mice, providing an experimental model to investigate the underlying pathogenesis (Xia et al., 2016; Song et al., 2019).

In addition to increasing POCD risk, aging increases susceptibility to metabolic syndrome (MetS) and type 2 diabetes mellitus (T2DM) (Ford et al., 2002; Menke et al., 2015). It is also well accepted that MetS can induce cognitive impairments, including of memory and executive function (Kim and Feldman, 2015; Ng et al., 2016). Moreover, MetS increases the risk of POCD (Hudetz et al., 2011). A decline in brain tissue volume can be detected even in early onset MetS patients (Sala et al., 2014). Similarly, T2DM disrupts brain structure and function, especially in cognition-related regions, and increases the risks of both POCD and age-related cognitive decline compared to age-matched non-diabetics (Feinkohl et al., 2017; Sanjari Moghaddam et al., 2019). Our pilot study also found that T2DM predicts POCD at 1 week after orthopedic surgery in elderly patients (over 60 years of age) and patients with T2DM had a 2.6-fold higher risk of POCD compared with patients without diabetes at 1 week after surgery (**Supplementary Table 1**). Collectively, these observations suggest that the molecular signaling mechanisms disrupted in T2DM may also contribute to POCD.

A decrease in insulin-induced molecular signaling, termed insulin resistance (IR), is a major pathogenic mechanism in MetS and T2DM, and may contribute to the associated cognitive impairments (Biessels and Reagan, 2015; Kim and Feldman, 2015). Experimental models of diabetes not only show remarkable peripheral and central nervous system IR, but also deficits in the neuroplastic processes linked to cognition (Biessels and Reagan, 2015). Moreover, brain and peripheral IR increase with advanced age (Petersen et al., 2015; Martín-Segura et al., 2019). Insulin resistance is also a common complication after anesthesia and surgery, and the degree of postoperative IR is associated with surgical magnitude (Thorell et al., 1993). In aged rats as well, surgical procedures impair central insulin signaling and increase susceptibility to hippocampus-related cognitive impairments (Kawano et al., 2016). Isoflurane and sevoflurane reduced peripheral insulin sensitivity by about 50% and almost completely suppressed liver insulin responses in a canine model (Kim et al., 2016). These anesthetics also significantly reduced mean cerebral glucose utilization during anesthesia in rats (Lenz et al., 1998). Recently, we found that long-term isoflurane exposure induced peripheral and central IR in adult mice and aggravated IR in T2DM mice (Fang et al., 2020). Clinical studies show that preoperative IR predicts POCD in elderly gastrointestinal patients and that the IR index is significantly higher in patients with POCD than patients without POCD (Tang et al., 2017; He et al., 2019). Collectively, these results provide compelling evidence that IR contributes to POCD development.

Hippocampal accumulation of hyperphosphorylated tau protein may link MetS/T2DM, IR, POCD, and AD risk. Hyperphosphorylated tau proteins are a core component of neurofibrillary tangles, a pathological hallmark of AD (Ittner et al., 2010), and IR can prevent hippocampal tau dephosphorylation in rats (Kim et al., 2015). Both clinical and preclinical studies have found an association between impaired insulin signaling and tau pathology in AD and other tauopathies (Yarchoan et al., 2014). Further, inhalational anesthetic exposure, especially prolonged or repeated exposure, induced a long-lasting increase in tau phosphorylation associated with cognitive impairment (Dong et al., 2012; Le Freche et al., 2012). Conversely, insulin-sensitizing strategies have been shown to improve memory performance, reduce cerebrospinal fluid biomarkers of disease, and enhance cerebral glucose utilization in mild cognitive impairment (MCI) and AD patients (Hölscher, 2014).

Based on these findings, we speculated that isoflurane-induced hippocampal IR and ensuing tau hyperphosphorylation contribute to POCD and progression of AD pathology, while amelioration of hippocampal IR may mitigate tau hyperphosphorylation and POCD caused by long-term isoflurane anesthesia. Metformin, a first-line antidiabetic drug, exerts its therapeutic glucose-lowering effects by suppressing hepatic gluconeogenesis, decreasing insulin resistance, and increasing insulin sensitivity (Giannarelli et al., 2003). Here we examine whether pretreatment with metformin can alleviate hippocampal IR and tau hyperphosphorylation as well as cognitive impairment caused by long-term isoflurane anesthesia in adult and T2DM mice.

MATERIALS AND METHODS

Animals and Treatment

Animal care and study protocols were approved by the Laboratory Animal Ethics Committee of Drum Tower Hospital. Animals were housed (6–7 per cage) with free access to food and water and were kept in temperature-controlled facilities at

Abbreviations: AD, Alzheimer's disease; Anes Isoflurane anesthesia; DM T2DM model mice; Glu 25% glucose solution; HFD, High-fat diet; IR, Insulin resistance; IRS1, Insulin receptor substrates 1; IRS2, Insulin receptor substrates 2; MCI, Mild cognitive impairment; Met Metformin injection; MetS, Metabolic syndrome; POCD, Postoperative cognitive dysfunction; STZ, Streptozotocin; T2DM, Type 2 diabetes mellitus; WT, Wild type.

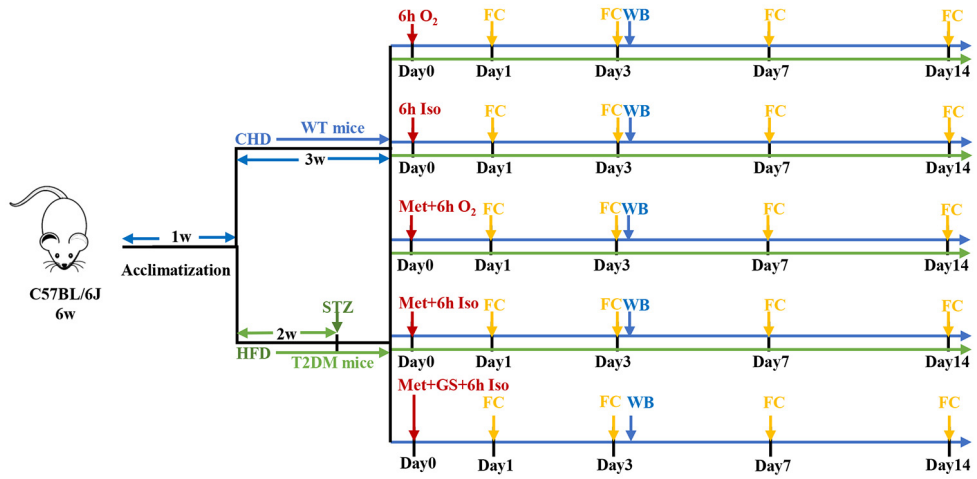

FIGURE 1 | Schematic presentation of experimental design. CHD, chow diet; HFD, high-fat diet; STZ, streptozotocin; Iso, isoflurane; Met, metformin; GS, 25% glucose solution; FC, fear conditioning test; WB, Western blot.

22–25°C under a 12 h light/dark cycle. Diabetic mellitus type 2 (T2DM) mice model was prepared as we described previously (Fang et al., 2020). After 1 week of acclimatization, 7-week-old male C57BL/6J wild type (WT) mice from the Model Animal Research Center of Nanjing University were fed either chow diet or high-fat diet (HFD, 60% kcal fat, 20% carbohydrate). After fed with HFD for 2 weeks, inducible diabetic mellitus type 2 mice were fasted overnight and intraperitoneally injected with streptozotocin (STZ, Sigma-Aldrich, United States) freshly dissolved in 0.1 mM citrate buffer (pH 4.5) at a dose of 60 mg/kg body weight and tested for fasting 12 h tail vein blood glucose levels 1-week post-injection. Mice fed with chow diet were injected intraperitoneally with the citrate buffer vehicle. Mice with typical features of T2DM (polyphagia, polydipsia and polyuria) and fasting blood glucose levels more than 11.1 mmol/L were considered to be T2DM and were used in the experiment. Animals were maintained with their respective diets and body weight was measured every 3 days during the experiment. WT mice fed a standard chow diet were randomly divided into five subgroups receiving vehicle injection (Con), isoflurane anesthesia (Anes), metformin injection (Met), metformin pretreatment plus isoflurane anesthesia (Met + Anes), or metformin plus gavage 25% glucose solution prior to isoflurane (Glu + Met + Anes). Another group of T2DM model mice was randomly divided into a control group (DM), isoflurane anesthesia group (DM + Anes), metformin group (DM + Met), and metformin pretreatment plus isoflurane anesthesia group (DM + Met + Anes). Mice in Anes, Met + Anes, Glu + Met + Anes, DM + Anes, and DM + Met + Anes groups were exposed to isoflurane anesthesia in a chamber prefilled with 4% isoflurane (Lunan Better Pharmaceutical Co.) in 100% oxygen and then maintained with 1.3% isoflurane in 100% oxygen flowing at 2.5 L/min for 6 h. The respiratory activities of mice were monitored during anesthesia. To prevent the effect of hypothermia on tau protein phosphorylation, mice were placed on heating pads to maintain body temperature during anesthesia and lasted until full recovery. Mice in Met, Met + Anes, Glu + Met + Anes, DM + Met, and DM + Met + Anes groups were injected intraperitoneally with metformin (Sigma-Aldrich, D150959) 50 mg/kg body weight 1 h before anesthesia or at the corresponding time. Mice in the Glu + Met + Anes group were administered 25% glucose solution 0.1 ml (25%Glu 0.1 ml + Met + Anes) or 0.2 ml (25%Glu 0.2 ml + Met + Anes) by gavage before anesthesia (**Figure 1**).

Measurements of Blood Glucose

To eliminate interference from cage mates, mice were housed singly during tail vein blood sampling. Experienced researchers cautiously snip 1–2 mm of tissue from the tail tip distal with sharp scissors, and blood was obtained by gently massaging the tail. Squeezing the tail violently should be avoided because it might be painful for the mice and affect the quality of the sample. Stroking over the incision gently with sterile swabs dipped in saline reopened it and several blood samples could be collected in subsequent experiments. Blood glucose levels were tested by a hand-held glucometer (ACCU-CHEK Active, Roche, Switzerland).

Fear Conditioning Test

The fear conditioning test was conducted in 30 cm × 37 cm × 25 cm chambers equipped with a sound amplifier to produce auditory cues and a metal grid floor to deliver conditioning foot shocks. During the training phase, a mouse was placed in the chamber and allowed to explore freely for 3 min as habituation. After habitation, the sound (4,000 Hz, 100 dB) was presented for 30 s (conditioned stimulus, CS) and co-terminated with a foot shock (2 s, 0.8 mA) as an unconditional stimulus (US). Freezing behavior (a sign of conditioned fear) was scored for 1 min after foot shock. The chamber was then cleaned and descented with 75% ethanol between trials. Contextual fear conditioning was tested 24 h

later in the same chamber by scoring freezing behavior (% of total time) for 3 min in the absence of sound or foot shock. A cued fear memory test was performed 2 h after the contextual fear conditioning test. Briefly, the sensory environment of the chamber (textures, odors, and colors) was modified and animals allowed 3 min of exploration as an accommodation period, followed by delivery of the CS (4,000 Hz, 100 db, 30 s). Freezing time (% of total time) was recorded automatically and the data were analyzed using Packwin 2.0 software.

Real-Time Reverse Transcription Polymerase Chain Reaction (RT-PCR)

The total RNA of hippocampus was extracted using PureLink RNA mini kit (Biotek, RP1202) and cDNAs were synthesized using cDNA synthesis kit (TakaRa, RR036A). RNA quality and quantity were measured by ultraviolet spectroscopy (Biotek, United States). RT-PCR was performed using SYBR Premix Ex Taq (Takara, RR420A) in the ABI StepOne Plus Real-Time PCR system (Applied Biosystems). The primers (TSINGKE, China) were shown as follows: β-actin (F: 5′-CTGTCCCTGTATGCCTCTG-3′, R: 5′-ATGTCACGCACGATTTCC-3′). GSK3β (F: 5′-ATTCCCTCAAATTAAGGCACATCC-3′, R: 5′-ATACTCCAGCAGACGGCTACACAG-3′); AKT (F: 5′-TGCATTGCCGAGTCCAGAA-3′, R: 5′-GCATCCGAGAAACAAAACATCA-3′); IRS1 (F: 5′-GTTTCCAGAAGCAGCCAGAG-3′, R: 5′-ACTCTCTCCACCCAACGTGA-3′); IRS2 (F: 5′-CATCGACTTCCTGTCCCATCA-3′, R: 5′-CCCATCCTCAAGGTCAAAGG-3′); Gene expression data were normalized to β -actin.

Western Blotting

The expression of tau, NR2B and insulin-signaling proteins were detected in the hippocampus by western blotting. Tissues were washed with ice-cold PBS and then lysed in proteinase and phosphatase inhibitors (Sigma, United States) containing RIPA buffer. The samples were centrifuged at 12,000 rpm, 4°C for 20 min. BSA method was performed to determine the protein contents. Twenty to forty microgram proteins per lane were separated by electrophoresis in 8% SDS-PAGE gels (KayGen Biotech, Co., Ltd.) and blotted onto polyvinylidene difluoride membranes (PVDF; Bio-Rad Laboratories, United States). The membranes were blocked with 5% non-fat milk for 2 h at normal temperature and then were incubated with the following primary antibodies overnight at 4°C: anti-tau (phospho Ser396) (1:500, 9632S, CST), anti-tau (phospho Ser202 and Thr205, AT8) (1:500, MN1020, Invitrogen), anti-tau (1:500, BS3738, Bioworld technology), anti-NR2B (phospho Tyr1472) (1:500, ab3856, Abcam), anti-NR2B (1:500, ab65783, Abcam), anti-IRS1(phospho Ser636/639) (1:500,2388, CST), anti-IRS1 (phospho Tyr896) (1:500, ab46800, Abcam), anti-IRS1 (1:500,ab52167, Abcam), anti-IRS2 (phospho Ser731) (1:500, ab3690, Abcam), anti-IRS2 (1:500,4502, CST), anti-AKT (phospho Ser473)(1:1,000, 4060, CST), anti-AKT (1:1,000, 4685, CST), anti-β-actin (1:1,000, ab8226, Abcam), anti-GSK3β (1:1,000, 12456, CST), and anti-GSK3β (phospho Ser9)(1:1,000, 5558, CST). β-actin were used as loading controls, respectively. Antibodies were diluted with 5% Bovine serum albumin (BSA; Gentihold) solvents. The membranes were washed three times with TBST and then incubated with HRP-conjugated antibodies for 2 h. The proteins were visualized using a chemiluminescence kit (ECL; Pierce, Illinois, United States). Band densities of protein were quantified via ImageJ (National Institutes of Health, United States).

Statistical Analysis

All data were parametric and summarized as mean ± standard deviation (SD). Results from cognitive behavioral tests, Western blotting, RT-PCR and light absorbance were analyzed by a one-way ANOVA test, followed by Bonferroni multiple comparison test. Changes in blood glucose levels over time were analyzed using multivariate analyses of variance for repeated measures followed by Bonferroni *post hoc* analysis. Statistical analysis was carried out using SPSS 25.0 software (IBM Corporation, Armonk, NY). Statistical significance referred to differences at the level of $P < 0.05$.

RESULTS

Isoflurane and T2DM Synergistically Induce Hippocampus-Dependent Cognitive Dysfunction in Adult Mice

In our previous studies, we found that long-term (6 h) isoflurane inhalation induced hippocampal IR and exacerbated pre-existing hippocampal IR (Fang et al., 2020). Furthermore, both clinical and preclinical studies have found that hippocampal IR is associated with cognitive decline (Biessels and Reagan, 2015; Grillo et al., 2015). We investigated whether long-term isoflurane inhalation also induces cognitive deficits in adult mice and aggravates cognitive dysfunction in T2DM mice. In adult wild type (WT) mice, 6 h of isoflurane anesthesia (Anes group) significantly reduced contextual fear memory as measured by freezing (%) compared to control mice (Con group) from Days 1 to 7 post-treatment (Day 1: 68.96 ± 7.32% vs. 84.70 ± 10.95%, $P = 0.034$; Day 3: 62.14 ± 7.04% vs. 87.97 ± 7.52%, $P < 0.001$; Day 7: 57.88 ± 7.04% vs. 87.97 ± 7.52%, $P = 0.004$), indicating disruption of hippocampal function (**Figure 2A**). In T2DM model mice as well, isoflurane exposure (DM + Anes group) significantly reduced freezing to context compared to controls (DM group) from Days 1 to 7 (Day 1: 52.73 ± 12.27% vs. 69.66 ± 7.27%, $P = 0.02$; Day 3: 50.75 ± 9.83% vs. 64.33 ± 10.44%, $P = 0.028$; Day 7: 52.77 ± 9.70 vs. 69.43 ± 7.54%, $P = 0.046$). Compared to the Anes group, DM + Anes mice demonstrated even lower freezing on Day 1 (68.96 ± 7.32% vs. 52.73 ± 12.27%, $P = 0.027$) and Day 3 (64.17 ± 7.04% vs. 50.75 ± 9.83%, although the difference did not reach significance, $P = 0.092$), suggesting that pre-existing IR and isoflurane synergistically impair hippocampal function (**Figure 2A**). By Day 14, no significant differences in contextual fear conditioning were observed in any group. In contrast,

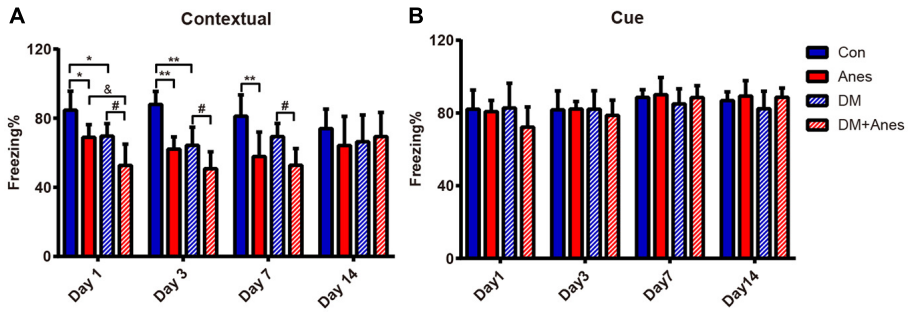

FIGURE 2 | Isoflurane inhalation selectively impairs contextual fear memory and this effect is exacerbated in diabetic mice. **(A)** Freezing (% time) in response to the foot-shock context (chamber) among adult WT mice and T2DM mice (DM groups) exposed to 1.3% isoflurane inhalation for 6 h (Anes and DM + Anes groups) or control inhalation (100% O_2 for 6 h). **(B)** Freezing time during exposure to the conditioned sound cue in a different context. Data are expressed as mean ± SD of 7–8 mice for each treated group and analyzed with one-way ANOVA test followed by Bonferroni multiple comparison test. $^{*}P < 0.05$ and $^{**}P < 0.01$ vs. Con group; $^{\&}P < 0.05$ vs. Anes group; $^{\#}P < 0.05$ vs. DM group.

there were no significant effects on cued fear conditioning, suggesting that these effects are selective for hippocampal function (**Figure 2B**).

Metformin Alleviates Hippocampal IR and Cognitive Dysfunction Caused by Long-Term Isoflurane Inhalation

Decrease insulin resistance and increased insulin sensitivity are the main mechanisms underlying the therapeutic effects of metformin (Giannarelli et al., 2003), so we examined changes in the insulin signaling pathway components insulin receptor substrates 1 and 2 (IRS1 and IRS2), Akt, and GSK-3β among adult WT mice and T2DM mice intraperitoneally pretreated with metformin 50 mg/kg or vehicle 1 h before long-term isoflurane or control inhalation. In adult WT mice, metformin alone had no effect on the mRNA and protein expression levels of IRS1, IRS2, Akt, and GSK-3b (**Supplementary Figure 1**, all the $P > 0.05$). The phosphorylation levels of IRS1 at Ser639 (pIRS1-Ser639) and IRS2 at Ser731 (pIRS2-Ser731) were upregulated significantly after long-term isoflurane inhalation (Anes group) compared to controls (Con group) (pIRS1-Ser639 1.90 ± 0.38% vs. 1.00 ± 0.08%, $P = 0.043$; pIRS2-Ser731: 2.34 ± 0.42% vs. 1.00 ± 0.32% $P = 0.033$), and these effects were significantly suppressed by intraperitoneal metformin (pIRS1-Ser639 down to 0.79 ± 0.43%, $P = 0.013$; pIRS2-Ser731 down to 1.26 ± 0.24%, $P = 0.035$) (**Figure 3A**). In contrast, long-term isoflurane inhalation reduced phosphorylation of IRS1 at Tyr896 (pIRS1-Tyr896 0.38 ± 0.04% vs. 1.00 ± 0.27%, $P = 0.020$), phosphorylation of Akt at Ser473 (pAkt-Ser473, 0.34 ± 0.06% vs. 1.00 ± 0.25, $P = 0.023$), and phosphorylation of GSK-3β at Ser9 (pGSK-3β-Ser9, 0.60 ± 0.02% vs. 1.00 ± 0.14, $P = 0.023$), while pretreatment with metformin significantly reversed the downregulation of pIRS1-Tyr896 (to 1.20 ± 0.15%, $P = 0.004$), pAkt-Ser473 (to 1.26 ± 0.26%, $P = 0.003$), and pGSK-3β-Ser9 (to 1.02 ± 0.12%, $P = 0.018$) (**Figure 3A**). Compared with HFD/STZ induced T2DM mice (DM group), isoflurane also induced the upregulation of pIRS1-Ser639 (1.00 ± 0.15% vs. 2.12 ± 0.13%, $P = 0.001$) and pIRS2-Ser731 (1.00 ± 0.07% vs. 1.83 ± 0.23%, $P = 0.027$), as well as the downregulation of pIRS1-Tyr896 (1.00 ± 0.05% vs. 0.52 ± 0.11%, $P = 0.007$), pAkt-Ser473 (1.00 ± 0.14% vs. 0.45 ± 0.03%, $P = 0.013$), and pGSK-3β-Ser9 (1.00 ± 0.12% vs. 0.54 ± 0.08%, $P = 0.002$) in T2DM mice (**Figure 3B**). Compared to vehicle pretreatment before isoflurane (DM + Anes group), metformin pretreatment (DM + Met + Anes group) reversed the upregulation of pIRS1-Ser639 (to 1.23 ± 0.11%, $P = 0.006$) and pIRS2-Ser731 (to 0.76 ± 0.39%, $P = 0.006$), induced by isoflurane, as well as the downregulation of pIRS1-Tyr896 (to 1.01 ± 0.13%, $P = 0.007$), pAkt-Ser473 (to 1.01 ± 0.12%, $P = 0.012$), and pGSK-3β-Ser9 (to 0.94 ± 0.03%, $P = 0.005$) in T2DM mice (**Figure 3B**). Although we previously demonstrated that induction of diabetic pathology by HFD/STZ treatment also markedly induced hippocampal IR (Fang et al., 2020), metformin treatment (DM + Met) failed to activate hippocampal insulin signaling pathways in T2DM mice (all $P > 0.05$).

In addition to normalizing hippocampal insulin signaling following isoflurane anesthesia among adult WT mice, intraperitoneal metformin treatment 1 h before anesthesia (Met + Anes group) also alleviated the impairment in contextual fear memory observed in the Anes group on Day 1 (91.20 ± 7.74% vs. 63.58 ± 11.91%, $P < 0.001$), Day 3 (89.93 ± 6.19% vs. 75.35 ± 11.40%, $P = 0.004$) and Day 7 (82.24 ± 11.64% vs. 64.46 ± 8.04%, $P = 0.004$) (**Figure 3C**). Similarly, in T2DM mice, isoflurane inhalation (DM + Anes group) decreased freezing time to context compared to untreated controls (DM group) on Day 1 (52.73 ± 12.27% vs. 69.66 ± 7.27%, $P = 0.017$), Day 3 (49.03 ± 9.23% vs. 66.12 ± 9.87%, $P = 0.047$), and Day 7(52.77 ± 9.70% vs. 69.43 ± 7.54%, $P = 0.033$), while metformin pretreatment (DM + Met + Anes group) increased freezing time compared to DM + Anes group mice on Day 1 (73.05 ± 0.61% vs. 52.73 ± 12.27%, $P = 0.003$) and Day 3 (66.34 ± 11.60% vs. 49.03 ± 9.23%, $P = 0.034$), but had no effect on Day 7 (**Figure 3D**). Further, there were no significant differences in cued freezing among T2DM mice (**Supplementary Figure 2B**, all the $P > 0.05$).

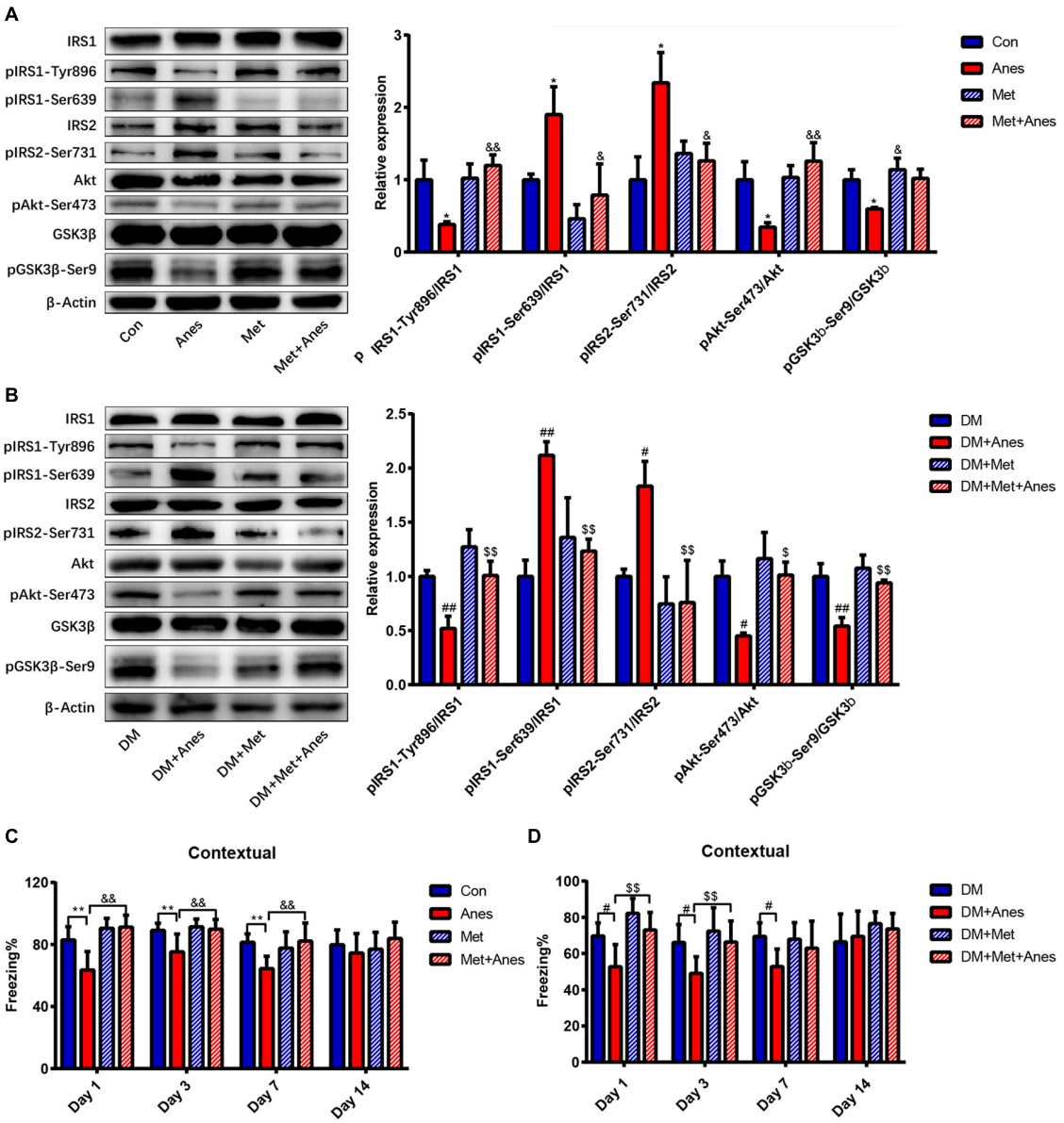

FIGURE 3 | Metformin alleviates hippocampal insulin resistance and impairs contextual fear memory induced by long-term isoflurane anesthesia, but not diabetic pathology. **(A,B)** Representative western blots (left panels) and densitometric analysis (right panels) showing the effects of isoflurane anesthesia, metformin, and anesthesia plus metformin pretreatment on the protein expression levels of hippocampal insulin-signaling pathway components in adult WT mice **(B)** and T2DM mice **(C)** (n = 3 mice per group). **(C)** Freezing time to context by adult WT mice receiving vehicle (Con), anesthesia (Anes), metformin (Met, 50 mg/kg), or metformin before anesthesia (Met + Anes) (n = 7–8). **(D)** Freezing time to context by T2DM mice receiving vehicle (DM), anesthesia (DM + Anes), metformin (DM + Met, 50 mg/kg), or metformin before anesthesia (DM + Met + Anes) (n = 7–8 mice per group). Data are expressed as mean ± SD and analyzed with one-way ANOVA test followed by Bonferroni multiple comparison test. $^{*}P < 0.05$ and $^{**}P < 0.01$ vs. Con group; $^{\&}P < 0.05$ and $^{\&\&}P < 0.01$ vs. Anes group; $^{\#}P < 0.05$ and $^{\#\#}P < 0.01$ vs. DM group; $^{\$}P < 0.05$ and $^{\$\$}P < 0.01$ vs. DM + Anes group.

Metformin Inhibits Hippocampal Tau Hyperphosphorylation and Increases NR2B Tyr1472 Phosphorylation in Isoflurane-Anesthetized Mice

Clinical and preclinical studies have found that impaired insulin signaling induces tau hyperphosphorylation and that insulin-sensitizing strategies improve cerebrospinal fluid biomarkers of tauopathy in patients with MCI/AD (Hölscher, 2014; Yarchoan et al., 2014; Kim et al., 2015). As a cytoskeleton-associated protein, tau plays an important role in postsynaptic targeting of the Src family tyrosine kinase Fyn to NMDA receptors and in phosphorylating the NR2B subunit at Tyr1472 (pNR2B-Tyr1472), which is associated with NMDA receptor-dependent plasticity (Ittner et al., 2010). Conversely, hyperphosphorylated tau

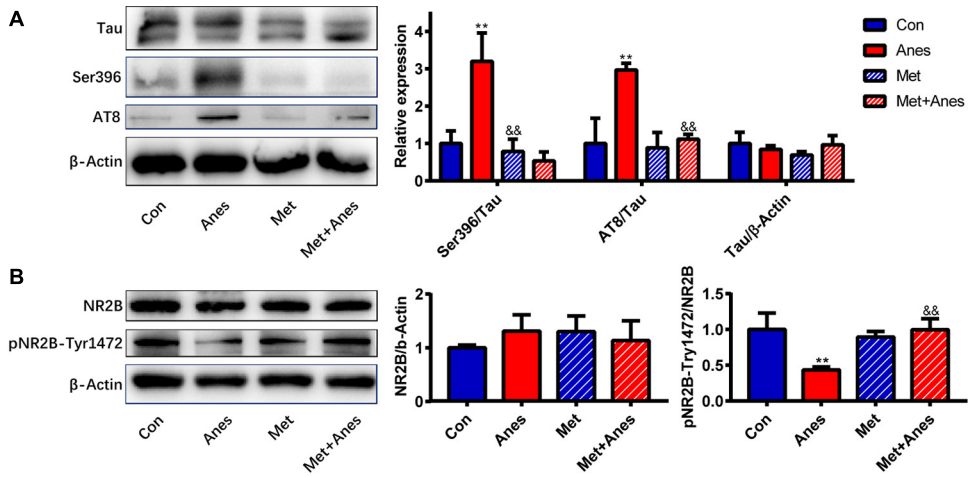

FIGURE 4 | Metformin alleviates tau hyperphosphorylation and pNR2B-Tyr1472 downregulation caused by long-term isoflurane anesthesia. Representative western blots (left panels) and densitometric analysis (right panels, $n = 3$ mice per group) showing the effects of isoflurane anesthesia (Anes group), metformin (Met group), and anesthesia plus metformin pretreatment (Met + Anes group) on expression levels of total tau (Tau) and phosphorylated tau (Ser396 and AT8) **(A)**, as well as total NR2B (NR2B) and phosphorylated NR2B at Tyr1472 (pNR2B-Tyr1472) **(B)** in the hippocampus. β-Actin was used as a gel loading control. Data are expressed as mean ± SD and compared by one-way ANOVA followed by Bonferroni multiple comparisons tests. $^{**}P < 0.01$ compared to the Con group; $^{\&\&}P < 0.01$ compared to the Anes group.

was shown to reduce Fyn binding (Reynolds et al., 2008), suggesting that tau hyperphosphorylation may decrease the expression of hippocampal pNR2B-Tyr1472 after long-term isoflurane anesthesia. Our previous studies indeed found that isoflurane inhalation inhibited hippocampal pNR2B-Tyr1472 expression and that this response was associated with cognitive decline3 (Xia et al., 2016). We further examined whether metformin can alleviate hippocampal IR and improve both tau hyperphosphorylation and pNR2B-Tyr1472 downregulation caused by long-term isoflurane anesthesia. Isoflurane (Anes group) increased tau phosphorylation at Ser396 (pTau-Ser396) and AT8 compared to the Con group (pTau-Ser396: 3.20 ± 0.76% vs. 1.00 ± 0.34, $P = 0.002$; AT8: 2.970 ± 0.18% vs. 1.00 ± 0.68, $P = 0.002$) (**Figure 4A**). Conversely, isoflurane reduced hippocampal pNR2B-Tyr1472/NR2B compared to the Con group (0.44 ± 0.04% vs. 1.00 ± 0.23%, $P = 0.008$) (**Figure 4B**). Pretreatment with metformin (Met + Anes group) reversed the increase in hippocampal pTau-Ser396/Tau and AT8/Tau compared to isoflurane alone (pTau-Ser396: 0.53 ± 0.24% vs. 3.20 ± 0.76%, $P = 0.001$; AT8: 1.12 ± 0.13% vs. 2.970 ± 0.18%, $P = 0.003$), as well as the isoflurane-induced reduction in hippocampal pNR2B-Tyr1472/NR2B (1.00 ± 0.15% vs. 0.44 ± 0.04%, $P = 0.009$), while metformin alone (Met group) had no effect on the expression levels of hippocampal pTau-Ser396/Tau, AT8/Tau and pNR2B-Tyr1472 compared to the Con group (**Figure 4**).

Glycemic Control Did Not Contribute to the Effects of Metformin on Contextual Fear Memory

Previous studies have shown that intraoperative hyperglycemia is associated with increased risk of postoperative cognitive dysfunction, and our previous studies found that long-term isoflurane increased blood glucose in adult WT and T2DM mice (Puskas et al., 2007; Fang et al., 2020). Thus, metformin may alleviate cognitive decline by reducing anesthesia-induced hyperglycemia. To examine this possibility, we compared blood glucose levels among adult WT and T2DM mice receiving anesthesia alone, metformin alone, and anesthesia plus metformin pretreatment with or without glucose supplementation. Repeated measures ANOVA with treatments (Con, Anes, Met and Met + Anes) and time as within-subject factors revealed a significant effect of treatment in adult WT mice [$F_{(3,\ 18)} = 84.091$, $P < 0.001$] and T2DM mice [$F_{(3,\ 13)} = 30.604$, $P < 0.001$], as well as a treatment × time interaction (Adult mice: [$F_{(18,\ 45)} = 3.281$, $P = 0.001$]; T2DM mice: [$F_{(18,\ 30)} = 2.149$, $P < 0.001$] (**Figures 5A,B**). There was also a marked effect of time in adult WT mice [$F_{(6,\ 13)} = 8.552$, $P = 0.001$], but not T2DM mice [$F_{(6,\ 8)} = 2.534$, $P = 0.112$] (**Figures 5A,B**). Simple contrasts indicated that blood glucose levels were significantly higher in Anes group mice compared to Con mice ($P < 0.001$), whereas Met + Anes mice had lower blood glucose levels than Con, Anes, and Met group mice (all the $P < 0.001$). Isoflurane anesthesia upregulated blood glucose levels in adult WT mice at 0.5 h (14.70 ± 2.46 mmol/L vs. 7.12 ± 0.72 mmol/L, $P < 0.001$), 1 h (15.38 ± 3.50 mmol/L vs. 7.50 ± 1.34 mmol/L, $P < 0.001$), 2 h (13.68 ± 0.97 mmol/L vs. 8.00 ± 1.46 mmol/L, $P < 0.001$), and 3 h (13.33 ± 2.08 mmol/L vs. 7.10 ± 0,83 mmol/L, $P < 0.001$), while intraperitoneal pretreatment with metformin 50 mg/kg 1 h before anesthesia not only completely reversed the hyperglycemic impact of isoflurane but also further decreased blood glucose levels compared to the Con group at 1 h (3.15 ± 1.15 mmol/L vs. 7.50 ± 1.34 mmol/L, $P = 0.017$)–6 h (2.65 ± 0.82 mmol/L vs. 6.67 ± 0.77 mmol/L, $P < 0.001$) (**Figure 5A**). A similar

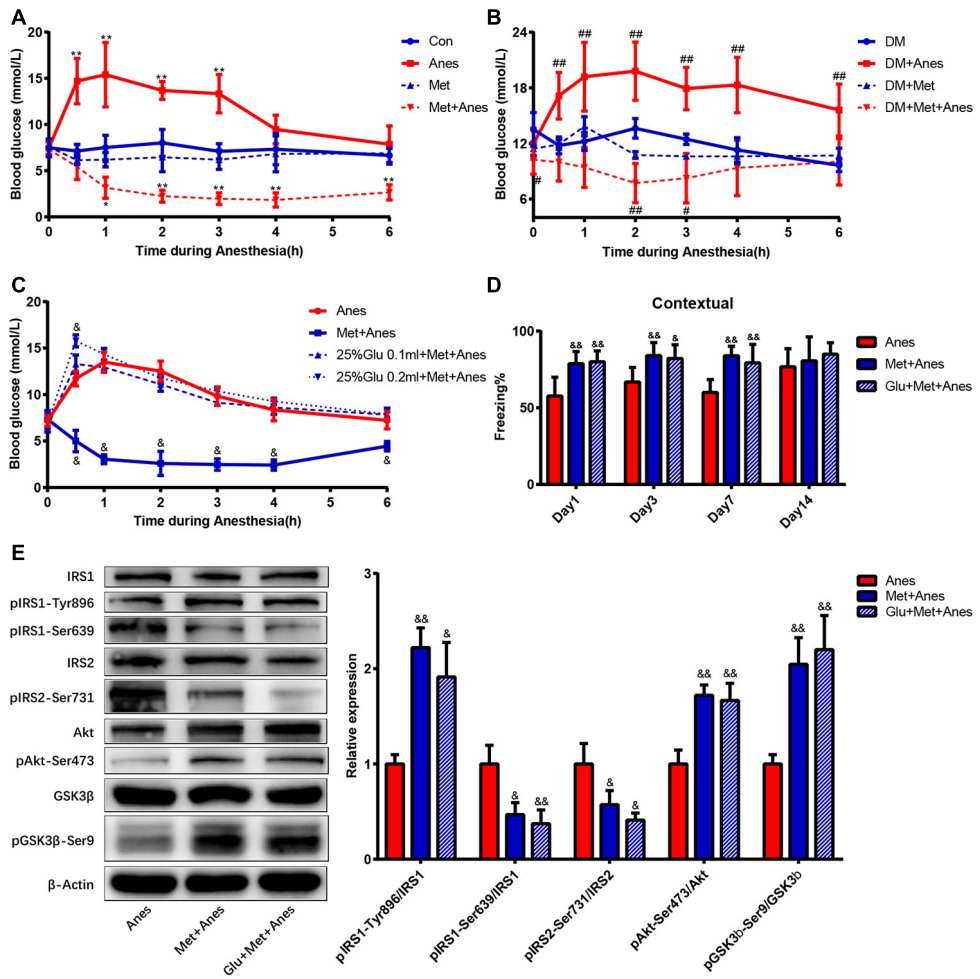

FIGURE 5 | Metformin improves hippocampal IR and contextual fear memory, independent of antiglycemic effects. **(A,B)** Changes in blood glucose levels during anesthesia among adult WT mice **(A)** and T2DM mice **(B)** with or without metformin pretreatment (n = 4–6). **(C)** Changes in blood glucose levels during isoflurane anesthesia among WT mice receiving pretreatment with vehicle (Anes), metformin (Met + Anes), 25% glucose 0.1 ml plus metformin (25% Glu 0.1 ml + Met + Anes), or 25% glucose 0.2 ml plus metformin (25% Glu 0.2 ml + Met + Anes) (n = 4 for each group). Blood glucose levels are expressed as mean ± SD and compared by repeated measures ANOVA followed by Bonferroni multiple comparisons tests. Repeated measures ANOVA revealed a significant effect of treatment in adult WT mice [$F_{(3,\ 18)} = 84.091$, $P < 0.001$] and T2DM mice [$F_{(3,\ 13)} = 30.604$, $P < 0.001$], as well as a treatment × time interaction [WT mice: $F_{(18,\ 45)} = 3.281$, $P = 0.001$; T2DM mice: $F_{(18,\ 30)} = 2.149$, $P < 0.001$]. There was also a marked effect of time in WT mice [$F_{(6,\ 13)} = 8.552$, $P = 0.001$], but not T2DM mice [$F_{(6,\ 8)} = 2.534$, $P = 0.112$]. Simple contrasts indicated administration of 25% glucose 0.1 ml or 0.2 ml to metformin-pretreated mice induced obvious hyperglycemia (both $P < 0.001$) and no substantial differences in blood glucose levels among Anes, 25%Glu 0.1 ml + Met + Anes, and 25%Glu 0.2 ml + Met + Anes group mice (all $P > 0.05$). **(D)** Freezing times to context by adult WT mice receiving vehicle, metformin, or 25% glucose 0.1 ml plus metformin (Glu + Met + Anes) prior to isoflurane anesthesia (n = 7–8). **(E)** Representative western blots (left panels) and densitometric analysis (right panels, n = 3 for each group) showing the effects of vehicle, metformin, and 25% glucose 0.1 ml plus metformin on the protein expression levels of hippocampal insulin signaling components in isoflurane anesthetized adult WT mice. Data of freezing conditional test and Western blots are expressed as mean ± SD and analyzed with one-way ANOVA test followed by Bonferroni multiple comparison test. $^{*}P < 0.05$ and $^{**}P < 0.01$ vs. Con group, $^{\#}P < 0.05$ and $^{\#\#}P < 0.01$ vs. DM group. $^{\&}P < 0.05$ and $^{\&\&}P < 0.01$ vs. Anes group.

glycemic effect of isoflurane was also found in T2DM mice, but was much longer lasting [from 0.5 h (17.15 ± 2.51 mmol/L vs. 11.78 ± 0.92 mmol/L, $P < 0.001$) to 6 h (15.60 ± 2.80 mmol/L vs. 9.64 ± 0.67 mmol/L, $P < 0.001$)]. Although metformin still reversed the glycemic impact of isoflurane ($P < 0.001$) in T2DM model mice and decreased blood glucose levels compared to control T2DM mice ($P = 0.019$), the duration was much shorter than in adult WT mice (0 h: 10.24 ± 1.55 mmol/L vs. 13.50 ± 1.83 mmol/L, $P = 0.018$; 2 h: 7.72 ± 2.13 mmol/L vs. 13.62 ± 1.06 mmol/L, $P = 0.003$; 3 h: 8.24 ± 2.67 mmol/L vs. 12.45 ± 0.56 mmol/L, $P = 0.031$). The blood glucose levels of Met and DM + Met groups were generally lower than in Con and DM groups, respectively, but the differences did not reach statistical significance (**Figure 5B**).

To eliminate the contribution of glycemic control to metformin effects on contextual fear memory, 0.1 or 0.2 ml 25% glucose solution was given by gavage before anesthesia. Simple contrasts indicated administration of 25% glucose 0.1 or 0.2 ml to metformin-pretreated mice induced obvious hyperglycemia (both $P < 0.001$) and no substantial differences in blood

glucose levels among Anes, 25%Glu 0.1 ml + Met + Anes, and 25%Glu 0.2 ml + Met + Anes group mice (all $P > 0.05$). Moreover, blood glucose levels did not differ between Anes and 25%Glu 0.1 ml + Met + Anes groups at any time point during anesthesia (**Figure 5C**). Thus, administration of 25% glucose solution essentially eliminated the antiglycemic effect of metformin. However, metformin pretreatment still markedly improved hippocampal insulin resistance in WT mice also receiving glucose prior to anesthesia (25%Glu 0.1 ml + Met + Anes group) compared to anesthesia alone (Anes group) (pIRS1-Tyr896: 1.91 ± 0.36% vs. 1.00 ± 0.10%, $P = 0.012$; pIRS1-Ser639: 0.37 ± 0.14% vs. 1.00 ± 0.20%, $P = 0.009$; pIRS2-Ser731: 0.41 ± 0.07% vs. 1.00 ± 0.21%, $P = 0.011$, pAkt-Ser47: 1.67 ± 0.18% vs. 1.00 ± 0.15%, $P = 0.004$; pGSK-3β-Ser9: 2.20 ± 0.36% vs. 1.00 ± 0.10%, $P = 0.005$). Moreover, metformin still enhanced contextual fear memory compared to the Anes group on Day 1 (57.67 ± 12.26% vs. 79.99 ± 7.14%, $P = 0.001$), Day 3 (66.79 ± 9.51% vs. 82.17 ± 8.94%, $P = 0.015$), and Day 7 (60.00 ± 8.44% vs. 79.31 ± 12.04%, $P = 0.003$) (**Figure 5E**). In addition, neither hippocampal insulin signing nor contextual fear memory differed between 25%Glu 0.1 ml + Met + Anes and control mice (**Figure 5D**), indicating complete reversal of anesthesia-induced IR and memory impairment even when the antiglycemic effect was blocked.

DISCUSSION

Our present study demonstrated that prolonged (6 h) isoflurane anesthesia can induce hippocampal insulin resistance and impair hippocampus-dependent contextual fear memory in adult WT mice. Further, these deleterious effects were exacerbated in HDF/STZ-induced T2DM model mice. Intraperitoneal pretreatment with metformin (50 mg/kg body weight) attenuated isoflurane-induced hippocampal IR and contextual fear memory impairment in WT mice, but had a more blunted effect in T2DM model mice. Metformin also reduced hippocampal tau hyperphosphorylation and increased expression of hippocampal pNR2B-Tyr1472, which may have contributed to the improvement in hippocampus-dependent memory. Metformin also successfully reversed isoflurane-induced hyperglycemia, but elimination of glycemic control by high oral glucose did not influence the effects on IR and memory impairment, suggesting a novel independent mechanism for the therapeutic benefits of this antidiabetic drug.

Isoflurane and HFD/STZ Synergistically Induce Hippocampus-Dependent Cognitive Decline

As T2DM is one of the most common, costly, and disabling conditions in the industrialized world (Cho et al., 2018), we focused on the role of preoperative IR created by HFD/STZ treatment and postoperative IR caused by long-term isoflurane inhalation on POCD. The combination of HFD feeding and low-dose STZ treatment is a classic method for inducing a T2DM-like phenotype in mice (Srinivasan et al., 2005). Indeed, our previous study demonstrated that HFD/STZ could induce marked peripheral and brain IR in mice (Fang et al., 2020). Brain insulin action is required for neuronal survival, synaptic plasticity, and cognitive function (van der Heide et al., 2006; Biessels and Reagan, 2015; Grillo et al., 2015). Both adult WT mice and T2DM mice demonstrated impairments in contextual fear conditioning after long-term isoflurane inhalation. However, isoflurane had no effects on cued fear conditioning. While the amygdala is critical for the expression of both cued and contextual conditioned fear responses, contextual fear memories are consolidated and maintained by the hippocampus (Chaaya et al., 2018). Thus, isoflurane and HFD/STZ treatment appear to selectively impair hippocampus-dependent fear learning and memory. Compared to adult WT mice receiving anesthesia (Anes group), T2DM model mice (DM + Anes group) displayed significantly weaker context-dependent freezing responses on Day 1 and a very weak freezing response on Day 3 that did not differ after long-term isoflurane inhalation, suggesting that contextual fear learning and memory were more severely impaired in T2DM mice. This is consistent with clinical studies reporting that diabetes patients are more susceptible to POCD (Feinkohl et al., 2017). Thus, preoperative IR and postoperative IR have synergistic effects on POCD.

Metformin Attenuated Hippocampal IR and Tau Hyperphosphorylation and Increase Hippocampal pNR2B-Tyr1472 Expression

To examine potential mechanisms underlying the memory impairments induced by isoflurane and HFD/STZ treatment, we measured the effects of the first-line antidiabetic drug metformin on cognitive performance, IR, and phosphorylation of the NMDA receptor, which is essential for many forms of synaptic plasticity underlying hippocampus-dependent learning and memory (Rostas et al., 1996; Petrone et al., 2003). Metformin has been shown to cross the blood-brain barrier rapidly and effectively ameliorate IR (Giannarelli et al., 2003; Łabuzek et al., 2010). Increases in IRS1 and IRS2 serine phosphorylation, as well as decreases in downstream Akt and GSK3β phosphorylation are hallmark features of brain IR (Fang et al., 2020). Consistent with hippocampal IR, long-term isoflurane inhalation increased pIRS1-Ser639 and pIRS2-Ser731 expression levels and downregulated pIRS1-Tyr896, pAkt-Ser473, and pGSK3β-Ser9 expression levels in the hippocampus, while metformin reversed these responses. A similar pattern of changes was also observed in long-term isoflurane anesthetized T2DM mice. Concomitant with improved hippocampal IR, metformin pretreatment ameliorated the impairment in fear learning induced by long-term isoflurane inhalation in adult WT mice, but was less effective in T2DM mice. These results are consistent with numerous studies implicating hippocampal IR as a key mediator of cognitive dysfunction (Reviewed in Biessels and Reagan, 2015). Clinical and preclinical studies have also revealed that impaired insulin signaling induces tau hyperphosphorylation

and that insulin-sensitizing strategies improve cerebrospinal fluid biomarkers of disease in patients with mild cognitive impairment or AD (Hölscher, 2014; Yarchoan et al., 2014; Kim et al., 2015). Consistent with these clinical findings, isoflurane upregulated the expression of p-tau in hippocampus, while metformin decreased the expression of hippocampal p-tau. As a cytoskeleton-associated protein, tau plays an important role in the postsynaptic targeting of the Scr kinase Fyn to NMDA receptors, where it phosphorylates the NR2B subunit at Tyr-1472 and promotes NMDAR-dependent synaptic plasticity (Rostas et al., 1996; Petrone et al., 2003; Ittner et al., 2010). Moreover, hyperphosphorylated tau has been shown to reduce Fyn binding (Reynolds et al., 2008). Metformin not only attenuated IR, but also inhibited the phosphorylation of tau protein and prevented isoflurane-induced downregulation of pNR2B-Tyr-1472, providing a feasible mechanism for the improvement in contextual fear memory following metformin treatment. Therefore, metformin pretreatment may effectively alleviate hippocampal IR, prevent tau hyperphosphorylation, enhance the phosphorylation of Tyr-1472 in the NR2B, and reverse cognitive impairment caused by long-term isoflurane inhalation.

Metformin Mitigated Cognitive Decline Through a Mechanism Independent of Glycemic Control

Previous studies have shown that hyperglycemia contributes to cognitive decline in diabetes patients (Cox et al., 2005). Higher glycated hemoglobin, an index of more severe and prolonged hyperglycemia, is associated with a greater magnitude of cognitive impairment, and even acute hyperglycemia can impair cognitive performance in persons with type 1 or type 2 diabetes mellitus (Sommerfield et al., 2004; Gao et al., 2015; Šuput Omladič et al., 2020). Intraoperative hyperglycemia also increases the risk of POCD (Puskas et al., 2007; Schricker et al., 2014). Our previous animal studies and related clinical studies have shown that isoflurane inhalation significantly increases blood glucose (Behdad et al., 2014; Fang et al., 2020). In addition to relieving insulin resistance, metformin reduces blood sugar by suppressing hepatic glucose production, increasing glucose uptake into muscle, and promoting the transport of blood glucose into stool (Giannarelli et al., 2003; Morita et al., 2020). Our present studies did find that intraperitoneal injection of metformin (50 mg/kg body weight) not only decreased blood glucose in adult WT and T2DM mice, but also dramatically reversed the hyperglycemic effect of isoflurane during anesthesia. Surprisingly, however, glycemic control did not contribute to the improvement in hippocampus-dependent fear memory under the current experimental conditions, as gavage treatment with 25% glucose solution elevated blood glucose even under metformin treatment, but did not influence metformin-associated improvements in insulin signaling pathways and fear learning following isoflurane anesthesia. The mechanism by which acute hyperglycemia causes cognitive decline remains unclear. Whether hyperglycemia impair cognitive performance through insulin signaling need further study.

Pretreatment of Metformin Had No Therapeutic Effects on HFD/STZ-Induced T2DM

Our present study found that metformin had no effects on the activation of hippocampal insulin signaling and intraperitoneal injection of metformin also had no effects on cognitive performance of T2DM mice. However, preclinical studies have shown that metformin treatment improved cognitive deficits in db/db mice and chronic HFD-fed mice (Li et al., 2012; Pintana et al., 2012; Chen et al., 2019). Clinical studies also demonstrated that long-term usage can lower the risk of cognitive impairment in older adults with diabetes (Ng et al., 2014). Different research models and drug treatment times may explain this discrepancy. Ramos-Rodriguez and colleagues found that the central pathologies and cognitive impairments differed among diabetes models (Ramos-Rodriguez et al., 2013). Db/db mice may be more amenable to metformin treatment that C57BL/6J mice used in this study and longer-term HFD treatment (12 weeks) was used for T2DM model animals in previous studies (Li et al., 2012; Pintana et al., 2012; Chen et al., 2019). In previous studies, metformin administration time has varied from 21 days or 8 weeks (Li et al., 2012; Pintana et al., 2012; Chen et al., 2019). Clinical studies reported that short-term metformin treatment (36 weeks) had no effect on cognitive performance in diabetes patients, while longer-term treatment (more than 6 years) was beneficial (Abbatecola et al., 2010; Ng et al., 2014). Whether long-term metformin treatment has therapeutic effects on HFD/STZ-induced T2DM mice requires further study.

CONCLUSION

Hippocampal IR, tau hyperphosphorylation, and downregulation of pNR2B-Tyr1472 contribute to prolonged isoflurane-induced cognitive dysfunction. Brief metformin treatment can mitigate these effects through a mechanism independent of glycemic control. However, a single intraperitoneal injection of metformin had less therapeutic effects on cognitive decline induced by isoflurane in T2DM mice. A single-dose pretreatment of metformin had no effects on the changes of hippocampal IR and cognitive decline induced by HFD/STZ. Future studies are needed to investigate whether long-term metformin treatment can also prevent HFD/STZ -induced hippocampal IR and cognitive decline.

DATA AVAILABILITY STATEMENT

The raw data supporting the conclusions of this article will be made available by the authors, without undue reservation.

ETHICS STATEMENT

The studies involving human participants were reviewed and approved by the Medical Ethics Committee of the Affiliated Drum Tower Hospital of Medical Department of Nanjing

University. The patients/participants provided their written informed consent to participate in this study. The animal study was reviewed and approved by Laboratory Animal Ethics Committee of Drum Tower Hospital. Written informed consent was obtained from the individual(s) for the publication of any potentially identifiable images or data included in this article.

AUTHOR CONTRIBUTIONS

XGu, TX, and ZM conceived the original idea. FX, XF, and SL performed the animal experiments. FX, XGo, and XF carried out the clinical study. LP, YQ, and XZ generated and analyzed data and wrote the manuscript with input from all authors. All authors read and approved the final manuscript.

FUNDING

This study was supported by the National Natural Science Foundation of China (81730033, 81701371, and 81801380); the Natural Science Foundation of Jiangsu Province of China (BK20170129 and BK20170654); and the Key Talents of 13th 5 Year Plan for Strengthening Health of Jiangsu Province (ZDRCA2016069).

SUPPLEMENTARY MATERIAL

The Supplementary Material for this article can be found online at: https://www.frontiersin.org/articles/10.3389/fnagi.2021.686506/full#supplementary-material

Supplementary Figure 1 | Metformin had no effects on the mRNA expression levels of hippocampal insulin-signaling pathway components Real-time quantitative RT-PCR showing the effects of isoflurane anesthesia, metformin, and anesthesia plus metformin pretreatment on the mRNA expression levels of IRS1, IRS2, Akt, and GSK3β in hippocampus (n = 3 mice per group).

Supplementary Figure 2 | Metformin and blood glucose changes had no effects on the cued fear memory. **(A)** Freezing time to cue by adult WT mice receiving vehicle (Con), anesthesia (Anes), metformin (Met, 50 mg/kg), or metformin before anesthesia (Met + Anes) (n = 7–8). **(B)** Freezing time to cue by T2DM mice receiving vehicle (DM), anesthesia (DM + Anes), metformin (DM + Met, 50 mg/kg), or metformin before anesthesia (DM + Met + Anes) (n = 7–8 mice per group). **(C)** Freezing time to cue by adult WT mice receiving vehicle (Anes), metformin (Met + Anes), or 25% glucose 0.1 ml plus metformin (Glu + Met + Anes) prior to isoflurane anesthesia (n = 7–8). Data are expressed as mean ± SD and analyzed with one-way ANOVA test followed by Bonferroni multiple comparison test.

REFERENCES

Abbatecola, A., Lattanzio, F., Molinari, A., Cioffi, M., Mansi, L., Rambaldi, P., et al. (2010). Rosiglitazone and cognitive stability in older individuals with type 2 diabetes and mild cognitive impairment. *Diabetes Care* 33, 1706–1711. doi: 10.2337/dc09-2030

Behdad, S., Mortazavizadeh, A., Ayatollahi, V., Khadiv, Z., and Khalilzadeh, S. (2014). The effects of propofol and isoflurane on blood glucose during abdominal hysterectomy in diabetic patients. *Diabetes Metab. J.* 38, 311–316. doi: 10.4093/dmj.2014.38.4.311

Biessels, G., and Reagan, L. (2015). Hippocampal insulin resistance and cognitive dysfunction. *Nat. Rev. Neurosci.* 16, 660–671. doi: 10.1038/nrn4019

Chaaya, N., Battle, A., and Johnson, L. (2018). An update on contextual fear memory mechanisms: transition between Amygdala and Hippocampus. *Neurosci. Biobehav. Rev.* 92, 43–54. doi: 10.1016/j.neubiorev.2018.05.013

Chen, J., Luo, C., Pu, D., Zhang, G., Zhao, Y., Sun, Y., et al. (2019). Metformin attenuates diabetes-induced tau hyperphosphorylation *in vitro* and *in vivo* by enhancing autophagic clearance. *Exp. Neurol.* 311, 44–56. doi: 10.1016/j.expneurol.2018.09.008

Cho, N., Shaw, J., Karuranga, S., Huang, Y., da Rocha Fernandes, J., Ohlrogge, A. W., et al. (2018). IDF Diabetes Atlas: global estimates of diabetes prevalence for 2017 and projections for 2045. *Diabetes. Res. Clin. Pract.* 138, 271–281. doi: 10.1016/j.diabres.2018.02.023

Cox, D., Kovatchev, B., Gonder-Frederick, L., Summers, K., McCall, A., Grimm, K., et al. (2005). Relationships between hyperglycemia and cognitive performance among adults with type 1 and type 2 diabetes. *Diabetes Care* 28, 71–77. doi: 10.2337/diacare.28.1.71

Dong, Y., Wu, X., Xu, Z., Zhang, Y., and Xie, Z. (2012). Anesthetic isoflurane increases phosphorylated tau levels mediated by caspase activation and Aβ generation. *PLoS One* 7:e39386. doi: 10.1371/journal.pone.0039386

Fang, X., Xia, T., Xu, F., Wu, H., Ma, Z., Zhao, X., et al. (2020). Isoflurane aggravates peripheral and central insulin resistance in high-fat diet/streptozocin-induced type 2 diabetic mice. *Brain Res.* 1727:146511. doi: 10.1016/j.brainres.2019.146511

Feinkohl, I., Winterer, G., and Pischon, T. (2017). Diabetes is associated with risk of postoperative cognitive dysfunction: a meta-analysis. *Diabetes Metab. Res. Rev.* 33:e2884. doi: 10.1002/dmrr.2884

Ford, E., Giles, W., and Dietz, W. (2002). Prevalence of the metabolic syndrome among US adults: findings from the third National Health and Nutrition Examination Survey. *JAMA* 287, 356–359. doi: 10.1001/jama.287.3.356

Gao, Y., Xiao, Y., Miao, R., Zhao, J., Zhang, W., Huang, G., et al. (2015). The characteristic of cognitive function in Type 2 diabetes mellitus. *Diabetes. Res. Clin. Pract.* 109, 299–305. doi: 10.1016/j.diabres.2015.05.019

Giannarelli, R., Aragona, M., Coppelli, A., and Del Prato, S. (2003). Reducing insulin resistance with metformin: the evidence today. *Diabetes Metab.* 29(4 Pt 2):S28. doi: 10.1016/s1262-3636(03)72785-2

Grillo, C., Piroli, G., Lawrence, R., Wrighten, S., Green, A., Wilson, S., et al. (2015). Hippocampal insulin resistance impairs spatial learning and synaptic plasticity. *Diabetes Metab. Res. Rev.* 64, 3927–3936. doi: 10.2337/db15-0596

He, X., Long, G., Quan, C., Zhang, B., Chen, J., and Ouyang, W. (2019). Insulin resistance predicts postoperative cognitive dysfunction in elderly gastrointestinal patients. *Front. Aging Neurosci.* 11:197. doi: 10.3389/fnagi.2019.00197

Hölscher, C. (2014). First clinical data of the neuroprotective effects of nasal insulin application in patients with Alzheimer's disease. *Alzheimers Dement.* 10 1(Suppl.), S33–S37. doi: 10.1016/j.jalz.2013.12.006

Hudetz, J., Patterson, K., Amole, O., Riley, A., and Pagel, P. (2011). Postoperative cognitive dysfunction after noncardiac surgery: effects of metabolic syndrome. *J. Anesth.* 25, 337–344. doi: 10.1007/s00540-011-1137-0

Ittner, L., Ke, Y., Delerue, F., Bi, M., Gladbach, A., Van Eersel, J., et al. (2010). Dendritic function of tau mediates amyloid-beta toxicity in Alzheimer's disease mouse models. *Cell* 142, 387–397. doi: 10.1016/j.cell.2010.06.036

James, E., et al. (2020). Anesthesia and cognitive outcome in elderly patients: a narrative viewpoint. *J. Neurosurg. Anesthesiol.* 32, 9–17. doi: 10.1097/ANA.0000000000000640

Kawano, T., Iwata, H., Aoyama, B., Nishigaki, A., Yamanaka, D., Tateiwa, H., et al. (2016). The role of hippocampal insulin signaling on postoperative cognitive dysfunction in an aged rat model of abdominal surgery. *Life Sci.* 162, 87–94. doi: 10.1016/j.lfs.2016.08.020

Kim, B., and Feldman, E. (2015). Insulin resistance as a key link for the increased risk of cognitive impairment in the metabolic syndrome. *Exp. Mol. Med.* 47:e149. doi: 10.1038/emm.2015.3

Kim, B., Figueroa-Romero, C., Pacut, C., Backus, C., and Feldman, E. (2015). Insulin resistance prevents AMPK-induced Tau Dephosphorylation through

Akt-mediated Increase in AMPKSer-485 Phosphorylation. *J. Biol. Chem.* 290, 19146–19157. doi: 10.1074/jbc.M115.636852

Kim, S., Broussard, J., and Kolka, C. (2016). Isoflurane and sevoflurane induce severe hepatic insulin resistance in a canine model. *PLoS One* 11:e0163275. doi: 10.1371/journal.pone.0163275

Łabuzek, K., Suchy, D., Gabryel, B., Bielecka, A., Liber, S., and Okopień, B. (2010). Quantification of metformin by the HPLC method in brain regions, cerebrospinal fluid and plasma of rats treated with lipopolysaccharide. *Pharmacol. Rep.* 62, 956–965. doi: 10.1016/s1734-1140(10)70357-1

Le Freche, H., Brouillette, J., Fernandez-Gomez, F., Patin, P., Caillierez, R., Zommer, N., et al. (2012). Tau phosphorylation and sevoflurane anesthesia: an association to postoperative cognitive impairment. *Anesthesiology* 116, 779–787. doi: 10.1097/ALN.0b013e31824be8c7

Lenz, C., Rebel, A., van Ackern, K., Kuschinsky, W., and Waschke, K. (1998). Local cerebral blood flow, local cerebral glucose utilization, and flow-metabolism coupling during sevoflurane versus isoflurane anesthesia in rats. *Anesthesiology* 89, 1480–1488. doi: 10.1097/00000542-199812000-00026

Li, J., Deng, J., Sheng, W., and Zuo, Z. (2012). Metformin attenuates Alzheimer's disease-like neuropathology in obese, leptin-resistant mice. *Pharmacol. Biochem. Behav.* 101, 564–574. doi: 10.1016/j.pbb.2012.03.002

Martín-Segura, A., Ahmed, T., Casadomé-Perales, Á., Palomares-Perez, I., Palomer, E., Kerstens, A., et al. (2019). Age-associated cholesterol reduction triggers brain insulin resistance by facilitating ligand-independent receptor activation and pathway desensitization. *Aging Cell* 18:e12932. doi: 10.1111/acel.12932

Menke, A., Casagrande, S., Geiss, L., and Cowie, C. (2015). Prevalence of and trends in diabetes among adults in the United States, 1988-2012. *JAMA* 314, 1021–1029. doi: 10.1001/jama.2015.10029

Moller, J., Cluitmans, P., Rasmussen, L., Houx, P., Rasmussen, H., Canet, J., et al. (1998). Long-term postoperative cognitive dysfunction in the elderly ISPOCD1 study. ISPOCD investigators. International Study of Post-Operative Cognitive Dysfunction. *Lancet* 351, 857–861. doi: 10.1016/s0140-6736(97)07382-0

Morita, Y., Nogami, M., Sakaguchi, K., Okada, Y., Hirota, Y., Sugawara, K., et al. (2020). Enhanced Release of Glucose Into the Intraluminal Space of the Intestine Associated With Metformin Treatment as Revealed by [F]Fluorodeoxyglucose PET-MRI. *Diabetes Care* 43, 1796–1802. doi: 10.2337/dc20-0093

Ng, T., Feng, L., Nyunt, M., Feng, L., Gao, Q., Lim, M., et al. (2016). Metabolic syndrome and the risk of mild cognitive impairment and progression to dementia: follow-up of the singapore longitudinal ageing study cohort. *JAMA Neurol.* 73, 456–463. doi: 10.1001/jamaneurol.2015.4899

Ng, T., Feng, L., Yap, K., Lee, T., Tan, C., and Winblad, B. (2014). Long-term metformin usage and cognitive function among older adults with diabetes. *J. Alzheimers Dis.* 41, 61–68. doi: 10.3233/jad-131901

Petersen, K., Morino, K., Alves, T., Kibbey, R., Dufour, S., Sono, S., et al. (2015). Effect of aging on muscle mitochondrial substrate utilization in humans. *Proc. Natl. Acad. Sci. U.S.A.* 112, 11330–11334. doi: 10.1073/pnas.1514844112

Petrone, A., Battaglia, F., Wang, C., Dusa, A., Su, J., Zagzag, D., et al. (2003). Receptor protein tyrosine phosphatase alpha is essential for hippocampal neuronal migration and long-term potentiation. *EMBO J.* 22, 4121–4131. doi: 10.1093/emboj/cdg399

Pintana, H., Apaijai, N., Pratchayasakul, W., Chattipakorn, N., and Chattipakorn, S. (2012). Effects of metformin on learning and memory behaviors and brain mitochondrial functions in high fat diet induced insulin resistant rats. *Life Sci.* 91, 409–414. doi: 10.1016/j.lfs.2012.08.017

Puskas, F., Grocott, H., White, W., Mathew, J., Newman, M., and Bar-Yosef, S. (2007). Intraoperative hyperglycemia and cognitive decline after CABG. *Ann. Thorac. Surg.* 84, 1467–1473. doi: 10.1016/j.athoracsur.2007.06.023

Ramos-Rodriguez, J., Ortiz, O., Jimenez-Palomares, M., Kay, K., Berrocoso, E., Murillo-Carretero, M., et al. (2013). Differential central pathology and cognitive impairment in pre-diabetic and diabetic mice. *Psychoneuroendocrinology* 38, 2462–2475. doi: 10.1016/j.psyneuen.2013.05.010

Reynolds, C., Garwood, C., Wray, S., Price, C., Kellie, S., Perera, T., et al. (2008). Phosphorylation regulates tau interactions with Src homology 3 domains of phosphatidylinositol 3-kinase, phospholipase Cgamma1, Grb2, and Src family kinases. *J. Biol. Chem.* 283, 18177–18186. doi: 10.1074/jbc.M709715200

Rostas, J., Brent, V., Voss, K., Errington, M., Bliss, T., and Gurd, J. (1996). Enhanced tyrosine phosphorylation of the 2B subunit of the N-methyl-D-aspartate receptor in long-term potentiation. *Proc. Natl. Acad. Sci. U.S.A.* 93, 10452–10456. doi: 10.1073/pnas.93.19.10452

Sala, M., de, Roos, A., van den Berg, A., Altmann-Schneider, I., Slagboom, P., et al. (2014). Microstructural brain tissue damage in metabolic syndrome. *Diabetes Care* 37, 493–500. doi: 10.2337/dc13-1160

Sanjari Moghaddam, H., Ghazi Sherbaf, F., and Aarabi, M. (2019). Brain microstructural abnormalities in type 2 diabetes mellitus: a systematic review of diffusion tensor imaging studies. *Front. Neuroendocrinol.* 55:100782. doi: 10.1016/j.yfrne.2019.100782

Schricker, T., Sato, H., Beaudry, T., Codere, T., Hatzakorzian, R., and Pruessner, J. (2014). Intraoperative maintenance of normoglycemia with insulin and glucose preserves verbal learning after cardiac surgery. *PLoS One* 9:e99661. doi: 10.1371/journal.pone.0099661

Sommerfield, A., Deary, I., and Frier, B. (2004). Acute hyperglycemia alters mood state and impairs cognitive performance in people with type 2 diabetes. *Diabetes Care* 27, 2335–2340. doi: 10.2337/diacare.27.10.2335

Song, Y., Li, X., Gong, X., Zhao, X., Ma, Z., Xia, T., et al. (2019). Green tea polyphenols improve isoflurane-induced cognitive impairment via modulating oxidative stress. *J. Nutr. Biochem.* 73:108213. doi: 10.1016/j.jnutbio.2019.07.004

Srinivasan, K., Viswanad, B., Asrat, L., Kaul, C., and Ramarao, P. (2005). Combination of high-fat diet-fed and low-dose streptozotocin-treated rat: a model for type 2 diabetes and pharmacological screening. *Pharmacol. Res.* 52, 313–320. doi: 10.1016/j.phrs.2005.05.004

Steinmetz, J., Christensen, K., Lund, T., Lohse, N., and Rasmussen, L. (2009). Long-term consequences of postoperative cognitive dysfunction. *Anesthesiology* 110, 548–555. doi: 10.1097/ALN.0b013e318195b569

Šuput Omladič, J., Slana Ozimič, A., Vovk, A., Šuput, D., Repovš, G., Dovc, K., et al. (2020). Acute hyperglycemia and spatial working memory in adolescents with type 1 diabetes. *Diabetes Care* 43, 1941–1944. doi: 10.2337/dc20-0171

Tang, N., Jiang, R., Wang, X., Wen, J., Liu, L., Wu, J., et al. (2017). Insulin resistance plays a potential role in postoperative cognitive dysfunction in patients following cardiac valve surgery. *Brain Res.* 1657, 377–382. doi: 10.1016/j.brainres.2016.12.027

Thorell, A., Efendic, S., Gutniak, M., Häggmark, T., and Ljungqvist, O. (1993). Development of postoperative insulin resistance is associated with the magnitude of operation. *Eur. J. Surg.* 159, 593–599.

van der Heide, L., Ramakers, G., and Smidt, M. (2006). Insulin signaling in the central nervous system: learning to survive. *Prog. Neurobiol.* 79, 205–221. doi: 10.1016/j.pneurobio.2006.06.003

Xia, T., Cui, Y., Chu, S., Song, J., Qian, Y., Ma, Z., et al. (2016). Melatonin pretreatment prevents isoflurane-induced cognitive dysfunction by modulating sleep-wake rhythm in mice. *Brain Res.* 1634, 12–20. doi: 10.1016/j.brainres.2015.10.036

Yarchoan, M., Toledo, J., Lee, E., Arvanitakis, Z., Kazi, H., Han, L., et al. (2014). Abnormal serine phosphorylation of insulin receptor substrate 1 is associated with tau pathology in Alzheimer's disease and tauopathies. *Acta Neuropathol.* 128, 679–689. doi: 10.1007/s00401-014-1328-5

Conflict of Interest: The authors declare that the research was conducted in the absence of any commercial or financial relationships that could be construed as a potential conflict of interest.

Publisher's Note: All claims expressed in this article are solely those of the authors and do not necessarily represent those of their affiliated organizations, or those of the publisher, the editors and the reviewers. Any product that may be evaluated in this article, or claim that may be made by its manufacturer, is not guaranteed or endorsed by the publisher.

frontiers in Aging Neuroscience

ORIGINAL RESEARCH
published: 17 September 2021
doi: 10.3389/fnagi.2021.736580

Functional Metabolic Mapping Reveals Highly Active Branched-Chain Amino Acid Metabolism in Human Astrocytes, Which Is Impaired in iPSC-Derived Astrocytes in Alzheimer's Disease

Claudia Salcedo[1†], Jens V. Andersen[1†], Kasper Tore Vinten[1], Lars H. Pinborg[2], Helle S. Waagepetersen[1], Kristine K. Freude[3] and Blanca I. Aldana[1]*

[1] Department of Drug Design and Pharmacology, Faculty of Health and Medical Sciences, University of Copenhagen, Copenhagen, Denmark, [2] Epilepsy Clinic and Neurobiology Research Unit, Copenhagen University Hospital, University of Copenhagen, Copenhagen, Denmark, [3] Department of Veterinary and Animal Sciences, Faculty of Health and Medical Sciences, University of Copenhagen, Frederiksberg, Denmark

OPEN ACCESS

Edited by:
Paula I. Moreira, University of Coimbra, Portugal

Reviewed by:
Marco G. Alves, Independent Researcher, Porto, Portugal
Milan Holeček, Charles University, Czechia

***Correspondence:**
Blanca I. Aldana
blanca.aldana@sund.ku.dk

[†] These authors have contributed equally to this work and share first authorship

Received: *05 July 2021*
Accepted: *04 August 2021*
Published: *17 September 2021*

Citation:
Salcedo C, Andersen JV, Vinten KT, Pinborg LH, Waagepetersen HS, Freude KK and Aldana BI (2021) Functional Metabolic Mapping Reveals Highly Active Branched-Chain Amino Acid Metabolism in Human Astrocytes, Which Is Impaired in iPSC-Derived Astrocytes in Alzheimer's Disease. Front. Aging Neurosci. 13:736580. doi: 10.3389/fnagi.2021.736580

The branched-chain amino acids (BCAAs) leucine, isoleucine, and valine are important nitrogen donors for synthesis of glutamate, the main excitatory neurotransmitter in the brain. The glutamate carbon skeleton originates from the tricarboxylic acid (TCA) cycle intermediate α-ketoglutarate, while the amino group is derived from nitrogen donors such as the BCAAs. Disturbances in neurotransmitter homeostasis, mainly of glutamate, are strongly implicated in the pathophysiology of Alzheimer's disease (AD). The divergent BCAA metabolism in different cell types of the human brain is poorly understood, and so is the involvement of astrocytic and neuronal BCAA metabolism in AD. The goal of this study is to provide the first functional characterization of BCAA metabolism in human brain tissue and to investigate BCAA metabolism in AD pathophysiology using astrocytes and neurons derived from human-induced pluripotent stem cells (hiPSCs). Mapping of BCAA metabolism was performed using mass spectrometry and enriched [^{15}N] and [^{13}C] isotopes of leucine, isoleucine, and valine in acutely isolated slices of surgically resected cerebral cortical tissue from human brain and in hiPSC-derived brain cells carrying mutations in either amyloid precursor protein (APP) or presenilin-1 (PSEN-1). We revealed that both human astrocytes of acutely isolated cerebral cortical slices and hiPSC-derived astrocytes were capable of oxidatively metabolizing the carbon skeleton of BCAAs, particularly to support glutamine synthesis. Interestingly, hiPSC-derived astrocytes with APP and PSEN-1 mutations exhibited decreased amino acid synthesis of glutamate, glutamine, and aspartate derived from leucine metabolism. These results clearly demonstrate that there is an active BCAA metabolism in human astrocytes, and that leucine metabolism is selectively impaired in astrocytes derived from the hiPSC models of AD. This impairment in astrocytic BCAA metabolism may contribute to neurotransmitter and energetic imbalances in the AD brain.

Keywords: AD, astrocytes, BCAA, glutamate, glutamine, neuron, induced pluripotent stem cell, energy metabolism

INTRODUCTION

Branched-chain amino acids (BCAAs) comprise three essential amino acids, leucine, isoleucine, and valine, which all have multiple functions in the brain (Yudkoff, 1997; Conway and Hutson, 2016). BCAAs are important nitrogen donors essential for nitrogen homeostasis and neurotransmitter cycling (Yudkoff, 1997; Sperringer et al., 2017). Furthermore, BCAAs can be utilized by brain cells as energy substrates in the tricarboxylic acid (TCA) cycle. BCAA metabolism is initiated by reversible transamination catalyzed by the branched-chain amino acid transaminase (BCAT) producing the corresponding branched-chain α-keto acids (BCKAs) and glutamate. BCAT exists as two isozymes, one cytosolic (BCATc/BCAT1), which is only found in brain, ovaries and testes, and one mitochondrial (BCATm/BCAT2), which is expressed in most tissues (Conway and Hutson, 2016). The subsequent irreversible oxidative decarboxylation of BCKAs is catalyzed by the branched-chain α-keto acid dehydrogenase (BCKDH) complex, followed by multiple other reactions (**Figure 1**), ultimately yielding acetyl coenzyme A (CoA) or succinyl CoA (Sperringer et al., 2017), which may support the TCA cycle and amino acid synthesis. Discrepancies on the cellular location of the metabolic machinery of BCAA metabolism have prompted the suggestion that astrocytes have a limited BCAA metabolism capacity (Conway and Hutson, 2016; Sperringer et al., 2017). Based on immunohistochemical studies, it has been suggested that human astrocytes do not express BCAT or BCKDH (Hull et al., 2012, 2015, 2018), which has led to the conclusion that human astrocytes are incapable of metabolizing BCAAs (Sperringer et al., 2017). However, this matter has not been functionally investigated.

Alzheimer's disease (AD) is a complex neurodegenerative disorder characterized by a heterogeneous pathology comprising defective protein clearance (Braak and Braak, 1991), disrupted energy metabolism (Cunnane et al., 2020), neuroinflammation (Leng and Edison, 2021), and oxidative stress (Butterfield and Halliwell, 2019). AD pathology gradually leads to common clinical manifestations, such as cognitive and memory impairment (Winblad et al., 2016). Although research has mainly focused on neurons, increasing evidence points toward the involvement of non-neuronal cells, namely, astrocytes, microglia, and oligodendrocytes, in the progression of the disease (De Strooper and Karran, 2016; Acosta et al., 2017). However, the glial contribution in AD is yet to be fully unraveled (De Strooper and Karran, 2016; Aldana, 2019; Bogetofte et al., 2019). Alterations in brain glucose metabolism is one of the earliest biomarkers of AD development (Gordon et al., 2018). Brain energy metabolism is closely related to neurotransmission (Yu et al., 2018). Interestingly, disrupted excitatory glutamate signaling is strongly implicated in AD as well as several other neurodegenerative disorders (Liu et al., 2019; Conway, 2020). Only a small fraction of glutamate from the circulating peripheral blood plasma crosses the blood-brain barrier (BBB), thus the majority of brain glutamate must be *de novo* synthesized (Sperringer et al., 2017). In the brain, glutamate is synthesized from TCA cycle intermediate α-ketoglutarate, providing the carbon backbone (Brekke et al., 2016), while the amino group is derived from a nitrogen donor such as BCAAs, aspartate, or alanine (Conway and Hutson, 2016). Particularly, BCAAs play an essential role as nitrogen donors, and they account for approximately one-third of the amino groups used for brain glutamate synthesis (Yudkoff, 1997). Furthermore, the carbon skeleton of BCAAs, entering cellular metabolism as either acetyl CoA or succinyl CoA, may serve as auxiliary fuels for brain cells, hereby supporting the failing energy metabolism in AD (Cunnane et al., 2020). Astrocytes take up the majority of synaptic glutamate released from neurons and hereby play a crucial role in terminating excitatory signaling. In astrocytes, most of the synaptic glutamate is converted into glutamine by the action of the enzyme glutamine synthetase (GS), which is selectively expressed in astrocytes (Norenberg and Martinez-Hernandez, 1979; Schousboe et al., 2013). The glutamine is subsequently released and taken up by neurons, which is essential to replenish the neuronal glutamate pool. This exchange of metabolites between neurons and astrocytes is known as the glutamate-glutamine cycle and is particularly important during extensive glutamatergic signaling (Shen, 2013; Tani et al., 2014; Andersen et al., 2021b). Given the involvement of astrocytes in AD pathology, the importance of brain BCAA metabolism for neurotransmitter homeostasis, and the energetic crisis of AD, it is important to functionally investigate astrocyte BCAA metabolism in relation to AD pathology.

The goals of this study were to perform the first functional profiling of BCAA metabolism in human astrocytes and identify metabolic alterations in BCAA metabolism in the pathophysiology of AD using human induced pluripotent stem cell-derived astrocytes and neurons. First, we demonstrate that astrocytes of acutely isolated human brain slices as well as astrocytes derived from hiPSCs are capable to oxidatively metabolizing the carbon skeleton of BCAAs, particularly for the synthesis of glutamine. Furthermore, astrocytes with mutations in the amyloid precursor protein (APP) or presenilin-1 (PSEN-1) genes known to result in familial forms of AD exhibited decreased synthesis of glutamate, glutamine, and aspartate derived from leucine metabolism. These results uncover highly active astrocytic BCAA metabolism and suggest a possible neurotransmitter imbalance in AD related to leucine metabolism.

MATERIALS AND METHODS

Materials

The stable isotopes [^{15}N]leucine, [^{15}N]isoleucine, [^{15}N]valine, [U-^{13}C]leucine, [U-^{13}C]isoleucine, [U-^{13}C]valine (all L-isomers of 98% chemical purity) were purchased from Cambridge Isotope Laboratories (Tewksbury, MA, United States). All the other chemicals and reagents used were of purest grade available from regular commercial sources.

Animals

Male NMRI mice were purchased from Harlan (Horst, The Netherlands) and housed at the Department of Drug Design and

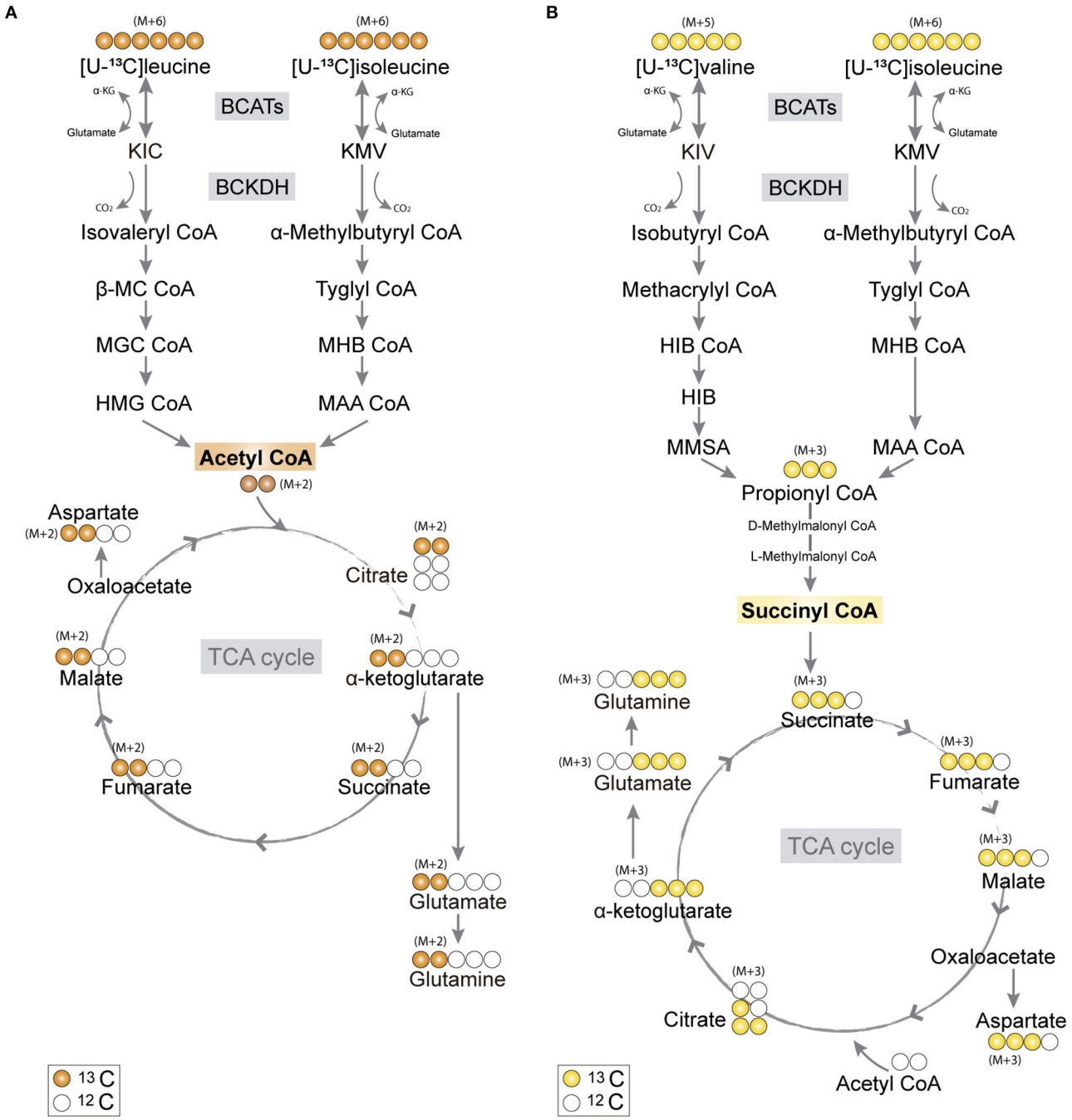

FIGURE 1 | Primary ^{13}C-labeling patterns from [U-^{13}C]branched-chain amino acid (BCAA) metabolism. **(A)** Metabolism of [U-^{13}C]leucine and [U-^{13}C]isoleucine (M+6) will result in acetyl coenzyme A (CoA), a process initiated by branched-chain aminotransferase (BCAT) catalyzing BCAA transamination and hereby producing branched-chain α-keto acids (BCKAs), α-ketoisocaproate (KIC), and α-keto-β-methylvalerate (KMV), respectively. Subsequently, irreversible oxidative decarboxylation of the BCKAs occurs by the branched-chain α-keto acid dehydrogenase (BCKDH) enzyme complex and through multiple enzymatic reactions entering the TCA cycle as double-labeled acetyl CoA (M+2). Filled circles (orange) represent labeled ^{13}C and empty circles unlabeled ^{12}C. **(B)** Valine and isoleucine can also enter into the TCA cycle *via* succinyl CoA. [U-^{13}C]valine (M+5) and [U-^{13}C]isoleucine (M+6) will be transaminated, resulting in BCKAs, α-ketoisovaleric (KIV), and KMV, respectively, and then decarboxylated, entering TCA cycle metabolism, after numerous reactions, as succinate (M+3). Filled circles (yellow) represent labeled ^{13}C and empty circles unlabeled ^{12}C. BCATs, branched-chain aminotransferase; BCKDH, branched-chain α-keto acid dehydrogenase; α-KG, α-ketoglutarate; KIC, α-ketoisocaproate; KMV, α-keto-β-methylvalerate; KIV, α-ketoisovaleric; β-MC CoA, β-methylcrotonyl CoA; MGC CoA, β-methylglutaconyl CoA; HIB CoA, β-hydroxyisobutyryl CoA; MHB CoA, α-methyl-β-hydroxyisobutyryl CoA; HMG CoA, β-hydroxy-β-methylglutaryl CoA; MAA CoA, α-methylacetoacetyl CoA; HIB, β-hydroxyisobutyrate; MMSA, methylmalonate semialdehyde; MAA CoA, α-methylacetoacetyl CoA.

Pharmacology, University of Copenhagen, in a specific pathogen-free and humidity- and temperature-controlled facility with a 12-h light/dark cycle. The mice were acclimatized for 2 weeks before the experiments and single-housed in individually ventilated cages with free access to food and water. In total, six 12- to 13-week-old mice were used for the experiments (body weight: 42.4 ± 0.4 g). The experiments were approved by the Danish National Ethics Committee and performed according to the European Convention (ETS 123 of 1986).

Brain Tissue

Human neocortical tissue was obtained from six patients (four females, two males) aged 25–52 years. Additional information on patient cohort characteristics can be found in Andersen et al. (2020). The use of human neocortical tissue was approved by the local Ethics Committee in Copenhagen (H-2-2011-104) with written informed consent from all the patients prior to surgery. Human neocortical tissue of the temporal lobe was resected at Rigshospitalet (Copenhagen, Denmark) in order to facilitate access to the mesial temporal lobe, e.g., amygdala, hippocampus, and parahippocampal gyrus, involved in generating epileptic seizures. Immediately after resection, the tissue was transferred to ice-cold artificial cerebrospinal fluid (ACSF) containing (in mM): NaCl 128, $NaHCO_3$ 25, D-glucose 10, KCl 3, $CaCl_2$ 2, $MgSO_4$ 1.2, and KH_2PO_4 0.4 with pH = 7.4, and transported on ice to the laboratory. Histopathological examination of the neocortical tissue revealed no abnormal pathological features for any of the patients. The metabolic integrity of resected cerebral cortical human tissue has been established previously (Andersen et al., 2020).

Cell Lines

Human-induced pluripotent stem cell lines were plated on Matrigel-coated plates (BD Matrigel; STEMCELL Technologies, Canada Inc.) with an E8 essential culture medium (STEMCELL Technologies, Canada Inc.). A fresh E8 medium was added every day until the cells reached 90–100% confluency, usually achieved after 7 days of culturing. The hiPSCs used in this study have been previously characterized by Frederiksen et al. (2019a,b) where specific pathogenic mutations in the amyloid precursor protein (APP) or presenilin-1 (PSEN-1) gene were introduced into a healthy iPSC line obtained from the skin biopsy of a healthy person by CRISPR-Cas9. The APP cell line contains a heterozygous double KM670/671NL mutation resulting in an amino acid change from lysine (K) and methionine (M) to asparagine (N) and leucine (L) into the APP gene. The PSEN-1 cell line contains a homozygous E280A mutation resulting in an amino acid change from glutamic acid (E) to alanine (A) into the PSEN-1 gene (Frederiksen et al., 2019a,b). Nucleotide substitution was confirmed by restriction digest and followed by DNA sequencing. Pluripotency of the gene-edited lines was confirmed by immunocytochemistry and quantified by flow analysis. The hiPSC lines used in this study will be referred to as AD astrocytes or AD neurons. These mutations are hallmarks of familial forms of AD with early onset. The healthy hiPSC line was used as the parental control (wild type).

Neural Progenitor Cell Generation and Cell Differentiation

Neural induction was achieved by dual SMAD inhibition using LDN193189 (S2618, Selleck Chemicals, Houston, TX, United States) and SB431542 (S1067, Selleck Chemicals, Houston, TX, United States), inhibiting the BMP and TGFß pathways, respectively, through a three-dimensional (3D)-sphere method (Chandrasekaran et al., 2017). After 7 days of induction, neuronal progenitor cells (NPCs) were plated on Matrigel in a medium supplemented with basic fibroblast growth factor (bFGF) (10 ng/ml) (CYT-557; ProSpec, Rehovot, Israel) and EGF (10 ng/ml) (CYT-217; ProSpec, Rehovot, Israel). Neuronal rosettes were selected for further passages.

Astrocytic Differentiation

The astrocytes were differentiated based on a modified protocol by Shaltouki et al. (2013), described elsewhere (Salcedo et al., 2021). Briefly, when the NPCs reached 70% confluency, they were plated on Matrigel in an astrocytic maintenance medium (AMM), which promotes the generation of astrocyte progenitor cells (APCs). To switch from neurogenesis to gliogenesis, the APCs were re-plated several times until passage five. The APCs (last passage) were plated at a seeding density of 50,000 cells/cm^2 in an astrocytic differentiation medium (ADM). The ADM was changed every other day, and the cells were kept under differentiation conditions for 7 weeks until they reached maturation for metabolic assays.

Neuronal Differentiation

The neurons were differentiated according to Zhang et al. (2017). When the NPCs reached 70% confluency, they were plated on Matrigel in a neural expansion media (NEM). The NEM was supplemented with 20 ng/ml of bFGF, and EGF. The NPCs were re-plated several times until passage three. Then, they (for last passage) were plated on 0.001% Poly-L-Ornithine (P4957; Sigma-Aldrich, St. Louis, MO, United States) and a 5 μg/ml laminin (L2020; Sigma-Aldrich, St. Louis, MO, United States) coating in a neural maturation media (NMM) for 10 days. The NMM was supplemented with 20 ng/μl brain-derived neurotrophic factor (BDNF) (CYT-207; Prospec, Rehovot, Israel), 10 ng/μl glial cell line-derived neurotrophic factor (GDNF) (CYT-305; Prospec, Rehovot, Israel), 200 μM L-ascorbic acid 2-phosphate (A8960, Sigma-Aldrich, St. Louis, MO, United States), and 50 μM dibutyryl-cyclic adenosine monophosphate (db-cAMP) (A6885; Sigma-Aldrich, St. Louis, MO, United States). Half media change was performed every 3 days. Ten-day immature neurons were passaged a last time on PLO-Laminin coated plates with the NMM at a seeding density of 50,000 cells/cm^2 until they reached maturation for the metabolic assays.

Brain Slice Incubations

Incubation of acutely isolated cerebral cortical brain slices of mice and humans was performed as described previously (Andersen et al., 2019, 2020). For mouse brain slices, the experiments were performed one mouse at a time. The mouse was euthanized by cervical dislocation and decapitated. The brain was quickly excised from the cranial vault and submerged

in slushed ice-cold ACSF. Cerebral cortices of the mouse brain were dissected, and the rest of the brain was discarded. The isolated mouse cerebral cortices or human neocortical tissue was sliced (350 μm) on a McIlwain tissue chopper (The Vibratome Company, O'Fallon, MO, United States), and slices were separated under a microscope. Two to six mouse cerebral cortical slices or one human slice (gray matter only) was kept just below the surface of 10 ml 37°C oxygenated (5% CO_2/95% O_2) ACSF and pre-incubated for 60 min to recover from slicing in a custom-made incubation apparatus (McNair et al., 2017). Subsequently, the media was exchanged for ACSF containing 2 mM ^{15}N or ^{13}C-labeled leucine, isoleucine, or valine, with a D-glucose concentration of 5 mM, for additional 60 min. Incubations were terminated by transferring the slices to ice-cold 70% ethanol. The slices were sonicated, centrifuged (20,000 g × 20 min), and the supernatant was lyophilized before gas chromatography–mass spectrometry (GC–MS) and high-performance liquid chromatography (HPLC) analysis. Protein content of the pellet was determined by the Pierce method using bovine serum albumin (BSA) as standard protein.

Cell Culture Incubations

Cultures of 7-week-old human-induced pluripotent stem cell-derived astrocytes and neurons were used for dynamic metabolic mapping. The culturing medium was removed, and the cells were washed twice with phosphate-buffered saline (PBS) at 37°C. The cells were then incubated for 90 min at 37°C in ACSF containing 2 mM [U-^{13}C]valine, [U-^{13}C]leucine, or [U-^{13}C]isoleucine plus 2.5 mM unlabeled glucose. These BCAA concentrations were chosen based on previous studies (Andersen et al., 2019). The glucose concentration represents physiological conditions. After incubation, the medium was collected, and the cells were washed with cold PBS (4°C) to stop metabolic reactions. The cells were lysed and extracted with 70% ethanol and centrifuged at 20,000 g for 20 min at 4°C to separate soluble and insoluble components. Cell extracts were lyophilized and solubilized in water for further GC-MS and HPLC analysis. Pellets were dissolved in 1 M potassium hydroxide (KOH) at room temperature and analyzed for protein content by the Pierce BSA assay.

Dynamic Metabolic Mapping by Gas Chromatography–Mass Spectrometry (GC–MS)

The ^{15}N and ^{13}C-enrichment of TCA cycle metabolites and amino acids was determined by GC–MS analyses, according to a previous method (Walls et al., 2014). Briefly, the extracts were reconstituted in water and acidified, and the metabolites were extracted into an organic phase with 96% ethanol/benzene and derivatized using N-tert-butyldimethylsilyl-N-methyltrifluoroacetamide. Natural ^{15}N and ^{13}C-abundance was corrected and calculated as described elsewhere (Biemann and McCloskey, 1962). Data are presented as percentage of labeling of the isotopolog M+X, where M corresponds to the molecular weight of the unlabeled molecule, and X is the number of ^{15}N or ^{13}C-enriched carbon atoms in the molecule (Andersen et al., 2019).

Quantitative Analysis of Amino Acid Amounts Performed by High Performance Liquid Chromatography (HPLC)

Reconstituted extracts were used for the quantification of amino acid amounts, by reverse phase high-performance liquid chromatography using 1260 Infinity (Agilent Technologies, Sta. Clara, CA, United States), as described elsewhere (Salcedo et al., 2021). Amino acid separation and detection were performed by precolumn o-phthalaldehyde (OPA) online derivatization and fluorescent detection (λex = 338 nm, 10-nm bandwidth; λem = 390 nm, 20-nm bandwidth). A gradient elution with Mobile phase A (10 mM NaH_2PO_4, 10 mM $Na_2B_4O_7$, 0.5 mM NaN_3, pH 6.8) and mobile phase B (acetonitrile 45%: methanol 45%: H_2O 10% V:V:V) was performed with a flow of 1.5 ml/min. The quantification of the amino acid amounts was achieved using calibration curves of external standards of the amino acids of interest with known increasing concentration ranging from 5 to 1,000 μM.

Statistical Analyses

Data are presented as mean (±) standard error of the mean (SEM) of values. Experimental values from the brain tissue were biological replicates, and values from cell cultures were obtained from three independent experiments derived from at least two separate cell differentiations (batches) of three different cell lines, namely the parental control cell line and the two cell lines with the APP- and PSEN-1-introduced mutations, respectively. Statistically significant differences were set at $p < 0.05$ and tested by either one-way or two-way ANOVA with Bonferroni multiple comparison test or with paired t-test, as indicated in Figure legends.

RESULTS

BCAA Nitrogen Metabolism in Human and Mouse Cortical Slices

The BCAAs, leucine, isoleucine, and valine, have been widely described as key nitrogen donors vital for neurotransmission and aid to maintain nitrogen balance in the brain (Conway and Hutson, 2016; Sperringer et al., 2017). The transamination of BCAAs is catalyzed by branched-chain aminotransferase (BCAT) transferring the BCAA nitrogen into glutamate. The nitrogen can subsequently be transferred to connected amino acids. To assess the nitrogen metabolism of the BCAAs, mouse and human cerebral cortical slices were incubated with [^{15}N]leucine, [^{15}N]isoleucine, and [^{15}N]valine. The labeling patterns from the human tissue were compared with the ones obtained from mouse cortical slices in order to distinguish specie-specific functional metabolic differences among cellular compartments (**Figure 2**). Substantial ^{15}N-enrichment was found for all three BCAAs in both mouse and human slices, suggesting a large BCAA uptake capacity. BCAA ^{15}N-incorporation was slightly lower in the mouse cortical slices after incubation with [^{15}N]leucine and [^{15}N]isoleucine when compared with that of the human slices. Increased

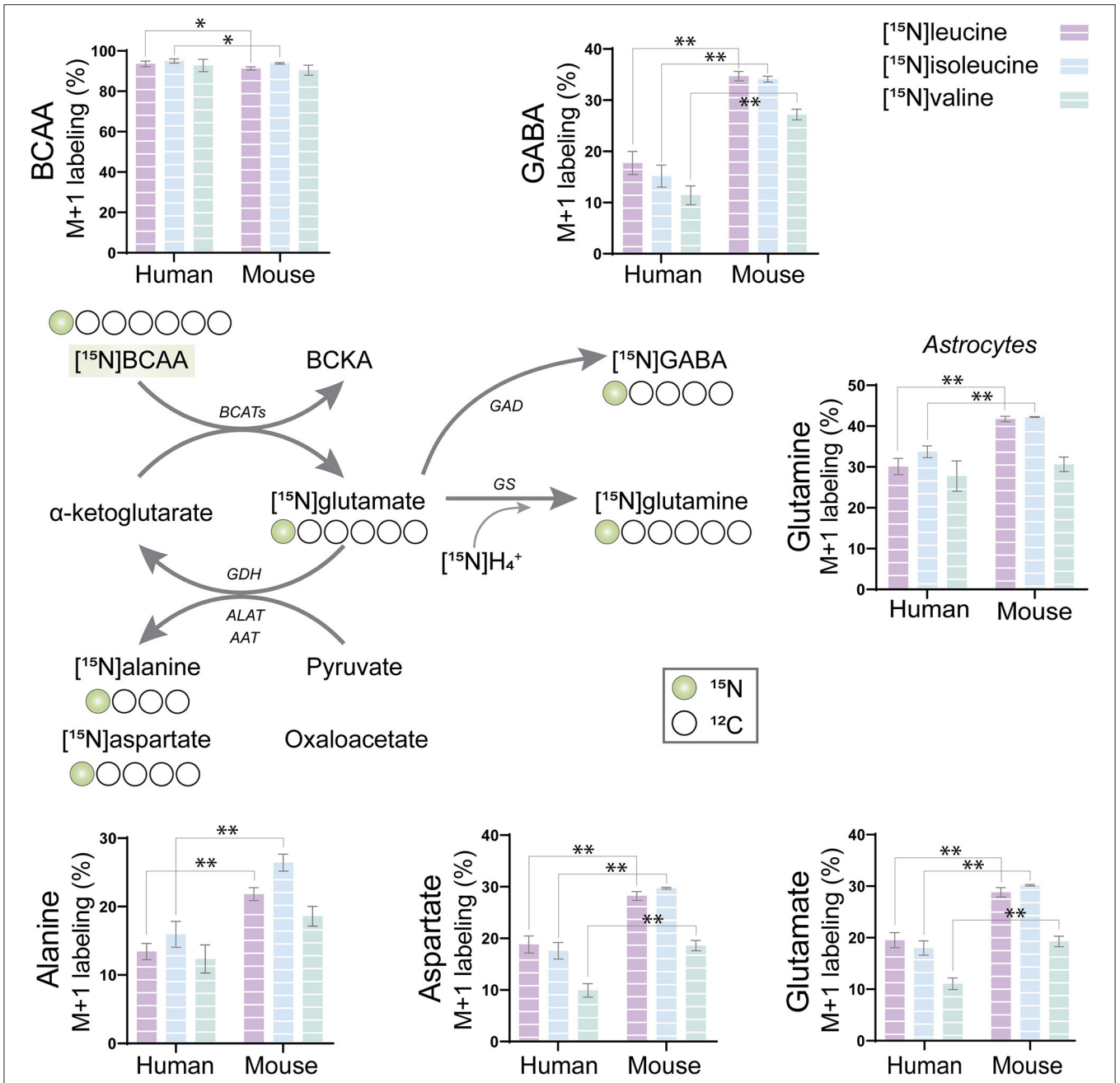

FIGURE 2 | BCAA nitrogen metabolism of human and mouse brain slices. After incubation with [^{15}N]BCAA (valine, leucine, or isoleucine), M+1 labeling was observed in glutamate, glutamine, gamma-aminobutyric acid (GABA), alanine, and aspartate, indicating significant nitrogen incorporation into amino acids supported by BCAA metabolism. ^{15}N-enrichment in intracellular amino acids was determined by gas chromatography–mass spectrometry (GC-MS). Values represent mean (±) standard error of the mean (SEM) ($n = 6$), $^{*}p < 0.05$, $^{**}p < 0.01$ (when compared with human cortical slices) analyzed by Student's paired t-test. BCAA, branched-chain amino acid; BCKA, branched-chain α-keto acids; BCATs, branched-chain aminotransferase; GAD, glutamate decarboxylase; GDH, glutamate dehydrogenase; ALAT, alanine aminotransferase; AAT, aspartate aminotransferase; GS, glutamine synthetase.

^{15}N-incorporation was observed in gamma-aminobutyric acid (GABA), aspartate, and glutamine after incubation with [^{15}N]leucine, [^{15}N]isoleucine, and [^{15}N]valine in the mouse cortical slices when compared with the human cortical slices. Furthermore, ^{15}N-incorporation in glutamine and alanine was increased after incubation with [^{15}N]leucine and [^{15}N]isoleucine in the mouse cortical slices. These results may suggest a higher BCAT activity in the mouse brain compared with the human brain. Interestingly, of all the amino acids, the ^{15}N-enrichment was highest in glutamine for all the three

[^{15}N]BCAAs in both mouse and human cortical slices. This observation could indicate that a large proportion of BCAA nitrogen metabolism is being utilized for glutamine synthesis in astrocytes.

BCAA Oxidative Metabolism in Human and Mouse Cortical Slices

The carbon skeleton of the branched-chain keto acid derived from BCAAs can enter the TCA cycle as either acetyl CoA or succinyl CoA (illustrated in **Figure 1**). The metabolic oxidation of BCAAs is initiated by BCKDH complex activity where irreversible oxidative decarboxylation of the BCKAs occur and *via* multiple subsequent enzymatic reactions yield acetyl CoA or succinyl CoA. To assess BCAA oxidative metabolism, the human and mouse cortical slices were incubated with [U-^{13}C]isoleucine, [U-^{13}C]leucine, or [U-^{13}C]valine, and ^{13}C-enrichment of TCA cycle intermediates and amino acids were determined by GC–MS (**Figure 3**) and amino acid amounts quantified by HPLC (**Supplementary Table 1**). The metabolism of [U-^{13}C]leucine and [U-^{13}C]isoleucine (M+6) (**Figure 1A**) will result in acetyl CoA M+2, whereas the metabolism of [U-^{13}C]valine (M+5) and [U-^{13}C]isoleucine (M+6) will result in succinyl CoA M+3 (**Figure 1B**).

Following incubation with [U-^{13}C]leucine, ^{13}C-enrichment in M+2 (*via* acetyl CoA) was higher in citrate (**Figure 3A**), glutamate, glutamine, and GABA (**Figure 3B**) in the mouse cortical slices when compared with the human cortical slices. When incubating with [U-^{13}C]isoleucine, we observed increased M+3 labeling (*via* succinyl CoA) in α-ketoglutarate, succinate, and glutamate in the mouse cortical slices when compared with the human cortical slices. Similarly, after incubation with [U-^{13}C]valine, ^{13}C-incorporation was higher in α-ketoglutarate and succinate in the mouse cortical slices. Decreased ^{13}C-incorporation in malate, citrate, and glutamine was observed in the mouse cortical slices when compared with the human cortical slices after incubation with [U-^{13}C]valine. The overall highest ^{13}C-enrichment was derived from [U-^{13}C]leucine metabolism in both the mouse and human cortical slices. In accordance with the results of [^{15}N]BCAA metabolism, glutamine and citrate reached the highest ^{13}C-enrichment after incubation with all the three [U-^{13}C]BCAAs in both the mouse and human cortical slices. These results demonstrate that oxidative metabolism of the BCAA carbon skeleton is utilized for amino acid synthesis, particularly for glutamine synthesis in astrocytes from both the mouse and human cerebral cortical slices.

BCAA Oxidative Metabolism in Human Astrocytes

The incubation experiments revealed that the brain slices of both mouse and humans have a large capacity for BCAA metabolism particularly supporting astrocyte glutamine synthesis. To further substantiate these results, we next assessed if hiPSC-derived astrocytes could metabolize BCAAs through ^{13}C-incorporation into the TCA cycle. Incubation with the three [U-^{13}C]BCAAs (**Figure 4**) is presented as the molecular carbon labeling (MCL), which is the average of the carbon labeling in a given molecule (Andersen et al., 2021a). ^{13}C-enrichment was recovered in all TCA cycle metabolites and amino acids from [U-^{13}C]BCAA metabolism, which demonstrates that human astrocytes are capable of introducing and metabolizing the carbon skeleton of leucine, isoleucine, and valine in the TCA cycle. Interestingly, the MCL obtained from incubation with [U-^{13}C]isoleucine appeared to be higher throughout all the TCA cycle intermediates and amino acids compared with leucine and valine. However, as the metabolism of [U-^{13}C]isoleucine gave rise to both M+2 and M+3 labeling, the MCL is expected to be higher. [U-^{13}C]valine had the lowest overall ^{13}C-enrichment in the TCA cycle intermediates and amino acids, which is in accordance with the results from mouse and human brain slices. These results functionally demonstrate that hiPSC-derived astrocytes are able to oxidatively metabolize BCAAs.

Altered BCAA Oxidative Metabolism in AD hiPSC-Derived Astrocytes With APP or PSEN-1 Mutations

Studies on postmortem AD brains have reported alterations in the expression of enzymes involved in the metabolism of BCAAs, such as BCAT (Hull et al., 2015). However, functional BCAA metabolism in relation to AD pathophysiology has not been explored. Given the central metabolic role of BCAAs in neurotransmission, we sought to determine whether BCAA oxidative metabolism is affected in hiPSC-derived astrocytes with APP or PSEN-1 mutation as models of AD pathology (referred to as AD astrocytes). hiPSC-derived astrocytes from either AD-mutated or parental control cell lines were, thus, incubated with [U-^{13}C]leucine, [U-^{13}C]isoleucine, or [U-^{13}C]valine, and ^{13}C-incorporation into the TCA cycle intermediates and amino acid were assessed (**Figure 5**). After incubation with [U-^{13}C]leucine, AD astrocytes with APP mutation exhibited increased labeling in glutamate and citrate (M+2) but reduced ^{13}C-enrichment was found in aspartate and malate when compared with control astrocytes. The AD astrocytes with PSEN-1 mutation only exhibited increased labeling in citrate (M+2) but otherwise similar labeling patterns when compared with the control astrocytes (**Figure 5A**). When incubated with [U-^{13}C]isoleucine, similar changes between AD and control astrocytes were observed in amino acid labeling (M+2) as observed in the [U-^{13}C]leucine incubation (**Figure 5B**). For instance, in the AD astrocytes with APP mutation, glutamate (M+2) labeling was increased, while labeling in aspartate was decreased although not significantly, compared with the control astrocytes. In the AD astrocytes with PSEN-1 mutation, however, the decrease in aspartate labeling was significantly different from that of the control astrocytes. ^{13}C-incorporation in citrate was increased only in the AD astrocytes with APP mutation, while labeling in malate (M+2) was decreased in both AD astrocytes when compared with the control astrocytes. No significant differences were found in the labeling of α-ketoglutarate, succinate, and fumarate (**Supplementary Table 2**). Furthermore, after incubation with [U-^{13}C]valine (**Figure 5C**), no significant differences between the AD and control astrocytes in amino acid

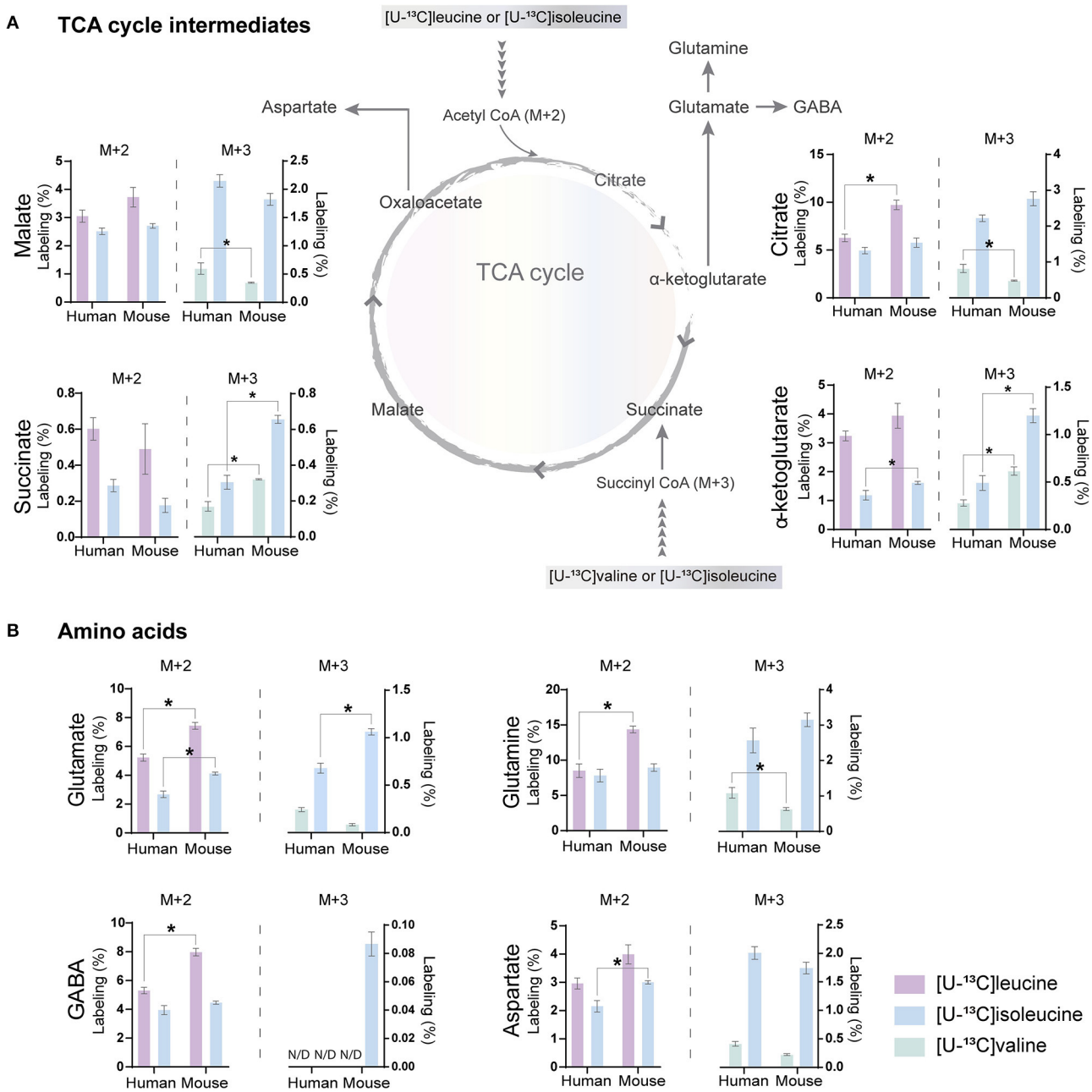

FIGURE 3 | BCAA oxidative metabolism in human and mouse brain slices. ^{13}C-enrichment of tricarboxylic acid (TCA) cycle metabolites and amino acids in human and mouse cerebral cortical slices after incubation with [U-^{13}C]isoleucine, [U-^{13}C]leucine, or [U-^{13}C]valine. M+2 and M+3 ^{13}C-enrichment in **(A)** TCA cycle intermediates. Increased M+2 ^{13}C-enrichment in **(B)** glutamate, glutamine, and GABA after incubation with [U-^{13}C]leucine in mouse cortical slices when compared with human cortical slices. ^{13}C-enrichment in intracellular metabolites was determined by GC-MS. Values represent mean (±) SEM ($n = 6$), $^{*}p < 0.05$ analyzed by two-way ANOVA. N/D, not detectable.

labeling (M+3) were found. However, the TCA cycle metabolites, citrate, and malate showed increased ^{13}C-enrichment in both mutated AD astrocytes when compared with control. Following [U-^{13}C]isoleucine metabolism, the AD astrocytes only exhibited lower labeling in aspartate (M+3) compared with the control astrocytes (**Figure 5D**). No significant differences were found in the labeling of α-ketoglutarate, succinate, and fumarate (**Supplementary Table 3**). Collectively, these results suggest that BCAA oxidative metabolism in AD astrocytes is impaired particularly when the BCAAs enter the TCA cycle *via* acetyl CoA.

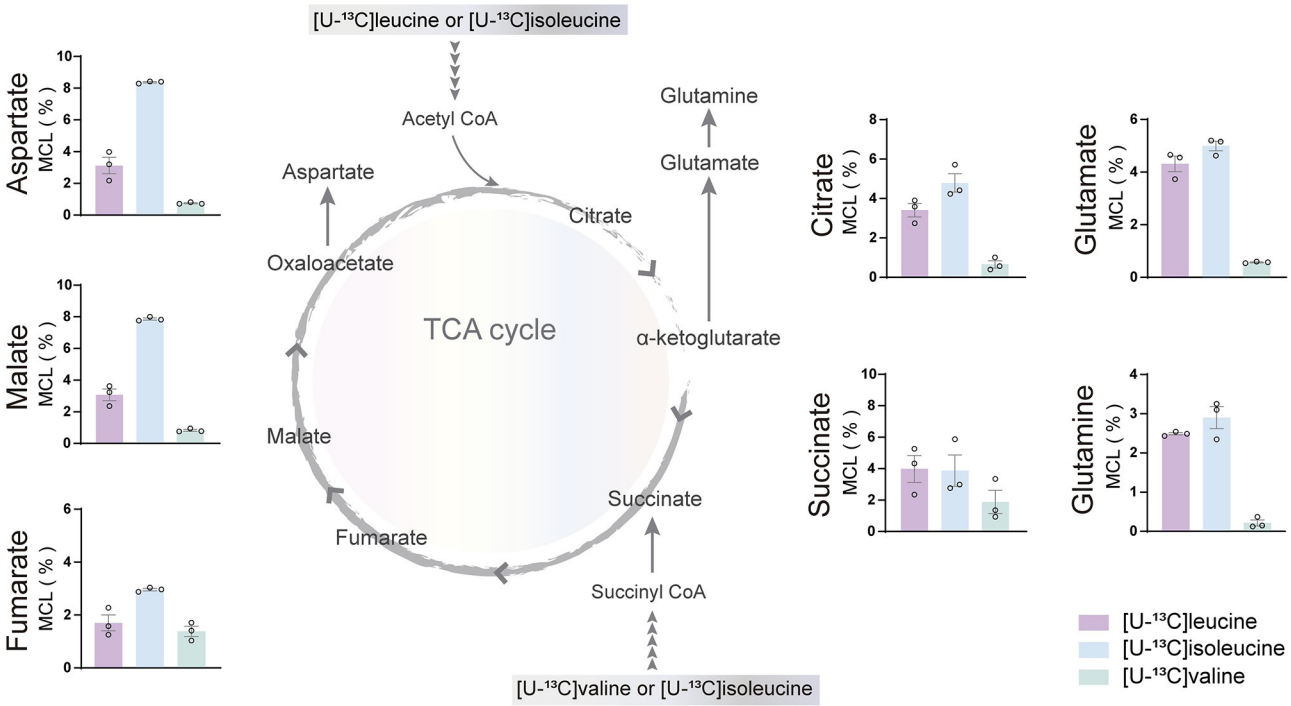

FIGURE 4 | BCAA oxidative metabolism in human induced pluripotent stem cell (hiPSC)-derived astrocytes. hiPSC-derived astrocytes were incubated with [U-^{13}C]isoleucine, [U-^{13}C]leucine, or [U-^{13}C]valine. Labeling in TCA cycle intermediates and amino acids represented as molecular carbon labeling (MCL) confirms hiPSC-derived astrocytes capability to oxidatively metabolize the BCAA isoleucine, leucine, and, to a lesser extent, valine by incorporating them in the TCA cycle. Values represent mean ± SEM ($n = 3$) from different hiPSC-derived astrocyte set-ups individually depicted as circles.

Decreased Aspartate Labeling in AD hiPSC-Derived Neurons With APP or PSEN-1 Mutations After Incubation With BCAAs

Astrocytes and neurons maintain tight metabolic interactions critical for cerebral homeostasis. After finding alterations in the BCAA metabolism of AD hiPSC-derived astrocytes, we next assessed if BCAA oxidative metabolism could be affected in hiPSC-derived neurons with APP or PSEN-1 mutation as models of AD pathology (referred to as AD neurons). hiPSC-derived neurons from AD-mutated or parental control cell lines were incubated with [U-^{13}C]leucine, [U-^{13}C]isoleucine, or [U-^{13}C]valine, and ^{13}C-incorporation into the TCA cycle intermediates and amino acids was assessed (**Figure 6**). After incubation with [U-^{13}C]leucine, no significant differences were observed in the labeling of glutamate or aspartate (M+2) in the AD neurons compared with the control neurons (**Figure 6A**). In contrast, following incubation with [U-^{13}C]isoleucine (**Figure 6B**), decreased glutamate labeling (M+2) in the AD neurons with APP mutation and decreased aspartate (M+2) labeling in the AD neurons with PSEN-1 mutation were found compared with the control neurons. No significant differences between the AD and control neurons were observed in glutamate or aspartate labeling after incubation with [U-^{13}C]valine (**Figure 6C**). Finally, reduced labeling in aspartate (M+3) derived from [U-^{13}C]isoleucine metabolism (*via* succinyl CoA) was found in both mutated AD neurons when compared with the control neurons (**Figure 6D**). No significant differences were found in the labeling of citrate, α-ketoglutarate, succinate, fumarate, and malate (**Supplementary Tables 4, 5**). These results demonstrate decreased ^{13}C-incorporation in aspartate (M+2 and M+3) after incubation with [U-^{13}C]isoleucine in AD neurons, suggesting that BCAA oxidative metabolism in AD hiPSC-derived neurons is largely maintained in contrast to the AD hiPSC-derived astrocytes.

Decreased Amino Acids Amounts in AD hiPSC-Derived Astrocytes and Neurons After Incubation With BCAAs

Total and labeled amounts of intracellular amino acids from the hiPSC-derived astrocytes and neurons were determined by HPLC. AD hiPSC-derived astrocytes with APP and PSEN-1 mutations showed decreased total and labeled M+2 amounts in glutamate, glutamine, and aspartate after [U-^{13}C]leucine-derived carbons entered the TCA cycle *via* acetyl CoA (**Figure 7A**). As mentioned previously, [U-^{13}C]isoleucine-derived carbons can enter the TCA cycle *via* acetyl CoA or succinyl CoA, giving rise to double labeled (M+2) or three labeled (M+3) intermediates, respectively. Labeled M+2 amounts and total amounts of aspartate were lower in the AD astrocytes with APP mutation when compared with the control astrocytes after incubation with [U-^{13}C]isoleucine (**Figure 7B**). In contrast,

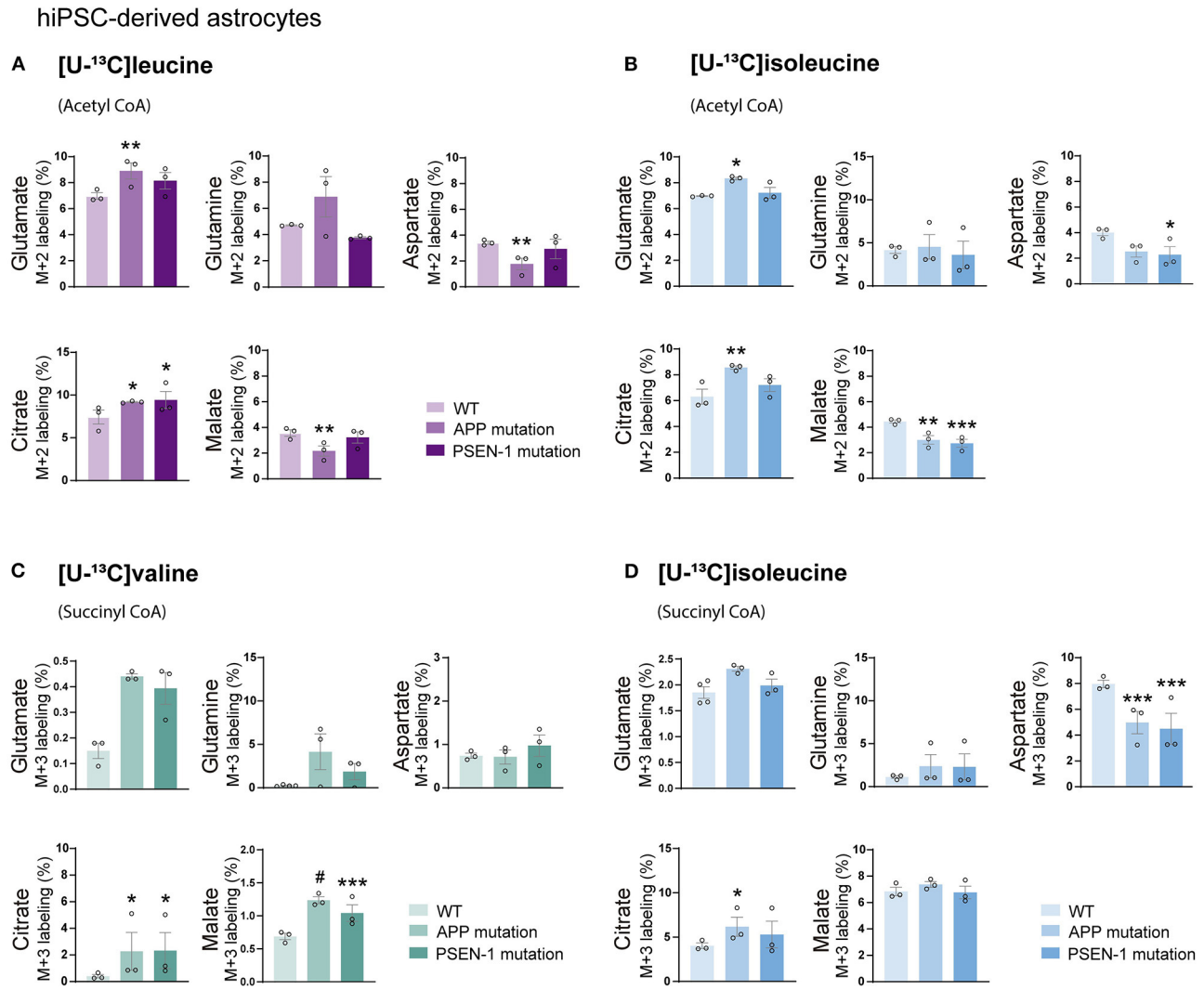

FIGURE 5 | Reduced oxidative BCAA metabolism entering as acetyl CoA in Alzheimer's disease (AD) astrocytes. **(A)** Increased glutamate and citrate M+2 labeling but decreased aspartate and malate ^{13}C-enrichment after incubation with [U-^{13}C]leucine and **(B)** [U-^{13}C]isoleucine in human AD astrocytes when entering *via* acetyl CoA. **(C)** Increased TCA cycle metabolites M+3 labeling after incubation with [U-^{13}C]valine but **(D)** decreased aspartate ^{13}C-enrichment after incubation with [U-^{13}C]isoleucine in human AD astrocytes when entering *via* succinyl CoA. Values represent mean (±) SEM ($n = 3$), $^{*}p < 0.05$, $^{**}p < 0.01$, $^{***}p < 0.001$, $^{\#}p < 0.0001$, analyzed by two-way ANOVA. WT, wild type; APP, amyloid precursor protein; PSEN-1, presenilin-1.

no differences were observed in labeled M+3 amounts of any amino acid or in the total amounts of glutamate and glutamine in both mutated AD astrocytes when compared with the control astrocytes after [U-^{13}C]isoleucine incubation. No significant differences were observed in labeled M+3 amounts of mutated AD astrocytes after [U-^{13}C]valine incubation (**Figure 7C**). However, total amounts of glutamine were lower in the AD astrocytes with APP mutation compared with control.

After incubation with [U-^{13}C]leucine, total amounts of glutamate and aspartate (**Figure 7D**) were decreased only in the AD neurons with PSEN-1 mutation compared with the control neurons. Similarly, the AD neurons with PSEN-1 mutation exhibited decreased amounts of labeled M+3 in aspartate (**Figure 7E**) after [U-^{13}C]isoleucine entry *via* succinyl CoA when compared with control. No significant differences were found in labeled or total amino acid amounts after incubation with [U-^{13}C]valine in the AD neurons when compared with the control neurons (**Figure 7F**). These results confirm that synthesis of the amino acids glutamate, glutamine, and aspartate, derived from leucine metabolism, is impaired to a larger extent compared with isoleucine and valine metabolism in AD hiPSC-derived astrocytes. Lastly, only the synthesis of aspartate derived from leucine and isoleucine metabolism was decreased in the AD hiPSC-derived neurons compared with the control neurons, which indicates that the metabolism of BCAAs is significantly affected in the AD astrocytes but generally maintained in the AD neurons.

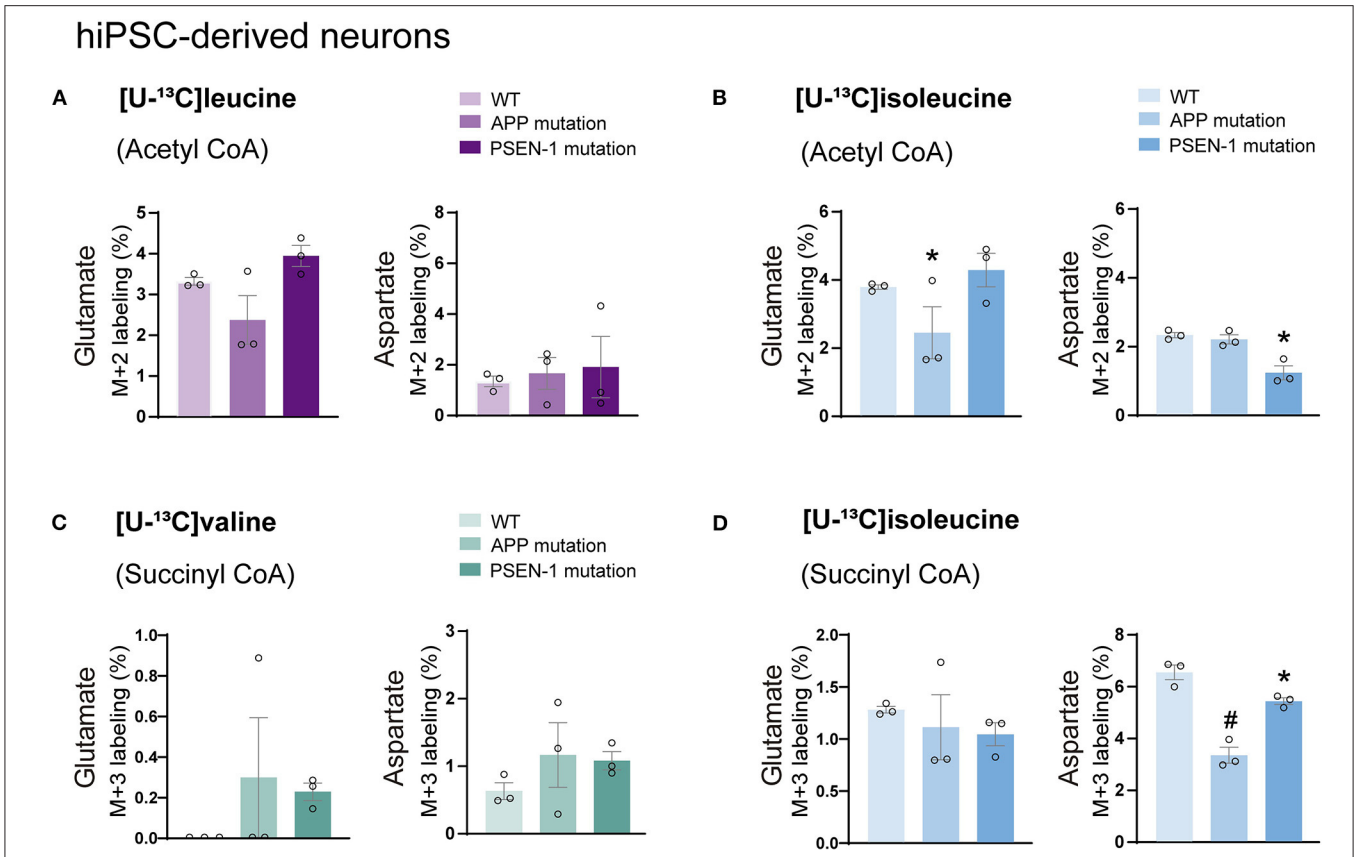

FIGURE 6 | Decreased aspartate synthesis from oxidative isoleucine metabolism in AD neurons. **(A)** No significant differences were found in AD neurons after incubation with [U-^{13}C]leucine. **(B)** Decreased glutamate M+2 and aspartate M+2 labeling after incubation with [U-^{13}C]isoleucine in AD neurons. **(C)** No significant differences were found in AD neurons after incubation with [U-^{13}C]valine in AD neurons. **(D)** Decreased aspartate M+3 labeling after incubation with [U-^{13}C]isoleucine in AD neurons when compared with control. No significant differences were found in TCA cycle intermediates. Values represent mean (±) SEM ($n = 3$), $^{*}p < 0.05$, $^{\#}p < 0.0001$ analyzed by two-way ANOVA. WT, wild type; APP, amyloid precursor protein; PSEN-1, presenilin-1.

DISCUSSION

This study represents the first functional evidence of active BCAA metabolism in human astrocytes. We found that the metabolism of the BCAA carbon skeleton supported astrocyte glutamine synthesis in acutely isolated human brain slices, which was also observed in hiPSC-derived astrocytes. Interestingly, we found reduced synthesis of amino acids derived from leucine metabolism in AD hiPSC-derived astrocytes when compared with the control astrocytes. Furthermore, the synthesis of glutamate and aspartate derived from leucine metabolism was decreased in the AD neurons with PSEN-1 mutation. Our findings are summarized in **Figure 8** along with a new proposed model of BCAA nitrogen and oxidative metabolism in the human brain.

BCAA Metabolism in Mouse and Human Brain Slices

BCAA metabolism is important for cerebral nitrogen homeostasis and neurotransmitter recycling, as these amino acids are nitrogen donors for glutamate and GABA synthesis, whereas the carbon skeleton can be utilized as oxidative fuels (Yudkoff, 1997; Conway and Hutson, 2016). From incubations of acutely isolated brain slices, we found that brain slices of both mice and humans have a large capacity for BCAA nitrogen and oxidative metabolism (**Figures 2**, **3**). Generally, we observed a higher fractional enrichment of both ^{15}N and ^{13}C in the brain slices of mice when compared with human slices, which may suggest that the rodent brain have a higher capacity for BCAA metabolism. Interestingly, immunohistochemistry studies have suggested that the cellular distribution of enzymes related to BCAA metabolism differs between the rodent and human brains (Sperringer et al., 2017). Specific isoforms of the initiating enzyme of BCAA metabolism, BCAT, have been located in both neurons (BCAT1 corresponding to BCATc) and astrocytes (BCAT2 corresponding to BCATm) in the rodent brain (Sweatt et al., 2004), whereas BCKDH was only found in neurons (Cole et al., 2012). This contrasts with the reported expression in the human brain, where both the BCAT and BCKDH expressions were found in neurons and endothelial cells, but were absent in astrocytes (Hull et al., 2012, 2018). These studies imply that both mouse and human astrocytes

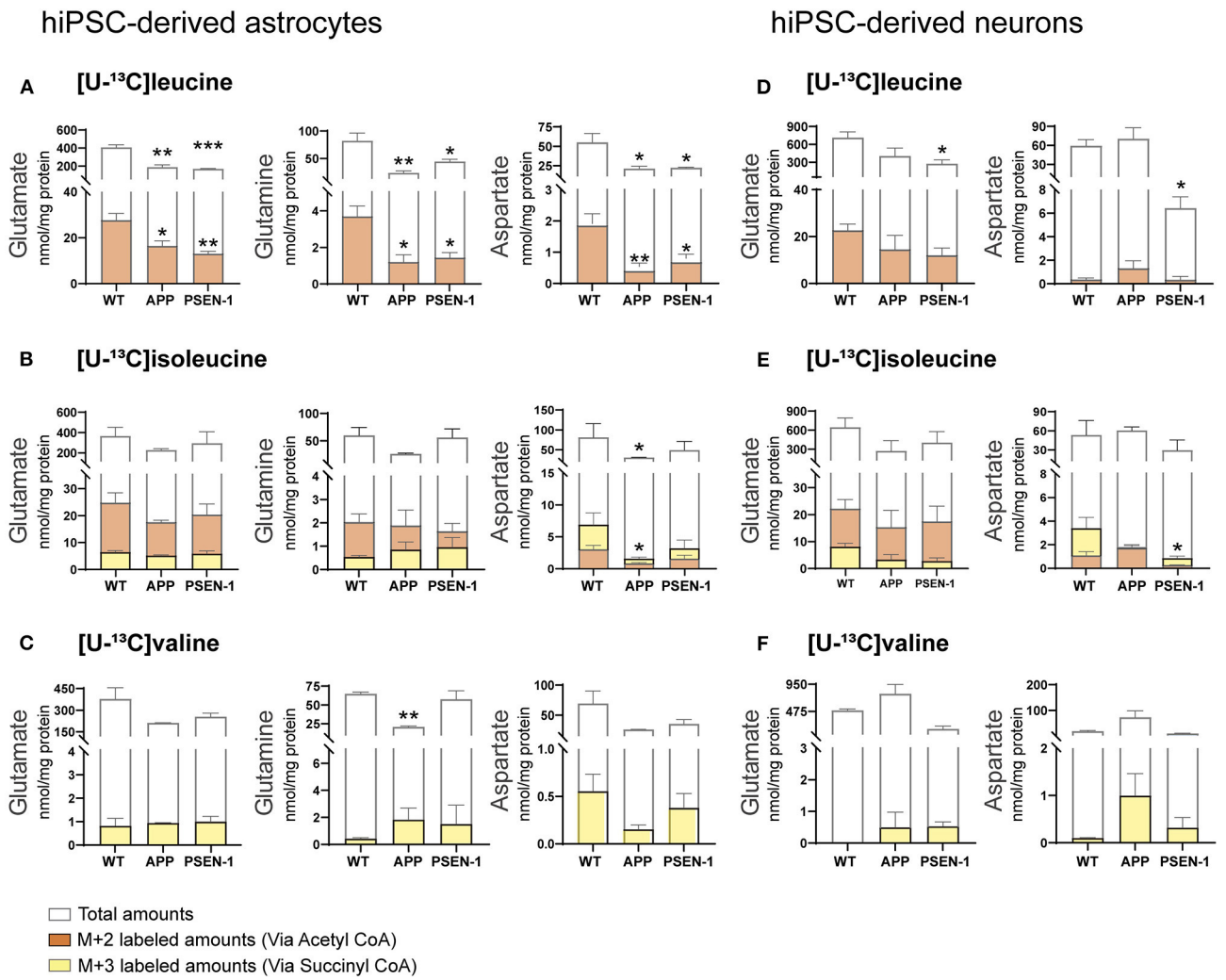

FIGURE 7 | Selective disruptions of amino acid amounts in AD astrocytes with APP and PSEN-1 mutations following incubation with [U-^{13}C]leucine. **(A)** nmol/mg protein in M+2 (*via* acetyl CoA) labeling and total amounts after incubation with [U-^{13}C]leucine. **(B)** nmol/mg protein in M+2 (*via* acetyl CoA) and M+3 (*via* succinyl CoA) labeling and total amounts after incubation with [U-^{13}C]isoleucine. **(C)** nmol/mg protein in M+3 (*via* succinyl CoA) labeling and total amounts after incubation with [U-^{13}C]valine in hiPSC-derived astrocytes. **(D)** nmol/mg protein in M+2 (*via* acetyl CoA) labeling and total amounts after incubation with [U-^{13}C]leucine. **(E)** nmol/mg protein in M+2 (*via* acetyl CoA) and M+3 (*via* succinyl CoA) labeling and total amounts after incubation with [U-^{13}C]isoleucine. **(F)** nmol/mg protein in M+3 (*via* succinyl CoA) labeling and total amounts after incubation with [U-^{13}C]valine in hiPSC-derived neurons. Values represent mean (±) SEM ($n = 3$), $^{*}p < 0.05$, $^{**}p < 0.01$, $^{***}p < 0.001$ when compared with control, analyzed by one-way ANOVA. No significant differences were found in M+3 labeling amounts in AD astrocytes. WT, wild type; APP, amyloid precursor protein; PSEN-1, presenilin-1.

have a limited enzymatic capacity for BCAA metabolism. Particularly, the complete absence of the rate-limiting enzyme BCKDH in astrocytes would imply that this cell type is unable to oxidatively metabolize the BCAA carbon skeleton in the TCA cycle. However, multiple studies using mouse astrocyte cultures have functionally shown that astrocytes are able to metabolize BCAAs (Yudkoff et al., 1996; Johansen et al., 2007; Murín et al., 2009a,b). Although most of the carbon skeleton may be released as the corresponding ketoacid or as ketone bodies (Bixel and Hamprecht, 1995; Yudkoff et al., 1996), a significant fraction enters the astrocytic TCA cycle, which will require astrocyte BCKDH activity. A recent proteomic study resolving the cellular protein expression of the mouse brain confirmed the differential expression BCATc in neurons and BCATm in astrocytes (Sharma et al., 2015). However, the same study found higher expression of the two BCKDH isoforms (BCKDHA and BCKDHB) in both cultured and isolated astrocytes when compared with neurons (Sharma et al., 2015). In the brain slices, we found the largest fractional ^{13}C-enrichment from ^{13}C-BCAA metabolism in glutamine (**Figure 3**), which is in line with a recent study by the group of the authors in a mouse model of Huntington's disease (Andersen et al., 2019). Since glutamine is exclusively synthesized in astrocytes, because of the selective expression of the enzyme glutamine

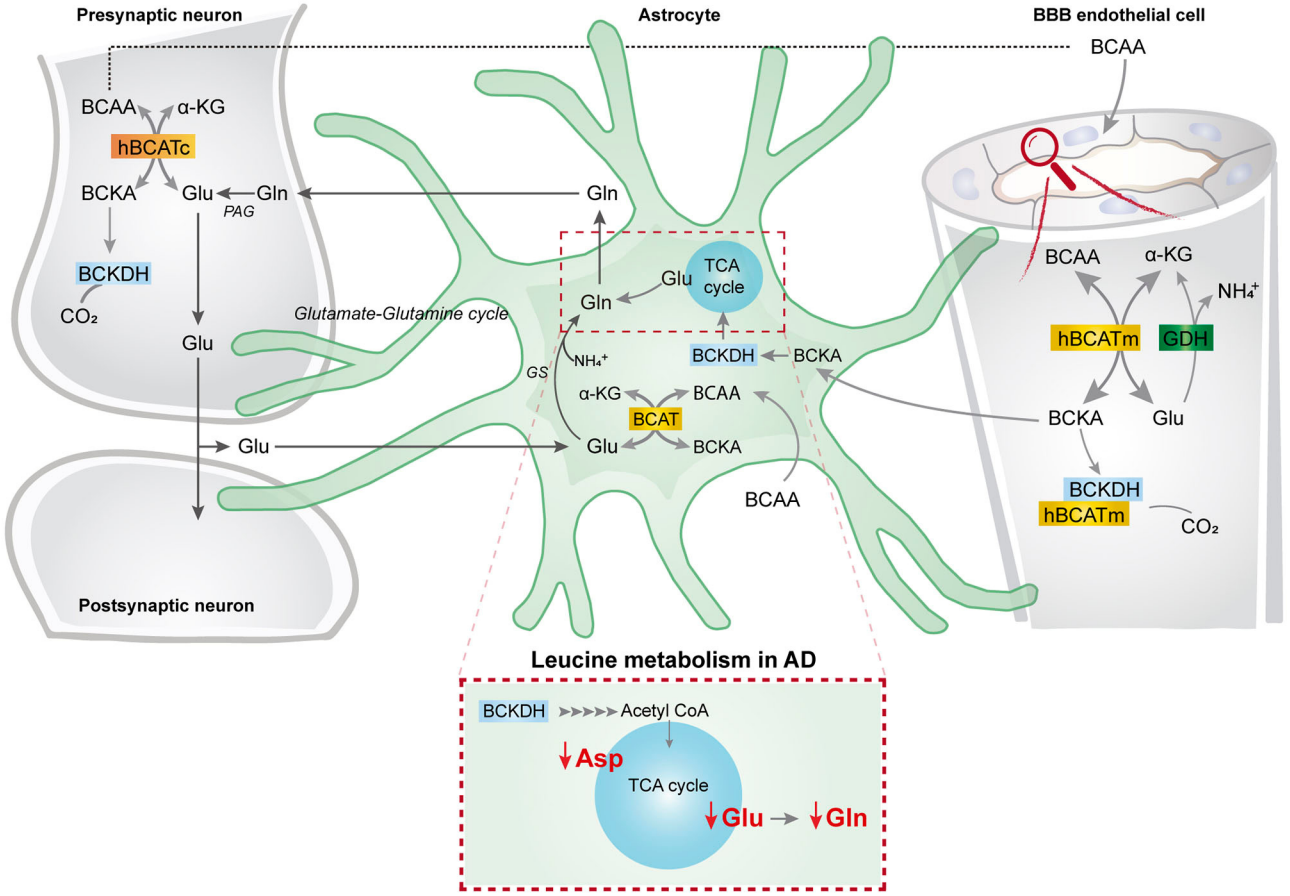

FIGURE 8 | BCAA oxidative metabolism and nitrogen transfer in human astrocytes and potential blood brain barrier-astrocyte-neuron axis. BCAAs are taken up by the blood brain barrier (BBB) endothelial cells, and then BCAAs can undergo transamination by the action of BCATm, forming glutamate and the branched-chain α-keto acids (BCKAs), KIC, KIV, and KVM. In the reverse reaction when α-ketoglutarate is formed from glutamate, the BCAT/GDH metabolon in the endothelial cells may release ammonia, and BCAAs can be released and taken up by neurons or astrocytes. Alternatively, BCKAs from endothelial cells can be released or metabolized by the BCKDH/BCATm metabolon. Likewise, in neurons, BCAAs can also be transaminated, producing BCKAs and glutamate. BCKAs can be further metabolized by BCKDH, and glutamate can be used for neurotransmission. Glutamate from neurons in the synaptic cleft can be taken up by astrocytes. Astrocytes synthesize glutamine from glutamate and ammonia which is catalyzed by glutamine synthetase (GS) and is released for neuronal uptake to replenish the glutamate pool, in the so-called glutamate-glutamine cycle. The data indicate that in astrocytes, BCAAs may be transaminated by the action of BCAT, and that the BCAA carbon skeleton can be oxidized by BCKDH activity. This set of metabolic reactions give rise to acetyl CoA or succinyl CoA, replenishing TCA cycle intermediates and amino acids in the astrocytes. Furthermore, we present evidence of reduced aspartate, glutamate, and glutamine total and labeling amounts after incubation with [U-^{13}C]leucine in AD astrocytes (represented within the dotted box). This altered leucine metabolism in AD astrocytes may contribute to the disrupted neurotransmitter homeostasis observed in the AD brain. BBB, blood brain barrier; BCATm, mitochondrial branched-chain aminotransferase; Glu, glutamate; α-KG, α-ketoglutarate, GDH, glutamate dehydrogenase, NH_4^+, ammonium; BCKA, branched-chain α-keto acids; KIC, α-ketoisocaproate; KIV, α-ketoisovaleric; KMV, α-keto-β-methylvalerate; BCAT, branched-chain aminotransferase; BCKDH, branched-chain α-keto acid dehydrogenase; Gln, glutamine; GS, glutamine synthetase; BCATc, cytosolic branched-chain aminotransferase; PAG, phosphate-activated glutaminase.

synthetase (GS) (Norenberg and Martinez-Hernandez, 1979), the large ^{13}C-enrichment in glutamine from BCAA metabolism strongly indicates active astrocyte BCAA oxidative metabolism. Furthermore, of the TCA cycle intermediates, citrate displayed the highest ^{13}C-enrichment from ^{13}C-BCAA metabolism, which is also an indicator of astrocyte metabolism in acute brain slices (Andersen et al., 2017; McNair et al., 2017). Finally, we also characterized oxidative BCAA metabolism in cultured human iPSC-derived astrocytes, where we likewise observed a conserved capacity for BCAA oxidative metabolism (**Figure 4**). Hence, the functional metabolic analyses conflict with the previous immunohistochemical investigations, and demonstrate active BCAA metabolism in both mouse and human astrocytes. The discrepancy between the functional metabolic studies and the immunohistochemical studies may be related to methodological limitations of immunohistochemistry, as discussed in (Danbolt et al., 2016).

BCAA Metabolism in AD

Branched-chain amino acid metabolism has been described to be altered in several neurological disorders. These alterations can arise from deficiencies in the expression and function

of metabolic enzymes as observed in Maple syrup urine disease, which is caused by deficiency in BCKDH and leads to severe neurological symptoms (Chuang and Chuang, 2000). Interestingly, decreased plasma and brain concentrations of BCAAs have consistently been reported in patients with Huntington's disease (HD), which correlates with disease severity (Perry et al., 1972; Mochel et al., 2011). Using a mouse model of HD, we have previously reported an elevated capacity of BCAA metabolism in cerebral cortical and striatal slices (Andersen et al., 2019). The enhanced BCAA metabolism was related to an increased expression of BCAA metabolic proteins and suggests that the reduced BCAA concentrations in HD may be due to compensatory increases in BCAA brain metabolism (Andersen et al., 2019). Evidence from both disease models and patients strongly indicate involvement of BCAA metabolism in AD pathology. For instance, it was found in patients with AD that genetic predisposition to elevated isoleucine plasma levels, but not leucine or valine, is positively associated with AD (Larsson and Markus, 2017). Furthermore, a large reduction in the concentration of valine has been detected in the cerebrospinal fluid (Basun et al., 1990) and plasma (González-domínguez et al., 2015; Toledo et al., 2017) of patients with AD patients, and the expression of hippocampal BCATc in patients with AD was increased by 28% compared with control brains (Hull et al., 2015). Interestingly, elevated BCAA levels have been found in the APP/PS1 mouse model of AD (Ruiz et al., 2016). BCAA supplementation has been shown to be beneficial in disorders with systemic elevated ammonia levels, e.g., hepatic encephalopathy (Holecek, 2018). In the periphery, BCAAs stimulate glutamine synthesis in muscles, hereby fixating ammonia (Holecek et al., 2011). In the brain, glutamine synthesis is also the primary pathway of ammonia fixation and is strictly located in astrocytes (Norenberg and Martinez-Hernandez, 1979; Brusilow et al., 2010). Interestingly, AD has been associated with elevated cerebral levels of ammonia (Seiler, 2002), which may be caused by insufficient astrocyte glutamine synthesis (Smith et al., 1991; Olabarria et al., 2011; Andersen et al., 2021a). Since glutamine is derived from the TCA cycle intermediate α-ketoglutarate *via* glutamate, astrocyte TCA cycle function is crucial for glutamine synthesis (Swanson and Graham, 1994). Multiple studies have revealed impaired astrocytic energy metabolism in AD (Oksanen et al., 2017; Dematteis et al., 2020; Andersen et al., 2021a; Ryu et al., 2021). It could, therefore, be speculated that the reduced synthesis of glutamate from oxidative leucine metabolism observed in the AD astrocytes may be caused by deficient astrocyte TCA cycle function, which may further hamper glutamine synthesis in AD. Furthermore, ammonia has been shown to inhibit oxidative astrocyte metabolism (Lerchundi et al., 2015), potentially further reducing glutamine synthesis. Further studies are needed to explore the potential link of disrupted ammonia homeostasis and BCAA metabolism in AD.

Here we found that in the AD astrocytes, the TCA cycle oxidation of leucine, isoleucine, and valine was largely maintained (**Figure 5**). However, citrate from metabolism of [U-^{13}C]leucine, [U-^{13}C]isoleucine, and [U-^{13}C]valine displayed increased ^{13}C-enrichment in AD astrocytes. It has been proposed that the astrocytic release of citrate may modulate neuronal excitability through the regulation of extracellular concentrations of Ca^{2+} and Mg^{2+} (Westergaard et al., 1994a,b). Furthermore, disruptions in brain citrate levels can alter neuronal excitability in the hippocampus, resulting in epileptic seizures (Henke et al., 2020). The results of increased citrate labeling from BCAA metabolism may reflect a supportive role of citrate transfer from astrocytes to neurons (Hertz et al., 1992).

BCAA metabolism is closely associated to the fate of glutamate. Glutamate acts as the link between neurotransmission and energy metabolism (Mckenna et al., 1996, 2019; Mckenna, 2013). Glutamate synthesis in astrocytes occurs mainly as transamination, particularly *via* aspartate aminotransferase (AAT) (Westergaard et al., 1996). The conversion of α-ketoglutarate to glutamate may depend on nitrogen from BCAAs, primarily leucine, *via* BCAT activity. It has been suggested that at least 20% of all glutamate nitrogen is derived from leucine in cultured astrocytes (Yudkoff et al., 1994). Interestingly, the results show reduced amino acid synthesis derived from leucine metabolism in AD astrocytes (**Figure 7**). Since AD astrocytes exhibited decreased amounts of glutamate derived from leucine metabolism, it can be speculated that impaired leucine nitrogen metabolism could reduce glutamate metabolic pools in the AD astrocytes. Leucine is also an efficient nitrogen donor for glutamine synthesis (Yudkoff et al., 1994, 2005). This is in line with the results showing that nitrogen metabolism of BCAAs is mainly utilized for glutamine synthesis in human and mouse cortical slices. Since glutamine is synthesized from glutamate, it can be suggested that the observed alterations in the glutamate pools could have a direct influence on glutamine synthesis, as observed in AD astrocytes. Metabolism of the BCAA carbon skeleton will result in net transfer of nitrogen to nonessential amino acids (Conway and Hutson, 2016), with the possibility of replenishing neurotransmitter pools. Interestingly, we found decreased amounts of labeling in amino acids derived from the oxidative metabolism of leucine in AD astrocytes. This reduction in amino acid synthesis derived from leucine metabolism, particularly in glutamine, could influence neurotransmitter recycling and homeostasis in AD astrocytes. Furthermore, one-third of the ^{13}C-incorporation from leucine metabolism will give rise to M+1 labeling in TCA cycle intermediates and amino acids. AD astrocytes, not AD neurons, displayed altered M+1 labeling (**Supplementary Table 6**). The labeling of succinate, malate, and aspartate (M+1) from leucine metabolism was reduced in the AD astrocytes with APP mutation. However, citrate (M+1) labeling was increased in both mutated AD astrocytes. These results further confirm that oxidative leucine metabolism is altered in AD astrocytes but maintained in AD neurons.

We found that glutamate labeling amounts from the metabolism of BCAAs in AD neurons were unaltered (**Figure 7**). However, glutamate and aspartate total amounts from leucine metabolism were decreased in the AD neurons with PSEN-1 mutation. BCAT isoforms are redox-sensitive proteins and are in their reduced form part of a metabolon with glutamate dehydrogenase (GDH) catalyzing the conversion of glutamate into α-ketoglutarate (Conway et al., 2002, 2004, 2008). An

increase in oxidative stress (OS) might change the redox status, preventing this metabolon formation (Harris et al., 2020). The reduced glutamate and aspartate total amounts observed in AD neurons may be due to changes in the redox state of BCAT, causing reduced amino acid synthesis. Furthermore, leucine is a positive allosteric modulator of GDH activity (Li et al., 2011), and changes in leucine amounts may hereby perturb glutamate homeostasis *via* GDH activity in AD. Imbalanced redox states, caused by an excessive accumulation of reactive oxygen species (ROS) and a decrease in antioxidant enzymes, leads to OS in AD (Zhao and Zhao, 2013; Wang et al., 2014; Kim et al., 2015). Alterations in glutathione (GSH), the most abundant brain antioxidant, have been described to be reduced in patients with AD (Mandal et al., 2012, 2015; Saharan and Mandal, 2014). In several studies using different AD models, OS can also be induced by Aβ accumulation (Pappolla et al., 1998; Butterfield, 2002; Cheignon et al., 2018), which could eventually lead to mitochondrial dysfunction (Zhao and Zhao, 2013; Wang et al., 2014). Alterations in the mitochondria might represent the major source of OS observed in AD (Castellani et al., 2002; Wang et al., 2014), since the majority of endogenous ROS is produced by the mitochondria (Wang et al., 2014). These alterations in OS could contribute further to mitochondrial impairments, such as metabolic imbalances.

Branched-chain amino acids also have a regulatory role in the mammalian target of rapamycin (mTOR) pathway. The mTOR pathway is an environmental sensor, which regulates cell proliferation, protein synthesis, and autophagy through multiple signaling pathways (Jewell et al., 2015; Shafei et al., 2017; Liu and Sabatini, 2020). mTOR constitutes the catalytic subunit of two distinct complexes (Shafei et al., 2017). mTOR complex 1 (mTORC1) plays a role in neuronal synaptic plasticity and phosphorylates substrates to promote synthesis of proteins, lipids, nucleotides, etc., while repressing the autophagic breakdown of cellular components. mTORC1 activation is regulated by nutrients such as several amino acids, particularly leucine and arginine (Liu and Sabatini, 2020). Depletion of amino acids, low glucose concentrations, and OS can negatively impact mTORC1 regulation while stimulating autophagy (Shafei et al., 2017). Some studies have reported that mitochondrial ROS are increased by high concentrations of BCAAs in human endothelial and peripheral blood cells (Zhenyukh et al., 2017, 2018). However, inhibition of the mTORC1 pathway, decreased BCAAs-induced pro-oxidant effects. Likewise, alterations in mTORC1 regulation in AD pathology may result in accumulation of amyloid-β (Aβ) aggregates. Increased mTOR activity and signaling were found in APP-transfected cell lines and in brains of 3xTg-AD mice (Caccamo et al., 2010, 2011). Interestingly, mTOR activity was reduced when preventing Aβ accumulation in the 3xTg-AD mice. Apparently, high Aβ levels can exert toxicity through increased mTOR activity. In addition, the use of rapamycin ameliorated cognitive deficits, and Aβ and Tau pathology in 3xTg-AD mice by increasing autophagy (Caccamo et al., 2010). It has been suggested that the alteration of mTOR signaling and autophagy occurs at early stages of AD. The status of the mTOR pathway in AD post-mortem brain tissue has been investigated, where increased reduction in autophagy was observed as the disease progressed (Tramutola et al., 2015). Since leucine regulates the mTOR pathway, mTOR signaling in AD astrocytes could be impaired, leading to reduction in amino acids pools. Leucine metabolism appears to be more affected in AD astrocytes than in AD neurons. It can be speculated that the metabolic alterations in astrocytes may be an early event in AD progression, possibly influencing neuronal metabolic and neurotransmitter homeostasis. The findings demonstrate reduced amino acid synthesis derived from leucine metabolism in AD astrocytes, possibly contributing further to neurotransmitter imbalances involved in AD.

Together, the results demonstrate extensive branched-chain amino acid metabolism in human astrocytes, identify disturbances in their metabolism in an AD pathological context, and highlight the need for further investigation on branched-chain amino acids metabolism, particularly in astrocytes, to possibly unravel additional pathological mechanisms implicated in neurodegenerative diseases.

DATA AVAILABILITY STATEMENT

The raw data supporting the conclusions of this article will be made available by the authors, without undue reservation.

ETHICS STATEMENT

The studies involving human participants were reviewed and approved by the local Ethics Committee in Copenhagen (H-2-2011-104). The patients/participants provided their written informed consent to participate in this study. The animal study was reviewed and approved by the Danish National Ethics Committee and performed according to the European Convention (ETS 123 of 1986).

AUTHOR CONTRIBUTIONS

BA, CS, and JA: study concept and design. LP provided the brain tissue from patients. CS, KV, and JA: acquisition of data. CS, BA, KV, and JA: analysis and interpretation of data and drafting of the manuscript. BA, KF, HW, JA, and LP: critical revision of the manuscript for intellectual content. CS: statistical analysis. BA, JA, HW, and KF: obtained funding. BA, KF, and HW: study supervision. All authors contributed to the article and approved the submitted version.

FUNDING

This study was supported by grants from The National Council of Science and Technology (CONACYT), (PhD Grant No: 2018-000009-01EXTF-00121 to CS), The Scholarship of Peter & Emma Thomsen (to JA), Aase and Ejnar Danielsen Foundation (Grant No: 10-002028 to JA), the Augustinus Foundation (Grant No: 17-4115 to JA), and Innovation Fund Denmark Brainstem (Grant No: 4108-00008B) and NeuroStem (to KF).

ACKNOWLEDGMENTS

The authors would like to thank Henriette Haukedal (KF lab) for providing some of the NPCs used in this project.

SUPPLEMENTARY MATERIAL

The Supplementary Material for this article can be found online at: https://www.frontiersin.org/articles/10.3389/fnagi.2021.736580/full#supplementary-material

REFERENCES

Acosta, C., Anderson, H. D., and Anderson, C. M. (2017). Astrocyte dysfunction in Alzheimer disease. *J. Neurosci. Res.* 95, 2430–2447. doi: 10.1002/jnr.24075

Aldana, B. I. (2019). Microglia-specific metabolic changes in neurodegeneration. *J. Mol. Biol.* 431, 1830–1842. doi: 10.1016/j.jmb.2019.03.006

Andersen, J. V., Christensen, S., Westi, E., Diaz-delCastillo, M., Tanila, H., Schousboe, A., et al. (2021a). Deficient astrocyte metabolism impairs glutamine synthesis and neurotransmitter homeostasis in a mouse model of Alzheimer's disease. *Neurobiol. Dis.* 148:105198. doi: 10.1016/j.nbd.2020.105198

Andersen, J. V., Jakobsen, E., Westi, E. W., Lie, M. E. K., Voss, C. M., Aldana, B. I., et al. (2020). Extensive astrocyte metabolism of γ-aminobutyric acid (GABA) sustains glutamine synthesis in the mammalian cerebral cortex. *Glia* 68, 2601–2612. doi: 10.1002/glia.23872

Andersen, J. V., Markussen, K. H., Jakobsen, E., Schousboe, A., Waagepetersen, H. S., Rosenberg, P. A., et al. (2021b). Glutamate metabolism and recycling at the excitatory synapse in health and neurodegeneration. *Neuropharmacology* 14:108719. doi: 10.1016/j.neuropharm.2021.108719

Andersen, J. V., McNair, L. F., Schousboe, A., and Waagepetersen, H. S. (2017). Specificity of exogenous acetate and glutamate as astrocyte substrates examined in acute brain slices from female mice using methionine sulfoximine (MSO) to inhibit glutamine synthesis. *J. Neurosci. Res.* 95, 2207–2216. doi: 10.1002/jnr.24038

Andersen, J. V., Skotte, N. H., Aldana, B. I., Nørremølle, A., and Waagepetersen, H. S. (2019). Enhanced cerebral branched-chain amino acid metabolism in R6/2 mouse model of Huntington's disease. *Cell. Mol. Life Sci.* 76, 2449–2461. doi: 10.1007/s00018-019-03051-2

Basun, H., Forssell, L., Almkvist, O., Cowburn, R., Eklof, R., Winblad, B., et al. (1990). Amino acid concentrations in cerebrospinal fluid and plasma in Alzheimer's disease and healthy control subjects. *J Neural Transm Park Dis Dement Sect* 2, 295–304. doi: 10.1007/BF02252924

Biemann, K., and McCloskey, J. A. (1962). Application of mass spectrometry to structure problems.1 VI. Nucleosides. *J. Am. Chem. Soc.* 84, 2005–2007. doi: 10.1021/ja00869a048

Bixel, M. G., and Hamprecht, B. (1995). Generation of ketone bodies from leucine by cultured astroglial cells. *J. Neurochem.* 65, 2450–2461. doi: 10.1046/j.1471-4159.1995.65062450.x

Bogetofte, H., Jensen, P., Ryding, M., Schmidt, S. I., Okarmus, J., Ritter, L., et al. (2019). PARK2 mutation causes metabolic disturbances and impaired survival of human iPSC-derived neurons. *Front. Cell. Neurosci.* 13:297. doi: 10.3389/fncel.2019.00297

Braak, H., and Braak, E. (1991). Neuropathological stageing of Alzheimer-related changes. *Acta Neuropathol.* 82, 239–259. doi: 10.1007/BF00308809

Brekke, E., Morken, T. S., Walls, A. B., Waagepetersen, H., Schousboe, A., and Sonnewald, U. (2016). Anaplerosis for glutamate synthesis in the neonate and in adulthood. *Adv. Neurobiol.* 4:3. doi: 10.1007/978-3-319-45096-4_3

Brusilow, S. W., Koehler, R. C., Traystman, R. J., and Cooper, A. J. L. (2010). Astrocyte glutamine synthetase: importance in hyperammonemic syndromes and potential target for therapy. *Neurotherapeutics* 7, 452–470. doi: 10.1016/j.nurt.2010.05.015

Butterfield, D. A. (2002). Amyloid β-peptide (1-42)-induced oxidative stress and neurotoxicity: Implications for neurodegeneration in Alzheimer's disease brain. A review. *Free Radic. Res.* 36, 1307–1313. doi: 10.1080/1071576021000049890

Butterfield, D. A., and Halliwell, B. (2019). Oxidative stress, dysfunctional glucose metabolism and Alzheimer disease. *Nat. Rev. Neurosci.* 20, 148–160. doi: 10.1038/s41583-019-0132-6

Caccamo, A., Majumder, S., Richardson, A., Strong, R., and Oddo, S. (2010). Molecular Interplay between Mammalian Target of Rapamycin (mTOR), Amyloid- β, and Tau: effects on cognitive impairments. *J. Biol. Chem.* 285, 13107–13120. doi: 10.1074/jbc.M110.100420

Caccamo, A., Maldonado, M. A., Majumder, S., Medina, D. X., Holbein, W., Magrí, A., et al. (2011). Naturally secreted amyloid-β increases mammalian target of rapamycin (mTOR) activity *via* a PRAS40-mediated. *J. Biol. Chem.* 286, 8924–8932. doi: 10.1074/jbc.M110.180638

Castellani, R., Hirai, K., Aliev, G., Drew, K. L., Nunomura, A., Takeda, A., et al. (2002). Role of mitochondrial dysfunction in Alzheimer's disease. *J. Neurosci. Res.* 70, 357–360. doi: 10.1002/jnr.10389

Chandrasekaran, A., Avci, H. X., Ochalek, A., Rösingh, L. N., Molnár, K., László, L., et al. (2017). Comparison of 2D and 3D neural induction methods for the generation of neural progenitor cells from human induced pluripotent stem cells. *Stem Cell Res.* 25, 139–151. doi: 10.1016/j.scr.2017.10.010

Cheignon, C., Tomas, M., Bonnefont-Rousselot, D., Faller, P., Hureau, C., and Collin, F. (2018). Oxidative stress and the amyloid beta peptide in Alzheimer's disease. *Redox Biol.* 14, 450–464. doi: 10.1016/j.redox.2017.10.014

Chuang, J. L., and Chuang, D. T. (2000). Diagnosis and mutational analysis of maple syrup urine disease using cell cultures. *Methods Enzymol.* 324, 413–423. doi: 10.1016/S0076-6879(00)24250-X

Cole, J. T., Sweatt, A. J., and Hutson, S. M. (2012). Expression of mitochondrial branched-chain aminotransferase and α-keto-acid dehydrogenase in rat brain: implications for neurotransmitter metabolism. *Front. Neuroanat.* 6:18. doi: 10.3389/fnana.2012.00018

Conway, M. E. (2020). Alzheimer's disease: targeting the glutamatergic system. *Biogerontology* 21, 257–274. doi: 10.1007/s10522-020-09860-4

Conway, M. E., Coles, S. J., Islam, M. M., and Hutson, S. M. (2008). Regulatory control of human cytosolic branched-chain aminotransferase by oxidation and S-glutathionylation and its interactions with redox sensitive neuronal proteins. *Biochemistry* 47, 5465–5479. doi: 10.1021/bi800303h

Conway, M. E., and Hutson, S. M. (2016). BCAA metabolism and NH3 homeostasis. *Adv. Neurobiol.* 13, 99–132. doi: 10.1007/978-3-319-45096-4_5

Conway, M. E., Poole, L. B., and Hutson, S. M. (2004). Roles for cysteine residues in the regulatory CXXC motif of human mitochondrial branched chain aminotransferase enzyme. *Biochemistry* 43, 7356–7364. doi: 10.1021/bi0498050

Conway, M. E., Yennawar, N., Wallin, R., Poole, L. B., and Hutson, S. M. (2002). Identification of a peroxide-sensitive redox switch at the CXXC motif in the human mitochondrial branched chain aminotransferase. *Biochemistry* 41, 9070–9078. doi: 10.1021/bi020200i

Cunnane, S. C., Trushina, E., Morland, C., Prigione, A., Casadesus, G., Andrews, Z. B., et al. (2020). Brain energy rescue: an emerging therapeutic concept for neurodegenerative disorders of ageing. *Nat. Rev. Drug Discov.* 19, 609–633. doi: 10.1038/s41573-020-0072-x

Danbolt, N. C., Zhou, Y., Furness, D. N., and Holmseth, S. (2016). Strategies for immunohistochemical protein localization using antibodies : what did we learn from neurotransmitter transporters in glial cells and neurons. *Glia* 64, 2045–2064. doi: 10.1002/glia.23027

De Strooper, B., and Karran, E. (2016). The cellular phase of Alzheimer's disease. *Cell* 164, 603–615. doi: 10.1016/j.cell.2015.12.056

Dematteis, G., Vydmantaite, G., Ruffinatti, F. A., Chahin, M., Farruggio, S., Barberis, E., et al. (2020). Proteomic analysis links alterations of bioenergetics, mitochondria-ER interactions and proteostasis in hippocampal astrocytes from 3xTg-AD mice. *Cell Death Dis.* 11, 1–16. doi: 10.1038/s41419-020-02911-1

Frederiksen, H. R., Holst, B., Mau-Holzmann, U. A., Freude, K., and Schmid, B. (2019a). Generation of two isogenic iPSC lines with either a heterozygous or a homozygous E280A mutation in the PSEN1 gene. *Stem Cell Res.* 35:101403. doi: 10.1016/j.scr.2019.101403

Frederiksen, H. R., Holst, B., Ramakrishna, S., Muddashetty, R., Schmid, B., and Freude, K. (2019b). Generation of two iPSC lines with either a heterozygous

V717I or a heterozygous KM670/671NL mutation in the APP gene. *Stem Cell Res.* 34:101368. doi: 10.1016/j.scr.2018.101368

González-domínguez, R., García-barrera, T., and Gómez-Ariza, J. L. (2015). Metabolite profiling for the identification of altered metabolic pathways in Alzheimer's disease. *J. Pharm. Biomed. Anal.* 107, 75–81. doi: 10.1016/j.jpba.2014.10.010

Gordon, B. A., Blazey, T. M., Su, Y., Hari-Raj, A., Dincer, A., Flores, S., et al. (2018). Spatial patterns of neuroimaging biomarker change in individuals from families with autosomal dominant Alzheimer's disease: a longitudinal study. *Lancet Neurol.* 17, 241–250. doi: 10.1016/S1474-4422(18)30028-0

Harris, M., Hindy, M., El, Usmari-moraes, M., Hudd, F., Shafei, M., Dong, M., et al. (2020). BCAT-induced autophagy regulates Aβ load through an interdependence of redox state and PKC phosphorylation-implications in Alzheimer 's disease. *Free Radic. Biol. Med.* 152, 755–766. doi: 10.1016/j.freeradbiomed.2020.01.019

Henke, C., Töllner, K., van Dijk, R. M., Miljanovic, N., Cordes, T., Twele, F., et al. (2020). Disruption of the sodium-dependent citrate transporter SLC13A5 in mice causes alterations in brain citrate levels and neuronal network excitability in the hippocampus. *Neurobiol. Dis.* 143:105018. doi: 10.1016/j.nbd.2020.105018

Hertz, L., Yu, A. C. H., and Schousboe, A. (1992). Uptake and metabolism of malate in neurons and astrocytes in primary cultures. *J. Neurosci. Res.* 33, 289–296. doi: 10.1002/jnr.490330212

Holecek, M. (2018). Branched-chain amino acids in health and disease: metabolism, alterations in blood plasma, and as supplements. *Nutr. Metab.* 15, 1–12. doi: 10.1186/s12986-018-0271-1

Holecek, M., Kandar, R., Sispera, L., and Kovarik, M. (2011). Acute hyperammonemia activates branched-chain amino acid catabolism and decreases their extracellular concentrations: different sensitivity of red and white muscle. *Amino Acids* 2, 575–584. doi: 10.1007/s00726-010-0679-z

Hull, J., Hindy, M., El Kehoe, P., Chalmers, K., Love, S., and Conway, M. E. (2012). Distribution of the branched chain aminotransferase proteins in the human brain and their role in glutamate regulation. *J. Neurochem.* 123, 997–1009. doi: 10.1111/jnc.12044

Hull, J., Patel, V. B., Hutson, S. M., and Conway, M. E. (2015). New insights into the role of the branched-chain aminotransferase proteins in the human brain. *J. Neurosci. Res.* 93, 987–998. doi: 10.1002/jnr.23558

Hull, J., Usmari, M., Brookes, E., Love, S., and Conway, M. E. (2018). Distribution of the branched-chain α-ketoacid dehydrogenase complex E1α subunit and glutamate dehydrogenase in the human brain and their role in neuro-metabolism. *Neurochem. Int.* 112, 49–58. doi: 10.1016/j.neuint.2017.10.014

Jewell, J. J., Kim, Y. C., Russell, R. C., Yu, F.-X., Park, H. W., Plouffe, S. W., et al. (2015). Differential regulation of mTORC1 by leucine and glutamine. *Science* 347, 194–198. doi: 10.1126/science.1259472

Johansen, M. L., Bak, L. K., Schousboe, A., Iversen, P., Sørensen, M., Keiding, S., et al. (2007). The metabolic role of isoleucine in detoxification of ammonia in cultured mouse neurons and astrocytes. *Neurochem. Int.* 50, 1042–1051. doi: 10.1016/j.neuint.2007.01.009

Kim, G. H., Kim, J. E., Rhie, S. J., and Yoon, S. (2015). The role of oxidative stress in neurodegenerative diseases. *Exp. Neurobiol.* 24, 325–340. doi: 10.5607/en.2015.24.4.325

Larsson, S. C., and Markus, H. S. (2017). Branched-chain amino acids and Alzheimer's disease: a Mendelian randomization analysis. *Sci. Rep.* 7:13604. doi: 10.1038/s41598-017-12931-1

Leng, F., and Edison, P. (2021). Neuroinflammation and microglial activation in Alzheimer disease: where do we go from here? *Nat. Rev. Neurol.* 17, 157–172. doi: 10.1038/s41582-020-00435-y

Lerchundi, R., Fernández-Moncada, I., Contreras-Baeza, Y., Sotelo-Hitschfeld, T., Machler, P., Wyss, M. T., et al. (2015). NH4(+) triggers the release of astrocytic lactate *via* mitochondrial pyruvate shunting. *Proc. Natl. Acad. Sci. U. S. A.* 112, 11090–11095. doi: 10.1073/pnas.1508259112

Li, M., Li, C., Allen, A., Stanley, C. A., and Smith, T. J. (2011). The structure and allosteric regulation of glutamate dehydrogenase. *Neurochem. Int.* 59, 445–455. doi: 10.1016/j.neuint.2010.10.017

Liu, G. Y., and Sabatini, D. M. (2020). mTOR at the nexus of nutrition, growth, ageing and disease. *Nat. Rev. Mol. Cell Biol.* 21, 183–203. doi: 10.1038/s41580-019-0199-y

Liu, J., Chang, L., Song, Y., Li, H., and Wu, Y. (2019). The role of NMDA receptors in Alzheimer's disease. *Front. Neurosci.* 13:43. doi: 10.3389/fnins.2019.00043

Mandal, P. K., Saharan, S., Tripathi, M., and Murari, G. (2015). Brain glutathione levels - a novel biomarker for mild cognitive impairment and Alzheimer's disease. *Biol. Psychiatry* 78, 702–710. doi: 10.1016/j.biopsych.2015.04.005

Mandal, P. K., Tripathi, M., and Sugunan, S. (2012). Brain oxidative stress: detection and mapping of anti-oxidant marker "Glutathione" in different brain regions of healthy male/female, MCI and Alzheimer patients using non-invasive magnetic resonance spectroscopy. *Biochem. Biophys. Res. Commun.* 417, 43–48. doi: 10.1016/j.bbrc.2011.11.047

Mckenna, M. C. (2013). Glutamate pays its own way in astrocytes. *Front. Endocrinol.* 4:191. doi: 10.3389/fendo.2013.00191

Mckenna, M. C., Schuck, P. F., and Ferreira, G. C. (2019). Fundamentals of CNS energy metabolism and alterations in lysosomal storage diseases. *J. Neurochem.* 148, 590–599. doi: 10.1111/jnc.14577

Mckenna, M. C., Sonnewald, U., Huang, X., Stevenson, J., and Zielke, H. R. (1996). Exogenous glutamate concentration regulates the metabolic fate of glutamate in astrocytes. *J. Neurochem.* 66, 386–393. doi: 10.1046/j.1471-4159.1996.66010386.x

McNair, L. F., Kornfelt, R., Walls, A. B., Andersen, J. V., Aldana, B. I., Nissen, J. D., et al. (2017). Metabolic characterization of acutely isolated hippocampal and cerebral cortical slices using [U-13C]glucose and [1,2-13C]acetate as substrates. *Neurochem. Res.* 42, 810–826. doi: 10.1007/s11064-016-2116-5

Mochel, F., Benaich, S., Rabier, D., and Durr, A. (2011). Validation of plasma branched chain amino acids as biomarkers in Huntington disease. *Arch. Neurol.* 68, 265–267. doi: 10.1001/archneurol.2010.358

Murín, R., Mohammadi, G., Leibfritz, D., and Hamprecht, B. (2009a). Glial metabolism of isoleucine. *Neurochem. Res.* 34, 194–204. doi: 10.1007/s11064-008-9840-4

Murín, R., Mohammadi, G., Leibfritz, D., and Hamprecht, B. (2009b). Glial metabolism of valine. *Neurochem. Res.* 34, 1195–1203. doi: 10.1007/s11064-008-9895-2

Norenberg, M. D., and Martinez-Hernandez, A. (1979). Fine structural localization of glutamine synthetase in astrocytes of rat brain. *Brain Res.* 161, 303–310. doi: 10.1016/0006-8993(79)90071-4

Oksanen, M., Petersen, A. J., Naumenko, N., Puttonen, K., Saraja, T., Viitanen, M., et al. (2017). PSEN1 mutant iPSC-derived model reveals severe astrocyte pathology in Alzheimer's disease. *Stem Cell Reports* 9, 1885–1897. doi: 10.1016/j.stemcr.2017.10.016

Olabarria, M., Noristani, H. N., Verkhratsky, A., and Rodríguez, J. J. (2011). Age-dependent decrease in glutamine synthetase expression in the hippocampal astroglia of the triple transgenic Alzheimer's disease mouse model: mechanism for deficient glutamatergic transmission? *Mol. Neurodegener.* 6, 1–9. doi: 10.1186/1750-1326-6-55

Pappolla, M. A., Chyan, Y. J., Omar, R. A., Hsiao, K., Perry, G., Smith, M. A., et al. (1998). Evidence of oxidative stress and *in vivo* neurotoxicity of β-amyloid in a transgenic mouse model of Alzheimer's disease: a chronic oxidative paradigm for testing antioxidant therapies *in vivo*. *Am. J. Pathol.* 152, 871–877.

Perry, T. L., Hansen, S., and Lesk, D. (1972). Plasma amino acid levels in children of patients with Huntington's chorea. *Neurology* 22, 68–70. doi: 10.1212/WNL.22.1.68

Ruiz, H. H., Chi, T., Shin, A. C., Lindtner, C., Hsieh, W., Ehrlich, M., et al. (2016). Increased susceptibility to metabolic dysregulation in a mouse model of Alzheimer's disease is associated with impaired hypothalamic insulin signaling and elevated BCAA levels. *Alzheimer's Dement.* 12, 851–861. doi: 10.1016/j.jalz.2016.01.008

Ryu, W., Bormann, M. K., Shen, M., Kim, D., Forester, B., Park, Y., et al. (2021). Brain cells derived from Alzheimer's disease patients have multiple specific innate abnormalities in energy metabolism. *Mol. Psychiatry*. doi: 10.1038/s41380-021-01068-3. [Epub ahead of print].

Saharan, S., and Mandal, P. K. (2014). The emerging role of glutathione in Alzheimer's disease. *J. Alzheimer's Dis.* 40, 519–529. doi: 10.3233/JAD-132483

Salcedo, C., Wagner, A., Andersen, J. V., Vinten, K. T., Waagepetersen, H. S., Schousboe, A., et al. (2021). Downregulation of GABA transporter 3 (GAT3) is associated with deficient oxidative GABA metabolism in human induced pluripotent stem cell-derived astrocytes in Alzheimer's disease. *Neurochem. Res.* doi: 10.1007/s11064-021-03276-3. [Epub ahead of print].

Schousboe, A., Bak, L. K., and Waagepetersen, H. S. (2013). Astrocytic control of biosynthesis and turnover of the neurotransmitters glutamate and GABA. *Front. Endocrinol.* 4:102. doi: 10.3389/fendo.2013.00102

Seiler, N. (2002). Ammonia and Alzheimer's disease. *Neurochem. Int.* 41, 189–207. doi: 10.1016/S0197-0186(02)00041-4

Shafei, M. A., Harris, M., and Conway, M. E. (2017). Divergent metabolic regulation of autophagy and mTORC1—early events in Alzheimer's disease? *Front. Aging Neurosci.* 9:173. doi: 10.3389/fnagi.2017.00173

Shaltouki, A., Peng, J., Liu, Q., Rao, M. S., and Zeng, X. (2013). Efficient generation of astrocytes from human pluripotent stem cells in defined conditions. *Stem Cells* 5, 941–952. doi: 10.1002/stem.1334

Sharma, K., Schmitt, S., Bergner, C. G., Tyanova, S., Kannaiyan, N., Manrique-Hoyos, N., et al. (2015). Cell type – and brain region – resolved mouse brain proteome. *Nat. Neurosci.* 18, 1819–1831. doi: 10.1038/nn.4160

Shen, J. (2013). Modeling the glutamate-glutamine neurotransmitter cycle. *Front. Neuroenerget.* 5:1. doi: 10.3389/fnene.2013.00001

Smith, C. D., Carney, J. M., Starke-Reed, P. E., Oliver, C. N., Stadtman, E. R., Floyd, R. A., et al. (1991). Excess brain protein oxidation and enzyme dysfunction in normal aging and in Alzheimer disease. *Proc. Natl. Acad. Sci. U. S. A.* 88, 10540–10543. doi: 10.1073/pnas.88.23.10540

Sperringer, J. E., Addington, A., and Hutson, S. M. (2017). Branched-chain amino acids and brain metabolism. *Neurochem. Res.* 42, 1697–1709. doi: 10.1007/s11064-017-2261-5

Swanson, R. A., and Graham, S. H. (1994). Fluorocitrate and fluoroacetate effects on astrocyte metabolism *in vitro*. *Brain Res.* 664, 94–100. doi: 10.1016/0006-8993(94)91958-5

Sweatt, A. J., Garcia-Espinosa, M. A., Wallin, R., and Hutson, S. M. (2004). Branched-chain amino acids and neurotransmitter metabolism: expression of cytosolic branched-chain aminotransferase (BCATC) in the cerebellum and hippocampus. *J. Comp. Neurol.* 477, 360–370. doi: 10.1002/cne.20200

Tani, H., Dulla, C. G., Farzampour, Z., Taylor-Weiner, A., Huguenard, J. R., and Reimer, R. J. (2014). A local glutamate-glutamine cycle sustains synaptic excitatory transmitter release. *Neuron* 81, 888–900. doi: 10.1016/j.neuron.2013.12.026

Toledo, J. B., Arnold, M., Chang, R., Rebecca, A., Han, X., Thambisetty, M., et al. (2017). Metabolic network failures in Alzheimer's disease: a biochemical road map. *Alzheimer's Dement.* 13, 965–984. doi: 10.1016/j.jalz.2017.01.020

Tramutola, A., Triplett, J. C., Di Domenico, F., Niedowicz, D. M., Murphy, M. P., Coccia, R., et al. (2015). Alteration of mTOR signaling occurs early in the progression of Alzheimer disease (AD): analysis of brain from subjects with pre-clinical AD, amnestic mild cognitive impairment and late-stage AD. *J. Neurochem.* 133, 739–749. doi: 10.1111/jnc.13037

Walls, B. A., Bak, L. K., Sonnewald, U., Schousboe, A., and Waagepetersen, H. S. (2014). Metabolic mapping of astrocytes and neurons in culture using stable isotopes and gas chromatography-mass spectrometry (GC-MS), chapter 4 in "brain energy metabolism." *J. Am. Chem. Soc.* 90, 73–105. doi: 10.1007/978-1-4939-1059-5_4

Wang, X., Wang, W., Li, L., Perry, G., Lee, H., and Zhu, X. (2014). Oxidative stress and mitochondrial dysfunction in Alzheimer's disease. *Biochim. Biophys. Acta* 1842, 1240–1247. doi: 10.1016/j.bbadis.2013.10.015

Westergaard, N., Drejer, J., Schousboe, A., and Sonnewald, U. (1996). Evaluation of the importance of transamination vs. deamination in astrocytic metabolism of [U-13C] glutamate. *Glia* 17, 160–168. doi: 10.1002/(SICI)1098-1136(199606)17:2<160::AID-GLIA7>3.0.CO;2-6

Westergaard, N., Sonnewald, U., and Schousboe, A. (1994a). Release of alpha-ketoglutarate, malate and succinate from cultured astrocytes: possible role in amino acid neurotransmitter homeostasis. *Neurosci. Lett.* 176, 105–109.

Westergaard, N., Sonnewald, U., Unsgård, G., Peng, L., Hertz, L., and Schousboe, A. (1994b). Uptake, release, and metabolism of citrate in neurons and astrocytes in primary cultures. *J. Neurochem.* 62, 1727–1733.

Winblad, B., Amouyel, P., Andrieu, S., Ballard, C., Brayne, C., Brodaty, H., et al. (2016). Defeating Alzheimer's disease and other dementias: a priority for European science and society. *Lancet Neurol.* 15, 455–532. doi: 10.1016/S1474-4422(16)00062-4

Yu, Y., Herman, P., Rothman, D. L., Agarwal, D., and Hyder, F. (2018). Evaluating the gray and white matter energy budgets of human brain function. *J. Cereb. Blood Flow Metabolism* 39, 1339–1353. doi: 10.1177/0271678X17708691

Yudkoff, M. (1997). Brain metabolism of branched-chain amino acids. *Glia* 21, 92–98. doi: 10.1002/(SICI)1098-1136(199709)21:1<92::AID-GLIA10>3.0.CO;2-W

Yudkoff, M., Daikhin, Y., Grunstein, L., Nissim, I., Stern, J., Pleasure, D., et al. (1996). Astrocyte leucine metabolism: significance of branched-chain amino acid transamination. *J. Neurochem.* 66, 378–385. doi: 10.1046/j.1471-4159.1996.66010378.x

Yudkoff, M., Daikhin, Y., Lin, Z., Nissim, I., Stern, J., Pleasure, D., et al. (1994). Interrelationships of leucine and glutamate metabolism in cultured astrocytes. *J. Neurochem.* 62, 1192–1202. doi: 10.1046/j.1471-4159.1994.62031192.x

Yudkoff, M., Daikhin, Y., Nissim, I., Horyn, O., Luhovyy, B., Lazarow, A., et al. (2005). Brain amino acid requirements and toxicity: the example of leucine. *J. Nutr.* 135, 1531S—8S. doi: 10.1093/jn/135.6.1531S

Zhang, Y., Schmid, B., Nikolaisen, N. K., Rasmussen, M. A., Aldana, B. I., Agger, M., et al. (2017). Patient iPSC-derived neurons for disease modeling of frontotemporal dementia with mutation in CHMP2B. *Stem Cell Rep.* 8, 648–658. doi: 10.1016/j.stemcr.2017.01.012

Zhao, Y., and Zhao, B. (2013). Oxidative stress and the pathogenesis of Alzheimer's disease. *Oxid. Med. Cell. Longev.* 2013, 1–10. doi: 10.1155/2013/316523

Zhenyukh, O., Civantos, E., Ruiz-Ortega, M., Sánchez, M. S., Vázquez, C., Peir,ó, C., et al. (2017). High concentration of branched-chain amino acids promotes oxidative stress, inflammation and migration of human peripheral blood mononuclear cells *via* mTORC1 activation. *Free Radic. Biol. Med.* 104, 165–177. doi: 10.1016/j.freeradbiomed.2017.01.009

Zhenyukh, O., González-Amor, M., Rodrigues-Diez, R. R., Esteban, V., Ruiz-Ortega, M., Salaices, M., et al. (2018). Branched-chain amino acids promote endothelial dysfunction through increased reactive oxygen species generation and inflammation. *J. Cell. Mol. Med.* 22, 4948–4962. doi: 10.1111/jcmm.13759

Conflict of Interest: The authors declare that the research was conducted in the absence of any commercial or financial relationships that could be construed as a potential conflict of interest.

Publisher's Note: All claims expressed in this article are solely those of the authors and do not necessarily represent those of their affiliated organizations, or those of the publisher, the editors and the reviewers. Any product that may be evaluated in this article, or claim that may be made by its manufacturer, is not guaranteed or endorsed by the publisher.

frontiers in Aging Neuroscience

REVIEW
published: 20 September 2021
doi: 10.3389/fnagi.2021.738686

Relieving Cellular Energy Stress in Aging, Neurodegenerative, and Metabolic Diseases, SIRT1 as a Therapeutic and Promising Node

Yang Fang[1,2], *Xifeng Wang*[3], *Danying Yang*[1,2], *Yimei Lu*[1,2], *Gen Wei*[1,2], *Wen Yu*[1,2], *Xing Liu*[1,2], *Qingcui Zheng*[1,2], *Jun Ying*[1,2]* *and Fuzhou Hua*[1,2]*

[1]*Department of Anesthesiology, The Second Affiliated Hospital of Nanchang University, Nanchang, China,* [2]*Key Laboratory of Anesthesiology of Jiangxi Province, Nanchang, China,* [3]*Department of Anesthesiology, The First Affiliated Hospital of Nanchang University, Nanchang, China*

The intracellular energy state will alter under the influence of physiological or pathological stimuli. In response to this change, cells usually mobilize various molecules and their mechanisms to promote the stability of the intracellular energy status. Mitochondria are the main source of ATP. Previous studies have found that the function of mitochondria is impaired in aging, neurodegenerative diseases, and metabolic diseases, and the damaged mitochondria bring lower ATP production, which further worsens the progression of the disease. Silent information regulator-1 (SIRT1) is a multipotent molecule that participates in the regulation of important biological processes in cells, including cellular metabolism, cell senescence, and inflammation. In this review, we mainly discuss that promoting the expression and activity of SIRT1 contributes to alleviating the energy stress produced by physiological and pathological conditions. The review also discusses the mechanism of precise regulation of SIRT1 expression and activity in various dimensions. Finally, according to the characteristics of this mechanism in promoting the recovery of mitochondrial function, the relationship between current pharmacological preparations and aging, neurodegenerative diseases, metabolic diseases, and other diseases was analyzed.

Keywords: silent information regulator-1, cellular energy stress, aging, age-related diseases, NAD+, AMP-dependent protein kinases, SIRT1-activating compounds

OPEN ACCESS

Edited by:
Carlos J. Rodriguez-Ortiz, University of California, Irvine, United States

Reviewed by:
Kaoru Tominaga, Jichi Medical University, Japan
Yujun Hou, National Institutes of Health (NIH), United States

***Correspondence:**
Fuzhou Hua
huafuzhou@126.com
Jun Ying
yingjun.80@163.com

Received: *09 July 2021*
Accepted: *26 August 2021*
Published: *20 September 2021*

Citation:
Fang Y, Wang X, Yang D, Lu Y, Wei G, Yu W, Liu X, Zheng Q, Ying J and Hua F (2021) Relieving Cellular Energy Stress in Aging, Neurodegenerative, and Metabolic Diseases, SIRT1 as a Therapeutic and Promising Node. Front. Aging Neurosci. 13:738686. doi: 10.3389/fnagi.2021.738686

INTRODUCTION

Energy stress caused by increased energy demand and decreased energy supply can activate intracellular energy sensors and achieve energy homeostasis through further activation of other pathways. It is important to maintain a sufficient energy supply according to the availability of nutrients and the ability to produce ATP. ATP is produced mainly by mitochondrial oxidative

phosphorylation (OXPHOS) and glycolysis in the cytoplasm which also generates a small portion (Cunnane et al., 2020). Under the low cellular ATP levels, it is urgent to take emergency measures to redistribute intracellular energy and restore it through enhancing the ability of mitochondrial biogenesis and OXPHOS which is a more efficient ATP-producing pathway than glycolysis.

SIRT1, a mammalian ortholog highly closed to Sir2, belongs to the Sirtuins family (SIRT1-SIRT7) whose function depends on nicotinamide adenine dinucleotide (NAD+) and is highly conserved in evolution (Hong et al., 2020). SIRT1 widely plays a key role in cell survival and apoptosis, inflammatory stress adaptation to cell growth, differentiation, metabolism, and senescence, and prevents mitochondrial dysfunction through regulating its transcriptional activity and protein expression levels by changing the acetylation state of substrates (Jiao and Gong, 2020; Chelladurai et al., 2021; Lou et al., 2021). In addition, SIRT1 not only catalyzes the deacetylation of lysine residues in histone substrates such as H1, H3, and H4, but also removes many acetyl groups from non-histone substrates, including peroxisome proliferator-activated receptor-gamma coactivator-1alpha (PGC-1α), forkhead box class O family (Foxos), peroxisome proliferator-activated receptor-γ (PPAR-γ), nuclear respiratory factors 1/2 (NRF1/2), liver X receptor (LXR), P53, P73, E2F transcription factor 1 (E2F1), nuclear factor-kappaB (NF-κB), and so on. Such deacetylation of transcription factors related to metabolism could lead to changes in intracellular metabolism (Ren et al., 2019; Gong et al., 2020; Maiese, 2021).

Mitochondria, which originate from prokaryotes in the endosymbiosis hypothesis, are semi-autonomous organelles that are composed of proteins encoded by transcription and translation *via* Mitochondrial DNA (MtDNA), but most protein structures are found in mitochondria are encoded by nuclear DNA (Popov, 2020). Mitochondrial dysfunction is a common feature in aging, neurodegenerative, and metabolic diseases. Therefore, mitochondria are identified as therapeutic intervention targets for many common diseases. And improvement of mitochondrial dysfunction, elimination of mutations in mitochondrial coding DNA, and mutations in nuclear gene encoding mitochondrial proteins are regarded as the three main strategies of mitochondrial therapy at present (Murphy and Hartley, 2018). Mitochondrial homeostasis depends on the balance between mitochondrial biogenesis and mitophagy. Mitochondrial biogenesis is the source of new mitochondria, which is largely regulated by transcriptional level. Mitophagy, a process that selectively clears dysfunctional mitochondria through the autophagy mechanism, is mainly mediated by PRKN (parkin RBR E3 ubiquitin protein ligase)-dependent and PRKN-independent pathways. As a molecule widely involved in the regulation of cellular processes, SIRT1 not only promotes mitochondrial biogenesis, but also regulates mitophagy, functions to clear damaged and aging mitochondria, and maintains mitochondrial quality and homeostasis (Sun et al., 2020).

In this overview article, the energy stress in some physiological and pathophysiological conditions will be discussed. And promoting the expression and activity of SIRT1 at different levels can relieve intracellular energy stress and become a promising treatment.

ENERGY STRESS IN MULTIFARIOUS SITUATIONS

Maintaining the dynamic homeostasis of cellular energy states involves a delicate balance between the consumption of energy and the generation of energy. In response to energy demands triggered by body activity and environmental stress, cells constantly adjust their metabolism, redistribute the use of energy and promote the mechanism of energy production (Herzig and Shaw, 2018).

Calorie restriction (CR) is defined as a sustained decline in energy intake compared to pre-intervention requirements without causing malnutrition (typically 20–50% less than average), and it has been shown to mediate a life-extending effect in the lower organisms through a key molecule Sir2 which previously mentioned to be highly homologous to SIRT1 in mammals (Yang N.-C. et al., 2019). The core of calorie restriction is to fully meet nutrient requirements and then gradually reduce the supply of energy-rich substrates. It can produce metabolic adaptation to reduce the metabolic rate by inducing a moderate energy deficit (Dorling et al., 2020).

The same metabolic adaptations that affect resting metabolic rate as calorie restriction were not observed in exercise-induced weight loss. This may be because exercise-induced acute energy deficits are insufficient to trigger metabolic adaptation (Karstoft et al., 2017). However, physical activity induces an acute energy deficit which activates AMP-dependent protein kinases (AMPK), uptake of substrates from plasma and lipolysis, promotes mitochondrial function and fat oxidation. Furthermore, these effects chronically improve the metabolic function of almost every organ in the body through increasing cardiorespiratory capacity, mitochondrial oxidative capacity, reducing lipid in plasma, tissues, and cells, and improving insulin sensitivity (Gao et al., 2020).

Aging is one of the powerful risk factors for the development of many diseases, particularly neurodegenerative and metabolic diseases. Alterations of metabolism caused by aging occur at different functional levels. And aging shows progressive impairment of mitochondrial respiratory function, not only displays in the antioxidant stress system but mitochondrial oxidative phosphorylation related enzymes may also be affected, results in the decrease of mitochondrial function, insulin resistance, and lipid metabolism diseases (Ma and Li, 2015), thereby reducing the production of ATP, to make the body energy stress state for a long time.

Mitochondrial homeostasis also plays a crucial role in maintaining the central function, once the homeostasis imbalance can lead to a reduction of brain energy production and activation of oxidative stress, leading to the central inflammatory response. Impaired mitochondrial function and central nervous system inflammatory microenvironment are the main characteristics of age-related neurodegenerative diseases, both of which are involved in aggravating cell energy stress. In

addition, changes in energy metabolism appear to deteriorate in a gradual, regional, and disease-specific manner. Alzheimer's disease (AD) is the most special type, and the decline in glucose metabolism begins early in the symptoms. After the onset of the disease, the activation of glial cells mediated by central nervous system inflammation increases the consumption of glucose, which further worsens the energy balance of neurons, and the persistence of neuronal energy stress further aggravates the progress of the disease (Joshi et al., 2019; Cunnane et al., 2020).

Metabolic diseases such as diabetes, obesity, and hypertension are characterized by decreased mitochondrial energy efficiency associated with impaired mitochondrial structure and function, including diminished OXPHOS, and reduced ATP production (Feng et al., 2019). Energy stress generated by insufficient energy production and metabolic substrates utilization disorder affects the physiological functions of various systems in the body which can further promote the pathological progress of these diseases (Zhang et al., 2019; Juszczak et al., 2020).

EXPRESSION AND ACTIVITY OF SIRT1 DECREASED IN AGING, NEURODEGENERATIVE AND METABOLIC DISEASES

As a multi-effector signaling molecule, SIRT1 can be found in both the nucleus and cytoplasm. However, there were differences in subcellular localization in different tissues and developmental stages of adult mice (Tanno et al., 2007). And existing data suggest that its subcellular localization can be altered by two nuclear localization signals (NLSs) and two nuclear export signals (NESs) which are located on the protein's amino acid sequences (Yang T. et al., 2019). Under normal physiological conditions, the activity and expression of SIRT1 are simultaneously regulated by multiple mechanisms and maintained at a normal level to adapt to environmental stress. However, deteriorated SIRT1 expression and activity in different subcellular localization is implicated in aging, neurodegenerative and metabolic diseases.

In the last decade, researchers have found that the level of yeast Sir2 (a homolog of Sirt1) decreases as the increasing number of replications, which is one of the causes of yeast aging (Dang et al., 2009). Until now, accumulating scientific evidence indicates that the expression and activity of SIRT1 in mammalian cells decreased progressively with aging (Lamichane et al., 2019; Lin et al., 2020; Lan et al., 2021). This may be due to NAD+, the major cofactor of SIRT1, also shows a progressive decline with aging (Covarrubias et al., 2021b). Recent studies have reported a possible mechanism for this phenomenon, namely autophagy-mediated down-regulation of mammalian SIRT1 protein during aging and *in vivo* aging. As a nuclear substrate for autophagy, SIRT1 in the nucleus is recognized by autophagy protein LC3 and transferred to the cytoplasmic autophagosome for degradation (Xu et al., 2020). And study reveals that SIRT1-mediated beneficial effects could be promoted by selectively inhibiting the autophagy degradation pathway of SIRT1 in the nucleus (Wang et al., 2021).

Aging is strongly associated with the incidence of neurodegenerative diseases, particularly AD and Parkinson's disease (PD). The decrease in serum SIRT1 protein level was more significant in patients with neurodegenerative diseases than in normal aging individuals, these results indicate the decreased expression and activity of SIRT1 are involved in the pathological process of neurodegenerative diseases (Cao et al., 2018). This is because some enzymes such as poly-ADP-ribose polymerases 1 (PARP1) are overexpressed and activated to compete with SIRT1 to utilize NAD+ during senescence, which reduces the content of NAD+ in tissues and cells, inhibits the activity of SIRT1 and its downstream pathways. And the inhibition of NAD+-SIRT1-PPARGC1A-UCP2 axis activity, resulting in increased mitochondrial membrane potential, PTEN induced putative kinase 1 (PINK1) cleavage, mitochondrial autophagy deficiency, and accelerating aging phenotype and neurodegenerative diseases, PINK1, as an autophagy-related protein attached to the outer mitochondrial membrane, is transported to the mitochondria in a membrane potential-dependent manner and degraded by mitochondrial protease, thus unable to trigger mitochondrial autophagy (Scheibye-Knudsen et al., 2014). A study has also been found that overactivation of PARP1 can also trigger the defect of mitochondrial autophagy by inhibiting the NAD+-SIRT1-PGC-1α pathway, which is related to the regulation of mitochondrial autophagy by SIRT1 through a variety of pathways, and this can be partially normalized with PARP1 inhibitors or pharmacological interventions with compounds that increase NAD+ abundance (Fang et al., 2014). There is also evidence that toxic proteins associated with neurodegenerative diseases can also reduce the expression of SIRT1, or directly interact with SIRT1 protein to inhibit its affinity with substrates and increase the acetylation of their substrates (Jiang et al., 2011; Manjula et al., 2020). Such as the expression of SIRT1 protein in the parietal cortex of patients with AD is significantly decreased and is closely related to the accumulation of Aβ and tau proteins (Kerr et al., 2017).

Metabolic diseases are a global public problem associated with overnutrition and are defined as a group of metabolic disorders including obesity, insulin resistance, type 2 diabetes, hypertension, and hyperlipidemia (Saklayen, 2018). SIRT1 is widely involved in the metabolic control of intracellular substrates in the body. The decrease of SIRT1 expression and activity is a major characteristic of metabolic diseases, and its mechanism partly explains the influence of a high-fat diet on metabolic syndrome, obese diabetes, cardiovascular disease, and other related metabolic diseases (Kosgei et al., 2020). Decrease of SIRT1 expression can also lead to lipid accumulation and impaired insulin signaling in hepatocytes. Conversely, mice on a high-fat diet to some extent avoid these diseases through the restoration of SIRT1 expression and activity (Nguyen et al., 2019; Li Z. et al., 2020).

Taken together, these data highlight the decreased expression and activity of SIRT1 as a key component of the molecular mechanisms that participate in the process of aging, neurodegenerative and metabolic diseases. However, some scientific evidence reveals that there is no inevitable connection

between SIRT1 protein content and activity (Gurd et al., 2010; Ryall et al., 2015). This may be because SIRT1 is regulated by different mechanisms from multiple levels at different developmental stages, and the subcellular distribution and localization of SIRT1 also change during this process. Therefore, the accurate elaboration of the regulatory mechanism of SIRT1 in different stages of cell activity is expected to be used in the design and development of pharmacological agents for the treatment of a variety of diseases.

THE EXPRESSION AND ACTIVITY OF SIRT1 ARE REGULATED BY MANY DIMENSIONS

Due to the importance of extensive participation in the regulation of energy metabolism and other cell life activities, SIRT1 activity and expression are tightly regulated in multiple dimensions. Therefore, a clear understanding of the regulatory mechanism by which SIRT1 plays a role is the basis for the development of therapeutic target drugs. In this review, we mainly attempt to expand from NAD+ to further discuss the regulation of SIRT1 expression and activity in energy metabolism.

NAD+

SIRT1 is a key regulatory protein in life activities. Under normal physiological conditions, the activity and expression of SIRT1 are simultaneously regulated by multiple mechanisms to adapt to environmental stress. Since NAD+ is a necessary cofactor for the deacetylation activity of SIRT1, it has become a research hotspot of scientists to regulate the level of NAD+ in the cell to promote the activity of SIRT1.

As a driving force and signal molecule for energy production, NAD+ has shown that its distribution is highly differentiated. Each subcellular NAD+ pool is regulated to varying degrees and participates in various NAD+-dependent signaling mechanisms (Zhu et al., 2019). Although the overall NAD+ level will decline in the process of aging, the activity of SIRT1 is mainly dependent on the NAD+ level in the nucleus, rather than the NAD+ pool in the mitochondria or cytoplasm (Gomes et al., 2013). Sufficient experiments have shown that NAD+ levels in mitochondria and nuclei in wild-type mouse cells or tissues can be restored by supplementing NAD+ precursors such as nicotinamide riboside (NR) and nicotinamide mononucleotide (NMN). And sufficient intracellular NAD+ levels can enhance oxidative metabolism and protect mice from metabolic abnormalities induced by a high-fat diet and improve age-related pathophysiology and diseases, thereby reflecting the effect of prevention and treatment (Schöndorf et al., 2018; Yoshino et al., 2018). Promoting the activity of NAM phosphoribosyltransferase (NAMPT), the first step of the rate-limiting enzyme in NAD+ remediation synthesis, can also increase NAD+ levels. Experimental studies have found that exercise can induce an increase in NAMPT activity and promote the salvage synthesis of NAD+ (Lamb et al., 2020), and overexpression of NAMPT can also activate the SIRT1-dependent P53-CD38 pathway and SIRT1-independent NRF2-PPARα/AMPKα pathway to maintain mitochondrial content and integrity (Yu et al., 2020). However, we should consider other potential effects of enhanced NAD+ metabolism, including pro-inflammatory and cancer-promoting effects. Studies have shown that NAMPT and NAD+ play a key role in cancer. NAD+ biosynthesis is usually up-regulated in tumor cells, and increased levels of NAMPT promote pro-inflammatory aging-related secretion phenotypes (Nacarelli et al., 2019). This presents a new challenge for us to regulate the activity of SIRT1 by influencing NAD+ metabolism.

It is widely known that lactic dehydrogenase (LDH) catalyzes the redox reaction between pyruvic acid and lactic acid, and promotes the conversion of lactic acid to pyruvate under alkaline conditions. In contrast, the neutral condition promotes the reverse conversion of pyruvate to lactic acid, which can consume NADH and produce NAD+. Therefore, studies have shown that supplementing L-serine can increase the expression of mitochondrial biogenesis-related genes in C2C12 myotubes, improves the quality and function of mitochondria, and reverses insulin resistance. This is because L-serine is converted to pyruvate, which is subsequently converted to lactic acid by LDH and increases intracellular NAD+ levels, thereby activating NAD+ dependent SIRT1 activity (Sim et al., 2019).

The activation of SIRT1 by amino acids was first identified as involving leucine. Researchers found that it can increase the expression and activity of SIRT1, improve the quality and function of mitochondria, and prevent mitochondrial dysfunction and metabolic disorders in obese mice induced by a high-fat diet (Sun and Zemel, 2009). Further studies have found that leucine may not only induce the increase of NAMPT expression (Li et al., 2012), but also affect the kinetics of SIRT1, reduce the activation energy of NAD+, and have a synergistic effect with AMPK or SIRT1 activators (Zemel, 2020). Taurine, a non-protein amino acid, also can alleviate oxidative stress and apoptosis of cardiomyocytes through increasing NAD+/NADH ratio, activate SIRT1 and suppress p53 acetylation (Liu et al., 2020). SIRT1 stimulated and activated by Taurine also can alleviate the mitochondrial dysfunction induced by amyloid β 1–42 in SK-N-SH cells (Sun et al., 2014) which provides a suggestion for the diet list of patients with neurodegenerative diseases. The kynurenine pathway, the main pathway for tryptophan metabolism to produce NAD+, also regulates the activity of SIRT1 (Yin et al., 2021). Since then, the addition of amino acids to food as a method for actively regulating the function of SIRT1 has become a research hotspot.

The current view is that except nuclear sirtuins is consuming NAD+ pool, PARPs (poly-ADP-ribose polymerases) and CD38 (a NAD glycohydrolase) are competing for the same NAD+ pool, and studies have found that inhibition or knockout of PARP or CD38 can increase intracellular NAD+ levels and show an effect similar to sirtuins activation (Wang et al., 2019; Chini et al., 2020; Covarrubias et al., 2021b). The competition between PARP and SIRT1 for the NAD+ pool is age-dependent. Studies have shown that the level of NAD+ itself decreases with age and age-related diseases (Covarrubias et al., 2021a; Hikosaka et al., 2021), while the activation of PARP with age aggravates a small number of NAD+ pools. This may be because PARP appears to be related to

DNA damage repair function, while aging can lead to an increase in chronic nuclear DNA damage (Shao et al., 2020).

AMPK

Metabolic stress is characterized by a decrease in the ratio of ATP to AMP/ADP, which activates AMPK, resulting in phosphorylation that activates a series of pathways that up-regulate ATP (Herzig and Shaw, 2018; Yan et al., 2018). As a sensor for the energy state of cells, researchers found that AMPK can be activated when skeletal muscle energy is exhausted, and directly phosphorylate PGC-1α at threonine-177 and serine-538 (Spinelli et al., 2021). Moreover, researchers discovered that AMPK regulates NAD+/NADH ratio and SIRT1 activity in a manner independent of NAMPT shortly after the activation, and this process relies on mitochondrial β-oxidation (Cantó et al., 2009). Subsequently, NAMPT can be activated and involved in the regulation of NAD+ metabolism. The increased NAD+/NADH ratio directly enhanced the activity of SIRT1. However, the interaction between AMPK and SIRT1 is not a simple one-way interaction, but a more complex functional interaction. This may be due to SIRT1-mediated deacetylation of LKB1, a mammalian AMPKK, which promotes the phosphorylation and activation of AMPK subunits (Sharma A. et al., 2021).

Consistent with this, under a low-energy state caused by exercise in skeletal muscle, AMPK was activated by the decrease in the ratio of ATP/AMP. Activated AMPK not only increases the ratio of NAD+/NADH, but also phosphorylates PGC-1α which can subsequently reduce insulin resistance, enhance glucose metabolism, and promote the recovery of energy state in skeletal muscle through improving mitochondrial biogenesis (Yang B. et al., 2021). Since the incomplete oxidation of fatty acids in skeletal muscle is caused by lipid intermediates related to insulin resistance (Koves et al., 2005), the ability of cells to maintain the oxidation of fatty acids and couple them with mitochondrial respiration is essential in the case of nutritional deficiency. A detailed explanation of their coordination mechanism can provide effective therapeutic targets for related metabolic diseases. PGC-1α phosphorylated by AMPK before deacetylation by SIRT1 may be used to distinguish which substrates are deacetylated, thus preventing the random deacetylation of SIRT1. In this case, AMPK is involved in the regulation of SIRT1 and PGC-1α and maintains its stable and sustained effect. These effectors include the activators of pyruvate dehydrogenase kinase 4 (PDK4), forkhead box O1 (FoxO1), ERRα, and PPARs gene expression. And enhanced PDK4 can phosphorylate PDH to inactivate it and prevent pyruvate from entering TCA, converting cells from glucose metabolism to lipid metabolism and then meet the energy needs of exercise (Knuiman et al., 2018). In addition, as a downstream factor activated by the SIRT1-PGC-1α axis, TFAM can play a role in diseases such as diabetes and diabetic peripheral neuropathy by enhancing the function of mitochondria, promote the complete oxidation of fatty acids in mitochondria, and provide a large number of sources of ATP for cells (Chandrasekaran et al., 2019). At the same time, the role of forkhead box O3 (FoxO3) in the SIRT1-PGC-1α axis is also very important. Activated AMPK further activates FoxO3 through phosphorylation, promoting its nuclear translocation. FoxO3 in the nucleus can be deacetylated by SIRT1, and participate in enhancing the transcription of NAMPT, PGC-1α, and LKB1, thus producing a stable and continuous role in the regulation of mitochondrial function (Sorrenti et al., 2020; **Figure 1A**).

The acetylation state of PGC-1α is regulated by SIRT1, histone acetyltransferase GCN5 (Mutlu and Puigserver, 2021), and steroid receptor coactivator 3 (SRC3; Hu et al., 2018). According to the availability of nutrition and the energy state of the cell, SIRT1 deacetylation and GCN5/SRC-3 acetylation jointly controls the acetylation state of PGC-1α. Under the basic energy state, AMPK is not activated and does not promote the catalytic effect of SIRT1 on PGC-1α, while GCN5 acetylates several lysine residues on PGC-1α, thus changing its location in the nucleus and inhibiting transcriptional activity (Dominy et al., 2010). The researchers discovered that hypoxia-inducible factor-1α (HIF-1α) is involved in regulating mitochondrial biogenesis and nuclear-mitochondrial communication during aging in a pathway independent of PGC-1α. In subsequent experiments, SIRT1 needs to regulate Von Hippel-Lindau (VHL) E3 ubiquitin ligase activity through post-transcriptional modification to ensure effective hydroxylation and degradation of HIF-1 in the nucleus, thus reducing the binding of HIF-1α to c-Myc, promoting the interaction between c-Myc and the binding site on the mitochondrial transcription factor A (TFAM) promoter, and enhancing the transcription and expression of mitochondrial biosynthetic genes (Gomes et al., 2013; **Figure 1B**).

Regulation by Transcriptional Level

There are many binding sites of transcriptional regulatory factors in the SIRT1 promoter, therefore, SIRT1 can be regulated by multiple regulatory mechanisms at the transcriptional activity level. The transcriptional regulatory factors in this regulatory mechanism are usually the substrate of SIRT1. Researchers reported that there are two p53 binding sites on the SIRT1 promoter under basic conditions, and the P53 (activated by CBP/p300 mediated acetylation) can bind and inhibit SIRT1 gene expression, while under a low energy state, the activated FOXO3a can undergo nuclear translocation, bind and remove p53 binding to the SIRT1 promoter, then induce SIRT1 transcription and alleviate energy stress (Luo et al., 2004). At the same time, the increased expression of SIRT1 can in turn mediate the deacetylation of P53 at lysine 382, reduce its stability and activity, prevent the inhibition of SIRT1 transcription, and produce a stable and sustained effect (Vaziri et al., 2001). Consistent with this, hypoxia-induced HIF-1α and HIF-2α can directly bind to the HIF response element (HRE) on the SIRT1 promoter, increasing the transcriptional activity and expression of SIRT1 (Li T. et al., 2020). However, as mentioned earlier, the increase in SIRT1 activity and expression can destabilize and degrade HIF-1α in a VHL E3 ubiquitin ligase-dependent manner (Gomes et al., 2013). Furthermore, scientists found that the interaction between SIRT1 and FoxO1 and deacetylation can promote the auto-transcription of SIRT1 driven by FoxO1. This may be because FOXO1 could directly bind to insulin receptor substrate

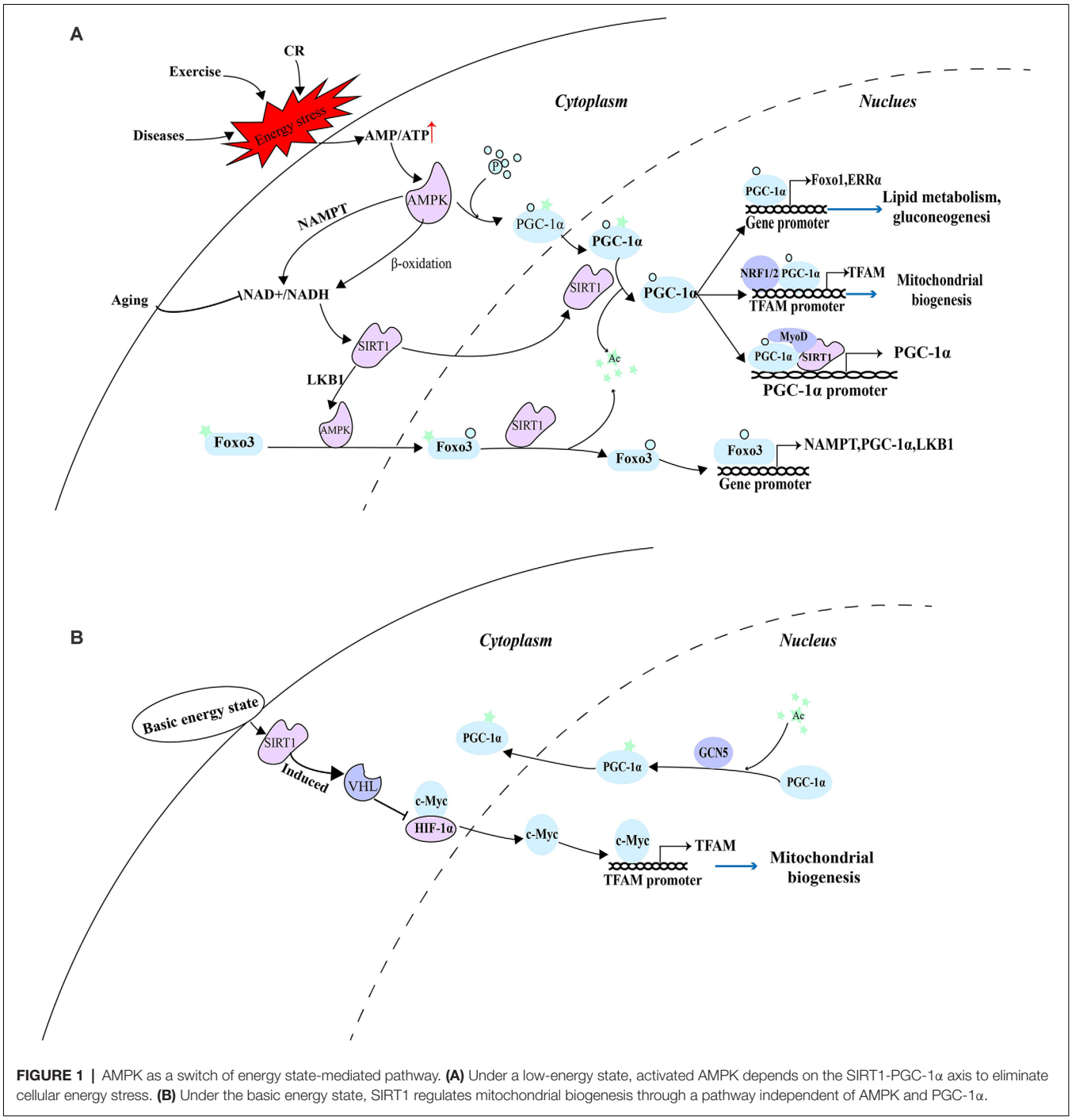

FIGURE 1 | AMPK as a switch of energy state-mediated pathway. **(A)** Under a low-energy state, activated AMPK depends on the SIRT1-PGC-1α axis to eliminate cellular energy stress. **(B)** Under the basic energy state, SIRT1 regulates mitochondrial biogenesis through a pathway independent of AMPK and PGC-1α.

1 (IRS-1) and forkhead-like consensus binding site (FKHD-L) on the SIRT1 promoter, increasing the transcription and expression of SIRT1 (Xiong et al., 2011). In response to low nutrient availability, cAMP response element-binding protein (CREB) can be activated and bind to the cAMP response element (CRE) transcriptional site on the SIRT1 promoter, thereby promoting the transcriptional activity of SIRT1 (Noriega et al., 2011). In turn, a recent study shows that CREB is also the substrate of SIRT1, and SIRT1 can deacetylate and inactivate CREB (Lu et al., 2020). In addition, as nuclear receptors, peroxisome proliferator-activated receptor (PPAR) also can increase the expression of SIRT1. Fasting for 24 h can increase the expression level of SIRT1 in mice, which may be due to the binding of PPARα to the PPAR-responsive element (PPRE) on the SIRT1 promoter (Hayashida et al., 2010). PPARβ/δ is another transcription factor, which can increase the expression of SIRT1 by binding to the Sp1 binding site in a state of starvation (Okazaki et al., 2010).

Conversely, under a high energy state, carbohydrate response element-binding protein (ChREBP) decreases the expression of SIRT1 by interacting with ChRE binding site on the SIRT1 promoter (Noriega et al., 2011). Another transcription factor is PPARγ, which not only can be initiated by the SIRT1-PGC-1α axis, but also PPARγ itself can directly bind to the SIRT1 promoter to inhibit the expression of SIRT1, thus PPARγ and SIRT1 compose a negative feedback loop (Han et al., 2010). Consistent with this, the hypermethylated in Cancer 1 (HIC1) negatively regulate SIRT1 expression by relying on carboxyl-terminal-binding protein (CtBP), and HIC1 also can be deacetylated and inactivated by SIRT1, thus reducing its inhibitory effect on SIRT1 expression (Paget et al., 2021). Moreover, recent studies have shown that HIC2, which is highly homologous to HIC1, is a transcriptional activator of SIRT1 due to the opposite activity of their intermediate domains, and it has been found that ectopic overexpression of HIC2 may protect the heart from ischemia-reperfusion injury (Song J.-Y. et al., 2019). In summary, it is suggested that the expression of SIRT1 is regulated by multiple negative feedback loops (**Figure 2**).

Regulation by Post-transcriptional Level

MicroRNAs (miRNAs), a small non-coding RNA, can regulate the transcription or post-transcriptional regulation of protein-coding genes by degrading mRNA or inhibiting translation (Włodarski et al., 2020). The micro-regulation of SIRT1 mRNA by different miRNA has a variety of functions in different cells and tissues, including from physiology and metabolism to disease pathologies such as cardiovascular disease and cancer. These miRNAs can inhibit the transcription and expression of SIRT1 by directly binding to the 3′ non-coding region of SIRT1 or indirectly by regulating the level of human antigen R (HUR). HUR is an RNA binding protein that is usually combined with miR-16, miR-125a, and miR-519 to indirectly regulate the stability of SIRT1 mRNA (Zhang et al., 2021). Most miRNAs inhibit the expression of SIRT1 (Yamakuchi, 2012).

Nowadays, the micro-regulation of mRNA by miRNA remains a research hotspot. In addition to the high expression of miR-22, miR-29a, miR-34a, miR-132, miR-138-5p, miR-143/145, miR-195, miR-199a, miR-217, and so on in the cardiovascular system (Mao et al., 2019; Ding et al., 2020; Zhou et al., 2020), the high expression of miR-9, miR-93, miR-100, miR-122, miR-132, miR-135a, miR-137, miR-155, miR-181a/b/c, miR-182-5p, miR-199b, miR-204, miR-221, and so on in other tissues can also directly inhibit the expression of SIRT1 (Ge et al., 2019; Guo et al., 2019; Long et al., 2019; Xie et al., 2019; Zhao et al., 2019). On the contrary, miR-16, miR-125a, and miR-519 can indirectly regulate SIRT1 by regulating HUR (Yuan et al., 2016). MiR-34a was the first miRNA, to be found to regulate Sirt1, so it is the most studied. Aging and pathological conditions can increase the expression of intracellular miR-34a, thus inhibit the expression of SIRT1, and further promote aging and disease progression (Chen et al., 2019; Song L. et al., 2019; Wang L. et al., 2020). Recent studies have shown that miR-141 mimics can reduce the expression of SIRT1 mRNA, inhibit hepatocyte autophagy, reduce HBV replication (Yang et al., 2017), and promote the progress of intervertebral disc degeneration (IDD; Ji et al., 2018). Overexpression of miR-449 inhibits the osteogenic differentiation of bone marrow mesenchymal stem cells in hyperglycemia and free fatty acid microenvironment in which SIRT1 was involved, which may play a role in the fight against diabetic osteoporosis (Qu et al., 2018). Further exploration of miRNA-based therapeutic ideas can provide new intervention approaches for clinical multiple diseases (**Figure 2**).

Regulation by Post-translational Modification

In addition to the above-mentioned regulation of SIRT1 activity and expression based on NAD+ level and AMPK activation, all sirtuins contain N-terminal and C-terminal domains (NTDs and CTDs), which are evolutionarily highly conserved catalytic domains, and both contain residues modified by post-translational mechanisms, of which the catalytic domain of SIRT1 is the largest (Dong, 2012). Fifteen phosphorylated residues have been identified in SIRT1, eight in CTDs, and seven in NTDs (Sasaki et al., 2008). Their phosphorylation status can be regulated by different phosphokinases. For example, under starvation (low-energy state), the enhanced cAMP signal can not only induce the phosphorylation of the highly conserved Ser434 site in the catalytic domain of SIRT1 (Hu et al., 2020), but also can be modified by intermediate phosphokinase at Ser 47,605 and 615 sites of SIRT1 and promote the dissociation of SIRT1 and DBC1, which is dependent on AMPK, then promote fatty acid oxidation, adapt to stress and meet the needs of cell energy metabolism through activating SIRT1 in an NAD+-independent manner (Gerhart-Hines et al., 2011; Nin et al., 2012).

When cell mitosis increases, cell cycle-dependent kinase (Cyclin-B/CDK1) can mediate the phosphorylation of SIRT1 at Thr530 and Ser540 to up-regulate SIRT1 activity, which is beneficial to provide energy for mitosis and promote mitochondrial division (Sasaki et al., 2008). Furthermore, c-Jun N-terminal kinase-1 (JNK1) can phosphorylate the Ser27, Ser47, and Thr530 sites of human SIRT1 and this modification of SIRT1 increased its enzymatic activity and nuclear localization (Nasrin et al., 2009). Under high glucose conditions (high nutritional availability), JNK1 phosphorylates the Ser27 site and temporarily activates the SIRT1 activity, then it is degraded through the ubiquitin-proteasome pathway, decreases the expression of SIRT1 in general (Gao et al., 2011). However, inhibition of CDK5 phosphorylation at Ser47 to modify SIRT1 not only blocks the degradation of SIRT1 through the ubiquitin-proteasome pathway (Zhang Q. et al., 2018), but also the podocyte injury and mitochondrial dysfunction in diabetic patients were significantly reduced (Wang S. et al., 2020). In addition, CK2-mediated phosphorylation of SIRT1 at the Ser164 site inhibits its nuclear localization and promotes the progress of non-alcoholic fatty liver (Choi et al., 2017), which provides evidence that SIRT1 is involved in the improvement of metabolic diseases. However, A recent study showed that in senescent cells, down-regulation of CK2 can mediate the inactivation of SIRT1, thus activating NF-KB and inducing the expression of senescence-associated secretory phenotype (SASP)

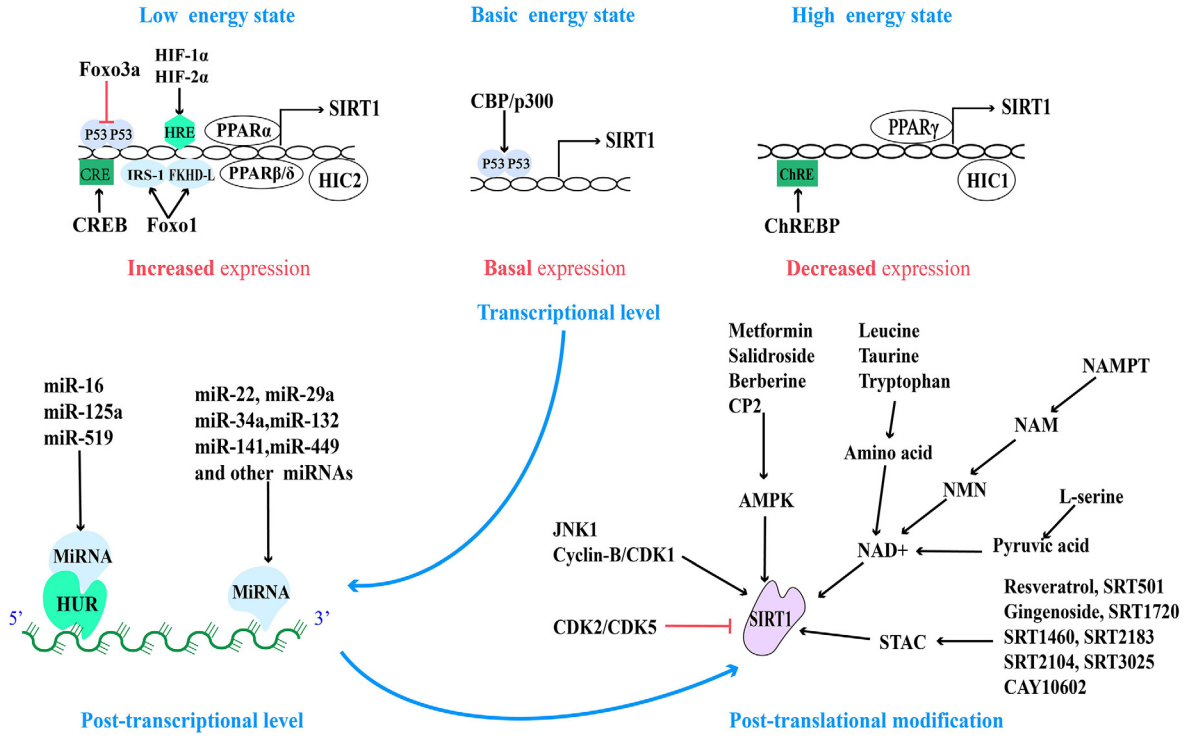

FIGURE 2 | Regulatory sites for SIRT1 protein expression and activity and related pharmacological agents. Based on the different energy states of cells, the activity of the SIRT1 promoter is regulated by a variety of transcriptional regulatory factors. And at the post-transcriptional level, SIRT1 mRNA is regulated by a variety of miRNA. Finally, the activity of post-translational SIRT1 proteins is regulated by different post-translational modification mechanisms.

factors (Song and Bae, 2021). This suggests that SIRT1 accepts negative regulation from CK2, but more evidence is needed to guide us to accurately understand the role of CK2 in different pathological models.

The strict multi-level regulation mechanism of SIRT1 is beneficial for cells to adapt to various stress states including energy stress. Post-transcriptional modification mostly regulates the activity of proteins. In light of this, the rapid regulation of SIRT1 activity may be the starting point for cells to rely on SIRT1 to adapt to stimulation, and effective regulation of this metabolic node will be of great benefit to rapid cell response. On the other hand, transcriptional activity regulation and post-transcriptional regulation play an vital role in maintaining the abundance and stability of SIRT1 protein. Due to the extensive involvement of SIRT1 in cell life activities, an in-depth understanding of these regulatory mechanisms may soon provide effective interventions for the improvement of human health (**Figure 2**).

PROMOTING THE EXPRESSION AND ACTIVITY OF SIRT1 EXERT BENEFICIAL ROLES

At the present moment, the activation of the SIRT1 pathway has become an attractive therapeutic intervention target, and this momentum prompted researchers to actively seek SIRT1-activating compounds (STACs). The chemical nature of most STAC is polyphenolic compounds with the coplanar arrangement of hydroxyl groups on the benzene ring. In addition, some pharmacological agents can enhance the activity of SIRT1 in other ways and bring beneficial effects for diseases.

Resveratrol

Resveratrol, a natural polyphenol compound found in the last century, as a classical activator of the SIRT1 pathway, the activation of downstream signal molecular mechanism still has not been elucidated in detail. Early studies have found that resveratrol mimics the life-prolonging effect of CR in yeast and multicellular organisms through SIRT1/Sir2-dependent pathway (Wood et al., 2004). Most of the currently recognized mechanisms are: (1) resveratrol directly interacts with the NTD domain of SIRT1, promoting the closer binding of SIRT1 to the effector protein and stimulating the activity of SIRT1 protein (Cao et al., 2015); and (2) resveratrol can also increase the level of intracellular NAD+ by activating AMPK and through NAMPT-dependent salvage synthesis pathway, and then enhance the activity of SIRT1 (Lan et al., 2017), which plays a beneficial role in energy metabolism and age-related diseases.

Injection of resveratrol into mice can not only simulate the effects of CR, such as anti-aging, promoting browning of white adipocytes, and improving metabolic disorders in mice (Li Z. et al., 2020; Pyo et al., 2020), but also play

a protective role in neurodegenerative diseases such as AD, amyotrophic lateral sclerosis, and PD (Zhang L.-F. et al., 2018; Ma et al., 2019). A study has demonstrated that long-term resveratrol supplementation can improve the homeostasis between mitochondrial biogenesis and mitochondrial autophagy by activating miR-34a/SIRT1-mediated signaling pathways, and strikingly reduce age-related cochlear hair cells loss and hearing loss in mice (Xiong et al., 2019). Furthermore, accumulating scientific evidence indicates that Amyloid-β (Aβ) protein can inhibit the AMPK-SIRT1-PGC-1α pathway, inhibit mitochondrial biogenesis, and reduce glucose metabolism (Dong et al., 2016; Carbonell et al., 2020). However, it has been recently reported that resveratrol not only reduces the expression of Aβ and p-tau protein in AD model mice, increase the activity of toxic protein degradation pathway, and improve the protein balance between normal mice and AD model mice, but also up-regulate SIRT1-mediated mitochondrial biogenetic pathway and promote the recovery of mitochondrial function and energy supply by increasing the level of AMPK protein (Corpas et al., 2019). Because the new strategy to improve obese patients is to reduce the fat burden of patients by "browning" white adipose tissue to burn excess fat. And it has been demonstrated that resveratrol can activate the SIRT1-mediated white fat browning pathway and improve hyperglycemia and hyperlipidemia in mice (Li Z. et al., 2020). This may be due to the deacetylation of Lys268 and Lys293 sites on PPARγ, which can lead to the recruitment of BAT program coactivator Prdm16 to PPARγ, resulting in browning of white adipose tissue and inhibition of genes related to insulin resistance. Therefore, resveratrol has become a promising therapeutic strategy in the fight against metabolic diseases such as obesity and diabetes.

However, resveratrol did not have a lasting beneficial effect in the experiment. Researchers found that the dose of resveratrol as a key factor makes it possible to activate AMPK, in a SIRT1-dependent/SIRT1-independent manner. Moderate doses of resveratrol (25 μM) can stimulate AMPK *in vitro* and *in vivo* through the SIRT1-dependent pathway, resulting in more sustained improvement of mitochondrial function. On the contrary, a high dose of resveratrol (50μM) not only leads to the activation of AMPK in a SIRT1-independent manner, but also leads to a significant reduction in mitochondrial function and intracellular ATP level (Price et al., 2012). If the dose of resveratrol has a significant effect on the results, then the low bioavailability of resveratrol itself in humans is also one of the problems that researchers urgently need to solve. Given the rapid metabolism of resveratrol in the liver and the influence of intestinal microflora in the intestine, researchers have developed a series of drug delivery systems such as embedding resveratrol in lipid nanoparticles or liposomes, using emulsions or micelles. Resveratrol derivatives such as SRT501 have also been developed, and preparations such as resVida and Longivinex that can greatly improve the bioavailability of resveratrol have been designed (Chimento et al., 2019; Singh et al., 2019).

Other STACs

Currently, the direction of searching for STAC is mainly extracted from natural products or artificially designed compounds according to the structure of SIRT1. In the latest screening, scientists found 19 kinds of STAC with anti-mitochondrial oxidative damage from traditional medicinal plants. Further studies on several of these activators have found that these compounds (including ginsenoside Rb2, ginsenoside F1, ginsenoside Rc, and schisandrin A) can enhance SIRT1 deacetylation activity, promote mitochondrial functional recovery by restoring oxygen consumption and increasing mitochondrial biogenesis, increase ATP production, decrease intracellular ROS levels, and strengthen antioxidant mechanisms (Wang et al., 2016).

Ginsenoside is the main active component of the pharmacological activity of Panax ginseng. Ginsenosides are classified according to different structural types, recent studies found that ginsenoside Rg3 can enhance the endurance of aged rats during exercise by affecting the activity of SIRT1 and the expression of PGC-1α (Yang et al., 2018), and six ginsenosides, including ginsenosides Rg1, Rb1, Rh2, Rg3, Rg5, and Re can protect the brain from ischemic injury by relying on SIRT1-activated signal pathways, among which ginsenosides Rb1 and Rg3 have the strongest therapeutic activity (Cheng et al., 2019). Consistent with this, as a STAC, ginsenoside Rc can promote energy metabolism in cardiomyocytes and neurons by activating the SIRT1-PGC-1α pathway to induce mitochondrial biosynthesis (Huang et al., 2021).

SRT1720 is a small molecular activator that is structurally independent of resveratrol, but its activation effect is hundreds of times that of resveratrol. It has the same effect as SRT501 and resveratrol and effectively solves the weakness of the low bioavailability of resveratrol. Resveratrol and SRT1720 bind at the same molecular site to activate SIRT1 activity and play a similar role in regulating the stability between mitochondrial biogenesis and mitochondrial autophagy. Activation of SIRT1 by SRT1720 increased mitochondrial biosynthesis *via* PGC-1α-dependent pathways, promoted the recovery of mitochondrial protein and function, and induced the protective effect of brain injury after intracerebral hemorrhage in rats (Zhou et al., 2017). SRT1720 can produce neuroprotective effects similar to resveratrol, reduce the content of Aβ in the brain of PD patients, and repair the autophagy dysfunction (Bai et al., 2021). Studies have also shown that SRT1720 plays an active role in the treatment of diabetes and insulin resistance, SRT1720 can promote wound healing and angiogenesis in diabetic mice *in vivo* and *in vitro* by activating SIRT1 (Li et al., 2019). However, studies have shown that the metabolic role of SRT1720 depends on AMPK, which is because SRT1720 cannot promote mitochondrial function and improve glucose tolerance in AMPKα 2 knockout mice (Park et al., 2017).

At present, several other STACs: such as SRT1460, SRT2183, RT2104, SRT3025, and CAY10602, have been developed (**Figure 2**), although there are few related studies, preliminary experiments have shown that they activate SIRT1 to mimic the anti-aging effects of resveratrol and improve the metabolic function of diabetic (type 2 diabetes) and obese mice (Zhang Y. et al., 2018; Cheang et al., 2019). Based on this effect, new drug strategies can be provided for the treatment of metabolic disorders and age-related diseases.

However, some scholars have put forward their views on the mechanism of STAC. They reported that SRT1720 and SRT2183 can effectively reduce acetylated p53 in cells treated with DNA damage agents by inhibiting the activity of P300 histone acetyltransferase even in cells lacking SIRT1 (Huber et al., 2010), indicating that the level of acetylation *in vivo* may be affected by various factors when using STAC. Recently, scholars have revealed the epigenetic alterations in patients with AD through an integrated multi-omics approach, in which the up-regulation of histone acetyltransferase expression in H3K27ac and H3K9ac leads to an increase in their acetylation level, and the activity and expression of SIRT1 in AD patients are also decreased (Nativio et al., 2020), which leads us to wonder whether restoring histone acetylation levels in patients with AD might reverse epigenetic alterations and provide new therapeutic targets for improving AD?

AMPK Activator

Part of the mechanism of metformin in the anti-aging and treatment of type 2 diabetes and neurodegenerative diseases is achieved by stimulating AMPK. The researchers found that AMPK activated by metformin preconditioning can effectively reduce the disorder of glucose and lipid metabolism, cellular oxidative stress, and renal function damage in diabetic rats through the SIRT1-dependent pathway, which has a protective effect on the pathological process of diabetes and diabetic nephropathy (Ren et al., 2020). In addition, the effects of metformin vary by cell and age. Metformin can activate AMPK and its downstream signal pathways in neurocytes, promote the recovery of mitochondrial function and reduce the accumulation of toxic proteins. Metformin combination therapy can even restore broken mitochondria to an almost normal state, thus meeting the energy needs of cells and improving age-related neurodegenerative diseases (Sharma S. et al., 2021). However, in cancer cells, AMPK activated by metformin can further activate the SIRT1/NF- κB pathway, induce mitochondrial dysfunction, and trigger cancer cell pyroptosis (Zheng et al., 2020). Furthermore, a recent study pointed out that the body's response to metformin is affected by age. Contrary to the anti-aging effect observed in young nematodes, metformin can aggravate aging-related mitochondrial dysfunction and lead to a shortening of life span in old *Caenorhabditis elegans* (Espada et al., 2020). The observed "cell and age discrimination" of metformin once again urges us to critically review the conventional wisdom and further explore the role of metformin in aging and aging-related diseases. Metformin plays a beneficial role by activating SIRT1-mediated, AMPK-independent autophagy pathways, and also combats the inhibition of intracytoplasmic P53 on parkin-mediated mitophagy, thus maintain mitochondrial quality (Song et al., 2016). This result is similar to another study, metformin promotes the expression of mitophagy-related genes to restore parkin-mediated mitophagy pathway activity, maintain mitochondrial integrity and cell survival, protect cells from high glucose-induced damage (Zhao and Sun, 2020). However, the association between mitophagy and SIRT1 has not been fully elucidated.

Other AMPK activators such as berberine and salidroside can significantly up-regulate the expression of phosphorylated AMPK, promote mitochondrial quality, improve insulin resistance and glucose uptake through stimulating AMPK/SIRT1 and its downstream signaling pathway (Shan et al., 2020; You et al., 2020). Moreover, the tricyclopyranone compound CP2 (Zhang et al., 2015), designed to have anti-central neurotoxic proteins and other neuroprotective effects, also activates AMPK, promoting mitochondrial function and reducing toxic protein accumulation (**Figure 2**).

CONCLUSION AND DISCUSSION

The imbalance of energy supply and demand make the body in a state of energy stress. Cells often redistribute the energy generated to important mechanisms and activities when the energy supply cannot meet the energy demand. As the main energy producer, the energy production of mitochondria is closely regulated by a variety of energy receptors in cells. Promoting the biosynthesis and function of mitochondria to produce enough ATP to meet the energy gap of cells has become an important means to break the energy stress state of cells.

SIRT1, the "hub" of intracellular signal, is widely involved in the processes of cell survival, apoptosis, inflammation, stress adaptation, cell growth and differentiation, metabolism, and senescence by regulating intracellular acetylation. However, the expression and activity of SIRT1 decreased significantly in pathological conditions such as aging or age-related diseases. In this review, we discussed that precise regulation of SIRT1 activity at all levels can eliminate cellular energy stress. We also discussed that SIRT1 molecular activator can promote the activity and expression of SIRT1 and play a useful role, which can be used as promising methods for the treatment of aging, neurodegenerative diseases, metabolic diseases, and other diseases.

As artificial energy stress can be tolerated by the body, previous studies have shown that different degrees of CR (20–50%) can cause beneficial metabolic adaptation in humans or mice, including the promotion of mitochondrial capacity and mitochondrial efficiency. Other studies also have found that a long-term CR diet can improve metabolism and promote fat loss, but the effect of fat loss will be quickly reversed once stopped (Melo et al., 2019). Therefore, I think we can implement CR with a continuous and progressive degree on mice to observe the effect on the body compared with the effect of CR with a constant degree of persistence. At the same time, the effect on weight reversal was observed by progressively reducing the extent of the CR diet rather than abruptly stopping the CR diet at the end.

NAD+ is the core prosthetic group for SIRT1 to exert its deacetylation activity, many pathways to increase SIRT1 activity are achieved by increasing the NAD+/NADH ratio. At present, some NMN-related preparations have been marketed as anti-aging products, but the effects of NAD+ metabolism have been objectively analyzed. Studies have revealed that a high NAD+/NADH ratio can drive the inflammation-related secretion phenotype of cancer-induced aging (Nacarelli et al.,

2019). This is a wake-up call for the future clinical development of NAD+-enhanced supplements: we should use dietary NAD+-enhanced supplements precisely to balance their pros and cons.

On the other hand, our study found that mitochondrial function is impaired under pathological conditions, which may be partly due to changes in mitochondrial dynamics and increased mitochondrial fragmentation (Yang D. et al., 2021). The SIRT1 pathway is beneficial to restore the quality and efficiency of mitochondria, so promoting the dynamic recovery of mitochondria is expected to be achieved by promoting the biosynthesis of mitochondria. Previous studies mainly focused on the nuclear-cytoplasmic shuttle of SIRT1. The subcellular localization of SIRT1 shows that SIRT1 in mitochondria can also communicate with SIRT1 in the cytoplasm, which provides a basis for us to accurately regulate the function of mitochondria through SIRT1.

In conclusion, although the mechanisms of SIRT1 and SIRT1-related activators in anti-aging and age-related diseases have not been clarified in detail, there is a complex and inseparable relationship between the fine regulation mechanism of SIRT1 activity and expression and the mitochondria function. Therefore, it is extremely important to further clarify the causal relationship between them to provide direction for the promotion of human health and anti-aging.

AUTHOR CONTRIBUTIONS

YF, JY and FH: conception, designing, and writing of the manuscript. XW, JY, DY, WY, XL and QZ: assisted in literature search, conception, and writing of the manuscript. FH, YL and GW: conception and revising the manuscript. All authors contributed to the article and approved the submitted version.

FUNDING

This work was supported by grants from the National Natural Science Foundation of China (81760261 and 82060219), Natural Science Foundation of Jiangxi Province (20192BCB23024 and 20202BABL206016), and Youth Team Project of the Second Affiliated Hospital of Nanchang University (2019YNTD12003).

ACKNOWLEDGMENTS

We apologize in advance to those researchers who contributed to the field and their publications were not listed in this review.

REFERENCES

Bai, L., Liu, R., Wang, R., Xin, Y., Wu, Z., Ba, Y., et al. (2021). Attenuation of Pb-induced Aβ generation and autophagic dysfunction *via* activation of SIRT1: neuroprotective properties of resveratrol. *Ecotoxicol. Environ. Saf.* 222:112511. doi: 10.1016/j.ecoenv.2021.112511

Cantó, C., Gerhart-Hines, Z., Feige, J. N., Lagouge, M., Noriega, L., Milne, J. C., et al. (2009). AMPK regulates energy expenditure by modulating NAD+ metabolism and SIRT1 activity. *Nature* 458, 1056–1060. doi: 10.1038/nature07813

Cao, K., Dong, Y.-T., Xiang, J., Xu, Y., Hong, W., Song, H., et al. (2018). Reduced expression of SIRT1 and SOD-1 and the correlation between these levels in various regions of the brains of patients with Alzheimer's disease. *J. Clin. Pathol.* 71, 1090–1099. doi: 10.1136/jclinpath-2018-205320

Cao, D., Wang, M., Qiu, X., Liu, D., Jiang, H., Yang, N., et al. (2015). Structural basis for allosteric, substrate-dependent stimulation of SIRT1 activity by resveratrol. *Genes Dev.* 29, 1316–1325. doi: 10.1101/gad.265462.115

Carbonell, F., Zijdenbos, A. P., and Bedell, B. J. (2020). Spatially distributed amyloid-β reduces glucose metabolism in mild cognitive impairment. *J. Alzheimers Dis.* 73, 543–557. doi: 10.3233/JAD-190560

Chandrasekaran, K., Anjaneyulu, M., Choi, J., Kumar, P., Salimian, M., Ho, C.-Y., et al. (2019). Role of mitochondria in diabetic peripheral neuropathy: influencing the nad+-dependent SIRT1-PGC-1α-TFAM pathway. *Int. Rev. Neurobiol.* 145, 177–209. doi: 10.1016/bs.irn.2019.04.002

Cheang, W. S., Wong, W. T., Wang, L., Cheng, C. K., Lau, C. W., Ma, R. C. W., et al. (2019). Resveratrol ameliorates endothelial dysfunction in diabetic and obese mice through sirtuin 1 and peroxisome proliferator-activated receptor δ. *Pharmacol. Res.* 139, 384–394. doi: 10.1016/j.phrs.2018.11.041

Chelladurai, P., Boucherat, O., Stenmark, K., Kracht, M., Seeger, W., Bauer, U.-M., et al. (2021). Targeting histone acetylation in pulmonary hypertension and right ventricular hypertrophy. *Br. J. Pharmacol.* 178, 54–71. doi: 10.1111/bph.14932

Chen, P., Chen, F., Lei, J., Li, Q., and Zhou, B. (2019). Activation of the miR-34a-mediated SIRT1/mTOR signaling pathway by urolithin A attenuates D-galactose-induced brain aging in mice. *Neurotherapeutics* 16, 1269–1282. doi: 10.1007/s13311-019-00753-0

Cheng, Z., Zhang, M., Ling, C., Zhu, Y., Ren, H., Hong, C., et al. (2019). Neuroprotective effects of ginsenosides against cerebral ischemia. *Molecules* 24:1102. doi: 10.3390/molecules24061102

Chimento, A., De Amicis, F., Sirianni, R., Sinicropi, M. S., Puoci, F., Casaburi, I., et al. (2019). Progress to improve oral bioavailability and beneficial effects of resveratrol. *Int. J. Mol. Sci.* 20:1381. doi: 10.3390/ijms20061381

Chini, C. C. S., Peclat, T. R., Warner, G. M., Kashyap, S., Espindola-Netto, J. M., de Oliveira, G. C., et al. (2020). CD38 ecto-enzyme in immune cells is induced during aging and regulates NAD+ and NMN levels. *Nat. Metab.* 2, 1284–1304. doi: 10.1038/s42255-020-00298-z

Choi, S. E., Kwon, S., Seok, S., Xiao, Z., Lee, K. W., Kang, Y., et al. (2017). Obesity-linked phosphorylation of SIRT1 by casein kinase 2 inhibits its nuclear localization and promotes fatty liver. *Mol. Cell. Biol.* 37:e00006-17. doi: 10.1128/MCB.00006-17

Corpas, R., Griñán-Ferré, C., Rodríguez-Farré, E., Pallàs, M., and Sanfeliu, C. (2019). Resveratrol induces brain resilience against alzheimer neurodegeneration through proteostasis enhancement. *Mol. Neurobiol.* 56, 1502–1516. doi: 10.1007/s12035-018-1157-y

Covarrubias, A. J., Kale, A., Perrone, R., Lopez-Dominguez, J. A., Pisco, A. O., Kasler, H. G., et al. (2021a). Author correction: senescent cells promote tissue NAD+ decline during ageing *via* the activation of CD38+ macrophages. *Nat. Metab.* 3, 120–121. doi: 10.1038/s42255-020-00328-w

Covarrubias, A. J., Perrone, R., Grozio, A., and Verdin, E. (2021b). NAD+ metabolism and its roles in cellular processes during ageing. *Nat. Rev. Mol. Cell Biol.* 22, 119–141. doi: 10.1038/s41580-020-00313-x

Cunnane, S. C., Trushina, E., Morland, C., Prigione, A., Casadesus, G., Andrews, Z. B., et al. (2020). Brain energy rescue: an emerging therapeutic concept for neurodegenerative disorders of ageing. *Nat. Rev. Drug Discov.* 19, 609–633. doi: 10.1038/s41573-020-0072-x

Dang, W., Steffen, K. K., Perry, R., Dorsey, J. A., Johnson, F. B., Shilatifard, A., et al. (2009). Histone H4 lysine 16 acetylation regulates cellular lifespan. *Nature* 459, 802–807. doi: 10.1038/nature08085

Ding, S., Liu, D., Wang, L., Wang, G., and Zhu, Y. (2020). Inhibiting MicroRNA-29a protects myocardial ischemia-reperfusion injury by targeting SIRT1 and suppressing oxidative stress and NLRP3-mediated pyroptosis pathway. *J. Pharmacol. Exp. Ther.* 372, 128–135. doi: 10.1124/jpet.119.256982

Dominy, J. E. Jr., Lee, Y., Gerhart-Hines, Z., and Puigserver, P. (2010). Nutrient-dependent regulation of PGC-1α's acetylation state and metabolic function through the enzymatic activities of Sirt1/GCN5. *Biochim. Biophys. Acta* 1804, 1676–1683. doi: 10.1016/j.bbapap.2009.11.023

Dong, X. C. (2012). Sirtuin biology and relevance to diabetes treatment. *Diabetes Manag.* 2, 243–257. doi: 10.2217/dmt.12.16

Dong, W., Wang, F., Guo, W., Zheng, X., Chen, Y., Zhang, W., et al. (2016). Aβ25–35 suppresses mitochondrial biogenesis in primary hippocampal neurons. *Cell. Mol. Neurobiol.* 36, 83–91. doi: 10.1007/s10571-015-0222-6

Dorling, J. L., Martin, C. K., and Redman, L. M. (2020). Calorie restriction for enhanced longevity: the role of novel dietary strategies in the present obesogenic environment. *Ageing Res. Rev.* 64:101038. doi: 10.1016/j.arr.2020.101038

Espada, L., Dakhovnik, A., Chaudhari, P., Martirosyan, A., Miek, L., Poliezhaieva, T., et al. (2020). Loss of metabolic plasticity underlies metformin toxicity in aged Caenorhabditis elegans. *Nat. Metab.* 2, 1316–1331. doi: 10.1038/s42255-020-00307-1

Fang, E. F., Scheibye-Knudsen, M., Brace, L. E., Kassahun, H., SenGupta, T., Nilsen, H., et al. (2014). Defective mitophagy in XPA *via* PARP-1 hyperactivation and NAD(+)/SIRT1 reduction. *Cell* 157, 882–896. doi: 10.1016/j.cell.2014.03.026

Feng, X., Sureda, A., Jafari, S., Memariani, Z., Tewari, D., Annunziata, G., et al. (2019). Berberine in cardiovascular and metabolic diseases: from mechanisms to therapeutics. *Theranostics* 9, 1923–1951. doi: 10.7150/thno.30787

Gao, Z., Zhang, J., Kheterpal, I., Kennedy, N., Davis, R. J., and Ye, J. (2011). Sirtuin 1 (SIRT1) protein degradation in response to persistent c-Jun N-terminal kinase 1 (JNK1) activation contributes to hepatic steatosis in obesity. *J. Biol. Chem.* 286, 22227–22234. doi: 10.1074/jbc.M111.228874

Gao, Y., Zhang, W., Zeng, L.-Q., Bai, H., Li, J., Zhou, J., et al. (2020). Exercise and dietary intervention ameliorate high-fat diet-induced NAFLD and liver aging by inducing lipophagy. *Redox Biol.* 36:101635. doi: 10.1016/j.redox.2020.101635

Ge, X., Xu, B., Xu, W., Xia, L., Xu, Z., Shen, L., et al. (2019). Long noncoding RNA GAS5 inhibits cell proliferation and fibrosis in diabetic nephropathy by sponging miR-221 and modulating SIRT1 expression. *Aging* 11, 8745–8759. doi: 10.18632/aging.102249

Gerhart-Hines, Z., Dominy, J. E., Blättler, S. M., Jedrychowski, M. P., Banks, A. S., Lim, J.-H., et al. (2011). The cAMP/PKA pathway rapidly activates SIRT1 to promote fatty acid oxidation independently of changes in NAD(+). *Mol. Cell* 44, 851–863. doi: 10.1016/j.molcel.2011.12.005

Gomes, A. P., Price, N. L., Ling, A. J. Y., Moslehi, J. J., Montgomery, M. K., Rajman, L., et al. (2013). Declining NAD+ induces a pseudohypoxic state disrupting nuclear-mitochondrial communication during aging. *Cell* 155, 1624–1638. doi: 10.1016/j.cell.2013.11.037

Gong, C., Qiao, L., Feng, R., Xu, Q., Zhang, Y., Fang, Z., et al. (2020). IL-6-induced acetylation of E2F1 aggravates oxidative damage of retinal pigment epithelial cell line. *Exp. Eye Res.* 200:108219. doi: 10.1016/j.exer.2020.108219

Guo, Q., Zhang, H., Zhang, B., Zhang, E., and Wu, Y. (2019). Tumor necrosis factor-α (TNF-α) enhances miR-155-mediated endothelial senescence by targeting sirtuin1 (SIRT1). *Med. Sci. Monit.* 25, 8820–8835. doi: 10.12659/MSM.919721

Gurd, B. J., Perry, C. G. R., Heigenhauser, G. J. F., Spriet, L. L., and Bonen, A. (2010). High-intensity interval training increases SIRT1 activity in human skeletal muscle. *Appl. Physiol. Nutr. Metab.* 35, 350–357. doi: 10.1139/H10-030

Han, L., Zhou, R., Niu, J., McNutt, M. A., Wang, P., and Tong, T. (2010). SIRT1 is regulated by a PPARγ-SIRT1 negative feedback loop associated with senescence. *Nucleic Acids Res.* 38, 7458–7471. doi: 10.1093/nar/gkq609

Hayashida, S., Arimoto, A., Kuramoto, Y., Kozako, T., Honda, S.-I., Shimeno, H., et al. (2010). Fasting promotes the expression of SIRT1, an NAD+ -dependent protein deacetylase, via activation of PPARα in mice. *Mol. Cell. Biochem.* 339, 285–292. doi: 10.1007/s11010-010-0391-z

Herzig, S., and Shaw, R. J. (2018). AMPK: guardian of metabolism and mitochondrial homeostasis. *Nat. Rev. Mol. Cell Biol.* 19, 121–135. doi: 10.1038/nrm.2017.95

Hikosaka, K., Yaku, K., Okabe, K., and Nakagawa, T. (2021). Implications of NAD metabolism in pathophysiology and therapeutics for neurodegenerative diseases. *Nutr. Neurosci.* 24, 371–383. doi: 10.1080/1028415X.2019.1637504

Hong, Y. A., Kim, J. E., Jo, M., and Ko, G.-J. (2020). The role of sirtuins in kidney diseases. *Int. J. Mol. Sci.* 21:6686. doi: 10.3390/ijms21186686

Hu, M., Zeng, H., Chen, S., Xu, Y., Wang, S., Tang, Y., et al. (2018). SRC-3 is involved in maintaining hematopoietic stem cell quiescence by regulation of mitochondrial metabolism in mice. *Blood* 132, 911–923. doi: 10.1182/blood-2018-02-831669

Hu, C., Zhang, X., Song, P., Yuan, Y.-P., Kong, C.-Y., Wu, H.-M., et al. (2020). Meteorin-like protein attenuates doxorubicin-induced cardiotoxicity via activating cAMP/PKA/SIRT1 pathway. *Redox Biol.* 37:101747. doi: 10.1016/j.redox.2020.101747

Huang, Q., Su, H., Qi, B., Wang, Y., Yan, K., Wang, X., et al. (2021). A SIRT1 activator, ginsenoside Rc, promotes energy metabolism in cardiomyocytes and neurons. *J. Am. Chem. Soc.* 143, 1416–1427. doi: 10.1021/jacs.0c10836

Huber, J. L., McBurney, M. W., Distefano, P. S., and McDonagh, T. (2010). SIRT1-independent mechanisms of the putative sirtuin enzyme activators SRT1720 and SRT2183. *Future Med. Chem.* 2, 1751–1759. doi: 10.4155/fmc.10.257

Ji, M.-L., Jiang, H., Zhang, X.-J., Shi, P.-L., Li, C., Wu, H., et al. (2018). Preclinical development of a microRNA-based therapy for intervertebral disc degeneration. *Nat. Commun.* 9:5051. doi: 10.1038/s41467-018-07360-1

Jiang, M., Wang, J., Fu, J., Du, L., Jeong, H., West, T., et al. (2011). Neuroprotective role of Sirt1 in mammalian models of Huntington's disease through activation of multiple Sirt1 targets. *Nat. Med.* 18, 153–158. doi: 10.1038/nm.2558

Jiao, F., and Gong, Z. (2020). The beneficial roles of SIRT1 in neuroinflammation-related diseases. *Oxid. Med. Cell. Longev.* 2020:6782872. doi: 10.1155/2020/6782872

Joshi, A. U., Minhas, P. S., Liddelow, S. A., Haileselassie, B., Andreasson, K. I., Dorn, G. W., et al. (2019). Fragmented mitochondria released from microglia trigger A1 astrocytic response and propagate inflammatory neurodegeneration. *Nat. Neurosci.* 22, 1635–1648. doi: 10.1038/s41593-019-0486-0

Juszczak, F., Caron, N., Mathew, A. V., and Declèves, A.-E. (2020). Critical role for AMPK in metabolic disease-induced chronic kidney disease. *Int. J. Mol. Sci.* 21:7994. doi: 10.3390/ijms21217994

Karstoft, K., Brinkløv, C. F., Thorsen, I. K., Nielsen, J. S., and Ried-Larsen, M. (2017). Resting metabolic rate does not change in response to different types of training in subjects with type 2 diabetes. *Front. Endocrinol.* 8:132. doi: 10.3389/fendo.2017.00132

Kerr, J. S., Adriaanse, B. A., Greig, N. H., Mattson, M. P., Cader, M. Z., Bohr, V. A., et al. (2017). Mitophagy and Alzheimer's disease: cellular and molecular mechanisms. *Trends Neurosci.* 40, 151–166. doi: 10.1016/j.tins.2017.01.002

Knuiman, P., Hopman, M. T. E., Wouters, J. A., and Mensink, M. (2018). Select skeletal muscle mRNAs related to exercise adaptation are minimally affected by different pre-exercise meals that differ in macronutrient profile. *Front. Physiol.* 9:28. doi: 10.3389/fphys.2018.00028

Kosgei, V. J., Coelho, D., Guéant-Rodriguez, R.-M., and Guéant, J.-L. (2020). Sirt1-PPARS cross-talk in complex metabolic diseases and inherited disorders of the one carbon metabolism. *Cells* 9:1882. doi: 10.3390/cells9081882

Koves, T. R., Li, P., An, J., Akimoto, T., Slentz, D., Ilkayeva, O., et al. (2005). Peroxisome proliferator-activated receptor-γ co-activator 1α-mediated metabolic remodeling of skeletal myocytes mimics exercise training and reverses lipid-induced mitochondrial inefficiency. *J. Biol. Chem.* 280, 33588–33598. doi: 10.1074/jbc.M507621200

Lamb, D. A., Moore, J. H., Mesquita, P. H. C., Smith, M. A., Vann, C. G., Osburn, S. C., et al. (2020). Resistance training increases muscle NAD+ and NADH concentrations as well as NAMPT protein levels and global sirtuin activity in middle-aged, overweight, untrained individuals. *Aging* 12, 9447–9460. doi: 10.18632/aging.103218

Lamichane, S., Baek, S. H., Kim, Y.-J., Park, J. H., Dahal Lamichane, B., Jang, W. B., et al. (2019). MHY2233 attenuates replicative cellular senescence in human endothelial progenitor cells SIRT1 signaling. *Oxid. Med. Cell. Longev.* 2019:6492029. doi: 10.1155/2019/6492029

Lan, Y., Dong, M., Li, Y., Diao, Y., Chen, Z., and Li, Y. (2021). SIRT1-induced deacetylation of Akt expedites platelet phagocytosis and delays HEMEC aging. *Mol. Ther. Nucleic Acids* 23, 1323–1333. doi: 10.1016/j.omtn.2021.01.023

Lan, F., Weikel, K. A., Cacicedo, J. M., and Ido, Y. (2017). Resveratrol-induced AMP-activated protein kinase activation is cell-type dependent: lessons from

basic research for clinical application. *Nutrients* 9:751. doi: 10.3390/nu9070751

Li, T., Mao, C., Wang, X., Shi, Y., and Tao, Y. (2020). Epigenetic crosstalk between hypoxia and tumor driven by HIF regulation. *J. Exp. Clin. Cancer Res.* 39:224. doi: 10.1186/s13046-020-01733-5

Li, X., Wu, G., Han, F., Wang, K., Bai, X., Jia, Y., et al. (2019). SIRT1 activation promotes angiogenesis in diabetic wounds by protecting endothelial cells against oxidative stress. *Arch. Biochem. Biophys.* 661, 117–124. doi: 10.1016/j.abb.2018.11.016

Li, H., Xu, M., Lee, J., He, C., and Xie, Z. (2012). Leucine supplementation increases SIRT1 expression and prevents mitochondrial dysfunction and metabolic disorders in high-fat diet-induced obese mice. *Am. J. Physiol. Endocrinol. Metab.* 303, E1234–E1244. doi: 10.1152/ajpendo.00198.2012

Li, Z., Zhang, Z., Ke, L., Sun, Y., Li, W., Feng, X., et al. (2020). Resveratrol promotes white adipocytes browning and improves metabolic disorders in Sirt1-dependent manner in mice. *FASEB J.* 34, 4527–4539. doi: 10.1096/fj.201902222R

Lin, J.-Y., Kuo, W.-W., Baskaran, R., Kuo, C.-H., Chen, Y.-A., Chen, W. S.-T., et al. (2020). Swimming exercise stimulates IGF1/ PI3K/Akt and AMPK/SIRT1/PGC1α survival signaling to suppress apoptosis and inflammation in aging hippocampus. *Aging* 12, 6852–6864. doi: 10.18632/aging.103046

Liu, J., Ai, Y., Niu, X., Shang, F., Li, Z., Liu, H., et al. (2020). Taurine protects against cardiac dysfunction induced by pressure overload through SIRT1–p53 activation. *Chem. Biol. Interact.* 317:108972. doi: 10.1016/j.cbi.2020.108972

Long, J.-K., Dai, W., Zheng, Y.-W., and Zhao, S.-P. (2019). miR-122 promotes hepatic lipogenesis via inhibiting the LKB1/AMPK pathway by targeting Sirt1 in non-alcoholic fatty liver disease. *Mol. Med.* 25:26. doi: 10.1186/s10020-019-0085-2

Lou, T., Huang, Q., Su, H., Zhao, D., and Li, X. (2021). Targeting Sirtuin 1 signaling pathway by ginsenosides. *J. Ethnopharmacol.* 268:113657. doi: 10.1016/j.jep.2020.113657

Lu, S., Yin, X., Wang, J., Gu, Q., Huang, Q., Jin, N., et al. (2020). SIRT1 regulates O-GlcNAcylation of tau through OGT. *Aging* 12, 7042–7055. doi: 10.18632/aging.103062

Luo, J., Li, M., Tang, Y., Laszkowska, M., Roeder, R. G., and Gu, W. (2004). Acetylation of p53 augments its site-specific DNA binding both *in vitro* and *in vivo*. *Proc. Natl. Acad. Sci. U S A* 101, 2259–2264. doi: 10.1073/pnas.0308762101

Ma, Y., and Li, J. (2015). Metabolic shifts during aging and pathology. *Compr. Physiol.* 5, 667–686. doi: 10.1002/cphy.c140041

Ma, X., Sun, Z., Han, X., Li, S., Jiang, X., Chen, S., et al. (2019). Neuroprotective effect of resveratrol *via* activation of Sirt1 signaling in a rat model of combined diabetes and Alzheimer's disease. *Front. Neurosci.* 13:1400. doi: 10.3389/fnins.2019.01400

Maiese, K. (2021). Targeting the core of neurodegeneration: FoxO, mTOR, and SIRT1. *Neural Regen. Res.* 16, 448–455. doi: 10.4103/1673-5374.291382

Manjula, R., Anuja, K., and Alcain, F. J. (2020). SIRT1 and SIRT2 activity control in neurodegenerative diseases. *Front. Pharmacol.* 11:585821. doi: 10.3389/fphar.2020.585821

Mao, Q., Liang, X.-L., Zhang, C.-L., Pang, Y.-H., and Lu, Y.-X. (2019). LncRNA KLF3-AS1 in human mesenchymal stem cell-derived exosomes ameliorates pyroptosis of cardiomyocytes and myocardial infarction through miR-138–5p/Sirt1 axis. *Stem Cell Res. Ther.* 10:393. doi: 10.1186/s13287-019-1522-4

Melo, D. D. S., Santos, C. S., Pereira, L. C., Mendes, B. F., Jesus, L. S., Pelaez, J. M. N., et al. (2019). Refeeding abolishes beneficial effects of severe calorie restriction from birth on adipose tissue and glucose homeostasis of adult rats. *Nutrition* 66, 87–93. doi: 10.1016/j.nut.2019.03.022

Murphy, M. P., and Hartley, R. C. (2018). Mitochondria as a therapeutic target for common pathologies. *Nat. Rev. Drug Discov.* 17, 865–886. doi: 10.1038/nrd.2018.174

Mutlu, B., and Puigserver, P. (2021). GCN5 acetyltransferase in cellular energetic and metabolic processes. *Biochim. Biophys. Acta Gene Regul. Mech* 1864:194626. doi: 10.1016/j.bbagrm.2020.194626

Nacarelli, T., Lau, L., Fukumoto, T., Zundell, J., Fatkhutdinov, N., Wu, S., et al. (2019). NAD+ metabolism governs the proinflammatory senescence-associated secretome. *Nat. Cell Biol.* 21, 397–407. doi: 10.1038/s41556-019-0287-4

Nasrin, N., Kaushik, V. K., Fortier, E., Wall, D., Pearson, K. J., de Cabo, R., et al. (2009). JNK1 phosphorylates SIRT1 and promotes its enzymatic activity. *PLoS One* 4:e8414. doi: 10.1371/journal.pone.0008414

Nativio, R., Lan, Y., Donahue, G., Sidoli, S., Berson, A., Srinivasan, A. R., et al. (2020). An integrated multi-omics approach identifies epigenetic alterations associated with Alzheimer's disease. *Nat. Genet.* 52, 1024–1035. doi: 10.1038/s41588-020-0696-0

Nguyen, L. T., Chen, H., Zaky, A., Pollock, C., and Saad, S. (2019). SIRT1 overexpression attenuates offspring metabolic and liver disorders as a result of maternal high-fat feeding. *J. Physiol.* 597, 467–480. doi: 10.1113/JP276957

Nin, V., Escande, C., Chini, C. C., Giri, S., Camacho-Pereira, J., Matalonga, J., et al. (2012). Role of deleted in breast cancer 1 (DBC1) protein in SIRT1 deacetylase activation induced by protein kinase A and AMP-activated protein kinase. *J. Biol. Chem.* 287, 23489–23501. doi: 10.1074/jbc.M112.365874

Noriega, L. G., Feige, J. N., Canto, C., Yamamoto, H., Yu, J., Herman, M. A., et al. (2011). CREB and ChREBP oppositely regulate SIRT1 expression in response to energy availability. *EMBO Rep.* 12, 1069–1076. doi: 10.1038/embor.2011.151

Okazaki, M., Iwasaki, Y., Nishiyama, M., Taguchi, T., Tsugita, M., Nakayama, S., et al. (2010). PPARbeta/delta regulates the human SIRT1 gene transcription via Sp1. *Endocr. J.* 57, 403–413. doi: 10.1507/endocrj.k10e-004

Paget, S., Dubuissez, M., Page, A., Dehennaut, V., Loison, I., Spruyt, N., et al. (2021). Phosphorylation of HIC1 (Hypermethylated in Cancer 1) Ser694 by ATM is essential for DNA repair. *Biochem. Biophys. Res. Commun.* 553, 51–57. doi: 10.1016/j.bbrc.2021.03.060

Park, S.-J., Ahmad, F., Um, J.-H., Brown, A. L., Xu, X., Kang, H., et al. (2017). Specific Sirt1 activator-mediated improvement in glucose homeostasis requires Sirt1-independent activation of AMPK. *EBioMedicine* 18, 128–138. doi: 10.1016/j.ebiom.2017.03.019

Popov, L.-D. (2020). Mitochondrial biogenesis: an update. *J. Cell Mol. Med.* 24, 4892–4899. doi: 10.1111/jcmm.15194

Price, N. L., Gomes, A. P., Ling, A. J. Y., Duarte, F. V., Martin-Montalvo, A., North, B. J., et al. (2012). SIRT1 is required for AMPK activation and the beneficial effects of resveratrol on mitochondrial function. *Cell Metab.* 15, 675–690. doi: 10.1016/j.cmet.2012.04.003

Pyo, I. S., Yun, S., Yoon, Y. E., Choi, J.-W., and Lee, S.-J. (2020). Mechanisms of aging and the preventive effects of resveratrol on age-related diseases. *Molecules* 25:4649. doi: 10.3390/molecules25204649

Qu, B., Gong, K., Yang, H.-S., Li, Y.-G., Jiang, T., Zeng, Z.-M., et al. (2018). MiR-449 overexpression inhibits osteogenic differentiation of bone marrow mesenchymal stem cells via suppressing Sirt1/Fra-1 pathway in high glucose and free fatty acids microenvironment. *Biochem. Biophys. Res. Commun.* 496, 120–126. doi: 10.1016/j.bbrc.2018.01.009

Ren, Z., He, H., Zuo, Z., Xu, Z., Wei, Z., and Deng, J. (2019). The role of different SIRT1-mediated signaling pathways in toxic injury. *Cell. Mol. Biol. Lett.* 24:36. doi: 10.1186/s11658-019-0158-9

Ren, H., Shao, Y., Wu, C., Ma, X., Lv, C., and Wang, Q. (2020). Metformin alleviates oxidative stress and enhances autophagy in diabetic kidney disease via AMPK/SIRT1-FoxO1 pathway. *Mol. Cell. Endocrinol.* 500:110628. doi: 10.1016/j.mce.2019.110628

Ryall, J. G., Dell'Orso, S., Derfoul, A., Juan, A., Zare, H., Feng, X., et al. (2015). The NAD+-dependent SIRT1 deacetylase translates a metabolic switch into regulatory epigenetics in skeletal muscle stem cells. *Cell Stem Cell* 16, 171–183. doi: 10.1016/j.stem.2014.12.004

Saklayen, M. G. (2018). The global epidemic of the metabolic syndrome. *Curr. Hypertens. Rep.* 20:12. doi: 10.1007/s11906-018-0812-z

Sasaki, T., Maier, B., Koclega, K. D., Chruszcz, M., Gluba, W., Stukenberg, P. T., et al. (2008). Phosphorylation regulates SIRT1 function. *PLoS One* 3:e4020. doi: 10.1371/journal.pone.0004020

Scheibye-Knudsen, M., Fang, E. F., Croteau, D. L., and Bohr, V. A. (2014). Contribution of defective mitophagy to the neurodegeneration in DNA repair-deficient disorders. *Autophagy* 10, 1468–1469. doi: 10.4161/auto.29321

Schöndorf, D. C., Ivanyuk, D., Baden, P., Sanchez-Martinez, A., De Cicco, S., Yu, C., et al. (2018). The NAD+ precursor nicotinamide riboside rescues mitochondrial defects and neuronal loss in iPSC and fly models of Parkinson's disease. *Cell Rep.* 23, 2976–2988. doi: 10.1016/j.celrep.2018.05.009

Shan, Y., Zhang, S., Gao, B., Liang, S., Zhang, H., Yu, X., et al. (2020). Adipose tissue SIRT1 regulates insulin sensitizing and anti-inflammatory effects of berberine. *Front. Pharmacol.* 11:591227. doi: 10.3389/fphar.2020.591227

Shao, Z., Lee, B. J., Rouleau-Turcotte, É., Langelier, M.-F., Lin, X., Estes, V. M., et al. (2020). Clinical PARP inhibitors do not abrogate PARP1 exchange at DNA damage sites *in vivo*. *Nucleic Acids Res.* 48, 9694–9709. doi: 10.1093/nar/gkaa718

Sharma, A., Anand, S. K., Singh, N., Dwarkanath, A., Dwivedi, U. N., and Kakkar, P. (2021). Berbamine induced activation of the SIRT1/LKB1/AMPK signaling axis attenuates the development of hepatic steatosis in high-fat diet-induced NAFLD rats. *Food Funct.* 12, 892–909. doi: 10.1039/d0fo02501a

Sharma, S., Nozohouri, S., Vaidya, B., and Abbruscato, T. (2021). Repurposing metformin to treat age-related neurodegenerative disorders and ischemic stroke. *Life Sci.* 274:119343. doi: 10.1016/j.lfs.2021.119343

Sim, W.-C., Kim, D. G., Lee, W., Sim, H., Choi, Y. J., and Lee, B. H. (2019). Activation of SIRT1 by L-serine increases fatty acid oxidation and reverses insulin resistance in C2C12 myotubes. *Cell Biol. Toxicol.* 35, 457–470. doi: 10.1007/s10565-019-09463-x

Singh, A. P., Singh, R., Verma, S. S., Rai, V., Kaschula, C. H., Maiti, P., et al. (2019). Health benefits of resveratrol: evidence from clinical studies. *Med. Res. Rev.* 39, 1851–1891. doi: 10.1002/med.21565

Song, J., and Bae, Y.-S. (2021). CK2 down-regulation increases the expression of senescence-associated secretory phenotype factors through NF-κB activation. *Int. J. Mol. Sci.* 22:406. doi: 10.3390/ijms22010406

Song, L., Chen, T.-Y., Zhao, X.-J., Xu, Q., Jiao, R.-Q., Li, J.-M., et al. (2019). Pterostilbene prevents hepatocyte epithelial-mesenchymal transition in fructose-induced liver fibrosis through suppressing miR-34a/Sirt1/p53 and TGF-β1/Smads signalling. *Br. J. Pharmacol.* 176, 1619–1634. doi: 10.1111/bph.14573

Song, J.-Y., Lee, S.-H., Kim, M.-K., Jeon, B.-N., Cho, S.-Y., Lee, S.-H., et al. (2019). HIC2, a new transcription activator of SIRT1. *FEBS Lett.* 593, 1763–1776. doi: 10.1002/1873-3468.13456

Song, Y. M., Lee, W. K., Lee, Y.-H., Kang, E. S., Cha, B.-S., and Lee, B.-W. (2016). Metformin restores parkin-mediated mitophagy, suppressed by cytosolic p53. *Int. J. Mol. Sci.* 17:122. doi: 10.3390/ijms17010122

Sorrenti, V., Davinelli, S., Scapagnini, G., Willcox, B. J., Allsopp, R. C., and Willcox, D. C. (2020). Astaxanthin as a putative geroprotector: molecular basis and focus on brain aging. *Mar. Drugs* 18:351. doi: 10.3390/md18070351

Spinelli, S., Begani, G., Guida, L., Magnone, M., Galante, D., D'Arrigo, C., et al. (2021). LANCL1 binds abscisic acid and stimulates glucose transport and mitochondrial respiration in muscle cells via the AMPK/PGC-1α/Sirt1 pathway. *Mol. Metab.* 53:101263. doi: 10.1016/j.molmet.2021.101263

Sun, Q., Hu, H., Wang, W., Jin, H., Feng, G., and Jia, N. (2014). Taurine attenuates amyloid β 1–42-induced mitochondrial dysfunction by activating of SIRT1 in SK-N-SH cells. *Biochem. Biophys. Res. Commun.* 447, 485–489. doi: 10.1016/j.bbrc.2014.04.019

Sun, K., Jing, X., Guo, J., Yao, X., and Guo, F. (2020). Mitophagy in degenerative joint diseases. *Autophagy* doi: 10.1080/15548627.2020.1822097. [Epub ahead of print].

Sun, X., and Zemel, M. B. (2009). Leucine modulation of mitochondrial mass and oxygen consumption in skeletal muscle cells and adipocytes. *Nutr. Metab.* 6:26. doi: 10.1186/1743-7075-6-26

Tanno, M., Sakamoto, J., Miura, T., Shimamoto, K., and Horio, Y. (2007). Nucleocytoplasmic shuttling of the NAD+-dependent histone deacetylase SIRT1. *J. Biol. Chem.* 282, 6823–6832. doi: 10.1074/jbc.M609554200

Vaziri, H., Dessain, S. K., Ng Eaton, E., Imai, S. I., Frye, R. A., Pandita, T. K., et al. (2001). hSIR2(SIRT1) functions as an NAD-dependent p53 deacetylase. *Cell* 107, 149–159. doi: 10.1016/s0092-8674(01)00527-x

Wang, L.-F., Cao, Q., Wen, K., Xiao, Y.-F., Chen, T.-T., Guan, X.-H., et al. (2019). CD38 deficiency alleviates D-galactose-induced myocardial cell senescence through NAD^+/Sirt1 signaling pathway. *Front. Physiol.* 10:1125. doi: 10.3389/fphys.2019.01125

Wang, Y., Liang, X., Chen, Y., and Zhao, X. (2016). Screening SIRT1 activators from medicinal plants as bioactive compounds against oxidative damage in mitochondrial function. *Oxid. Med. Cell. Longev.* 2016:4206392. doi: 10.1155/2016/4206392

Wang, L., Sun, M., Cao, Y., Ma, L., Shen, Y., Velikanova, A. A., et al. (2020). miR-34a regulates lipid metabolism by targeting SIRT1 in non-alcoholic fatty liver disease with iron overload. *Arch. Biochem. Biophys.* 695:108642. doi: 10.1016/j.abb.2020.108642

Wang, L., Xu, C., Johansen, T., Berger, S. L., and Dou, Z. (2021). SIRT1—a new mammalian substrate of nuclear autophagy. *Autophagy* 17, 593–595. doi: 10.1080/15548627.2020.1860541

Wang, S., Yang, Y., He, X., Yang, L., Wang, J., Xia, S., et al. (2020). Cdk5-mediated phosphorylation of sirt1 contributes to podocyte mitochondrial dysfunction in diabetic nephropathy. *Antioxid. Redox Signal.* 34, 171–190. doi: 10.1089/ars.2020.8038

Włodarski, A., Strycharz, J., Wróblewski, A., Kasznicki, J., Drzewoski, J., and Śliwińska, A. (2020). The role of microRNAs in metabolic syndrome-related oxidative stress. *Int. J. Mol. Sci.* 21:6902. doi: 10.3390/ijms21186902

Wood, J. G., Rogina, B., Lavu, S., Howitz, K., Helfand, S. L., Tatar, M., et al. (2004). Sirtuin activators mimic caloric restriction and delay ageing in metazoans. *Nature* 430, 686–689. doi: 10.1038/nature02789

Xie, L., Huang, W., Fang, Z., Ding, F., Zou, F., Ma, X., et al. (2019). CircERCC2 ameliorated intervertebral disc degeneration by regulating mitophagy and apoptosis through miR-182–5p/SIRT1 axis. *Cell Death Dis.* 10:751. doi: 10.1038/s41419-019-1978-2

Xiong, H., Chen, S., Lai, L., Yang, H., Xu, Y., Pang, J., et al. (2019). Modulation of miR-34a/SIRT1 signaling protects cochlear hair cells against oxidative stress and delays age-related hearing loss through coordinated regulation of mitophagy and mitochondrial biogenesis. *Neurobiol. Aging* 79, 30–42. doi: 10.1016/j.neurobiolaging.2019.03.013

Xiong, S., Salazar, G., Patrushev, N., and Alexander, R. W. (2011). FoxO1 mediates an autofeedback loop regulating SIRT1 expression. *J. Biol. Chem.* 286, 5289–5299. doi: 10.1074/jbc.M110.163667

Xu, C., Wang, L., Fozouni, P., Evjen, G., Chandra, V., Jiang, J., et al. (2020). SIRT1 is downregulated by autophagy in senescence and ageing. *Nat. Cell Biol.* 22, 1170–1179. doi: 10.1038/s41556-020-00579-5

Yamakuchi, M. (2012). MicroRNA regulation of SIRT1. *Front. Physiol.* 3:68. doi: 10.3389/fphys.2012.00068

Yan, Y., Zhou, X. E., Xu, H. E., and Melcher, K. (2018). Structure and physiological regulation of AMPK. *Int. J. Mol. Sci.* 19:3534. doi: 10.3390/ijms19113534

Yang, N.-C., Cho, Y.-H., and Lee, I. (2019). The lifespan extension ability of nicotinic acid depends on whether the intracellular NAD+ level is lower than the sirtuin-saturating concentrations. *Int. J. Mol. Sci.* 21:142. doi: 10.3390/ijms21010142

Yang, Q.-Y., Lai, X.-D., Ouyang, J., and Yang, J.-D. (2018). Effects of Ginsenoside Rg3 on fatigue resistance and SIRT1 in aged rats. *Toxicology* 409, 144–151. doi: 10.1016/j.tox.2018.08.010

Yang, Y., Liu, Y., Xue, J., Yang, Z., Shi, Y., Shi, Y., et al. (2017). MicroRNA-141 targets Sirt1 and inhibits autophagy to reduce HBV replication. *Cell. Physiol. Biochem.* 41, 310–322. doi: 10.1159/000456162

Yang, B., Yu, Q., Chang, B., Guo, Q., Xu, S., Yi, X., et al. (2021). MOTS-c interacts synergistically with exercise intervention to regulate PGC-1α expression, attenuate insulin resistance and enhance glucose metabolism in mice via AMPK signaling pathway. *Biochim. Biophys. Acta Mol. Basis Dis.* 1867:166126. doi: 10.1016/j.bbadis.2021.166126

Yang, D., Ying, J., Wang, X., Zhao, T., Yoon, S., Fang, Y., et al. (2021). Mitochondrial dynamics: a key role in neurodegeneration and a potential target for neurodegenerative disease. *Front. Neurosci.* 15:654785. doi: 10.3389/fnins.2021.654785

Yang, T., Zhou, R., Yu, S., Yu, S., Cui, Z., Hu, P., et al. (2019). Cytoplasmic SIRT1 inhibits cell migration and invasion by impeding epithelial-mesenchymal transition in ovarian carcinoma. *Mol. Cell. Biochem.* 459, 157–169. doi: 10.1007/s11010-019-03559-y

Yin, J., Zhang, B., Yu, Z., Hu, Y., Lv, H., Ji, X., et al. (2021). Ameliorative effect of dietary tryptophan on neurodegeneration and inflammation in d-galactose-induced aging mice with the potential mechanism relying on AMPK/SIRT1/PGC-1α pathway and gut microbiota. *J. Agric. Food Chem.* 69, 4732–4744. doi: 10.1021/acs.jafc.1c00706

Yoshino, J., Baur, J. A., and Imai, S.-I. (2018). NAD+ intermediates: the biology and therapeutic potential of NMN and NR. *Cell Metab.* 27, 513–528. doi: 10.1016/j.cmet.2017.11.002

You, B., Dun, Y., Zhang, W., Jiang, L., Li, H., Xie, M., et al. (2020). Anti-insulin resistance effects of salidroside through mitochondrial quality control. *J. Endocrinol.* 244, 383–393. doi: 10.1530/JOE-19-0393

Yu, A., Zhou, R., Xia, B., Dang, W., Yang, Z., and Chen, X. (2020). NAMPT maintains mitochondria content via NRF2-PPARα/AMPKα pathway to promote cell survival under oxidative stress. *Cell. Signal.* 66:109496. doi: 10.1016/j.cellsig.2019.109496

Yuan, Y., Cruzat, V. F., Newsholme, P., Cheng, J., Chen, Y., and Lu, Y. (2016). Regulation of SIRT1 in aging: roles in mitochondrial function and biogenesis. *Mech. Ageing Dev.* 155, 10–21. doi: 10.1016/j.mad.2016.02.003

Zemel, M. B. (2020). Modulation of energy sensing by leucine synergy with natural sirtuin activators: effects on health span. *J. Med. Food* 23, 1129–1135. doi: 10.1089/jmf.2020.0105

Zhang, S., Sheng, H., Zhang, X., Qi, Q., Chan, C. B., Li, L., et al. (2019). Cellular energy stress induces AMPK-mediated regulation of glioblastoma cell proliferation by PIKE-A phosphorylation. *Cell Death Dis.* 10:222. doi: 10.1038/s41419-019-1452-1

Zhang, Y., Thai, K., Jin, T., Woo, M., and Gilbert, R. E. (2018). SIRT1 activation attenuates α cell hyperplasia, hyperglucagonaemia and hyperglycaemia in STZ-diabetic mice. *Sci. Rep.* 8:13972. doi: 10.1038/s41598-018-32351-z

Zhang, F., Wang, K., Hu, G., Fu, F., Fan, R., Li, J., et al. (2021). Genetic ablation of fas-activated serine/threonine kinase ameliorates alcoholic liver disease through modulating HuR-SIRT1 mRNA complex stability. *Free Radic. Biol. Med.* 166, 201–211. doi: 10.1016/j.freeradbiomed.2021.02.002

Zhang, L.-F., Yu, X.-L., Ji, M., Liu, S.-Y., Wu, X.-L., Wang, Y.-J., et al. (2018). Resveratrol alleviates motor and cognitive deficits and neuropathology in the A53T α-synuclein mouse model of Parkinson's disease. *Food Funct.* 9, 6414–6426. doi: 10.1039/c8fo00964c

Zhang, Q., Zhang, P., Qi, G. J., Zhang, Z., He, F., Lv, Z. X., et al. (2018). Cdk5 suppression blocks SIRT1 degradation via the ubiquitin-proteasome pathway in Parkinson's disease models. *Biochim. Biophys. Acta Gen. Subj.* 1862, 1443–1451. doi: 10.1016/j.bbagen.2018.03.021

Zhang, L., Zhang, S., Maezawa, I., Trushin, S., Minhas, P., Pinto, M., et al. (2015). Modulation of mitochondrial complex I activity averts cognitive decline in multiple animal models of familial Alzheimer's Disease. *EBioMedicine* 2, 294–305. doi: 10.1016/j.ebiom.2015.03.009

Zhao, Y., and Sun, M. (2020). Metformin rescues Parkin protein expression and mitophagy in high glucose-challenged human renal epithelial cells by inhibiting NF-κB via PP2A activation. *Life Sci.* 246:117382. doi: 10.1016/j.lfs.2020.117382

Zhao, M.-W., Yang, P., and Zhao, L.-L. (2019). Chlorpyrifos activates cell pyroptosis and increases susceptibility on oxidative stress-induced toxicity by miR-181/SIRT1/PGC-1α/Nrf2 signaling pathway in human neuroblastoma SH-SY5Y cells: implication for association between chlorpyrifos and Parkinson's disease. *Environ. Toxicol.* 34, 699–707. doi: 10.1002/tox.22736

Zheng, Z., Bian, Y., Zhang, Y., Ren, G., and Li, G. (2020). Metformin activates AMPK/SIRT1/NF-κB pathway and induces mitochondrial dysfunction to drive caspase3/GSDME-mediated cancer cell pyroptosis. *Cell Cycle* 19, 1089–1104. doi: 10.1080/15384101.2020.1743911

Zhou, Y., Li, K.-S., Liu, L., and Li, S.-L. (2020). MicroRNA-132 promotes oxidative stress-induced pyroptosis by targeting sirtuin 1 in myocardial ischaemia-reperfusion injury. *Int. J. Mol. Med.* 45, 1942–1950. doi: 10.3892/ijmm.2020.4557

Zhou, Y., Wang, S., Li, Y., Yu, S., and Zhao, Y. (2017). SIRT1/PGC-1α signaling promotes mitochondrial functional recovery and reduces apoptosis after intracerebral hemorrhage in rats. *Front. Mol. Neurosci.* 10:443. doi: 10.3389/fnmol.2017.00443

Zhu, Y., Liu, J., Park, J., Rai, P., and Zhai, R. G. (2019). Subcellular compartmentalization of NAD+ and its role in cancer: a sereNADe of metabolic melodies. *Pharmacol. Ther.* 200, 27–41. doi: 10.1016/j.pharmthera.2019.04.002

Conflict of Interest: The authors declare that the research was conducted in the absence of any commercial or financial relationships that could be construed as a potential conflict of interest.

Publisher's Note: All claims expressed in this article are solely those of the authors and do not necessarily represent those of their affiliated organizations, or those of the publisher, the editors and the reviewers. Any product that may be evaluated in this article, or claim that may be made by its manufacturer, is not guaranteed or endorsed by the publisher.

frontiers in Aging Neuroscience

ORIGINAL RESEARCH
published: 27 October 2021
doi: 10.3389/fnagi.2021.765252

Effects of Sex, Age, and Apolipoprotein E Genotype on Brain Ceramides and Sphingosine-1-Phosphate in Alzheimer's Disease and Control Mice

Sandra den Hoedt[1†], Simone M. Crivelli[2†], Frank P. J. Leijten[1], Mario Losen[2], Jo A. A. Stevens[2], Marina Mané-Damas[2], Helga E. de Vries[3], Jochen Walter[4], Mina Mirzaian[5], Eric J. G. Sijbrands[1], Johannes M. F. G. Aerts[6], Adrie J. M. Verhoeven[1], Pilar Martinez-Martinez[2‡] and Monique T. Mulder[1*‡]*

[1] Department of Internal Medicine, Erasmus University Medical Center, Rotterdam, Netherlands, [2] Department of Psychiatry and Neuropsychology, School for Mental Health and Neuroscience, Maastricht University, Maastricht, Netherlands, [3] Department of Molecular Cell Biology and Immunology, Amsterdam Neuroscience, VU Medical Center, Amsterdam UMC, Amsterdam, Netherlands, [4] Department of Neurology, University Hospital Bonn, Venusberg Campus, Bonn, Germany, [5] Department of Clinical Chemistry, Erasmus University Medical Center, Rotterdam, Netherlands, [6] Leiden Institute of Chemistry, Leiden University, Leiden, Netherlands

OPEN ACCESS

Edited by:
Kristine Freude,
University of Copenhagen, Denmark

Reviewed by:
Malin Wennström,
Lund University, Sweden
Robert Piotr Strosznajder,
Mossakowski Medical Research Centre, Polish Academy of Sciences (PAN), Poland

***Correspondence:**
Pilar Martinez-Martinez
p.martinez@maastrichtuniversity.nl
Monique T. Mulder
m.t.mulder@erasmusmc.nl

[†]These authors share first authorship

[‡]These authors share senior authorship

Received: 26 August 2021
Accepted: 29 September 2021
Published: 27 October 2021

Citation:
den Hoedt S, Crivelli SM, Leijten FPJ, Losen M, Stevens JAA, Mané-Damas M, de Vries HE, Walter J, Mirzaian M, Sijbrands EJG, Aerts JMFG, Verhoeven AJM, Martinez-Martinez P and Mulder MT (2021) Effects of Sex, Age, and Apolipoprotein E Genotype on Brain Ceramides and Sphingosine-1-Phosphate in Alzheimer's Disease and Control Mice. Front. Aging Neurosci. 13:765252. doi: 10.3389/fnagi.2021.765252

Apolipoprotein ε4 (*APOE*)4 is a strong risk factor for the development of Alzheimer's disease (AD) and aberrant sphingolipid levels have been implicated in AD. We tested the hypothesis that the *APOE4* genotype affects brain sphingolipid levels in AD. Seven ceramides and sphingosine-1-phosphate (S1P) were quantified by LC-MSMS in hippocampus, cortex, cerebellum, and plasma of <3 months and >5 months old human *APOE3* and *APOE4*-targeted replacement mice with or without the familial AD (FAD) background of both sexes (145 animals). *APOE4* mice had higher Cer(d18:1/24:0) levels in the cortex (1.7-fold, $p = 0.002$) than *APOE3* mice. Mice with AD background showed higher levels of Cer(d18:1/24:1) in the cortex than mice without (1.4-fold, $p = 0.003$). S1P levels were higher in all three brain regions of older mice than of young mice (1.7-1.8-fold, all $p \leq 0.001$). In female mice, S1P levels in hippocampus ($r = -0.54$ [−0.70, −0.35], $p < 0.001$) and in cortex correlated with those in plasma ($r = -0.53$ [−0.71, −0.32], $p < 0.001$). Ceramide levels were lower in the hippocampus (3.7–10.7-fold, all $p < 0.001$), but higher in the cortex (2.3–12.8-fold, $p < 0.001$) of female than male mice. In cerebellum and plasma, sex effects on individual ceramides depended on acyl chain length (9.5-fold lower to 11.5-fold higher, $p \leq 0.001$). In conclusion, sex is a stronger determinant of brain ceramide levels in mice than *APOE* genotype, AD background, or age. Whether these differences impact AD neuropathology in men and women remains to be investigated.

Keywords: ceramide, S1P, apolipoprotein E4, Alzheimer's disease, aging, sex differences

INTRODUCTION

Alzheimer's disease (AD) is the most common cause of late-onset dementia with a prevalence of approximately 50 million cases worldwide (Prince et al., 2013). It is a progressive neurodegenerative disorder characterized by a gradual loss of memory and other cognitive functions. Less than 3% of AD is early onset, caused by mutations including those in the APP, PS1, or PS2 genes (Kang et al., 1987; Levy-Lahad et al., 1995; Sherrington et al., 1995). There is no single cause for late-onset, sporadic AD, but important risk factors are age and being female (Liesinger et al., 2018). A major genetic risk factor for sporadic AD is the ε4 allele of the *APOE* gene encoding for apolipoprotein (Apo)E4 in comparison to the other *APOE* isoforms, ε2 and ε3 (Corder et al., 1993; Strittmatter et al., 1993; Zhang and Hong, 2015). Compared to the general population, individuals heterozygous for *APOE4* have a ∼3-fold higher risk of developing AD, and homozygous *APOE4* individuals have a ∼15-fold increased risk (Chartier-Harlin et al., 1994; Farrer et al., 1997; Kloske and Wilcock, 2020). How ApoE4 affects AD development remains to be clarified. Besides genome wide associations studies have identified *APOE* as a longevity gene, with *APOE4* being associated with lower odds for a long live (Partridge Nature 2018, 561, 45–56 and Deelen Nature comm 2019, 10:3669).

ApoE is best known for its role in peripheral lipid trafficking, and there is evidence supporting a similar role for ApoE in the brain (Holtzman et al., 2012). Glial cells, which are the predominant source of brain ApoE, secrete it associated with lipids as high density lipoprotein-like particles (Abildayeva et al., 2006; Mahley, 2016). Brain lipid homeostasis is strictly regulated (Bjorkhem and Meaney, 2004; Strazielle and Ghersi-Egea, 2013). Imbalances in brain (sphingo)lipid homeostasis are associated with intellectual disability and with neurodegenerative disease (Liu et al., 1998; Haughey et al., 2010; Crivelli et al., 2020a) and possibly also with AD. In mice, deletion of *Apoe* or replacement with human *APOE4* leads to a dysfunctional cerebrovascular unit (Mulder et al., 2001; Bell et al., 2012), which may affect trafficking of lipids, including sphingolipids, across the blood–brain barrier. Such a disturbance in brain lipid homeostasis by *APOE4* may accelerate the pathogenesis of AD. Presently, the knowledge on trafficking of sphingolipids across the blood–brain barrier is limited (Zimmermann et al., 2001).

Alterations in brain and plasma sphingolipid homeostasis have been observed in patients with cognitive impairment and with AD (Mielke et al., 2010a,b, 2014, 2017; Martinez Martinez and Mielke, 2017; Crivelli et al., 2020a). Sphingolipids consist of a sphingosine backbone and can have various head groups and an acyl chain that differs in length. Besides their role as plasma membrane components (Olsen and Faergeman, 2017), sphingolipids are involved in neuronal plasticity (Wheeler et al., 2009), neurogenesis (Schwarz and Futerman, 1997; Olsen and Faergeman, 2017), and inflammation (Hannun, 1994; van Echten-Deckert et al., 2014). The sphingolipid acyl chain length is an important determinant of their function. Sphingolipids with long chains (C16:0) increase apoptosis, while very-long chains (C22:0-C24:0/C24:1) offer partial protection from apoptosis (Park and Park, 2015). In addition, the ratio between saturated (i.e., C24:0) and unsaturated (i.e., C24:1) acyl chains affects plasma membrane properties, thereby affecting signal transduction, membrane fusion, and cellular integrity (Pinto et al., 2008; Lazzarini et al., 2015).

Ceramides are the central hub of sphingolipid metabolism and are derived via *de novo* synthesis or from the degradation of more complex sphingolipids. Low ceramide levels promote neuronal cell growth, development, survival and division (Schwarz and Futerman, 1997; Brann et al., 1999; Mullen et al., 2012), while high levels may cause (neuronal) cell death (Jana et al., 2009; Mullen and Obeid, 2012; Czubowicz and Strosznajder, 2014). Sphingosine-1-phosphate (S1P) is formed in a reversible process from ceramide. S1P is an important signaling molecule that regulates cell survival, differentiation and immunity (van Echten-Deckert et al., 2014). The balance between ceramides and S1P is considered a major determinant of cell survival and death (Van Brocklyn and Williams, 2012).

The effect of *APOE4* on cholesterol and phospholipid homeostasis in the brain has been reported, but little attention has been paid, so far, to its relation with sphingolipid homeostasis. In patients with late-onset AD, *APOE4* was associated with higher ceramide levels in brain, but this was not observed in healthy controls (Bandaru et al., 2009; Couttas et al., 2018). Minor differences in total brain ceramide levels were found between *APOE4*, *APOE3*, and *APOE2* knock-in mice (Sharman et al., 2010; den Hoedt et al., 2016). Therefore, we aimed at investigating the modulatory effect of *APOE* genotype on brain sphingolipid homeostasis, in the context of the development of AD pathology. To this end, we assessed brain and plasma ceramide and S1P profiles in *APOE4* and *APOE3* transgenic mice with or without five familial AD mutations (*E4FAD* or *E3FAD*; K670N/M671L, I716V, and V717I in the APP gene and M146L and L286V in the PS1 gene) (Tai et al., 2011; Youmans et al., 2012a,b). The mice with the FAD mutations develop an AD phenotype, including Aβ accumulation, neuroinflammation, and cognitive impairment, from as early as 4 months of age (Youmans et al., 2012b; Tai et al., 2017). Therefore, sphingolipids were analyzed in different brain regions of mice younger than 3 months and older than 5 months. As sex potentially modulates AD incidence (Jorm and Jolley, 1998; Fratiglioni et al., 2000; Liesinger et al., 2018) and pathology (Maynard et al., 2006; Schafer et al., 2007), both female and male mice were included in the analyses.

MATERIALS AND METHODS

Animals

This study was not pre-registered. Transgenic *APOE3*-targeted replacement (TR), *E3FAD*-TR (*APOE3*-TR mice with 5xFAD mutations), *APOE4*-TR, and *E4FAD*-TR (*APOE4*-TR mice with 5xFAD mutations) mice were purchased from Dr. Mary Jo LaDu (University of Illinois at Chicago) and have been fully characterized by Oakley et al. (2006) and Youmans et al. (2012a,b). Colonies were maintained at Maastricht University. Young [<3 months, (2.1–2.6 months old)] and older [>5 months (5.4–14.3 months old)] male and female mice of all four genotypes were included in this study. An alternative analysis

TABLE 1 | Animal groups.

Brain regions	**Female**		**Male**		**Total**
Genotype	**Young (<3 months)**	**Older (>5 months)**	**Young (<3 months)**	**Older (>5 months)**	
APOE3	9	9	10	9	37
APOE4	10	9	10	7	36
E3FAD	9	10	8	7	34
E4FAD	10	10	10	8	38
Total	38	38	38	31	145
Plasma	**Female**		**Male**		**Total**
Genotype	**Young (<3 months)**	**Older (>5 months)**	**Young (<3 months)**	**Older (>5 months)**	
APOE3	9	5	8	6	28
APOE4	10	7	10	4	31
E3FAD	9	8	9	6	32
E4FAD	9	6	10	6	31
Total	37	26	37	22	122

Brain and plasma of these animals were analyzed.

excluding 3 animals 5 months and 3 animals 14 months to narrow age range to 7–12 was carried out and the data is reported in **Supplementary Information 1**. Exclusion of these 6 animals did not affect the results qualitatively. All female mice were breeders. Animals were housed socially on a reverse 12-h day-night cycle under standardized environmental conditions (ambient temperature 20 ± 1°C; humidity 40–60%, background noise, cage enrichment) at the central animal facility of Maastricht University and had *ad libitum* access to food and water. All experiments were approved by the Animal Welfare Committee of Maastricht University and were performed according to Dutch federal regulations for animal protection (DEC 2015-002).

No sample size calculation was performed prior to the experiments, but based on previous studies on sphingolipids in mice we aimed at 10 mice per group (Barrier et al., 2010; den Hoedt et al., 2016). The in total 145 mice were divided in groups consisting of 7–10 animals for brain analysis and of 4–10 animals for plasma analysis (**Table 1**). Animals were sacrificed by CO_2 inhalation in the morning (09:00 – 12:00 h) and subsequent decapitation. Blood was collected in a Microvette® CB 300 LH tube (order no. 16.443, Sarstedt group, Etten-Leur, Netherlands) and subsequently centrifuged (2,000 g, 4°C, 10 min) to isolate plasma, which was stored at −80°C until analysis. From all animals the brain was removed, cut through the midline sagittal section, snap frozen in liquid nitrogen, and stored at −80°C until analysis. Before sphingolipid analysis, brain hemispheres were dissected into cortex, hippocampus, and cerebellum on ice and samples were powdered on dry ice and stored at −80°C until analysis.

Sphingolipid Analysis

Group allocation of experimental animals was unknown to the experimenter prior to sphingolipid analysis.

Lipid Extraction

Sphingolipids were extracted as described (de Wit et al., 2016, 2019). In short, frozen tissue samples were weighed and homogenized in cold Millipore water (MQ, 18.2 MΩ cm filter) from a Milli-Q® PF Plus system (Merck Millipore B.V., Amsterdam, Netherlands). To 10 μL tissue homogenates and plasma samples, the internal standards Cer(d18:1/17:0), Cer(d17:0/24:1), and S1P(d18:1)-D7 were added (10 μL of 2, 2 and 0.2 μg/mL in methanol, respectively; IS: Avanti Polar Lipids, Alabaster, AL, United States; methanol: Merck Millipore B.V.). After addition of 10 μL of 10% TEA solution [triethylamine (10/90, v/v) in methanol/dichloromethane (DCM) (50/50, v/v); TEA: Merck Millipore B.V., DCM: Merck Millipore B.V.]. Lipids were extracted with 450 μL methanol/DCM (50/50, v/v). Samples were vortexed and incubated under constant agitation for 30 min at 4°C followed by centrifugation at 18,500 *g* for 20 min at 4°C (Hettich mikro 200R, Geldermalsen, Netherlands). Supernatants were transferred to glass vials, freeze dried and reconstituted in 100 μL methanol prior to liquid chromatography-tandem mass spectrometry (LC-MSMS).

Liquid Chromatography-Tandem Mass Spectrometry Analysis

An LC-30A autosampler (Shimadzu, Kyoto, Japan) injected 10 μL brain lipid extracts or 5 μL plasma lipid extracts into a Shimadzu HPLC system (Shimadzu) equipped with a Kinetex C8 column (50 mm × 2.1 mm, 2.6 μm, 00B-4497-AN, Phenomenex, Maarssen, Netherlands) at 30°C. After washing with 95% mobile phase A [MQ/methanol (50/50, v/v) containing 1.5 mM ammonium formate and 0.1% formic acid] and 5% mobile phase B (methanol containing 1 mM ammonium formate and 0.1% formic acid) for 2 min, elution was performed by a linear gradient from 95% mobile phase A and 5% mobile phase B to 7% mobile phase A and 93% mobile phase B in 5.5 min, which was held for 4.5 min. After 10 min the column was flushed with 99% mobile phase B for 2 min followed by a

2 min re-equilibration. The flow rate was set at 0.25 mL/min and total run time was 14 min. The effluent was directed to a Sciex Qtrap 5500 quadruple mass spectrometer (AB Sciex Inc., Thornhill, ON, Canada) and analyzed in positive ion mode following electrospray ionization using multiple reaction monitoring. Detailed LC-MS/MS settings for each sphingolipid species are given in **Supplementary Table 1**.

We quantified S1P and the seven most abundant ceramide species for which standards were commercially available. Nine-point calibration curves were constructed by plotting analyte to internal standard peak area ratios versus the corresponding analyte concentration for Cer(d18:1/14:0), Cer(d18:1/16:0), Cer(d18:1/18:0), Cer(d18:1/20:0), Cer(d18:1/22:0), Cer(d18:1/24:1), Cer(d18:1/24:0), and S1P(d18:1) (all Avanti polar lipids). Correlation coefficients (R^2) were >0.99. Sphingolipid levels were determined from these standard curves based on sphingolipid species acyl chain length. Instrument control and quantification of spectral data was performed using MultiQuant software (AB Sciex Inc.). Brain sphingolipid levels were normalized to mg tissue weight and plasma sphingolipid levels to mL plasma used for analysis.

Statistical Analyses

All outcome parameters were analyzed with IBM SPSS Statistics version 24.0. Group allocation of all experimental animals was known prior to statistical analysis. For sphingolipid parameters *Z*-values were calculated and individual values that corresponded to a *Z*-value that deviated more than 4 from the center were considered outliers. Of all data points, 0.84% were excluded as outliers. Normal distribution of the data was confirmed by the Shapiro–Wilk test.

Four main parameters, *APOE* genotype, FAD mutations, age, and sex, determined to which group mice were assigned, with a total of sixteen groups. The interaction between these four main parameters was analyzed by a generalized linear model to assess whether a combination of these four parameters affected the S1P and ceramide levels and ceramide distribution differently than the individual parameters. Relative ceramide levels were calculated by dividing the level of the individual species by the sum of all the variants measured. Univariate analysis was used to assess the effects of the four parameters on S1P(d18:1), while multivariate analysis was used to assess the effects on the individual ceramide species. The Benjamini–Hochberg procedure (false discover rate = 0.05) was used to correct for multiple testing (Benjamini and Hochberg, 1995). Pearson's test was used to assess the correlation between sphingolipid levels in plasma and brain regions in female or in male mice.

RESULTS

For the present study, 5xFAD mice were cross-bred with *APOE3*-TR and *APOE4*-TR mice to obtain the *E3FAD* and *E4FAD* mice. To confirm an AD phenotype in the *E3FAD* and *E4FAD* mice (Tai et al., 2011; Youmans et al., 2012a,b) Aβ deposition was determined in the hippocampus (Youmans et al., 2012b) by enzyme-linked immunoassay (Crivelli et al., 2021) as described in **Supplementary Information 2**. Tris-buffered saline (TBS) soluble, TBS-1% Triton-X (TBS-T) soluble, and formic acid (FA) soluble Aβ depositions were detectable in the hippocampus of the *E3FAD* and *E4FAD* mice. Older mice showed a higher extent of Aβ depositions than young mice, irrespective of *APOE* genotype or sex (all $p < 0.001$; **Supplementary Figure 1**).

Overall Effect of *APOE4* Genotype, Familial Alzheimer's Disease Mutations, Age, and Sex on Sphingosine-1-Phosphate and Ceramide Levels in Brain and in Plasma

The effect of *APOE* genotype, FAD mutations, age, and sex on S1P and ceramide levels in the hippocampus, cortex, cerebellum and plasma of mice is shown in **Figures 1–3** (individual ceramides in **Supplementary Figures 2–8**). **Figure 1** shows that S1P levels in all brain regions tended to be higher in older than in younger mice. Total ceramide levels were mostly affected by sex (**Figure 2**). In the hippocampus, total ceramide levels tended to be lower in female than in male mice, while in the cortex they tended to be higher. When examining the overall differences in total and specific ceramide and S1P levels in all groups, we found no significant interaction between the four independent parameters, *APOE* genotype, FAD mutations, age, and sex (**Supplementary Tables 2, 3**). This allowed us to assess the effect of each parameter separately and independently and hence only the main effects of *APOE* genotype, FAD mutations, age, and sex are displayed below (**Figure 3**).

Limited Effects of *APOE* Genotype on Levels of Sphingosine-1-Phosphate and Ceramide in Brain and in Plasma

APOE4 compared to *APOE3* showed limited impact on few sphingolipids in brain and in plasma (**Figure 3**). S1P(d18:1) levels were not affected by *APOE* genotype. Ceramide levels in the cortex were higher in *APOE4* than in *APOE3* carriers (1.1-fold, $p < 0.001$). When analyzing individual ceramides, levels of Cer(d18:1/24:0) exclusively were significantly higher in the cortex of *APOE4* than of *APOE3* carriers (1.7-fold, $p = 0.002$). *APOE4* compared to *APOE3* mice also displayed higher levels of total ceramide levels in plasma (1.1-fold, $p = 0.001$), mostly due to higher levels of Cer(d18:1/20:0) (1.4-fold, $p = 0.012$).

Limited Effects of Familial Alzheimer's Disease Mutations on Sphingolipid Profiles in Brain and Plasma

Familial Alzheimer's disease mutations hardly affected sphingolipids in brain or in plasma (**Figure 3**). While mice with *APOE4* display higher levels of Cer(d18:1/24:0), mice with FAD mutations displayed higher levels of Cer(d18:1/24:1) in the cortex than in mice without the FAD mutations (1.4-fold, $p = 0.003$).

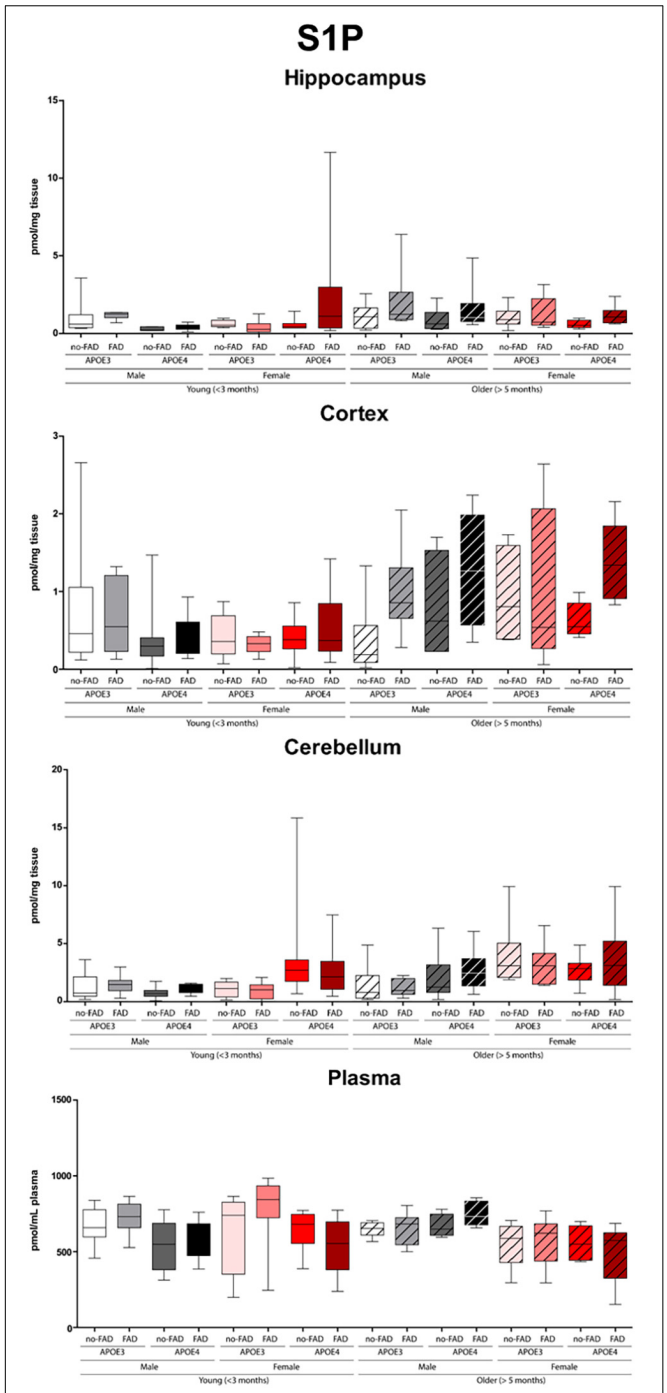

FIGURE 1 | Sphingosine-1-phosphate (S1P) levels in hippocampus, cortex, cerebellum, and plasma. Data are provided as median (line, box dimensions 25th–75th percentile, whiskers min–max) in pmol/mg tissue or pmol/mL plasma (n = 7–10 mice per group for brain samples and n = 4–10 per group for plasma samples).

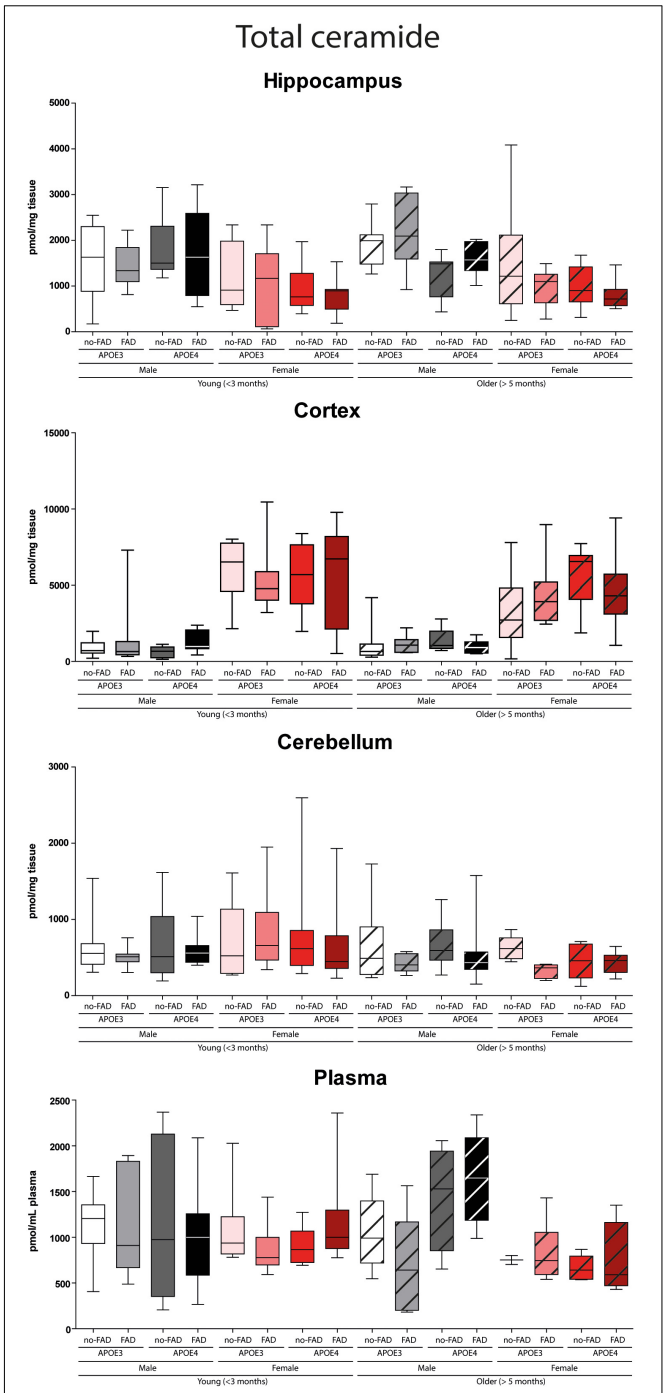

FIGURE 2 | Total determined ceramide levels in hippocampus, cortex, cerebellum, and plasma. Data are given as median (line, box dimensions 25th–75th percentile, whiskers min–max) in pmol/mg tissue or pmol/mL plasma (n = 7–10 mice per group for brain samples and n = 4–10 per group for plasma samples).

Limited Effects of Age on Sphingolipid Profiles in Brain and Plasma

Older mice displayed higher levels of S1P(d18:1) in the hippocampus, cortex, and cerebellum than younger mice (1.7 – 1.8-fold, all $p < 0.001$), while there were no differences in plasma (**Figure 3**). On the other hand, total cortex and cerebellum ceramide levels were lower in older than in young mice (1.1 – 1.2-fold, all $p \leq 0.003$), which could not

be attributed to individual ceramide species. Total ceramide levels in plasma were also lower in older than in young mice (1.1-fold, $p < 0.001$), which was due to lower levels of most of the individual ceramides (1.6 – 4.4-fold, all $p \leq 0.012$).

Effects of Sex on Sphingolipid Profiles in Brain and Plasma

In the cerebellum S1P(d18:1) levels were higher in female than in male mice (1.9-fold, $p < 0.001$), while levels did not differ in the hippocampus, cortex, and in plasma (**Figure 3**).

Total ceramide levels in the hippocampus were lower in female than in male mice (4.3-fold, $p < 0.001$). In line, levels of five out of seven individual ceramide species were lower in female than in male mice (2.7 – 9.7-fold, all $p < 0.001$), whereas Cer(d18:1/24:0) levels were fourfold higher ($p < 0.001$). In contrast with the findings in the hippocampus, total ceramide levels in cortex were higher in female than in male mice (5.1-fold, $p < 0.001$), as were all individual ceramide species (2.3 – 12.8-fold, all $p < 0.001$). Also in the cerebellum total ceramide levels were slightly, but significantly, higher in female than in male mice (1.05-fold, $p < 0.001$), due to three out of seven individual ceramide species (1.3 – 11.5-fold, all $p < 0.001$), whereas Cer(d18:1/24:1) was 9.5-fold lower ($p < 0.001$). In line with findings in the hippocampus, total ceramide levels in plasma, were lower in female than in male mice (3.4-fold, $p < 0.001$), mostly due to lower Cer(d18:1/22:0) and Cer(d18:1/24:1) levels (6.2 – 9.5-fold, both $p < 0.001$). However, Cer(d18:1/18:0) levels were higher (1.3-fold, $p < 0.001$).

Effect of *APOE4* Genotype, Familial Alzheimer's Disease Mutations, Age, and Sex on Ceramide Acyl Chain Length Distribution

As ceramide acyl chain composition can affect sphingolipid function we examined the acyl chain length distribution in further detail. The effects of *APOE* genotype, FAD mutations, age and sex on ceramide acyl chain length distribution were in line with the data on the absolute levels (**Supplementary Figure 9**).

Cortex and Hippocampus Sphingosine-1-Phosphate Levels Correlate With Plasma Levels in Female Mice

In female mice, plasma S1P(d18:1) levels negatively associated with those in the cortex ($r = -0.53$, [95%CI: −0.71, −0.32], $p < 0.001$) and hippocampus ($r = -0.54$, [95%CI: −0.70, −0.35], $p < 0.001$), regardless of age, *APOE* genotype and presence of FAD mutations. In male mice, no correlation was found between S1P or ceramide levels in plasma and any of the brain regions analyzed.

Validation of Effects of *APOE4* Genotype, Age, and Sex on Sphingosine-1-Phosphate and Ceramide Levels in a Small Cohort of Mice

To confirm our findings that sex greatly affected ceramide and to a smaller extent S1P levels in the hippocampus and cortex of our mice we reanalyzed brain tissues from a selection of mice ($n = 20$ per region) by a different extraction, sample preparation, and LC-MSMS method. S1P levels were determined as previously described (Mirzaian et al., 2016). Total ceramide levels were determined by microwave-induced deacylation followed by quantification of the sphingoid base (Mirzaian et al., 2017). The latter method somewhat overestimates total ceramide levels since some of the sulfatides also lose their sulfate group during deacylation. These results showed qualitatively similar results to our study with total ceramide levels being lower in the hippocampus and higher in the cortex of female than of male mice (**Table 2**). No effect of *APOE* genotype or age on ceramide levels was found, whereas S1P levels in the hippocampus were lower in the *APOE4* mice than in *APOE3* mice.

DISCUSSION

The data of this explorative study revealed that *APOE* genotype, FAD mutations, and age affect overall brain and plasma sphingolipids to a very limited extent. Unexpectedly, sex notably affected ceramide levels, e.g., with ceramide levels being in the hippocampus and higher in the cortex of female than of male mice. The limited effect of *APOE* genotype on sphingolipid levels, even in AD mice, might be due to the fact that the mice in our study were relatively younger (5.4–14.3 months, only 3 mice ≥ 10 months) than in previously published papers. Previously, we found *APOE4* knock-in mice > 15 months old to display lower ceramide levels in the brain than wild-type mice (den Hoedt et al., 2016) suggesting an effect of *APOE* genotype on sphingolipids may become apparent with increasing age or that human *APOE3* affects ceramide differently from mouse *apoE*. The observed and externally validated profound effects of sex on sphingolipids may provide an avenue to further explore sex-specific mechanisms contributing to disease progression in men and women with Alzheimer's disease.

Although, the ε4 allele of the *APOE* gene is long known to be the strongest genetic risk factor for the development of late-onset AD, the underlying mechanisms contributing to disease progression remain to be established. Differences in lipidation of ApoE4 and ApoE3 secreted by astrocytes have been detected in AD (Verghese et al., 2013; Grimm et al., 2017), with potential consequences for the clearance of Aß from the brain. So far, no major effects of *APOE* genotype on brain lipids, such as sterols, phospholipids, fatty acids or ceramides have been observed (Mulder et al., 1998; Martins et al., 2006; Sharman et al., 2010; Lim et al., 2014). Our data show minor modulatory effects of the *APOE* genotype on overall sphingolipid homeostasis. Interestingly, only Cer(d18:1/24:0) levels were significantly higher in the cortex of *APOE4* mice irrespective of

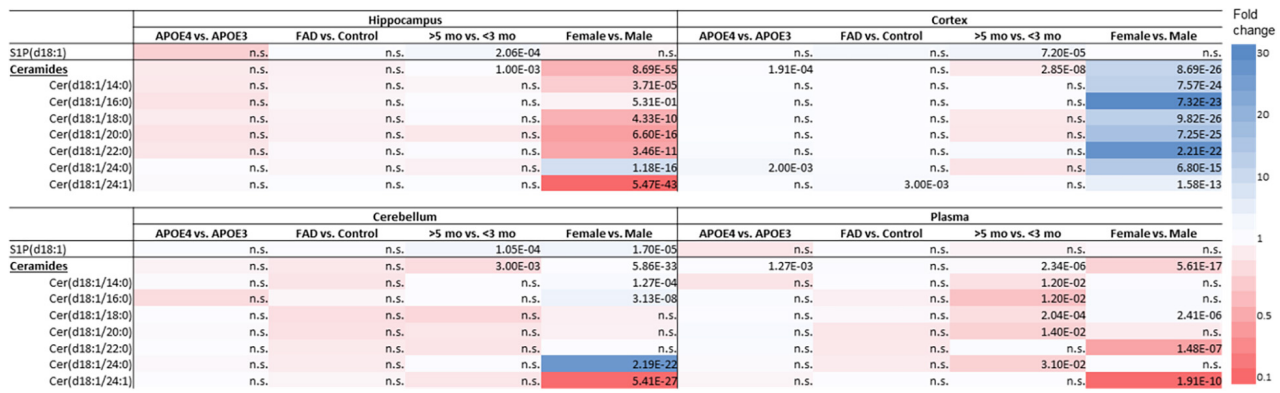

FIGURE 3 | Effect of *APOE* genotype (*APOE4* vs. *APOE3*), familial AD mutations (FAD vs. non-FAD), age (>5 mo vs. <3 mo), and sex (♂ vs. ♀) on sphingolipid levels in hippocampus, cortex, cerebellum and in plasma of mice. Color-scale indicates the differences in sphingolipid levels; blue indicates up to 30-fold higher levels and red indicates up to 10-fold lower sphingolipid levels. *P*-values of significant differences after correction for multiple testing are indicated in the table, n.s., non-significant (n = 45–76 mice per group).

TABLE 2 | Effect of *APOE* genotype (*APOE4* vs. *APOE3*), age (>5 months vs. <3 months), and sex (female vs. male) on S1P and ceramide levels (mean ± sd pmol/mg protein) in hippocampus and cortex of a selection of mice to validate study results (n = 20).

	S1P (d18)		**Ceramide (d18)**	
	Hippocampus	**Cortex**	**Hippocampus**	**Cortex**
APOE3	28 (±9)	25 (±14)	17927 (±9021)	20763 (±9203)
APOE4	18 (±10)	21 (±21)	23601 (±11789)	22244 (±8663)
Fold difference	0.66	0.85	1.32	1.07
p-value	**0.032**	0.923	0.063	0.541
<3 months	20 (±10)	17 (±14)	16985 (±4879)	21586 (±9277)
>5 months	26 (±11)	29 (±20)	24542 (±13517)	21570 (±8592)
Fold difference	1.27	1.72	1.44	1.00
p-value	0.118	0.363	0.111	0.871
Male	20 (±12)	33 (±20)	26970 (±11277)	17664 (±4695)
Female	26 (±9)	12 (±7)	14557 (±5047)	25492 (±10188)
Fold difference	1.31	0.37	0.54	1.44
p-value	0.096	**0.036**	**0.003**	**0.011**

P-values are not corrected for multiple testing, $p < 0.05$ is marked bold, red indicates lower levels and blue indicates higher levels.

sex, age, and FAD mutations. Higher levels of Cer(d18:1/24:0) were also observed in the brain of AD patients (Cutler et al., 2004a). Increased levels of intracellular Cer(d18:1/24:0) have been found to induce apoptosis in cultured neutrophils (Seumois et al., 2007), but Cutler et al. (2004a) could not detect any direct link with apoptosis. It cannot be excluded that the increased Cer(d18:1/24:0) levels observed in the cortex of the *APOE4* mice in our study contribute, via inducing apoptosis, to the neuronal loss that is a prominent pathological feature of AD. With aging this may further exacerbate the neurodegenerative processes.

Minor effects of the FAD mutations on brain sphingolipids were observed. Our observation that mice with the FAD mutations show significantly higher levels of Cer(d18:1/24:1) in the cortex than mice without the mutations is in line with previously reported data of the APP(SL)/PS1 knock-in AD mouse model (Barrier et al., 2010). Ceramides have been suggested to play a role in neuroinflammatory processes occurring in neurodegenerative diseases like AD. In reactive astrocytes of patients with late-onset AD, frontotemporal lobar dementia, and capillary cerebral amyloid angiopathy, high ceramide levels and an increased expression of ceramide synthase 5, the enzyme responsible for Cer(d18:1/16:0) production, were observed (van Doorn et al., 2012; de Wit et al., 2016, 2019). Additionally, in individuals with a parental history of late-onset AD, cerebral spinal fluid Cer(d18:1/18:0) levels correlated with Aβ and T-tau levels (Mielke et al., 2014). On the other hand high serum ceramide levels, especially Cer(d18:1/16:0) and Cer(d18:1/24:0), were also observed to be associated with the risk of developing sporadic late-onset AD (Mielke et al., 2012). Although we observed only Cer(d18:1/24:1) levels increased because of the FAD mutations on brain ceramide levels, these effects are in line with the proposed role of ceramides in the pathogenesis of AD.

Effects of aging on sphingolipid profiles have previously been reported. Age-related increases in ceramide levels and decrease in S1P were detected in the hippocampus of cognitively normal individuals of 65 years or older (Cutler et al., 2004b;

Couttas et al., 2018). An accumulation upon aging of ceramide in the cortex and hippocampus has also been reported in wild-type mice and rats (Cutler et al., 2004b; Durani et al., 2017; Vozella et al., 2017), suggesting that these changes reflect normal aging processes. In contrast, we observed a modest increase in S1P and a modest decrease in ceramides in all brain regions upon maturation of the mice, irrespective of *APOE* genotype, FAD mutations, and sex. However, the previously reported increase in ceramides were detected in mice that were almost twice as old as the eldest mice in this study, which may explain the lack of such a difference. Interestingly, S1P levels were significantly higher in the brain regions of older than of younger mice. S1P has been suggested to modulate synaptic strength (Kanno et al., 2010), brain inflammation, and cerebrovascular integrity (Chua et al., 2020). Upon aging, the increased S1P levels in combination with higher Aß$_{42}$ levels may deteriorate synaptic function and blood–brain barrier integrity during the progression of AD. However, the origin of the S1P needs to be further investigated, because region-specific differences in sphingolipid metabolism have been observed (Blot et al., 2021). In plasma, S1P levels were reported to be higher in females compared to males in response to estradiol starting at a relatively young age (Guo et al., 2014). Yet with aging and menopause S1P plasma levels were downregulated (Guo et al., 2014). In our study, we could not reproduce these findings probably because of small samples size or because of the fact that the older females were employed as breeders. During pregnancy the levels of estradiol fluctuate (Bai et al., 2020), with possible consequences for S1P regulation (Guo et al., 2014).

So far reports on sex-specific effects on sphingolipid profiles in the brain of mice are limited. Sex-specific differences in sphingolipid levels in the cortex of APP^{SL}/PS1 mice, but not in PS1 mice have been reported (Barrier et al., 2010). Female APP^{SL}/PS1 mice display lower levels of saturated fatty acid ceramides [i.e., Cer(d18:1/24:0)], and higher levels of unsaturated fatty acid ceramides [Cer(d18:1/24:1)], than male mice in the cortex at the age of 3 and 6 months (Barrier et al., 2010). In contrast with these data, we found statistically relevant higher levels of saturated fatty acid ceramides and lower levels of unsaturated fatty acid ceramides in the cortex of female as compared to male mice. This discrepancy might be due to the different backgrounds of the mice (Casas et al., 2004). Moreover, it has to be noticed that our female mice were former breeders.

Sex-dependent effects on ceramide levels have also been reported for human hippocampus, where ceramide levels correlated with age in men exclusively (Couttas et al., 2018). In addition, the elevated plasma ceramide levels in (menopausal) women, as compared to men, without cognitive impairment negatively correlated with estradiol levels (Mielke et al., 2015; Vozella et al., 2019). Estradiol was found to decrease hypothalamic ceramide levels and thereby endoplasmatic reticulum stress in female rats (Gonzalez-Garcia et al., 2018), which is in line with the lower ceramide levels we observed in the hippocampus of female compared to male mice. Estradiol was also found to modulate plasma membrane lipid rafts, highly enriched in ceramides and other sphingolipids and where the amyloidogenic processing of APP takes place (Cordy et al., 2006). The reduction of estradiol associated with menopause could contribute to the development of AD via a modulatory effect on lipid raft composition (Marin and Diaz, 2018). The differences in sphingolipids between sexes might provide insight into metabolism-related differences between men and women that may contribute to the development of AD and underline the importance of the use of both sexes in future studies.

Notably, we found ceramide levels to be higher in the cortex than in the hippocampus. This may have critical implications when designing drugs to control ceramide levels in the brain (Giles et al., 2017). In fact, the response to the ceramide modulators may be different depending on brain region or even cell type (Fitzner et al., 2020).

There are several limitations in this study. First, the AD model used reflects familial (early-onset) AD, whereas *APOE4* is a genetic risk factor for sporadic late-onset AD and most studies reporting a link between sphingolipid levels and cognitive decline were performed in patients with sporadic late-onset AD (Mielke et al., 2010a, 2011; Mielke and Haughey, 2012). Although, the FAD mouse is a model for familial AD, similar to sporadic AD the mice display Aβ deposition, neuroinflammation, and cognitive impairment (Tai et al., 2017; Youmans et al., 2012b). Secondly, although the older mice (>5 months) did show increased Aß levels, our mice were relatively young. Senescence effects in mice are generally not observed before the age of 10 months when they are considered middle aged (Jonas, 2007; Dutta and Sengupta, 2016). We did observe changes in sphingolipid levels in relatively young mice depending on FAD mutations, *APOE4* genotype, or sex which may suggest these contribute to the later development of AD. Thirdly, due to the nature of the study and the four parameters that determined the sixteen different groups there were relatively few mice per individual group, especially considering plasma analysis. However, the very limited interaction effects between *APOE* genotype, FAD mutations, age, and sex allowed us to address their effect on S1P and ceramide levels as independent parameters in groups of sufficient size (n = 45–76 per group). The sex-specific findings were externally validated further strengthening our findings. Finally, our analysis comprised a selected number of sphingolipids, e.g., S1P and seven ceramides. Though the analysis of additional sphingolipids, such as hexosylceramides and sulfatides, is undoubtedly interesting in association to FAD mutation and age (Crivelli et al., 2020b), we here focused on S1P and ceramide as they are important signaling sphingolipids and commercial MS standards were available for these lipids. Brain sphingosine levels were below the detection limit of our LC-MSMS setup and were therefore not reported.

CONCLUSION

Our data shows very limited effects of *APOE* genotype on very-long chain ceramides [Cer(d18:1/24:0)], which might represent one of the early signs of neuroinflammation that may worsen with aging. Unexpectedly, sex was found to profoundly affect ceramide levels in plasma and in brain in particular in the

cortex and hippocampus. A role for sex hormones needs further investigation. If and how these brain ceramide profiles affect the pathogenesis of AD differently in men and women remains to be examined. S1P levels in the brain increased with aging and in female mice S1P levels in cortex and hippocampus negatively correlate with levels in plasma. Therefore, plasma S1P might be of interest for future investigation as proxy for alterations in brain sphingolipid metabolism, and to explore if these are related to the progression of neurodegenerative processes.

DATA AVAILABILITY STATEMENT

The raw data supporting the conclusions of this article will be made available by the authors, without undue reservation.

ETHICS STATEMENT

The animal study was reviewed and approved by Animal Welfare Committee of Maastricht University.

AUTHOR CONTRIBUTIONS

SH: methodology, formal analysis, investigation, data curation, writing – original draft, and visualization. SC, ML, JS, and MM-D: methodology, resources, and writing – review and editing. FL: methodology, investigation, and writing – review and editing. HV: conceptualization, writing – review and editing, and funding acquisition. JW: conceptualization and writing – review and editing, and funding acquisition. ES: writing – review and editing. AV: methodology and writing – original draft. PM-M: conceptualization, methodology, resources, writing – review and editing, and funding acquisition. MTM: conceptualization, methodology, writing – original draft, supervision, project administration, and funding acquisition. All authors contributed to the article and approved the submitted version.

FUNDING

This work was supported by grants to SH, SC, JW, HV, PM-M, and MTM from ZonMw Memorabel program (projectnr: 733050105). PM-M was also supported by the International Foundation for Alzheimer Research (ISAO) (projectnr: 14545).

SUPPLEMENTARY MATERIAL

The Supplementary Material for this article can be found online at: https://www.frontiersin.org/articles/10.3389/fnagi.2021.765252/full#supplementary-material

REFERENCES

Abildayeva, K., Jansen, P. J., Hirsch-Reinshagen, V., Bloks, V. W., Bakker, A. H., Ramaekers, F. C., et al. (2006). 24(S)-hydroxycholesterol participates in a liver X receptor-controlled pathway in astrocytes that regulates apolipoprotein E-mediated cholesterol efflux. *J. Biol. Chem.* 281, 12799–12808. doi: 10.1074/jbc.m601019200

Bai, J., Qi, Q. R., Li, Y., Day, R., Makhoul, J., Magness, R. R., et al. (2020). Estrogen Receptors and Estrogen-Induced Uterine Vasodilation in Pregnancy. *Int. J. Mol. Sci.* 21:4349. doi: 10.3390/ijms21124349

Bandaru, V. V., Troncoso, J., Wheeler, D., Pletnikova, O., Wang, J., Conant, K., et al. (2009). ApoE4 disrupts sterol and sphingolipid metabolism in Alzheimer's but not normal brain. *Neurobiol. Aging* 30, 591–599. doi: 10.1016/j.neurobiolaging.2007.07.024

Barrier, L., Ingrand, S., Fauconneau, B., and Page, G. (2010). Gender-dependent accumulation of ceramides in the cerebral cortex of the APP(SL)/PS1Ki mouse model of Alzheimer's disease. *Neurobiol. Aging* 31, 1843–1853. doi: 10.1016/j.neurobiolaging.2008.10.011

Bell, R. D., Winkler, E. A., Singh, I., Sagare, A. P., Deane, R., Wu, Z., et al. (2012). Apolipoprotein E controls cerebrovascular integrity via cyclophilin A. *Nature* 485, 512–516. doi: 10.1038/nature11087

Benjamini, Y., and Hochberg, Y. (1995). Controlling the False Discovery Rate - a Practical and Powerful Approach to Multiple Testing. *J. R. Statist. Soc. Ser. B Methodol.* 57, 289–300. doi: 10.1111/j.2517-6161.1995.tb02031.x

Bjorkhem, I., and Meaney, S. (2004). Brain cholesterol: long secret life behind a barrier. *Arterioscler. Thromb. Vasc. Biol.* 24, 806–815. doi: 10.1161/01.atv.0000120374.59826.1b

Blot, F. G. C., Krijnen, W. H. J. J., Hoedt, S. D., Osório, C., White, J. J., Mulder, M. T., et al. (2021). Sphingolipid metabolism governs Purkinje cell patterned degeneration in *Atxn1[82Q]/+* mice. *Proc. Natl. Acad. Sci. U. S. A.* 118:e2016969118. https://doi.org/10.1073/pnas.2016969118

Brann, A. B., Scott, R., Neuberger, Y., Abulafia, D., Boldin, S., Fainzilber, M., et al. (1999). Ceramide signaling downstream of the p75 neurotrophin receptor mediates the effects of nerve growth factor on outgrowth of cultured hippocampal neurons. *J. Neurosci.* 19, 8199–8206. doi: 10.1523/jneurosci.19-19-08199.1999

Casas, C., Sergeant, N., Itier, J. M., Blanchard, V., Wirths, O., van der Kolk, N., et al. (2004). Massive CA1/2 neuronal loss with intraneuronal and N-terminal truncated Abeta42 accumulation in a novel Alzheimer transgenic model. *Am. J. Pathol.* 165, 1289–1300. doi: 10.1016/s0002-9440(10)63388-3

Chartier-Harlin, M. C., Parfitt, M., Legrain, S., Perez-Tur, J., Brousseau, T., Evans, A., et al. (1994). Apolipoprotein E, epsilon 4 allele as a major risk factor for sporadic early and late-onset forms of Alzheimer's disease: analysis of the 19q13.2 chromosomal region. *Hum. Mol. Genet.* 3, 569–574. doi: 10.1093/hmg/3.4.569

Chua, X. Y., Ho, L. T. Y., Xiang, P., Chew, W. S., Lam, B. W. S., Chen, C. P., et al. (2020). Preclinical and Clinical Evidence for the Involvement of Sphingosine 1-Phosphate Signaling in the Pathophysiology of Vascular Cognitive Impairment. *Neuromolecular. Med.* 23, 47–67. doi: 10.1007/s12017-020-08632-0

Corder, E. H., Saunders, A. M., Strittmatter, W. J., Schmechel, D. E., Gaskell, P. C., Small, G. W., et al. (1993). Gene dose of apolipoprotein E type 4 allele and the risk of Alzheimer's disease in late onset families. *Science* 261, 921–923. doi: 10.1126/science.8346443

Cordy, J. M., Hooper, N. M., and Turner, A. J. (2006). The involvement of lipid rafts in Alzheimer's disease. *Mol. Membr. Biol.* 23, 111–122. doi: 10.1080/09687860500496417

Couttas, T. A., Kain, N., Tran, C., Chatterton, Z., Kwok, J. B., and Don, A. S. (2018). Age-Dependent Changes to Sphingolipid Balance in the Human Hippocampus are Gender-Specific and May Sensitize to Neurodegeneration. *J. Alzheimers Dis.* 63, 503–514. doi: 10.3233/jad-171054

Crivelli, S. M., Giovagnoni, C., Visseren, L., Scheithauer, A. L., de Wit, N., den Hoedt, S., et al. (2020a). Sphingolipids in Alzheimer's disease, how can we target them? *Adv. Drug Deliv. Rev.* 159, 214–231. doi: 10.1016/j.addr.2019.12.003

Crivelli, S. M., Luo, Q., Stevens, J. A. A., Giovagnoni, C., van Kruining, D., Bode, G., et al. (2021). CERTL reduces C16 ceramide, amyloid-beta levels, and inflammation in a model of Alzheimer's disease. *Alzheimers Res. Ther.* 13:45.

Crivelli, S. M., van Kruining, D., Luo, Q., Stevens, J. A. A., Giovagnoni, C., Paulus, A., et al. (2020b). Ceramide analog [18F]F-HPA-12 detects sphingolipid

disbalance in the brain of Alzheimer's disease transgenic mice by functioning as a metabolic probe. *Sci. Rep.* 2020:19354.

Cutler, R. G., Haughey, N. J., Tammara, A., McArthur, J. C., Nath, A., Reid, R., et al. (2004a). Dysregulation of sphingolipid and sterol metabolism by ApoE4 in HIV dementia. *Neurology* 63, 626–630.

Cutler, R. G., Kelly, J., Storie, K., Pedersen, W. A., Tammara, A., Hatanpaa, K., et al. (2004b). Involvement of oxidative stress-induced abnormalities in ceramide and cholesterol metabolism in brain aging and Alzheimer's disease. *Proc. Natl. Acad. Sci. U S A.* 101, 2070–2075. doi: 10.1073/pnas.0305799101

Czubowicz, K., and Strosznajder, R. (2014). Ceramide in the molecular mechanisms of neuronal cell death. The role of sphingosine-1-phosphate. *Mol. Neurobiol.* 50, 26–37. doi: 10.1007/s12035-013-8606-4

de Wit, N. M., den Hoedt, S., Martinez-Martinez, P., Rozemuller, A. J., Mulder, M. T., and de Vries, H. E. (2019). Astrocytic ceramide as possible indicator of neuroinflammation. *J. Neuroinflamm.* 16, 48.

de Wit, N. M., Snkhchyan, H., den Hoedt, S., Wattimena, D., de Vos, R., Mulder, M. T., et al. (2016). Altered Sphingolipid Balance in Capillary Cerebral Amyloid Angiopathy. *J. Alzheimers Dis.* 60, 795–807. doi: 10.3233/jad-160551

den Hoedt, S., Janssen, C. I., Astarita, G., Piomelli, D., Leijten, F. P., Crivelli, S. M., et al. (2016). Pleiotropic Effect of Human ApoE4 on Cerebral Ceramide and Saturated Fatty Acid Levels. *J. Alzheimers Dis.* 60, 769–781.

Durani, L. W., Hamezah, H. S., Ibrahim, N. F., Yanagisawa, D., Makpol, S., Damanhuri, H. A., et al. (2017). Age-related changes in the metabolic profiles of rat hippocampus, medial prefrontal cortex and striatum. *Biochem. Biophys. Res. Commun.* 493, 1356–1363. doi: 10.1016/j.bbrc.2017.09.164

Dutta, S., and Sengupta, P. (2016). Men and mice: Relating their ages. *Life Sci.* 152, 244–248. doi: 10.1016/j.lfs.2015.10.025

Farrer, L. A., Cupples, L. A., Haines, J. L., Hyman, B., Kukull, W. A., Mayeux, R., et al. (1997). Effects of age, sex, and ethnicity on the association between apolipoprotein E genotype and Alzheimer disease. A meta-analysis. APOE and Alzheimer Disease Meta Analysis Consortium. *JAMA* 278, 1349–1356.

Fitzner, D., Bader, J. M., Penkert, H., Bergner, C. G., Su, M., Weil, M. T., et al. (2020). Cell-Type- and Brain-Region-Resolved Mouse Brain Lipidome. *Cell Rep.* 32:108132. doi: 10.1016/j.celrep.2020.108132

Fratiglioni, L., Launer, L. J., Andersen, K., Breteler, M. M., Copeland, J. R., Dartigues, J. F., et al. (2000). . Incidence of dementia and major subtypes in Europe: A collaborative study of population-based cohorts. Neurologic Diseases in the Elderly Research Group. *Neurology* 54, S10–S15.

Giles, C., Takechi, R., Mellett, N. A., Meikle, P. J., Dhaliwal, S., and Mamo, J. C. (2017). Differential regulation of sphingolipid metabolism in plasma, hippocampus, and cerebral cortex of mice administered sphingolipid modulating agents. *J. Neurochem.* 141, 413–422.

Gonzalez-Garcia, I., Contreras, C., Estevez-Salguero, A., Ruiz-Pino, F., Colsh, B., Pensado, I., et al. (2018). Estradiol Regulates Energy Balance by Ameliorating Hypothalamic Ceramide-Induced ER Stress. *Cell Rep.* 25, 413–423e415.

Grimm, M. O. W., Michaelson, D. M., and Hartmann, T. (2017). Omega-3 fatty acids, lipids, and apoE lipidation in Alzheimer's disease: a rationale for multi-nutrient dementia prevention. *J. Lipid Res.* 58, 2083–2101. doi: 10.1194/jlr.r076331

Guo, S., Yu, Y., Zhang, N., Cui, Y., Zhai, L., Li, H., et al. (2014). Higher level of plasma bioactive molecule sphingosine 1-phosphate in women is associated with estrogen. *Biochim. Biophys. Acta* 1841, 836–846. doi: 10.1016/j.bbalip.2014.02.005

Hannun, Y. A. (1994). The sphingomyelin cycle and the second messenger function of ceramide. *J. Biol. Chem.* 269, 3125–3128. doi: 10.1016/s0021-9258(17)41834-5

Haughey, N. J., Bandaru, V. V., Bae, M., and Mattson, M. P. (2010). Roles for dysfunctional sphingolipid metabolism in Alzheimer's disease neuropathogenesis. *Biochim. Biophys. Acta* 1801, 878–886. doi: 10.1016/j.bbalip.2010.05.003

Holtzman, D. M., Herz, J., and Bu, G. (2012). Apolipoprotein E and apolipoprotein E receptors: normal biology and roles in Alzheimer disease. *Cold Spring Harb. Perspect. Med.* 2:a006312. doi: 10.1101/cshperspect.a006312

Jana, A., Hogan, E. L., and Pahan, K. (2009). Ceramide and neurodegeneration: susceptibility of neurons and oligodendrocytes to cell damage and death. *J. Neurol. Sci.* 278, 5–15. doi: 10.1016/j.jns.2008.12.010

Jonas, A. M. (2007). The Mouse in Biomedical Research. *Physiologist* 27, 330–346.

Jorm, A. F., and Jolley, D. (1998). The incidence of dementia: a meta-analysis. *Neurology* 51, 728–733. doi: 10.1212/wnl.51.3.728

Kang, J., Lemaire, H. G., Unterbeck, A., Salbaum, J. M., Masters, C. L., Grzeschik, K. H., et al. (1987). The precursor of Alzheimer's disease amyloid A4 protein resembles a cell-surface receptor. *Nature* 325, 733–736. doi: 10.1038/325733a0

Kanno, T., Nishizaki, T., Proia, R. L., Kajimoto, T., Jahangeer, S., Okada, T., et al. (2010). Regulation of synaptic strength by sphingosine 1-phosphate in the hippocampus. *Neuroscience* 171, 973–980. doi: 10.1016/j.neuroscience.2010.10.021

Kloske, C. M., and Wilcock, D. M. (2020). The Important Interface Between Apolipoprotein E and Neuroinflammation in Alzheimer's Disease. *Front. Immunol.* 11:754. doi: 10.3389/fimmu.2020.00754

Lazzarini, A., Macchiarulo, A., Floridi, A., Coletti, A., Cataldi, S., Codini, M., et al. (2015). Very-long-chain fatty acid sphingomyelin in nuclear lipid microdomains of hepatocytes and hepatoma cells: can the exchange from C24:0 to C16:0 affect signal proteins and vitamin D receptor? *Mol. Biol. Cell* 26, 2418–2425. doi: 10.1091/mbc.e15-04-0229

Levy-Lahad, E., Wasco, W., Poorkaj, P., Romano, D. M., Oshima, J., Pettingell, W. H., et al. (1995). Candidate gene for the chromosome 1 familial Alzheimer's disease locus. *Science* 269, 973–977. doi: 10.1126/science.7638622

Liesinger, A. M., Graff-Radford, N. R., Duara, R., Carter, R. E., Hanna Al-Shaikh, F. S., Koga, S., et al. (2018). Sex and age interact to determine clinicopathologic differences in Alzheimer's disease. *Acta Neuropathol.* 136, 873–885. doi: 10.1007/s00401-018-1908-x

Lim, W. L., Martins, I. J., and Martins, R. N. (2014). The involvement of lipids in Alzheimer's disease. *J. Genet. Genomics* 41, 261–274. doi: 10.1016/j.jgg.2014.04.003

Liu, Y., Peterson, D. A., and Schubert, D. (1998). Amyloid beta peptide alters intracellular vesicle trafficking and cholesterol homeostasis. *Proc. Natl. Acad. Sci. U S A.* 95, 13266–13271. doi: 10.1073/pnas.95.22.13266

Mahley, R. W. (2016). Central Nervous System Lipoproteins: ApoE and Regulation of Cholesterol Metabolism. *Arterioscler. Thromb. Vasc. Biol.* 36, 1305–1315. doi: 10.1161/ATVBAHA.116.307023

Marin, R., and Diaz, M. (2018). Estrogen Interactions With Lipid Rafts Related to Neuroprotection. Impact of Brain Ageing and Menopause. *Front. Neurosci.* 12:128. doi: 10.3389/fnins.2018.00128

Martinez Martinez, P., and Mielke, M. M. (2017). Sphingolipids in Alzheimer's Disease and Related Disorders. *J. Alzheimers Dis.* 60, 753–756. doi: 10.3233/JAD-170735

Martins, I. J., Hone, E., Foster, J. K., Sunram-Lea, S. I., Gnjec, A., Fuller, S. J., et al. (2006). Apolipoprotein E, cholesterol metabolism, diabetes, and the convergence of risk factors for Alzheimer's disease and cardiovascular disease. *Mol. Psychiatry* 11, 721–736. doi: 10.1038/sj.mp.4001854

Maynard, C. J., Cappai, R., Volitakis, I., Cherny, R. A., Masters, C. L., Li, Q. X., et al. (2006). Gender and genetic background effects on brain metal levels in APP transgenic and normal mice: implications for Alzheimer beta-amyloid pathology. *J. Inorg. Biochem.* 100, 952–962. doi: 10.1016/j.jinorgbio.2006.02.010

Mielke, M. M., and Haughey, N. J. (2012). Could plasma sphingolipids be diagnostic or prognostic biomarkers for Alzheimer's disease? *Clin. Lipidol.* 7, 525–536. doi: 10.2217/clp.12.59

Mielke, M. M., Bandaru, V. V., Han, D., An, Y., Resnick, S. M., Ferrucci, L., et al. (2015). Demographic and clinical variables affecting mid- to late-life trajectories of plasma ceramide and dihydroceramide species. *Aging Cell* 2015, 1014–1023. doi: 10.1111/acel.12369

Mielke, M. M., Bandaru, V. V., Haughey, N. J., Rabins, P. V., Lyketsos, C. G., and Carlson, M. C. (2010a). Serum sphingomyelins and ceramides are early predictors of memory impairment. *Neurobiol. Aging* 31, 17–24. doi: 10.1016/j.neurobiolaging.2008.03.011

Mielke, M. M., Bandaru, V. V., Haughey, N. J., Xia, J., Fried, L. P., Yasar, S., et al. (2012). Serum ceramides increase the risk of Alzheimer disease: the Women's Health and Aging Study II. *Neurology* 79, 633–641. doi: 10.1212/WNL.0b013e318264e380

Mielke, M. M., Haughey, N. J., Bandaru, V. V., Schech, S., Carrick, R., Carlson, M. C., et al. (2010b). Plasma ceramides are altered in mild cognitive impairment and predict cognitive decline and hippocampal volume loss. *Alzheimers Dement.* 6, 378–385. doi: 10.1016/j.jalz.2010.03.014

Mielke, M. M., Haughey, N. J., Bandaru, V. V., Weinberg, D. D., Darby, E., Zaidi, N., et al. (2011). Plasma sphingomyelins are associated with cognitive progression in Alzheimer's disease. *J. Alzheimers Dis.* 27, 259–269. doi: 10.3233/JAD-2011-110405

Mielke, M. M., Haughey, N. J., Bandaru, V. V., Zetterberg, H., Blennow, K., Andreasson, U., et al. (2014). Cerebrospinal fluid sphingolipids, beta-amyloid,

and tau in adults at risk for Alzheimer's disease. *Neurobiol. Aging* 35, 2486–2494. doi: 10.1016/j.neurobiolaging.2014.05.019

Mielke, M. M., Haughey, N. J., Han, D., An, Y., Bandaru, V. V. R., Lyketsos, C. G., et al. (2017). The Association Between Plasma Ceramides and Sphingomyelins and Risk of Alzheimer's Disease Differs by Sex and APOE in the Baltimore Longitudinal Study of Aging. *J. Alzheimers Dis.* 60, 819–828. doi: 10.3233/JAD-160925

Mirzaian, M., Wisse, P., Ferraz, M. J., Marques, A. R. A., Gabriel, T. L., van Roomen, C., et al. (2016). Accurate quantification of sphingosine-1-phosphate in normal and Fabry disease plasma, cells and tissues by LC-MS/MS with (13)C-encoded natural S1P as internal standard. *Clin. Chim. Acta* 459, 36–44. doi: 10.1016/j.cca.2016.05.017

Mirzaian, M., Wisse, P., Ferraz, M. J., Marques, A. R. A., Gaspar, P., Oussoren, S. V., et al. (2017). Simultaneous quantitation of sphingoid bases by UPLC-ESI-MS/MS with identical (13)C-encoded internal standards. *Clin. Chim. Acta* 466, 178–184. doi: 10.1016/j.cca.2017.01.014

Mulder, M., Blokland, A., van den Berg, D. J., Schulten, H., Bakker, A. H., Terwel, D., et al. (2001). Apolipoprotein E protects against neuropathology induced by a high-fat diet and maintains the integrity of the blood-brain barrier during aging. *Lab. Invest.* 81, 953–960. doi: 10.1038/labinvest.3780307

Mulder, M., Ravid, R., Swaab, D. F., de Kloet, E. R., Haasdijk, Julk, J., et al. (1998). Reduced levels of cholesterol, phospholipids, and fatty acids in cerebrospinal fluid of Alzheimer disease patients are not related to apolipoprotein E4. *Alzheimer Dis. Assoc. Disord.* 12, 198–203. doi: 10.1097/00002093-199809000-00012

Mullen, T. D., and Obeid, L. M. (2012). Ceramide and apoptosis: exploring the enigmatic connections between sphingolipid metabolism and programmed cell death. *Anticancer Agents Med. Chem.* 12, 340–363. doi: 10.2174/187152012800228661

Mullen, T. D., Hannun, Y. A., and Obeid, L. M. (2012). Ceramide synthases at the centre of sphingolipid metabolism and biology. *Biochem. J.* 441, 789–802. doi: 10.1042/BJ20111626

Oakley, H., Cole, S. L., Logan, S., Maus, E., Shao, P., Craft, J., et al. (2006). Intraneuronal beta-amyloid aggregates, neurodegeneration, and neuron loss in transgenic mice with five familial Alzheimer's disease mutations: potential factors in amyloid plaque formation. *J. Neurosci.* 26, 10129–10140. doi: 10.1523/JNEUROSCI.1202-06.2006

Olsen, A. S. B., and Faergeman, N. J. (2017). Sphingolipids: membrane microdomains in brain development, function and neurological diseases. *Open Biol.* 7:170069. doi: 10.1098/rsob.170069

Park, W. J., and Park, J. W. (2015). The effect of altered sphingolipid acyl chain length on various disease models. *Biol. Chem.* 396, 693–705. doi: 10.1515/hsz-2014-0310

Pinto, S. N., Silva, L. C., de Almeida, R. F., and Prieto, M. (2008). Membrane domain formation, interdigitation, and morphological alterations induced by the very long chain asymmetric C24:1 ceramide. *Biophys. J.* 95, 2867–2879. doi: 10.1529/biophysj.108.129858

Prince, M., Bryce, R., Albanese, E., Wimo, A., Ribeiro, W., and Ferri, C. P. (2013). The global prevalence of dementia: a systematic review and metaanalysis. *Alzheimers Dement.* 9, 63–75e62. doi: 10.1016/j.jalz.2012.11.007

Schafer, S., Wirths, O., Multhaup, G., and Bayer, T. A. (2007). Gender dependent APP processing in a transgenic mouse model of Alzheimer's disease. *J. Neural Transm.* 114, 387–394. doi: 10.1007/s00702-006-0580-9

Schwarz, A., and Futerman, A. H. (1997). Distinct roles for ceramide and glucosylceramide at different stages of neuronal growth. *J. Neurosci. Offic. J. Soc. Neurosci.* 17, 2929–2938. doi: 10.1523/JNEUROSCI.17-09-02929.1997

Seumois, G., Fillet, M., Gillet, L., Faccinetto, C., Desmet, C., Francois, C., et al. (2007). De novo C16- and C24-ceramide generation contributes to spontaneous neutrophil apoptosis. *J. Leukoc. Biol.* 81, 1477–1486. doi: 10.1189/jlb.0806529

Sharman, M. J., Shui, G., Fernandis, A. Z., Lim, W. L., Berger, T., Hone, E., et al. (2010). Profiling brain and plasma lipids in human APOE epsilon2, epsilon3, and epsilon4 knock-in mice using electrospray ionization mass spectrometry. *J. Alzheimers Dis.* 20, 105–111. doi: 10.3233/JAD-2010-1348

Sherrington, R., Rogaev, E. I., Liang, Y., Rogaeva, E. A., Levesque, G., Ikeda, M., et al. (1995). Cloning of a gene bearing missense mutations in early-onset familial Alzheimer's disease. *Nature* 375, 754–760. doi: 10.1038/375754a0

Strazielle, N., and Ghersi-Egea, J. F. (2013). Physiology of blood-brain interfaces in relation to brain disposition of small compounds and macromolecules. *Mol. Pharm.* 10, 1473–1491. doi: 10.1021/mp300518e

Strittmatter, W. J., Saunders, A. M., Schmechel, D., Pericak-Vance, M., Enghild, J., Salvesen, G. S., et al. (1993). Apolipoprotein E: high-avidity binding to beta-amyloid and increased frequency of type 4 allele in late-onset familial Alzheimer disease. *Proc. Natl. Acad. Sci. U S A.* 90, 1977–1981. doi: 10.1073/pnas.90.5.1977

Tai, L. M., Balu, D., Avila-Munoz, E., Abdullah, L., Thomas, R., Collins, N., et al. (2017). EFAD transgenic mice as a human APOE relevant preclinical model of Alzheimer's disease. *J. Lipid Res.* 58, 1733–1755. doi: 10.1194/jlr.R076315

Tai, L. M., Youmans, K. L., Jungbauer, L., Yu, C., and Ladu, M. J. (2011). Introducing Human APOE into Abeta Transgenic Mouse Models. *Int. J. Alzheimers Dis.* 2011:810981. doi: 10.4061/2011/810981

Van Brocklyn, J. R., and Williams, J. B. (2012). The control of the balance between ceramide and sphingosine-1-phosphate by sphingosine kinase: oxidative stress and the seesaw of cell survival and death. *Comp. Biochem. Physiol. B Biochem. Mol. Biol.* 163, 26–36. doi: 10.1016/j.cbpb.2012.05.006

van Doorn, R., Nijland, P. G., Dekker, N., Witte, M. E., Lopes-Pinheiro, M. A., van het Hof, B., et al. (2012). Fingolimod attenuates ceramide-induced blood-brain barrier dysfunction in multiple sclerosis by targeting reactive astrocytes. *Acta Neuropathol.* 124, 397–410. doi: 10.1007/s00401-012-1014-4

van Echten-Deckert, G., Hagen-Euteneuer, N., Karaca, I., and Walter, J. (2014). Sphingosine-1-phosphate: boon and bane for the brain. *Cell Physiol. Biochem.* 34, 148–157. doi: 10.1159/000362991

Verghese, P. B., Castellano, J. M., Garai, K., Wang, Y., Jiang, H., Shah, A., et al. (2013). ApoE influences amyloid-beta (Abeta) clearance despite minimal apoE/Abeta association in physiological conditions. *Proc. Natl. Acad. Sci. U S A.* 110, E1807–E1816. doi: 10.1073/pnas.1220484110

Vozella, V., Basit, A., Misto, A., and Piomelli, D. (2017). Age-dependent changes in nervonic acid-containing sphingolipids in mouse hippocampus. *Biochim. Biophys. Acta Mol. Cell Biol. Lipids* 1862, 1502–1511. doi: 10.1016/j.bbalip.2017.08.008

Vozella, V., Basit, A., Piras, F., Realini, N., Armirotti, A., Bossu, P., et al. (2019). Elevated plasma ceramide levels in post-menopausal women: a cross-sectional study. *Aging* 11, 73–88. doi: 10.18632/aging.101719

Wheeler, D., Knapp, E., Bandaru, V. V., Wang, Y., Knorr, D., Poirier, C., et al. (2009). Tumor necrosis factor-alpha-induced neutral sphingomyelinase-2 modulates synaptic plasticity by controlling the membrane insertion of NMDA receptors. *J. Neurochem.* 109, 1237–1249. doi: 10.1111/j.1471-4159.2009.06038.x

Youmans, K. L., Tai, L. M., Kanekiyo, T., Stine, W. B. Jr., Michon, S. C., Nwabuisi-Heath, E., et al. (2012a). Intraneuronal Abeta detection in 5xFAD mice by a new Abeta-specific antibody. *Mol. Neurodegener.* 7:8. doi: 10.1186/1750-1326-7-8

Youmans, K. L., Tai, L. M., Nwabuisi-Heath, E., Jungbauer, L., Kanekiyo, T., Gan, M., et al. (2012b). APOE4-specific changes in Abeta accumulation in a new transgenic mouse model of Alzheimer disease. *J. Biol. Chem.* 287, 41774–41786. doi: 10.1074/jbc.M112.407957

Zhang, L., and Hong, H. (2015). Genomic Discoveries and Personalized Medicine in Neurological Diseases. *Pharmaceutics* 7, 542–553. doi: 10.3390/pharmaceutics7040542

Zimmermann, C., Ginis, I., Furuya, K., Klimanis, D., Ruetzler, C., Spatz, M., et al. (2001). Lipopolysaccharide-induced ischemic tolerance is associated with increased levels of ceramide in brain and in plasma. *Brain Res.* 895, 59–65. doi: 10.1016/s0006-8993(01)02028-5

Conflict of Interest: The authors declare that the research was conducted in the absence of any commercial or financial relationships that could be construed as a potential conflict of interest.

Publisher's Note: All claims expressed in this article are solely those of the authors and do not necessarily represent those of their affiliated organizations, or those of the publisher, the editors and the reviewers. Any product that may be evaluated in this article, or claim that may be made by its manufacturer, is not guaranteed or endorsed by the publisher.

frontiers in Aging Neuroscience

REVIEW
published: 05 November 2021
doi: 10.3389/fnagi.2021.736734

Nicotinamide Adenine Dinucleotide Phosphate Oxidases Are Everywhere in Brain Disease, but Not in Huntington's Disease?

*Luisana Villegas[1], Anne Nørremølle[1], Kristine Freude[2] and Frederik Vilhardt[1]**

[1] Department of Cellular and Molecular Medicine, University of Copenhagen, Copenhagen, Denmark, [2] Department of Veterinary and Animal Sciences, Faculty of Health and Medical Sciences, University of Copenhagen, Frederiksberg, Denmark

Huntington's disease (HD) is an inherited neurodegenerative disorder characterized by neuronal loss and tissue atrophy mainly in the striatum and cortex. In the early stages of the disease, impairment of neuronal function, synaptic dysfunction and white matter loss precedes neuronal death itself. Relative to other neurodegenerative diseases such as Alzheimer's and Parkinson's disease and Amyotrophic Lateral Sclerosis, where the effects of either microglia or NADPH oxidases (NOXs) are recognized as important contributors to disease pathogenesis and progression, there is a pronounced lack of information in HD. This information void contrasts with evidence from human HD patients where blood monocytes and microglia are activated well before HD clinical symptoms (PET scans), and the clear signs of oxidative stress and inflammation in post mortem HD brain. Habitually, NOX activity and oxidative stress in the central nervous system (CNS) are equated with microglia, but research of the last two decades has carved out important roles for NOX enzyme function in neurons. Here, we will convey recent information about the function of NOX enzymes in neurons, and contemplate on putative roles of neuronal NOX in HD. We will focus on NOX-produced reactive oxygen species (ROS) as redox signaling molecules in/among neurons, and the specific roles of NOXs in important processes such as neurogenesis and lineage specification, neurite outgrowth and growth cone dynamics, and synaptic plasticity where NMDAR-dependent signaling, and long-term depression/potentiation are redox-regulated phenomena. HD animal models and induced pluripotent stem cell (iPSC) studies have made it clear that the very same physiological processes are also affected in HD, and we will speculate on possible roles for NOX in the pathogenesis and development of disease. Finally, we also take into account the limited information on microglia in HD and relate this to any contribution of NOX enzymes.

Keywords: Huntington's (disease), NADPH (nicotinamide adenine dinucleotide phosphate) oxidase, neuron, Huntingtin (HTT), NMDAR (NMDA receptor), LTP (long term potentiation), LTD (long term depression)

OPEN ACCESS

Edited by:
Christian Gonzalez-Billault, University of Chile, Chile

Reviewed by:
Aslihan Terzi, Stanford University, United States
Andréa Cristina Paula-Lima, University of Chile, Chile

****Correspondence:***
Frederik Vilhardt
vilhardt@sund.ku.dk

Received: *05 July 2021*
Accepted: *08 October 2021*
Published: *05 November 2021*

Citation:
Villegas L, Nørremølle A, Freude K and Vilhardt F (2021) Nicotinamide Adenine Dinucleotide Phosphate Oxidases Are Everywhere in Brain Disease, but Not in Huntington's Disease? Front. Aging Neurosci. 13:736734. doi: 10.3389/fnagi.2021.736734

INTRODUCTION

Microglia express NADPH oxidases (NOX) and in many neurodegenerative diseases (NDDs) microglia activation and the ensuing oxidant production through NOX2, together with proinflammatory response including cytokine secretion, play major roles in disease pathogenesis (Block et al., 2007; Tejera and Heneka, 2019). However, more recently NOX expression in neurons have attracted attention in physiological and pathological settings (Nayernia et al., 2014). Hence, changes in NOX activity in NDD's are not necessarily restricted to microglia but may also take place in neurons as a cell-autonomous mechanism, all though evidence for direct involvement of neuronal NOX isoforms in NDD is still scarce.

Here, we will convey recent information about the function of NOXs in the Central Nervous System (CNS) and contemplate on the putative role of neuronal NOX in the neurodegenerative disorder Huntington's Disease (HD). We will focus on NOX-produced reactive oxygen species (ROS) as a signaling molecule in/among neurons and the specific roles of NOXs in important processes in the synapses and neurites. We will thus compare the processes where NOXs are involved to the pathogenic mechanisms of HD, asking if NOXs are likely to be players in the initial synaptic dysfunction that characterizes HD, as well as later in disease progression. Given the high expression of NOX in microglia, we will also review the limited literature of NOX derived ROS in this particular cell type in relation to HD.

NOX AND OXIDANTS: OXIDATIVE STRESS VERSUS REDOX SIGNALING

Before we delve into the intricacies of NOX activity and oxidant production in neurons it is justified to briefly put into perspective the phenomenon of oxidative eustress versus oxidative stress. Oxidative stress is a condition with an imbalance in oxidant and antioxidant production, such that antioxidant defense mechanisms are overwhelmed by excessive oxidants. As such, oxidative stress is thought to be an inherent property of many neurodegenerative diseases (Singh et al., 2019). In the early days, oxidative stress was synonymous with the indiscriminate and irreversible oxidation and destruction of biomolecules and detected as molecular signs of oxidative modification of biomolecules (nitrosylation, sulfonation, carbonylation, and peroxidation). Today we know that under physiological circumstances cellular redox balance (oxidative eustress) is tightly maintained to allow oxidants to act as signaling molecules typically by their reversible oxidation of low pKa cysteines in target redox proteins, with a wide spectrum of functions that are still not fully discovered (Sies and Jones, 2020). Therefore, the concept of oxidative stress has since been expanded to account for the fact that even small perturbations of local or global redox milieu can seriously disrupt redox signaling circuits (Sies, 2014).

The CNS itself is highly susceptible to oxidative stress due to its fast rate of oxygen consumption and high iron content (Bresgen and Eckl, 2015), resulting in an increased generation of ROS. In addition, the antioxidant machinery that exists to counteract oxidative stress has lower levels of expression in the CNS, and in neurons particularly (Kamat et al., 2008; Teleanu et al., 2019). This relatively low neuronal antioxidant level could be due to a tradeoff; as ROS is required for exit from the neurogenic stem cell niche and neuronal induction (Nayernia et al., 2017), nerve cells habitually express low levels of nuclear factor erythroid 2-related factor 2 (NRF2) (Bell et al., 2015), a major transcriptional regulator of antioxidant genes (Hardingham and Do, 2016).

HUNTINGTON'S DISEASE

HD is an autosomal dominant inherited, neurodegenerative disease caused by an expansion of a CAG repeat in exon 1 of the HD gene, encoding an elongated poly-glutamine stretch in the huntingtin protein (The Huntington Disease Collaborative Research Group, 1993). Symptoms of HD include motor, psychiatric and cognitive changes usually emerging in midlife (with an earlier onset in those patients with larger poly-glutamine expansions), progressing to eventually cause fatal multi-system failure. Death of neurons, in particular striatal medium spiny neurons (MSNs) and cortical projection neurons but also neuron populations in other brain regions, is a prominent feature in late-stage HD. The MSNs are gamma-aminobutyric acid-ergic (GABAergic) inhibitory neurons receiving glutamatergic input from cortex, as well as dopaminergic input from the substantia nigra pars compacta (Blumenstock and Dudanova, 2020). MSNs affect the activity of neurons in the thalamus and cortex, thereby regulating the initiation and execution of movements. MSNs are divided in two classes, where the MSNs of the direct pathway project to output nuclei in the substantia nigra pars reticulate and the internal part of the globus pallidus (which connect to the thalamus), whereas the MSNs of the indirect pathway project to inhibitory neurons in the external part of the globus pallidus. These inhibitory neurons in turn affects the same output nuclei as the direct pathway, leading to opposing effect on the activity of these: the MSN direct pathway inhibits, and the MSN indirect pathway activates, the GABAergic neurons of the substantia nigra pars reticulate and the internal part of the globus pallidus (Blumenstock and Dudanova, 2020). In HD progression, the MSNs of the indirect pathway are the first to degenerate, which correlate well with the prominent involuntary movements (hyperkinesia) which are among the early symptoms of HD.

Before reaching final stage of neurodegeneration, at which symptoms of HD are evident and widespread, patients endure an extended period of gradual disease progression. Increasing neuronal dysfunction, specifically synaptic dysfunctions such as impaired synaptic plasticity and dysregulation of synaptic transmission are observed, most likely starting already at the prodromal, pre-symptomatic phase (Smith-Dijak et al., 2019). In particular, aberration of cortico-striatal connections are prominent and may (at least in part) explain the early hyperkinetic motor symptoms of HD (Plotkin and Surmeier, 2015). Because motor symptoms of the disease manifest before there is overt nerve cell death, HD is sometimes referred to as a 'synaptopathy'. Indeed, both cortical and striatal neurons of

HD mouse models display synaptic dysfunction at very early, pre-symptomatic stages (reviewed in Cepeda and Levine (2020)). These functional changes are supported by proteomic analysis, in which early HD-related changes predominantly occur in proteins involved in synaptic function (Skotte et al., 2018; Sapp et al., 2020). According to the "dying-back" theory, such early synaptic changes can lead to synapse and neurite degeneration and loss, which may eventually result in neuronal death (Han et al., 2010).

Huntingtin (Htt) is ubiquitously expressed and localizes mainly in the cytoplasm, but also in the nucleus; within the cell, huntingtin associates with numerous cellular structures and molecules (Saudou and Humbert, 2016). Htt has a tremendous number of protein interaction partners (> 100), which perhaps point to a general function of Htt as scaffolding protein, and in part dictates the many proposed roles of Htt as well as the subcellular localization of Htt. In neurons Htt can be found along neurites and in terminals, in part due to its interaction with the dynein-dynactin complex (Rui et al., 2015), which drives vesicular transport along microtubules. Htt has a major role in the regulation of autophagosome (Wong and Holzbaur, 2014; Rui et al., 2015), endosomal (Caviston et al., 2007), or stress granule (Ma et al., 2011) dynamics and positioning, and the very same processes and organelles (among others) are affected adversely by mHtt (Gunawardena et al., 2003; Morfini et al., 2009; Martinez-Vicente et al., 2010; Wong and Holzbaur, 2014). Htt also interacts with the actin cytoskeleton through binding to a-actinin, an actin anchoring and cross-linking protein, and in fibroblasts co-localizes with actin stress fibers and adhesion structures (Tousley et al., 2019a). In mHtt-expressing cells, a large fractional area of the cytosol is occupied by spherical inclusion bodies of aggregated mHtt surrounded by markers of autophagy (p62/SQSTM1) and intermediate filaments. Inclusion formation can have negative effects on organelles (Bauerlein et al., 2017), trafficking systems (Woerner et al., 2016), and cause the sequestration of other glutamine-rich and prion domain-containing proteins (Ramdzan et al., 2017) but may also have cytoprotective function (Miller et al., 2010).

In HD patients, mutant huntingtin is expressed throughout life, including during embryogenesis (Saudou and Humbert, 2016). In line with this, the expression of mutant huntingtin has been shown to affect not only adult neuronal function, leading to neurodegeneration, but also neurodevelopment including neuronal differentiation and establishment of connectivity through neurite outgrowth (Conforti et al., 2018; Barnat et al., 2020; van der Plas et al., 2020). Intriguingly, mouse models expressing mutant huntingtin solely during embryonic and early development develop HD-like symptoms (Molero et al., 2016). As hypothesized by Lu and Lu, these data indicate that neurodevelopmental dysregulation may play an important role in HD pathogenesis developing in adulthood (Lu and Lu, 2021).

Although the initial cause of the pathology is known – expression of huntingtin carrying an expanded poly-glutamine stretch – the downstream pathogenic processes are still not well understood. As excellently reviewed by Bates et al., mutant huntingtin has been shown to lead to (among others) transcriptional dysregulation, impairment of axonal vesicular transport, synaptic dysfunction and impaired mitochondrial function (Bates et al., 2015). In both human post mortem HD brain (Sorolla et al., 2008) and HD animal models (Bogdanov et al., 2001) there are tell-tale signs of oxidative stress, but focus has almost exclusively been on mitochondria-generated ROS (Zheng et al., 2018; Fão and Rego, 2021) ignoring the major oxidant producing enzymes, the family of NOXs (Brown and Borutaite, 2012; Lambeth and Neish, 2014; Sies and Jones, 2020).

THE FAMILY OF NICOTINAMIDE ADENINE DINUCLEOTIDE PHOSPHATE OXIDASES

NOXs are transmembrane, superoxide-producing enzyme complexes. Once activated, the NOX complexes transfer electrons from nicotinamide adenine dinucleotide phosphate (NADPH) in the cytosol to molecular oxygen on the other side of the membrane, thus producing superoxide ($O_2^{\cdot -}$) in the extracellular space or the topologically identical luminal space of organelles and vesicles. Superoxide quickly dismutation to hydrogen peroxide spontaneously, or more commonly at high levels of oxidants, via superoxide dismutase activity.

The NOX family is comprised of 7 isoforms (NOX1-5 and DUOX1-2) (**Figure 1**; Bedard and Krause, 2007). The first prototypical member of the family to be characterized was the classical phagocyte NADPH oxidase, now called NOX2, consisting of a membrane-anchored flavocytochrome b_{558}, itself composed of two membrane proteins gp91^{phox} (also confusingly referred to as NOX2), containing heme redox relay stations for electron transfer, and p22^{phox}. Activation of the NOX2 enzyme involves further recruitment of four cytosolic proteins which translocate to the membrane: p67^{phox} and the small GTP-binding protein Rac1/2, which together regulate electron transfer from NADPH to redox centers in gp91^{phox}, and p40^{phox} or p47^{phox} as organizers of assembly (Vignais, 2002). While introduction of dominant active Rac1 is sufficient to induce NOX activation in a heterologous cell model with NOX2 overexpression (Price et al., 2002), it is insufficient in phagocytes, where the critical step in NOX2 activation (at least in microglia) is phosphorylation of p47^{phox} (Roepstorff et al., 2008). Multiple phosphorylation events on serines uncovers the latent SH3 domains of p47^{phox}, making them available for binding to p22^{phox} (Sumimoto et al., 1996). In addition, PX domains contained in the SH3 domains of p47^{phox} and p40^{phox} contributes to membrane recruitment through binding to phosphoinositide lipids (Zhan et al., 2002; Ago et al., 2003).

NOX1 consists of the membrane-anchored subunits NOX1 and p22^{phox}, which interacts with NOXO1 and NOXA1, homologs of p47^{phox} and p67^{phox}, respectively, as well as Rac. Likewise, NOX3 interacts with p22^{phox} in addition to NOXO1 (Cheng et al., 2004). In contrast, the NOX4-p22^{phox} complex, as well as the NOX5, DUOX1 and DUOX2 isoforms can be activated independently of cytosolic phox proteins (Bedard and Krause, 2007). NOX4 is thought to be constitutively active, while NOX5

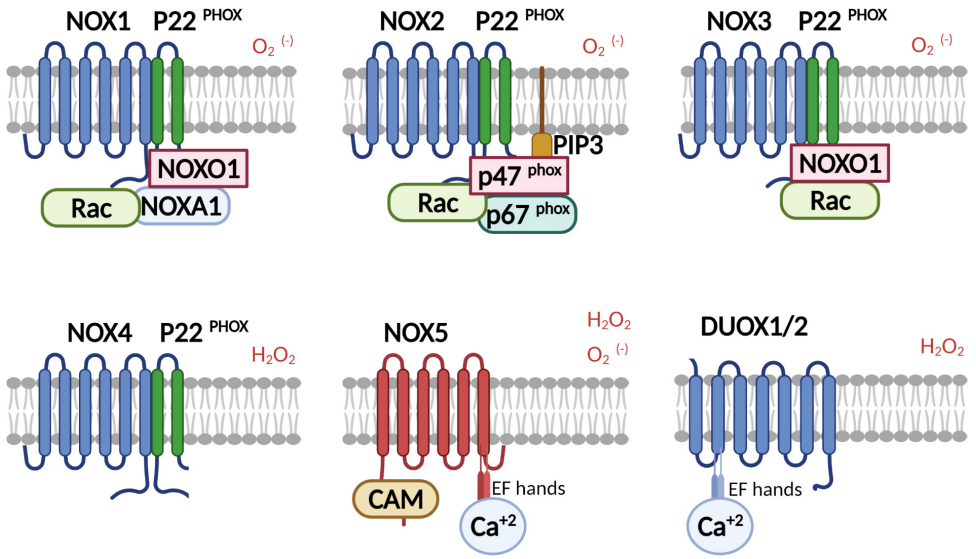

FIGURE 1 | Schematic representation of the family of NADPH oxidases. NOX isoforms and regulatory subunits: NOX1-3 are activated in the presence of cytosolic phox proteins, where PIP3 serves as a membrane anchor for $p47^{phox}$ in the case of NOX2 activation. NOX1-3, and NOX5 release superoxide (in some cases NOX5 also hydrogen peroxide), whereas NOX4 and the DUOXes release only hydrogen peroxide. NOX4 is constitutively active and is regulated by expression. NOX5 and DUOX1/2 are calcium dependent through calcium-calmodulin binding or by the direct binding of Ca^{2+} to EF-hands in DUOXes, respectively.

and DUOX1/2 have N-terminal extensions containing 2 to 4 EF-hand Ca^{+2} binding domains allowing their activation through calcium sensing (Banfi et al., 2004) (see **Figure 1** for schematic representation of NOX isoforms). Both NOX4 and the DUOX enzymes release hydrogen peroxide rather than superoxide.

NOX2, the classical phagocyte NADPH oxidase, is well known for its bactericidal role in innate immune defense (Nauseef, 2019), but with the advent of the NOX superfamily it was quickly realized that these enzymes occupies an important role as oxidant producers in an intricate network of cellular redox signaling circuits. Hydrogen peroxide is here believed to be the redox-relevant signaling messenger, and controls the activity of target proteins typically by the reversible oxidation of low pKa cysteines or metal centers (Sies and Jones, 2020; Petersen et al., 2021). The redox targets are diverse, but for the purpose of this review it is worth mentioning that many ion channels, kinases, and phosphatases are regulated or modulated by hydrogen peroxide (Winterbourn, 2013; Sies, 2014; Sies and Jones, 2020).

In the CNS, mainly NOX2 and NOX4 isoforms are expressed under basal conditions, while other NOX isoforms can be induced by stimulation (Massaad and Klann, 2011; Nayernia et al., 2014). Different neuronal populations (cortical, hippocampal, hypothalamic paraventricular nucleus neurons, cerebellar granule neurons, neurons of the sympathetic system, parvalbumin-positive GABAergic interneurons) mainly express the phagocyte NOX2, but dopaminergic neurons express NOX1, and dorsal root ganglion neurons (DRGs) express NOX4 (Massaad and Klann, 2011; Nayernia et al., 2014; Sorce et al., 2017). Glial cells and the vascular compartment also express NOX isoforms (Nayernia et al., 2014), and in particular microglia express NOX2. Because only NOX2 function in CNS has been addressed with some weight, we will in the following sections focus on neuronal expression of this isoform in CNS neurons and microglia.

SUBCELLULAR LOCALIZATION OF NOX IN NEURONS

Virtually all cells of our body express NOX isoforms. Many cell types express more than one NOX isoform, and despite their high homology, they localize differentially in a cell type-specific manner. For example, in endothelial cells, NOX1 is present in caveolae while NOX4 segregates to focal adhesions (Helmcke et al., 2009); in microglia, NOX1 seems to reside in lysosomes (Cheret et al., 2008), while NOX2 is localized to agonist-responsive secretory vesicles and the plasma membrane (Ejlerskov et al., 2012). Because of the large and polarized shape of neurons it is reasonable to assume that the same can occur in neurons, such that separate redox signaling circuits can function simultaneously in the same cell (see discussion in Petersen et al. (2021)). No sorting receptors for NOX have been identified, and there are very few clues to the differential and cell-specific subcellular distribution of the different NOX isoforms, as very few interaction partners of NOX family members have been identified (Park et al., 2004; Ikeda et al., 2005; Gianni et al., 2009). In microglia, the small GTPases Rab27A/B determine the distribution of intracellular to cell surface-resident NOX2 (Ejlerskov et al., 2012), which in essence determines the release to the surroundings of either hydrogen peroxide or superoxide, respectively, because of their different membrane permeabilities.

In the following sections, we have compiled the available data of NOX2 localization in neurons (summarized in **Table 1**). The data have been compiled from ultrastructural studies, most

TABLE 1 | The subcellular distribution of NOX2, $p22^{phox}$, and $p47^{phox}$ observed by immunolabeling in neurons (Wang G. et al., 2004; Glass et al., 2006; Brennan et al., 2009; Girouard et al., 2009; Minnella et al., 2018).

Somata	Plasma membrane	$gp91^{phox}$ (Wang G. et al., 2004; Glass et al., 2006), $p47^{phox}$ (Coleman et al., 2013)
	Mitochondria	$gp91^{phox}$ (Wang G. et al., 2004; Girouard et al., 2009; Coleman et al., 2013)
	MVBs	$gp91^{phox}$ (Glass et al., 2006), $p47^{phox}$ (Coleman et al., 2013)
	Vesicular organelles of the cytoplasm	$gp91^{phox}$ (Glass et al., 2006; Girouard et al., 2009), $p22^{phox}$, $p47^{phox}$ (Glass et al., 2006) $p47^{phox}$ (Coleman et al., 2013)
	Rough ER	$gp91^{phox}$ (Glass et al., 2006), $p47^{phox}$ (Coleman et al., 2013)
	Golgi Complex	$gp91^{phox}$ (Wang G. et al., 2004), $p22^{phox}$ (Glass et al., 2006), $p47^{phox}$ (Glass et al., 2006)
	Cytosol	$p47^{phox}$ (Coleman et al., 2013)
Dendrites	Plasma membrane	$gp91^{phox}$ (Glass et al., 2006), $p47^{phox}$ (Coleman et al., 2013)
	Perisynaptic plasma membrane	$gp91^{phox}$ (Glass et al., 2006; Wang et al., 2015), $p22^{phox}$, $p47^{phox}$ (Coleman et al., 2013) (Glass et al., 2006; Coleman et al., 2013)
	Mitochondria	$gp91^{phox}$ (Glass et al., 2006), $p22^{phox}$ (Glass et al., 2006), $p47^{phox}$ (Coleman et al., 2013)
	Smooth ER	$gp91^{phox}$ (Wang G. et al., 2004)
	MVBs	$gp91^{phox}$ (Wang G. et al., 2004)
	Vesicular organelles of the cytoplasm	$gp91^{phox}$ (Glass et al., 2006), $p22^{phox}$, $p47^{phox}$ (Glass et al., 2006)
	Undefined endomembrane beneath synapse	$gp91^{phox}$ (Glass et al., 2006; Girouard et al., 2009), $p47^{phox}$ (Coleman et al., 2013)
	Cytosol	$gp91^{phox}$ (Glass et al., 2006; Coleman et al., 2013)
Axons	The plasma membrane of an axon terminal	$gp91^{phox}$ (Wang et al., 2015)
	Clear vesicles of an axon terminal	$gp91^{phox}$ (Wang G. et al., 2004; Wang et al., 2015)

The most thorough studies used immunogold labeling and immunoperoxidase staining to reveal co-localization of $cytb_{558}$ and $p47^{phox}$ in mainly intracellular vesicular organelles, or cell surface in dendrites of the nucleus tractus solitarius (Glass et al., 2006); or localization of $p47^{phox}$ in the paraventricular thalamic nucleus (Coleman et al., 2013).

of them performed by the groups of Iadecola and Wilkens. The immunolocalization is of high quality, and in several cases quantitation of NOX2 subunits distribution was performed (Glass et al., 2006; Coleman et al., 2013). The expression and subcellular distribution of other NOX family members in neurons has not been analyzed in detail.

NOX2 in the Soma of Neurons

NOX2 can be found at various sites in neuronal cell bodies including the plasmalemma, rough ER, smooth ER, Golgi Complex, mitochondria, multivesicular bodies (MVBs) and vesicles (Wang G. et al., 2004; Girouard et al., 2009; Coleman et al., 2013). However, detection of $gp91^{phox}$ and $p22^{phox}$ at some of these sites is likely due to their biosynthesis.

NOX2 in Neurites

In developing neurons NOX2 localizes to growth cones, including filopodia and lamella (Munnamalai et al., 2014; Terzi et al., 2021), as we will later discuss. Here, we will mainly focus on mature neurons *in vivo*, where most ultrastructural studies have been performed. Within dendrites, $p22^{phox}$, $p47^{phox}$, and $gp91^{phox}$ are predominantly found on intracellular vesicular organelles, but also at the plasma membrane close to dendritic spines (Wang G. et al., 2004; Glass et al., 2006; Girouard et al., 2009). In a quantitative study, the majority of NOX2 labeling ($gp91^{phox}$, $p22^{phox}$, and $p47^{phox}$ labeling) was in fact associated with dendrites and less with soma, axons, and terminals (Glass et al., 2006). Intracellularly, $p47^{phox}$ and $gp91^{phox}$ can be detected in association with vesicular organelles and mitochondria (Glass et al., 2006). Additionally, the $gp91^{phox}$ subunit has been found on membranes resembling smooth endoplasmic reticulum (Glass et al., 2006) and in multivesicular bodies (endosomes) (Wang G. et al., 2004).

NOX2 in Synapses

Two separate studies have used electron microscopy to dissect the subcellular distribution of NOX2 in neurons of the nucleus tractus solitarius (brain stem). One study shows that immunogold-labeled NOX2 is present in pre-synaptic axon terminals, possibly belonging to the vagus nerve. More specifically, NOX2 is found at the plasma membrane and associated with small clear vesicles of the terminal and some MVB's (Wang G. et al., 2004). A different study that systematically quantified the $p47^{phox}$, $gp91^{phox}$, and $p22^{phox}$ distribution concludes that only a fraction of these subunits localize to axon terminals or axons in general (Glass et al., 2006). Both studies, however, agree that $gp91^{phox}$, $p22^{phox}$, and $p47^{phox}$ can be found on or just beneath the peri-synaptic portions of the post-synaptic (dendritic) plasma membrane (Wang G. et al., 2004; Glass et al., 2006). Interestingly, in a quantitative approach, angiotensin II stimulation was shown to induce $p47^{phox}$ translocation from cytosol to undefined endomembranes in close proximity to post-synaptic membranes of non-vassopressin hypothalamic paraventricular neurons (Coleman et al., 2013). Taken together, NOX2 can be found at synaptic sites, especially in the post-synaptic (dendritic) part, which is also confirmed by biochemical analysis of synaptosome

preparations (isolated pre- and post-synaptic structures) prepared from hippocampal neurons (Tejada-Simon et al., 2005; Brennan et al., 2009), as well as synaptosome preparations from aged mice (Ali et al., 2011).

NOX AND MUTANT HUNTINGTIN; A DIRECT INTERACTION?

While there is good evidence for expression of NOX2 in cortical projection neurons (Massaad and Klann, 2011; Nayernia et al., 2014), some of which project to innervate striatal GABAergic MSNs, there are no data on the expression of NOX isoforms in the MSNs themselves. One of the few studies that relates expression of the HD mutation and cellular pathology to NOX expression applied immunoprecipitation which suggests a direct interaction between NOX2 and mutant huntingtin (Bertoni et al., 2011). This study by Bertoni et al. indicated that mutant huntingtin from patient fibroblasts was selectively sequestered in cholesterol- and glycosphingolipid-enriched membrane microdomains (lipid rafts) (Bertoni et al., 2011), which are central platforms for organization and signaling. Interestingly, NOX2 also segregates to lipid rafts (Vilhardt and van Deurs, 2004). Moreover, using an inducible polyQ expression system on PC12 cells, they propose that expanded polyQ proteins interact with gp91^{phox}, as indicated by co-immunoprecipitation, which promotes NOX2-related oxidative stress in the cells (Bertoni et al., 2011). In accordance with the above, expanded polyQ tracts in Ataxin-7 have been shown to activate NOX in a cell model (Ajayi et al., 2012). Remarkably, treatment of polyQ-GFP-expressing PC12 cells with gp91ds-Tat (inhibiting NOX2 complex assembly) not only prevented the formation of new polyQ aggregates (which are typical of polyQ expanded diseases such as HD), but also dissolved the already existing ones (Bertoni et al., 2011). Moreover, a single *in vivo* study shows that instrastriatal injection of quinolinic acid in Wistar rats causes HD like symptoms, as well as increased NOX activity. Inhibition with apocynin resulted in less ROS production and prevented excitotoxicity (Maldonado et al., 2010).

These few studies constitute the entirety of NOX-related research on a HD background, which compared to the wealth of information available on the role of NOX-derived oxidants (mainly from microglia) in other NDDs is surprisingly limited. In the following sections of this review, we will speculate on the possible pathways in HD pathogenesis where NOX could play a role. Therefore, we will look into the known physiological functions of NOXs in neuronal development, differentiation, and synaptic function and plasticity with the purpose of discussing and speculating where in these processes NOXs may be contributing to the pathogenesis of HD. For a wider view of NOX roles in the CNS, we refer to a recent review by Terzi and Suter (2020).

Before we venture into the literature addressing any role of NOX isoforms in neuron function *in vivo* or *in vitro*, a technical *caveat* is warranted. In many studies, various synthetic inhibitors purported to specifically inhibit NOX2 have been used, and the results should be interpreted with caution. For example, apocynin, purported to inhibit p47^{phox} translocation to the membrane, is most likely a general antioxidant and has no specificity for NOX2 (Sorce et al., 2017). Therefore, the use of particularly knockout animal models of NOX isoforms, but also shRNA knockdown or expression of dominant negative constructs of NOX subunits, is the golden standard to affirm specific involvement of any NOX isoform in a given process. The use of gp91 ds-tat is also generally accepted by most as being a specific inhibitor of NOX2. The inhibitor consists of a 9 amino acid peptide of gp91^{phox} (amino acids 86–94) which binds to p47^{phox}, therefore preventing endogenous complex assembly. The tat portion is a 9 amino acid sequence of the HIV-tat transport region, allowing it to enter into the cells (Rey et al., 2001).

ROLE OF NOXS IN NEUROGENESIS/NEURODEVELOPMENT

A few studies have delineated a role for NOX2 in neurogenesis in the subventricular zone (SVZ) of the mammal brain, and in human iPSC-derived neurons. Thus maintenance of the neurogenic niche and neuroprogenitor proliferation depends on a sustained oxidant production through NOX2, which is expressed by neurogenic stem cells and their progenitors (Yoneyama et al., 2010; Le Belle et al., 2011; Kokovay et al., 2012; Nayernia et al., 2017). Some details have been unraveled. Thus, vascular cell adhesion protein 1 (VCAM1) expression in neuronal stem cells is essential to uphold the neurogenic niche, and VCAM1 in turn activates NOX2 to produce superoxide (Kokovay et al., 2012). Others have identified upregulation of Akt signaling as important for neuroprogenitor proliferation. NOX2-derived oxidants inhibit the opposing phosphatase and tensin homolog (PTEN) (although only chemical NOX2 inhibitors were used to arrive at this conclusion) (Le Belle et al., 2011), and Akt membrane association and activation is itself redox-modulated (Su et al., 2019). The most careful study has been performed using knock-out models to substantiate NOX involvement both *in vivo* and *in vitro* during iPSC differentiation to neurons (Nayernia et al., 2017). The authors find that gp91^{phox}, specifically, is strongly upregulated to allow the passage from pluripotency to neural induction and then disappears during neuronal differentiation and maturation. Interestingly, the downregulation of p22^{phox} is less impressive which could hint at a role for other NOX family members in differentiated cells.

REGULATION OF THE NEUROGENIC STEM CELL NICHE IN HD

While HD is a neurodegenerative disease, it is also apparent that there is a neurodevelopmental aspect to it, which is played out in iPSC and embryonic stem cell (ESC) models of disease and in animal models. As mentioned earlier, a study using a mouse model conditionally expressing mutant huntingtin (97Q) only until postnatal day 21 showed that many of the

pathological phenotypes observed in other HD mouse models are recapitulated in the aged mice, indicating that mutant huntingtin expression during development is sufficient for disease induction (Molero et al., 2016). It has been shown that mutant huntingtin expression is associated with a lower rate of progenitor cell division in isogenic ESC models (Ooi et al., 2019), as well as in cortical tissue from HD carrier fetuses at gestation week 13 (Barnat et al., 2020). Moreover, HD neural progenitor cells (NPCs) enter earlier into neuronal lineage fate, in comparison to their WT controls. Studies using mutant huntingtin knock-in cell lines showed that NPCs displayed impaired lineage restriction, lower proliferation rates, and aberrant MSN subtype specification (Molero et al., 2016). In unrelated studies by Xu et al. (2017), they corrected the huntingtin mutation in isogenic lines (Control: CAG33, mutant: CAG180) with a CRISPR-Cas9 and piggyBac transposon-based approach. Correction of the mutation reverted the phenotype to proper establishment of neural rosettes in culture, as opposed to what was seen in the non-modified CAG180 line. The latter was a specific effect of the HD mutation given the same genomic background of the isogenic lines (Xu et al., 2017). Given the role of NOX2 in progression from the stem cell niche to neuronal induction (Nayernia et al., 2017), it is possible that derangement of NOX activity could contribute to these phenomena of altered neuronal induction and differentiation in HD.

ROLE OF NOXS IN NEURITE GROWTH, SPECIFICATION, AND CONNECTIVITY DURING DEVELOPMENT AND AFTER NERVE INJURY

A few *in vitro* studies first indicated a role for NOX activity in neurite outgrowth and extension in the commonly used catecholaminergic PC12 nerve cell line (Suzukawa et al., 2000; Ibi et al., 2006). But only recently has the involvement of NOX in neurite extension, specification (dendrite or axon), and targeting been addressed in different animal models or *in vitro* models of nerve cell sprouting (Munnamalai et al., 2014; Olguin-Albuerne and Moran, 2015; Wilson et al., 2015, 2016; Weaver et al., 2018; Terzi and Suter, 2020).

One of the first studies supporting a role of NOX in neurite growth demonstrated the presence of gp91^{phox} in growth cones of *Aplysia* bag cell neurons. NOX2 was shown to orchestrate actin dynamics in growth cones, since chemical NOX2 inhibition reduced F-actin levels, and lowered retrograde transport, accompanied by shorter neurites (Munnamalai et al., 2014). When neurite growth was induced, an increase in co-localization of p40^{phox} with gp91^{phox} at apCAM (neural cell adhesion molecule (NCAM) homolog) adhesion sites was observed, indicating NOX2 complex formation and activation.

Related studies showed that chemical or genetic inhibition of NOX2 activity significantly diminished neurite outgrowth in primary cerebellar granule neurons (Olguin-Albuerne and Moran, 2015). *In vitro* peaks of ROS production correlated with high expression and activity of NOX1 and NOX2; also, the majority of hydrogen peroxide production, as measured by the hydrogen peroxide-specific biosensor Hyper, was in focal sites of axonal and dendritic growth cones, as well as in filopodia, with the highest peak before elongation of the latter.

In rat primary hippocampal neurons, NOX2 inhibition by chemical, biological, or genetic (dominant negative -p22^{phox} expression or p47$^{phox(-/-)}$ mice) means, resulted in decreased axonal growth and loss of cell polarization *in vitro* (Wilson et al., 2015). Expression of dominant negative -p22^{phox} (which would inhibit NOX1-3) also interfered with the lamellae area (region of outgrowth of axons and minor neurites). NOX2 inhibition also reduced the number, length and lifetime of filopodia on axonal tips.

Further studies from the same group using the fluorescent Hyper biosensor (specific for hydrogen peroxide, and amenable for imaging) revealed that the highest hydrogen peroxide production was found at the periphery of the soma as well as at the axonal tip (Wilson et al., 2016). This study also represents the only documented example of a gain-of-function effect (increased neurite growth) when NOX2 activity is increased, in this case by p47^{phox} over-expression. NOX2 is also present in the growth cones of retinal ganglion cells of zebra fish and is required for proper axonal targeting and connection with the optical tectum (Weaver et al., 2018).

Altogether, the studies suggest a positive role for physiological levels of oxidant production by NOX2 in neuritic outgrowth and arborization in diverse neuronal populations, which may also translate to other neuronal subtypes of the CNS. Interestingly, PC12 cells express both NOX1 and NOX2, which are differentially regulated during NGF-induced differentiation such that NOX2 promotes neurite extension, and is down-regulated during the process, while NOX1 opposes neurite extension and is upregulated (Ibi et al., 2006), suggesting different signaling roles depending on the specific NOX isoform. However, the CNS of chronic granulomatous disease (CGD) patients, who lack NOX2 activity, and NOX2 knock-out animal models, develop with only mild cognitive deficits (Kishida et al., 2006). Thus, while a certain redundancy between NOX isoforms can perhaps be expected (Weaver et al., 2018), it seems prudent to conclude that NOX2-mediated redox signaling is a modulating factor, but physiologically important (Terzi et al., 2021), among many, in the development of neurite outgrowth, polarity, targeting, and connections in the brain.

NOX may also have neuroprotective roles. NOX2 activity is required in at least one example of axonal regeneration following peripheral nerve injury. Studies by Hervera and colleagues on mechanically lesioned dorsal root ganglia (DRGs) neurons from mouse, showed that oxidants (hydrogen peroxide) are required for axonal regrowth after nerve injury, indicating a neuroprotective role (Hervera et al., 2018). Unexpectedly, the NOX2 complex is 'delivered' to the DRGs by tissue macrophages by emission of CD63-positive exosomes that contain the full package of NOX2 subunits and are oxidant production proficient. The exosomes are internalized by the DRGs, and traffic to Rab7- and Trk-positive signaling endosomes. Interestingly, only those exosomes deriving from WT bone-marrow-derived macrophages (BMDMs), but not Ncf1−/− (human homolog of p47^{phox}) or

Nox2−/− BMDMs, were capable of inducing axonal regrowth after nerve injury (Hervera et al., 2018).

AXONAL PATHFINDING IN HD NEURODEVELOPMENT

In neurodevelopment axonal pathfinding is crucial to create a proper connectivity in the brain, and here, as is described above, NOX2 has been shown to have a role in growth and neurite guidance of developing neurons, and to localize in growth cones, associated with site specific peaks of ROS production (Olguin-Albuerne and Moran, 2015; Weaver et al., 2018; Terzi et al., 2021). Recent studies have shown that NOX acts as downstream effector of guidance cue molecules in developing neurons, with NOX2 mutants displaying aberrant axonal projections (Terzi et al., 2021). Interestingly, other oxidoreductases may be involved in pathfinding. Members of the cytosolic MICAL (molecule interacting with CaL) family of oxidoreductases have been shown to exert an essential function in mediating semaphorin–plexin repulsive axon guidance and cell morphological changes by direct redox modification (cysteine oxidation by hydrogen peroxide) of actin (Hung et al., 2010, 2011). The modification greatly increases affinity of actin for cofilin, an actin-severing protein, and promotes growth cone collapse.

RNAseq analysis of HD iPSCs-derived GABAergic neuronal cultures show a decreased expression of genes that are key for correct axonal guidance (HD IPSCs consortium). Moreover, Htt is required for newborn neuron migration and for the multipolar to bipolar transition during corticogenesis, as three-dimensional reconstructions of dendritic trees of conditional knockout Htt cells (timely done when developing neurons have migrated to the different cortical layers targets, and synaptic connectivity needs to be established) resulted in a decrease of the dendritic length and dendritic branching in comparison to control cells (Barnat et al., 2020). Furthermore, in HD human iPSCs derived cortical neurons, longer CAG repeats correlated with shorter neurites. The latter was confirmed by alterations in transcriptomics that corresponded to altered cellular morphology (Mehta et al., 2018). Therefore, it would be interesting to assess if mutant huntingtin changes the pattern of expression and/or activity of NADPH oxidases during neurodevelopment.

NMDAR SIGNALING AND NOX2 ACTIVATION

Stimulation of N-methyl-D-aspartate (NMDA) glutamate receptors induces oxidant production both physiologically and in relation to excitotoxic cell death (Bindokas et al., 1996; Massaad and Klann, 2011). At first it was surmised that oxidants derived mostly from mitochondria (see discussions in Massaad and Klann (2011), Oswald et al. (2018), Wang and Swanson (2020)), but later it was established that NOX2 is activated subsequent to NMDAR ligation and constitutes the oxidant response (Brennan et al., 2009; Girouard et al., 2009; Brennan-Minnella et al., 2013; **Figure 2**).

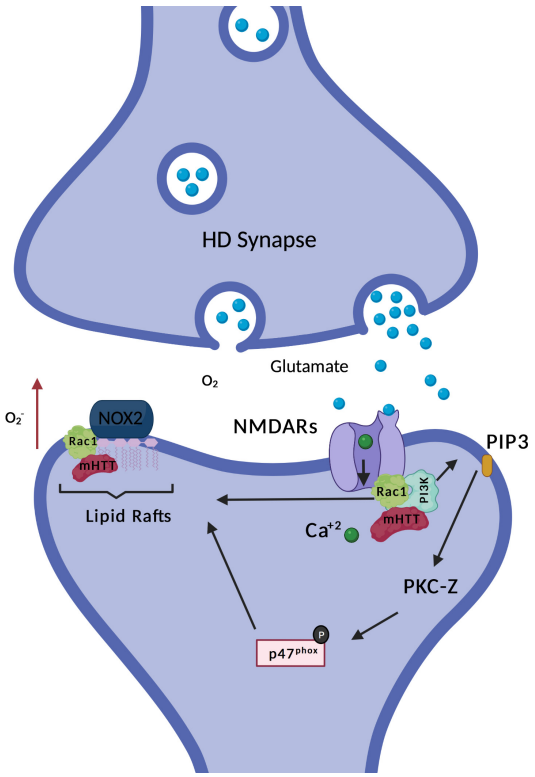

FIGURE 2 | HD and NOX2 interaction. Non-ionotropic activation of PI3K (explained with more details in **Figure 3**) promotes association of $p47^{phox}$ with the rest of the subunits of NOX2, inducing its enzymatic activation. Mutant Huntingtin (mHtt) is found in complex with Rac1 and PI3K. Expression of mHtt is associated with hyperactive Rac1, which could further contribute to enzymatic activation of NOX2. Moreover, NOX2 is sequestered in lipid rafts together with mHtt, also associated with higher super oxide production, as indicated by the red arrow. The figure here depicts the few data currently available on NOX and HD, it does not illustrates the putative roles of NOX in HD which are discussed in the review.

Protein kinase C (PKC) is an important kinase family that phosphorylates $p47^{phox}$ (Fontayne et al., 2002), which can be activated downstream of NMDAR activation and calcium influx. Early observations, just after the discovery of the expanded NOX family, demonstrated the necessity of both PKC and oxidant production for synaptic potentiation (Knapp and Klann, 2002), and since then, further evidence for the involvement of different PKC isoforms in NOX2 activation following NMDAR stimulation and synaptic plasticity in neurons has been provided (Brennan et al., 2009; Brennan-Minnella et al., 2013; Yi et al., 2018; Wang and Swanson, 2020).

In an *in vitro* study of mouse cortical neuronal cultures, NMDAR activation-related calcium influx activated PKC-zeta (indirectly, as this novel type PKC does not require calcium for activity) which subsequently phosphorylated $p47^{phox}$ and caused its translocation to the cell membrane for NOX2 activation. When using neuronal cultures from transgenic $p47^{phox-/-}$ mice, as well as when using peptide inhibitors for PKC-zeta,

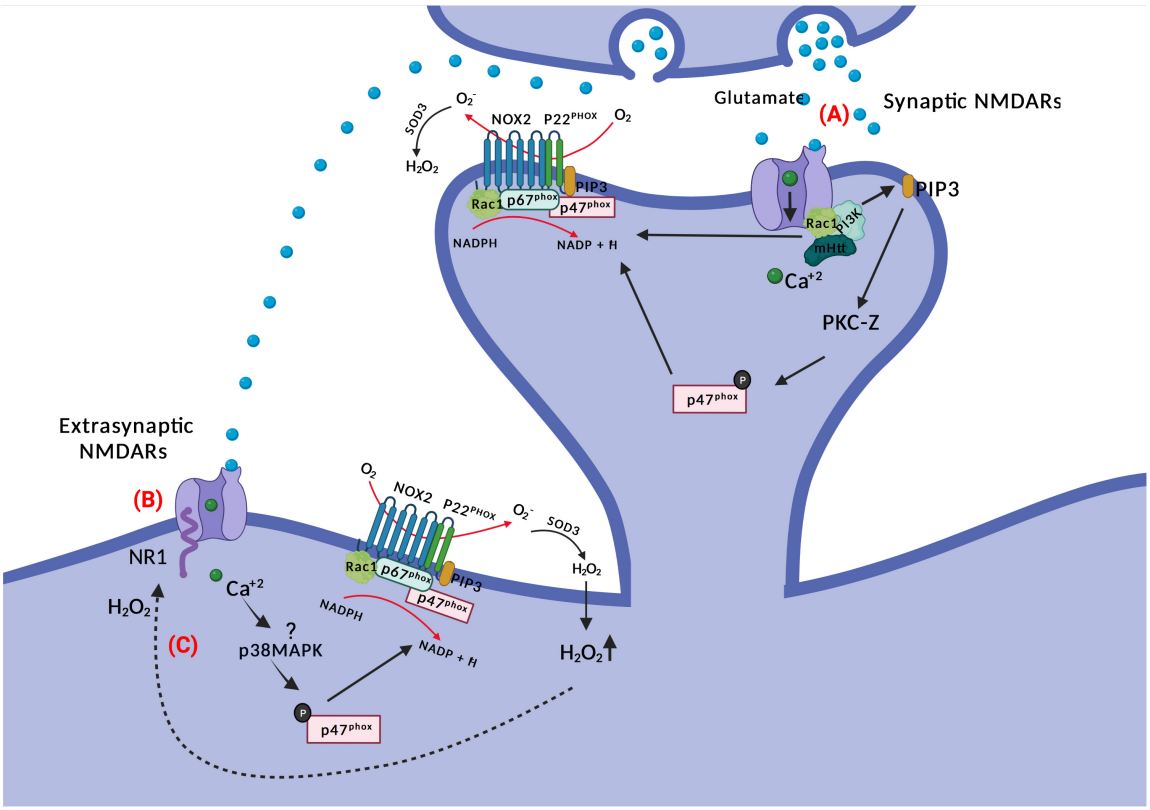

FIGURE 3 | NOX and NMDAR signaling. **(A)** Glutamate binding to NMDARs activates PI3K non-ionotropically (through conformational changes in the receptor) and subsequent PIP3 production. PIP3 activates PKC-zeta, which phosphorylates $p47^{phox}$. The latter translocates to the membrane for NOX2 complex assembly. There is also a requirement for Ca^{2+} for NMDAR-mediated NOX2 activation; potentially through Rac1. **(B)** Glutamate spillover can activate extra-synaptic NMDARs, where activated p38MAPK may phosphorylate $p47^{phox}$ inducing ROS production by NOX2. Extrasynaptic NMDARs activation is associated with neuronal death in HD. **(C)** NR1 subunits of NMDARs are redox targets of hydrogen peroxide, which alters their function and conductivity.

oxidant production and excitotoxic cell death was blocked (Brennan et al., 2009).

The evidence for activation of PKC-zeta downstream of NR2B-containing NMDARs is particularly strong (Wang and Swanson, 2020). NR2B-dependent calcium influx through NMDAR leads to activation of phosphoinositide 3-kinase (PI3K) and production of PIP3, the latter activating the atypical PKC-zeta, which then phosphorylates $p47^{phox}$ (Brennan-Minnella et al., 2013). Excitotoxic neuron death and superoxide formation could be prevented by the PI3K inhibitor wortmannin (and $p47^{phox}$ knockout). The involvement of PKC-zeta has been further refined, as it has been demonstrated that specifically phosphorylation at position 316 of $p47^{phox}$ is required for induction of LTD (Yi et al., 2018). Incidentally, generation of phosphoinositide species in the vesicular or plasma membrane by PI3K is also a direct recruitment factor for $p40^{phox}$ and $p47^{phox}$, respectively, via their PX domains (Zhan et al., 2002; Ago et al., 2003; Ellson et al., 2006).

In phagocytes, activation of p47phox seems dominant in relation to Rac1 activation for NOX2 assembly and enzyme function (Roepstorff et al., 2008), however in artificial systems (Price et al., 2002), and potentially other cell types, Rac1 activation is sufficient to drive NOX2 activation. Tousley and colleagues have contributed with another study possibly linking NOXs and HD, through Rac1 (Tousley et al., 2019b). Rac1 activity is required for actin remodeling, a process that is required for the change in morphology and structure of dendritic spines. Moreover, actin remodeling is also necessary for the formation of new axonal branches and end-feet, therefore giving it a role in synaptic plasticity and connectivity (Spence and Soderling, 2015). Interestingly, specifically the active form of Rac1 (GTP bound Rac1) is necessary for NOX1, NOX2 and NOX3 enzymatic activation. Huntingtin is found in complex with GTP-Rac1 and p87α (component of the kinase PI3K) together with alpha-actinin1 and other proteins (Tousley et al., 2019b). This interaction is increased when mutant huntingtin (mHtt) is expressed and is accompanied by Rac1 hyperactivity. In the HD scenario, higher activity of GTP-Rac1 could be translated to an increased ROS production by Rac1-dependent NOXs (see **Figure 2**). Increased ROS production by NOXs could further contribute to impaired neuronal arborization dynamics, which in part is coordinated by NOX derived oxidants. The role of NOX derived oxidants in neuronal arborization is explained with more details in

one of the sections of this review: "Role of NOXs in neurite growth, specification, and connectivity during development and after nerve injury". Remarkably, hyperactivity of Rac1 is associated with dysfunctional neuritogenesis of cortical projection neurons (Zamboni et al., 2018), a neuronal subtype highly affected in HD.

Evidence has been forwarded that the activation of PI3K by NMDAR activation is non-ionotropic, meaning that although Ca^{2+}-conductance is required for NOX2 activation (Wang and Swanson, 2020), PI3K is activated directly by ligand-induced conformational changes in the cytosolic aspect of NMDAR subunits alone (Minnella et al., 2018). This would provide for an exceptionally rapid activation of PKC and NOX2 assembly for oxidant production upon NMDAR ligation by glutamate, in particular if the NOX2 complex is in a primed state and active Rac1 is available.

In an excitotoxic setting, the NMDAR-stimulated oxidant release from neurons is sufficiently robust that it can induce oxidative stress even in neighboring neurons *in vitro* (Reyes et al., 2012; Brennan-Minnella et al., 2013) and cause their bystander cell death. This may also occur *in vivo*. Thus, social isolation dramatically upregulates NOX2 in pyramidal neurons of the prefrontal cortex. Nevertheless, it is the small, parvalbumin-positive GABAergic inhibitory interneurons, without NOX2 immunoreactivity, dispersed between the pyramidal neurons that are eventually progressively lost in this psychosocial stress model (Schiavone et al., 2012). When active NOX2 is surface-localized, superoxide, rather than hydrogen peroxide, for an intracellular superoxide source, will be released directly into the surroundings, where it reacts promptly and diffusion-limited with available NO to form the highly toxic peroxynitrite (NO_3^-), which is the main driver of oxidative damage and cell death (Wang and Swanson, 2020). A fraction of ROS is released to the surroundings, and in astrocyte-neuron co-cultures, with neurons coming from E14 mice cortices, it has been shown that NMDAR activation causes oxidative stress in neighboring neurons and glia cells (Reyes et al., 2012). Notably, this does not happen in cultures established from $p47^{phox-/-}$ neurons, indicating the crucial role of NOX2 in the matter (Reyes et al., 2012).

Whether NMDA promotes NOX2 activation also extrasynaptically is not settled. A single study has linked NR2B (a subunit of the NMDAR receptors which is enriched in extrasynaptic sites and associated with cell death (Hardingham, 2009; Martel et al., 2009)) with superoxide production. Treatment of neuronal cultures with N2RB antagonists resulted in blockage of NMDAR-induced NOX2 superoxide production and excitotoxic cell death (Brennan-Minnella et al., 2013), indicating a crosslink between NOX and excitotoxic neuronal cell death. But interestingly, the authors showed that after blocking specifically synaptic NMDARs with MK801, activation of the remaining (extrasynaptic) NMDARs with bicuculline and 4-aminopyridine still provoked an increase in dihydroethidium (DHE) fluorescence, suggesting that extrasynaptic NMDARs can also activate oxidant generation. Moreover, adding NADPH into the bath triggered a rise in DHE fluorescence which was higher than without synaptic receptors blockage (Brennan et al., 2009), implicating NOX activity rather than mitochondria as the oxidant source. Extrasynaptic NMDAR signaling upregulates the activity of p38MAPK, and this stress kinase is known to phosphorylate and partially activate (prime) $p47^{phox}$ and NOX2 (Brown et al., 2004; Dang et al., 2006).

NMDAR EXCITOTOXICITY IN HD

Excitotoxic cell death, caused by overactivation of NMDA receptors, has been considered in the pathogenesis of HD, and specifically extrasynaptic NMDAR are associated with striatal neuronal loss in HD (Heng et al., 2009). Synaptic versus extrasynaptic NMDAR signaling, or hypofunction of NMDAR, already causes a reduced balance of transcription of antioxidant genes (Hardingham and Bading, 2010; Hardingham and Do, 2016). Intriguingly, the signaling processes that emanate from synaptic versus extrasynaptic NMDARs are radically different. Thus, glutamate stimulation of synaptic NMDAR initiates pro-survival pathways including the PI3K-Akt pathway and ERK signaling, suppresses death gene transcription, and stimulates transcription of antioxidant genes and CREB-dependent transcription (Hardingham and Bading, 2010). In contrast, extrasynaptic NMDAR stimulation leads to activation of p38MAPK and FOXO1 transcription factor activation, which in effect oppose the signaling pathways and transcription imposed by synaptic NMDAR signaling, including a lessened transcription of antioxidant genes. The end result is a disruption of prosurvival pathways and an altered redox balance (Hardingham and Bading, 2010; Szlachcic et al., 2015; Hardingham and Do, 2016). The situation is exacerbated by the inhibition of peroxisome proliferator-activated receptor gamma coactivator 1-alpha (PGC-1α) function by mutant huntingtin. Normally, PGC-1α directs the transcription of several antioxidant genes (St-Pierre et al., 2006), and regulates the flow of electrons through the respiratory chain in mitochondria, but through a direct interaction mutant huntingtin inhibits PGC-1α-assisted transcription (Cui et al., 2006; Weydt et al., 2006). Thus, in the HD brain the stage is set for any subsequent overproduction or unwarranted production of oxidants in time and space – e.g., from NOX activation - to do damage.

NOX AND OXIDANTS IN THE PRE-SYNAPTIC COMPARTMENT

NOX-derived oxidants could play a role pre-synaptically by producing oxidants in close proximity to the protein machinery responsible for neurotransmission. Alternatively, oxidants produced in the post-synapse may trans-synaptically modulate pre-synaptic mechanisms such as glutamate release. Such a role is already documented for NO (Stanton et al., 2003) and is a form of synaptic plasticity. The SNARE complex is necessary for docking and fusion of the synaptic vesicles into the pre-synaptic membrane in active synapses. Interestingly, it has been shown that SNAP25, one of the components of the core SNARE complex, is specifically sensitive to oxidation by hydrogen peroxide, and that pre-exposure to 100 μM levels

of hydrogen peroxide is sufficient to prevent SNARE complex assembly. Oxidants could be supplied by NOX2 in the pre-synapse itself or extrinsically by either activated microglia or post-synaptic NOX2 activity. In the latter case, oxidants would modulate pre-synaptic function across the synaptic cleft similar to other short-lived metabolites such as NO or endocannabinoids (Gerdeman et al., 2002; Stanton et al., 2003). Furthermore, protein levels of specifically SNAP25 in the pre-synaptic plasma membrane are reduced in neurons that are subjected to oxidative stress and SNAP25 knockout experiments in non-diseased cortical projection neurons (CPNs) has been shown to induce neurodegeneration (Hoerder-Suabedissen et al., 2019). Deficits in SNAP25 expression and function has been reported in HD (Smith et al., 2007). Therefore, deficits in the SNAREs machinery function of HD synapses, as a result of exposure to NOX-derived ROS, could be a potential contributor to the synaptopathology of the disease.

NOX INVOLVEMENT IN LONG-TERM DEPRESSION/POTENTIATION AND SYNAPTIC PLASTICITY

Synaptic plasticity is in part orchestrated by long-term potentiation (LTP) and long-term depression (LTD) (**Figure 4**). LTP is a persistent rise in synaptic strength following high-frequency stimulation of a synapse. On the other hand, LTD is an activity-dependent decrease in the strength of synaptic connectivity. Both processes play a crucial role in the formation of specific types of memories and learning (Massaad and Klann, 2011). For example, recognition memory (the capacity to recognize formerly encountered events, objects or individuals) is processed through LTD by neural circuits in the perirhinal cortex, specifically, through an activity-dependent decrease in the efficacy of neurotransmission at glutamatergic synapses. Even though LTP and LTD effect on synaptic excitability are opposite, they can both happen at the same synapse in response to different patterns of activation of NMDARs combined with membrane depolarization. Typically, the final outcome is in one way or the other a modulation of the number and functionality of Na^+-conducting α-amino-3-hydroxy-5-methyl-4-isoxazolepropionic acid (AMPA) receptors in the post-synaptic membrane, but other mechanisms exist (Collingridge et al., 2010).

In relation to NOX2, it was first shown that hippocampal plasticity and LTP was impaired in mouse models of CGD with no $gp91^{phox}$ or $p47^{phox}$ expression (Kishida et al., 2006). Studies have since then shown that oxidants and NOX2 are essential for LTP induction (see Massaad and Klann (2011) for a good historical review).

LTP can be blocked by the use of different oxidant scavengers (Lee et al., 2010), including mouse models with overexpression of extracellular SOD3 (Thiels et al., 2000), and conversely, LTP can be induced by application of xanthine/xanthine oxidase (a superoxide source) to the extracellular medium of hippocampal brain slices (Knapp and Klann, 2002). However, the latter is clearly context-dependent, as NOX2-derived oxidants from inflammatory microglia can in fact inhibit LTP induction (Wang Q. et al., 2004; Di Filippo et al., 2016). Presumably the outcome is modulated by additional reciprocal interactions between microglia and neurons (Hanisch and Kettenmann, 2007; Kettenmann et al., 2013), and it should also be noted that the effect of hydrogen peroxide concentration on LTP induction is bimodal (Kamsler and Segal, 2003).

Most studies have found that NOX2 expression in the spinal cord lies with either microglia or macrophages, where its activity plays a role in altered pain perception (Kallenborn-Gerhardt et al., 2013, 2014; Lim et al., 2013). Others have found that DRG expression of NOX4 is required for maintenance of the late phase of neuropathic pain after peripheral neurons injury, and conditional deletion of NOX4 in adult mice reduced pain-related behavior (Kallenborn-Gerhardt et al., 2012). However, one recent study proposes that LTP induction by high frequency train stimulation of the sciatic nerve in the dorsal spinal cord depends on NOX2 expression in neurons, and further describes upregulation of $gp91^{phox}$ (Xu et al., 2020). LTP induction, but not maintenance, could be inhibited by gp91ds-tat, and further, $gp91^{phox}$ knock-down inhibited allodynia in this mouse model of pain perception.

Post-synaptic NOX2 activity is also required for NMDAR-dependent LTD (Yi et al., 2018). LTD induced by low frequency stimulation on acute neuronal slices was dependent on post-synaptic expression of NOX2 as verified by shRNA knockdown of $gp91^{phox}$ and $p47^{phox}$. They also demonstrated that $p47^{phox}$ phosphorylation at serine 316 by PKC-zeta is specifically required for LTD induction.

In some cases, oxidants do not have to be produced by neurons themselves to affect synapse function. In a pathological setting, Aβ provokes superoxide production by microglia through NOX2, and this accounts for the Aβ-induced inhibition of LTP in brain slices from mice (Wang Q. et al., 2004), and similarly, in the remitting phase of an experimental multiple sclerosis model, hippocampal LTP is impaired because of microglial NOX2 activity (Di Filippo et al., 2016). It has later been shown in an experimental LTD paradigm of combined hypoxia/LPS-stimulation in mouse models, that microglia through LPS activation of complement receptor 3 (CR3) within minutes activates NOX2 to release superoxide, which initiates a signaling cascade in the post-synapse of hippocampal neurons to down-regulate AMPA glutamate receptors, a known mechanism of LTD and synapse weakening (Zhang et al., 2014).

The opposing actions of oxidants on plasticity, dependent on context and oxidant concentration, and similarly, the participation of NOX2-derived oxidants in both LTP and LTD induction, can seem contradictory and puzzling, and clearly calls for more research into the area. A part of a reconciliatory explanation may reside in the precise subcellular localization of the oxidant source, and the differing membrane permeabilities of superoxide versus hydrogen peroxide.

In the redox signaling business proximity of oxidant producer and redox target is essential for redox modification, because the penetration range of hydrogen peroxide in cytosol is on the border of only 1–2 μm before extinction by the cellular antioxidant machinery (Winterbourn, 2008; Jones and Sies, 2015). It follows, that if two redox signaling circuits, with

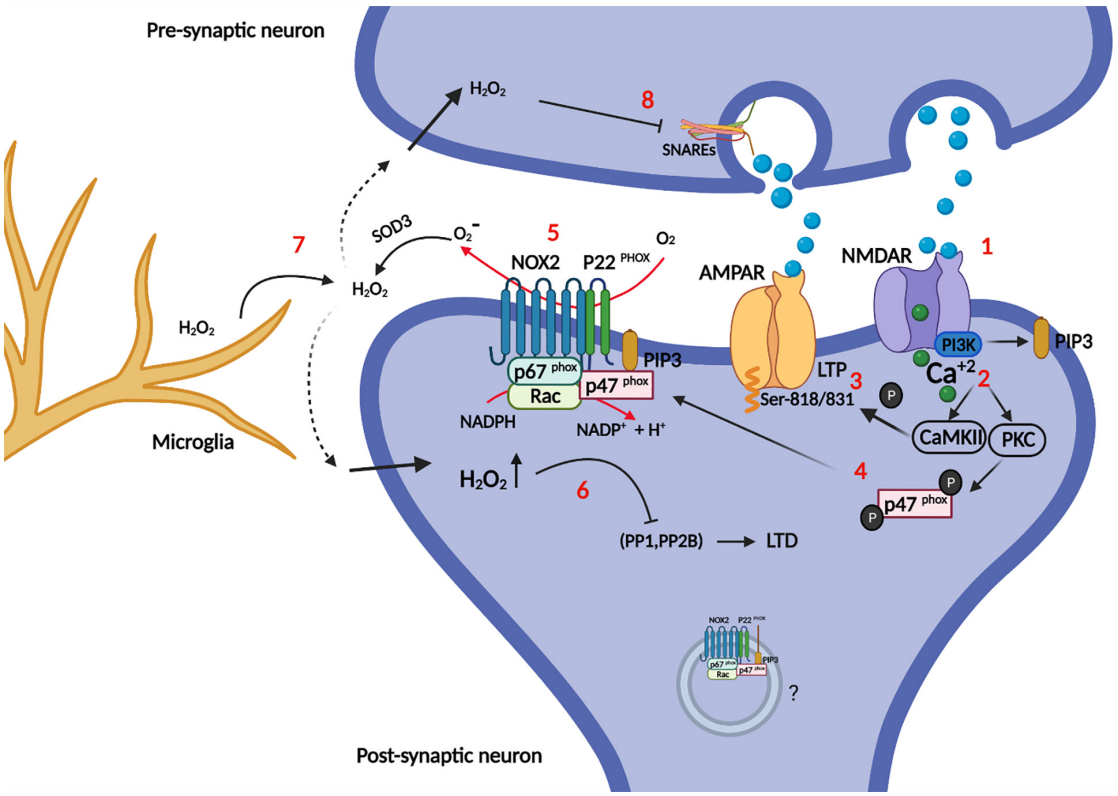

FIGURE 4 | Role of NOX in synapse plasticity. Briefly, synaptic plasticity is governed mainly by LTP: Synapse enhancement through recruitment of AMPA receptors into the post-synaptic membrane and LTD: synapse weakening (AMPA receptors endocytosis). **(1)** Glutamate binding to NMDARs opens the calcium channel, and activates PI3K directly. **(2)** Calcium activates CaMKII and PKC (the latter also requires PIP3 as explained in **Figure 2**), which can both **(3)** phosphorylate AMPARs at specific serines, increasing their conductance and recruitment into the post-synaptic membrane (LTP). Moreover **(4)** $p47^{phox}$ is phosphorylated by PKC, which recruits it for complex assembly and activation of NOX2. **(5)** Enzymatically active NOX2 produces superoxide in the extracellular space, which is cycled back into the cytosol as hydrogen peroxide after dismutation by SOD3. **(6)** Intracellular hydrogen peroxide potentially redox-regulates phosphatases PP1, and PP2B by oxidation. These phosphatases dephosphorylate AMPARs, promoting their endocytosis and removal from the post-synaptic membrane (LTD). The intra-synaptic pool (depicted inside a vesicle) of NOX2 may be activated differentially from the perisynaptic NOX2 in the plasma membrane and could represent a layer of specificity to redox signaling. **(7)** NOX2 derived oxidants from microglia may impair instillation of LTP or conversely promote LTD. **(8)** Hydrogen peroxide can also enter the presynaptic neuron and impair the SNAREs machinery, which is required for synaptic vesicle release.

different outcomes, are to arise from the same oxidant source either different redox targets must be recruited dynamically to the immediate vicinity of a fixed oxidant source, or physically separated pools of oxidant producer affects different redox targets. It is therefore intriguing, that NOX2 in post-synapses is also located to endosomal elements and small unidentified vesicles and membranes (Coleman et al., 2013) in addition to the peri-synaptic surface membrane (Wang G. et al., 2004; Glass et al., 2006). Further, NOX2 activation can be directed spatially, and the proximal assembly of the holoenzyme adapted to the stimuli for activation. For example, $p40^{phox}$ is specifically required for IgG-FcgR induced activation of NOX2 in phagocytes, where it assists the function of $p47^{phox}$ as organizer of NOX2 assembly (Anderson et al., 2011; Ueyama et al., 2011). In addition, because of differing affinities for phosphoinositide species, $p40^{phox}$ is recruited mainly to intracellular vesicles, whereas $p47^{phox}$ associates with the plasma membrane (Zhan et al., 2002). In phagocytes, there is good evidence for the differential activation of cell surface resident versus intracellular pools of NOX2 (Serrander et al., 1999; Li et al., 2010), and potentially similar mechanisms could be at work in the post-synapse.

However, the penetration range of hydrogen peroxide exceeds with a good measure the size of most synapses, which speaks against a resolution of LTD/LTP-associated differential redox signaling based on physical distance alone. Another, independent or reinforcing, speculative mechanism therefore lies in the different membrane permeabilities of superoxide (charged and impermeable) and hydrogen peroxide (fairly permeable). It is curious that extracellular SOD3 abolishes LTP induction (Thiels et al., 2000), even though the enzyme converts superoxide into hydrogen peroxide, the generally accepted relayer of redox signals (Winterbourn, 2013; Sies and Jones, 2020). Could it be that specificity for one form of plasticity over the other could in part be achieved by cell surface-resident NOX2 and superoxide-mediated oxidation of cell surface proteins on the extracellular aspect? Being membrane-impenetrable, superoxide action would be restricted to redox targets on the surface

in the immediate vicinity of NOX2, further reinforced by the quick dismutation to hydrogen peroxide. Only a few examples of superoxide in redox signaling are known however (Sies and Jones, 2020), and the proposed mechanism breaks with the current dogmatic view of cell surface receptor-induced NOX activation, which relies on back-diffusion of hydrogen peroxide through the membrane directly or through aquaporins to modulate intracellular redox targets. It is unknown whether synapses express aquaporins (which allows hydrogen peroxide to move along its concentration gradient), and to what extent vesicular NOX2 in synapses contributes to oxidant production, but endosomal NOX2-mediated oxidant production has been proposed in other cell types (Oakley et al., 2009; Lamb et al., 2012), and NOX2 storage vesicles also have oxidant production capability (Moreland et al., 2007; Ejlerskov et al., 2012).

The redox targets of NOX2 in synapses are entirely unknown. However, a major function of NOX2 is to regulate, by oxidative inactivation, the activity of both tyrosine and serine/threonine phosphatases (Sies, 2014). LTD and LTP are governed by a balance of kinases like PKC and Ca^{2+}-calmodulin-dependent protein kinase II (CaMKII) (promotes LTP), and opposing phosphatases calcineurin (PP2B), PP1 and PP2A (promotes LTD) (Collingridge et al., 2010). Phosphorylation of AMPA receptors increases conductance and their synaptic incorporation during LTP, while dephosphorylation promotes their endocytosis, and LTD and synapse weakening. Interestingly, calcineurin, PP1A, and PP2A are all inactivated by hydrogen peroxide (Rhee et al., 2000). and NOX2 derived oxidants could activate PKC (in a feedback loop) (Knapp and Klann, 2002), and similarly, Akt, which also phosphorylates and activates $p47^{phox}$ (Hoyal et al., 2003), is in part positively regulated by redox modification (Luo et al., 2012) (Su et al., 2019). Finally, NMDARs are targets for redox modification themselves. Redox modifications of cysteine residues in the cytosolic tails of particularly NR1B modulate NMDAR function (Lipton et al., 2002), and there is evidence that NOX2 contributes to this process (Di Maio et al., 2011). Interestingly, evidence for NOX2-derived oxidant alteration of the stoichiometric composition of the NMDAR (upregulation of NR2B) has been presented following cholinergic stimulation of m1R metabotropic receptors (Di Maio et al., 2011). In addition, metabotropic receptors can be redox modified (Campanucci et al., 2008; Coddou et al., 2009).

Outside of synapses it has been shown that NOX2 activity is required for axonal development by causing Ca^{2+} release from endoplasmatic reticulum through Ryanodine receptors (Wilson et al., 2016). However, it was not investigated whether the ryanodine receptor was a direct target of redox modification, as observed in other cell types where evidence of NOX4 participation is particularly strong (Sun et al., 2011). Notably, store operated calcium entry is affected in HD (Czeredys, 2020) likely downstream of an interaction between mHtt and the IP3R1 receptor in the rER, which sensitizes the IP3R calcium channel, such that calcium in rER is depleted and subsequently activates the store operated entry of calcium (Wu et al., 2016).

NOX2, LTD/LTP AND HD PATHOLOGY

The memory deficits that are characteristic of HD, and demonstrated in patients as well as mouse models, include failure in recognition memory (Giralt et al., 2011), and cognitive dysfunction (Milnerwood et al., 2006) which are manifest early in the disease (Montoya et al., 2006).

Electrophysiological measurements in brain slices from several different genetic mouse models have consistently shown LTP dysfunction in HD, not only the most commonly characterized hippocampal LTP (Hodgson et al., 1999; Usdin et al., 1999; Murphy et al., 2000; Quirion and Parsons, 2019) but also in the cortico-striatal synapse (Kung et al., 2007; Dallérac et al., 2011; Plotkin et al., 2014; Sepers et al., 2018). The effect of mutant huntingtin on the ability to evoke stimulation-induced LTD, also studied in various HD mouse models, is less clear. LTD evocation has been shown to be diminished in the perirhinal cortex in the R6/1 mouse model (Cummings et al., 2007) and in cortico-striatal synapses (Ghiglieri et al., 2019; Kim et al., 2020), but reports of similar changes in hippocampus has not been consistent (Murphy et al., 2000; Milnerwood and Raymond, 2007; Ghilan et al., 2014).

Different mechanisms have been proposed to convey these effects, including changes in dopamine receptor function and endocannabinoid receptor activity (Sepers et al., 2018; Ghiglieri et al., 2019). Dopamine D1 receptor activity has been shown to regulate the expression and activity of NMDAR, which as described above is essential for LTP and LTD; as D1 receptor hypersensitivity has been shown in HD this presents a potential mechanism for the involvement of mutant huntingtin in synaptic plasticity (Ghiglieri et al., 2019). Another potential mechanism involves the "alternative" brain-derived neurotrophic factor (BDNF) receptor $p75^{NRT}$: BDNF exerts neurotrophic actions and stimulates LTP and LTD through activation of the TrkB receptors, however, BDNF binding to $p75^{NRT}$ has been proposed to have antagonistic effects on synaptic plasticity (Brito et al., 2014). Interestingly, increased protein levels of $p75^{NRT}$ has been shown in HD patients and mouse models (Brito et al., 2014), and in cortico-striatal synapses HD-associated abnormalities in LTP were restored by inhibiting $p75^{NRT}$ (Plotkin et al., 2014). $p75^{NRT}$ activation acts through PTEN, which, as described previous in this review, may be inhibited by NOX-derived ROS (Le Belle et al., 2011).

MICROGLIA AND NOX2 IN HD

Glial cells might be contributors to the pathology of HD (Wilton and Stevens, 2020), and when it concerns NADPH oxidases, by far, the most literature on NOX2 in the brain involves microglia, the resident CNS phagocytes, which additionally express NOX1 (Cheret et al., 2008). As phagocytes, they are equipped for high level oxidant production following pathogen encounter, and the very same pattern of recognition receptors come into play in the recognition of extracellular amyloids (Fellner et al., 2012; Qiao et al., 2015; Wang et al., 2015).

Relative to the common neurodegenerative diseases like Alzheimer's (AD) and Parkinson's disease (PD), the mass of literature on microglia in HD is limited. Search terms 'AD/PD/HD' AND 'microglia' retrieves 5755, 2600, and 257 records from PubMed, respectively. The information on NOX2 activity in microglia of animal models of HD is virtually non-existent and has only been addressed peripherally *in vitro*.

This despite the fact that PET scanning of HD patients with peripheral benzodiazepine receptor ligands (11C-(R)-PK11195), as measure of microglia activation, indicates that microglia are activated well before clinical disease onset (Pavese et al., 2006; Tai et al., 2007). Post mortem HD brains show typical signs of neuroinflammation including cytokine production and complement deposition (Singhrao et al., 1999) as well as markers of oxidative stress (see references in Bono-Yagüe et al. (2020)).

Transcriptional profiling of AD brain shows a clear inflammatory signature (Block et al., 2007) (Malik et al., 2015), and a significant correlation between NOX activity and cognitive decline exists (Ansari and Scheff, 2011). In PD models, dopaminergic neuron death can be instilled by the mere stereotactic infusion of LPS into the substantia nigra to activate microglia and NOX2 specifically (Qin et al., 2004).

The situation is somewhat different in animal models of HD, where microglia activation and neuroinflammation seems more subdued. While microglia in early disease in the R6/2 HD model decrease ramification and assume more activated shapes, indicating that microglia are detecting (Kraft et al., 2012) and responding to a deviation from homeostasis, possibly derangement of synaptic function (Milnerwood and Raymond, 2007), a neuroinflammatory profile with full blown microglia activation and proinflammatory cytokine production is observed only late in the disease (see Wilton and Stevens (2020) for an overview). At this point microglia activation is not necessarily disease-specific but represents a prototypical response to neuronal death processes, particularly so in the R6/2 mouse model where the course of disease is very aggressive (mice die at 16 weeks of age). Therefore, the recent demonstration that shRNA knock-down of Galectin 3 in R6/2 mice dampens microglia activation, neuroinflammatory profile, and ameliorates disease (increasing survival) is surprising (Siew et al., 2019). It will be interesting to see whether microglia activation also plays out as a driver of pathology in other HD animal models with a more protracted disease course than R6/2 mice (Plotkin and Surmeier, 2015).

In contrast to idiopathic brain disease, where microglia are typically initially activated down-stream of neuronal dysfunction or extracellular amyloid aggregates, all glia cells in HD endogenously express mutant huntingtin, which affects their activation and function from within (Wilton and Stevens, 2020). In the R6/2 model, microglia display pro-inflammatory transcriptional activation by increasing the expression and transcriptional activities of the myeloid lineage-determining factors PU.1 and C/EBPs (Crotti et al., 2014). Of note, increased transcription of PU.1 and C/EBP target genes was microglia specific in the R6/2 model, which contrasts with the monocytic priming by mutant huntingtin expression observed early in human patients (Bjorkqvist et al., 2008). It has also been noted that microglia, and myeloid cells in general, in experimental HD models or patients show a reduced migratory response versus chemotactic stimuli *in vitro* or laser-induced injury *in vivo* (Kwan et al., 2012). However, selective depletion of mutant huntingtin in myeloid cells, including microglia, has no bearing on disease development in the BACHD HD mouse model (Petkau et al., 2019).

Whereas both amyloid-β (Bianca et al., 1999; Zhang et al., 2011) and α-synuclein (Fellner et al., 2012; Qiao et al., 2015; Wang et al., 2015) aggregates induce NOX2-dependent superoxide production in microglia through specific scavenger receptors, no such data are available for mutant huntingtin aggregates. In fact, no internalization or signaling cell surface receptors are known for mutant huntingtin in microglia (or in any other cell type for that matter). To date therefore, no publications have specifically addressed microglial NOX-mediated oxidant production in an *in vitro* or *in vivo* setting of HD models, discounting studies that, too optimistically, rely only on apocynin or other general anti-oxidant inhibition as measure of NOX involvement (Maldonado et al., 2010; O'Regan et al., 2021).

CONCLUSION

While the role of microglia and NOX2-mediated oxidant production in the progression of late stage neurodegenerative disease is undisputed, the involvement of neuronal NOX isoforms in physiology and brain pathology are just in the process of being unraveled. From the early recognition of a requirement for superoxide for LTD/LTP instigation, several groups have now contributed to the delineation of the pathways that lead to NOX2 activation following NMDAR engagement in synaptic parts of neurons. However, the redox circuits downstream of NOX2 oxidant production, and in particular how both LTD and LTP are redox controlled by NOX2, awaits further elucidation, and presumably identification of protein redox targets. It will also be interesting to see whether the deleterious effects of extrasynaptic NMDAR signaling are mediated in part by NOX2 activity and by which pathway; if different from synaptic NOX2 activation they could perhaps be uncoupled pharmacologically.

Any specific effects of neuronal NOX activity in HD would depend in the (1) stage of the disease, (2) specific cell type and NOX isoform involved, and (3) subcellular localization of the enzyme – the latter given the complex neuronal morphology and extensive length of the axons, allowing for several redox signaling microcircuits to occur within the same cell. And last but not least, (4) NOX-derived ROS from other cell types, in this particular case microglia, may also play a role in HD disease progression, which has not been fully explored yet.

We have presented evidence that NOX function could potentially participate from the very start of developmental defects seen in HD, including altered neurogenesis, neurite growth, and axonal pathfinding, while also having a possible role in mature neurons where NOX2 regulates NMDAR signaling and synaptic plasticity, known to be affected in presymptomatic

HD. It will be essential to follow up on the present isolated findings of mHtt modulation of PI3K and Rac1 signaling, as it will be important to establish whether mHtt interacts with NOX2 in lipid raft compartments of the membrane to interfere with crucial synaptic processes that mediate synaptic plasticity and maintenance. To the extent that the "dying back" pattern of degeneration in which loss of synaptic connectivity and axonal degeneration precedes and provokes neuronal death over time (Han et al., 2010), a lot could potentially be gained by remedying initial synaptic dysfunction in the striatum, which would also presumably ameliorate early motor symptoms.

We hope that it can be conjectured from the present review that the relative 'under-representation' of literature on NOX in HD compared to other NDDs cannot simply be explained by the different prevalence of these diseases; there is certainly room for future research into the roles of NOX and oxidants in HD.

AUTHOR CONTRIBUTIONS

All authors listed have made a substantial, direct and intellectual contribution to the work, and approved it for publication.

REFERENCES

Ago, T., Kuribayashi, F., Hiroaki, H., Takeya, R., Ito, T., Kohda, D., et al. (2003). Phosphorylation of p47phox directs phox homology domain from SH3 domain toward phosphoinositides, leading to phagocyte NADPH oxidase activation. *Proc. Natl. Acad. Sci. U.S.A.* 100, 4474–4479. doi: 10.1073/pnas.073571 2100

Ajayi, A., Yu, X., Lindberg, S., Langel, U., and Ström, A. L. (2012). Expanded ataxin-7 cause toxicity by inducing ROS production from NADPH oxidase complexes in a stable inducible Spinocerebellar ataxia type 7 (SCA7) model. *BMC Neurosci.* 13:86. doi: 10.1186/1471-2202-13-86

Ali, S. S., Young, J. W., Wallace, C. K., Gresack, J., Jeste, D. V., Geyer, M. A., et al. (2011). Initial evidence linking synaptic superoxide production with poor short-term memory in aged mice. *Brain Res.* 1368, 65–70. doi: 10.1016/j.brainres. 2010.11.009

Anderson, K. E., Chessa, T. A., Davidson, K., Henderson, R. B., Walker, S., Tolmachova, T., et al. (2011). PtdIns3P and Rac direct the assembly of the NADPH oxidase on a novel, pre-phagosomal compartment during FcR-mediated phagocytosis in primary mouse neutrophils. *Blood* 116, 4978–4989. doi: 10.1182/blood-2010-03-275602

Ansari, M. A., and Scheff, S. W. (2011). NADPH-oxidase activation and cognition in Alzheimer disease progression. *Free Radic. Biol. Med.* 51, 171–178. doi: 10.1016/j.freeradbiomed.2011.03.025

Banfi, B., Tirone, F., Durussel, I., Knisz, J., Moskwa, P., Molnar, G. Z., et al. (2004). Mechanism of Ca2+ activation of the NADPH oxidase 5 (NOX5). *J. Biol. Chem.* 279, 18583–18591. doi: 10.1074/jbc.M310268200

Barnat, M., Capizzi, M., Aparicio, E., Boluda, S., Wennagel, D., Kacher, R., et al. (2020). Huntington's disease alters human neurodevelopment. *Science* 369, 787–793. doi: 10.1126/science.aax3338

Bates, G. P., Dorsey, R., Gusella, J. F., Hayden, M. R., Kay, C., Leavitt, B. R., et al. (2015). Huntington disease. *Nat. Rev. Dis. Primers* 1:15005. doi: 10.1038/nrdp. 2015.5

Bauerlein, F. J. B., Saha, I., Mishra, A., Kalemanov, M., Martinez-Sanchez, A., Klein, R., et al. (2017). *In situ* architecture and cellular interactions of PolyQ inclusions. *Cell* 171, 179–187.e10. doi: 10.1016/j.cell.2017.08.009

Bedard, K., and Krause, K. H. (2007). The NOX family of ROS-generating NADPH oxidases: physiology and pathophysiology. *Physiol. Rev.* 87, 245–313. doi: 10. 1152/physrev.00044.2005

Bell, K. F., Al-Mubarak, B., Martel, M. A., McKay, S., Wheelan, N., Hasel, P., et al. (2015). Neuronal development is promoted by weakened intrinsic antioxidant defences due to epigenetic repression of Nrf2. *Nat. Commun.* 6:7066. doi: 10.1038/ncomms8066

Bertoni, A., Giuliano, P., Galgani, M., Rotoli, D., Ulianich, L., Adornetto, A., et al. (2011). Early and late events induced by polyQ-expanded proteins: identification of a common pathogenic property of polYQ-expanded proteins. *J. Biol. Chem.* 286, 4727–4741. doi: 10.1074/jbc.M110.156521

Bianca, V. D., Dusi, S., Bianchini, E., Dal Pra, I., and Rossi, F. (1999). beta-amyloid activates the O-2 forming NADPH oxidase in microglia, monocytes, and neutrophils. A possible inflammatory mechanism of neuronal damage in Alzheimer's disease. *J. Biol. Chem.* 274, 15493–15499. doi: 10.1074/jbc.274.22. 15493

Bindokas, V. P., Jordán, J., Lee, C. C., and Miller, R. J. (1996). Superoxide production in rat hippocampal neurons: selective imaging with hydroethidine. *J. Neurosci.* 16, 1324–1336. doi: 10.1523/JNEUROSCI.16-04-01324.1996

Bjorkqvist, M., Wild, E. J., Thiele, J., Silvestroni, A., Andre, R., Lahiri, N., et al. (2008). A novel pathogenic pathway of immune activation detectable before clinical onset in Huntington's disease. *J. Exp. Med.* 205, 1869–1877. doi: 10. 1084/jem.20080178

Block, M. L., Zecca, L., and Hong, J. S. (2007). Microglia-mediated neurotoxicity: uncovering the molecular mechanisms. *Nat. Rev. Neurosci.* 8, 57–69. doi: 10. 1038/nrn2038

Blumenstock, S., and Dudanova, I. (2020). Cortical and striatal circuits in Huntington's disease. *Front. Neurosci.* 14:82. doi: 10.3389/fnins.2020.00082

Bogdanov, M. B., Andreassen, O. A., Dedeoglu, A., Ferrante, R. J., and Beal, M. F. (2001). Increased oxidative damage to DNA in a transgenic mouse model of Huntington's disease. *J. Neurochem.* 79, 1246–1249. doi: 10.1046/j.1471-4159. 2001.00689.x

Bono-Yagüe, J., Gómez-Escribano, A. P., Millán, J. M., and Vázquez-Manrique, R. P. (2020). Reactive species in Huntington disease: Are they really the radicals you want to catch? *Antioxidants* 9:577. doi: 10.3390/antiox9070577

Brennan, A. M., Suh, S. W., Won, S. J., Narasimhan, P., Kauppinen, T. M., Lee, H., et al. (2009). NADPH oxidase is the primary source of superoxide induced by NMDA receptor activation. *Nat. Neurosci.* 12, 857–863. doi: 10.1038/nn.2334

Brennan-Minnella, A. M., Shen, Y., El-Benna, J., and Swanson, R. A. (2013). Phosphoinositide 3-kinase couples NMDA receptors to superoxide release in excitotoxic neuronal death. *Cell Death Dis.* 4:e580. doi: 10.1038/cddis.2013.111

Bresgen, N., and Eckl, P. M. (2015). Oxidative stress and the homeodynamics of iron metabolism. *Biomolecules* 5, 808–847. doi: 10.3390/biom5020808

Brito, V., Giralt, A., Enriquez-Barreto, L., Puigdellívol, M., Suelves, N., Zamora-Moratalla, A., et al. (2014). Neurotrophin receptor p75(NTR) mediates Huntington's disease-associated synaptic and memory dysfunction. *J. Clin. Invest.* 124, 4411–4428. doi: 10.1172/JCI74809

Brown, G. C., and Borutaite, V. (2012). There is no evidence that mitochondria are the main source of reactive oxygen species in mammalian cells. *Mitochondrion* 12, 1–4. doi: 10.1016/j.mito.2011.02.001

Brown, G. E., Stewart, M. Q., Bissonnette, S. A., Elia, A. E., Wilker, E., and Yaffe, M. B. (2004). Distinct ligand-dependent roles for p38 MAPK in priming and activation of the neutrophil NADPH oxidase. *J. Biol. Chem.* 279, 27059–27068. doi: 10.1074/jbc.M314258200

Campanucci, V. A., Krishnaswamy, A., and Cooper, E. (2008). Mitochondrial reactive oxygen species inactivate neuronal nicotinic acetylcholine receptors and induce long-term depression of fast nicotinic synaptic transmission. *J. Neurosci.* 28, 1733–1744. doi: 10.1523/JNEUROSCI.5130-07.2008

Caviston, J. P., Ross, J. L., Antony, S. M., Tokito, M., and Holzbaur, E. L. (2007). Huntingtin facilitates dynein/dynactin-mediated vesicle transport. *Proc. Natl. Acad. Sci. U.S.A.* 104, 10045–10050. doi: 10.1073/pnas.0610628104

Cepeda, C., and Levine, M. S. (2020). Synaptic dysfunction in Huntington's disease: lessons from genetic animal models. *Neuroscientist.* [Epub ahead of print]. doi: 10.1177/1073858420972662

Cheng, G., Ritsick, D., and Lambeth, J. D. (2004). Nox3 regulation by NOXO1, p47phox, and p67phox. *J. Biol. Chem.* 279, 34250–34255. doi: 10.1074/jbc. M400660200

Cheret, C., Gervais, A., Lelli, A., Colin, C., Amar, L., Ravassard, P., et al. (2008). Neurotoxic activation of microglia is promoted by a nox1-dependent NADPH oxidase. *J. Neurosci.* 28, 12039–12051. doi: 10.1523/JNEUROSCI.3568-08.2008

Coddou, C., Codocedo, J. F., Li, S., Lillo, J. G., Acuña-Castillo, C., Bull, P., et al. (2009). Reactive oxygen species potentiate the P2X2 receptor activity through intracellular Cys430. *J. Neurosci.* 29, 12284–12291. doi: 10.1523/JNEUROSCI.2096-09.2009

Coleman, C. G., Wang, G., Faraco, G., Marques Lopes, J., Waters, E. M., Milner, T. A., et al. (2013). Membrane trafficking of NADPH oxidase p47(phox) in paraventricular hypothalamic neurons parallels local free radical production in angiotensin II slow-pressor hypertension. *J. Neurosci.* 33, 4308–4316. doi: 10.1523/JNEUROSCI.3061-12.2013

Collingridge, G. L., Peineau, S., Howland, J. G., and Wang, Y. T. (2010). Long-term depression in the CNS. *Nat. Rev. Neurosci.* 11, 459–473. doi: 10.1038/nrn2867

Conforti, P., Besusso, D., Bocchi, V. D., Faedo, A., Cesana, E., Rossetti, G., et al. (2018). Faulty neuronal determination and cell polarization are reverted by modulating HD early phenotypes. *Proc. Natl. Acad. Sci. U.S.A.* 115, E762–E771. doi: 10.1073/pnas.1715865115

Crotti, A., Benner, C., Kerman, B. E., Gosselin, D., Lagier-Tourenne, C., Zuccato, C., et al. (2014). Mutant Huntingtin promotes autonomous microglia activation via myeloid lineage-determining factors. *Nat. Neurosci.* 17, 513–521. doi: 10.1038/nn.3668

Cui, L., Jeong, H., Borovecki, F., Parkhurst, C. N., Tanese, N., and Krainc, D. (2006). Transcriptional repression of PGC-1alpha by mutant huntingtin leads to mitochondrial dysfunction and neurodegeneration. *Cell* 127, 59–69. doi: 10.1016/j.cell.2006.09.015

Cummings, D. M., Milnerwood, A. J., Dallerac, G. M., Vatsavayai, S. C., Hirst, M. C., and Murphy, K. P. (2007). Abnormal cortical synaptic plasticity in a mouse model of Huntington's disease. *Brain Res. Bull.* 72, 103–107. doi: 10.1016/j.brainresbull.2006.10.016

Czeredys, M. (2020). Dysregulation of neuronal calcium signaling via store-operated channels in Huntington's disease. *Front. Cell. Dev. Biol.* 8:611735. doi: 10.3389/fcell.2020.611735

Dallérac, G. M., Vatsavayai, S. C., Cummings, D. M., Milnerwood, A. J., Peddie, C. J., Evans, K. A., et al. (2011). Impaired long-term potentiation in the prefrontal cortex of Huntington's disease mouse models: rescue by D1 dopamine receptor activation. *Neurodegener. Dis.* 8, 230–239. doi: 10.1159/000322540

Dang, P. M., Stensballe, A., Boussetta, T., Raad, H., Dewas, C., Kroviarski, Y., et al. (2006). A specific p47phox -serine phosphorylated by convergent MAPKs mediates neutrophil NADPH oxidase priming at inflammatory sites. *J. Clin. Invest.* 116, 2033–2043. doi: 10.1172/JCI27544

Di Filippo, M., de Iure, A., Giampà, C., Chiasserini, D., Tozzi, A., Orvietani, P. L., et al. (2016). Persistent activation of microglia and NADPH oxidase [corrected] drive hippocampal dysfunction in experimental multiple sclerosis. *Sci. Rep.* 6:20926. doi: 10.1038/srep23855

Di Maio, R., Mastroberardino, P. G., Hu, X., Montero, L., and Greenamyre, J. T. (2011). Pilocapine alters NMDA receptor expression and function in hippocampal neurons: NADPH oxidase and ERK1/2 mechanisms. *Neurobiol. Dis.* 42, 482–495. doi: 10.1016/j.nbd.2011.02.012

Ejlerskov, P., Christensen, D. P., Beyaie, D., Burritt, J. B., Paclet, M. H., Gorlach, A., et al. (2012). NADPH oxidase is internalized by clathrin-coated pits and localizes to a Rab27A/B GTPase-regulated secretory compartment in activated macrophages. *J. Biol. Chem.* 287, 4835–4852. doi: 10.1074/jbc.M111.293696

Ellson, C., Davidson, K., Anderson, K., Stephens, L. R., and Hawkins, P. T. (2006). PtdIns3P binding to the PX domain of p40phox is a physiological signal in NADPH oxidase activation. *EMBO J.* 25, 4468–4478. doi: 10.1038/sj.emboj.7601346

Fão, L., and Rego, A. C. (2021). Mitochondrial and redox-based therapeutic strategies in Huntington's disease. *Antioxid. Redox Signal.* 34, 650–673. doi: 10.1089/ars.2019.8004

Fellner, L., Irschick, R., Schanda, K., Reindl, M., Klimaschewski, L., Poewe, W., et al. (2012). Toll-like receptor 4 is required for alpha-synuclein dependent activation of microglia and astroglia. *Glia* 2012:22437. doi: 10.1002/glia.22437

Fontayne, A., Dang, P. M., Gougerot-Pocidalo, M. A., and El-Benna, J. (2002). Phosphorylation of p47phox sites by PKC alpha, beta II, delta, and zeta: effect on binding to p22phox and on NADPH oxidase activation. *Biochemistry* 41, 7743–7750. doi: 10.1021/bi011953s

Gerdeman, G. L., Ronesi, J., and Lovinger, D. M. (2002). Postsynaptic endocannabinoid release is critical to long-term depression in the striatum. *Nat. Neurosci.* 5, 446–451. doi: 10.1038/nn832

Ghiglieri, V., Campanelli, F., Marino, G., Natale, G., Picconi, B., and Calabresi, P. (2019). Corticostriatal synaptic plasticity alterations in the R6/1 transgenic mouse model of Huntington's disease. *J. Neurosci. Res.* 97, 1655–1664. doi: 10.1002/jnr.24521

Ghilan, M., Bostrom, C. A., Hryciw, B. N., Simpson, J. M., Christie, B. R., and Gil-Mohapel, J. (2014). YAC128 Huntington's disease transgenic mice show enhanced short-term hippocampal synaptic plasticity early in the course of the disease. *Brain Res.* 1581, 117–128. doi: 10.1016/j.brainres.2014.06.011

Gianni, D., Diaz, B., Taulet, N., Fowler, B., Courtneidge, S. A., and Bokoch, G. M. (2009). Novel p47(phox)-related organizers regulate localized NADPH oxidase 1 (Nox1) activity. *Sci. Signal.* 2:ra54. doi: 10.1126/scisignal.2000370

Giralt, A., Saavedra, A., Carretón, O., Xifró, X., Alberch, J., and Pérez-Navarro, E. (2011). Increased PKA signaling disrupts recognition memory and spatial memory: role in Huntington's disease. *Hum. Mol. Genet.* 20, 4232–4247. doi: 10.1093/hmg/ddr351

Girouard, H., Wang, G., Gallo, E. F., Anrather, J., Zhou, P., Pickel, V. M., et al. (2009). NMDA receptor activation increases free radical production through nitric oxide and NOX2. *J. Neurosci.* 29, 2545–2552. doi: 10.1523/JNEUROSCI.0133-09.2009

Glass, M. J., Huang, J., Oselkin, M., Tarsitano, M. J., Wang, G., Iadecola, C., et al. (2006). Subcellular localization of nicotinamide adenine dinucleotide phosphate oxidase subunits in neurons and astroglia of the rat medial nucleus tractus solitarius: relationship with tyrosine hydroxylase immunoreactive neurons. *Neuroscience* 143, 547–564. doi: 10.1016/j.neuroscience.2006.08.051

Gunawardena, S., Her, L. S., Brusch, R. G., Laymon, R. A., Niesman, I. R., Gordesky-Gold, B., et al. (2003). Disruption of axonal transport by loss of huntingtin or expression of pathogenic polyQ proteins in *Drosophila*. *Neuron* 40, 25–40. doi: 10.1016/S0896-6273(03)00594-4

Han, I., You, Y., Kordower, J. H., Brady, S. T., and Morfini, G. A. (2010). Differential vulnerability of neurons in Huntington's disease: the role of cell type-specific features. *J. Neurochem.* 113, 1073–1091. doi: 10.1111/j.1471-4159.2010.06672.x

Hanisch, U. K., and Kettenmann, H. (2007). Microglia: active sensor and versatile effector cells in the normal and pathologic brain. *Nat. Neurosci.* 10, 1387–1394. doi: 10.1038/nn1997

Hardingham, G. E. (2009). Coupling of the NMDA receptor to neuroprotective and neurodestructive events. *Biochem. Soc. Trans.* 37, 1147–1160. doi: 10.1042/BST0371147

Hardingham, G. E., and Bading, H. (2010). Synaptic versus extrasynaptic NMDA receptor signalling: implications for neurodegenerative disorders. *Nat. Rev. Neurosci.* 11, 682–696. doi: 10.1038/nrn2911

Hardingham, G. E., and Do, K. Q. (2016). Linking early-life NMDAR hypofunction and oxidative stress in schizophrenia pathogenesis. *Nat. Rev. Neurosci.* 17, 125–134. doi: 10.1038/nrn.2015.19

Helmcke, I., Heumüller, S., Tikkanen, R., Schröder, K., and Brandes, R. P. (2009). Identification of structural elements in Nox1 and Nox4 controlling localization and activity. *Antioxid. Redox Signal.* 11, 1279–1287. doi: 10.1089/ars.2008.2383

Heng, M. Y., Detloff, P. J., Wang, P. L., Tsien, J. Z., and Albin, R. L. (2009). In vivo evidence for NMDA receptor-mediated excitotoxicity in a murine genetic model of Huntington disease. *J. Neurosci.* 29, 3200–3205. doi: 10.1523/JNEUROSCI.5599-08.2009

Hervera, A., De Virgiliis, F., Palmisano, I., Zhou, L., Tantardini, E., Kong, G., et al. (2018). Publisher Correction: reactive oxygen species regulate axonal regeneration through the release of exosomal NADPH oxidase 2 complexes into injured axons. *Nat. Cell Biol.* 20, 307–319. doi: 10.1038/s41556-018-0039-x

Hodgson, J. G., Agopyan, N., Gutekunst, C. A., Leavitt, B. R., LePiane, F., Singaraja, R., et al. (1999). A YAC mouse model for Huntington's disease with full-length mutant huntingtin, cytoplasmic toxicity, and selective striatal neurodegeneration. *Neuron* 23, 181–192. doi: 10.1016/S0896-6273(00)80764-3

Hoerder-Suabedissen, A., Korrell, K. V., Hayashi, S., Jeans, A., Ramirez, D. M. O., Grant, E., et al. (2019). Cell-specific loss of SNAP25 from cortical projection

neurons allows normal development but causes subsequent neurodegeneration. *Cereb. Cortex* 29, 2148–2159. doi: 10.1093/cercor/bhy127

Hoyal, C. R., Gutierrez, A., Young, B. M., Catz, S. D., Lin, J. H., Tsichlis, P. N., et al. (2003). Modulation of p47PHOX activity by site-specific phosphorylation: Akt-dependent activation of the NADPH oxidase. *Proc. Natl. Acad. Sci. U.S.A.* 100, 5130–5135. doi: 10.1073/pnas.1031526100

Hung, R. J., Pak, C. W., and Terman, J. R. (2011). Direct redox regulation of F-actin assembly and disassembly by Mical. *Science* 334, 1710–1713. doi: 10.1126/science.1211956

Hung, R. J., Yazdani, U., Yoon, J., Wu, H., Yang, T., Gupta, N., et al. (2010). Mical links semaphorins to F-actin disassembly. *Nature* 463, 823–827. doi: 10.1038/nature08724

Ibi, M., Katsuyama, M., Fan, C., Iwata, K., Nishinaka, T., Yokoyama, T., et al. (2006). NOX1/NADPH oxidase negatively regulates nerve growth factor-induced neurite outgrowth. *Free Radic. Biol. Med.* 40, 1785–1795. doi: 10.1016/j.freeradbiomed.2006.01.009

Ikeda, S., Yamaoka-Tojo, M., Hilenski, L., Patrushev, N. A., Anwar, G. M., Quinn, M. T., et al. (2005). IQGAP1 regulates reactive oxygen species-dependent endothelial cell migration through interacting with Nox2. *Arterioscler. Thromb. Vasc. Biol.* 25, 2295–2300. doi: 10.1161/01.ATV.0000187472.55437.af

Jones, D. P., and Sies, H. (2015). The redox code. *Antioxid. Redox Signal.* 23, 734–746. doi: 10.1089/ars.2015.6247

Kallenborn-Gerhardt, W., Hohmann, S. W., Syhr, K. M., Schroder, K., Sisignano, M., Weigert, A., et al. (2014). Nox2-dependent signaling between macrophages and sensory neurons contributes to neuropathic pain hypersensitivity. *Pain* 155, 2161–2170. doi: 10.1016/j.pain.2014.08.013

Kallenborn-Gerhardt, W., Schroder, K., Del Turco, D., Lu, R., Kynast, K., Kosowski, J., et al. (2012). NADPH oxidase-4 maintains neuropathic pain after peripheral nerve injury. *J. Neurosci.* 32, 10136–10145. doi: 10.1523/JNEUROSCI.6227-11.2012

Kallenborn-Gerhardt, W., Schroder, K., Geisslinger, G., and Schmidtko, A. (2013). NOXious signaling in pain processing. *Pharmacol. Ther.* 137, 309–317. doi: 10.1016/j.pharmthera.2012.11.001

Kamat, C. D., Gadal, S., Mhatre, M., Williamson, K. S., Pye, Q. N., and Hensley, K. (2008). Antioxidants in central nervous system diseases: preclinical promise and translational challenges. *J. Alzheimers Dis.* 15, 473–493. doi: 10.3233/JAD-2008-15314

Kamsler, A., and Segal, M. (2003). Hydrogen peroxide modulation of synaptic plasticity. *J. Neurosci.* 23, 269–276. doi: 10.1523/JNEUROSCI.23-01-00269.2003

Kettenmann, H., Kirchhoff, F., and Verkhratsky, A. (2013). Microglia: new roles for the synaptic stripper. *Neuron* 77, 10–18. doi: 10.1016/j.neuron.2012.12.023

Kim, A., García-García, E., Straccia, M., Comella-Bolla, A., Miguez, A., Masana, M., et al. (2020). Reduced Fractalkine levels lead to striatal synaptic plasticity deficits in Huntington's Disease. *Front. Cell. Neurosci.* 14:163. doi: 10.3389/fncel.2020.00163

Kishida, K. T., Hoeffer, C. A., Hu, D., Pao, M., Holland, S. M., and Klann, E. (2006). Synaptic plasticity deficits and mild memory impairments in mouse models of chronic granulomatous disease. *Mol. Cell. Biol.* 26, 5908–5920. doi: 10.1128/MCB.00269-06

Knapp, L. T., and Klann, E. (2002). Potentiation of hippocampal synaptic transmission by superoxide requires the oxidative activation of protein kinase C. *J. Neurosci.* 22, 674–683. doi: 10.1523/JNEUROSCI.22-03-00674.2002

Kokovay, E., Wang, Y., Kusek, G., Wurster, R., Lederman, P., Lowry, N., et al. (2012). VCAM1 is essential to maintain the structure of the SVZ niche and acts as an environmental sensor to regulate SVZ lineage progression. *Cell Stem Cell* 11, 220–230. doi: 10.1016/j.stem.2012.06.016

Kraft, A. D., Kaltenbach, L. S., Lo, D. C., and Harry, G. J. (2012). Activated microglia proliferate at neurites of mutant huntingtin-expressing neurons. *Neurobiol. Aging* 33, 621.e17–621.e33. doi: 10.1016/j.neurobiolaging.2011.02.015

Kung, V. W., Hassam, R., Morton, A. J., and Jones, S. (2007). Dopamine-dependent long term potentiation in the dorsal striatum is reduced in the R6/2 mouse model of Huntington's disease. *Neuroscience* 146, 1571–1580. doi: 10.1016/j.neuroscience.2007.03.036

Kwan, W., Trager, U., Davalos, D., Chou, A., Bouchard, J., Andre, R., et al. (2012). Mutant huntingtin impairs immune cell migration in Huntington disease. *J. Clin. Invest.* 122, 4737–4747. doi: 10.1172/JCI64484

Lamb, F. S., Hook, J. S., Hilkin, B. M., Huber, J. N., Volk, A. P., and Moreland, J. G. (2012). Endotoxin priming of neutrophils requires endocytosis and NADPH oxidase-dependent endosomal reactive oxygen species. *J. Biol. Chem.* 287, 12395–12404. doi: 10.1074/jbc.M111.306530

Lambeth, J. D., and Neish, A. S. (2014). Nox enzymes and new thinking on reactive oxygen: a double-edged sword revisited. *Annu. Rev. Pathol.* 9, 119–145. doi: 10.1146/annurev-pathol-012513-104651

Le Belle, J. E., Orozco, N. M., Paucar, A. A., Saxe, J. P., Mottahedeh, J., Pyle, A. D., et al. (2011). Proliferative neural stem cells have high endogenous ROS levels that regulate self-renewal and neurogenesis in a PI3K/Akt-dependant manner. *Cell Stem Cell* 8, 59–71. doi: 10.1016/j.stem.2010.11.028

Lee, K. Y., Chung, K., and Chung, J. M. (2010). Involvement of reactive oxygen species in long-term potentiation in the spinal cord dorsal horn. *J. Neurophysiol.* 103, 382–391. doi: 10.1152/jn.90906.2008

Li, X., Marchal, C. C., Stull, N. D., Stahelin, R. V., and Dinauer, M. C. (2010). p47phox PX domain regulates plasma membrane but not phagosome neutrophil NADPH oxidase activation. *J. Biol. Chem.* 285, 35169–35179. doi: 10.1074/jbc.M110.164475

Lim, H., Kim, D., and Lee, S. J. (2013). Toll-like receptor 2 mediates peripheral nerve injury-induced NADPH oxidase 2 expression in spinal cord microglia. *J. Biol. Chem.* 288, 7572–7579. doi: 10.1074/jbc.M112.414904

Lipton, S. A., Choi, Y. B., Takahashi, H., Zhang, D., Li, W., Godzik, A., et al. (2002). Cysteine regulation of protein function–as exemplified by NMDA-receptor modulation. *Trends Neurosci.* 25, 474–480. doi: 10.1016/S0166-2236(02)02245-2

Lu, S., and Lu, B. (2021). Degeneration versus development: hunting-out the D-Unit of Huntington's disease. *Neurosci. Bull.* 37, 757–760. doi: 10.1007/s12264-021-00649-0

Luo, L., Kaur Kumar, J., and Clément, M. V. (2012). Redox control of cytosolic Akt phosphorylation in PTEN null cells. *Free Radic. Biol. Med.* 53, 1697–1707. doi: 10.1016/j.freeradbiomed.2012.08.566

Ma, B., Savas, J. N., Yu, M. S., Culver, B. P., Chao, M. V., and Tanese, N. (2011). Huntingtin mediates dendritic transport of beta-actin mRNA in rat neurons. *Sci. Rep.* 1:140. doi: 10.1038/srep00140

Maldonado, P. D., Molina-Jijón, E., Villeda-Hernández, J., Galván-Arzate, S., Santamaría, A., and Pedraza-Chaverrí, J. (2010). NAD(P)H oxidase contributes to neurotoxicity in an excitotoxic/prooxidant model of Huntington's disease in rats: protective role of apocynin. *J. Neurosci. Res.* 88, 620–629. doi: 10.1002/jnr.22240

Malik, M., Parikh, I., Vasquez, J. B., Smith, C., Tai, L., Bu, G., et al. (2015). Genetics ignite focus on microglial inflammation in Alzheimer's disease. *Mol. Neurodegener.* 10:52. doi: 10.1186/s13024-015-0048-1

Martel, M. A., Wyllie, D. J., and Hardingham, G. E. (2009). In developing hippocampal neurons, NR2B-containing N-methyl-D-aspartate receptors (NMDARs) can mediate signaling to neuronal survival and synaptic potentiation, as well as neuronal death. *Neuroscience* 158, 334–343. doi: 10.1016/j.neuroscience.2008.01.080

Martinez-Vicente, M., Talloczy, Z., Wong, E., Tang, G., Koga, H., Kaushik, S., et al. (2010). Cargo recognition failure is responsible for inefficient autophagy in Huntington's disease. *Nat. Neurosci.* 13, 567–576. doi: 10.1038/nn.2528

Massaad, C. A., and Klann, E. (2011). Reactive oxygen species in the regulation of synaptic plasticity and memory. *Antioxid. Redox Signal.* 14, 2013–2054. doi: 10.1089/ars.2010.3208

Mehta, S. R., Tom, C. M., Wang, Y., Bresee, C., Rushton, D., Mathkar, P. P., et al. (2018). Human Huntington's disease iPSC-derived cortical neurons display altered transcriptomics, morphology, and maturation. *Cell Rep.* 25, 1081–1096.e6. doi: 10.1016/j.celrep.2018.09.076

Miller, J., Arrasate, M., Shaby, B. A., Mitra, S., Masliah, E., and Finkbeiner, S. (2010). Quantitative relationships between huntingtin levels, polyglutamine length, inclusion body formation, and neuronal death provide novel insight into huntington's disease molecular pathogenesis. *J. Neurosci.* 30, 10541–10550. doi: 10.1523/JNEUROSCI.0146-10.2010

Milnerwood, A. J., Cummings, D. M., Dallérac, G. M., Brown, J. Y., Vatsavayai, S. C., Hirst, M. C., et al. (2006). Early development of aberrant synaptic plasticity in a mouse model of Huntington's disease. *Hum. Mol. Genet.* 15, 1690–1703. doi: 10.1093/hmg/ddl092

Milnerwood, A. J., and Raymond, L. A. (2007). Corticostriatal synaptic function in mouse models of Huntington's disease: early effects of huntingtin repeat

length and protein load. *J. Physiol.* 585, 817–831. doi: 10.1113/jphysiol.2007.142448

Minnella, A. M., Zhao, J. X., Jiang, X., Jakobsen, E., Lu, F., Wu, L., et al. (2018). Excitotoxic superoxide production and neuronal death require both ionotropic and non-ionotropic NMDA receptor signaling. *Sci. Rep.* 8:17522. doi: 10.1038/s41598-018-35725-5

Molero, A. E., Arteaga-Bracho, E. E., Chen, C. H., Gulinello, M., Winchester, M. L., Pichamoorthy, N., et al. (2016). Selective expression of mutant huntingtin during development recapitulates characteristic features of Huntington's disease. *Proc. Natl. Acad. Sci. U.S.A.* 113, 5736–5741. doi: 10.1073/pnas.1603871113

Montoya, A., Pelletier, M., Menear, M., Duplessis, E., Richer, F., and Lepage, M. (2006). Episodic memory impairment in Huntington's disease: a meta-analysis. *Neuropsychologia* 44, 1984–1994. doi: 10.1016/j.neuropsychologia.2006.01.015

Moreland, J. G., Davis, A. P., Matsuda, J. J., Hook, J. S., Bailey, G., Nauseef, W. M., et al. (2007). Endotoxin priming of neutrophils requires NADPH oxidase-generated oxidants and is regulated by the anion transporter ClC-3. *J. Biol. Chem.* 282, 33958–33967. doi: 10.1074/jbc.M705289200

Morfini, G. A., You, Y. M., Pollema, S. L., Kaminska, A., Liu, K., Yoshioka, K., et al. (2009). Pathogenic huntingtin inhibits fast axonal transport by activating JNK3 and phosphorylating kinesin. *Nat. Neurosci.* 12, 864–871. doi: 10.1038/nn.2346

Munnamalai, V., Weaver, C. J., Weisheit, C. E., Venkatraman, P., Agim, Z. S., Quinn, M. T., et al. (2014). Bidirectional interactions between NOX2-type NADPH oxidase and the F-actin cytoskeleton in neuronal growth cones. *J. Neurochem.* 130, 526–540. doi: 10.1111/jnc.12734

Murphy, K. P., Carter, R. J., Lione, L. A., Mangiarini, L., Mahal, A., Bates, G. P., et al. (2000). Abnormal synaptic plasticity and impaired spatial cognition in mice transgenic for exon 1 of the human Huntington's disease mutation. *J. Neurosci.* 20, 5115–5123. doi: 10.1523/JNEUROSCI.20-13-05115.2000

Nauseef, W. M. (2019). The phagocyte NOX2 NADPH oxidase in microbial killing and cell signaling. *Curr. Opin. Immunol.* 60, 130–140. doi: 10.1016/j.coi.2019.05.006

Nayernia, Z., Colaianna, M., Robledinos-Anton, N., Gutzwiller, E., Sloan-Bena, F., Stathaki, E., et al. (2017). Decreased neural precursor cell pool in NADPH oxidase 2-deficiency: From mouse brain to neural differentiation of patient derived iPSC. *Redox Biol.* 13, 82–93. doi: 10.1016/j.redox.2017.04.026

Nayernia, Z., Jaquet, V., and Krause, K. H. (2014). New insights on NOX enzymes in the central nervous system. *Antioxid. Redox Signal.* 20, 2815–2837. doi: 10.1089/ars.2013.5703

Oakley, F. D., Smith, R. L., and Engelhardt, J. F. (2009). Lipid rafts and caveolin-1 coordinate interleukin-1beta (IL-1beta)-dependent activation of NFkappaB by controlling endocytosis of Nox2 and IL-1beta receptor 1 from the plasma membrane. *J. Biol. Chem.* 284, 33255–33264. doi: 10.1074/jbc.M109.042127

Olguin-Albuerne, M., and Moran, J. (2015). ROS produced by NOX2 control *in vitro* development of cerebellar granule neurons development. *ASN Neuro* 7:1759091415578712. doi: 10.1177/1759091415578712

Ooi, J., Langley, S. R., Xu, X., Utami, K. H., Sim, B., Huang, Y., et al. (2019). Unbiased profiling of isogenic Huntington disease hPSC-Derived CNS and peripheral cells reveals strong cell-type specificity of CAG length effects. *Cell Rep.* 26:2494. doi: 10.1016/j.celrep.2019.02.008

O'Regan, G. C., Farag, S. H., Casey, C. S., Wood-Kaczmar, A., Pocock, J. M., Tabrizi, S. J., et al. (2021). Human Huntington's disease pluripotent stem cell-derived microglia develop normally but are abnormally hyper-reactive and release elevated levels of reactive oxygen species. *J. Neuroinflammation* 18:94. doi: 10.1186/s12974-021-02147-6

Oswald, M. C. W., Garnham, N., Sweeney, S. T., and Landgraf, M. (2018). Regulation of neuronal development and function by ROS. *FEBS Lett.* 592, 679–691. doi: 10.1002/1873-3468.12972

Park, H. S., Jung, H. Y., Park, E. Y., Kim, J., Lee, W. J., and Bae, Y. S. (2004). Cutting edge: direct interaction of TLR4 with NAD(P)H oxidase 4 isozyme is essential for lipopolysaccharide-induced production of reactive oxygen species and activation of NF-kappa B. *J. Immunol.* 173, 3589–3593. doi: 10.4049/jimmunol.173.6.3589

Pavese, N., Gerhard, A., Tai, Y. F., Ho, A. K., Turkheimer, F., Barker, R. A., et al. (2006). Microglial activation correlates with severity in Huntington disease: a clinical and PET study. *Neurology* 66, 1638–1643. doi: 10.1212/01.wnl.0000222734.56412.17

Petersen, S. V., Poulsen, N. B., Linneberg Matthiesen, C., and Vilhardt, F. (2021). Novel and converging ways of NOX2 and SOD3 in trafficking and redox signaling in macrophages. *Antioxidants* 10:172. doi: 10.3390/antiox10020172

Petkau, T. L., Hill, A., Connolly, C., Lu, G., Wagner, P., Kosior, N., et al. (2019). Mutant huntingtin expression in microglia is neither required nor sufficient to cause the Huntington's disease-like phenotype in BACHD mice. *Hum. Mol. Genet.* 28, 1661–1670. doi: 10.1093/hmg/ddz009

Plotkin, J. L., Day, M., Peterson, J. D., Xie, Z., Kress, G. J., Rafalovich, I., et al. (2014). Impaired TrkB receptor signaling underlies corticostriatal dysfunction in Huntington's disease. *Neuron* 83, 178–188. doi: 10.1016/j.neuron.2014.05.032

Plotkin, J. L., and Surmeier, D. J. (2015). Corticostriatal synaptic adaptations in Huntington's disease. *Curr. Opin. Neurobiol.* 33, 53–62. doi: 10.1016/j.conb.2015.01.020

Price, M. O., Atkinson, S. J., Knaus, U. G., and Dinauer, M. C. (2002). Rac activation induces NADPH oxidase activity in transgenic COSphox cells and level of superoxide production is exchange factor-dependent. *J. Biol. Chem.* 277, 19220–19228. doi: 10.1074/jbc.M200061200

Qiao, H., Zhang, Q., Yuan, H., Li, Y., Wang, D., Wang, R., et al. (2015). Elevated neuronal alpha-synuclein promotes microglia activation after spinal cord ischemic/reperfused injury. *Neuroreport* 26, 656–661. doi: 10.1097/WNR.0000000000000406

Qin, L., Liu, Y., Wang, T., Wei, S. J., Block, M. L., Wilson, B., et al. (2004). NADPH oxidase mediates lipopolysaccharide-induced neurotoxicity and proinflammatory gene expression in activated microglia. *J. Biol. Chem.* 279, 1415–1421. doi: 10.1074/jbc.M307657200

Quirion, J. G., and Parsons, M. P. (2019). The onset and progression of hippocampal synaptic plasticity deficits in the Q175FDN mouse model of Huntington disease. *Front. Cell. Neurosci.* 13:326. doi: 10.3389/fncel.2019.00326

Ramdzan, Y. M., Trubetskov, M. M., Ormsby, A. R., Newcombe, E. A., Sui, X., Tobin, M. J., et al. (2017). Huntingtin inclusions trigger cellular quiescence, deactivate apoptosis, and lead to delayed necrosis. *Cell Rep.* 19, 919–927. doi: 10.1016/j.celrep.2017.04.029

Rey, F. E., Cifuentes, M. E., Kiarash, A., Quinn, M. T., and Pagano, P. J. (2001). Novel competitive inhibitor of NAD(P)H oxidase assembly attenuates vascular O(2)(-) and systolic blood pressure in mice. *Circ. Res.* 89, 408–414. doi: 10.1161/hh1701.096037

Reyes, R. C., Brennan, A. M., Shen, Y., Baldwin, Y., and Swanson, R. A. (2012). Activation of neuronal NMDA receptors induces superoxide-mediated oxidative stress in neighboring neurons and astrocytes. *J. Neurosci.* 32, 12973–12978. doi: 10.1523/JNEUROSCI.1597-12.2012

Rhee, S. G., Bae, Y. S., Lee, S. R., and Kwon, J. (2000). Hydrogen peroxide: a key messenger that modulates protein phosphorylation through cysteine oxidation. *Sci. STKE* 2000:e1. doi: 10.1126/scisignal.532000pe1

Roepstorff, K., Rasmussen, I., Sawada, M., Cudre-Maroux, C., Salmon, P., Bokoch, G., et al. (2008). Stimulus-dependent regulation of the phagocyte NADPH Oxidase by a VAV1, Rac1, and PAK1 Signaling Axis. *J. Biol. Chem.* 283, 7983–7993. doi: 10.1074/jbc.M708281200

Rui, Y. N., Xu, Z., Patel, B., Chen, Z., Chen, D., Tito, A., et al. (2015). Huntingtin functions as a scaffold for selective macroautophagy. *Nat. Cell Biol.* 17, 262–275. doi: 10.1038/ncb3101

Sapp, E., Seeley, C., Iuliano, M., Weisman, E., Vodicka, P., DiFiglia, M., et al. (2020). Protein changes in synaptosomes of Huntington's disease knock-in mice are dependent on age and brain region. *Neurobiol. Dis.* 141:104950. doi: 10.1016/j.nbd.2020.104950

Saudou, F., and Humbert, S. (2016). The biology of Huntingtin. *Neuron* 89, 910–926. doi: 10.1016/j.neuron.2016.02.003

Schiavone, S., Jaquet, V., Sorce, S., Dubois-Dauphin, M., Hultqvist, M., Backdahl, L., et al. (2012). NADPH oxidase elevations in pyramidal neurons drive psychosocial stress-induced neuropathology. *Transl. Psychiatry* 2:e111. doi: 10.1038/tp.2012.36

Sepers, M. D., Smith-Dijak, A., LeDue, J., Kolodziejczyk, K., Mackie, K., and Raymond, L. A. (2018). Endocannabinoid-specific impairment in synaptic plasticity in striatum of Huntington's Disease mouse model. *J. Neurosci.* 38, 544–554. doi: 10.1523/JNEUROSCI.1739-17.2017

Serrander, L., Larsson, J., Lundqvist, H., Lindmark, M., Fallman, M., Dahlgren, C., et al. (1999). Particles binding beta(2)-integrins mediate intracellular production of oxidative metabolites in human neutrophils independently of phagocytosis. *Biochim. Biophys. Acta* 1452, 133–144. doi: 10.1016/S0167-4889(99)00123-8

Sies, H. (2014). Role of metabolic H2O2 generation: redox signaling and oxidative stress. *J. Biol. Chem.* 289, 8735–8741. doi: 10.1074/jbc.R113.544635

Sies, H., and Jones, D. P. (2020). Reactive oxygen species (ROS) as pleiotropic physiological signalling agents. *Nat. Rev. Mol. Cell Biol.* 21, 363–383. doi: 10.1038/s41580-020-0230-3

Siew, J. J., Chen, H. M., Chen, H. Y., Chen, H. L., Chen, C. M., Soong, B. W., et al. (2019). Galectin-3 is required for the microglia-mediated brain inflammation in a model of Huntington's disease. *Nat. Commun.* 10:3473. doi: 10.1038/s41467-019-11441-0

Singh, A., Kukreti, R., Saso, L., and Kukreti, S. (2019). Oxidative stress: a key modulator in neurodegenerative diseases. *Molecules* 24:1583. doi: 10.3390/molecules24081583

Singhrao, S. K., Neal, J. W., Morgan, B. P., and Gasque, P. (1999). Increased complement biosynthesis by microglia and complement activation on neurons in Huntington's disease. *Exp. Neurol.* 159, 362–376. doi: 10.1006/exnr.1999.7170

Skotte, N. H., Andersen, J. V., Santos, A., Aldana, B. I., Willert, C. W., Nørremølle, A., et al. (2018). Integrative characterization of the R6/2 mouse model of Huntington's disease reveals dysfunctional astrocyte metabolism. *Cell Rep.* 23, 2211–2224. doi: 10.1016/j.celrep.2018.04.052

Smith, R., Klein, P., Koc-Schmitz, Y., Waldvogel, H. J., Faull, R. L., Brundin, P., et al. (2007). Loss of SNAP-25 and rabphilin 3a in sensory-motor cortex in Huntington's disease. *J. Neurochem.* 103, 115–123. doi: 10.1111/j.1471-4159.2007.04703.x

Smith-Dijak, A. I., Sepers, M. D., and Raymond, L. A. (2019). Alterations in synaptic function and plasticity in Huntington disease. *J. Neurochem.* 150, 346–365. doi: 10.1111/jnc.14723

Sorce, S., Stocker, R., Seredenina, T., Holmdahl, R., Aguzzi, A., Chio, A., et al. (2017). NADPH oxidases as drug targets and biomarkers in neurodegenerative diseases: What is the evidence? *Free Radic. Biol. Med.* 112, 387–396. doi: 10.1016/j.freeradbiomed.2017.08.006

Sorolla, M. A., Reverter-Branchat, G., Tamarit, J., Ferrer, I., Ros, J., and Cabiscol, E. (2008). Proteomic and oxidative stress analysis in human brain samples of Huntington disease. *Free Radic. Biol. Med.* 45, 667–678. doi: 10.1016/j.freeradbiomed.2008.05.014

Spence, E. F., and Soderling, S. H. (2015). Actin out: regulation of the synaptic cytoskeleton. *J. Biol. Chem.* 290, 28613–28622. doi: 10.1074/jbc.R115.655118

Stanton, P. K., Winterer, J., Bailey, C. P., Kyrozis, A., Raginov, I., Laube, G., et al. (2003). Long-term depression of presynaptic release from the readily releasable vesicle pool induced by NMDA receptor-dependent retrograde nitric oxide. *J. Neurosci.* 23, 5936–5944. doi: 10.1523/JNEUROSCI.23-13-05936.2003

St-Pierre, J., Drori, S., Uldry, M., Silvaggi, J. M., Rhee, J., Jäger, S., et al. (2006). Suppression of reactive oxygen species and neurodegeneration by the PGC-1 transcriptional coactivators. *Cell* 127, 397–408. doi: 10.1016/j.cell.2006.09.024

Su, Z., Burchfield, J. G., Yang, P., Humphrey, S. J., Yang, G., Francis, D., et al. (2019). Global redox proteome and phosphoproteome analysis reveals redox switch in Akt. *Nat. Commun.* 10:5486. doi: 10.1038/s41467-019-13114-4

Sumimoto, H., Hata, K., Mizuki, K., Ito, T., Kage, Y., Sakaki, Y., et al. (1996). Assembly and activation of the phagocyte NADPH oxidase. Specific interaction of the N-terminal Src homology 3 domain of p47phox with p22phox is required for activation of the NADPH oxidase. *J. Biol. Chem.* 271, 22152–22158. doi: 10.1074/jbc.271.36.22152

Sun, Q. A., Hess, D. T., Nogueira, L., Yong, S., Bowles, D. E., Eu, J., et al. (2011). Oxygen-coupled redox regulation of the skeletal muscle ryanodine receptor-Ca2+ release channel by NADPH oxidase 4. *Proc. Natl. Acad. Sci. U.S.A.* 108, 16098–16103. doi: 10.1073/pnas.1109546108

Suzukawa, K., Miura, K., Mitsushita, J., Resau, J., Hirose, K., Crystal, R., et al. (2000). Nerve growth factor-induced neuronal differentiation requires generation of Rac1-regulated reactive oxygen species. *J. Biol. Chem.* 275, 13175–13178. doi: 10.1074/jbc.275.18.13175

Szlachcic, W. J., Switonski, P. M., Krzyzosiak, W. J., Figlerowicz, M., and Figiel, M. (2015). Huntington disease iPSCs show early molecular changes in intracellular signaling, the expression of oxidative stress proteins and the p53 pathway. *Dis. Models Mech.* 8, 1047–1057. doi: 10.1242/dmm.019406

Tai, Y. F., Pavese, N., Gerhard, A., Tabrizi, S. J., Barker, R. A., Brooks, D. J., et al. (2007). Microglial activation in presymptomatic Huntington's disease gene carriers. *Brain* 130, 1759–1766. doi: 10.1093/brain/awm044

Tejada-Simon, M. V., Serrano, F., Villasana, L. E., Kanterewicz, B. I., Wu, G. Y., Quinn, M. T., et al. (2005). Synaptic localization of a functional NADPH oxidase in the mouse hippocampus. *Mol. Cell. Neurosci.* 29, 97–106. doi: 10.1016/j.mcn.2005.01.007

Tejera, D., and Heneka, M. T. (2019). Microglia in neurodegenerative disorders. *Methods Mol. Biol.* 2034, 57–67. doi: 10.1007/978-1-4939-9658-2_5

Teleanu, R. I., Chircov, C., Grumezescu, A. M., Volceanov, A., and Teleanu, D. M. (2019). Antioxidant therapies for neuroprotection-a review. *J. Clin. Med.* 8:1659. doi: 10.3390/jcm8101659

Terzi, A., Roeder, H., Weaver, C. J., and Suter, D. M. (2021). Neuronal NADPH oxidase 2 regulates growth cone guidance downstream of slit2/robo2. *Dev. Neurobiol.* 81, 3–21. doi: 10.1002/dneu.22791

Terzi, A., and Suter, D. M. (2020). The role of NADPH oxidases in neuronal development. *Free Radic. Biol. Med.* 154, 33–47. doi: 10.1016/j.freeradbiomed.2020.04.027

The Huntington Disease Collaborative Research Group (1993). A novel gene containing a trinucleotide repeat that is expanded and unstable on Huntington's disease chromosomes. The Huntington's Disease Collaborative Research Group. *Cell* 72, 971–983. doi: 10.1016/0092-8674(93)90585-e

Thiels, E., Urban, N. N., Gonzalez-Burgos, G. R., Kanterewicz, B. I., Barrionuevo, G., Chu, C. T., et al. (2000). Impairment of long-term potentiation and associative memory in mice that overexpress extracellular superoxide dismutase. *J. Neurosci.* 20, 7631–7639. doi: 10.1523/JNEUROSCI.20-20-07631.2000

Tousley, A., Iuliano, M., Weisman, E., Sapp, E., Richardson, H., Vodicka, P., et al. (2019a). Huntingtin associates with the actin cytoskeleton and α-actinin isoforms to influence stimulus dependent morphology changes. *PLoS One* 14:e0212337. doi: 10.1371/journal.pone.0212337

Tousley, A., Iuliano, M., Weisman, E., Sapp, E., Zhang, N., Vodicka, P., et al. (2019b). Rac1 Activity is modulated by huntingtin and dysregulated in models of Huntington's disease. *J. Huntingtons Dis.* 8, 53–69. doi: 10.3233/JHD-180311

Ueyama, T., Nakakita, J., Nakamura, T., Kobayashi, T., Kobayashi, T., Son, J., et al. (2011). Cooperation of p40phox with p47phox for Nox2-based NADPH Oxidase Activation during Fcgamma Receptor (FcgammaR)-mediated Phagocytosis: MECHANISM FOR ACQUISITION OF p40phox PHOSPHATIDYLINOSITOL 3-PHOSPHATE (PI(3)P) BINDING. *J. Biol. Chem.* 286, 40693–40705. doi: 10.1074/jbc.M111.237289

Usdin, M. T., Shelbourne, P. F., Myers, R. M., and Madison, D. V. (1999). Impaired synaptic plasticity in mice carrying the Huntington's disease mutation. *Hum. Mol. Genet.* 8, 839–846. doi: 10.1093/hmg/8.5.839

van der Plas, E., Schultz, J. L., and Nopoulos, P. C. (2020). The neurodevelopmental hypothesis of Huntington's Disease. *J. Huntingtons Dis.* 9, 217–229. doi: 10.3233/JHD-200394

Vignais, P. V. (2002). The superoxide-generating NADPH oxidase: structural aspects and activation mechanism. *Cell. Mol. Life Sci.* 59, 1428–1459. doi: 10.1007/s00018-002-8520-9

Vilhardt, F., and van Deurs, B. (2004). The phagocyte NADPH oxidase depends on cholesterol-enriched membrane microdomains for assembly. *EMBO J.* 23, 739–748. doi: 10.1038/sj.emboj.7600066

Wang, G., Anrather, J., Huang, J., Speth, R. C., Pickel, V. M., and Iadecola, C. (2004). NADPH oxidase contributes to angiotensin II signaling in the nucleus tractus solitarius. *J. Neurosci.* 24, 5516–5524. doi: 10.1523/JNEUROSCI.1176-04.2004

Wang, J., and Swanson, R. A. (2020). Superoxide and non-ionotropic signaling in neuronal excitotoxicity. *Front. Neurosci.* 4:861. doi: 10.3389/fnins.2020.00861

Wang, Q., Rowan, M. J., and Anwyl, R. (2004). Beta-amyloid-mediated inhibition of NMDA receptor-dependent long-term potentiation induction involves activation of microglia and stimulation of inducible nitric oxide synthase and superoxide. *J. Neurosci.* 24, 6049–6056. doi: 10.1523/JNEUROSCI.0233-04.2004

Wang, S., Chu, C. H., Stewart, T., Ginghina, C., Wang, Y., Nie, H., et al. (2015). alpha-Synuclein, a chemoattractant, directs microglial migration via H2O2-dependent Lyn phosphorylation. *Proc. Natl. Acad. Sci. U.S.A.* 112, E1926–E1935. doi: 10.1073/pnas.1417883112

Weaver, C. J., Terzi, A., Roeder, H., Gurol, T., Deng, Q., Leung, Y. F., et al. (2018). nox2/cybb deficiency affects zebrafish retinotectal connectivity. *J. Neurosci.* 38, 5854–5871. doi: 10.1523/JNEUROSCI.1483-16.2018

Weydt, P., Pineda, V. V., Torrence, A. E., Libby, R. T., Satterfield, T. F., Lazarowski, E. R., et al. (2006). Thermoregulatory and metabolic defects in Huntington's disease transgenic mice implicate PGC-1alpha in Huntington's disease neurodegeneration. *Cell Metab.* 4, 349–362. doi: 10.1016/j.cmet.2006.10.004

Wilson, C., Munoz-Palma, E., Henriquez, D. R., Palmisano, I., Nunez, M. T., Di Giovanni, S., et al. (2016). A feed-forward mechanism involving the NOX complex and RyR-Mediated Ca2+ release during axonal specification. *J. Neurosci.* 36, 11107–11119. doi: 10.1523/JNEUROSCI.1455-16.2016

Wilson, C., Nunez, M. T., and Gonzalez-Billault, C. (2015). Contribution of NADPH oxidase to the establishment of hippocampal neuronal polarity in culture. *J. Cell Sci.* 128, 2989–2995. doi: 10.1242/jcs.168567

Wilton, D. K., and Stevens, B. (2020). The contribution of glial cells to Huntington's disease pathogenesis. *Neurobiol. Dis.* 143:104963. doi: 10.1016/j.nbd.2020.104963

Winterbourn, C. C. (2008). Reconciling the chemistry and biology of reactive oxygen species. *Nat. Chem. Biol.* 4, 278–286. doi: 10.1038/nchembio.85

Winterbourn, C. C. (2013). The biological chemistry of hydrogen peroxide. *Methods Enzymol.* 528, 3–25. doi: 10.1016/B978-0-12-405881-1.00001-X

Woerner, A. C., Frottin, F., Hornburg, D., Feng, L. R., Meissner, F., Patra, M., et al. (2016). Cytoplasmic protein aggregates interfere with nucleocytoplasmic transport of protein and RNA. *Science* 351, 173–176. doi: 10.1126/science.aad2033

Wong, Y. C., and Holzbaur, E. L. (2014). The regulation of autophagosome dynamics by huntingtin and HAP1 is disrupted by expression of mutant huntingtin, leading to defective cargo degradation. *J. Neurosci.* 34, 1293–1305. doi: 10.1523/JNEUROSCI.1870-13.2014

Wu, J., Ryskamp, D. A., Liang, X., Egorova, P., Zakharova, O., Hung, G., et al. (2016). Enhanced Store-operated calcium entry leads to striatal synaptic loss in a Huntington's Disease mouse model. *J. Neurosci.* 36, 125–141. doi: 10.1523/JNEUROSCI.1038-15.2016

Xu, J., Wei, X., Gao, F., Zhong, X., Guo, R., Ji, Y., et al. (2020). Nicotinamide adenine dinucleotide phosphate oxidase 2-derived reactive oxygen species contribute to long-term potentiation of C-fiber-evoked field potentials in spinal dorsal horn and persistent mirror-image pain following high-frequency stimulus of the sciatic nerve. *Pain* 161, 758–772. doi: 10.1097/j.pain.0000000000001761

Xu, X., Tay, Y., Sim, B., Yoon, S. I., Huang, Y., Ooi, J., et al. (2017). Reversal of phenotypic abnormalities by CRISPR/Cas9-mediated gene correction in Huntington disease patient-derived induced pluripotent stem cells. *Stem Cell Rep.* 8, 619–633. doi: 10.1016/j.stemcr.2017.01.022

Yi, J. H., Kim, D. H., Piers, T. M., Kim, S. C., Whitcomb, D. J., Regan, P., et al. (2018). Postsynaptic p47phox regulates long-term depression in the hippocampus. *Cell Discov.* 4:44. doi: 10.1038/s41421-018-0046-x

Yoneyama, M., Kawada, K., Gotoh, Y., Shiba, T., and Ogita, K. (2010). Endogenous reactive oxygen species are essential for proliferation of neural stem/progenitor cells. *Neurochem. Int.* 56, 740–746. doi: 10.1016/j.neuint.2009.11.018

Zamboni, V., Armentano, M., Berto, G., Ciraolo, E., Ghigo, A., Garzotto, D., et al. (2018). Hyperactivity of Rac1-GTPase pathway impairs neuritogenesis of cortical neurons by altering actin dynamics. *Sci. Rep.* 8:7254. doi: 10.1038/s41598-018-25354-3

Zhan, Y., Virbasius, J. V., Song, X., Pomerleau, D. P., and Zhou, G. W. (2002). The p40phox and p47phox PX domains of NADPH oxidase target cell membranes via direct and indirect recruitment by phosphoinositides. *J. Biol. Chem.* 277, 4512–4518. doi: 10.1074/jbc.M109520200

Zhang, D., Hu, X., Qian, L., Chen, S. H., Zhou, H., Wilson, B., et al. (2011). Microglial MAC1 receptor and PI3K are essential in mediating beta-amyloid peptide-induced microglial activation and subsequent neurotoxicity. *J. Neuroinflammation* 8:3. doi: 10.1186/1742-2094-8-3

Zhang, J., Malik, A., Choi, H. B., Ko, R. W., Dissing-Olesen, L., and MacVicar, B. A. (2014). Microglial CR3 activation triggers long-term synaptic depression in the hippocampus via NADPH oxidase. *Neuron* 82, 195–207. doi: 10.1016/j.neuron.2014.01.043

Zheng, J., Winderickx, J., Franssens, V., and Liu, B. (2018). A mitochondria-associated oxidative stress perspective on Huntington's Disease. *Front. Mol. Neurosci.* 11:329. doi: 10.3389/fnmol.2018.00329

Conflict of Interest: The authors declare that the research was conducted in the absence of any commercial or financial relationships that could be construed as a potential conflict of interest.

Publisher's Note: All claims expressed in this article are solely those of the authors and do not necessarily represent those of their affiliated organizations, or those of the publisher, the editors and the reviewers. Any product that may be evaluated in this article, or claim that may be made by its manufacturer, is not guaranteed or endorsed by the publisher.

Advantages of publishing in Frontiers

OPEN ACCESS
Articles are free to read for greatest visibility and readership

FAST PUBLICATION
Around 90 days from submission to decision

HIGH QUALITY PEER-REVIEW
Rigorous, collaborative, and constructive peer-review

TRANSPARENT PEER-REVIEW
Editors and reviewers acknowledged by name on published articles

Frontiers
Avenue du Tribunal-Fédéral 34
1005 Lausanne | Switzerland

Visit us: www.frontiersin.org
Contact us: frontiersin.org/about/contact

REPRODUCIBILITY OF RESEARCH
Support open data and methods to enhance research reproducibility

DIGITAL PUBLISHING
Articles designed for optimal readership across devices

FOLLOW US
@frontiersin

IMPACT METRICS
Advanced article metrics track visibility across digital media

EXTENSIVE PROMOTION
Marketing and promotion of impactful research

LOOP RESEARCH NETWORK
Our network increases your article's readership